



Universidade de Aveiro
2023

**Sandra Cristina
Carvalho Hilário**

**O género *Diaporthe* em mirtilos em Portugal: da
diversidade de espécies à patogenicidade**

**The genus *Diaporthe* on blueberry plants in
Portugal: from species diversity to pathogenicity**



Universidade de Aveiro
2023

Sandra Cristina
Carvalho Hilário

O género *Diaporthe* em mirtilos em Portugal: da
diversidade de espécies à patogenicidade

The genus *Diaporthe* on blueberry plants in
Portugal: from species diversity to pathogenicity

Tese apresentada à Universidade de Aveiro para cumprimento dos requisitos necessários à obtenção do grau de Doutor em Biologia, realizada sob a orientação científica do Doutor Artur Jorge da Costa Peixoto Alves, Professor Auxiliar com Agregação do Departamento de Biologia da Universidade de Aveiro e sob coorientação da Doutora Liliana Tavares dos Santos, Investigadora Auxiliar do Departamento de Biologia da Universidade de Aveiro

Apoio financeiro da FCT e do FSE no âmbito do III Quadro Comunitário de Apoio.

Bolsa de doutoramento:
SFRH/BD/137394/2018



“If you ever made any valuable discoveries, it has been due more to patient attention, than to any other talent.”

Isaac Newton

o júri

presidente

Doutor Carlos Fernandes da Silva
professor Catedrático da Universidade de Aveiro

vogais

Doutor Artur Jorge da Costa Peixoto Alves
professor auxiliar com agregação da Universidade de Aveiro

Doutor António Manuel Santos Carriço Portugal
professor auxiliar da Universidade de Coimbra

Doutora Dora Cristina Vicente Batista Lyon de Castro
professora auxiliar da Universidade de Lisboa

Doutora Glória Catarina Cintra da Costa Pinto
professora auxiliar da Universidade de Aveiro

Joana Cardoso da Costa
investigadora da Universidade de Coimbra

agradecimentos

Embora uma tese seja um trabalho individual, há contributos diversos que não podem e nem devem deixar de ser realçados. Por essa razão, manifesto o meu agradecimento a todos aqueles que contribuíram, diretamente ou indiretamente, para a realização esta tese.

Aos meus orientadores. À Doutora Liliana Santos e ao Prof. Doutor Artur Alves. No entanto, não posso deixar de manifestar o meu especial agradecimento ao Prof. Artur. Por todo o incentivo, espírito crítico, confiança, compreensão, constante disponibilidade e por tudo o que me foi ensinando ao longo destes anos. Agradeço também a sua amizade que foi igualmente determinante para o desenvolvimento desta tese.

A todos os colegas do Microlab com quem tive um enorme prazer de trabalhar e partilhar esta experiência. Agradeço à Marta Tação pela sua constante boa disposição, ajuda, amizade e alegria contagiante. À Isabel Silva e à Diana pelo apoio, pelas conversas e por todo o companheirismo.

Ao colega Micael. Havia tanto a dizer. Deixo apenas um simples, mas profundo agradecimento por todo o apoio incondicional, pelos conselhos e ajuda. Pela eterna paciência em ouvir-me nos dias não. Pelas trocas de ideias que foram tantas e que contribuíram para a realização deste trabalho. Por todos os bons e maus momentos que partilhámos. Os risos, as lágrimas e as conversas que guardo com tanto carinho. Um amigo e colega com quem quero, seguramente, voltar a trabalhar.

Aos meus pais. Os que nunca desistem. Um obrigado especial por todos os conselhos, pelo apoio e incentivo constantes.

À minha irmã Bárbara. Pela paciência em ouvir os meus desabafos em fases menos boas. Pelo apoio e por todas as nossas conversas que me ajudaram tanto.

Às amigas Andreia e Nicole. Agradeço todo o apoio que me deram, a boa disposição e alegria contante. Foi tão importante ter a vossa presença nesta fase.

palavras-chave

Diversidade, filogenia, fisiologia vegetal, genómica, patogenicidade, taxonomia

resumo

O mirtilo (*Vaccinium corymbosum*) é uma planta não nativa, bastante cultivada em Portugal, sendo importante para a economia do país. No entanto, o rápido crescimento na sua produção tem levado ao aumento de doenças causadas por agentes fitopatogénicos, em particular por fungos. Por este motivo, esta tese teve como objetivo estudar a diversidade e patogenicidade de espécies do género *Diaporthe* em várias regiões do país, visto serem agentes patogénicos que afetam plantações de mirtilo.

Foram amostradas plantas sintomáticas de mirtilo, das quais se obteve uma coleção de 206 isolados fúngicos. Os isolados foram submetidos a tipagem por MSP-PCR para avaliar a diversidade genética. Com base nos perfis genéticos, foram selecionados isolados representativos para identificação molecular. Os isolados de *Diaporthe* foram identificados, representando 4 espécies conhecidas (*D. rudis*, *D. foeniculina*, *D. amygdali* e *D. ambigua*), 4 espécies novas (*D. crousii*, *D. phillipsii*, *D. rossmaniae* e *D. vacuae*) e um potencial híbrido (*D. hybrida*). Os ensaios de patogenicidade, permitiram perceber que *D. amygdali* e *D. vacuae* são as espécies mais agressivas, enquanto *D. foeniculina* revelou ser a menos agressiva.

Dada a importância de detetar e identificar estes fungos, foram aplicados diferentes métodos para obter uma correta delimitação de *D. amygdali* e *D. eres*, dois complexos de espécies (constituídos por várias espécies) sobre os quais ainda existem dúvidas. A aplicação destes métodos revelou que *D. amygdali* e *D. eres* são de facto espécies e não complexos de espécies, e que *D. vaccinii* (organismo de quarentena) é um sinónimo de *D. eres*.

Em ensaios de inoculação, foi estudado o efeito das espécies *D. amygdali* e *D. eres* (syn. *D. vaccinii*) na planta de mirtilo sob condições de défice de água. De uma forma geral, a infeção pelos fungos levou a uma diminuição dos rácios de fotossíntese e condutância estomática. A mortalidade causada por *D. amygdali* indica que o défice de água parece aumentar a patogenicidade desta espécie.

Por fim, as espécies *D. amygdali* e *D. eres* (syn. *D. vaccinii*) foram estudadas em mais detalhe através da sequenciação dos seus genomas. Ambas as espécies apresentam nos seus genomas, uma grande diversidade de grupos de genes biossintéticos, transportadores celulares, e enzimas hidrolíticas.

Esta tese demonstrou que em Portugal, existe uma grande diversidade de espécies de *Diaporthe* associadas á cultura do mirtilo. Algumas destas espécies podem causar cancro, murchidão apical e em alguns casos a morte da planta. Foi também demonstrado que estas espécies apresentam assinaturas genómicas que refletem a capacidade de produzir fitotoxinas e de degradar a parede celular do hospedeiro, facilitando o processo de infeção.

keywords

Diversity, genomics, pathogenicity, phylogeny, plant physiology, taxonomy

abstract

The blueberry (*Vaccinium corymbosum*) is a non-native plant, widely cultivated in Portugal, representing an important asset for the Portuguese economy. However, the fast growth in production has led to an increase in diseases caused by phytopathogenic agents, particularly by fungi. Thus, this work aimed to study the diversity and pathogenicity of species of the genus *Diaporthe* in several regions of the country, since they are pathogens affecting blueberry plantations.

Symptomatic plants were sampled, from which a collection of 206 fungal isolates was obtained. These isolates were subjected to MSP-PCR fingerprinting to assess the genetic diversity of the entire collection. Based on the genetic profiles obtained, representative isolates were selected for molecular identification.

Diaporthe isolates were identified representing 4 known species (*D. rudis*, *D. foeniculina*, *D. amygdali* and *D. ambigua*), 4 new species (*D. crousii*, *D. phillipsii*, *D. rossmaniae* and *D. vacuae*) and a potential hybrid (*D. hybrida*). Pathogenicity assays showed that *D. amygdali* and *D. vacuae* are the most aggressive species, while *D. foeniculina* proved to be the least aggressive. Since it is essential to detect and identify these fungal pathogens to avoid disease outbreaks, phylogenetic methods were applied to achieve a correct delimitation of the species *D. amygdali* (the most aggressive) and *D. vaccinii* (quarantine organism). The use of these methods revealed that both *D. amygdali* and *D. eres* represent species complexes, and that *D. vaccinii* is a synonym with *D. eres*.

In inoculation trials, the effect of *D. amygdali* and *D. eres* species (syn. *D. vaccinii*) on blueberry plants under water deficit conditions was studied. Overall, fungal infection caused a decrease of photosynthesis and stomatal conductance ratios. The mortality caused by *D. amygdali* indicates that the water deficit seems to trigger the pathogenicity of this species.

Finally, the species *D. amygdali* and *D. eres* (syn. *D. vaccinii*) were studied in more detail, by sequencing their genomes. Both species comprise a high diversity of biosynthetic gene clusters, transporters of ions and sugars, and hydrolytic enzymes.

This thesis demonstrated that the species of *Diaporthe* studied cause symptoms in blueberries, and in some cases their death. It was also demonstrated that these species have genomic signatures that reflect the ability to produce phytotoxins and to degrade the host cell wall, facilitating the infection process.

Table of Contents

List of Figures.....	VII
List of Tables.....	XII
List of Abbreviations.....	XV
Thesis Outline.....	XVII

CHAPTER 1 | General Introduction

The genus <i>Diaporthe</i>	3
<i>Diaporthe</i> vs <i>Phomopsis</i> : The abolishment of the dual nomenclature.....	3
Morphological characteristics of the genus.....	4
Position in Ascomycetes systematics and taxonomic history.....	5
The species in <i>Diaporthe</i>	7
How many species are there?.....	7
Species concepts in <i>Diaporthe</i>	8
How to delimit species in <i>Diaporthe</i>	10
<i>Diaporthe</i> : endophytes or pathogens?.....	11
<i>Diaporthe</i> on blueberry plants.....	14
The blueberry: The genus <i>Vaccinium</i> , diversity and distribution.....	14
The blueberries worldwide.....	14
The market of blueberries in Portugal.....	15
Diversity and pathogenicity of <i>Diaporthe</i>	16
A brief history of <i>Diaporthe vaccinii</i>	18
Host-pathogen interactions.....	22
Biotic and abiotic stresses.....	22
How fungi infect the host?.....	22
How plants respond to fungal infection?.....	24
Genomics of fungal plant pathogens.....	25
Aims of the work.....	28
References.....	29

CHAPTER 2 | Diversity and pathogenicity of *Diaporthe* species associated with blueberry plants in Portugal

SUBCHAPTER 2.1 | *Diaporthe* species associated with twig blight and dieback of *Vaccinium corymbosum* in Portugal, with description of four new species

Abstract.....	51
Introduction.....	51
Material and Methods.....	53
Fungal isolation.....	53

DNA extraction, PCR amplification, and sequencing.....	54
Phylogenetic analyses.....	55
Mating type assay.....	57
Temperature growth studies.....	57
Pathogenicity tests.....	59
Results.....	59
Fungal isolation.....	59
Molecular characterization.....	59
Temperature growth studies.....	64
Pathogenicity tests.....	64
Taxonomy.....	65
Discussion.....	74
Conclusions.....	78
Acknowledgments.....	78
References.....	80
Supplementary Material.....	85

SUBCHAPTER 2.2 | Diversity and pathogenicity of *Diaporthe* species revealed from a survey of blueberry orchards in Portugal

Abstract.....	91
Introduction.....	92
Material and Methods.....	94
Sampling and fungal isolates.....	94
Morphological characterization.....	95
DNA extraction, PCR amplification, and sequencing.....	95
Phylogenetic analysis.....	95
Mating type assay.....	96
Prevalence of <i>Diaporthe</i> species.....	96
Plant material and pathogenicity tests.....	96
Results.....	101
Fungal isolation.....	101
Molecular characterization.....	103
Distribution and prevalence of <i>Diaporthe</i> species.....	106
Plant mortality.....	107
Lesion length measurements.....	107
Taxonomy.....	111
Discussion.....	120
Conclusions.....	125
Acknowledgments.....	126

References.....	126
Supplementary Material.....	133

CHAPTER 3 | Coalescent models and phylogenetic networks to resolve species complexes in *Diaporthe*

SUBCHAPTER 3.1 | *Diaporthe amygdali*, a species complex or a complex species?

Abstract.....	143
Introduction.....	144
Material and Methods.....	146
Fungal isolation.....	146
DNA extraction and PCR amplification.....	146
Morphological characterization and temperature growth studies.....	146
Phylogenetic analyses.....	147
Pairwise homoplasy index test.....	147
Phylogenetic network analyses.....	148
Coalescent-based species delimitation.....	148
Population genetic diversity.....	149
Results.....	154
Phylogenetic analyses.....	154
Species delimitation based on GCPSR principle.....	154
Species delimitation based on coalescent methods.....	155
Pairwise homoplasy test and phylogenetic networks.....	156
Population genetic diversity.....	157
Morphological analysis.....	157
Taxonomy.....	161
Discussion.....	166
Conclusions.....	170
Acknowledgments.....	170
References.....	171
Supplementary Material.....	176

SUBCHAPTER 3.2 | Using genealogical concordance and coalescent-based species delimitation to assess species boundaries in the *Diaporthe eres* complex

Abstract.....	195
Introduction.....	195
Material and Methods.....	198
Fungal isolates.....	198
DNA extraction and PCR amplification.....	198

Phylogenetic analyses.....	198
Pairwise homoplasy index test and phylogenetic network analysis.....	199
Species delimitation analyses.....	199
Population genetic diversity.....	200
Morphology of the <i>Diaporthe eres</i> species complex.....	200
Results.....	204
Phylogenetic analyses and informative characters.....	204
Species delimitation based on GCPSR principle.....	204
Species delimitation based on Poisson Tree Processes (PTP).....	206
Pairwise homoplasy test and phylogenetic networks.....	210
Population genetic diversity.....	211
Morphology of the <i>Diaporthe eres</i> species complex.....	211
Taxonomy.....	211
Discussion.....	222
Conclusions.....	227
Acknowledgments.....	228
References.....	228
Supplementary Material.....	235

CHAPTER 4 | Caveats of the internal transcribed spacer region as a barcode to resolve species boundaries in *Diaporthe*

Abstract.....	249
Introduction.....	250
Material and Methods.....	252
Fungal isolation.....	252
DNA extraction and PCR amplification.....	252
Mating type assays.....	252
Phylogenetic analyses.....	252
Mating experiments.....	253
Morphology and culture characteristics.....	256
Population genetic diversity and haplotype network analysis.....	256
Results.....	256
Fungal isolation.....	256
Phylogenetic analyses.....	257
ITS rRNA cloning.....	263
Case studies.....	264
1. Intraspecific ITS variability.....	264
2. Intrasporocarpic and intragenomic ITS heterogeneity.....	265
3. Hybridization in <i>Diaporthe</i>	266

Mating type diagnosis and mating experiments.....	267
Polymorphism and population structure analysis.....	269
Morphological characterization.....	271
Taxonomy.....	273
Discussion.....	281
Guidelines for an appropriate species delimitation in the genus <i>Diaporthe</i>	287
Conclusions.....	288
Acknowledgments.....	289
References.....	289
Supplementary Material.....	297

CHAPTER 5 | The impact of two *Diaporthe* spp. on *Vaccinium corymbosum* physiological fitness under different water availability scenarios

Abstract.....	305
Introduction.....	306
Material and Methods.....	308
Fungal isolates.....	308
Plant material.....	308
Plant inoculation procedure.....	309
Experimental design.....	309
Disease progression.....	310
Water status.....	310
Leaf gas exchange.....	311
Biochemical parameters.....	311
Photosynthetic pigments, total soluble sugars, and starch.....	311
Malondialdehyde (MDA) content.....	312
Proline quantification.....	312
Total phenolic content and flavonoids quantification.....	312
Statistical analysis.....	313
Results.....	314
Disease progression.....	314
Necrosis length.....	314
Water potential.....	315
Relative water content.....	315
Leaf gas exchange measurements.....	317
Photosynthetic pigments content.....	318
Malondialdehyde content.....	319
Phenolic compounds and flavonoids content.....	320
Proline content.....	321

Total soluble sugars and starch content.....	321
Discussion.....	322
Conclusions.....	326
Acknowledgments.....	327
References.....	327

CHAPTER 6 | Genome analysis of two blueberry pathogens: *Diaporthe amygdali* CAA958 and *Diaporthe eres* CBS 160.32

Abstract.....	337
Introduction.....	338
Material and Methods.....	339
Fungal material and culture conditions.....	339
DNA extraction.....	340
Genome sequencing, assembly, and prediction.....	340
Dispersed repeat sequences and non-coding tRNA annotation.....	340
Gene annotation and functional analyses.....	341
Comparative analyses.....	342
Results.....	342
Genome assembly and genomic characteristics.....	342
Gene prediction and functional annotation.....	344
Fusicoccin A biosynthesis.....	345
Virulence factors, effectors and strategies to overcome host responses.....	346
Cellular transporters.....	348
Comparative analysis.....	349
Predicted genes and genome statistics.....	349
CAZymes.....	351
BGCs.....	353
Discussion.....	355
Conclusions.....	360
Acknowledgments.....	360
Data availability.....	360
References.....	361
Supplementary Material.....	370

CHAPTER 7 | Final Considerations

General discussion.....	373
Future perspectives.....	380
References.....	382

List of Figures

CHAPTER 1

Figure 1. Morphological characteristics of some <i>Diaporthe</i> species.....	4
Figure 2. The <i>Sordaryomycetes</i> class (<i>Pezizomycotina</i> sub-phylum), comprising 7 sub-classes and representative genera.....	6
Figure 3. Numbers of newly introduced species names of <i>Diaporthe</i> and <i>Phomopsis</i> for each decade from 1870 to 2020.....	8
Figure 4. An overview of <i>Diaporthe</i> and <i>Phomopsis</i> species distribution worldwide.....	13
Figure 5. Pathogenic invasion strategies from different trophic lifestyles.....	24

CHAPTER 2 | SUBCHAPTER 2.1

Figure 1. Maximum likelihood phylogenetic tree obtained from combined analysis of ITS, <i>tef1-α</i> , <i>tub2</i> , <i>cal</i> , and <i>his3</i> sequence data from <i>Diaporthe</i> species.....	63
Figure 2. Morphology of <i>Diaporthe crousii</i> from <i>Vaccinium corymbosum</i> (MUM 19.29).....	66
Figure 3. Morphology of <i>Diaporthe phillipsii</i> from <i>Vaccinium corymbosum</i> (MUM 19.28).....	69
Figure 4. Morphology of <i>Diaporthe rossmaniae</i> from <i>Vaccinium corymbosum</i> (MUM 19.30).....	71
Figure 5. Morphology of <i>Diaporthe vacuae</i> from <i>Vaccinium corymbosum</i> (MUM 19.31).....	73
Figure S1. Maximum Likelihood phylogenetic tree obtained from ITS sequences data from <i>Diaporthe</i> species.....	85
Figure S2. Maximum Likelihood phylogenetic tree obtained from <i>tef1-α</i> sequences data from <i>Diaporthe</i> species.....	86
Figure S3. Maximum Likelihood phylogenetic tree obtained from <i>tub2</i> sequences data from <i>Diaporthe</i> species.....	87
Figure S4. Maximum Likelihood phylogenetic tree obtained from <i>his3</i> sequences data from <i>Diaporthe</i> species.....	88
Figure S5. Maximum Likelihood phylogenetic tree obtained from <i>cal</i> sequences data from <i>Diaporthe</i> species.....	89

CHAPTER 2 | SUBCHAPTER 2.2

Figure 1. Map of Portugal indicating the distribution and frequency of each <i>Diaporthe</i> species within sampled regions.....	102
Figure 2. Symptoms on <i>Vaccinium corymbosum</i> with associated <i>Diaporthe</i> species.....	102
Figure 3. Phylogenetic relationships based on combined ITS, <i>tef1-α</i> , <i>tub2</i> , <i>his3</i> and <i>cal</i> sequence data from <i>Diaporthe</i> species.....	105
Figure 4. Representative symptoms of twig dieback induced by inoculation of blueberry plants...	107
Figure 5. Box plot of lesion length (cm) caused by isolates of <i>Diaporthe</i> on twigs.....	109
Figure 6. Morphology of <i>Diaporthe ambigua</i>	112

Figure 7. Morphology of <i>Diaporthe crousii</i>	114
Figure 8. Morphology of <i>Diaporthe foeniculina</i>	116
Figure 9. Morphology of <i>Diaporthe leucospermi</i>	118
Figure 10. Morphology of <i>Diaporthe rudis</i>	120
Figure S1. Phylogram generated from Maximum Likelihood analysis based on combined ITS sequence data from <i>Diaporthe</i> species.....	133
Figure S2. Phylogram generated from Maximum Likelihood analysis based on <i>tef1-α</i> sequence data from <i>Diaporthe</i> species.....	134
Figure S3. Phylogram generated from Maximum Likelihood analysis based on <i>tub2</i> sequence data from <i>Diaporthe</i> species.....	135
Figure S4. Phylogram generated from Maximum Likelihood analysis based on <i>cal</i> sequence data from <i>Diaporthe</i> species.....	136
Figure S5. Phylogram generated from Maximum Likelihood analysis based on combined <i>his3</i> sequence data from <i>Diaporthe</i> species.....	137
Figure S6. Time course percentage of mortality of cultivar ‘Duke’, after inoculation.....	138
Figure S7. Time course percentage of mortality of cultivar ‘Legacy’, after inoculation.....	138
Figure S8. Time course percentage of mortality of cultivar ‘Spartan’, after inoculation.....	138
Figure S9. Box plot of lesion length (cm) caused by <i>Diaporthe</i> species on blueberry twigs.....	139

CHAPTER 3 | SUBCHAPTER 3.1

Figure 1. Phylogenetic relationships and species boundaries of <i>Diaporthe amygdali</i> complex and related species.....	153
Figure 2. Phylogenetic network from the concatenated data (ITS, <i>tef1-α</i> , <i>tub2</i> , <i>his3</i> and <i>cal</i>) representing the structure of the <i>Diaporthe amygdali</i> complex and related taxa	158
Figure 3. Results of the GMYC analyses for the <i>Diaporthe amygdali</i> clade and related taxa.....	159
Figure 4. Results of the PTP analyses for the <i>Diaporthe amygdali</i> clade and related taxa, based on the Bayesian and Maximum Likelihood topologies.....	160
Figure 5. Morphology of <i>Diaporthe amygdali</i> CAA958 from <i>Vaccinium corymbosum</i>	163
Figure S1. Phylogram generated from maximum likelihood analysis based on ITS sequence data of the <i>Diaporthe amygdali</i> species complex.....	176
Figure S2. Phylogram generated from maximum likelihood analysis based on <i>tef1-α</i> sequence data of the <i>Diaporthe amygdali</i> species complex.....	177
Figure S3. Phylogram generated from maximum likelihood analysis based on <i>tub2</i> sequence data of the <i>Diaporthe amygdali</i> species complex.....	178
Figure S4. Phylogram generated from maximum likelihood analysis based on <i>his3</i> sequence data of the <i>Diaporthe amygdali</i> species complex.....	179
Figure S5. Phylogram generated from maximum likelihood analysis based on <i>cal</i> sequence data of the <i>Diaporthe amygdali</i> species complex.....	180

Figure S6. Phylogram generated from maximum likelihood analysis based on ITS sequence data for <i>Diaporthe amygdali</i> species complex and related species.....	181
Figure S7. Phylogram generated from maximum likelihood analysis based on <i>tef1-α</i> sequence data for <i>Diaporthe amygdali</i> species complex.....	182
Figure S8. Phylogram generated from maximum likelihood analysis based on <i>tub2</i> sequence data for <i>Diaporthe amygdali</i> species complex.....	183
Figure S9. Phylogram generated from maximum likelihood analysis based on <i>his3</i> sequence data for <i>Diaporthe amygdali</i> species complex.....	184
Figure S10. Phylogram generated from maximum likelihood analysis based on <i>cal</i> sequence data for <i>Diaporthe amygdali</i> species complex.....	185
Figure S11. Results of the PTP analysis for the <i>Diaporthe amygdali</i> complex.....	186
Figure S12. Phylogenetic network from ITS locus, representing the structure of the <i>Diaporthe amygdali</i> complex.....	187
Figure S13. Phylogenetic network from <i>tef1-α</i> locus, representing the structure of the <i>Diaporthe amygdali</i> complex.....	188
Figure S14. Phylogenetic network from <i>tub2</i> locus, representing the structure of the <i>Diaporthe amygdali</i> complex.....	189
Figure S15. Phylogenetic network from <i>his3</i> locus, representing the structure of the <i>Diaporthe amygdali</i> complex.....	190
Figure S16. Phylogenetic network from <i>cal</i> locus, representing the structure of the <i>Diaporthe amygdali</i> complex.....	191
Figure S17. Dendrogram based on the Ward's method showing the distribution of the lengths and width ratio (L/W) of alpha conidia and conidiophores.....	192

CHAPTER 3 | SUBCHAPTER 3.2

Figure 1. Maximum Likelihood (ML) tree of the <i>Diaporthe eres</i> complex and related species, based on ITS <i>tef1-α</i> , <i>tub2</i> , <i>his3</i> and <i>cal</i> loci.....	207
Figure 2. Results of the single PTP analyses for the <i>Diaporthe eres</i> species complex and related taxa, based on Bayesian and Maximum Likelihood topologies.....	208
Figure 3. Results of the mPTP analysis for the <i>Diaporthe eres</i> species complex.....	209
Figure 4. Phylogenetic network from the concatenated data (ITS, <i>tef1-α</i> , <i>tub2</i> , <i>his3</i> and <i>cal</i>) representing the structure of <i>Diaporthe eres</i> species complex.....	210
Figure 5. Dendrogram based on the Ward's method showing the distribution of the lengths and width ratio (L/W) of alpha conidia, beta conidia and conidiophores.....	212
Figure S1. Maximum Likelihood tree based on ITS sequences of the <i>Diaporthe eres</i> complex....	235
Figure S2. Maximum Likelihood tree based on <i>tef1-α</i> sequences of the <i>Diaporthe eres</i> complex....	236
Figure S3. Maximum Likelihood tree based on <i>tub2</i> sequences of the <i>Diaporthe eres</i> complex....	237
Figure S4. Maximum Likelihood tree based on <i>his3</i> sequences of the <i>Diaporthe eres</i> complex....	238
Figure S5. Maximum Likelihood tree based on <i>cal</i> sequences of the <i>Diaporthe eres</i> complex....	239

Figure S6. Maximum Likelihood tree based on ITS sequence data for the <i>Diaporthe eres</i> species complex and related species.....	240
Figure S7. Maximum Likelihood tree based on <i>tef1-α</i> sequence data for the <i>Diaporthe eres</i> species complex and related species.....	241
Figure S8. Maximum Likelihood tree based on <i>tub2</i> sequence data for the <i>Diaporthe eres</i> species complex and related species.....	242
Figure S9. Maximum Likelihood tree based on <i>his3</i> sequence data for the <i>Diaporthe eres</i> species complex and related species.....	243
Figure S10. Maximum Likelihood tree based on <i>cal</i> sequence data for the <i>Diaporthe eres</i> species complex and related species.....	244
Figure S11. Maximum Likelihood tree based on <i>tef-α</i> , <i>tub2</i> , <i>his3</i> and <i>cal</i> sequence data for the <i>Diaporthe eres</i> species complex and related species.....	245
Figure S12. Results of the single PTP analyses for the <i>Diaporthe eres</i> species complex and related taxa, based on <i>tef1-α</i> , <i>tub2</i> , <i>his3</i> and <i>cal</i> loci.....	246

CHAPTER 4

Figure 1. Maximum Likelihood phylogenetic tree obtained from ITS sequences data from <i>Diaporthe</i> species.....	261
Figure 2. Maximum Likelihood phylogenetic tree obtained from ITS, <i>tef1-α</i> , <i>tub2</i> , <i>his3</i> and <i>cal</i> sequences data from <i>Diaporthe</i> species.....	262
Figure 3. Sequencing chromatogram of PCR product of the rRNA ITS1-5.8S-ITS2 region of <i>Diaporthe novem</i> strain CAA300.....	263
Figure 4. Alignment of the nuclear ribosomal DNA of <i>Diaporthe portugallica</i> and <i>D. phillipsii</i> ex-types and the putative hybrids CAA998 and CAA999.....	267
Figure 5. Mating experiments between some isolates from ITS populations of <i>D. novem</i> and <i>D. malorum</i>	268
Figure 6. Median joining networks constructed for Internal Transcribed Spacer (ITS) sequences representing haplotypes of <i>Diaporthe malorum</i> and <i>D. novem</i>	270
Figure 7. Morphology of <i>Diaporthe malorum</i> isolates from <i>Vaccinium corymbosum</i>	271
Figure 8. Morphology of <i>Diaporthe novem</i> isolates from <i>Foeniculum vulgare</i>	272
Figure 9. Morphology of <i>Diaporthe xhybrida nothosp. nov.</i> from <i>Vaccinium corymbosum</i>	275
Figure 10. Morphology of <i>Diaporthe malorum</i> progenies.....	277
Figure S1. Maximum Likelihood phylogenetic tree obtained from <i>tef1-α</i> sequences data from <i>Diaporthe</i> species.....	297
Figure S2. Maximum Likelihood phylogenetic tree obtained from <i>tub2</i> sequences data from <i>Diaporthe</i> species.....	298
Figure S3. Maximum Likelihood phylogenetic tree obtained from <i>his3</i> sequences data from <i>Diaporthe</i> species.....	299

Figure S4. Maximum Likelihood phylogenetic tree obtained from <i>cal</i> sequences data from <i>Diaporthe</i> species.....	300
Figure S5. Maximum Likelihood phylogenetic tree obtained from <i>tef1-α</i> , <i>tub2</i> , <i>his3</i> and <i>cal</i> sequences data from <i>Diaporthe</i> species.....	301

CHAPTER 5

Figure 1. Experimental design to evaluate the physiological performance of blueberry plants, inoculated with two fungal species and under different water regimes.....	310
Figure 2. Blueberry mortality after inoculation with <i>Diaporthe amygdali</i> and <i>D. eres</i>	314
Figure 3. Lesion lengths on blueberry plants caused by <i>Diaporthe eres</i> and <i>D. amygdali</i>	315
Figure 4. Shoot water potential of blueberry plants (Ψ_{md}).....	315
Figure 5. Foliar net CO ₂ assimilation rate (<i>A</i>), intercellular CO ₂ concentration (<i>C_i</i>), stomatal conductance (<i>g_s</i>) and transpiration rate (<i>E</i>) of blueberry plants.....	316
Figure 6. Relative water content (RWC) of blueberry plants.....	317
Figure 7. Chlorophyll A, b, and carotenoids content of blueberry plants.....	318
Figure 8. MDA content of blueberry plants.....	320
Figure 9. Phenolic compounds and flavonoids content of blueberry plants.....	320
Figure 10. Proline content of blueberry plants.....	321
Figure 11. Total soluble sugars and starch content of blueberry plants.....	322

CHAPTER 6

Figure 1. Gene Ontology (GO) and EggNOG functional annotation of <i>Diaporthe amygdali</i> CAA958 and <i>Diaporthe eres</i> CBS 160.32.....	345
Figure 2. Fusicoccin A biosynthetic gene clusters found in <i>Diaporthe amygdali</i> CAA958.....	346
Figure 3. Number of predicted genes encoding for the most abundant carbohydrate-active enzymes identified in the genomes of <i>Diaporthe</i> analyzed.....	352
Figure 4. Biosynthetic gene clusters (BGC) identified in the genomes of <i>Diaporthe</i> analyzed.....	354

CHAPTER 7

Figure 1. Representation of the main steps to consider an accurate species delimitation in the genus <i>Diaporthe</i>	376
Figure 2. Schematic representation for the construction of phylogenetic trees in the genus <i>Diaporthe</i> , the main pitfalls associated to the use of the ITS region on species delimitation.....	377

List of Tables

CHAPTER 1

Table 1. Synopsis of all <i>Diaporthe</i> associated to diseases on <i>Vaccinium corymbosum</i>	20
Table 2. Synopsis of all <i>Diaporthe</i> strains with genomes sequenced.....	27

CHAPTER 2 | SUBCHAPTER 2.1

Table 1. Isolates obtained from <i>Vaccinium corymbosum</i> used in this study.....	58
Table 2. <i>Diaporthe</i> species used in the multilocus sequence analysis.....	61
Table 3. Estimated growth parameters for <i>Diaporthe crousii</i> , <i>D. phillipsii</i> , <i>D. rossmaniae</i> , and <i>D. vacuae</i>	64
Table 4. Means \pm SD of lesion lengths (cm) caused by <i>Diaporthe</i> species inoculated on <i>Vaccinium corymbosum</i>	65

CHAPTER 2 | SUBCHAPTER 2.2

Table 1. List of plantations included in this study.....	94
Table 2. List of <i>Diaporthe</i> species used in this study.....	98
Table 3. Fungal isolates used and obtained from a previous study.....	101
Table 4. <i>Diaporthe</i> isolates used in the phylogenetic analysis.....	104
Table 5. Number of isolates and prevalence of each <i>Diaporthe</i> species	106
Table S1. Cases of <i>Diaporthe</i> species found alone or co-existing with other species in the same plant material surveyed.....	140

CHAPTER 3 | SUBCHAPTER 3.1

Table 1. List of <i>Diaporthe</i> species used in this study.....	150
Table 2. Alignment properties and nucleotide substitution models used for phylogenetic analyses.....	155
Table 3. Polymorphism and genetic diversity data for the <i>Diaporthe amygdali</i> complex.....	157
Table 4. Synopsis of micromorphological characteristics of <i>Diaporthe amygdali</i> synonyms discussed in this study.....	164
Table S1. Pairwise homoplasly index (PHI) of paired clades in <i>Diaporthe amygdali</i> complex, based on the concatenation of five loci.....	193

CHAPTER 3 | SUBCHAPTER 3.2

Table 1. List of <i>Diaporthe</i> species used in this study.....	201
Table 2. Alignment properties and nucleotide substitution models used for phylogenetic analyses.....	205
Table 3. Polymorphism and genetic diversity data for the <i>Diaporthe eres</i> species complex.....	211

Table 4. Synopsis of morphological characteristics of <i>Diaporthe eres</i> synonymous discussed in this study.....	217
--	-----

CHAPTER 4

Table 1. <i>Diaporthe</i> isolates from <i>Magnolia soulangeana</i> , <i>Vaccinium corymbosum</i> , <i>Foeniculum vulgare</i> and <i>Eucalyptus globulus</i> used in this study.....	254
Table 2. <i>Diaporthe</i> species used in the phylogenetic analyses.....	258
Table 3. Alignment properties from individual and combined phylograms.....	260
Table 4. Polymorphism and genetic diversity data of <i>Diaporthe novem</i> and <i>D. malorum</i>	269
Table 5. Synopsis of characters of <i>Diaporthe malorum</i> , <i>D. novem</i> and their representative isolates from the different ITS populations.....	278

CHAPTER 5

Table 1. Two-way ANOVA table for morphological and physiological parameters considering two water availability scenarios and fungi as fixed factors.....	316
Table 2. One-way ANOVA summary table for morphological and physiological parameters considering the inoculation of <i>Diaporthe eres</i> and <i>D. amygdali</i>	319

CHAPTER 6

Table 1. Genome assembly overview for the genome of <i>Diaporthe amygdali</i> CAA958, and <i>Diaporthe eres</i> CBS 160.32.....	343
Table 2. Statistical results for repetitive sequences, tandem repeats and tRNAs in <i>Diaporthe amygdali</i> CAA958 and <i>Diaporthe eres</i> CBS 160.32.....	343
Table 3. Putative proteins involved in fungal pathogenesis, identified in the genome of <i>Diaporthe amygdali</i> CAA958 and <i>Diaporthe eres</i> CBS 160.32.....	347
Table 4. Number of genes predicted to code for transporters in the genome of <i>Diaporthe amygdali</i> CAA958 and <i>Diaporthe eres</i> CBS 160.32.....	348
Table 5. Genomic features of the <i>Diaporthe</i> species analyzed.....	350
Table 6. Predicted genes encoding for CAZymes in the genomes of <i>Diaporthe amygdali</i> CAA958 and <i>Diaporthe eres</i> CBS 160.32.....	351
Table S1. Gene annotation of <i>Diaporthe amygdali</i> CAA958.....	370
Table S2. Gene annotation of <i>Diaporthe eres</i> CBS 160.32.....	370
Table S3. Predicted proteins with signal peptides.....	370
Table S4. Predicted proteins with transmembrane structure.....	370
Table S5. Predicted secreted proteins.....	370
Table S6. Pathogen-Host Interaction database	370
Table S7. Effectors candidates.....	370
Table S8. Predicted cellular transporters.....	370

Table S9. Predicted CAZymes of <i>Diaporthe eres</i> CBS 160.32.....	370
Table S10. Predicted CAZymes of <i>D. amygdali</i> CAA958.....	370
Table S11. Biosynthetic Gene Clusters.....	370

List of Abbreviations

A	Net CO ₂ Assimilation Rate
AA	Auxiliary Activities
ANOVA	Analysis of Variance
BEAST	Bayesian Evolutionary Analysis Sampling Trees
BLAST	Local Alignment Search Tool
BGCs	Biosynthetic Gene Clusters
BI	Bayesian Inference
BSC	Biological Species Concept
<i>cal</i>	calmodulin
CAZymes	Carbohydrate-Active Enzymes
CE	Carbohydrate Esterases
<i>Ci</i>	Intercellular CO ₂ Concentration
CBM	Carbohydrate Binding Modules
COG/KOG	Eukaryotic Cluster of Orthologous Groups of Proteins
DRs	Dispersed Repeat Sequences
<i>E</i>	Transpiration Rate
EggNOG	Non-Supervised Orthologous Groups
FC	Field Capacity
GCPSR	Genealogical Concordance Phylogenetic Species Recognition
GH	Glycoside Hydrolases
GO	Gene Ontology
<i>gs</i>	Stomatal Conductance
GT	Glycosyltransferases
GMYC	Generalized Mixed Yule Coalescent
<i>his3</i>	histone
ITS	Internal Transcribed Spacer
JGI	Joint Genome Institute
KEGG	Kyoto Encyclopedia of Genes and Genomes
LINEs	Long Interspersed Nuclear Elements
LTRs	Long Terminal Repeats
MDA	Malondialdehyde
MCMC	Markov Chain Monte Carlo
ML	Maximum Likelihood

MP	Maximum Parsimony
mPTP	multi-rate Poisson Tree Processes
MSC	Morphological Species Concept
MSP-PCR	Microsatellite-Primed PCR
MUM	Micoteca da Universidade do Minho
NCBI	National Center for Biotechnology Information
NNI	Nearest-Neighbour-Interchange
NRPs	Non-Ribosomal Peptide Synthases
PDA	Potato Dextrose Agar
PDB	Potato Dextrose Broth
PHI	Pairwise Homoplasy Index
PSC	Phylogenetic Species Concept
PTP	Poisson Tree Processes
PKs	Polyketide Synthases
PL	Polysaccharide Lyases
PP	Posterior Probabilities
RWC	Relative Water Content
SINEs	Short Interspersed Nuclear Elements
TC	Transporter Classification
<i>tef1-α</i>	Translation Elongation Factor 1-alpha
TRF	Tandem Repeat Finder
TRs	Tandem Repeat Sequences
<i>tub2</i>	beta-tubulin
UPGMA	Unweighted Pair Group Method with Arithmetic Mean
WP	Water Potential

Thesis Outline

The present thesis documents the research work done to evaluate and improve the knowledge about the diversity of species of *Diaporthe* occurring on blueberry plants (*Vaccinium corymbosum*) in Portugal, the pathogenic potential on this host under two different water regimes, as well as genomic signatures involved in the pathogenicity of *Diaporthe*. Given that a correct disease diagnosis is essential to develop new strategies to manage disease, prevent outbreaks and consequently economic losses, this research presents useful approaches to be applied for an accurate species delimitation in the genus *Diaporthe*. Different procedures were applied to achieve that, being the thesis organized in seven chapters as shown below:

CHAPTER 1: The first chapter includes a general review of the literature, providing background for the work carried out, and the main goals of the research.

CHAPTER 2: In chapter 2, the diversity of *Diaporthe* species associated with *Vaccinium corymbosum* plants in Portugal is presented. Here, the isolates were identified using DNA sequencing tools, new fungal species were described and tested on different cultivars to evaluate their aggressiveness.

CHAPTER 3: Based on the taxonomic ambiguities found in Chapter 2, Chapter 3 provides the need to use additional molecular and phylogenetic approaches for an accurate delimitation of species in *Diaporthe*. In this chapter, it is demonstrated that coalescent models and phylogenetic networks are useful to resolve species complexes in the genus.

CHAPTER 4: Chapter 4 complements the information obtained in Chapter 3, providing clear evidence and practical examples of how the primary barcoding marker for fungi, the internal transcribed spacer region (ITS), is not suitable to delimit species in *Diaporthe*.

CHAPTER 5: To complement the information obtained in Chapter 2 and given that taxonomic ambiguities of *D. eres* (syn. *D. vaccinii*) and *D. amygdali* (two of the most aggressive species on blueberry plants) were reviewed and set in Chapters 3 and 4, the Chapter 5 aimed to evaluate the effects of these species on blueberry performance under two different water regimes.

CHAPTER 6: In chapter 6, *D. eres* (syn. *D. vaccinii*) and *D. amygdali* were analyzed in detail by sequencing their genomes to identify cellular transporters, biosynthetic gene clusters and pathogenicity genes, including candidate effectors and plant cell wall degrading enzymes to understand how *Diaporthe* species invade their hosts.

CHAPTER 7: Chapter 7 presents a general discussion of this thesis based on the proposed goals and hypothesis presented, as well as perspectives for future work.

The results presented in this thesis are published in the papers listed below:

CHAPTER 2

Hilário S, Amaral IA, Goncalves MFM, Lopes A, Santos L, Alves A. **2020**. *Diaporthe* species associated with twig blight and dieback of *Vaccinium corymbosum* in Portugal, with description of four new species. *Mycologia* 112, 293-308. <https://doi.org/10.1080/00275514.2019.1698926>

Hilário S, Santos L, Alves A. **2021**. Diversity and Pathogenicity of *Diaporthe* Species Revealed from a Survey of Blueberry Orchards in Portugal. *Agriculture* 11, 1271. <https://www.mdpi.com/2077-0472/11/12/1271>

CHAPTER 3

Hilário S, Santos L, Alves A. **2021**. *Diaporthe amygdali*, a species complex or a complex species? *Fungal Biology* 125, 505-518. <http://dx.doi.org/10.1016/j.funbio.2021.01.006>

Hilário S, Gonçalves MFM, Alves A. **2021**. Using Genealogical Concordance and Coalescent-Based Species Delimitation to Assess Species Boundaries in the *Diaporthe eres* Complex. *Journal of Fungi*, 7, 507. <https://www.mdpi.com/2309-608X/7/7/507>

CHAPTER 4

Hilário S, Santos L, Phillips AJL, Alves A. **2022**. Caveats of the Internal Transcribed Spacer region as a barcode to resolve species boundaries in *Diaporthe*. *Fungal Biology* 126, 54-74. <http://dx.doi.org/10.1016/j.funbio.2021.10.005>.

CHAPTER 5

Hilário S, Pinto G, Monteiro P, Santos L, Alves A. **(2023)**. The impact of two *Diaporthe* spp. on *Vaccinium corymbosum* physiological performance under different water availability scenarios. *European Journal of Plant Pathology* (in press). <https://doi.org/10.1007/s10658-023-02651-w>

CHAPTER 6

Hilário S, Gonçalves MFM, Tacão M, Alves A. **2022**. Genome sequencing of two blueberry pathogens: *Diaporthe amygdali* strain CAA958 and *D. eres* strain CBS 160.32. *Journal of Fungi* 8, 804. <https://doi.org/10.3390/jof8080804>



CHAPTER 1

General Introduction



The genus *Diaporthe*

***Diaporthe* vs *Phomopsis*: The abolishment of the dual nomenclature**

In 1870, Nitschke established the genus *Diaporthe* and described *D. eres* as the type species (Udayanga et al. 2014), that has been accepted since then (Brayford 1990; Castlebury et al 2002; Gomes et al. 2013; Udayanga et al. 2014; Guarnaccia et al. 2018). In 1884, Saccardo recognized the genus *Phomopsis* as the asexual morph of *Diaporthe* (Wehmeyer 1926). Thus, the asexual morph of *D. eres* has been known as *Phomopsis oblonga* (Desm.) Traverso (1906) (basionym: *Phoma oblonga* Desm. 1853) (Udayanga et al. 2011). However, considering the many older names listed as synonyms of *D. eres* (Wehmeyer 1933), Rossman et al. (2014) proposed to conserve the name *D. eres* *nom. cons. prop.* against competing older names published before 1870.

Some fungi with pleomorphic lifecycles (exhibiting asexual as well as sexual growth forms) held from many years two names: “*Deuteromycota*” and “*Eumycota*”, for asexual and sexual forms respectively (Taylor 2011). However, even before PCR had been developed in 1983, mycologists recognized that the two systems of nomenclature should be merged (Taylor 2011). Regarding this, mycologists proposed to apply the concept “One Fungus = One Name”, in which only one correct name should be accepted for one fungal taxon, regardless of the fungus reproduction. The first detailed assessment of this concept was provided by Crous et al. (2006), whose revision of the family *Botryosphaeriaceae* includes the following sentence: “Separate teleomorph and anamorph names are not provided for newly introduced genera, even where both morphs are known”.

In 2012, the change to one scientific name for pleomorphic fungi was accepted based in the Melbourne Code (currently known as the International Code of Nomenclature for algae, fungi, and plants; Shenzhen Code) (Turland et al. 2018). Therefore, following the abolishment of dual nomenclature for fungi, the names *Diaporthe* Nitschke (1870) and *Phomopsis* (Sacc.) (1884) are no longer used to distinguish different morphs of the genus (Guarnaccia et al. 2018; Rossman et al. 2014). Rossman et al. (2015) proposed that the genus *Diaporthe* should be preserved over *Phomopsis*, and it has priority because it was introduced first and presents most species. Regarding the asexual morph *Phomopsis*, it was proposed

that it should be referred to as “Phomopsis-like” rather than naming the genus in italics (Chepkirui & Stadler 2017).

Morphological characteristics of the genus

The sexual morph of *Diaporthe* is characterized by black spherical ascomata, erumpent pseudostroma, with single or multiple elongated perithecial necks (Wehmeyer 1993). Their asci are unitunicate, 8-spored, clavate to subclavate, straight to slightly curved with a visible apical ring (Fig. 1).

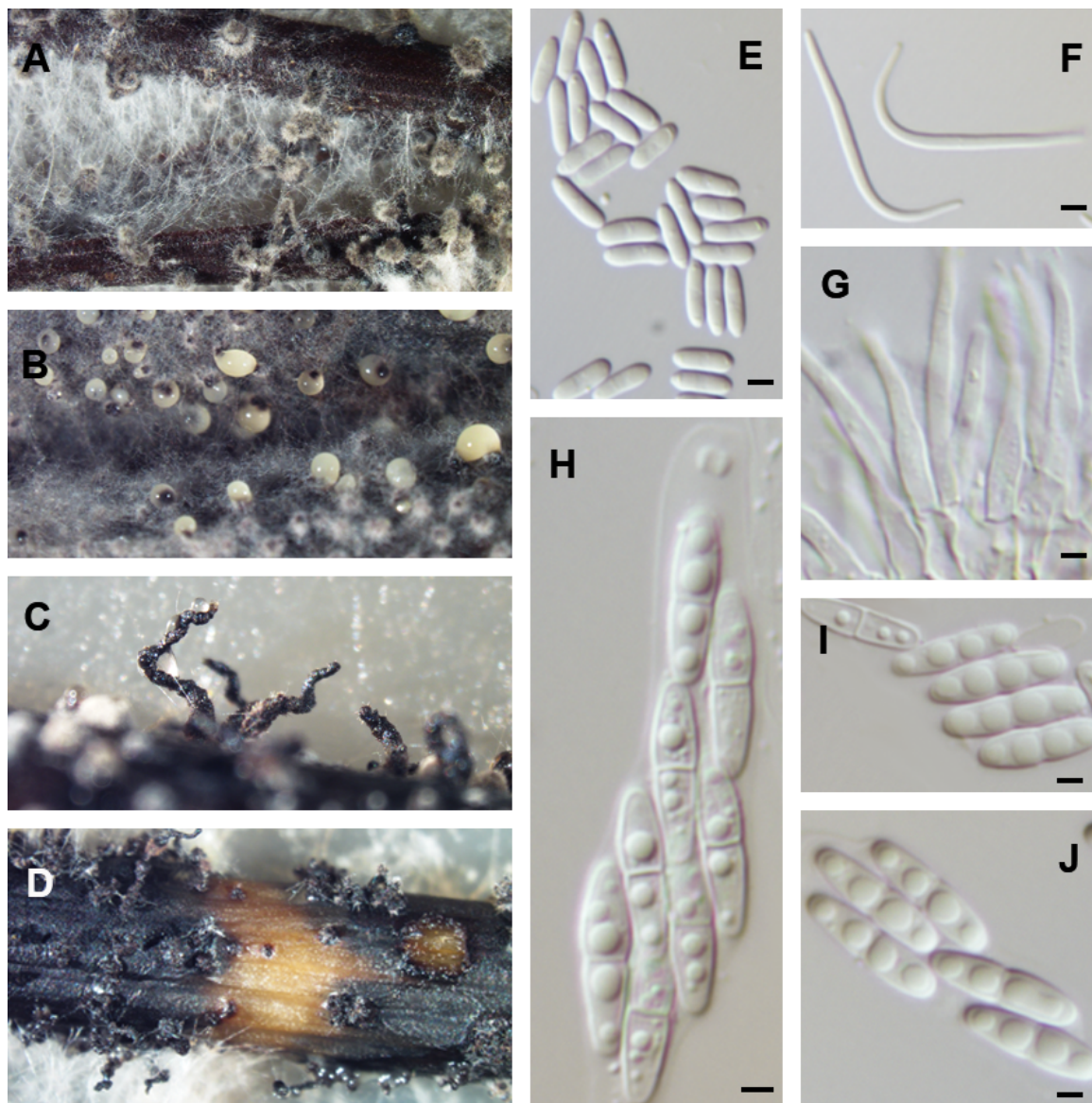


Figure 1. Morphological characteristics of some *Diaporthe* species. A. Pycnidial conidiomata on pine needles on culture (*D. novem*). B. Pycnidia oozing yellowish conidial cirrhuses. (*D. foeniculina*). C, D. Perithecial ascomata and necks emerging through fennel twigs on culture (*D. novem*). E. Alpha conidia (*D. ambigua*). F. Beta conidia (*D. leucospermi*). G. Conidiophores (*D. malorum*). H. Ascus with visible apical ring (*D. novem*). I, J. Ascospores (*D. novem*). Scale bars: 2.5 μ m.

The ascospores are hyaline, two-celled, often biguttulate, but sometimes eguttulate and tetraguttulate, and elliptical to fusiform (Fig. 1H, 1I and 1J) (Udayanga et al. 2015; Guo et al. 2020).

The asexual morph is characterized by black or dark brown conidiomata solitary or aggregated, with dimorphic conidia (alpha and beta) (Guo et al. 2020). In some species, there are intermediates between alpha and beta conidia named gamma conidia (Roskopf et al. 2000). Alpha conidia aseptate or biguttulate, hyaline, acute at both ends and sometimes with rounded ends (Fig. 1E). Beta conidia hyaline, aseptate, smooth, filiform, apex acute, slightly curved, hooked in apical part (Fig. 1F). Conidiophores are hyaline, smooth, densely aggregated, thick walled, cylindrical, straight to slightly curved with conidiogenous cells in the ends (Fig. 1G). Paraphyses when present are hyaline, subcylindrical, straight, 1-septate and branched (Gomes et al. 2013; Fan et al. 2018; Guarnaccia et al. 2018; Guo et al. 2020; Jiang et al. 2021; Wang et al. 2021).

Position in Ascomycetes systematics and taxonomic history

Ascomycota is the largest phylum in the kingdom *Fungi* with 3 subphyla, 21 classes, 148 orders, 630 families and over 6600 genera. *Pezizomycotina* is the largest subphylum of *Ascomycota* with 11 classes. The class *Sordariomycetes* is one of the main classes in the phylum and counts with 7 subclasses (Fig. 2), 45 orders and 167 families that include many important plant pathogens, as well as endophytes, occurring in terrestrial, freshwater, and marine habitats worldwide (Hyde et al. 2020; Wijayawardene et al. 2020).

The order *Diaporthales* was introduced to accommodate “true” diaporthean taxa and Eriksson & Winka (1997) accommodated it in the class *Sordariomycetidae*. Later, Maharachchikumbura et al. (2015) introduced the subclass *Diaporthomycetidae* to accommodate the order *Diaporthales*. Currently, the subclass *Diaporthomycetidae* comprises 21 orders and 66 families (Hyde et al. 2021).

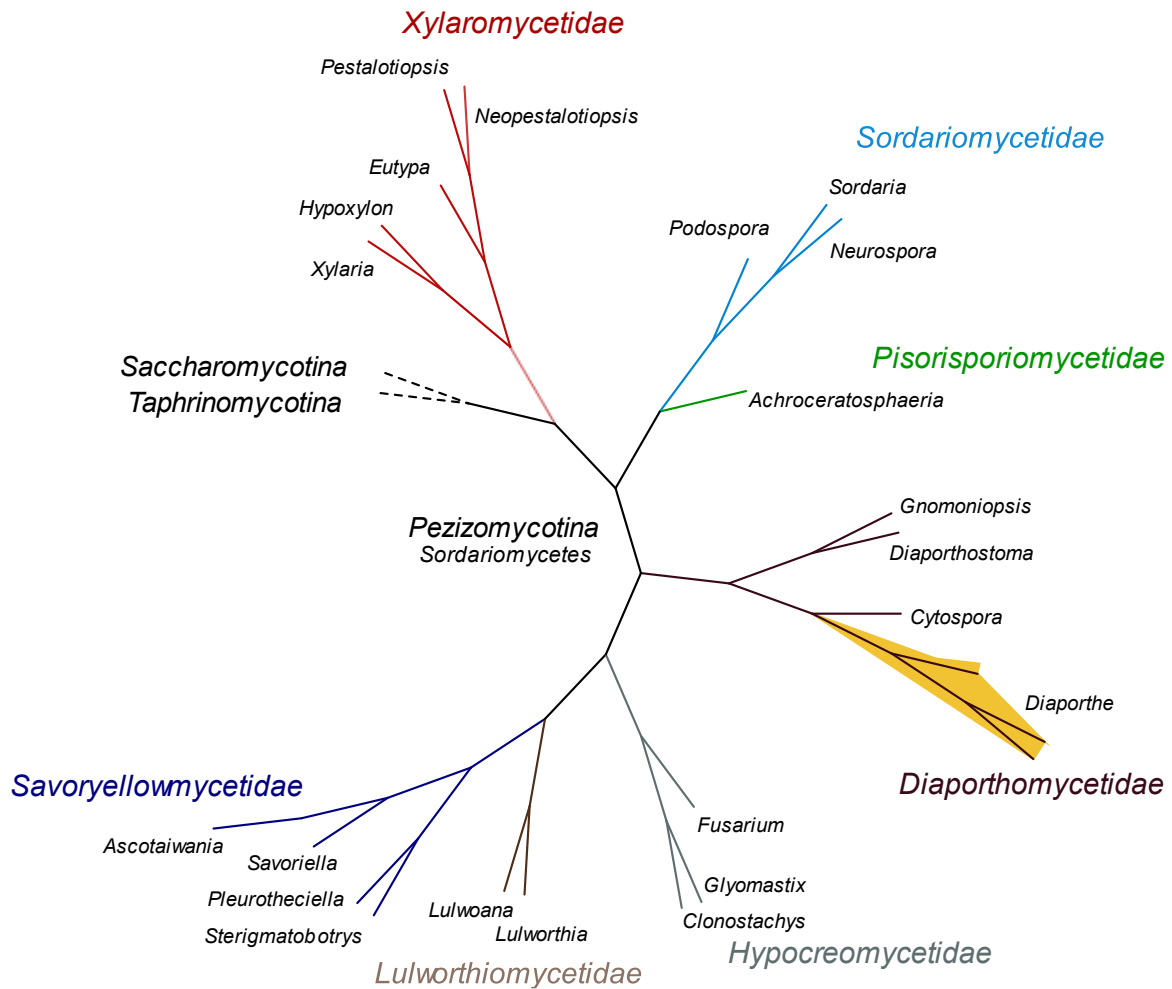


Figure 2. The Sordariomycetes class (*Pezizomycotina* sub-phylum), comprising 7 sub-classes and representative genera. The genus *Diaporthe* is highlighted in orange. The figure was created with iTOL.embl.de (accessed on 22 February 2022).

The position of the family *Diaporthaceae* and the genus *Diaporthe* within the Ascomycetes was subjected to taxonomic rearrangements over the years. Taxa initially placed in “*Diaporthaceae sensu lato*” were divided into two groups by von Höhnelt (1917) as “*Eu-Diaportheen*” and “*Valseen*” (Senanayake et al. 2017). Later, the family *Diaporthaceae* was established by Wehmeyer (1926) to accommodate *Diaporthe*, *Mazzantia*, *Melanconis*, and some other genera mainly based on morphological characters. In 1932, Nannfeldt introduced the order *Diaporthales* to accommodate von Höhnelt's “*Eu-Diaportheen*” group. And in 1975, Wehmeyer classified the *Diaporthales* to include three families: *Diaporthaceae*, *Cytosporaceae* and *Gnomoniaceae*. Based on the observation of characters such as the presence or absence of stromata and perithecial necks, ascospore shape and based on

analysis of LSU and SSU nrDNA sequence data, many other families have been accommodated in the order *Diaporthales*. (Barr 1978; Castlebury et al. 2002; Mostert et al. 2006; Senanayake et al. 2017; Wijayawardene et al. 2020).

In 2002, Castlebury and co-authors reported that the family *Diaporthaceae* comprised *Diaporthe* and *Mazzantia* based on LSU DNA sequence data, assigning the other genera to different families in *Diaporthales* (Castlebury et al. 2002). Later, additional genera were subsequently added to this family including *Leucodiaporthe* (Vasilyeva et al. 2007), *Stenocarpella* (Crous et al. 2006), *Phaeocytophoma* (Lamprecht et al. 2011), *Ophiodiaporthe* (Fu et al. 2013), *Pustulomyces* (Dai et al. 2014), *Paradiaporthe* and *Chiangraiomyces* (Senanayake et al. 2017).

Currently the order *Diaporthales* accommodates 29 families, and the family *Diaporthaceae* comprises 15 genera (Wijayawardene et al. 2020).

The species in *Diaporthe*

How many species are there?

The initial species concept applied to *Diaporthe*, based on the assumption of host-specificity and morphological traits (Uecker 1988), resulted in the introduction of over 2,000 species names for both *Diaporthe* and *Phomopsis*. A search of Index Fungorum (www.indexfungorum.org; accessed on 06 October 2022) database revealed 1178 epithets for *Diaporthe* and 984 for *Phomopsis* (Fig. 3).

A recent study demonstrated that *Diaporthe* is one of the most speciose genera, since it is referred as a species-rich phylogenetic group (Bhunjun et al. 2022). The genus *Diaporthe* has been reported as one of the most frequently found genera in a wide range of hosts (Gomes et al. 2013). It can be found co-occurring with other fungi (e.g., *Neofusicoccum*, *Pestalotiopsis*) on the same host or lesion under different lifestyles (e.g., endophyte, harmful pathogen) (Gomes et al. 2013; Guarnaccia and Crous 2017), thus explaining the high number of taxa. Although there are over 500 species names under *Diaporthe* as listed in Species Fungorum (<http://www.speciesfungorum.org>; accessed on 06 October 2022), with the advent of DNA sequencing, currently the genus comprises only 285 species well supported by ex-type cultures and supplemented with DNA barcodes (Bhunjun et al. 2022).

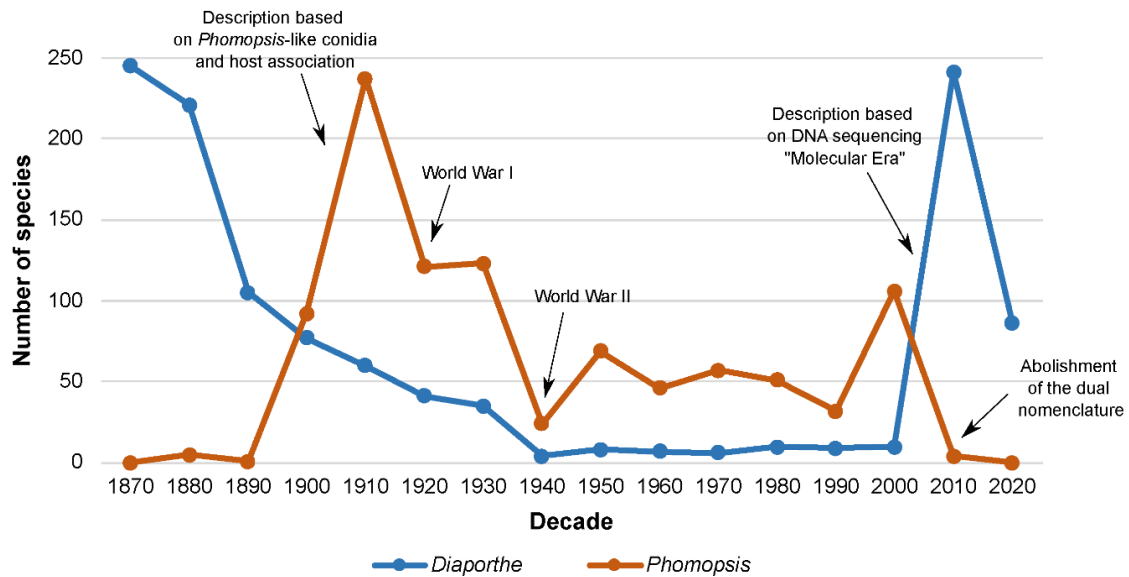


Figure 3. Numbers of newly introduced species names of *Diaporthe* and *Phomopsis* for each decade from 1870 to 2020, based on data from the Index Fungorum database (accessed on 06 September 2022).

Species concepts in *Diaporthe*

Fungi exhibit enormous species diversity due to their diverse morphologies, ecological roles, and nutritional modes (Chethana et al. 2021). Given that fungal identification has been based either on morphology or phylogeny or a combination of both, the rate of description of new fungal species has increased to over 1,800 per year (Antonelli 2020). However, the use of morphology in species identification can mislead the true fungal diversity due to gene exchange events, cryptic speciation, convergent evolution, and phenotypic plasticity (Matute & Sepulveda 2019).

The most used species concepts in fungi are the Morphological Species Concept (MSC), Biological Species Concept (BSC), Phylogenetic Species Concept (PSC) (Chethana et al. 2021). The species concept traditionally applied to *Diaporthe* was the MSC in which several characters such as the color of mycelium, shapes, color, and size of conidia, ascospores, asci, and conidiophores, were widely used, although with a reduced taxonomic value (Mostert et al. 2001; Uecker 1988). Moreover, in the past, the ability to infect a specific host was also considered an important trait to identify a species in *Diaporthe* (Rehner & Uecker 1994), which resulted in a proliferation of species names (both the asexual and sexual morphs).

Additionally, some studies have also revealed that host association is not a reliable character, since the same *Diaporthe* species can be found on different hosts and several species can occur on the same host (Diogo et al. 2010; Mostert et al. 2001). Furthermore, it has also been proven that morphology alone is inadequate to identify a species since morphological characters are often elusive, subjective and their interpretation may depend on the observer (Chethana et al. 2021).

In fungi, BSC has been used to identify groups of mating compatible individuals (Dettman et al. 2003). According to Mayr (1942), biological species are 'groups of actually or potentially interbreeding natural populations, which are reproductively isolated from other such groups.' This concept highlights the lack of gene flow between populations resulting from reproductive barriers preventing sexual reproduction or producing hybrids (Aldhebiani 2018; Taylor et al. 2000). Nevertheless, the possibility of hybridization in the genus *Diaporthe* (Hosseini et al. 2020), may reflect a lack of reproductive barriers between isolates. This fact hinders the application of the BSC in this genus.

The delimitation of species in the genus *Diaporthe* improved as soon as DNA sequence data and multiple gene genealogies were incorporated, since it facilitates the description of new species and unveils cryptic speciation (Marin-Felix et al. 2019; Santos et al. 2010; Udayanga et al. 2014). Under the PSC, species are "the smallest aggregation of populations with a common lineage that share unique, diagnosable phenotypic characters" (Harrington & Rizzo 1999). This was noted by Guo et al. (2020) for *Diaporthe* species who stated that some species of *Diaporthe* exhibit morphological characteristics that correspond to their DNA phylogeny. For instance, colonies of *D. eres* often secrete grey olivaceous pigments, *D. arecae* ooze deep brown pigments, whereas *D. sojiae* lacked pigments (Guo et al. 2020). Moreover, some studies also demonstrated that their alpha conidia morphologies differ among the above-mentioned species complexes. For instance, isolates in the *D. eres* complex show short alpha conidia (Guo et al. 2020; Udayanga et al. 2014), *D. sojiae* have oval conidia with rounded ends (Udayanga et al. 2015), while *D. arecae* exhibit alpha conidia with acutely rounded ends (Huang et al. 2013). Nevertheless, the same morphological characteristics can also be observed in different species. For example, Guarnaccia & Crous (2017) and Guo et al. (2020)

found that *D. limonicola* and *D. eres* produce gamma conidia hyaline, fusiform to subcylindrical with an acute or rounded apex. Therefore, as the presence of cryptic species and phenotypic plasticity in the genus *Diaporthe* hamper the accurate identification of species (Udayanga et al. 2014), it is of paramount importance to identify phylogenetic species using gene genealogies.

How to delimit species in *Diaporthe*?

Since the first molecular phylogenetic study in *Diaporthe*, using the nuclear ribosomal internal transcribed spacer (ITS) (Rehner & Uecker 1994), partial sequences of translation elongation factor 1- α (*tef1- α*) and mating type genes (*MAT 1-1-1/MAT1-2-1*) have been employed in molecular phylogenetic studies (Kanematsu et al. 2007; Santos et al. 2010; Van Niekerk et al. 2005). Later, to improve the accuracy of species identification in *Diaporthe*, Gomes et al. (2013) proposed the use of a five-loci dataset including ITS, *tef1- α* , β -tubulin (*tub2*), histone (*his3*) and calmodulin (*cal*), which have been adopted by many other authors (Guarnaccia et al. 2018; Guo et al. 2020; Santos et al. 2017; Sun et al. 2021; Yang et al. 2018; Wang et al. 2021). Besides phylogenetic analyses through the construction of gene trees, mycologists have also used morphological characteristics to describe species of *Diaporthe* (Gomes et al. 2013; Guarnaccia and Crous 2017; Guo et al. 2020; Udayanga et al. 2014, 2015; Wang et al. 2021). Briefly, a species is considered as a group of individuals that share similar morphological traits and sufficient DNA similarities (Steenkamp et al. 2018). However, this is not straightforward in the genus *Diaporthe*, given its morphological plasticity (Mostert et al. 2001), and its known intraspecific variability (Chaisiri et al. 2021; Udayanga et al. 2014) that have been used to describe novel taxa. Despite the role of ITS in fungal identification as a DNA barcode (Schoch et al. 2012), its use to delimit species has been disputed. Some authors have shown the presence of variation across the ITS in some genera (e.g., *Candida*, *Ceratocystis*, *Fusarium*, *Hypoxylon*, *Xylaria*) (Gazis et al. 2011; Harrington et al. 2014; O'Donnell & Cigelnik 1997; Stadler et al. 2020; Zhao et al. 2015) may overestimate the true diversity of species, leading to an increasing number of novel taxa (Stengel et al. 2022).

Regarding the genus *Diaporthe*, it has been recognized that the ITS region alone can cause confusion in defining closely related taxa (Chaisiri et al. 2021a; Murali et al. 2006; Santos et al. 2010; Udayanga et al. 2014). The occurrence of intrasporocarpic ITS variability, intragenomic ITS heterogeneity, intraspecific ITS variability and hybridization events are evidence that the ITS region may not be appropriate for species delimitation in the genus *Diaporthe*, as previously stated by Chaisiri et al. 2021a and Santos & Phillips (2009).

The Genealogical Concordance Phylogenetic Species Recognition (GCPSR) (Taylor 2000) represents an improved tool for species delimitation in the genus *Diaporthe*, that relies on the comparison of individual gene genealogies to detect incongruencies (Chaisiri et al. 2021a; Udayanga et al. 2014). However, despite the presence of incongruencies among gene genealogies, researchers have been combining those genes and considering distinct well-supported clades in multilocus trees as a species (Stewart et al. 2014). Moreover, gene concatenation has been shown to fail to recover true tree topologies when there are high levels of incomplete lineage sorting, recombination, or horizontal gene transfer, thus masking the true evolutionary relationship among taxa (Degnan & Rosenberg 2009; Mendes & Hahn 2018).

More recently, complementary methods as: haplotype network analyses, phylogenetic networks, and population genetic analyses, have also been implemented to clarify the boundaries of species complexes in the genus *Diaporthe* (Chaisiri et al. 2021). The coalescent-based delimitation, based on the coalescent theory reviewed by Fujita et al. (2012), involves understanding how several species are related by modeling their genealogical history regarding its common ancestor. Although coalescent models are considered to have a central role to identify independently evolving lineages through the construction of species trees (Bustamante et al. 2019; Fujita et al. 2012), it was never applied before in the genus *Diaporthe*.

***Diaporthe*: endophytes or pathogens?**

Species of *Diaporthe* are cosmopolitan (Fig. 4) and well-known as pathogens on several agricultural crops, forest trees and ornamental plants, causing diseases

including root and fruit rots, dieback, stem cankers, leaf spots, wilting, pod blights and seed decay (Arciuolo et al. 2020; Fan et al. 2018; Guarnaccia et al. 2018; Wang et al. 2021). For example, cankers caused by *D. limonicola* and *D. melitensis* were reported on lemon trees (Guarnaccia & Crous 2017), and *D. kongii*, *D. masirevicii*, and *D. ueckerae* were found causing stem and peg dieback on peanut trees (*Arachis hypogaea*) (Thompson et al. 2018). *Diaporthe ambigua*, *D. malorum*, *D. foeniculina*, *D. eres* and *D. actinidiae* are associated with cankers, shoot blight and fruit rot on apple tree (*Malus domestica*) (Santos et al. 2017b; Sessa et al. 2018; Udayanga et al. 2014).

Recent studies using molecular data have shown that while a few species are host-specific many others have an extensive host range (Dissanayake & Phillips 2017; Murali et al. 2006). For example, *Diaporthe ampelina* and *D. citri* are well-known pathogens associated only with *Phomopsis* cane and cankers of grapevines (*Vitis vinifera*), melanose and gummosis on *Citrus* sp. respectively (Cinelli et al. 2016; Guarnaccia & Crous 2017; Lawrence et al. 2015). Similarly, *D. helianthi* is exclusively pathogenic to sunflower (*Helianthus annuus*), causing stem canker and twig blight (Mathew et al. 2018) on crops in Europe, USA, and Australia (Thompson et al. 2011). Other *Diaporthe* species are non-specific and infect a wide range of hosts (Dissanayake & Phillips 2017; Yang et al. 2018). For instance, *D. novem* has been reported as pathogen on *Aspalathus linearis*, *Citrus* spp., *Glycine max*, *Helianthus annuus* and *Hydrangea macrophylla* (Santos et al. 2011). Sunflower stem blight is also caused by *D. gulyae*, *D. kochmanii*, *D. kongii*, *D. stewartii*, *D. phaseolorum* and *D. novem* (Mathew et al. 2018; Thompson et al. 2011). Similarly, several *Diaporthe* species have been found associated with *Phomopsis* cane and leaf spot disease as well as cankers of grapevine (Guarnaccia et al. 2018; Mostert et al. 2001, Van Niekerk et al. 2005).

Although species of *Diaporthe* are known as important plant pathogens and saprobes (Udayanga et al. 2014, Gomes et al. 2013), they are a major group of endophytes in stems and leaves of gymnosperms and angiosperms in tropical and temperate ecosystems (Huang et al. 2015; Lopes et al. 2021). The term “endophyte” was originally introduced by de Bary (1866), but the most used definition of endophytes was proposed by Petrini (1991). It refers to a group of organisms

“inhabiting plant organs that at some time in their life can colonize internal plant tissues without causing apparent harm to the host” (Chitnis et al. 2020; Hyde & Soyong 2008).

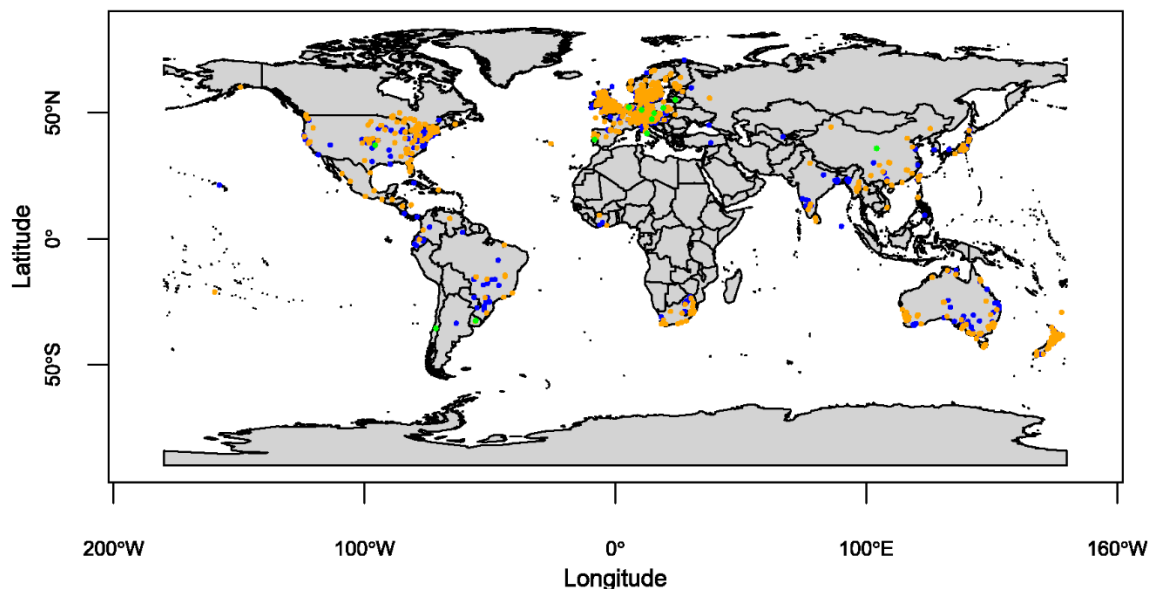


Figure 4. An overview of *Diaporthe* (orange dots), “Phomopsis-like” (blue dots) species distribution worldwide, and reports of *Diaporthe* spp. on *Vaccinium* spp. (green dots).

Due to intercontinental trade of plant material, species of *Diaporthe* are introduced into new areas as endophytes or latent pathogens, behaving as biotrophic at this stage. When the host is under stress conditions, the pathogen may switch to a necrotrophic stage inducing a phase of infection, and thus are called hemibiotrophs (Dissanayake et al. 2017; Udayanga et al. 2011). For example, it is assumed that *D. rudis* was imported to Chile via asymptomatic avocado fruit from California, causing then stem-end rot in avocados in Chile (Torres et al. 2016). Moreover, some endophytes have been shown to act as pathogens, depending on the host and its health (Gomes et al. 2013). *Diaporthe sojae*, previously found on *Citrus* as endophyte (Huang et al. 2015), was considered as the main causal agent of stem canker of soybean (*Glycine max*) (Udayanga et al. 2015). Moreover, *D. caulivora* (syn. *D. phaseolorum*) is pathogenic to soybean (Santos et al. 2011), but endophytic in mangroves (*Laguncularia racemosa*) (Sebastiane et al. 2011). Although species of *Diaporthe* can be found with different lifestyles in nature, the mechanisms of lifestyle shift are still unknown (Huang et al. 2015).

Diaporthe on blueberry plants

The blueberry: The genus *Vaccinium*, diversity and distribution

The plant genus *Vaccinium*, is very ancient and the species numbers range from 150 to 450 (Hancock et al. 2008; Luby et al. 1991). Most of the *Vaccinium* species are distributed in subtropical, temperate, and boreal regions of the Northern hemisphere, occurring in mountains, forests, and alpine regions at various altitudes (Camp 1945; Song & Hancock 2011). The 40% of the *Vaccinium* species are distributed in Southeast Asia, 25% in North America, 15% in South and Central America, 6% in Europe and the rest 14% are widely dispersed across the world (Fonseca & Oliveira 2007). This genus is divided in the subgenus *Oxycoccus* and *Vaccinium* each one with different sections within (Retamales & Hancock 2018). The most important *Vaccinium* species are found in the sections *Oxycoccus* (genus *Oxycoccus*), *Cyanococcus*, *Vitis-Idaea* and *Myrtillus* (genus *Vaccinium*).

Most of the blueberry production comes from species in the section *Cyanococcus* (Fonseca & Oliveira 2007). From this section we can highlight: the highbush blueberry (*V. corymbosum* L.), rabbiteye blueberry (*V. ashei* R.; syn. *V. virgatum*) and lowbush blueberry (*V. angustifolium*, *V. myrtilloides* and *V. boreale* Hall and Aald.) (Retamales & Hancock 2018; Song & Hancock 2011).

The blueberries worldwide

Cultivation of *Vaccinium* species is thought to have started when native Americans burned wild lowbush blueberries (*V. angustifolium*) to increase productivity (Nestby et al. 2011). After that, the habit of its consumption passed quickly to the European colonizers. For this reason, the first commercial plantations took place in the USA, growing endlessly after 1940 (Madeira 2016).

The Highbush blueberry plants, the most cultivated *Vaccinium* species, are separated into northern and southern cultivars depending on their chilling requirements (Retamales & Hancock 2018). Northern highbush blueberries (e.g., Bluecrop, Duke, Spartan) are by far the most frequently cultivated species due to high fruit quality and resistance to low temperatures (Rodriguez-Saona et al. 2019). Southern highbush cultivars (e.g., Ozarkblue, O'neal, Gup-ton) were developed through the introgression of genes from *V. darrowii* and *V. ashei* into *V. corymbosum*

to be more adaptable to warmer climates (Retamales & Hancock 2018). Regarding the blueberry plants market, highbush plants dominate worldwide production (75% northern highbush, 10% southern highbush) (Rodriguez-Saona et al. 2019).

The first blueberry plants planted in Australia and New Zealand were in the 1960s and 1970s, primarily as a crop for export markets (Retamales & Hancock 2012). A significant industry emerged in Japan in the late 1980s, but in China they were only introduced in 2010. In Europe, the first blueberry plants were imported to the Netherlands in 1923. In the 1950's, Germany had already 50 hectares planted (Retamales & Hancock 2018), but only in the 90's, the culture began professionally in the Iberian Peninsula (Madeira 2016). In 2020, the USA represented 35,8% of worldwide blueberries production (294,000 tons), followed by Peru (184,300 tons) representing 22,4%, Canada (146,370) with 17,8% and Poland (55,300 tons) that represented 6.7% of the worldwide production (FAOSTAT 2022).

The market of blueberries in Portugal

The interest in starting to produce the blueberry crop in Portugal occurred in the 1980's when the Lockhorn Foundation in the Netherlands, carried out a study in the central region of Portugal to confirm the possibility of the early production to supply the markets of the Nordic countries (Madureira et al. 2014).

In the last 10 years, blueberries in Portugal have received higher attention and their production and consumption have increased year by year (Madeira 2016). Many studies have focused on health promoting activities of blueberries such as bioactive phenols and flavonoids, which have had an impact on demand for its consumption and commercialization (Cheplick et al. 2015; Gonçalves et al. 2015; Silva et al. 2020). According to the Portuguese Agricultural Statistics, it has been observed an increase of the cultivated area and yield, evolving from 75 ha and 700 tons in 2011, to 2490 ha and a production of 15 418 tons in 2020 (INE 2012, 2021), making blueberries a highly profitable crop to the economy of the country. Nowadays, Portugal is ranked as the 7th biggest producer of blueberries, whose productions have increased 234% in the last 5 years. The notable exponential increase of blueberry production in the last years may explain the greater interest in the consumption and exportation of this berry fruit. In 2020, Portugal exported 5472

tons of this berry fruit that correspond to approximately 37 million euros (FAOSTAT 2022).

Diversity and pathogenicity of *Diaporthe*

Nowadays, blueberry plants have an increased value all over the world, with thousands of hectares spread across diversified soils and climates (Elfar et al. 2013). This extensive range of soil and climates may enhance the development of new diseases that did not occur in natural habitat of blueberries. The fast growing of blueberry yields worldwide, is accompanied by the emergence of diseases caused by plant pathogens leading to significant production losses (Espinoza et al. 2009; Lombard et al. 2014). These pathogenic agents can be bacteria, viruses, fungi, insects, or nematodes (Jagdale et al. 2013; Kalužna et al. 2013; Lombard et al. 2014; Martin et al. 2012).

A search in the SMML Fungus-Host Distribution Database (<http://nt.ars-grin.gov/fungaldatabases/> accessed on 06 October 2022) retrieved more than 581 fungal species associated with blueberry plants (*V. corymbosum*) worldwide (Fig. 7). However, the oomycete *Phytophthora* (Larach et al. 2009) and some fungal genera are frequently reported on this crop, such as *Alternaria* (Zhu and Xiao 2015), *Armillaria* (Prodorutti et al. 2009), *Botryosphaeria* (Hilário et al. 2020), *Botrytis* (Saito et al. 2014), *Colletotrichum* (Xu et al. 2013), *Diaporthe* (Lombard et al. 2014; Scarlett et al. 2018), *Fusarium* (Moya-Elizondo et al. 2019), *Lasiodiplodia* (Rodríguez-Gálvez et al. 2021), *Monilinia* (Burchhardt & Cubeta 2015), *Neofusicoccum* (Hilário et al. 2020), *Pestalotiopsis sensu lato* (Santos et al. 2021), and *Sclerotinia* (Lopez et al. 2015).

To our knowledge, the genus *Diaporthe* is the only genus from the family *Diaporthaceae* to cause diseases on blueberry plants worldwide (Farr & Rossman 2022). The main disease symptoms observed in blueberry growing areas worldwide are stem canker, twig blight and dieback (Cardinaals et al. 2018; Elfar et al. 2013; Lombard et al. 2014). These symptoms have been associated with several *Diaporthe* species such as *D. ambigua*, *D. australafricana*, *D. baccae*, *D. eres*, *D. foeniculina*, *D. oxe*, *D. passiflorae*, *D. rudis* and *D. vaccinii* (Cardinaals et al. 2018; Elfar et al. 2013; Lombard et al. 2014; Sessa et al. 2018; Yu et al. 2018) (Table 1).

Diaporthe australafricana is also known to cause cankers on blueberry plants in Chile (Latorre et al. 2012). Later in 2013, Elfar et al. carried out pathogenicity tests on blueberry plants and confirmed its virulence.

Diaporthe ambigua and *D. passiflorae* were found in Chile as a pathogen on blueberry plants but with differences in the aggressiveness. While *D. ambigua* was regarded as the least virulent species, *D. passiflorae* was found to cause cankers on shoots and stems and therefore regarded as highly virulent (Elfar et al. 2013).

Diaporthe baccae, was also described as a blueberry pathogen in Italy, causing brown lesions on stems, decay, and twig blight (Lombard et al. 2014).

Diaporthe foeniculina is known to be a common endophyte on several trees, and responsible to cause twig blight and dieback on several fruit and ornamental trees (Diogo et al. 2010; Farr & Rossman 2022; Golzar et al. 2012; Guarnaccia & Crous 2017; Santos & Phillips 2009). Its presence in blueberry plants was documented in Chile causing stem canker (Elfar et al. 2013) and later in Portugal causing twig blight.

Although *Diaporthe rudis* is a recognized fungal pathogen in Europe specially associated with *Vitis vinifera*, it has also been associated to other plants (Gomes et al. 2013; Lombard et al. 2014; Udayanga et al. 2014b). Regarding blueberry plants, Lombard et al. (2014) found for the first-time isolates of *D. rudis* occurring on blueberry plants in the Netherlands. Even though, it was not clear whether these isolates were obtained from diseased plants, nor whether pathogenicity tests were carried out. Later, Cardinaals et al. (2018) isolated *D. rudis* also in the Netherlands from blueberry plants showing shoot blight symptoms.

Diaporthe sterillis was also reported in Italy as causing stem cankers and twig blight on blueberry plants, although it is not clear whether pathogenicity tests were carried out (Lombard et al. 2014).

Diaporthe oxe, first reported in the Netherlands, was obtained as endophyte from blueberry plants (Cardinaals et al. 2018). This species revealed to be a pathogen producing necrosis and therefore considered as a latent pathogen in this host (Cardinaals et al. 2018).

Several studies conducted by Gomes et al. (2013) and Udayanga et al. (2014a) have shown that *D. eres* is the most common species found associated with

a wide range of families, including blueberry plants (Lombard et al. 2014). *Diaporthe eres* was previously isolated from blueberry plants in the Netherlands, Chile, and USA, from plants exhibiting necrotic stems (Lombard et al. 2014).

Diaporthe vaccinii has been considered a threat to plantations of blueberries for many years, causing several symptoms despite its unclear impact and pathogenicity on this host (Lombard et al. 2014; van Bruggen et al. 2018). Recent studies on the pathogenicity of *D. vaccinii*, based on the strain CPC 23811, showed that this species caused minor symptoms on blueberries, and was thus considered as a minor threat to blueberry plantations (Cardinaals et al. 2018).

A brief history of *Diaporthe vaccinii*

Diaporthe vaccinii, (formerly known as *Phomopsis vaccinii*) is native to North America and it was firstly reported in the USA causing cankers, dieback, and twig blight on blueberries in 1939 (Jeger et al. 2017). One year later, this pathogen was described based on its morphological characters (Wilcox 1940). Given that *D. vaccinii* was considered as globally threatening to blueberry plantations worldwide, it was recommended as a quarantine pathogen for the European Union (EU) (Regulation 2016/2031 of 26 October 2016) (Cardinaals et al. 2018).

The intercontinental spread of plant material has carried the potential to introduce plant pathogens into new areas (Lombard et al. 2014). For instance, in Chile, *D. vaccinii* was found in plants imported from the USA (Elfar et al. 2013). In Europe, the appearance of *D. vaccinii* was thought to be associated with imports of plant material from the USA after World War I (Nabetani et al. 2017; Teodorescu et al. 1985; Wilcox & Falconer 1961). However, many doubts have upsurged regarding the presence of *D. vaccinii* on blueberry plantations (Elfar et al. 2013; Jeger et al. 2017). Despite the known reports of *D. vaccinii* on Asia (van Bruggen et al. 2018), Europe (Lombard et al. 2014), North America (Farr et al. 2002; Nabetani et al. 2017) and South America (Elfar et al. 2013), its pathogenicity was never clarified. In addition, the literature seemed to be somehow unclear. For these reasons, it was suggested that the reports of *D. vaccinii* could be linked to an incorrect identification. Lombard et al. (2014) found that isolates from blueberries were wrongly identified as *D. vaccinii* since they were based only on morphological traits and host

association. Elfar et al. (2013) also suggested that *D. vaccinii* was wrongly identified as the only reports in Chile was in 1980, with no molecular analysis performed.

Despite these reports, the European Food Safety Authority (EFSA) stated that there were insufficient data available to get to a conclusion on the pest categorization of *D. vaccinii*. Moreover, some studies have proposed to reassess the status of this pathogen, and to understand if there were reasons to keep *D. vaccinii* as a quarantine organism (van Bruggen et al. 2018; Cardinaals et al. 2018; Jeger et al. 2017). Van Bruggen et al. (2018) and Cardinaals et al. (2018) have revealed in their studies that symptoms caused by *D. vaccinii* were considered as insignificant, thus affirming that this pathogen does not present a major threat to blueberry productions.

Table 1. Synopsis of all *Diaporthe* species associated to diseases on *Vaccinium corymbosum* plants.

Species	Reports	Symptoms	Morphology on PDA medium (Potato Dextrose Agar)	References	Reports on blueberry plants
<i>D. ambigua</i>	Chile / Portugal	Stem canker	Colonies flat, spreading, with sparse, white, dense aerial mycelium; surface with solid patches of olivaceous-black in the central part; outer region dirty-white to cream;	Van Rensburg et al. 2006	Elfar et al. 2013 Chapter 2.2
<i>D. amygdali</i>	Portugal	Stem canker	Colony growth woolly, pale olivaceous gray surface, with lighter shades to white tufts and a few patches of grayish sepia. Reverse olivaceous gray with patches of iron gray. Felty to woolly texture, colony raised with no growth zones.	Mostert et al. 2001	Chapter 2.2
<i>D. australafricana</i>	Chile	Stem canker	-	Van Niekerk et al. 2005	Latorre et al. 2012 Elfar et al. 2013
<i>D. baccae</i>	Italy	Stem canker	Surface smoke-grey mycelium, flattened, dense and felty; reverse greyish sepia	Lombard et al. 2014	Lombard et al. 2014
<i>D. crousii</i>	Portugal	Twig blight and dieback	Colonies spreading with white to grey sparse aerial mycelium and with reverse greenish concentric zones; fast growing, covering a Petri dish in 7 days at 25 °C.	Chapter 2.1	Chapter 2.1, 2.2
<i>D. eres</i>	Poland Chile / Netherlands / Portugal / USA / Lithuania / Germany	Stem canker Twig blight Dieback Blighted twigs	Colonies with fast growing, aerial, fluffy mycelium, reverse center dark pigmentation developing in center; producing abundant, black stromata at maturity.	Udayanga et al. 2014a	Chapter 2.1 Lombard et al. 2014a Cardinaals et al. 2018
<i>D. foeniculina</i>	Chile / Portugal	Stem canker / twig blight	Colonies with slow growing, white, sparse aerial mycelium, greenish yellow pigmentation developing in reverse center.	Udayanga et al. 2014b	Elfar et al., 2013 Chapter 2.1, 2.2
<i>D. malorum</i>	Portugal	Stem canker	Colonies spreading, flat, with sparse to moderate aerial mycelium, sometimes with a reddish exudate; exhibiting a pale brown to brown colonies with reverse pale brown to dark reddish-brown mycelia	Santos et al. 2017b Chapter 2.2	Chapter 2.2
<i>D. oxe</i>	Uruguay	twig bight	Colonies flat, with an entire edge, surface mycelium dense and felty, exudates rarely present as colourless drops; reverse umber, ochreous to fulvous.	Sessa et al. 2018	Sessa et al. 2018
<i>D. passiflorae</i>	Chile	Stem canker	Colonies fluffy, with abundant aerial mycelium; surface dirty white, with patches of pale olivaceous grey.	Elfar et al. 2013	Elfar et al. 2013

<i>D. phillipsii</i>	Portugal	Twig blight / dieback	Colonies spreading with white superficial mycelium flattened and dense with reverse white to ivory colour concentric zone, moderate growing rate, covering a Petri dish in 7 days at 25 °C.	Chapter 2.1	Chapter 2.1
<i>D. rossmaniae</i>	Portugal	Twig blight/dieback	White colonies spreading large with moderate aerial mycelium and reverse with greenish gray zones, fast growing, covering a Petri dish in 6 days at 25°C.	Crous et al. 2011	Chapter 2.1, 2.2
<i>D. rudis</i>	Netherlands / Portugal	Twig blight Dieback Blighted shoots	Colonies relatively slow growing, white, fluffy aerial mycelium, reverse with yellow pigmentation developing in centre.	Udayanga et al. 2014b	Lombard et al. 2014; Chapter 2.1, 2.2
<i>D. sterillis</i>	Italy	Stem cankers / twig blight	Colonies with sparse aerial mycelium, buff, honey to isabelline; reverse greyish sepia	Lombard et al. 2014	Lombard et al. 2014 Chapter 2.2
<i>D. vaccinii</i>	Netherlands / Canada / Lithuania Latvia / Poland / USA	Twig dieback Twig blight Blossom blight Stem dieback	White colonies, with yellowish gray to brownish-gray coloration around agar plug in some strains, surface mycelium felty to cottony, denser and aerial at outer margin of each zone	Shear et al. 1931	Farr et al. 2002; Lombard et al. 2014; Nabetani et al. 2017; Cardinaals et al. 2018 Vilka & Volkova 2015 Narouei-Khandan 2017
<i>D. vacuae</i>	Portugal	Twig blight / dieback	White to gray surface mycelium and reverse with yellowish zones, colonies spreading with appressed mycelium, with moderate growing on PDA media and covering a Petri dish in 10 days at 25 °C.	Chapter 2.1	Chapter 2.1

Host-pathogen interactions

Biotic and abiotic stresses

Plant hosts are often exposed to a wide range of environmental stimuli, such as abiotic (e.g., drought, salinity, heat, cold) and biotic (e.g., pathogens attack) stresses that compromise plants survival and their performance (Ali et al. 2018; Naika et al. 2013). To adjust their physiological mechanisms to changing external conditions, plants can respond by activating a complex biochemical and molecular responses (Vuković et al. 2022). For instance, some studies have addressed these responses upon fungal infections (Boloff et al. 2004; Gortari et al. 2018; Shen et al. 2017).

In the field, plants are exposed to a set of stresses. Combined stresses have different outcomes on plant performance, can either increase the plant susceptibility to pathogens (Ghanbary et al. 2021; Pedronceli et al. 2019), or even provide endurance of some plants (Pandey et al. 2017). Moreover, it is recognized that water stress can influence the development of fungal diseases by disturbing the physiological status of the host plants and, consequently, their capacity to resist to fungal infections (Desprez-Loustau et al. 2006). Due to climate change scenarios, it is expected that drought stress will be intensified, especially in the Mediterranean region, where the limited availability of water has proven to be a problem to some crops with (e.g., blueberries) (Tramblay et al. 2020). Additionally, such climate changes will also lead to shifts in the distribution of fungal species, expand the host range of pathogens and increase the pathogens aggressiveness (Nnadi & Carter 2021). However, studies on the effects of environmental stresses on disease development caused by *Diaporthe* are still scarce (Hrycan et al. 2020).

How fungi infect the host?

Pathogenic fungi use diverse strategies to colonize plants, to uptake nutrients and to cause disease, and can be classified as: biotrophs, that colonize the living tissues, utilize molecules to suppress plant cell death, manipulate plant metabolism and derive nutrients from living cells (Doehlemann et al. 2017); 2) necrotrophic pathogens that have traditionally been perceived to employ a “kill and feed” approach, using a plethora of secreted toxins and cell-wall degrading enzymes; 3) hemibiotrophs that deploy both biotrophic and necrotrophic

strategies, initially invading live cells preceding a transition to a necrotrophic lifestyle to get nutrients from killing the host cells (Rajarammohan 2021) (Fig. 5).

For a successful invasion, colonization and expansion into the host, fungal pathogens produce cell wall-degrading enzymes to break down and degrade the cell wall components (e.g., cellulose, hemicellulose, pectin, and lignin) (Garcia et al. 2021; Peng et al. 2021; Wang et al. 2022). Moreover, fungal pathogens are also able to develop specific infection structures to overcome the host physical barriers (Doehlemann et al. 2017). The fungal life cycle begins when a spore germinates and forms an appressorium to attach the surface of the host cell, producing a penetration peg. If the pathogen is a biotrophic fungi, it establishes then a close association with the host through the development of infection hyphae or haustoria within living plant cells from which nutrients are taken up (Fig. 5). At this stage, appressorial cells activate genes for hydrolases to facilitate penetration as well as small-secreted proteins to manipulate the host cell (Koeck et al. 2011). The biotrophic stage is followed by activation of necrotrophy, in which fungi secrete toxins and enzymes to destroy host cells. Key genes in this stage encode carbohydrate active enzymes, proteases, and nutrient transporters (Rajarammohan 2021). On the other hand, hemibiotrophic fungi, as the case of species of *Diaporthe* (Udayanga et al. 2011), combine both strategies. An initial biotrophic phase, during which the host's immune system is actively suppressed, allows secondary hyphae to spread throughout the infected plant tissue. This is followed by a necrotrophic phase during which toxins are secreted by the pathogen to induce host cell death (Koeck et al. 2011).

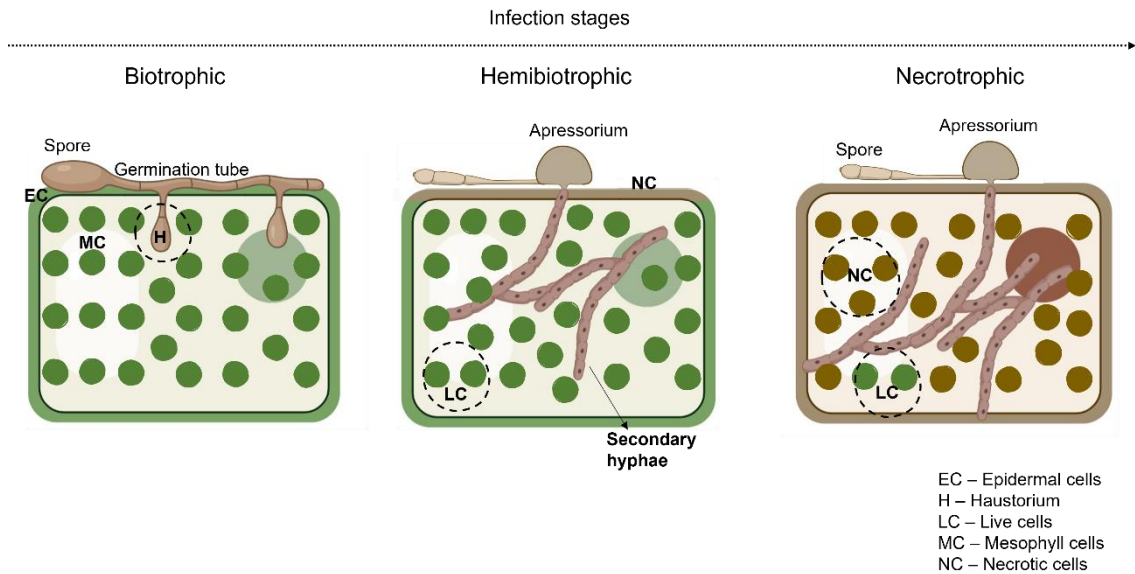


Figure 5. Pathogenic invasion strategies from different trophic lifestyles. Biotrophic pathogens form a haustorium inside the host cell to obtain nutrients. Hemibiotrophs form penetration pegs called apressoria to invade the host cell; and switch to necrotrophy when secondary hyphae are formed. The figure was created with BioRender.com (accessed on 22 February 2022).

How plants respond to fungal infection?

During fungal attack, plants activate several defense strategies to defend themselves against the pathogen entry and spread (Kaur et al. 2022). These strategies are classified as constitutive (e.g., composition of plant cell walls, waxy cuticles, and bark to give the plant strength and rigidity) and inducible defenses (e.g., antimicrobial, and toxic secondary metabolites, antioxidants, and pathogen-degrading enzymes) (Freeman & Beattie 2008).

Some endophytic fungi, such as members of the genus *Diaporthe* can promote plants growth through the secretion of plant growth promoters, contribution to nitrogen uptake (da Silva Santos et al. 2022) or by improving the biosynthesis of primary metabolites involved in plant self-defense (Lacerda et al. 2021). On the other hand, several other pathogenic fungi can produce phytotoxins and secondary metabolites that may have a negative effect on plant physiology (Cimmino et al. 2012; Perincherry et al. 2019).

Overall, some studies have reported changes on plant physiology after a pathogen attack, such as, decrease of total chlorophyll amount (Baghbani et al. 2019), increase of the amount of reactive oxygen species (ROS) (Zhang et al. 2020), accumulation or decrease of total soluble sugars (Morkunas & Ratajczak 2014), decrease of transpiration rates and stomatal conductance (Yang & Luo

2021), or increase of proline content (Christgen & Becker 2019). Nevertheless, the knowledge of how species of *Diaporthe* affect plant physiology is still virtually unknown.

Genomics of fungal plant pathogens

As mentioned above, pathogenic fungi can secrete toxins and decompose a broader diversity of cell wall carbohydrates, which can be unveiled through genomics. The sequencing and annotation of genomes unveil gene functions and open the opportunity for multi-omics analyses to further provide a thorough overview on plant-pathogen interactions (Ball et al. 2020; Félix et al. 2019; Gonçalves et al. 2019; Mena et al. 2022; Wang et al. 2022).

Since the sequencing of the first fungal genome, advances in next-generation sequencing (NGS) technology have led to an increase of genomes (Zhang et al. 2017), specifically from fungal pathogens affecting agriculture and forestry (Aylward et al. 2017). NGS is a rapid and high-throughput approach, and it is represented by different sequencing platforms such as AB SOLiD, Illumina HiSeq System, PacBio RS and Oxford Nanopore Technology (Goodwin et al. 2016; Yang et al. 2022). In 2011, the 1000 Fungal Genomes Project started with plans to sequence at least two reference genomes from each fungal family (<http://1000.fungalgenomes.org>). Currently, a search at the NCBI database (National Center for Biotechnology Information) (<https://www.ncbi.nlm.nih.gov/>; accessed on 06 October 2022) retrieved 12 287 fungal genomes, while searches at the Genome Portal (<https://genome.jgi.doe.gov/portal/>; accessed on 06 October 2022), retrieved 2682 fungal genomes. From all these fungal strains with sequenced genomes, 11 554 belong to *Ascomycota*, the phylum that contains more sequenced fungal genomes (Hill et al. 2021).

Despite the increasing number of fungal genomes over the last years, there is only a few genomes available in the genus *Diaporthe* (Table 2). This lack of information hampers researchers to understand which key genes may be involved in the infection process of *Diaporthe*. To fill this gap, some studies on the genome sequencing of *Diaporthe* species have been focused to unveil the presence of ligninolytic enzymes that degrade plant cell wall polysaccharides, cellular transporters of sugars and toxins, secondary metabolites, and pathogenicity-related genes (Gai et al. 2021; Mena et al. 2022). These studies

have also intended to provide useful resources to study pathogen-host interactions (Mena et al. 2022), for population genomic analyses (Gai et al. 2021), and to enrich the knowledge on the adaptation for plant cell wall degradation, as further expanded in Chapter 6. Moreover, further genome sequencing allied to comparative genome analysis and phylogenomic studies would be crucial to offer insights into phylogenetic inference of *Diaporthe* (Zhang et al. 2017), and to study the evolution of possible virulence factors (Garcia et al. 2021).

Table 2. Synopsis of all *Diaporthe* strains with genomes sequenced. (Note: NA stands for ‘not applicable’ which means that the genome is available at the JGI Portal but has no Project ID).

Species	Strain	Host	JGI Project	GenBank Accession number	Sequencing Platform	References
<i>Diaporthe ampelina</i>	DA912	<i>Vitis vinifera</i>	NA	LCUC00000000	Illumina HiSeq	Morales-Cruz et al. 2015
	S3MP	<i>Commiphora wightii</i>	-	LWAD00000000	Illumina HiSeq	Savitha et al. 2016
<i>Diaporthe amygdali</i>	CAA958	<i>Vaccinium corymbosum</i>	-	JAJATV000000000	Illumina HiSeq	This study
	DUCC20226	<i>Malus</i> sp.	-	JAJJOG000000000	PacBio Sequel and Illumina	-
<i>Diaporthe aspalathi</i>	MS-SSC91	<i>Glycine max</i>	-	LJJS00000000	Illumina HiSeq	Li et al. 2016
<i>Diaporthe batatas</i>	CRI 302-4	<i>Ipomoea batatas</i>	-	JAHWGW000000000	Oxford Nanopore PromethION	Yang et al. 2022
<i>Diaporthe capsici</i>	GY-Z16	<i>Juglans regia</i>	-	WNXA00000000	PacBio RSII	Fang et al. 2020
<i>Diaporthe caulivora</i>						
<i>Diaporthe cf. heveae</i>	LGMF1633	-	1251927	-	-	JGI Portal
<i>Diaporthe destruens</i>	CRI305-2	<i>Ipomoea batatas</i>	-	JACAAM010000000	Oxford Nanopore PromethION	Huang et al. 2021
<i>Diaporthe citrisiana</i>	ZJUD30	<i>Citrus unshiu</i>	-	JADAZS000000000	Illumina HiSeq	Gai et al. 2021
			-	JADWDH000000000		
<i>Diaporthe citrichinensis</i>	ZJUD34	<i>Citrus unshiu</i>	-	JADAZR000000000	Illumina HiSeq	Gai et al. 2021
	NFHF-8-4	<i>Citrus</i> sp.	-	JACTAD000000000	PacBio Sequel	Liu et al. 2021
<i>Diaporthe citri</i>	ZJUD2	<i>Citrus reticulata</i>	-	JADAZQ000000000	Illumina HiSeq	Gai et al. 2021
	ZJUD14	<i>Citrus reticulata</i>	-	JADAZP000000000	Illumina HiSeq	
	Q7	<i>Citrus reticulata</i>	-	JADAZO000000000	Illumina HiSeq	
<i>Diaporthe eres</i> (syn. <i>D. phragmitis</i>)	NJD1	<i>Actinidia deliciosa</i>	-	JACDXY000000000	PacBio RS	Wang et al. 2021
<i>Diaporthe eres</i> (syn. <i>D. vaccinii</i>)	CBS 160.32	<i>Vaccinium corymbosum</i>	-	JAJATR000000000	Illumina HiSeq	This study
<i>Diaporthe eres</i>	Phoaprs 18-02	<i>Malus</i> sp.	-	JAKJXL000000000	Illumina NovaSeq	Ali et al. 2020
	Phoaprs 18-03	<i>Malus</i> sp.	-	JAKJXM000000000	PacBio Sequel	
<i>Diaporthe helianthi</i>	7/96	<i>Helianthus annuus</i>	NA	MAVT02000001	Illumina MiSeq	Baroncelli et al. 2016
<i>Diaporthe inconspicua</i>	LGMF1612	-	1251935	-	-	-
<i>Diaporthe longicolla</i>	MSPL 10-6	<i>Glycine max</i>	-	AYRD000000000	Illumina HiSeq	Li et al. 2017
	TWH P74		-	JUJX000000000	Illumina HiSeq	Li et al. 2015
<i>Diaporthe vochysiae</i>	LGMF1583	<i>Vochysia divergens</i>	1251931 1251933	-	-	JGI Portal
<i>Diaporthe</i> sp. DP-2020a	DP-2020a	<i>Sequoia sempervirens</i>	-	JACVEP000000000	Illumina HiSeq	NCBI Genome database
<i>Diaporthe</i> sp. HANT25	HANT25	<i>Hydnocarpus anthelminthicus</i>	-	JACBFG000000000	Illumina HiSeq	Tulsook et al. 2020

Aims of the work

The starting point of any disease diagnostic is a thorough understanding and a correct identification of the pathogenic agent. Despite the recent advances in the taxonomy and systematics of the genus *Diaporthe*, some aspects concerning the species delimitation are still a challenge. Species of the genus *Diaporthe* are known to cause diseases on several plant hosts. However, very little is known regarding the occurrence of *Diaporthe* species associated with *Vaccinium corymbosum* in Portugal, as well as their pathogenic potential on this host. Therefore, given the high economic importance of blueberry plants in Portugal, this thesis was carried out with the main objective of assessing the diversity and the pathogenicity potential of species of *Diaporthe* occurring on this host. The objectives of this thesis are also aligned with the objectives of the UN “2030 Agenda for Sustainable Development, particularly with goals 8 and 12, by contributing to a sustainable consumption and economic growth, and by achieving higher levels of economic productivity.

Considering the main goal, the work presented here aimed to address the following questions:

- a. Which species of *Diaporthe* occur on blueberry in Portugal?
- b. Are these species able to cause disease on blueberry plants?
- c. Is *Diaporthe vaccinii* a threat to blueberry orchards?
- d. Is water deficit a disease trigger?
- e. Which genes may be involved in the pathogenicity of *Diaporthe*?

To answer these questions, several specific goals were proposed:

1. Collect and study species of *Diaporthe* that occur in association with dieback and twig blight of *Vaccinium corymbosum* in Portugal.
2. Assess the pathogenic potential of *Diaporthe* species on blueberry plants.
3. Evaluate the physiological fitness of blueberries under biotic (pathogen) and abiotic (water deficit) stresses.
4. Sequence the genomes of the most relevant species for blueberry plants, including *D. vaccinii*, to unveil genomic traits potentially involved in pathogenicity.

REFERENCES

- Aldhebiani AY. **2018**. Species concept and speciation. *Saudi Journal of Biological Sciences* 25, 437–440.
- Ali S, Ganai BA, Kamili AN, Bhat AA, Mir ZA, Bhat JA, Tyagi A, Islam ST, Mushtaq M, Yadav P, Rawat S. **2018**. Pathogenesis-related proteins and peptides as promising tools for engineering plants with multiple stress tolerance. *Microbiological Research* 212, 29–37.
- Ali S, Renderos W, Bevis E, Hebb J, Abbasi PA. **2020**. *Diaporthe eres* causes stem cankers and death of young apple rootstocks in Canada. *Canadian Journal of Plant Pathology* 42, 218–227.
- Antonelli A (e.d.). **2020**. State of the world's plants and fungi. Report. Royal Botanic Gardens, Kew.
- Arciuolo R, Santos C, Soares C, Castello G, Spigolon N, Chiusa G, Lima N, Battilani P. **2020**. Molecular characterization of *Diaporthe* species associated with hazelnut defects. *Frontiers in Plant Science* 11, 611655
- Aylward J, Steenkamp ET, Dreyer LL, Roets F, Wingfield BD, Wingfield MJ. **2007**. A plant pathology perspective of fungal genome sequencing. *IMA Fungus* 8, 1–15.
- Baghbani F, Lotfi R, Moharramnejad S, Bandehagh A, Roostaei M, Rastogi A, Kalaji HM. **2019**. Impact of *Fusarium verticillioides* on chlorophyll fluorescence parameters of two maize lines. *European Journal of Plant Pathology* 154, 337–346.
- Ball B, Langille M, Geddes-McAlister J. **2020**. Fun(gi)omics: advanced and diverse technologies to explore emerging fungal pathogens and define mechanisms of antifungal resistance. *MBio* 11, e01020–20.
- Baroncelli R, Scala F, Vergara M, Thon MR, Ruocco M. **2016**. Draft whole-genome sequence of the *Diaporthe helianthi* 7/96 strain, causal agent of sunflower stem canker. *Genomics Data* 10, 151–152.
- Barr ME. **1978**. The *Diaporthales* in North America: with emphasis on *Gnomonia* and its segregates. *Mycologia Memoirs* 7, 1–232.
- Bhunjun CS, Niskanen T, Suwannarach N, Wannathes N, Chen YJ, McKenzie EH, Maharachchikumbura SS, Buyck B, Zhao CL, Fan YG, ... Lumyong S. **2022**.

- The numbers of fungi: are the most speciose genera truly diverse? *Fungal Diversity* 114 387–462.
- Brayford D. **1990**. Variation in *Phomopsis* isolates from *Ulmus* species in the British Isles and Italy. *Mycological Research* 94, 691–697.
- Burchhardt KM, Cubeta MA. **2015**. Population structure of the blueberry pathogen *Monilinia vaccinii-corymbosi* in the United States. *Phytopathology* 105, 533–541.
- Bustamante DE, Oliva M, Leiva S, Mendoza JE, Bobadilla L, Angulo G, Calderon MS. **2019**. Phylogeny and species delimitations in the entomopathogenic genus *Beauveria* (*Hypocreales*, *Ascomycota*), including the description of *B. peruviansis* sp. nov. *MycoKeys* 58, 47–68.
- Camp WH. **1945**. The North American blueberries with notes on other groups of *Vaccinium*. *Brittonia* 5, 203–275.
- Cardinaals J, Wenneker M, Voogd B, Van Leeuwen M. **2018**. Pathogenicity of *Diaporthe* spp. on two blueberry cultivars (*Vaccinium corymbosum*). *EPPO Bulletin* 48, 128–134.
- Castlebury LA, Rossman AY, Jaklitsch WJ, Vasilyeva LN. **2002**. A preliminary overview of the *Diaporthales* based on large subunit nuclear ribosomal DNA sequences. *Mycologia* 94, 1017–1031.
- Chaisiri C, Liu X, Lin Y, Fu Y, Zhu F, Luo C. **2021**. Phylogenetic and haplotype network analyses of *Diaporthe eres* species in China based on sequences of multiple loci. *Biology* 10, 179.
- Chepkirui C, Stadler M. **2017**. The genus *Diaporthe*: a rich source of diverse and bioactive metabolites. *Mycological Progress* 16, 477–494.
- Chethana KW, Manawasinghe IS, Hurdeal VG, Bhunjun CS, Appadoo MA, Gentekaki E, Raspé O, Promputtha I, Hyde KD. **2021**. What are fungal species and how to delineate them? *Fungal Diversity* 109, 1–25.
- Chitnis VR, Suryanarayanan TS, Nataraja KN, Prasad SR, Oelmüller R, Shaanker RU. **2020**. Fungal endophyte-mediated crop improvement: the way ahead. *Frontiers in Plant Science* 11, 1588.
- Christgen SL, Becker DF. **2019**. Role of proline in pathogen and host interactions. *Antioxidants & Redox Signaling* 30, 683–709.

- Cimmino A, Andolfi A, Zonno MC, Troise C, Santini A, Tuzi A, Vurro M, Ash G, Evidente A. **2012**. Phomentrioloxin: A phytotoxic pentasubstituted geranylcylohexentriol produced by *Phomopsis* sp., a potential mycoherbicide for *Carthamus lanatus* biocontrol. *Journal of Natural Products* 75, 1130-1137.
- Cinelli T, Mondello V, Marchi G, Burrzano S, Alves A, Mugnai L. **2016**. First report of *Diaporthe eres* associated with cane blight of grapevine (*Vitis vinifera*) in Italy. *Plant Disease* 100, 532
- Crous PW, Groenewald JZ, Shivas RG, Edwards J, Seifert KA, Alfenas AC., Burgess TI, Carnegie AJ, Hardy GESTJ, Hiscock N, ... Quaedvlieg W. **2011**. Fungal Planet description sheets: 69–91. *Persoonia* 26, 108–156.
- Crous PW, Slippers B, Wingfield MJ, Rheeder J, Marasas WFO, Philips AJL, Alves A, Burgess T, Barber P, Groenewald JZ. **2006**. Phylogenetic lineages in the *Botryosphaeriaceae*. *Studies in Mycology* 55, 235–253.
- da Silva Santos SDS, da Silva AAD, Polonio JC, Polli AD, Orlandelli RC, dos Santos Oliveira JADS, Brandão Filho JUT, Azevedo JL, Pamphile JA. **2022**. Influence of plant growth-promoting endophytes *Colletotrichum siamense* and *Diaporthe masirevici* on tomato plants (*Lycopersicon esculentum* Mill.). *Mycology* 13, 257–270.
- Dai DQ, Wijayawardene NN, Bhat DJ, Chukeatirote E, Bahkali AH, Zhao RL, Xu JC, Hyde KD. **2014**. *Pustulomyces* gen. nov. accommodated in *Diaporthaceae*, *Diaporthales*, as revealed by morphology and molecular analyses. *Cryptogamie, Mycologie* 35, 63–72.
- Degnan JH, Rosenberg NA. **2009**. Gene tree discordance, phylogenetic inference and the multispecies coalescent. *Trends in Ecology and Evolution* 24, 332-340.
- Desprez-Loustau ML, Marçais B, Nageleisen LM, Piou D, Vannini A. **2006**. Interactive effects of drought and pathogens in forest trees. *Annals of Forest Science*, 63, 597–612.
- Dettman JR, Jacobson DJ, Turner E, Pringle A, Taylor JW. **2003**. Reproductive isolation and phylogenetic divergence in *Neurospora*: comparing methods of species recognition in a model eukaryote. *Evolution* 57, 2721–2741.

- Diogo EL, Santos JM, Phillips AJL. **2010**. Phylogeny, morphology and pathogenicity of *Diaporthe* and *Phomopsis* species on almond in Portugal. *Fungal Diversity* 44, 107–115.
- Dissanayake AJ, Camporesi E, Hyde KD, Zang W, Yan JY, Li XH. **2017**. Molecular phylogenetic analysis reveals seven new *Diaporthe* species from Italy. *Mycosphere* 8, 853–877.
- Dissanayake AJL & Phillips AJL. **2017**. Advances in understanding *Diaporthe* (Editorial). *Mycosphere* 8, 7019.
- Doehlemann G, Ökmen B, Zhu W, Sharon A. **2017**. Plant Pathogenic Fungi. *Microbiology Spectrum* 5, FUNK-0023–2016.
- Elfar K, Torres R, Díaz GA, Latorre B. **2013**. Characterization of *Diaporthe australafricana* and *Diaporthe* spp. associated with stem canker of blueberry in Chile. *Plant Disease* 97, 1042–1050.
- Eriksson OE, Winka K. **1997**. Supraordinal taxa of Ascomycota. *Myconet* 1, 1–16.
- Espinoza JG, Briceño EX, Chávez ER, Úrbez-Torres JR, Latorre BA. **2009**. *Neofusicoccum* spp. associated with stem canker and dieback of blueberry in Chile. *Plant Disease* 93, 1187–1194.
- Fan X, Yang Q, Bezerra JD, Alvarez LV, Tian C. **2018**. *Diaporthe* from walnut tree (*Juglans regia*) in China, with insight of the *Diaporthe eres* complex. *Mycological Progress* 17, 841–853.
- Fang X, Qin K, Li S, Han S, Zhu T. **2020**. Whole genome sequence of *Diaporthe capsici*, a new pathogen of walnut blight. *Genomics* 112, 3751–3761.
- Food and Agriculture Organization of the United Nations (FAOSTAT) **2022**. Retrieved from <http://www.fao.org/faostat/en/#home>.
- Farr DF, Castlebury LA, Rossman AY. **2002**. Morphological and molecular characterization of *Phomopsis vaccinii* and additional isolates of *Phomopsis* from blueberry and cranberry in the eastern United States. *Mycologia* 94, 494–504.
- Farr DF, Rossman AY. **2022**. Fungal Databases, Systematic Mycology and Microbiology Laboratory, ARS, USDA. Retrieved from <https://nt.arsgrin.gov/fungalDATABASES/>.

- Félix C, Meneses R, Gonçalves MFM, Tilleman L, Duarte AS, Jorrín-Novo JV, Van de Peer Y, Deforce, D., Van Nieuwerburgh F, Esteves AC, Alves A. **2019**. A multi-omics analysis of the grapevine pathogen *Lasiodiplodia theobromae* reveals that temperature affects the expression of virulence-and pathogenicity-related genes. *Scientific Reports* 9, 13144.
- Freeman BC, Beattie GA. **2008**. An overview of plant defenses against pathogens and herbivores. *The Plant Health Instructor*. The American Phytopathological Society.
- Fu CH, Hsieh HM, Chen CY, Chang TT, Huang YM, Ju YM. **2013**. *Ophiodiaporthe cyatheae* gen. et sp. nov., a diaporthalean pathogen causing a devastating wilt disease of *Cyathea lepifera* in Taiwan. *Mycologia* 105, 861–872.
- Fujita MK, Leaché AD, Burbrink FT, McGuire JA, Moritz C. **2012**. Coalescent-based species delimitation in an integrative taxonomy. *Trends in Ecology and Evolution* 27, 480–488.
- Gai Y, Xiong T, Xiao X, Li P, Zeng Y, Li L, Riely BK, Li H. **2021**. The Genome Sequence of the *Citrus* Melanose Pathogen *Diaporthe citri* and Two *Citrus*-Related *Diaporthe* Species. *Phytopathology* 111, 779–783.
- Garcia JF, Lawrence DP, Morales-Cruz A, Travadon R, Minio A, Hernandez-Martinez R, Rolshausen PE, Baumgartner K, Cantu D. **2021**. Phylogenomics of plant associated *Botryosphaeriaceae* species. *Frontiers in Microbiology* 12, 587.
- Gazis R, Rehner S, Chaverri P. **2011**. Species delimitation in fungal endophyte diversity studies and its implications in ecological and biogeographic inferences. *Molecular Ecology* 20, 3001–3013.
- Golzar H, Tan YP, Shivas RG, Wang C. **2012**. First report of shoot blight of persimmon caused by *Diaporthe neotheicola* in Australia. *Australasian Plant Disease Notes* 7, 115–117.
- Goodwin S, McPherson JD, McCombie WR. **2016**. Coming of age: Ten years of next-generation sequencing technologies. *Nature Reviews Genetics* 17, 333–351.

- Gomes RR, Glienke C, Videira SIR, Lombard L, Groenewald JZ, Crous PW. **2013**. *Diaporthe*: A genus of endophytic, saprobic and plant pathogenic fungi. *Persoonia* 31, 1–41.
- Gonçalves C, Guiné RPF, Teixeira D, Gonçalves FJ. **2015**. Evaluation of bioactive phenols in blueberries from different cultivars. *International Journal of Biological, Food, Veterinary and Agricultural Engineering* 9, 281–284.
- Gonçalves MFM, Nunes RB, Tilleman L, Van de Peer Y, Deforce D, Van Nieuwerburgh F, Esteves AC, Alves A. **2019**. Dual RNA sequencing of *Vitis vinifera* during *Lasiodiplodia theobromae* infection unveils host–pathogen interactions. *International Journal of Molecular Sciences* 20, 6083.
- Gortari F, Guamet JJ, Graciano C. **2018**. Plant–pathogen interactions: leaf physiology alterations in poplars infected with rust (*Melampsora medusae*). *Tree Physiology* 38, 925–935.
- Guarnaccia V, Crous PW. **2017**. Emerging citrus diseases in Europe caused by *Diaporthe* spp. *IMA Fungus* 8, 317–334.
- Guarnaccia V, Groenewald JZ, Woodhall J, Armengol J, Cinelli T, Eichmeier A, Ezra D, Fontaine F, Gramaje D, Gutierrez-Aguirregabiria A, ... Crous PW. **2018**. *Diaporthe* diversity and pathogenicity revealed from a broad survey of grapevine diseases in Europe. *Persoonia* 40, 135–153.
- Guo YS, Crous PW, Bai Q, Fu M, Yang MM, Wang XH, Du YM, Hong N, Xu WX, Wang GP. **2020**. High diversity of *Diaporthe* species associated with pear shoot canker in China. *Persoonia* 45, 132–162.
- Hancock J, Lyrene P, Finn C, Vorsa N, Lobos G. **2008**. Blueberries and Cranberries. In: Hancock JF, eds. *Temperate Fruit Crop Breeding*. Springer, Dordrecht. p. 115-150.
- Harrington TC, Kazmi MR, Al-Sadi AM, Ismail SI. **2014**. Intraspecific and intragenomic variability of ITS rDNA sequences reveals taxonomic problems in *Ceratocystis fimbriata sensu stricto*. *Mycologia* 106, 224–242.
- Harrington TC, Rizzo DM. **1999**. Defining species in the fungi. In: Worrall JJ, ed. *Structure and dynamics of fungal populations*. Dordrecht, Netherlands: Springer. p. 43–71.

- Hilário S, Lopes A, Santos L, Alves A. **2020**. *Botryosphaeriaceae* species associated with blueberry stem blight and dieback in the Centre Region of Portugal. *European Journal of Plant Pathology* 156, 31–44.
- Hill R, Leitch IJ, Gaya E. **2021**. Targeting Ascomycota genomes: what and how big?. *Fungal Biology Reviews* 36, 52–59.
- Hosseini B, El-Hasan A, Link T, Voegelé RT. **2020**. Analysis of the species spectrum of the *Diaporthe/Phomopsis* complex in European soybean seeds. *Mycological Progress* 19, 455–469.
- Hrycan J, Hart M, Bowen P, Forge T, Urbez-Torres JR. **2020**. Grapevine trunk disease fungi: their roles as latent pathogens and stress factors that favour disease development and symptom expression. *Phytopathologia Mediterranea* 59, 395–424.
- Huang F, Hou X, Dewdney MM, Fu Y, Chen G, Hyde KD, Li H. **2013**. *Diaporthe* species occurring on citrus in China. *Fungal Diversity* 61, 237–250.
- Huang F, Udayanga D, Wang X, Hou X, Mei X, Fu Y, Hyde KD, Li H. **2015**. Endophytic *Diaporthe* associated with Citrus: A phylogenetic reassessment with seven new species from China. *Fungal Biology* 119, 331–347.
- Huang L, Zhang X, Yang Y, Zou H, Fang B, Liu W. **2021**. High-Quality genome resource of *Diaporthe destruens* causing foot rot disease of sweet potato. *Plant Disease* 105, 3279–3281.
- Hyde KD, Bao DF, Hongsanan S, Chethana KW, Yang J, Suwannarach N. **2021**. Evolution of freshwater *Diaporthomycetidae* (*Sordariomycetes*) provides evidence for five new orders and six new families. *Fungal Diversity* 107, 71–105.
- Hyde KD, Norphanphoun C, Maharachchikumbura SSN, Bhat DJ, Jones EBG, Bundhun D, Chen YJ, Bao DF, Boonmee S, Calabon MS, ... Xiang MM. **2020**. Refined families of *Sordariomycetes*. *Mycosphere* 11, 305–1059.
- Hyde KD, Soyong K. **2008**. The fungal endophyte dilemma. *Fungal Diversity* 33, e173.
- Jagdale GB, Holladay T, Brannen PM, Cline WO, Agudelo P, Nyczepir AP, Noe JP. **2013**. Incidence and pathogenicity of plant-parasitic nematodes associated with

- blueberry (*Vaccinium* spp.) replant disease in Georgia and North Carolina. *Journal of Nematology* 45, 92.
- Jeger M, Bragard C, Caffier D, Candresse T, Chatzivassiliou E, Dehnen-Schmutz K, Gilioli G, Grégoire JC, Miret J, MacLeod A, ... van Bruggen AHC. **2017**. Pest risk assessment of *Diaporthe vaccinii* for the EU territory. *European Food Safety Authority Journal* 15, 1–185.
- Jiang N, Voglmayr H, Piao CG, Li Y. **2021**. Two new species of *Diaporthe* (*Diaporthaceae*, *Diaporthales*) associated with tree cankers in the Netherlands. *MycKeys* 85, 31.
- Kaluźna M, Puławska J. Meszka B. **2013**. A new bacterial disease on blueberry (*Vaccinium corymbosum*) caused by *Pseudomonas* spp. *Journal of Plant Protection Research* 53, 1–4
- Kanematsu S, Adachi Y, Ito T. **2007**. Mating-type loci of heterothallic *Diaporthe* spp.: homologous genes are present in opposite mating-types. *Current Genetics* 52, 11–22.
- Kaur S, Samota MK, Choudhary M, Choudhary M, Pandey AK, Sharma A, Thakur J. **2022**. How do plants defend themselves against pathogens-Biochemical mechanisms and genetic interventions. *Physiology and Molecular Biology of Plants* 28, 485–504.
- Koeck M, Hardham AR, Dodds PN. **2011**. The role of effectors of biotrophic and hemibiotrophic fungi in infection. *Cellular Microbiology* 13, 1849-1857.
- Lacerda JW, Siqueira KA, Vasconcelos LG, Bellete BS, Dall'Oglio EL, Sousa Junior PT, Faraggi TM, Vieira LC, Soares MA, Sampaio OM. **2021**. Metabolomic Analysis of *Combretum lanceolatum* Plants Interaction with *Diaporthe phaseolorum* and *Trichoderma spirale* Endophytic Fungi through 1H-NMR. *Chemistry & Biodiversity* 18, 2100350.
- Lamprecht SC, Crous PW, Groenewald JZ, Tewoldemedhin YT, Marasas WF. **2011**. *Diaporthaceae* associated with root and crown rot of maize. *IMA Fungus* 2, 13–24.
- Larach A, Besoain X, Salgado E. **2009**. Crown and root rot of highbush blueberry caused by *Phytophthora cinnamomi* and *P. citrophthora* and cultivar susceptibility. *Ciencia E Investigación Agraria* 36, 433–442.

- Latorre BA, Elfar K, Espinoza JG, Torres R, Díaz GA. **2012**. First report of *Diaporthe australafricana* associated with stem canker on blueberry in Chile. *Plant Disease* 96, 768–768.
- Li S, Darwish O, Alkharouf NW, Musungu B, Matthews BF. **2017**. Analysis of the genome sequence of *Phomopsis longicolla*: a fungal pathogen causing *Phomopsis* seed decay in soybean. *BMC Genomics* 18, 1–14.
- Li S, Song Q, Martins AM, Cregan P. **2016**. Draft genome sequence of *Diaporthe aspalathi* isolate MS-SSC91, a fungus causing stem canker in soybean. *Genomics Data* 7, 262–263.
- Li S, Song Q, Ji P, Cregan P. **2015**. Draft genome sequence of *Phomopsis longicolla* type strain TWH P74, a fungus causing *Phomopsis* seed decay in soybean. *Genome Announcements* 3, e00010–15.
- Liu XY, Chaisiri C, Lin Y, Yin WX, Luo CX. **2021**. Whole-Genome sequence of *Diaporthe citri* Isolate NFHF-8-4, the causal Agent of *Citrus* melanose. *Molecular Plant-Microbe Interactions* 34, 845–847.
- Lombard L, Van Leeuwen GCM, Guarnaccia V, Polizzi G, Van Rijswijk PCJ, Rosendahl CHM, Gabler J, Crous PW. **2014**. *Diaporthe* species associated with *Vaccinium*, with specific reference to Europe. *Phytopathologia Mediterranea* 53, 287–299.
- Lopes AF, Batista E, Hilário S, Santos L, Alves A. **2021**. Occurrence of *Diaporthe* species in *Eucalyptus globulus*, *Pinus pinaster* and *Quercus suber* in Portugal. *Forest Pathology* 51, e12674.
- Lopez MB, Spadaro D, Gullino ML. **2015**. First report of *Sclerotinia sclerotiorum* causing postharvest sclerotinia rot on highbush blueberry in Europe. *Plant Disease* 99, 1648–1648.
- Luby JJ, Ballington JR, Draper AD, Pliszka K, Austin ME. **1991**. Blueberries and cranberries (*Vaccinium*). *Acta Horticulture* 290, 393–456.
- Madeira BSP. **2006**. *Cultura do Mirtilo*. Agrobok: Portugal, 2016. pp. 200.
- Madureira L, Koehnen T, Pires M, Baptista A, Cristovão A, Ferreira D. **2014**. The effectiveness of advisory services to respond to demands of diverse types of small-scale farmers: New small-scale farmers in the small fruits sector in Portugal. (Report AKIS on the ground: focusing knowledge flow systems (WP4))

- of the PRO AKIS project). Available online: www.proakis.eu (accessed on 29 March 2022).
- Maharachchikumbura SSN, Hyde KD, Jones EBG, McKenzie EHC, Huang S-K, Abdel-Wahab MA, Daranagama DA, Dayarathne M, D'souza MJ, Goonasekara ID, ... Xu J. **2015**. Towards a natural classification and backbone tree for Sordariomycetes. *Fungal Diversity* 72, 199–301.
- Marin-Felix Y, Hernández-Restrepo M, Wingfield MJ, Akulov A, Carnegie AJ, Cheewangkoon R, Gramaje D, Groenewald JZ, Guarnaccia V, Halleen F, ... Crous PW. **2019**. Genera of phytopathogenic fungi: GOPHY 2. *Studies in Mycology* 92, 47–133.
- Martin RR, Polashock JJ, Tzanetakis IE. **2012**. New and emerging viruses of blueberry and cranberry. *Viruses* 4, 2831–2852.
- Mathew FM, Olson TR, Science P, Dakota S. **2018**. Identification of Sunflower (*Helianthus annuus*) accessions resistant to *Diaporthe helianthi* and *Diaporthe gulyae*. *Plant Health Progress* 19, 97–102.
- Matute DR, Sepúlveda VE. **2019**. Fungal species boundaries in the genomics era. *Fungal Genetics and Biology* 131, 103249.
- Mayr E. **1942**. *Systematics and the origin of species*. Columbia University Press, New York. p. 334.
- Mena E, Garaycochea S, Stewart S, Montesano M, Ponce De León I. **2022**. Comparative genomics of plant pathogenic *Diaporthe* species and transcriptomics of *Diaporthe caulivora* during host infection reveal insights into pathogenic strategies of the genus. *BMC Genomics* 23, 175.
- Mendes FK, Hahn MW. **2018**. Why concatenation fails near the anomaly zone. *Systematic Biology* 67, 158–169.
- Morales-Cruz A, Amrine KC, Blanco-Ulate B, Lawrence DP, Travadon R, Rolshausen PE, Baumgartner K, Cantu, D. **2015**. Distinctive expansion of gene families associated with plant cell wall degradation, secondary metabolism, and nutrient uptake in the genomes of grapevine trunk pathogens. *BMC Genomics* 16, 469.

- Morkunas I, Ratajczak L. **2014**. The role of sugar signaling in plant defense responses against fungal pathogens. *Acta Physiologiae Plantarum* 36, 1607–1619.
- Moya-Elizondo EA, Doussoulin H, San Martin J, Ruiz B, Del Valle P. **2019**. First report of *Fusarium oxysporum* causing Fusarium wilt on blueberry (*Vaccinium corymbosum*) in Chile. *Plant Disease* 103, 2669–2669.
- Mostert L, Crous PW, Kang JC, Phillips AJL. **2001**. Species of *Phomopsis* and a *Libertella* sp. occurring on grapevines with specific reference to South Africa: morphological, cultural, molecular and pathological characterization. *Mycologia* 93, 146–167.
- Mostert L, Groenewald JZ, Summerbell RC, Gams W, Crous PW. **2006**. Taxonomy and pathology of *Togninia* (*Diaporthales*) and its *Phaeoacremonium* anamorphs. *Studies in Mycology* 54, 1–113.
- Murali T, Suryanarayanan T, Geeta R. **2006**. Endophytic *Phomopsis* species: host range and implications for diversity estimates. *Canadian Journal of Microbiology* 52, 673–680.
- Nabetani K, Wood B, Sabaratnam S. **2017**. Role of pycnidia in twig and blossom blight and stem dieback of highbush blueberry caused by *Phomopsis vaccinii* in British Columbia. *Canadian Journal of Plant Pathology* 39, 405–421.
- Nagel JH, Wingfield MJ, Slippers B. **2021**. Increased abundance of secreted hydrolytic enzymes and secondary metabolite gene clusters define the genomes of latent plant pathogens in the *Botryosphaeriaceae*. *BMC Genomics* 22, 589.
- Naika M, Shameer K, Mathew OK, Gowda R, Sowdhamini R. **2013** STIFDB2: an updated version of plant stress-responsive transcription factor database with additional stress signals, stress-responsive transcription factor binding sites and stress-responsive genes in *Arabidopsis* and rice. *Plant Cell Physiology* 54, e8.
- Nannfeldt JA **1932**. Studien über die Morphologie und Systematik der nichlichenisierten inoperculaten Discomyceten. *Nova Acta Regiae Societatis Scientiarum Upsaliensis Series* 4, 1–368.

- Narouei-Khandan HA, Harmon CL, Harmon P, Olmstead J, Zelenev VV, Van Der Werf W, Van Bruggen AHC. **2017**. Potential global and regional geographic distribution of *Phomopsis vaccinii* on *Vaccinium* species projected by two species distribution models. *European Journal of Plant Pathology* 148, 919–930.
- Nestby R, Percival D, Martinussen I. **2011**. The European blueberry (*Vaccinium myrtillus* L.) and the potential for cultivation. A Review. *The European Journal of Plant Science and Biotechnology* 5, 5–16.
- Nnadi NE, Carter DA. **2021**. Climate change and the emergence of fungal pathogens. *PLoS Pathogens* 17, e1009503.
- O'Donnell K, Cigelnik E. **1997**. Two divergent intragenomic rDNA ITS2 types within a monophyletic lineage of the fungus *Fusarium* are nonorthologous. *Molecular Phylogenetics and Evolution* 7, 103–116.
- Pandey P, Irulappan V, Bagavathiannan MV, Senthil-Kumar M. **2017**. Impact of combined abiotic and biotic stresses on plant growth and avenues for crop improvement by exploiting physio-morphological traits. *Frontiers in Plant Science* 8, 537.
- Pedroncelli L, Carter-House D, Ginnan N, Andrews H, Drozd C, DiSalvo B. **2019**. The consequences of drought on plant pathology. *Journal of Science Policy & Governance*, 15, 1–6.
- Peng Y, Li, SJ, Yan J, Tang Y, Cheng JP, Gao AJ, Yao X, Ruan JJ, Xu BL. **2021**. Research progress on phytopathogenic fungi and their role as biocontrol agents. *Frontiers in Microbiology* 12, 670135
- Perincherry L, Lalak-Kańczugowska J, Stępień Ł. **2019**. *Fusarium*-produced mycotoxins in plant-pathogen interactions. *Toxins* 11, 664.
- Portal do Instituto Nacional de Estatística (INE). **2012**. Estatísticas agrícolas 2011. Available online <https://www.ine.pt/xurl/pub/142185148> (accessed on 01 March 2022).
- Portal do Instituto Nacional de Estatística (INE). **2021**. Estatísticas agrícolas 2020. Available online <https://www.ine.pt/xurl/pub/437147278> (accessed on 01 March 2022).

- Prodorutti D, Vanblaere T, Gobbin D, Pellegrini A, Gessler C, Pertot I. **2009**. Genetic diversity of *Armillaria* spp. infecting highbush blueberry in northern Italy (Trentino region). *Phytopathology* 99, 651–658.
- Rajarammohan S. **2021**. Redefining plant-necrotroph interactions: the thin line between hemibiotrophs and necrotrophs. *Frontiers in Microbiology* 12, 944.
- Rehner SA, Uecker FA. **1994**. Nuclear ribosomal internal transcribed spacer phylogeny and host diversity in the coelomycete *Phomopsis*. *Canadian Journal of Botany* 72, 1666–1674.
- Retamales JB, Hancock JF. **2018**. *Blueberries*, 2nd ed., CAB International. p. 424.
- Rodriguez-Saona C, Vincent C, Isaacs R. **2019**. Blueberry IPM: Past successes and future challenges. *Annual Review of Entomology* 64, 95–114.
- Roskopf EN, Charudattan R, Shabana YM, Benny GL. **2000**. *Phomopsis amaranthicola*, a new species from amaranthus sp. *Mycologia* 92, 114–122.
- Rossmann AY, Adams GC, Cannon PF, Castlebury LA, Crous PW, Gryzenhout M, Walker DM. **2015**. Recommendations of generic names in *Diaporthales* competing for protection or use. *IMA Fungus* 6, 145–154.
- Rossmann A, Udayanga D, Castlebury LA, Hyde KD. **2014**. (2304) Proposal to conserve the name *Diaporthe eres* against twenty-one competing names (*Ascomycota: Diaporthales: Diaporthaceae*). *Taxon* 63, 934–935.
- Saito S, Michailides TJ, Xiao CL. **2014**. First report of *Botrytis pseudocinerea* causing gray mold on blueberry in North America. *Plant Disease* 98, 1743–1743.
- Santos L, Alves A, Alves, R. **2017a**. Evaluating multi-locus phylogenies for species boundaries determination in the genus *Diaporthe*. *Peer J* 5, e3120.
- Santos JM, Correia VG, Phillips AJL. **2010**. Primers for mating-type diagnosis in *Diaporthe* and *Phomopsis*: their use in teleomorph induction in vitro and biological species definition. *Fungal Biology* 114, 255–270.
- Santos J, Hilário S, Pinto G, Alves A. **2022**. Diversity and pathogenicity of pestalotioid fungi associated with blueberry plants in Portugal, with description of three novel species of *Neopestalotiopsis*. *European Journal of Plant Pathology* 162, 539–555.

- Santos JM, Phillips AJL. **2009**. Resolving the complex of *Diaporthe* (*Phomopsis*) species occurring on *Foeniculum vulgare* in Portugal. *Fungal Diversity* 34, 111–125.
- Santos L, Phillips AJL, Crous PW, Alves A. **2017b**. *Diaporthe* species on *Rosaceae* with descriptions of *D. pyracanthae* sp. *Mycosphere* 8, 485–511.
- Santos JM, Vrandecic K, Cosic J, Duvnjak T, Phillips AJL. **2011**. Resolving the *Diaporthe* species occurring on soybean in Croatia. *Persoonia* 27, 9–19.
- Savitha J, Bhargavi SD, Praveen VK. **2016**. Complete genome sequence of the endophytic fungus *Diaporthe* (*Phomopsis*) *ampelina*. *Genome Announcements* 4, e00477–16.
- Scarlett KA, Shuttleworth LA, Collins D, Rothwell CT, Guest DI, Daniel R. **2018**. *Botryosphaeriales* associated with stem blight and dieback of blueberry (*Vaccinium* spp.) in New South Wales and Western Australia. *Australasian Plant Pathology* 48, 45–57.
- Schoch CL, Seifert KA, Huhndorf S, Robert V, Spouge JL, Levesque CA, Chen W, Fungal Barcoding Consortium. **2012**. Nuclear ribosomal internal transcribed spacer (ITS) region region as universal DNA barcode marker for Fungi. *Proceedings of the National Academy of Sciences of the United States of America* 109, 6241–6246.
- Sebastianes FL, Lacava PT, Fávoro LC, Rodrigues MB, Araújo WL, Azevedo JL, Pizzirani-Kleiner AA. **2012**. Genetic transformation of *Diaporthe phaseolorum*, an endophytic fungus found in mangrove forests, mediated by *Agrobacterium tumefaciens*. *Current Genetics* 58, 21–33.
- Senanayake IC, Crous PW, Groenewald JZ, Maharachchikumbura SSN, Jeewon R, Phillips AJL, Bhat JD, Perera RH, Li QR, Li WJ, ... Hyde KD. **2017**. Families of *Diaporthales* based on morphological and phylogenetic evidence. *Studies in Mycology* 86, 217–296.
- Sessa L, Abreo E, Lupu. **2018**. Diversity of fungal latent pathogens and true endophytes associated with fruit trees in Uruguay. *Journal of Phytopathology* 166, 633–647.
- Shear CL, Stevens NE, Bain HF. **1931**. Fungus diseases of the cultivated cranberry. *Technical Bulletin, United States Department of Agriculture* 258, 7–8.

- Shen Y, Liu N, Li C, Wang X, Xu X, Chen W, Xing G, Zheng W. **2017**. The early response during the interaction of fungal phytopathogen and host plant. *Open Biology* 7, 70057.
- Silva SCEM, Veiga M, Morais RM, Calhau C, Pintado M. **2020**. Health promoting properties of blueberries: A review. *Critical Reviews in Food Science and Nutrition* 60, 181–200.
- Song GQ, Hancock JF. **2011**. *Vaccinium*. In *Wild crop relatives: Genomic and breeding resources*. Springer, Berlin, Heidelberg. p. 197-221.
- Stadler M, Lambert C, Wibberg D, Kalinowski J, Cox RJ, Kolařík M, Kuhnert E. **2020**. Intragenomic polymorphisms in the ITS region of high-quality genomes of the *Hypoxylaceae* (*Xylariales*, *Ascomycota*). *Mycological Progress* 19, 235–245.
- Stengel A, Stanke KM, Quattrone AC, Herr JR. **2022**. Improving Taxonomic Delimitation of Fungal Species in the Age of Genomics and Phenomics. *Frontiers in Microbiology* 13, 847067
- Steenkamp ET, Wingfield MJ, McTaggart AR, Wingfield BD. **2018**. Fungal species and their boundaries matter – Definitions, mechanisms and practical implications. *Fungal Biology Reviews* 32, 104–116.
- Stewart JE, Timmer LW, Lawrence CB, Pryor BM, Peever TL. **2014**. Discord between morphological and phylogenetic species boundaries: incomplete lineage sorting and recombination results in fuzzy species boundaries in an asexual fungal pathogen. *BMC Evolutionary Biology* 14, 38.
- Sun W, Huang S, Xia J, Zhang X, Li Z. **2021**. Morphological and molecular identification of *Diaporthe* species in south-western China, with description of eight new species. *MycoKeys* 77, 65.
- Taylor JW. **2011**. One Fungus= One Name: DNA and fungal nomenclature twenty years after PCR. *IMA Fungus* 2, 113–120.
- Taylor JW, Jacobson DJ, Kroken S, Kasuga T, Geiser DM, Hibbett DS, Fisher MC, **2000**. Phylogenetic species recognition and species concepts in fungi. *Fungal Genetics and Biology* 31, 21–32.
- Teodorescu G, Copaescu V, Florea S. **1985**. The behaviour of some blueberry cultivars to the main mycoses in Romania. *Acta Horticulturae* 165, 159–166.

- Thompson SM, Tan YP, Young AJ, Neate SM, Aitken EAB, Shivas RG. **2011**. Stem cankers on sunflower (*Helianthus annuus*) in Australia reveal a complex of pathogenic *Diaporthe* (*Phomopsis*) species. *Persoonia* 27, 80–89.
- Torres C, Camps R, Aguirre R, Besoain XA. **2016**. First report of *Diaporthe rudis* in Chile causing stem-end rot on ‘Hass’ avocado fruit imported from California, USA. *Plant Disease* 100, 1951.
- Tramblay Y, Koutroulis A, Samaniego L, Vicente-Serrano SM, Volaire F, Boone A, Le Page M, Llasat MC, Albergel C, Burak S, Cailleret M. **2020**. Challenges for drought assessment in the Mediterranean region under future climate scenarios. *Earth-Science Reviews* 210, 103348.
- Traverso GB. **1906**. Flora Italica Cryptogama Pars 1, Fungi, fasc 1. Firenze, Italy: Rocca S. Casciano. pp. 700.
- Tulsook K, Isarangkul D, Sriubolmas N, Kittakoo P, Wiyakrutta S. **2020**. Draft genome sequence of *Diaporthe* sp. strain HANT25, an endophytic fungus producing mycoepoxydiene. *Microbiology Resource Announcements* 9, e00805–20.
- Turland NJ, Wiersema JH, Barrie FR, Greuter W, Hawksworth DL, Herendeen PS, Knapp S, Kusber W-H, Li D-Z, Marhold K, ... Smith GF, eds. **2018**. *International Code of Nomenclature for algae, fungi, and plants (Shenzhen Code) adopted by the Nineteenth International Botanical Congress Shenzhen, China, July 2017*. Regnum Vegetabile 159. Koeltz Botanical Books: Glashütten, Germany.
- Udayanga D, Castlebury LA, Rossman AY, Chukeatirote E, Hyde KD. **2014a**. Insights into the genus *Diaporthe*: phylogenetic species delimitation in the *D. eres* species complex. *Fungal Diversity* 67, 203–229.
- Udayanga D, Castlebury LA, Rossman AY, Chukeatirote E, Hyde KD. **2015**. The *Diaporthe sojae* species complex: Phylogenetic reassessment of pathogens associated with soybean, cucurbits and other field crops. *Fungal Biology* 119, 383–407.
- Udayanga D, Castlebury LA, Rossman AY, Hyde KD. **2014b**. Species limits in *Diaporthe*: Molecular re-assessment of *D. citri*, *D. cytospora*, *D. foeniculina* and *D. rudis*. *Persoonia* 32, 83–101.

- Udayanga D, Liu X, McKenzie EHC, Chukeatirote E, Bahkali AHA, Hyde KD. **2011**. The genus *Phomopsis*: Biology, applications, species concepts and names of common phytopathogens. *Fungal Diversity* 50, 189–225.
- Uecker FA. **1988**. A world list of *Phomopsis* names with notes on nomenclature, morphology and biology. *Mycologia Memoir* 13, 1–231.
- van Bruggen AHC, West JS, van der Werf W, Potting RPJ, Gardi C, Koufakis I, Zelenev VV, Narouei-Khandan H, Shilder A, Harmon P. **2018**. Input data needed for a risk model for the entry, establishment and spread of a pathogen (*Phomopsis vaccinii*) of blueberries and cranberries in the EU. *Annals of Applied Biology* 172, 126–147.
- van Niekerk JM, Groenewald JZ, Farr DF, Fourie PH, Haleen F, Crous PW. **2005**. Reassessment of *Phomopsis* on grapevine. *Australasian Plant Pathology* 34, 27–39.
- van Rensburg JCJ, Lamprecht SC, Groenewald JZ, Castlebury LA, Crous PW. **2006**. Characterisation of *Phomopsis* spp. associated with die-back of rooibos (*Aspalathus linearis*) in South Africa. *Studies in Mycology* 55, 65–74.
- Vasilyeva LN, Rossman AY, Farr DF. **2007**. New species of the *Diaporthales* from eastern Asia and eastern North America. *Mycologia* 99, 916–923.
- Vilka L, Volkova J. **2015**. Morphological diversity of *Phomopsis vaccinii* isolates from cranberry (*Vaccinium macrocarpon* Ait.) in Latvia. *Proceedings of the Latvia University of Agriculture* 33, 8–18.
- Vuković R, Čamagajevac IŠ, Vuković A, Šunić K, Begović L, Mlinarić S, Sekulić R, Sabo N, Španić V. **2022**. Physiological, Biochemical and Molecular Response of Different Winter Wheat Varieties under Drought Stress at Germination and Seedling Growth Stage. *Antioxidants* 11, 693.
- Wang X, Dong H, Lan J, Liu Y, Liang K, Lu Q, Fang Z, Liu P. **2021b**. High-quality genome resource of the pathogen of *Diaporthe* (*Phomopsis*) *phragmitis* causing kiwifruit soft rot. *Molecular Plant-Microbe Interactions* 34, 218–221.
- Wang X, Guo Y, Du Y, Yang Z, Huang X, Hong N, Xu W, Wang G. **2021a**. Characterization of *Diaporthe* species associated with peach constriction canker, with two novel species from China. *MycKeys* 80, 77.


- Wang Y, Wu J, Yan J, Guo M, Xu L, Hou L, Zou Q. **2022**. Comparative genome analysis of plant ascomycete fungal pathogens with different lifestyles reveals distinctive virulence strategies. *BMC Genomics* 23, 34.
- Wehmeyer LE. **1926**. A biologic and phylogenetic study of the stromatic *Sphaeriales*. *American Journal of Botany* 13, 575–645.
- Wehmeyer LE. **1933**. The genus *Diaporthe* Nitschke and its segregates. *University of Michigan Studies: Science Series* 9, 1–349.
- Wehmeyer LE. **1975**. The Pyrenomycetous Fungi. *Mycologia Memoirs* 6, 1–250.
- Wijayawardene NN, Hyde KD, Al-Ani LKT, Tedersoo L, Haelewaters D, Rajeshkumar KC, Zhao RL, Aptroot A, Leontyev DV, Saxena RK, Tokarev YS. **2020**. Outline of fungi and fungus-like taxa. *Mycosphere* 13, 53–453.
- Wilcox MS. **1940**. *Diaporthe vaccinii*, the ascigerous stage of *Phomopsis*, causing a twig blight of blueberry. *Phytopathology* 30, 441–443.
- Wilcox HJ, Falconer MA. **1961**. New or uncommon plant pests. *Plant Pathology* 10, 123–124.
- Yang Q, Fan XL, Guarnaccia V, Tian CM. **2018**. High diversity of *Diaporthe* species associated with dieback diseases in China, with twelve new species described. *MycoKeys* 39, 97–149
- Yang H, Luo P. **2021**. Changes in photosynthesis could provide important insight into the interaction between wheat and fungal pathogens. *International Journal of Molecular Sciences* 22, 8865.
- Yang Y, Yao X, Xhang X, Zou H, Chen J, Fang B, Huang L. **2022**. Draft genome sequence of *Diaporthe batatatis* causing dry rot disease in sweet potato. *Plant Disease* 106, 737–740.
- Yu C, Wu C, Li G, Wang C. **2018**. First report of *Diaporthe nobilis* causing postharvest rot of blueberry in Shandong Province, China. *Plant Disease* 102, 1856.
- Zhang Z, Chen Y, Li B, Chen T, Tian S. **2020**. Reactive oxygen species: A generalist in regulating development and pathogenicity of phytopathogenic fungi. *Computational and Structural Biotechnology Journal* 18, 3344–3349.
- Zhang N, Luo J, Bhattacharya D. **2017**. Advances in fungal phylogenomics and their impact on fungal systematics. *Advances in Genetics* 100, 309–328.

- Zhao Z, Liu H, Wang C, Xu JR. **2013**. Comparative analysis of fungal genomes reveals different plant cell wall degrading capacity in fungi. *BMC Genomics* *14*, 274.
- Zhao Y, Tsang CC, Xiao M, Cheng J, Xu Y, Lau SK, Woo PC. **2015**. Intragenomic internal transcribed spacer region sequence heterogeneity and molecular diagnosis in clinical microbiology. *International Journal of Molecular Sciences* *16*, 25067–25079.
- Zhu XQ, Xiao CL. **2015**. Phylogenetic, morphological, and pathogenic characterization of *Alternaria* species associated with fruit rot of blueberry in California. *Phytopathology* *105*, 1555–1567.



CHAPTER 2

Diversity and pathogenicity of *Diaporthe* species
associated with blueberry plants in Portugal



SUBCHAPTER 2.1

***Diaporthe* species associated with twig blight and dieback of *Vaccinium corymbosum* in Portugal, with description of four new species**

Hilário S, Amaral IA, Gonçalves MFM, Santos L, Lopes A, Alves A.

Mycologia 2020 112, 293-308

ABSTRACT

Blueberry, an increasingly cultivated fruit crop in Portugal, is known to be susceptible to twig blight and dieback caused by species of *Diaporthe*. The diversity of *Diaporthe* species associated with symptomatic and asymptomatic *Vaccinium corymbosum* plants in Portugal was assessed. A multilocus sequence analysis of the rRNA internal transcribed spacer (ITS) region and the translation elongation factor 1-alpha (*tef1- α*), β -tubulin (*tub2*), calmodulin (*cal*), and histone 3 (*his3*) genes revealed the presence of *Diaporthe foeniculina*, *Diaporthe rudis*, and four new species, which are described as *Diaporthe crousii*, *D. phillipsii*, *D. rossmaniae*, and *D. vacuae*. These new species were characterized in terms of their morphology, mating strategies, and temperature growth requirements. In artificial inoculation trials of *V. corymbosum* cv. 'Bluecrop' plants, all *Diaporthe* species caused minor symptoms. Further, no differences in aggressiveness were apparent between species. This study provides the first survey of *Diaporthe* species associated with blueberry twig blight and dieback in Portugal. It disclosed the occurrence of a diverse assemblage of *Diaporthe* species, whose status and impact as pathogens of blueberry is not yet fully understood.

keywords: blueberry; *Diaporthaceae*; pathogenicity; phylogeny; taxonomy; 4 new taxa

INTRODUCTION

Vaccinium corymbosum (blueberry) plantations in Portugal were first established in the 1990s. Since then, blueberry production has been increasing, especially in the last decade, making it an economically relevant fruit crop in the country (Madeira 2016). Although being planted throughout the country, the Severo do Vouga region, located in the center of Portugal, is one of the main producing

areas. Data from 2018 show that in Portugal, blueberry production occupied a total area of 9840 ha, with a production of 11 061 tones, representing the second most cultivated crop among the small fruits, which include raspberries, blackberries, among others (INE 2019).

The growing demand for blueberries, due to their recognized health benefits, increased plantation and consumption worldwide (Chen et al. 2019). However, the spread of blueberry plant material throughout the world has been accompanied by an increase of several plant pathogens, mainly fungi (Lombard et al. 2014). Among these fungal pathogens, the genus *Diaporthe* represents an important role because it includes known species affecting blueberry growing areas worldwide (Elfar et al. 2013; Lombard et al. 2014).

The genus *Diaporthe* (= *Phomopsis*) includes over 2000 species names, mostly based on host associations and morphological characteristics (Guarnaccia et al. 2018; Santos et al. 2010). This genus includes important plant pathogens infecting an extensive variety of hosts and threatening trees of agricultural and forestry importance (Cinelli et al. 2016; Dissanayake & Phillips 2017; Guarnaccia et al. 2018). However, the biology and lifestyle of some of these pathogens remains unclear (Vilka & Volkova 2015). They are also known to asymptotically colonize plant tissues, living as endophytes or opportunistic pathogens (Udayanga et al. 2011). Several studies revealed the presence of *Diaporthe* species on blueberry plants distributed mostly in the USA (Farr et al. 2002), Canada (Nabetani et al. 2017), the Netherlands (Cardinaals et al. 2018), Poland, Italy, and Lithuania (Lombard et al. 2014), Latvia (Vilka & Volkova 2015), Chile (Elfar et al. 2013), China (Yu et al. 2018), and Uruguay (Sessa et al. 2018). Twelve *Diaporthe* species have been reported on blueberry plants, including *Diaporthe ambigua*, *D. asheicola*, *D. australafricana*, *D. baccae*, *D. eres*, *D. foeniculina*, *D. nobilis*, *D. rudis*, *D. passiflorae*, *D. oxe*, *D. sterillis*, and *D. vaccinii* (Elfar et al. 2013; Gomes et al. 2013; Lombard et al. 2014; Sessa et al. 2018; Yu et al. 2018). Symptoms of twig blight, stem canker, and dieback caused by *Diaporthe* species are characterized by apical necrosis of the shoots, brown to red necrotic lesions on stems, discoloration of the vascular tissues, leaf spots, and fruit rot (Cardinaals et al. 2018; Elfar et al. 2013; Sessa et al. 2018). Furthermore, *Diaporthe vaccinii*, a quarantine pathogen in

Europe, is alleged to be quite threatening for blueberries, but there is a lack of information regarding its pathogenicity and virulence, as well as its lifestyle and host specificity (Cardinaals et al. 2018; Lombard et al. 2014; Vilka & Volkova 2015).

Blueberry twig blight and dieback symptoms typical of *Diaporthe* have been occasionally observed in Portugal. However, the impact of these diseases and pathogens on blueberry plantations in the country has not been studied before. Moreover, the presence of *Diaporthe* has been based solely on the observation of symptoms in plants. Therefore, this study aimed to assess the diversity of *Diaporthe* species occurring in blueberry (*V. corymbosum*) plants in Portugal, to identify the etiological agents of the symptoms observed as well as to evaluate their pathogenicity in this host.

MATERIAL AND METHODS

Fungal isolation.

Surveys were carried out during the summer of 2015 and 2016 in Sever do Vouga, the main blueberry growing area in the central region of Portugal. The cultivars 'Duke', 'Ozarkblue', 'Draper', 'Patriot', and 'Blue Ray' were selected. Twigs ($n = 38$) and stems ($n = 6$) with dieback, twig blight, and necrosis and leaves ($n = 3$) exhibiting a yellow and red discoloration were collected from symptomatic plants. Twigs ($n = 10$) were collected from healthy asymptomatic plants. The plant material was surface-sterilized in 5% sodium hypochlorite for 1 min, followed by 96% ethanol for 1 min and rinsed twice in sterile water for 1 min. Fungal isolations were made by placing pieces of diseased tissues (2–5 mm) and asymptomatic material on half-strength potato dextrose agar ($\frac{1}{2}$ PDA) (Merck, Darmstadt, Germany) plates. The plates were incubated at 25 °C and checked daily for fungal growth. Fungal isolates were obtained by transferring mycelial plugs from the margins of the expanding colonies and placed in fresh PDA plates supplemented with tetracycline and streptomycin at final concentrations of 100 mg/L, to inhibit bacterial growth. Typical *Diaporthe* colonies were initially selected based on micromorphological and culture characteristics, and then monosporic cultures were obtained.

To induce sporulation, fungal isolates were cultured on 2% water agar (WA) and on quarter-strength potato dextrose agar ($\frac{1}{4}$ PDA) plates containing sterilized

Pinus pinea needles and *Foeniculum vulgare* stems. Cultures were kept at room temperature under diffuse daylight. After sporulation, conidiomata and ascomata were observed with a Nikon SMZ1500 stereomicroscope (Nikon, Japan) and photographed with a Digital Sight DS-Fi1 camera (Nikon, Japan). The fruiting bodies were cut in a drop of sterile water in a microscope slide, mounted in 100% lactic acid and the micromorphological characters (e.g., conidia and conidiophores size) were observed. All preparations were visualized with a Nikon 80i microscope (Nikon, Japan) with interference contrast equipment and captured with a Nikon Digital Sight DS-Ri1 camera (Nikon, Japan).

DNA extraction, PCR amplification, and sequencing.

Genomic DNA was extracted from all fungal isolates grown in PDA for 5 days at 25 °C, according to a modified protocol by Möller et al. (1992). Microsatellite-primed polymerase chain reaction (MSP-PCR) fingerprinting was performed using the (GTG)₅ primer and based on the methodology described previously by Alves et al. (2007). Isolates were clustered based on their profiles in a consensus dendrogram built with GelCompar II software (Applied Maths) using Pearson's correlation coefficient and the unweighted pair group method with arithmetic mean (UPGMA). A cut-off of approximately 82.5% was chosen as the reproducibility level, since strains from a cluster above this level are deemed to belong to the same species, as previously described by Santos & Phillips (2009).

Five loci were selected for this study (ITS, rRNA internal transcribed spacer region; *tef1- α* , translation elongation factor 1-alpha; *tub2*, β -tubulin; *his3*, histone 3; and *cal*, calmodulin). Primers ITS5 and ITS4 were used to amplify the ITS region (White et al. 1990) as described by Alves et al. (2004). The remaining loci were amplified using the following primer sets: EF-688F/EF-1251R or EF-688F/EF-986R for *tef1- α* (Alves et al. 2008; Carbone & Kohn 1999), T1/Bt2b for *tub2* (Glass & Donaldson 1995; O'Donnell & Cigelnik 1997), CYLH3F/H3-1bR for *his3* (Crous et al. 2004; Glass & Donaldson 1995), and CAL-228F/CAL-737R for *cal* (Carbone & Kohn 1999). However, for some isolates, amplification of the *cal* region was impossible with the primer set CAL-228F and CAL-737R. Therefore, a new set of primers was designed based on the *cal* gene sequences from the available

genomes of *Diaporthe* (Baroncelli et al. 2016; Li et al. 2015, 2016; Savitha et al. 2016). The sequences were aligned and appropriate regions for primer design were visually identified, and the following set of primers: CALD-38F (5' CTGACCGAGGAACAAGTCTCC 3') and CALD-752R (5' GGAGATGAAGCCGTTGTTGTCG 3') were chosen. PCR conditions were as described by Santos et al. (2017a), except for the new primer set, whose conditions were as follows: initial denaturation for 5 min at 95 °C, followed by 30 cycles of 94 °C for 45 s, annealing at 58 °C for 30 s, and extension at 72 °C for 1 min, and a final elongation step at 72 °C for 10 min. The PCR reactions, with a final volume of 25 µL, were composed of 15.75 µL of sterile distilled water, 6.25 µL of NZYTaQ 2× green Master Mix (Nzytech™, Lisbon, Portugal), 1 µL of each primer at 10 pmol, and 1 µL of DNA template and performed in a Bio-Rad C1000 touch thermal cycler (BioRad, Hercules, California). PCR amplification products were checked using an electrophoresis in 1.5% agarose gels and visualized under ultraviolet (UV) light (Gel Doc XR+; Bio-Rad). Amplicons were purified using the NZYGelPure kit (Nzytech™, Lisbon, Portugal) and sequenced by GATC Biotech (Ebersberg, Germany). All sequences generated in this study were deposited in GenBank (www.ncbi.nlm.nih.gov) (Table 1).

Phylogenetic analyses.

Sequences were aligned with Clustal X 2.1 software (Larkin et al. 2007) using the following parameters: pairwise alignment: gap opening = 10, gap extension = 0.1; multiple alignment: gap opening = 10, gap extension = 0.2, transition weight = 0.5, delay divergent sequences = 25%. The alignments were optimized with BioEdit (Hall 1999) and concatenated using SequenceMatrix (Vaydia et al. 2011).

Phylogenetic analyses of sequence data were done using PAUP* v.4.0b10 (Swofford 2002) for Maximum Parsimony (MP) analyses, MrBayes v.3.0b4 (Ronquist & Huelsenbeck 2003) for Bayesian Inference (BI) analyses and MEGA v.7 (Kumar et al. 2016) for Maximum Likelihood (ML) analyses. The general time-reversible model of evolution, assuming invariant sites and a gamma distribution was used for BI analyses (Rodriguez et al. 1990). Trees were rooted to *Diaporthella corylina* and visualized with TreeView (Page 1996).

Maximum Parsimony analyses were performed using the heuristic search option with 100 random taxon additions and subtree pruning regrafting (SPR) method as the branch-swapping algorithm. All characters were unordered and of equal weight, and gaps were treated as missing data. Maxtrees were set to 100 and branches of zero length were collapsed. Clade stability was assessed using a bootstrap analysis with 1000 replicates.

Bayesian analyses employing a Markov Chain Monte Carlo sampling (MCMC) method were performed. Four MCMC chains were run simultaneously, starting from random trees for 1 000 000 generations and sampled every 100th generation for a total of 10 000 trees. The first 1000 were discarded as the burn-in phase of each analysis. Posterior probabilities (PP) were determined from a majority-rule consensus tree generated with the remaining trees.

Maximum likelihood analyses were performed on a Neighbour-Joining starting tree generated automatically by the software. Nearest-Neighbour-Interchange (NNI) was used as the heuristic method for tree inference and 1000 bootstrap replicates were performed. MEGA v.7 was also used to determine the best nucleotide substitution model to be in the ML trees (<https://www.megasoftware.net/>).

An initial ITS-only tree, containing all species currently accepted in the genus *Diaporthe*, was generated to determine the clades that contained the isolates obtained in this study. This analysis was further used to select the species to be included in multilocus phylogenetic analyses. To assess the possibility of combining the five loci (ITS, *tef1- α* , *tub2*, *his3*, and *cal*) in a multilocus phylogenetic analysis, single locus trees were generated using ML in MEGA7 and compared to detect conflict (Figs. S1–S5). MEGA7 was also used to calculate the pairwise distance among nucleotide sites in each locus and to determine the best nucleotide substitution model to be used for building the ML tree. The phylogenetic tree and alignments were deposited in TreeBASE (www.TreeBASE.org; study number 24787).

Mating type assay.

The mating strategy of the new species was determined by a PCR-based method, following the protocol described by Santos et al. (2010) with slight modifications. Given that the amplification with some primers described by the authors was unsuccessful for some isolates, two new primers were designed in the present study: MAT1 141F (5' GGTCAAGAAGAAGAAGTCC 3') and MAT2 188F (5' CCAGCTCCATCACAAC 3'). Then, the most suitable primer combinations for those isolates were selected: MAT1 141F and MAT1-1-1RV (5' GTCTMTGACCARGACCATG 3') (Santos et al. 2010) for the partial amplification of *MAT1-1-1* gene and MAT2 188F and MAT1-2-1RV (5' TTGACYTCAGAAGACTTGCGTG 3') (Santos et al. 2010) to amplify part of the *MAT1-2-1* gene. Primers were used at a concentration of 10 pmol. PCR conditions were as follows: initial denaturation for 5 min at 95 °C, followed by 40 cycles of 94 °C for 30 s, annealing at 51 °C for 30 s, and extension at 72 °C for 1 min, and a final elongation step at 72 °C for 10 min.

Temperature growth studies.

The putative new species identified, were inoculated on ½ PDA plates and incubated at 25 °C for 6 days or until the colonies reached the edges of the plate. From these cultures, a 5-mm plug for each isolate was placed in the center of PDA plates. Three replicate plates per isolate were incubated at 5, 10, 20, 25, 30, 35, and 40 °C. The effect of temperature on colonies growth was examined daily for 6 days and determined by measuring the diameter in two perpendicular directions in each replicate. Fungal radius plotted against time was used to calculate the growth rate (μ , mm/d) for each strain, using the primary model of the biphasic Baranyi's function (Baranyi & Roberts 1994), to estimate the growth parameters: minimum temperature (T_{min}), maximum temperature (T_{max}), optimum temperature (T_{opt}), and optimal growth rate (μ_{opt}). The estimates of optimal growth rate were fitted to a secondary model proposed by Rosso et al. (1995). Both models were fitted using the Statgraphics Centurion XVI 16.1.15 (StartPoint Technologies, The Plains, Virginia).

Table 1. Isolates obtained from *Vaccinium corymbosum* used in this study.

Species	Strain ¹	Symptoms	Cultivar	GenBank Accession Numbers					Mating-type	
				ITS	<i>tef1-α</i>	<i>tub2</i>	<i>his3</i>	<i>cal</i>	MAT1-1-1	MAT1-2-1
<i>D. crousii</i>	CAA819	healthy twigs	Ozarkblue	MK792299	MK828071	MK837922	MK871440	MK883827	(+)	(+)
	CAA820	yellow leaves	Ozarkblue	MK792300	MK828072	MK837923	MK871441	MK883828	(+)	(+)
	CAA821	yellow leaves	Blue Ray	MK792301	MK828073	MK837924	MK871442	MK883829	(+)	(+)
	CAA823 / MUM 19.29	dieback	Blue Ray	MK792311	MK828081	MK837932	MK871450	MK883835	(+)	(+)
	CAA825	dieback	Patriot	MK792313	MK828082	MK837933	MK871451	MK883836	(+)	(+)
	CAA828	dieback	Patriot	MK792317	MK828084	MK837935	MK871453	MK883837	(+)	(+)
<i>D. foeniculina</i>	CAA 810	dead twig	Duke	MK792296	MK828068	MK837919	MK871437	MN000345	n.d.	n.d.
	CAA 811	dead twig	Duke	MK792297	MK828069	MK837920	MK871438	MN000346	n.d.	n.d.
	CAA 812	dead twig	Duke	MK792298	MK828070	MK837921	MK871439	MN000347	n.d.	n.d.
	CAA 813	healthy twig	Ozarkblue	MK792303	MK828075	MK837926	MK871444	MN000348	n.d.	n.d.
	CAA 815	healthy twig	Duke	MK792308	MK828079	MK837930	MK871448	MN000349	n.d.	n.d.
	CAA 816	dead twig	Duke	MK792314	MK828083	MK837934	MK871452	MN000350	n.d.	n.d.
<i>D. phillipsii</i>	CAA817 / MUM 19.28	dead twig	Duke	MK792305	MK828076	MN000351	MK871445	MK883831	(-)	(+)
	CAA818	dead twig	Duke	MK792307	MK828078	MN000352	MK871447	MK883833	(-)	(+)
<i>D. rossmaniae</i>	CAA762 / MUM 19.30	twig canker	Duke	MK792290	MK828063	MK837914	MK871432	MK883822	(+)	(-)
	CAA763	twig canker	Duke	MK792291	MK828064	MK837915	MK871433	MK883823	(+)	(-)
<i>D. rudis</i>	CAA777	stem canker	Draper	MK792292	MK828065	MK837916	MK871434	MK883824	n.d.	n.d.
	CAA790	stem canker	Ozarkblue	MK792294	MK828066	MK837917	MK871435	MK883825	n.d.	n.d.
	CAA831	dead twig	Duke	MK792295	MK828067	MK837918	MK871436	MK883826	n.d.	n.d.
	CAA832	yellow and red leaves	Ozarkblue	MK792302	MK828074	MK837925	MK871443	MK883830	n.d.	n.d.
<i>D. vacuae</i>	CAA829	dead twig	Blue Ray	MK792306	MK828077	MK837928	MK871446	MK883832	(+)	(-)
	CAA830 / MUM 19.31	dieback	Blue Ray	MK792309	MK828080	MK837931	MK871449	MK883834	(+)	(-)

¹Acronyms of culture collection: **CAA** – Personal Culture Collection Artur Alves, University of Aveiro, Aveiro, Portugal; **MUM** – Culture collection from Micoteca da Universidade do Minho, Braga, Portugal

Pathogenicity tests.

One isolate from each species identified was selected to inoculate blueberry plants (9 plants per isolate). The pathogenicity assay was performed on 3-year-old potted *V. corymbosum* plants (cv. 'Bluecrop'). For inoculation, a piece of the bark tissue was cut using a sterile scalpel exposing the cambium. A 5-mm-diam mycelial plug was taken from 7-day-old cultures on ½ PDA and placed in the wounded area with the mycelium in contact with the plant tissue. The inoculation site was sealed with Parafilm to avoid rapid dehydration. Plugs of uninoculated ½ PDA were used as negative controls. The plants were maintained at room temperature for 2 months, after which the size of necrotic lesions was measured. Symptoms were checked regularly and registered. Data were checked for normality with the Shapiro-Wilk test and subjected to one-way analysis of variance (ANOVA). Differences between means were determined following a Tukey test ($p < 0.05$). Statistical analyses were performed with JMP 8.0.1 (SAS Institute, Cary, North Carolina).

RESULTS

Fungal isolation.

During the survey, three blueberry plantations were inspected for disease symptoms such as twig blight, dieback, stem canker, wilting, and necrotic leaves, mostly in the apex of the plant. Nineteen plants from the cultivars 'Duke' ($n = 8$), 'Draper' ($n = 2$), 'Ozarkblue' ($n = 4$), 'Patriot' ($n = 3$), and 'Blue Ray' ($n = 2$) were sampled, leading to a collection of 10 asymptomatic twigs and 47 diseased samples among leaves, stems, and twigs. Ninety fungal isolates obtained were initially selected based on culture and micromorphological characteristics typical of the genus *Diaporthe* (Gomes et al. 2013). Most isolates sporulated within 6 weeks and produced pycnidia oozing white to yellow conidial cirri on both pine needles and fennel stems.

Molecular characterization.

MSP-PCR fingerprinting was performed to evaluate the genetic diversity of the 90 fungal isolates. A total of 22 isolates representative of each cluster were selected for further molecular characterization, and new sequences were deposited

in GenBank (Table 1). A primary identification based on ITS sequences was done using BLASTn, which assigned the isolates to the genus *Diaporthe*. The analysis of single-locus phylogenies revealed no conflicts between them, indicating that the loci could be combined. Thus, a multilocus analysis using the loci ITS, *tef1- α* , *tub2*, *cal*, and *his3* was performed, including those *Diaporthe* species phylogenetically closely related to our isolates and whose sequences for all five loci were available (Table 2). The concatenated alignment contained 2546 characters (594 from ITS, 416 from *tef1-a*, 491 from *tub2*, 529 from *his3*, and 516 from *cal*). The analysis included one outgroup and 53 ingroup taxa (22 sequences from this study and 31 *Diaporthe* sequences from GenBank) (Fig. 1). Four isolates clustered in the *D. rudis* clade and six in *D. foeniculina* clade. The clade containing isolates CAA817 and CAA818 was supported by high bootstrap and posterior probability values (ML/MP/PP = 100/100/1.00) and is phylogenetically related to *D. portugallica*. However, a novel species was considered since a comparison of sequences showed differences in three loci only (ITS, *his3*, and *cal*). The isolates CAA819, CAA820, CAA821, CAA823, CAA825, and CAA828 formed a single and highly supported clade (ML/MP/PP = 100/100/1.00), representing a potential novel species. The isolates CAA762 and CAA763 were well supported (ML/MP/PP = 99/95/1.00) but phylogenetically close to *D. leucospermi* and *D. pyracanthae*. The nucleotide sequences of five loci (ITS, *tef1- α* , *tub2*, *cal*, and *his3*) of CAA762 and CAA763 were compared with the ones from *D. pyracanthae* and *D. leucospermi*. The comparison showed that these isolates differ from *D. leucospermi* and *D. pyracanthae* in several nucleotide positions and are therefore considered to be a novel species. Isolates CAA829 and CAA830 formed a highly supported (ML/MP/PP = 100/100/1.00) and separate clade but are phylogenetically related to *D. eres* (ML/MP/PP = 99/94/1.00). A pairwise alignment showed 3 unique polymorphisms in *tef1- α* sequences, 7 differences in *cal* sequences, and 20 differences in *tub2* sequences; hence, these isolates are regarded as a novel species.

Table 2. *Diaporthe* species used in the multilocus sequence analysis.

Species	Strain ¹	Host	Location	GenBank Accession numbers				
				ITS	<i>tef1-α</i>	<i>tub2</i>	<i>cal</i>	<i>his3</i>
<i>D. alleghaniensis</i>	CBS 495.72	<i>Betula alleghaniensis</i>	Canada	KC343007	KC343733	KC343975	KC343249	KC343491
<i>D. alnea</i>	CBS 146.46	<i>Alnus</i> sp.	-	KC343008	KC343734	KC343976	KC343250	KC343492
<i>D. anacardii</i>	CBS 720.97	<i>Anacardium occidentale</i>	East Africa	KC343024	KC343750	KC343992	KC343266	KC343508
<i>D. australafricana</i>	CBS 113487	<i>Vitis vinifera</i>	South Africa	KC343039	KC343765	KC344007	KC343281	KC343523
<i>D. beckhausii</i>	CBS 138.27	<i>Viburnum</i> sp.	-	KC343041	KC343767	KC344009	KC343283	KC343525
<i>D. betulae</i>	CFCC 50469	<i>Betula platyphylla</i>	China	KT732950	KT733016	KT733020	KT732997	KT732999
<i>D. betulina</i>	CFCC 52562	<i>Betula platyphylla</i>	China	MH121497	MH121539	MH121579	MH121421	MH121457
<i>D. bicincta</i>	CBS 121004	<i>Juglans</i> sp.	USA	KC343134	KC343860	KC344102	KC343376	KC343618
<i>D. celastrina</i>	CBS 139.27	<i>Celastrus scandens</i>	-	KC343047	KC343773	KC344015	KC343289	KC343531
<i>D. celeris</i>	CPC 28262	<i>Vitis vinifera</i>	Czech Republic	MG281017	MG281538	MG281190	MG281712	MG281363
<i>D. chamaeropsis</i>	CBS 454.81	<i>Chamaerops humilis</i>	Greece	KC343048	KC343774	KC344016	KC343290	KC343532
<i>D. chensiensis</i>	CFCC 52567	<i>Abies chensiensis</i>	China	MH121502	MH121544	MH121584	MH121426	MH121462
<i>D. conica</i>	CFCC 52571	<i>Alangium chinense</i>	China	MH121506	MH121548	MH121588	MH121426	MH121466
<i>D. cynaroidis</i>	CBS 122676	<i>Protea cynaroides</i>	South Africa	KC343058	KC343784	KC344026	KC343300	KC343542
<i>D. elaeagni</i>	CBS 504.72	<i>Elaeagnus</i> sp.	Netherlands	KC343064	KC343790	KC344032	KC343306	KC343548
<i>D. eres</i>	CBS 138594	<i>Ulmus laevis</i>	Germany	KJ210529	KJ210550	KJ420799	KJ434999	KC343574
<i>D. foeniculina</i>	CBS 123208	<i>Foeniculum vulgare</i>	Portugal	KC343101	KC343827	KC344069	KC343343	KC343585
<i>D. gardeniae</i>	CBS 288.56	<i>Gardenia florida</i>	Italy	KC343113	KC343839	KC344081	KC343355	KC343597
<i>D. helicis</i>	CBS 138596	<i>Hedera helix</i>	France	KJ210538	KJ210559	KJ420828	KJ435043	KJ420875
<i>D. inconspicua</i>	CBS 133813	<i>Maytenus ilicifolia</i>	Brazil	KC343123	KC343849	KC344091	KC343365	KC343607
<i>D. leucospermi</i>	CBS 111980	<i>Leucospermum</i> sp.	Australia	JN712460	KY435632	KY435673	KY435663	KY435653
<i>D. neilliae</i>	CBS 144.27	<i>Spiraea</i> sp.	-	KC343144	KC343870	KC344112	KC343386	KC343628
<i>D. nobilis</i>	CBS 113470	<i>Castanea sativa</i>	South Korea	KC343146	KC343872	KC344114	KC343388	KC343630
<i>D. padina</i>	CFCC 52590	<i>Prunus padus</i>	China	MH121525	MH121567	MH121604	MH121443	MH121483

<i>D. portugallica</i>	CBS 144228	<i>Camelia sinensis</i>	Portugal	MH063905	MH063911	MH063917	MH063893	MH063899
<i>D. pseudoinconspicua</i>	URM 7874	<i>Poincianella pyramidalis</i>	Brazil	MH122538	MH122533	MH122524	MH122528	MH122517
<i>D. pulla</i>	CBS 338.89	<i>Hedera helix</i>	Yugoslavia	KC343152	KC343878	KC344120	KC343394	KC343636
<i>D. pyracanthae</i>	CBS 142384	<i>Pyracantha coccinea</i>	Portugal	KY435635	KY435625	KY435666	KY435656	KY435645
<i>D. rudis</i>	CBS 113201	<i>Vitis vinifera</i>	Portugal	KC343234	KC343960	KC344202	KC343476	KC343718
<i>D. sennicola</i>	CFCC 51634	<i>Senna bicapsularis</i>	China	KY203722	KY228883	KY228889	KY228873	KY228879
<i>D. vaccinii</i>	CBS 160.32	<i>Vaccinium macrocarpon</i>	USA	KC343228	KC343954	KC344196	KC343470	KC343712
<i>Diaporthella corylina</i>	CBS 121124	<i>Corylus</i> sp.	China	KC343004	KC343730	KC343972	KC343246	KC343488

¹Acronyms of culture collection: **CBS** – Westerdijk Fungal Biodiversity Institute, Utrecht, the Netherlands; **CFCC** – China Forestry Culture Collection Center; **CPC** – personal culture collection of Pedro W. Crous, hosted at CBS; **URM** – fungal culture collection from Micoteca at Federal University of Pernambuco, Brazil. The ex-type isolates are highlighted in bold

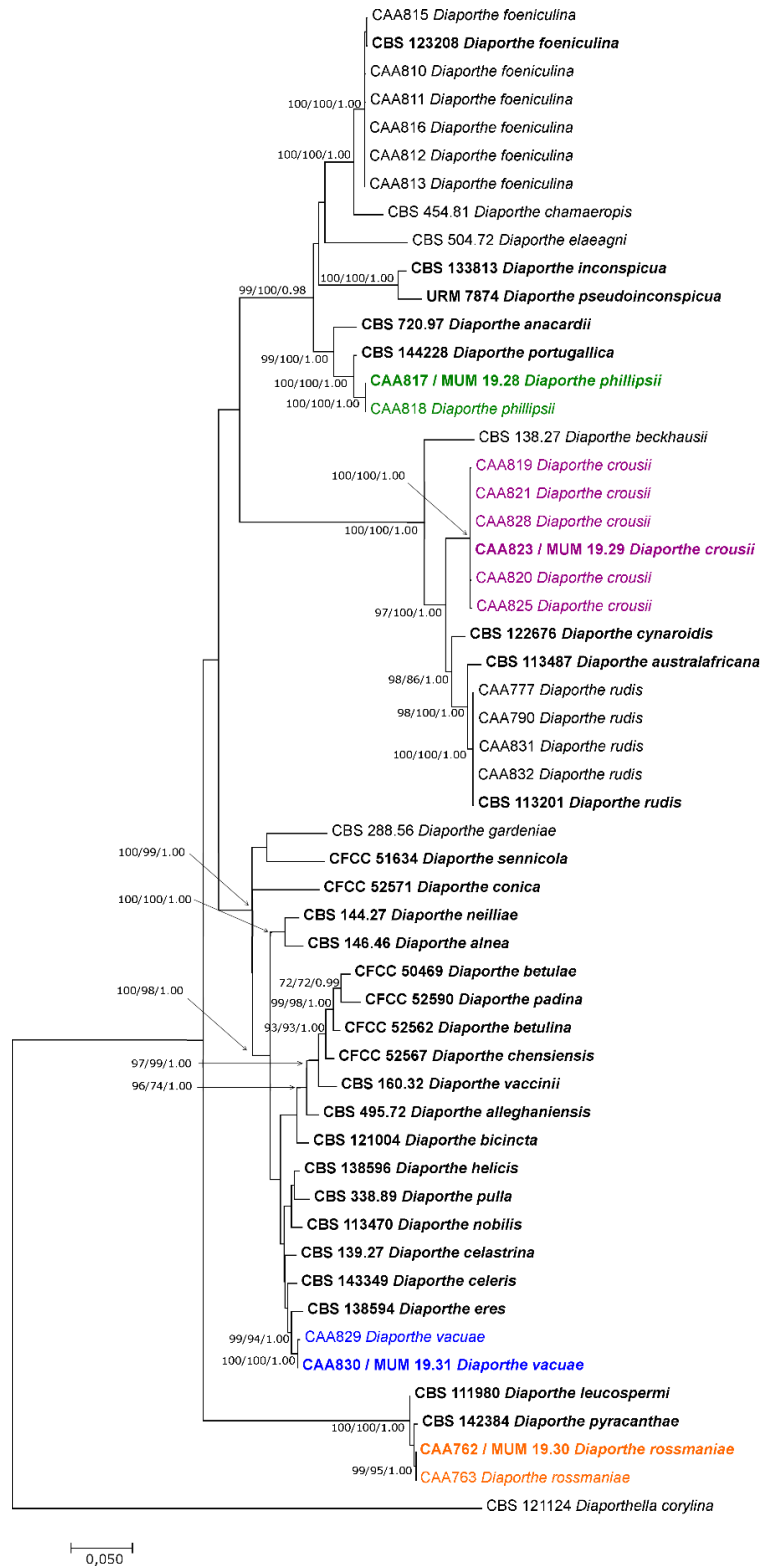


Figure 1. Maximum likelihood phylogenetic tree obtained from combined analysis of ITS, *tef1- α* , *tub2*, *cal*, and *his3* sequence data from *Diaporthe* species. The ML tree was built using the Tamura-Nei parameter model assuming a gamma distribution and invariant sites. *Diaporthella corylina* (CBS 121124) was used as outgroup. Bootstrap values of ML and MP above 70% and posterior probabilities above ≥ 0.70 (ML/MP/PP) are given at the nodes. Ex-type isolates are given in bold.

Temperature growth studies.

Temperature growth studies were made for isolates of new *Diaporthe* species. The colonies diameters were measured daily until the colonies reached the edges of the plate. At 5 °C, none of the isolates were able to grow. However, as soon as the plates were taken out the incubator and placed at room temperature, regrowth was observed. Forty-degree temperature was lethal to most of the isolates, since when returning to room temperature they did not recover. Table 3 summarizes the estimated growth parameters, with 95% confidence intervals, for the species tested.

Table 3. Estimated growth parameters with 95% confidence intervals for *Diaporthe crousii*, *D. phillipsii*, *D. rossmaniae*, and *D. vacuae* (E – Estimate; L – Lower; U – Upper).

Species	μ_{opt} (mm/day)			T_{max} (C)			T_{min} (C)			T_{opt} (C)			R^2 (%)
	E	L	U	E	L	U	E	L	U	E	L	U	
<i>Diaporthe crousii</i>	7.3	6.3	8.2	37.5	36.3	38.7	5.2	3.9	6.5	21.7	20.0	23.5	57.1
<i>Diaporthe phillipsii</i>	5.2	4.5	5.8	38.9	37.6	40.2	5.7	3.4	7.9	23.6	21.5	25.6	73.0
<i>Diaporthe rossmaniae</i>	9.3	8.2	10.4	39.2	37.9	40.5	5.3	1.0	9.6	23.6	21.4	25.8	86.9
<i>Diaporthe vacuae</i>	4.7	4.3	5.1	39.4	38.6	40.2	4.7	2.4	8.9	24.4	22.5	26.2	88.5

Pathogenicity tests.

For the pathogenicity tests, the following isolates were tested: CAA832 (*Diaporthe rudis*), CAA815 (*D. foeniculina*), and the representatives of the potential novel species (CAA829, CAA818, CAA825, and CAA762). A total of 54 blueberry plants (cv. 'Bluecrop') were inoculated. After 2 months, the Parafilm® was removed, and brown external lesions were observed at the fungal inoculation sites. No internal lesions were observed on the control plants. Plants inoculated with the isolate CAA762 started to exhibit yellow to brown leaves 15 days after inoculation. The rest of the inoculated blueberry plants showed healthy leaves and small lesions on the inoculated stems and twigs. The external lesions were mainly discoloration of the tissues that ranged from yellow to brown, and in some cases, cankers were visible as reaction to the infection. The internal lesions were characterized by brownish color of the inner vascular tissues, and the length varied depending on the species inoculated (Table 4). There were no significant differences in lesion size between

the *Diaporthe* isolates, although the isolate CAA762 caused the largest lesion lengths.

Table 4. Means \pm SD of lesion lengths (cm) caused by *Diaporthe* species inoculated on *Vaccinium corymbosum* (cv. 'Bluecrop').

Species	Isolate	External lesion	Internal lesion
<i>Diaporthe crousii</i>	CAA825	0.8 \pm 0.4 a	1.2 \pm 0.4 A
<i>Diaporthe foeniculina</i>	CAA815	0.7 \pm 0.3 a	0.9 \pm 0.5 A
<i>Diaporthe phillipsii</i>	CAA818	0.6 \pm 0.4 a	1.0 \pm 0.7 A
<i>Diaporthe rossmaniae</i>	CAA762	0.7 \pm 0.3 a	1.9 \pm 0.3 A
<i>Diaporthe rudis</i>	CAA832	0.5 \pm 0.3 a	0.7 \pm 0.4 A
<i>Diaporthe vacuae</i>	CAA829	0.9 \pm 0.5 a	0.8 \pm 0.5 A

Note: Means followed by the same letters are not significantly different ($p < 0.05$).

TAXONOMY

Diaporthe crousii S. Hilário, L. Santos & A. Alves, sp. nov. (Fig. 2)

Mycobank MB831439

Typification: Portugal. Sever do Vouga: Vila Fria (40°45'6.9"N 8°23'17.9"W), from dieback lesions of *V. corymbosum*, 10 Jul 2016, L. Santos CAA823 (holotype **AVE-F-3**, a dried culture sporulating on fennel stems, deposited in the Herbarium Universitatis Aveirensis from Universidade de Aveiro, Portugal). Ex-type culture **MUM 19.29**, deposited in the Micoteca da Universidade do Minho, Portugal.

Etymology: Named in honor of the mycologist Pedro Crous.

Known distribution: Portugal.

Mating type strategy: Homothallic.

Description: Asexual morph: brown to black pycnidial conidiomata secreting yellow conidial mass from ostiole; alpha conidia hyaline, smooth, aseptate, ellipsoid, rounded apex and obtuse to truncate base, biguttulate (mean \pm SD = 5.7 \pm 0.5 \times 2.3 \pm 0.2 μ m, $n = 100$); conidiophores hyaline, aggregated, cylindrical, straight, reduced to conidiogenous cells (mean \pm SD = 21.9 \pm 3.9 \times 1.5 \pm 0.3 μ m, $n = 30$); paraphyses not observed; beta conidia not observed; gamma conidia infrequent, aseptate, smooth, hyaline (mean \pm SD = 10.6 \pm 1.0 \times 1.5 \pm 0.2 μ m, $n = 8$). Sexual morph: perithecial ascomata, globose to subglobose, solitary or in clusters, black, ostiolate exuding a translucent white spores mass; brown ascomatal necks emerging through

fennel stems; asci (mean \pm SD = $46.9 \pm 3.2 \times 8.8 \pm 1.2 \mu\text{m}$, $n = 50$) 8-spored, unitunicate, clavate to subclavate, straight to slightly curved; ascospores (mean \pm SD = $12.8 \pm 1.2 \times 3.0 \pm 0.5 \mu\text{m}$, $n = 100$), 2-celled, septate and slightly constricted at the septum, frequently tetraguttulate, ellipsoidal, straight, hyaline, without appendages.

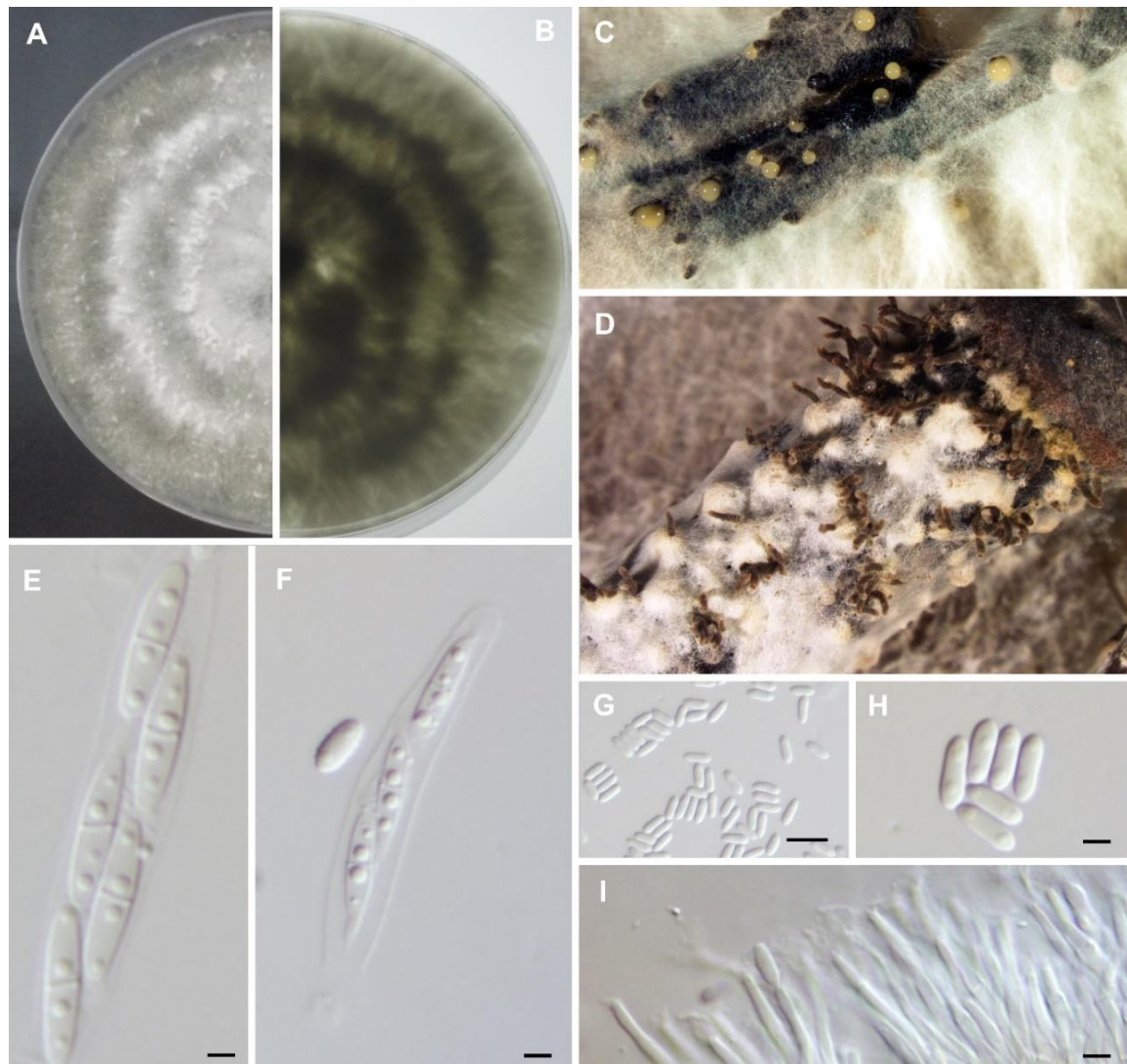


Figure 2. Morphology of *Diaporthe crousii* from *Vaccinium corymbosum* (MUM 19.29). **A.** Upper culture surface. **B.** Reverse culture surface. Both on PDA, 25 °C and 7 days **C.** Conidiomata on fennel stems exuding yellow conidial cirrus. **D.** Perithecial ascomata and necks emerging through fennel stems. **E.** Ascus with ascospores. **F.** left: alpha conidia; right: ascus. **G, H.** Alpha conidia. **I.** Conidiophores. Bars: **E, F, H, I,** = 2.5 μm ; **G** = 10 μm .

Culture characteristics: Colonies spreading with white to gray sparse aerial mycelium and with reverse greenish concentric zones; fast growing ($\mu_{\text{opt}} = 7.3 \pm 1.0$ mm/day, $n = 6$) and covering a Petri dish in 7 days at 25 °C. The colonies grew

better at 25 °C. Only after the fifth day, the culture started to exhibit some growth at 10 °C. At 30 and 35 °C, the culture did not grow but displayed a circular brown pigmentation; maximum temperature for growth is 37.5 ± 1.2 °C, minimum temperature is 5.2 ± 1.3 °C, and optimum temperature is 21.7 ± 1.8 °C.

Additional material examined: **Portugal. Sever do Vouga:** Vila Fria (40°45'6.9"N 8°23'17.9"W) and Azibal (40°44'17.5"N 8°22'25.1"W), isolated from *V. corymbosum*. L. Santos, living cultures CAA819, CAA820, CAA821, CAA825, and CAA828.

Notes: *Diaporthe crousii* is known only from *V. corymbosum* in Portugal. This new species clusters in a well-supported and separate clade (ML/MP/PP = 100/100/1.00), and it appears closely related to the clade containing *D. australafricana*, *D. cynaroidis*, and *D. rudis*. Morphologically, *D. crousii* differs from *D. australafricana* in its larger alpha conidia ($5.7 \pm 0.5 \times 2.3 \pm 0.2$ µm for *D. crousii* vs. $5.2 \pm 0.2 \times 1.7 \pm 0.2$ µm for *D. australafricana*), slightly larger ascospores ($12.8 \pm 1.2 \times 3.0 \pm 0.5$ µm for *D. crousii* vs. $12.2 \pm 0.7 \times 3.2 \pm 0.2$ µm for *D. australafricana*), and shorter but wider asci ($49.6 \pm 3.2 \times 8.8 \pm 1.2$ µm for *D. crousii* vs. $58.0 \pm 3.0 \times 6.7 \pm 1.8$ µm for *D. australafricana*) (van Niekerk et al. 2005). The new species also differs from *D. rudis* in its smaller alpha conidia ($5.7 \pm 0.5 \times 2.3 \pm 0.2$ µm for *D. crousii* vs. $7.5 \pm 0.5 \times 2.2 \pm 0.2$ µm for *D. rudis*), in the absence of beta conidia (known in *D. rudis*), in shorter gamma conidia ($10.6 \pm 1.0 \times 1.5 \pm 0.2$ µm for *D. crousii* vs. $14.5 \pm 0.5 \times 1.5 \pm 0.5$ µm for *D. rudis*), and in shorter and thinner asci ($49.6 \pm 3.2 \times 8.8 \pm 1.2$ µm for *D. crousii* vs. $56 \pm 2.5 \times 11.3 \pm 0.7$ µm for *D. rudis*) (Udayanga et al. 2014a). Morphological characters of *D. cynaroidis* were not available to be compared. A pairwise comparison shows that *D. crousii* can be distinguished from *D. cynaroidis* by 6 nucleotides (nt) of 594 bp in ITS (p-distance = 1.0%), 14 nt of 416 bp in *tef1-α* (p-distance = 3.4%), 16 nt of 491 bp in *tub2* (p-distance = 3.3%), 10 nt of 529 bp in *his3* (p-distance = 1.9%), and 5 nt of 516 bp in *cal* (p-distance = 0.9%); from *D. australafricana* by 9 nt of 594 bp in ITS (p-distance = 0.7%), 17 nt of 416 bp in *tef1-α* (p-distance = 4.1%), 16 nt of 491 bp in *tub2* (p-distance = 3.3%), 18 nt of 529 bp in *his3* (p-distance = 3.4%), and 11 nt of 516 bp in *cal* (p-distance = 2.1%); and from *D. rudis* by 6 nt of 594 bp in ITS (p-distance = 1.0%), 17 nt of 416 bp in *tef1-α* (p-distance = 4.1%), 13 nt of 491 bp in *tub2* (p-

distance = 2.6%), 17 nt of 529 bp in *his3* (p-distance = 3.2%), and 8 nt of 516 bp in *cal* (p-distance = 1.6%).

Diaporthe phillipsii S. Hilário, L. Santos & A. Alves, **sp. nov.** (Fig. 3)

MycoBank MB831438

Typification: **Portugal. Sever do Vouga.** Vila Fria (40°45'6.9"N 8°23'17.9"W), from *V. corymbosum* dead stem, 10 Jul 2016, L. Santos CAA817 (holotype **AVE-F-2**, a dried culture sporulating on fennel stems, deposited in the Herbarium Universitatis Aveirensis from Universidade de Aveiro, Portugal). Ex-type culture **MUM 19.28**, deposited in the Micoteca da Universidade do Minho, Portugal.

Etymology: Named in honor of the mycologist Alan J. L. Phillips.

Known distribution: Portugal.

Mating type strategy: heterothallic.

Description: Sexual morph: not observed. Asexual morph: brown to black pycnidial conidiomata, solitary or aggregated, secreting yellow conidial cirrhus from the ostioles; conidiophores hyaline, smooth, densely aggregated, cylindrical, straight and slightly curved, reduced to conidiogenous cells (mean \pm SD = $19.5 \pm 4.7 \times 1.4 \pm 0.2 \mu\text{m}$, $n = 30$); paraphyses not observed; alpha conidia aseptate, rarely found triguttulate, fusoid, hyaline, acute at both ends (mean \pm SD = $6.8 \pm 0.7 \times 2.2 \pm 0.2 \mu\text{m}$, $n = 100$); beta and gamma conidia were not observed.

Culture characteristics: Colonies spreading with white superficial mycelium flattened and dense with reverse white to ivory color concentric zone, moderate growing rate ($\mu_{\text{opt}} = 5.2 \pm 0.7 \text{ mm/day}$, $n = 6$), covering a Petri dish in 7 days at 25 °C. The colonies grew better at 30 °C than 25 °C in the first 3 days. After the fourth day, the growth was higher at 25 °C. No growth was observed at 5 °C nor at 40 °C; maximum temperature for growth is $38.9 \pm 1.3 \text{ °C}$, minimum temperature is $5.7 \pm 2.3 \text{ °C}$, and optimum temperature is $23.6 \pm 2.1 \text{ °C}$.

Additional material examined: Portugal. Sever do Vouga: Vila Fria (40°45'6.9"N 8°23'17.9"W), isolate from *V. corymbosum*, L. Santos, living culture CAA818.

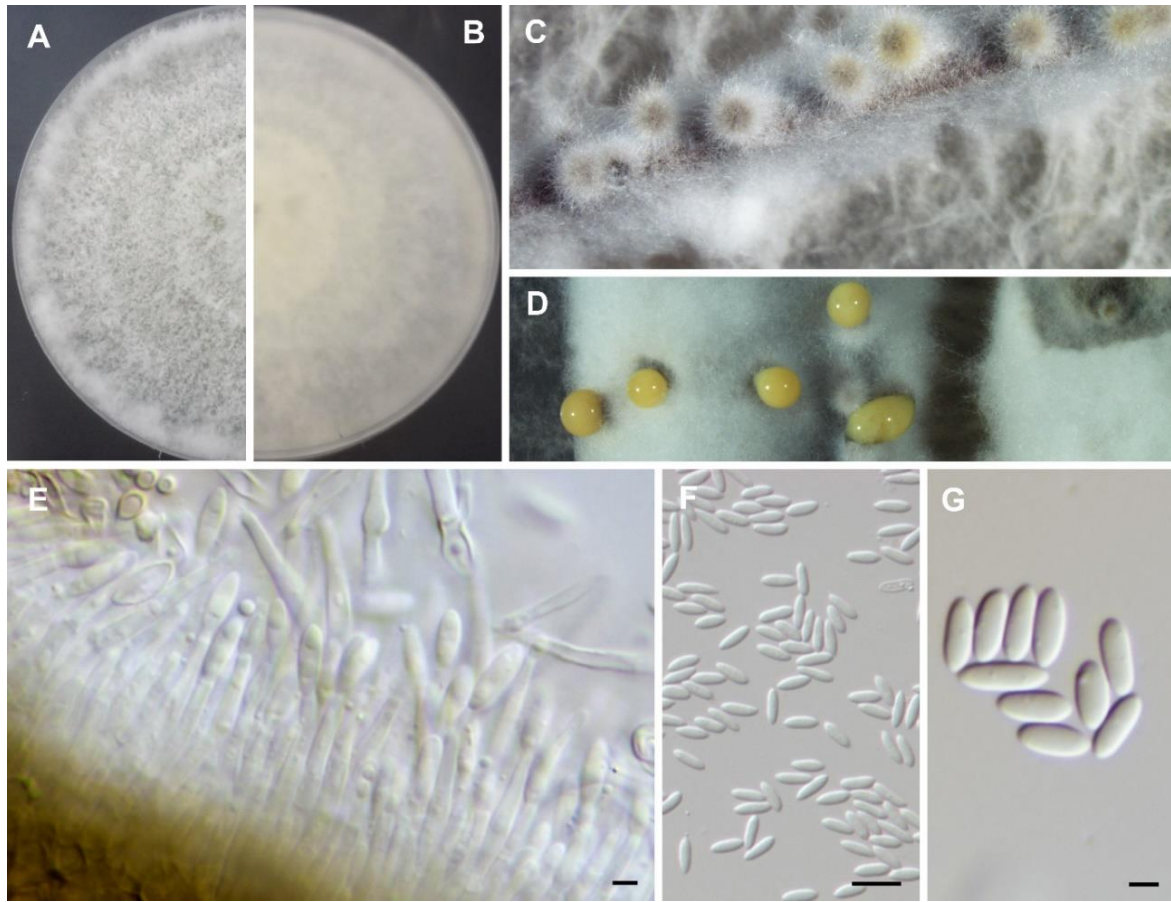


Figure 3. Morphology of *Diaporthe phillipsii* from *Vaccinium corymbosum* (MUM 19.28). **A.** Upper culture surface on PDA, 25 °C and 7 days. **B.** Reverse culture surface on PDA, 25 °C and 7 days. **C.** Conidiomata on pine needles in culture. **D.** Conidiomata on fennel stems in culture oozing yellow conidial cirrus. **E.** Conidiophores reduced to conidiogenous cells. **F, G.** Alpha conidia. Bars: **E, G** = 2.5 µm; **F** = 10 µm.

Notes: *Diaporthe phillipsii* is known only from *V. corymbosum* in Portugal. This species clusters in a subclade with *D. portugallica* supported by high bootstrap and posterior probability values (ML/MP/PP = 100/100/1.00) and is closely related to *D. anacardii* (ML/MP/PP = 99/100/1.00). *Diaporthe portugallica* was found only in Portugal (Azores Islands) from leaf lesions of *Camellia sinensis* (Guarnaccia & Crous 2018). Although conidial dimensions of *D. phillipsii* and *D. portugallica* are virtually undistinguishable ($6.8 \pm 0.7 \times 2.2 \pm 0.2 \mu\text{m}$ for *D. phillipsii* vs. $6.6 \pm 0.8 \times 2.2 \pm 0.3 \mu\text{m}$ for *D. portugallica*), *D. phillipsii* differs from *D. portugallica* in colony characters (reverse white to ivory color for *D. phillipsii* vs. reverse pale brown for *D. portugallica*) (Guarnaccia & Crous 2018). *Diaporthe phillipsii* differs from *D. anacardii* in its thinner alpha conidia ($6.8 \pm 0.7 \times 2.2 \pm 0.2 \mu\text{m}$ for *D. phillipsii* vs. $7.0 \pm 1.5 \times 7.7 \pm 1.2 \mu\text{m}$ for *D. anacardii*) and in the absence of beta conidia, which is

known in *D. anacardii* (Gomes et al. 2013). Molecularly, *D. phillipsii* differs from *D. anacardii* in 17 nt of 594 bp in ITS (p-distance = 2.8%), 15 nt of 416 bp in *tef1- α* (p-distance = 3.6%), 12 nt of 491 bp in *tub2* (p-distance = 2.4%), 13 nt of 529 in *his3* (p-distance = 2.5%), and 16 nt of 516 bp in *cal* (p-distance = 3.1%); and from *D. portugallica* in 19 nt of 594 bp in ITS (p-distance = 3.2%), 2 nt of 529 bp in *his3* (p-distance = 0.4%), and 2 nt of 516 bp in *cal* (p-distance = 0.4%).

Diaporthe rossmaniae S. Hilário, I. Amaral, L. Santos & A. Alves, **sp. nov.** (Fig. 4)
MycoBank MB831452

Typification: **Portugal. Sever do Vouga:** Azibal (40°44'17.5"N 8°22'25.1"W), from twig lesions of *V. corymbosum*, 8 Aug 2015, L. Santos CAA762 (holotype **AVE-F-4**, a dried culture sporulating on pine needles, deposited in the Herbarium Universitatis Aveirensis from Universidade de Aveiro, Portugal). Ex-type culture **MUM 19.30**, deposited in the Micoteca da Universidade do Minho, Portugal.

Etymology: Named in honor of the mycologist Amy Y. Rossman.

Known distribution: Portugal.

Mating type strategy: Heterothallic.

Description: Sexual morph: not observed. Asexual morph: brown to black pycnidial conidiomata, exuding a creamy white to yellow conidial cirrhous; conidiophores lining the inner cavity, subcylindrical, hyaline to gold, smooth, reduced to conidiogenous cells (mean \pm SD = $7.4 \pm 1.3 \times 1.9 \pm 0.4$ μ m, $n = 30$); paraphyses not observed; alpha conidia hyaline, uni- to biguttulate, smooth, aseptate, ellipsoid, rounded apex, obtuse to truncate base (mean \pm SD = $6.8 \pm 0.6 \times 2.5 \pm 0.2$ μ m, $n = 100$); beta conidia hyaline, aseptate, smooth, filiform, frequently hooked in apical part, apex acute, base truncate (mean \pm SD = $25.7 \pm 2.4 \times 1.2 \pm 0.2$ μ m, $n = 100$); gamma conidia not found.

Culture characteristics: White colonies spreading large with moderate aerial mycelium and reverse with greenish gray zones, fast growing ($\mu_{opt} = 9.3 \pm 1.1$ mm/day, $n = 6$), covering a Petri dish in 6 days at 25 °C. The colony grew better at 30 °C than at 25 °C in the first 3 days. After the fourth day, the growth was higher at 25 °C. It grew better at 35 °C than at 10 °C. However, at day 6, the growth at both temperatures was the same. The isolate CAA762 was the only that recovered after

being taken out from the 40 °C incubator; maximum temperature for growth is 39.2 ± 1.3 °C, minimum temperature is 5.3 ± 4.3 °C, and optimum temperature is 23.6 ± 2.2 °C.

Additional material examined: Portugal. Sever do Vouga: Azibal ($40^{\circ}44'17.5''\text{N}$ $8^{\circ}22'25.1''\text{W}$), isolate from *V. corymbosum*. L. Santos, living culture CAA763.

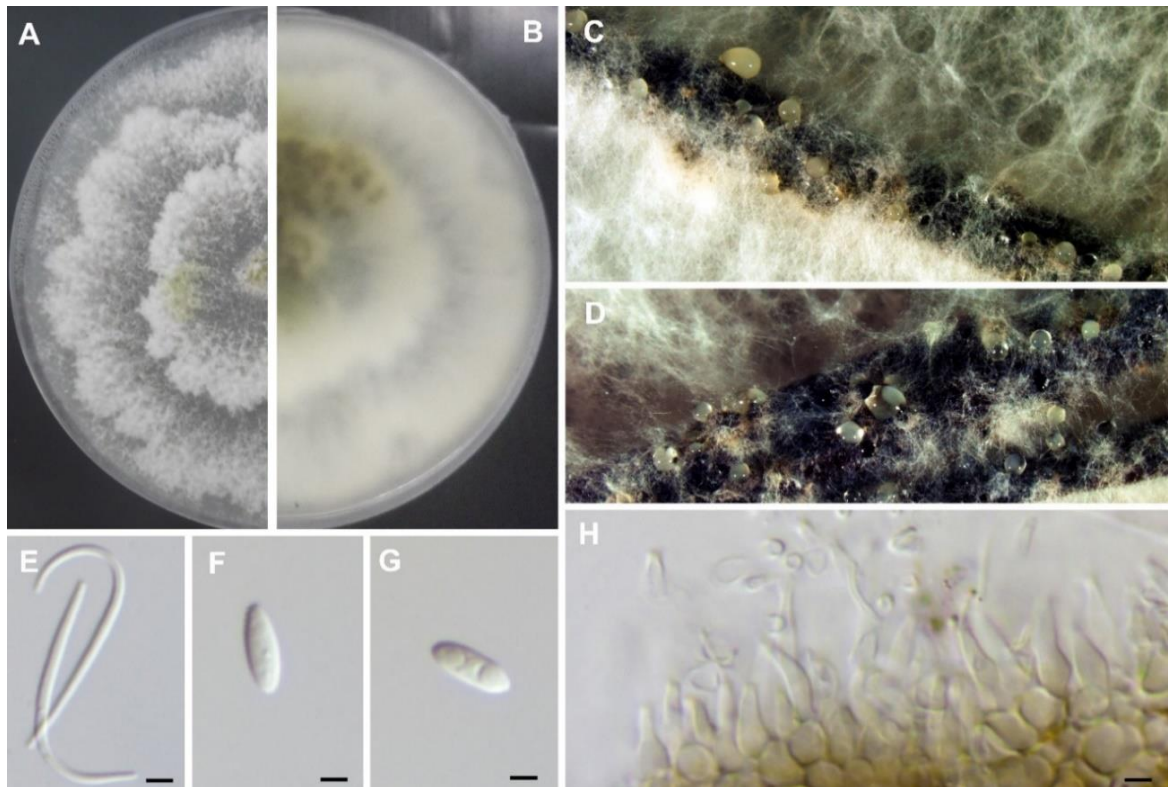


Figure 4. Morphology of *Diaporthe rossmaniae* from *Vaccinium corymbosum* (MUM 19.30). **A.** Upper culture surface. **B.** Reverse culture surface. Both on PDA, 25 °C and 7 days. **C, D.** Conidiomata on pine needles in culture exuding conidial cirrhous. **E.** Beta conidia. **F, G.** Alpha conidia. **H.** Conidiophores protruding on pseudoparenchyma. Bars = 2.5 μm.

Notes: *Diaporthe rossmaniae* is known only from *Vaccinium corymbosum* in Portugal. *Diaporthe rossmaniae* clusters in a highly supported clade (ML/MP/PP = 99/95/1.00) and is phylogenetically closely related to *D. pyracanthae* and *D. leucospermi* (ML/MP/PP = 100/100/1.00). Colony characters on PDA medium of *D. rossmaniae* are slightly different from those of *D. leucospermi* and *D. pyracanthae* (white colonies spreading large and reverse with greenish gray zones for *D. rossmaniae*; pale olivaceous-gray to smoke-gray colonies with reverse olivaceous-gray for *D. leucospermi*; pale brown to smoke-gray colonies with reverse pale brown

to smoke-gray for *D. leucospermi*). Although alpha conidia of these species are almost undistinguishable ($6.8 \pm 0.6 \times 2.5 \pm 0.2 \mu\text{m}$ for *D. rossmaniae* vs. $6.0 \pm 1.0 \times 2.7 \pm 0.2 \mu\text{m}$ for *D. leucospermi* vs. $6.8 \pm 0.4 \times 2.2 \pm 0.2 \mu\text{m}$ for *D. pyracanthae*); *D. rossmaniae* differs from *D. pyracanthae* and *D. leucospermi* in its smaller beta conidia ($25.7 \pm 2.4 \times 1.2 \pm 0.2 \mu\text{m}$ for *D. rossmaniae* vs. $27.5 \pm 2.5 \times 1.2 \pm 0.3 \mu\text{m}$ for *D. leucospermi* vs. $30.0 \pm 2.7 \times 1.3 \pm 0.8 \mu\text{m}$ for *D. pyracanthae*) (Crous et al. 2011; Santos et al. 2017b). A pairwise comparison showed that *D. rossmaniae* differs from *D. leucospermi* in 3 nt of 594 bp on ITS (p-distance = 0.5%), 3 nt of 416 bp in *tef1- α* (p-distance = 0.7%), 2 nt of 529 bp in *his3* (p-distance = 0.4%), and 1 nt of 491 in *tub2* (p-distance = 0.2%). Additionally, 5 nt of 491 bp in *tub2* (p-distance = 1.0%) and 2 nt of 416 bp in *tef1- α* (p-distance = 0.5%) separate *D. rossmaniae* from *D. pyracanthae*.

Diaporthe vacuae S. Hilário, L. Santos & A. Alves, **sp. nov.** (Fig. 5)

MycoBank MB831440

Typification: **Portugal. Sever do Vouga:** Vila Fria ($40^{\circ}45'6.9''\text{N}$ $8^{\circ}23'17.9''\text{W}$), from twig lesions of *V. corymbosum*, 10 Jul 2016, L. Santos CAA830 (holotype **AVE-F-5**, a dried culture sporulating on pine needles, deposited in the Herbarium Universitatis Aveirensis from Universidade de Aveiro, Portugal). Extype culture **MUM 19.31**, deposited in the Micoteca da Universidade do Minho, Portugal.

Etymology: Named after the ancient Latin name (*Vacua*) of the region Vouga where it was first isolated from.

Known distribution: Portugal.

Mating type strategy: Heterothallic.

Description: Sexual morph: not observed. Asexual morph: brown to black pycnidial conidiomata, broadly spherical, covered in white mycelium, with yellowish conidial cirrus extruding from ostiole; conidiophores reduced to conidiogenous cells, hyaline, smooth and straight to sinuous, broadening in the base, slightly tapering toward the apex (mean \pm SD = $10.9 \pm 2.2 \times 1.8 \pm 0.3 \mu\text{m}$, $n = 30$); paraphyses not observed; beta conidia were found hyaline, 1-celled, aseptate, smooth, filiform, frequently hooked in apical part, apex acute (mean \pm SD = $27.4 \pm$

$2.3 \times 1.6 \pm 0.2 \mu\text{m}$, $n = 100$); alpha conidia infrequent, hyaline, smooth, cylindrical (mean \pm SD = $9.3 \pm 1.1 \times 2.6 \pm 0.3 \mu\text{m}$, $n = 6$); gamma conidia were not observed.

Culture characteristics: White to gray surface mycelium and reverse with yellowish zones, colonies spreading with appressed mycelium, with moderate growing on PDA medium ($\mu_{\text{opt}} = 4.7 \pm 0.4 \text{ mm/day}$, $n = 6$) and covering a Petri dish in 10 days at 25 °C. Growth rates at 25 and 30 °C were quite similar. After the fourth day, the growth was higher at 25 °C. It grew better at 35 °C than at 10 °C; maximum temperature for growth is $39.4 \pm 0.8 \text{ °C}$, minimum temperature is $4.7 \pm 2.3 \text{ °C}$, and optimum temperature is $24.4 \pm 1.9 \text{ °C}$.

Additional material examined: Portugal. Sever do Vouga: Vila Fria ($40^{\circ}45'6.9''\text{N } 8^{\circ}23'17.9''\text{W}$), isolate from *V. corymbosum*. L. Santos, living culture CAA829.

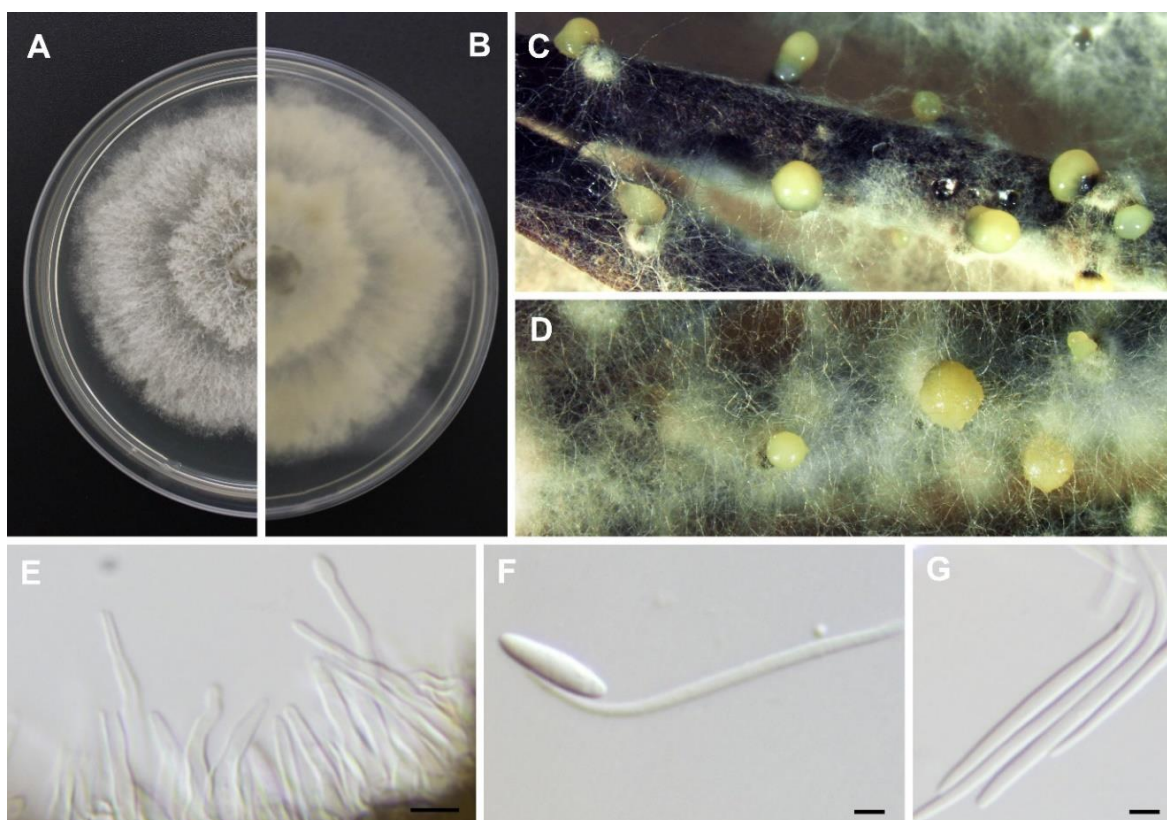


Figure 5. Morphology of *Diaporthe vacuae* from *Vaccinium corymbosum* (MUM 19.31). **A.** Upper culture surface. **B.** Reverse culture surface. Both on PDA, 25 °C and 7 days. **C, D.** Conidiomata on pine needles in culture exuding yellow conidial cirrus. **E.** Conidiophores. **F.** Alpha and beta conidia. **G.** Beta conidia. Bars = 2.5 μm .

Notes: *Diaporthe vacuae* is known only from *V. corymbosum* in Portugal. This species clusters in a highly supported clade (ML/MP/PP = 100/100/1.00) and is

phylogenetically closely related to *D. eres* and *D. celeris*. *Diaporthe vacuae* differs from *D. eres* and *D. celeris* in its larger beta and alpha conidia (alpha conidia: $9.3 \pm 1.1 \times 2.6 \pm 0.3 \mu\text{m}$ for *D. vacuae* vs. $7.5 \pm 0.5 \times 2.5 \pm 0.5 \mu\text{m}$ for *D. eres* vs. $6.0 \pm 1.5 \times 2.5 \pm 0.5 \mu\text{m}$ for *D. celeris*; beta conidia: $27.4 \pm 2.3 \times 1.6 \pm 0.2 \mu\text{m}$ for *D. vacuae* vs. $25.0 \pm 2 \times 1.3 \pm 0.3 \mu\text{m}$ for *D. eres* vs. $19.2 \pm 3.2 \times 1.5 \pm 0.5 \mu\text{m}$ for *D. celeris*). *Diaporthe vacuae* also differs from *D. eres* and *D. celeris* in colony characters in PDA medium (white to gray surface mycelium and reverse with yellowish zones for *D. vacuae*; white and fluffy mycelium with reverse dark pigmentation developing in center for *D. eres*; white colonies becoming cream to brown with reverse whitish to cream for *D. celeris*) (Guarnaccia et al. 2018; Udayanga et al. 2014b). Molecularly, *D. vacuae* differs from *D. eres* in several nucleotide positions: 3 nt of 416 bp in *tef1- α* (p-distance = 0.7%), 5 nt of 516 bp in *cal* (p-distance = 0.9%), and 18 nt of 491 bp in *tub2* (p-distance = 3.7%); and from *D. celeris* in 6 nt of 594 bp in ITS (p-distance = 1.0%), 7 nt of 416 bp in *tef1- α* (p-distance = 1.7%), 9 nt of 491 bp in *tub2* (p-distance = 1.8%), 6 nt of 529 bp in *his3* (p-distance = 1.1%), and 2 nt of 516 bp in *cal* (p-distance = 0.4%).

DISCUSSION

Given an overall lack of studies regarding blueberry fungal diseases occurring in Portugal, the current study addressed the diversity and pathogenicity of *Diaporthe* species associated with blueberry plants (*Vaccinium corymbosum*) in plantations from the central region of Portugal. A special emphasis was put on members of the genus *Diaporthe*, due to their relevance as known plant pathogens, affecting blueberry growing areas worldwide (Lombard et al. 2014).

Diaporthe is commonly associated with dieback, twig blight, stem canker, fruit rot, and even death of *Vaccinium* plants, occurring in the USA, Chile, and Europe (Elfar et al. 2013; Narouei-Khandan et al. 2017; van Bruggen et al. 2018). The plant symptoms are difficult to distinguish from those caused by other factors such as herbicide or fungicide injuries, stress caused by heat and drought, frost damages, and nutritional deficits (Gabler et al. 2004). Also, it can be mistaken with bacterial canker or even with other fungi such as *Pestalotiopsis*, *Colletotrichum*, and *Botryosphaeriaceae* (Michalecka et al. 2017). Moreover, the identification of some

Diaporthe species can be quite difficult due to pleomorphism (Gao et al. 2017). For this reason, a multilocus phylogenetic analysis combining ITS and the coding genes *tef1- α* , *tub2*, *cal*, and *his3* has become the most effective tool to identify cryptic fungal species in *Diaporthe*, known to be a highly complex genus (Guarnaccia et al. 2018; Santos et al. 2017b).

A search of the SMML Fungus-Host Distribution Database (<https://nt.ars-grin.gov/fungalatabases/>) retrieved several reports of *Diaporthe* species on *V. corymbosum* worldwide, such as *D. rudis*, *D. eres*, *D. asheicola*, *D. baccae*, *D. sterillis*, and *D. vaccinii* (Lombard et al. 2014), *D. australafricana*, *D. ambigua*, *D. passiflorae*, and *D. foeniculina* (Elfar et al. 2013), *D. oxe* (Sessa et al. 2018), and *D. nobilis* (Yu et al. 2018).

In the present study, *D. foeniculina*, *D. rudis*, and four new species (*D. phillipsii*, *D. crousii*, *D. rossmaniae*, and *D. vacuae*) were identified from blueberry plants. *Diaporthe crousii* was the most common species found, with an abundance of 49%, followed by *D. vacuae* and *D. rudis*, with abundance of 25% and 12%, respectively. *Diaporthe eres*, considered to be the most common species found, associated with a wide range of families including the *Ericaceae* (particularly the genus *Vaccinium*) (Lombard et al. 2014), was not found in the present study. *Diaporthe rudis* and *D. foeniculina* were previously reported on other host plants, thus showing that they are not host specific and may be present on a wide range of hosts (Gomes et al. 2013; Udayanga et al. 2014b). *Diaporthe foeniculina* is responsible for causing twig blight, cankers, and dieback on several fruit and ornamental trees (Diogo et al. 2010; Golzar et al. 2012; Santos et al. 2010). Its presence in blueberry plants was documented only in Chile, causing stem canker (Elfar et al. 2013). In the present study, we found isolates of *D. foeniculina* occurring as endophytes or latent pathogen in asymptomatic twigs. Also, this species was isolated from dead twigs, coexisting with *D. rudis*. This result is corroborated by Guarnaccia & Crous (2018) who stated that *Diaporthe* species could coexist in the same host. Moreover, *D. foeniculina*, known to be a common endophyte on several tropical trees (Gao et al. 2017), has been shown to cause cankers on *Castanea sativa* and *Citrus* species in Europe, proving that *Diaporthe* can be either pathogenic or endophytic depending on the host (Guarnaccia & Crous 2018).

Although *Diaporthe rudis* is a recognized fungal pathogen in Europe and New Zealand, specially associated with *Vitis vinifera*, it has also been found in a wide range of hosts (Gomes et al. 2013; Lombard et al. 2014; Udayanga et al. 2014b). Regarding blueberry plants, Lombard et al. (2014) found for the first-time isolates of *D. rudis* occurring on blueberry plants in the Netherlands, although it was not clear whether these isolates were obtained from diseased plants or whether pathogenicity tests were carried out. Later, Cardinaals et al. (2018) isolated *D. rudis* also in the Netherlands from blueberry plants showing shoot blight symptoms. However, in this study, *D. rudis* was not only isolated from plants showing symptoms but also recovered as endophyte from leaves with no apparent symptom of disease, apart from a red or yellow color.

In the multilocus analysis using ITS, *tef1- α* , *tub2*, *cal*, and *his3* sequences, the new *Diaporthe* species formed clades separated from other known species. *Diaporthe phillipsii* and *D. crousii* had very high support (ML/MP/PP = 100/100/1.00) and therefore are regarded as new species. *Diaporthe rossmaniae* was highly supported (ML/MP/PP = 99/95/1.00) but is phylogenetically closely related to *D. pyracanthae* and *D. leucospermi* (Fig. 1). A comparison of nucleotides showed that *D. rossmaniae* differs from *D. leucospermi* and *D. pyracanthae* in several nucleotide positions and therefore is described as a new species. *Diaporthe vacuae* isolates were also highly supported by bootstrap and posterior probability values (ML/MP/PP) (100/100/1.00) but are phylogenetically related to *D. eres*. A pairwise comparison of the sequences revealed differences only in *tef1- α* , *tub2*, and *cal* loci; thus, *D. vacuae* is considered to be a novel species.

The pathogenicity tests in cv. 'Bluecrop' showed that all *Diaporthe* species tested caused lesions on the inoculated plants and were regarded as pathogenic. No severe symptoms, apart from small necrosis of the outer epidermis and discoloration of the internal vascular tissues, were observed. Despite that *D. rossmaniae* produced the largest lesions compared with the other species, no significant differences in aggressiveness were observed between the different species tested (Table 4). Nevertheless, whereas some authors report *D. rudis* as the less aggressive on blueberry plants, other authors show that *D. foeniculina* can cause stem canker (Cardinaals et al. 2018; Elfar et al. 2013). The different

responses of blueberry plants to these pathogens may be related either to the high interspecific variability within *Diaporthe* species or to the choice of host tissue and age of wound (Dissanayake & Phillips 2017). Alternatively, the minor lesions caused by all *Diaporthe* species tested may be explained by the fact that the genus *Diaporthe*, although known to be plant pathogenic, has been reported as one of the most common genera of endophytic fungi, occurring in a wide range of hosts (Murali et al. 2006; Sessa et al. 2018). However, there is a lack of studies regarding the aggressiveness of *Diaporthe* species on blueberry plants that deserves further investigation.

Diaporthe vaccinii is native to North America and a threat to *Vaccinium* plantations worldwide. In Europe and New Zealand, it is a quarantine pathogen according to the European Plant Protection Organization (EPPO) and the New Zealand Government (Lombard et al. 2014; van Bruggen et al. 2018). Besides the USA (Farr et al. 2002) and Canada (Nabetani et al. 2017), *D. vaccinii* was previously reported on blueberry plants in China, Chile, Lithuania, Poland, UK, and Romania (EPPO 2019a), Latvia (Vilka & Volkova 2015), and the Netherlands (Lombard et al. 2014). Although *D. vaccinii* has also been reported in Russia and Belarus, these records are unreliable because confirmation using molecular tools has not been carried out (van Bruggen et al. 2018). Currently and according to EPPO, *D. vaccinii* has been eradicated in most European countries, except for Latvia where it is still present (EPPO 2019b).

Although no isolates of *D. vaccinii* were found in the present study, its presence in the north of Portugal was reported by some authors, who detected twig blight on blueberry plants, based merely on morphological features (Madeira 2016). However, such information needs to be clarified with molecular data, because it may be associated with an incorrect identification of the species, as previously shown by Lombard et al. (2014). In their study, it was found that isolates from blueberry plants were wrongly regarded as *D. vaccinii*, since this was based only on morphological traits and host association. Such fact is also supported by Elfar et al. (2013), who suggested that *D. vaccinii* isolates were misidentified because the only reports in Chile were in 1980, when no molecular analysis was conducted. Nevertheless, the occurrence of *D. vaccinii* in Portugal cannot be excluded, since Narouei-Khandan

et al. (2017) have shown that the northern region of the country seems to be highly suitable for the establishment of this pathogen due to the ideal environmental conditions.

CONCLUSIONS

To better understand the diversity, pathogenicity, distribution, and implications of *Diaporthe* species on blueberry plantations in Portugal, wider surveys on *V. corymbosum* plantations collecting a larger number of samples should be considered in future studies. Also, further research needs to be carried out to unravel the real status of *D. vaccinii*, to understand the mechanisms related to its pathogenicity and distribution in Portugal and Europe.

ACKNOWLEDGMENTS

The authors thank the Portuguese Foundation for Science and Technology (FCT/MCTES) for the financial support to CESAM (Centro de Estudos do Ambiente e do Mar) (UID/AMB/50017/2019) through national funds and the PhD grants of Sandra Hilário (SFRH/BD/137394/2018) and Micael Gonçalves (SFRH/BD/129020/2017). Liliana Santos is funded by national funds (OE), through FCT in the scope of the framework contract foreseen in the numbers 4, 5, and 6 of the article 23, of the Decree-Law 57/2016, of August 29, changed by Law 57/2017, of July 19. The authors are thankful to Mirtilusa, Lda, for providing the blueberry plants for pathogenicity tests and to Sandro Alves and Custódio Daniel Borges for supplying the plant material from their plantations.

REFERENCES

- Alves A, Correia A, Luque J, Phillips AJL. **2004**. *Botryosphaeria corticola*, sp. nov. on *Quercus* Species, with notes and description of *Botryosphaeria stevensii* and its anamorph, *Diplodia mutila*. *Mycologia* 96, 598–613.
- Alves A, Phillips AJL, Henriques I, Correia A. **2007**. Rapid differentiation of species of *Botryosphaeriaceae* by PCR fingerprinting. *Research in Microbiology* 58, 112–121.

- Alves A, Crous PW, Correia A, Phillips AJL. **2008**. Morphological and molecular data reveal cryptic speciation in *Lasiodiplodia theobromae*. *Fungal Diversity* 28, 1–13.
- Baranyi J, Roberts TA. **1994**. A dynamic approach to predicting bacterial growth in food. *International Journal of Food Microbiology* 23, 277–294.
- Baroncelli R, Scala F, Vergara M, Thon MR, Ruocco M. **2016**. Draft whole-genome sequence of the *Diaporthe helianthi* 7/96 strain, causal agent of sunflower stem canker. *Genomics Data* 10, 151–152.
- Carbone I, Kohn LM. **1999**. A method for designing primer set for speciation studies in filamentous ascomycetes. *Mycologia* 91, 553–556.
- Cardinaals J, Wenneker M, Voogd B, Van Leeuwen M. **2018**. Pathogenicity of *Diaporthe* spp. on two blueberry cultivars (*Vaccinium corymbosum*). *EPPO Bulletin* 48, 128–134.
- Chen S, Zhu Y, Shao T, Long X, Gao X, Zhou Z. **2019**. Relationship between rhizosphere soil properties and disease severity in highbush blueberry (*Vaccinium corymbosum*). *Applied Soil Ecology* 137, 187–194.
- Cinelli T, Mondello V, Marchi G, Burrano S, Alves A, Mugnai L. **2016**. First report of *Diaporthe eres* associated with cane blight of grapevine (*Vitis vinifera*) in Italy. *Plant Disease* 100, 532.
- Crous PW, Groenewald JZ, Risede JM, Hywe NL. **2004**. *Calonectria* species and their *Cylindrocladium* anamorphs: species with sphaeropedunculate vesicles. *Studies in Mycology* 50, 415–430.
- Crous PW, Summerell BA, Swart L, Denman S, Taylor JE, Bezuidenhout CM, Palm ME, Marinowitz S. **2011**. Fungal pathogens of Proteaceae. *Persoonia* 27, 20–45.
- Diogo ELF, Santos JM, Phillips AJL. **2010**. Phylogeny, morphology and pathogenicity of *Diaporthe* and *Phomopsis* species on almond in Portugal. *Fungal Diversity* 44, 107–115.
- Dissanayake AJ, Phillips AJL. **2017**. Advances in understanding *Diaporthe* (Editorial). *Mycosphere* 8, 7019.

- Elfar K, Torres R, Díaz GA, Latorre B. **2013**. Characterization of *Diaporthe australafricana* and *Diaporthe* spp. associated with stem canker of blueberry in Chile. *Plant Disease* 97, 1042–1050.
- European and Mediterranean Plant Protection Organization (EPPO). **2019a**. *Diaporthe vaccinii* reporting service articles. Available online <https://gd.eppo.int/taxon/DIAPVA> (accessed on 29 March 2019).
- European and Mediterranean Plant Protection Organization (EPPO). **2019b**. EPPO A2 List of pests recommended for regulation as quarantine pests. Available online https://www.eppo.int/ACTIVITIES/plant_quarantine/A2_list (accessed on 10 May 2019).
- Farr DF, Castlebury LA, Rossman AY. **2002**. Morphological and molecular characterization of *Phomopsis vaccinii* and additional isolates of *Phomopsis* from blueberry and cranberry in the eastern United States. *Mycologia* 94, 494–504.
- Gabler J, Kačergius A, Jovaišiene Z. **2004**. Detection of *Phomopsis vaccinii* on blueberry and cranberry in Europe by direct tissue blot immunoassay and plate-trapped antigen ELISA. *Journal of Phytopathology* 152, 630–632.
- Gao Y, Liu F, Duan W, Crous PW, Cai L. **2017**. *Diaporthe* is paraphyletic. *IMA Fungus* 8, 163–187.
- Golzar H, Tan YP, Shivas RG, Wang C. **2012**. First report of shoot blight of persimmon caused by *Diaporthe neotheicola* in Australia. *Australasian Plant Disease Notes* 7, 115–117.
- Glass NL, Donaldson GC. **1995**. Development of primer sets designed for use with the PCR to amplify conserved genes from filamentous Ascomycetes. *Applied Environment Microbiology* 61, 1323–1330.
- Gomes RR, Glienke C, Videira SIR, Lombard L, Groenewald JZ, Crous PW. **2013**. *Diaporthe*: A genus of endophytic, saprobic and plant pathogenic fungi. *Persoonia* 31, 1–41.
- Guarnaccia V, Crous PW. **2018**. Species of *Diaporthe* on *Camellia* and *Citrus* in the Azores Islands. *Phytopathologia Mediterranea* 57, 307–319.
- Guarnaccia V, Groenewald JZ, Woodhall J, Armengol J, Cinelli T, Eichmeier A, Ezra D, Fontaine F, Gramaje D, Gutierrez-Aguirregabiria A, ... Crous PW. **2018**.

- Diaporthe* diversity and pathogenicity revealed from a broad survey of grapevine diseases in Europe. *Persoonia* 40, 135–153.
- Hall TA. **1999**. BioEdit: A user-friendly biological sequence alignment editor and analysis program for Windows 95/98/NT. *Nucleic Acids Symposium Series* 41, 95–98.
- Jeger M, Bragard C, Caffier D, Candresse T, Chatzivassiliou E, Dehnen-Schmutz K, Gilioli G, Grégoire JC, Miret J, MacLeod A, ... van Bruggen AHC. **2017**. Pest risk assessment of *Diaporthe vaccinii* for the EU territory. *European Food Safety Authority Journal* 15, 1–185.
- Kumar S, Stecher G, Tamura K. **2016**. MEGA7: Molecular evolutionary genetics analysis version 7.0 for bigger datasets. *Molecular Biology and Evolution* 33, 1870–1874.
- Li S, Darwish O, Alkharouf N. **2015**. Draft genome sequence of *Phomopsis longicolla* isolate MSPL 10-6. *Genomics Data* 3, 55–56.
- Li S, Song Q, Martins AM, Cregan P. **2016**. Draft genome sequence of *Diaporthe aspalathi* isolate MS-SSC91, a fungus causing stem canker in soybean. *Genomics Data* 7, 262–263.
- Larkin MA, Blackshields G, Brown NP, Chenna R, McGettigan PA, McWilliam H, Higgins D.G. **2007**. Clustal W and Clustal X version 2.0. *Bioinformatics* 23, 2947–2948.
- Lombard L, Van Leeuwen GCM, Guarnaccia V, Polizzi G, Van Rijswijk PCJ, Rosendahl CHM, Gabler J, Crous PW. **2014**. *Diaporthe* species associated with *Vaccinium*, with specific reference to Europe. *Phytopathologia Mediterranea* 53, 287–299.
- Madeira BSP. **2016**. *Cultura do Mirtilo*. Lisbon: Agrobook Press. 185 p.
- Michalecka M, Bryk H, Seliga P. **2017**. Identification and characterization of *Diaporthe vaccinii* Shear causing upright dieback and viscid rot of cranberry in Poland. *European Journal of Plant Pathology* 148, 595–605.
- Möller EM, Bahnweg G, Sandermann H, Geiger HH. **1992**. A simple and efficient protocol for isolation of high molecular weight DNA from filamentous fungi, fruit bodies, and infected plant tissues. *Nucleic Acids Research* 20, 6115–6116.

- Murali T, Suryanarayanan T, Geeta R. **2006**. Endophytic *Phomopsis* species: host range and implications for diversity estimates. *Canadian Journal of Microbiology* 52, 673–680.
- Nabetani K, Wood B, Sabaratnam S. **2017**. Role of pycnidia in twig and blossom blight and stem dieback of highbush blueberry caused by *Phomopsis vaccinii* in British Columbia. *Canadian Journal of Plant Pathology* 39, 405–421.
- Narouei-Khandan HA, Harmon CL, Harmon P, Olmstead J, Zelenev VV, van der Werf W, van Bruggen AHC. **2017**. Potential global and regional geographic distribution of *Phomopsis vaccinii* on *Vaccinium* species projected by two species distribution models. *European Journal of Plant Pathology* 148, 919–930.
- O'Donnell K, Cigelnik E. **1997**. Two divergent intragenomic rDNA ITS2 types within a monophyletic lineage of the fungus *Fusarium* are nonorthologous. *Molecular Phylogenetics and Evolution* 7, 103–116.
- Page RDM. **1996**. TreeView: An application to display phylogenetic trees on personal computers. *Computer Applications in Biosciences* 12, 357–358.
- Portal do Instituto Nacional de Estatística (INE). **2019**. Estatísticas agrícolas 2018. Available online <https://www.ine.pt/xurl/pub/358629204> (accessed on 9 October 2019).
- Rodriguez F, Oliver JF, Marin A, Medina JR. **1990**. The general stochastic model of nucleotide substitutions. *Journal of Theoretical Biology* 142, 485–501.
- Ronquist F, Huelsenbeck JP. **2003**. MrBayes 3: Bayesian phylogenetic inference under mixed models. *Bioinformatics* 19, 1572–1574.
- Rosso L, Lobry JR, Bajard S, Flandrois JP. **1995**. Convenient model to describe combined effects of temperature and pH on microbial growth. *Applied and Environmental Microbiology* 61, 610–616.
- Santos JM, Correia VG, Phillips AJL. **2010**. Primers for mating-type diagnosis in *Diaporthe* and *Phomopsis*: their use in teleomorph induction in vitro and biological species definition. *Fungal Biology* 114, 255–270.
- Santos L, Alves A, Alves R, **2017b**. Evaluating multi-locus phylogenies for species boundaries determination in the genus *Diaporthe*. *Peer J* 5, e3120.

- Santos JM, Phillips AJL, **2009**. Resolving the complex of *Diaporthe* (*Phomopsis*) species occurring on *Foeniculum vulgare* in Portugal. *Fungal Diversity* 34, 111–125.
- Santos L, Phillips AJL, Crous PW, Alves A. **2017a**. *Diaporthe* species on Rosaceae with descriptions of *D. pyracanthae* sp. *Mycosphere* 8, 485–511.
- Savitha J, Bhargavi SD, Praveen VK. **2016**. Complete genome sequence of the endophytic fungus *Diaporthe* (*Phomopsis*) *ampelina*. *Genome Announcements* 4, e00477-16.
- Swofford DL. **2002**. PAUP*. Phylogenetic Analysis Using Parsimony (*and Other Methods). Version 4.0. Sinauer Associates: Sunderland, Massachusetts.
- Sessa L, Abreo E, Lupo S. **2018**. Diversity of fungal latent pathogens and true endophytes associated with fruit trees in Uruguay. *Journal of Phytopathology* 166, 633–647.
- Udayanga D, Liu X, McKenzie EHC, Chukeatirote E, Bahkali AHA, Hyde KD. **2011**. The genus *Phomopsis*: Biology, applications, species concepts and names of common phytopathogens. *Fungal Diversity* 50, 189–225.
- Udayanga D, Castlebury LA, Rossman AY, Hyde KD. **2014a**. Species limits in *Diaporthe*: Molecular re-assessment of *D. citri*, *D. cytospora*, *D. foeniculina* and *D. rudis*. *Persoonia* 32, 83–101.
- Udayanga D, Castlebury LA, Rossman AY, Chukeatirote E, Hyde KD. **2014b**. Insights into the genus *Diaporthe*: phylogenetic species delimitation in the *D. eres* species complex. *Fungal Diversity* 67, 203–229.
- van Bruggen AHC, West JS, van der Werf W, Potting RPJ, Gardi C, Koufakis I, Zelenev VV, Narouei-Khandan H, Shilder A, Harmon P. **2018**. Input data needed for a risk model for the entry, establishment and spread of a pathogen (*Phomopsis vaccinii*) of blueberries and cranberries in the EU. *Annals of Applied Biology* 172, 126–147.
- van Niekerk JM, Groenewald JZ, Farr DF, Fourie PH, Haleen F, Crous PW. **2005**. Reassessment of *Phomopsis* on grapevine. *Australasian Plant Pathology* 34, 27–39.

- Vaydia G, Lohman DJ, Meier R. **2011**. SequenceMatrix: Concatenation software for the last assembly of multi-gene datasets with character set and codon information. *Cladistics* 27, 171–180.
- Vilka L, Volkova J. **2015**. Morphological diversity of *Phomopsis vaccinii* isolates from cranberry (*Vaccinium macrocarpon* Ait.) in Latvia. *Proceedings of the Latvia University of Agriculture* 33, 8–18.
- White TJ, Bruns T, Lee S, Taylor JW. **1990**. Amplification and direct sequencing of fungal ribosomal RNA genes for phylogenetics. In: Innis MA, Gelfand DH, Sninsky JJ, White TJ, eds. *PCR protocols: A guide to the methods and applications*. New York: Academic Press. p. 315–322.
- Yu C, Wu C, Li G, Wang C. **2018**. First report of *Diaporthe nobilis* causing postharvest rot of blueberry in Shandong Province, China. *Plant Disease* 102, 1856.

SUPPLEMENTARY MATERIAL

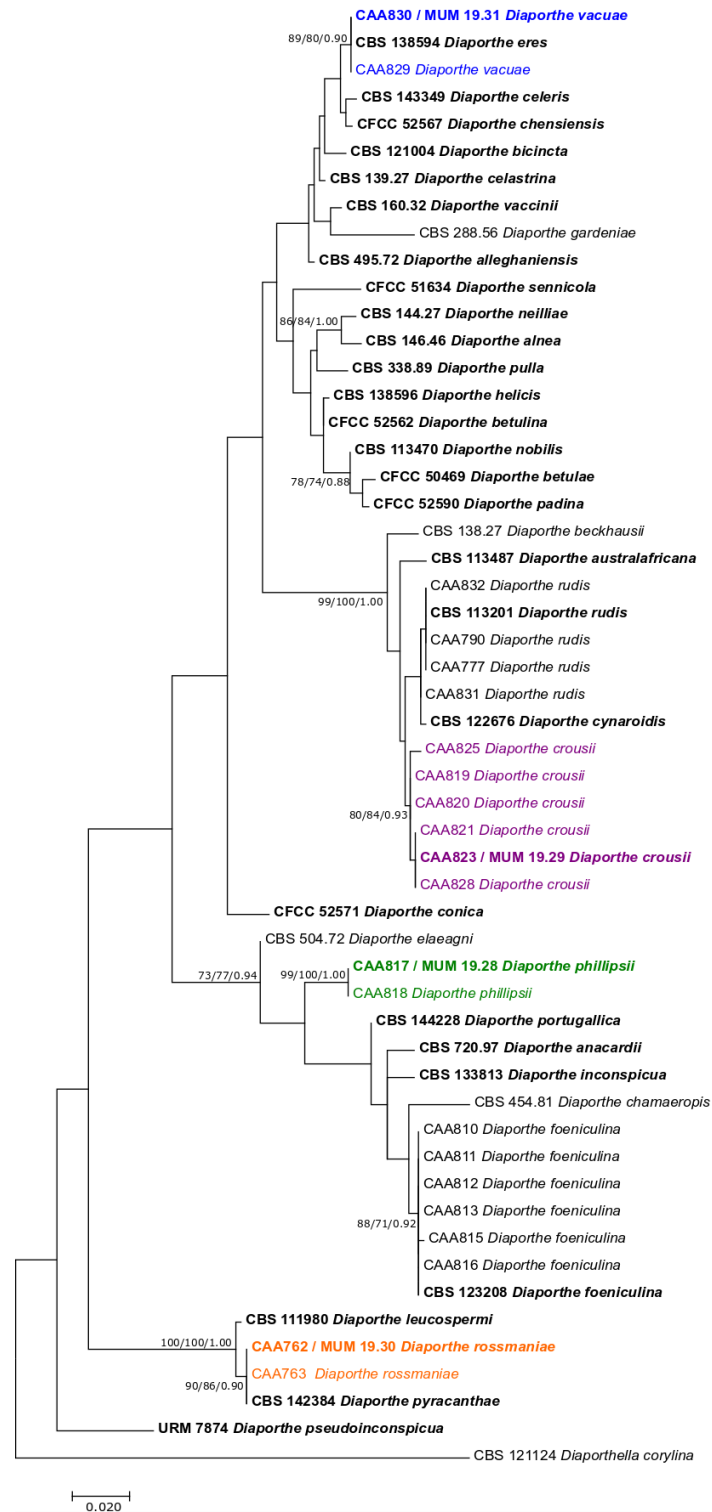


Figure S1. Maximum Likelihood phylogenetic tree obtained from ITS sequences data from *Diaporthe* species. The ML tree was built using the Kimura parameter model. *Diaporthella corylina* (CBS 121124) was used as outgroup. ML bootstrap ($\geq 70\%$), MP bootstrap ($\geq 70\%$) and posterior probabilities (≥ 0.70) are shown at the nodes (ML/MP/PP). Ex-type isolates are given in bold.

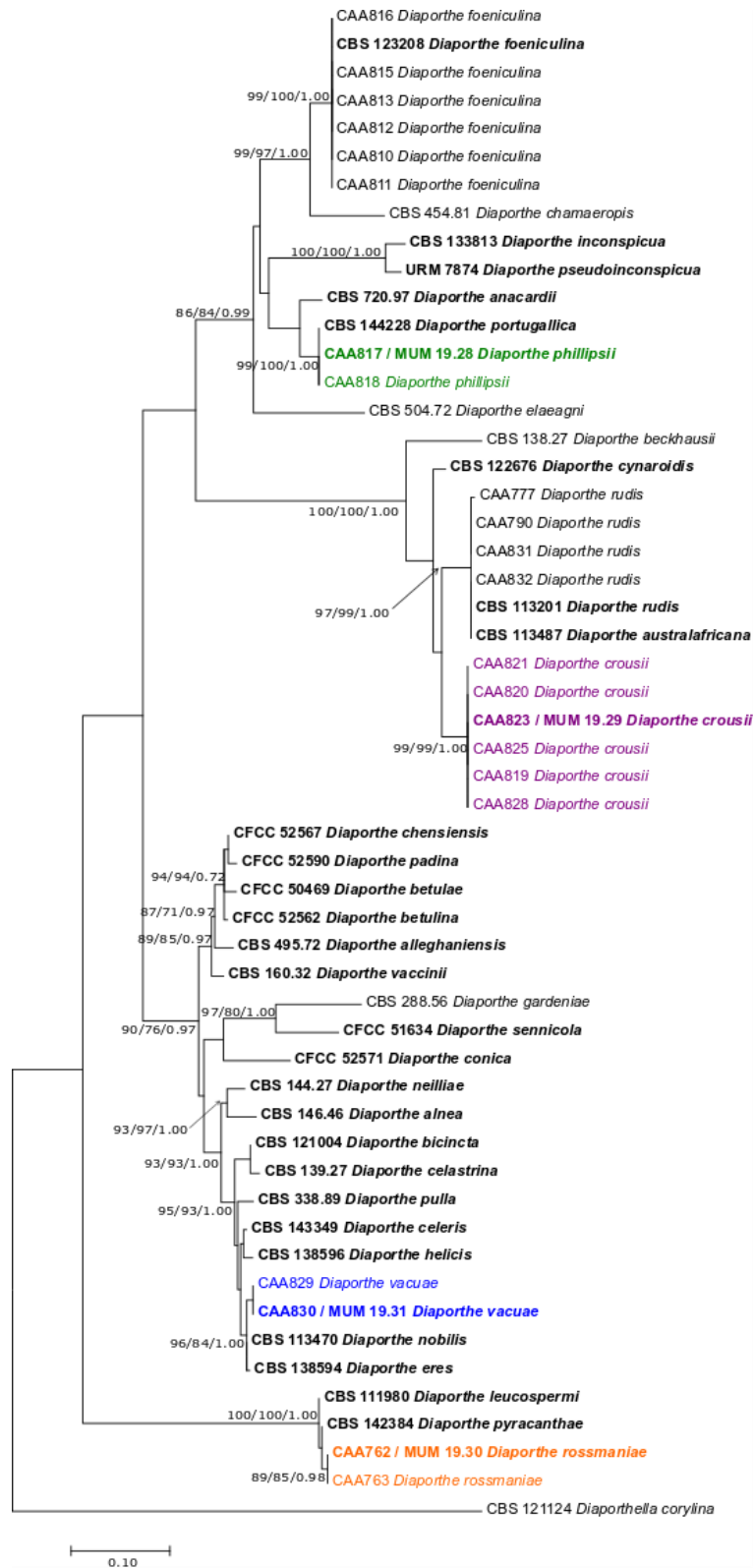


Figure S2. Maximum Likelihood phylogenetic tree obtained from *tef1-α* sequences data from *Diaporthe* species. The ML tree was built using the Kimura parameter model. *Diaporthella corylina* (CBS 121124) was used as outgroup. ML bootstrap ($\geq 70\%$), MP bootstrap ($\geq 70\%$) and posterior probabilities (≥ 0.70) are shown at the nodes (ML/MP/PP). Ex-type isolates are given in bold.

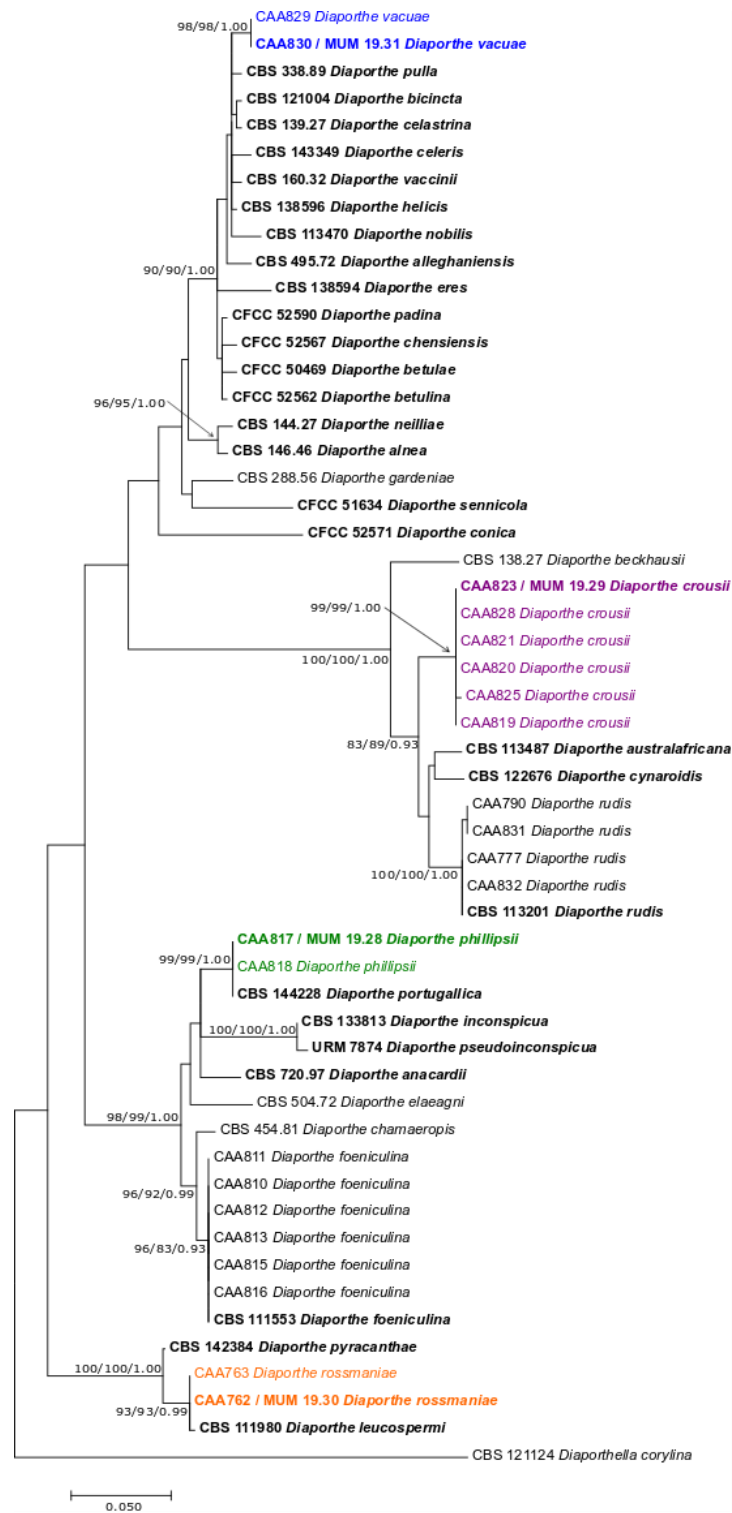


Figure S3. Maximum Likelihood phylogenetic tree obtained from *tub2* sequences data from *Diaporthe* species. The ML tree was built using the Kimura parameter model. *Diaporthella corylina* (CBS 121124) was used as outgroup. ML bootstrap ($\geq 70\%$), MP bootstrap ($\geq 70\%$) and posterior probabilities (≥ 0.70) are shown at the nodes (ML/MP/PP). Ex-type isolates are given in bold.

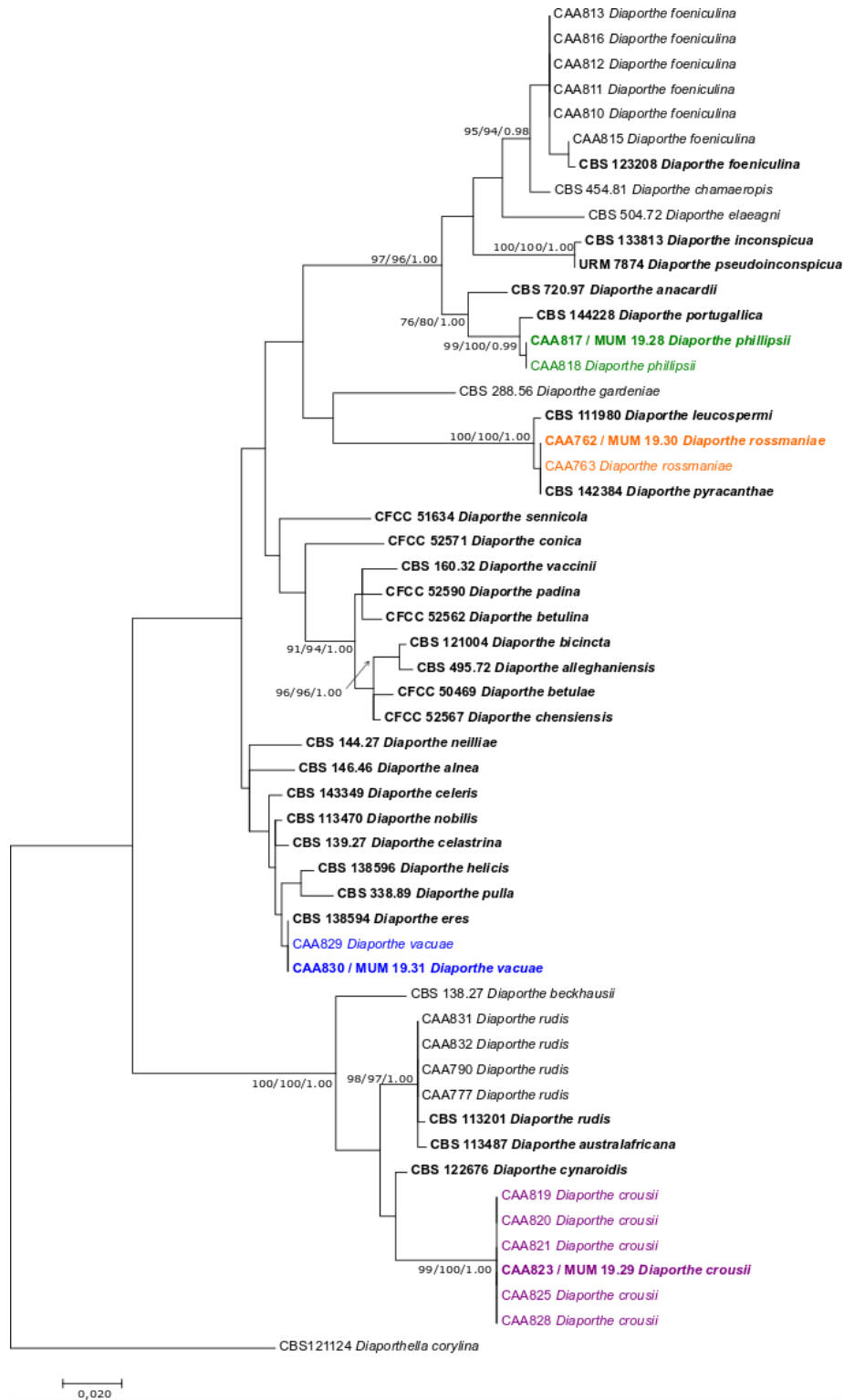


Figure S4. Maximum Likelihood phylogenetic tree obtained from *his3* sequences data from *Diaporthe* species. The ML tree was built using the Kimura parameter model. *Diaporthella corylina* (CBS 121124) was used as outgroup. ML bootstrap ($\geq 70\%$), MP bootstrap ($\geq 70\%$) and posterior probabilities (≥ 0.70) are shown at the nodes (ML/MP/PP). Ex-type isolates are given in bold.

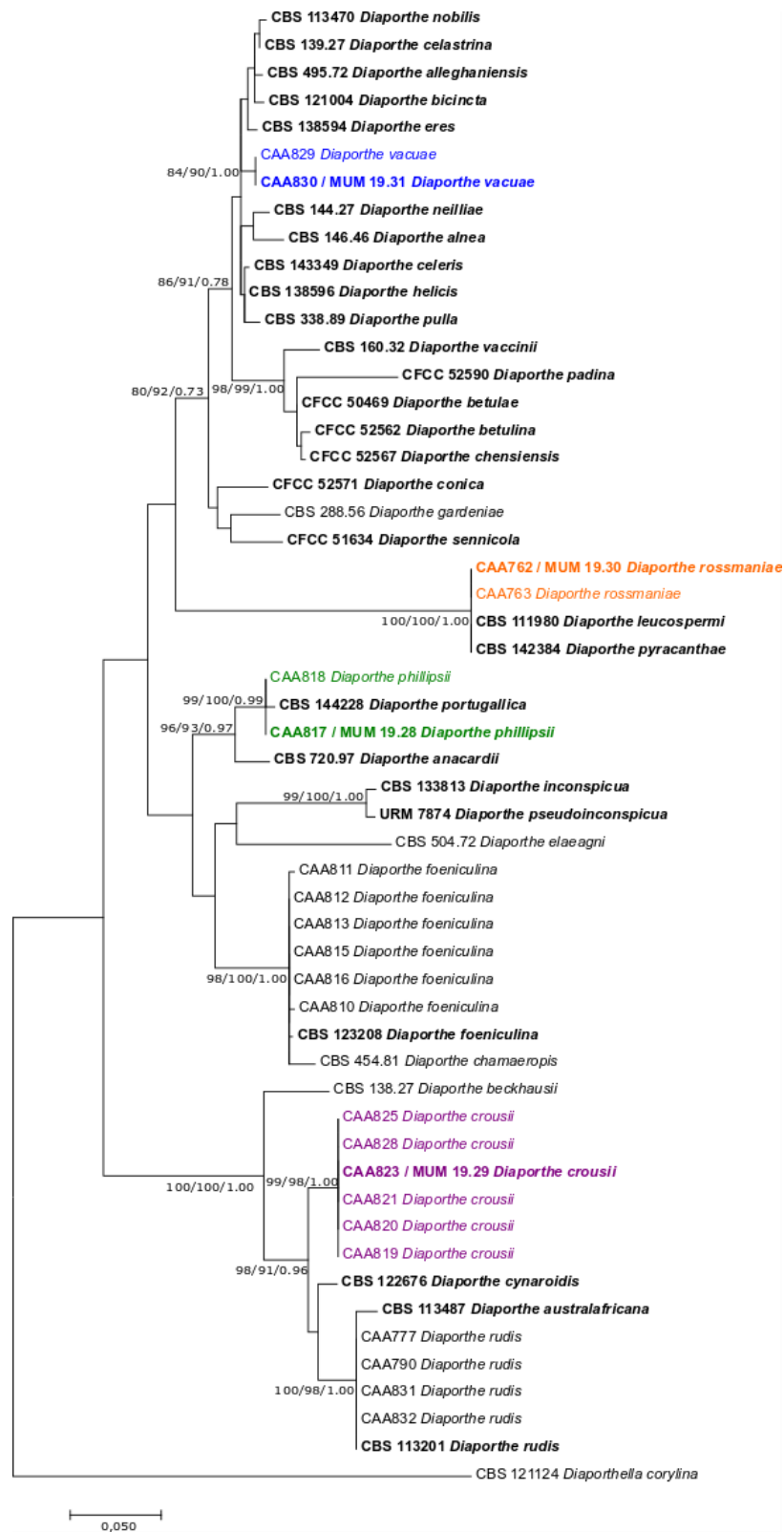


Figure S5. Maximum Likelihood phylogenetic tree obtained from *cal* sequences data from *Diaporthe* species. The ML tree was built using the Kimura parameter model. *Diaporthella corylina* (CBS 121124) was used as outgroup. ML bootstrap ($\geq 70\%$), MP bootstrap ($\geq 70\%$) and posterior probabilities (≥ 0.70) are shown at the nodes (ML/MP/PP). Ex-type isolates are given in bold.

SUBCHAPTER 2.2

Diversity and pathogenicity of *Diaporthe* species revealed from a survey of blueberry orchards in Portugal

Hilário S, Santos L, Alves A.

Agriculture 2021 11, 1271

ABSTRACT

Blueberries (*Vaccinium corymbosum*) are widely cultivated worldwide and largely consumed due to their known antioxidant and medicinal properties. Although *Diaporthe* species have been documented in Portugal as causal agents of blueberry twig blight and dieback, there is still scarce information on the species that cause these symptoms. Moreover, *Diaporthe vaccinii*, recently synonymized with *D. eres*, has been considered a concern to blueberry production worldwide. However, the current knowledge about its impact on blueberries remains unclear. The diversity of *Diaporthe* species associated with diseased blueberry plants were assessed through a national survey. A multilocus sequence analysis of the rRNA internal transcribed spacer (ITS) region, the translation elongation factor 1-alpha (*tef1-a*), tubulin (*tub2*), calmodulin (*cal*) and histone 3 (*his3*) genes unveiled the presence of *Diaporthe ambigua*, *D. amygdali*, *D. crousii*, *D. foeniculina*, *D. hybrida*, *D. leucospermi*, *D. malorum* and *D. rudis*. Moreover, all species were fully characterized based on a detailed morphological description. *Diaporthe amygdali*, *D. hybrida*, *D. leucospermi* and *D. malorum* are reported for the first time on diseased blueberries in Portugal. Results show that *D. eres* exhibited a high level of intraspecific variability within isolates, given that the strain CBS 160.32 might be a minor pathogen on blueberry plants, whereas CAA829 was revealed to be the most aggressive. Overall, this study also demonstrates that *Diaporthe amygdali* and *D. eres* may be two of the most aggressive species to blueberry plants. This study improves our understanding of the *Diaporthe* species and its causing of dieback and twig blight on Portuguese blueberry orchards. Additionally, the identification of these pathogens represents crucial information for blueberry producers to apply appropriate phytosanitary measures, as well as offering new insights into the potential pathogenicity of *D. eres* on this host.

keywords: *Diaporthaceae*; dieback; pathogens; phylogeny; twig blight; *Vaccinium corymbosum*

INTRODUCTION

The genus *Vaccinium* includes nearly 450 species of woody and perennial shrubs belonging to the family *Ericaceae*, adapted to several climates (Retamales & Hancock 2012). The northern highbush blueberry (*Vaccinium corymbosum*) is a small-fruit crop, native to North America and commercially cultivated in Europe (Lombard et al. 2014). Due to the recognized high nutritional and medicinal value of fruits (Gonçalves et al. 2015; Silva et al. 2020), blueberry production has been rapidly increasing world-wide.

In the last 10 years the production of this crop in Portugal has increased substantially. Although production initiated intensively only in 2011 with a yield of 700 tons and a cultivated area of 75 ha, in 2020 the country was ranked as the 7th largest producer worldwide (FAOSTAT 2021) with a production of 15 418 tons, and a total area of 2490 ha (INE 2021), making it a highly profitable crop to the economy of the country. However, due to the spread of blueberry plants across continents, and the increasing population demand for consumption, blueberry production has been affected by several fungal pathogens (Cardinaals et al. 2018). Some of these pathogens, such as members of *Botryosphaeriaceae*, *Pestalotiopsis sensu lato* and *Diaporthe* can cause twig blight, stem cankers and dieback on blueberry plants (Hilário et al. 2020; Rodríguez-Gálvez et al. 2020; Scarlett et al. 2018).

The genus *Diaporthe* encompasses endophytes, saprobes and plant pathogens associated with a wide variety of agricultural crops, ornamental plants, and forest trees (Gomes et al. 2013; Mathew et al. 2018; Udayanga et al. 2011; Yang et al. 2018). Members of this genus were previously found to colonize blueberry tissues as latent pathogens or endophytes (Hilário et al. 2020) and as pathogens causing numerous diseases on this crop such as apical necrosis of twigs and stems, cankers, necrosis of the vascular tissues, wilting of leaves, and leaf spots (Cardinaals et al. 2018; Elfar et al. 2013; van Bruggen et al. 2018). These symptoms have been associated with an assemblage of species comprising *D. ambigua*, *D. amygdali*, *D. australafricana*, *D. baccae*, *D. crousii*, *D. eres*, *D.*

foeniculina, *D. oxe*, *D. passiflorae*, *D. phillipsii*, *D. rossmaniae*, *D. rudis*, and *D. vaccinii* (syn. *D. eres*) (Elfar et al. 2013; Farr et al. 2002; Hilário et al. 2020; Lombard et al. 2014).

Diaporthe vaccinii, formerly known as *Phomopsis vaccinii*, is native to North America (Weingartner & Klos 1975) and it is recognized as a host-specific species on *Vaccinium* spp., causing severe losses to blueberry production worldwide (Lombard et al. 2014). Concerns about the damaging impacts of this pathogen on blueberry production led the European Food Safety Authority (EFSA) to recommend *D. vaccinii* as a quarantine pathogen for the European Union (Regulation (EU) 2016/2031 of 26 October 2016). Although *D. vaccinii* has been reported on blueberry plants in South America (Elfar et al. 2013), North America (Farr et al. 2022; Nabetani et al. 2017), Europe (Cardinaals et al. 2018; Lombard et al. 2014; Vilka & Volkova 2015) and Asia (van Bruggen et al. 2018), the current knowledge about its pathogenicity on blueberries was barely explored. However, the most recent EU Regulation of 29 November 2019 (2019/2072), has no longer included *D. vaccinii* into the list of EU quarantine pests. Moreover, to clarify the species boundaries of the *Diaporthe eres* complex, Hilário et al. (2021a) implemented the Genealogical Phylogenetic Species Recognition principle (GCPSR) and the coalescent-based model Poisson Tree Processes (PTPs) and considered *D. vaccinii* to be a synonym of *D. eres*. Nevertheless, despite the alleged presence of *D. vaccinii* in the North of Portugal based on the symptoms observed in the field (Madeira 2016), this species was not found in a recent survey carried out in one of the major blueberry productions in the country (Hilário et al. 2020). Given that species identification is essential to develop appropriate control measures, the focus of this study was the implementation of a large survey on *V. corymbosum* plantations across the country, aiming to understand the diversity and distribution of *Diaporthe* species associated with blueberry plants showing dieback and twig blight symptoms, as well as their pathogenic potential to different blueberry cultivars widely planted in the country.

MATERIAL AND METHODS

Sampling and fungal isolates.

Surveys were carried out between April and August of 2019 in 12 Portuguese blueberry orchards (Table 1): Braga, Porto, Aveiro, Viseu, Castelo Branco and Santarém. Plants from cultivars 'Duke', 'Ozarkblue', 'Aurora', 'Legacy', 'O'Neal', 'Liberty', 'Gupton', 'Bluecrop', 'Early Blue' and 'New Hanover' corresponding to a total area of 31 ha were evaluated. Nearly 0.5% of plants from each plantation were inspected for dis-ease symptoms such as twig blight, dieback, stem cankers, wilting and necrotic leaves in the apex of the plant. From the 531 plants inspected, only 95 showing these symptoms were collected. The samples were transported to the Fungal and Plant Biology Lab at University of Aveiro in paper bags, within 4–6 h. After arrival, one 10–30 cm long twig or stem per plant was taken for fungal isolation.

Fungal isolations and monosporic cultures were established following the procedures described in subchapter 2.1. Moreover, several other fungal isolates obtained from *V. corymbosum* plants sampled in a previous work (Table 2) (Hilário et al. 2020) and the ex-type strain of *Diaporthe vaccinii* (CBS 160.32) were also selected to perform the pathogenicity tests. This latter strain was obtained from the Westerdijk Fungal Biodiversity Institute in the Netherlands.

Table 1. List of plantations included in this study.

Region	Plantation	GPS coordinates		Area (ha)	Total of plants	Inspected plants	Sampled plants
		Latitude	Longitude				
Aveiro	Águeda	40°33'06.2"N	8°28'44.0"W	2.5	7 000	35	10
	Arouca	40°54'35.3"N	8°22'49.7"W	1.7	4 400	22	9
Braga	Urgezes	41°25'24.5"N	8°17'35.1"W	2	4 000	20	9
	Póvoa de Lanhoso	41°31'35.0"N	8°15'08.3"W	1.5	4 600	23	9
Castelo Branco	Idanha-a-Nova	39°52'58.4"N	7°17'23.2"W	2.5	10 416	52	4
Porto	Penafiel	41°08'07.0"N	8°22'42.5"W	0.6	500	3	3
	Agrela	41°08'07.0"N	8°28'09.7"W	1.8	6 200	31	8
	Arcozelo	41°15'31.8"N	8°28'57.8"W	2.3	8 000	40	8
	Monte Córdova	41°15'22.9"N	8°26'29.5"W	1	3 084	15	9
Santarém	Alpiarça	39°15'04.1"N	8°32'39.1"W	6	20 000	100	8
	Ourém	39°39'13.5"N	8°35'32.0"W	1.7	8 000	40	9
Viseu	Mangualde	40°37'43.2"N	7°51'51.8"W	7.4	31 091	150	9

Morphological characterization.

The procedures to induce sporulation and to record the micromorphological characters of our isolates, were as described in subchapter 2.1, with slight modifications. Briefly, at least 50 conidia or ascospores were selected randomly and measured on images taken with the ×100 objective lens. Dimensions of other fungal structures (e.g., conidiophores, asci) are given as the range of at least 20 measurements. Data for spores, conidiophores and asci measurements are presented as the lower and upper 95% confidence limits, with the minimum and maximum dimensions in parentheses, and followed by mean and standard deviation (S.D.). Colony colors were examined according to Syme (2021) after 7 days of growth on PDA in the dark at 25°C.

DNA Extraction, PCR Amplification, and sequencing.

Genomic DNA extraction, microsatellite-primed PCR (MSP-PCR) fingerprinting and amplification of ITS and the protein coding regions *tef1-a*, *tub2*, *his3* and *cal*, were as described in subchapter 2.1.

Phylogenetic analysis.

The nucleotide sequences were analyzed, and the phylogenetic trees were constructed based on Maximum Parsimony (MP), Maximum Likelihood (ML) and Bayesian Inference (BI) analyses, as described in subchapter 2.1. For the MP analyses, the following parameters were also calculated: consistency index (CI), retention index (RI), tree length (TL), rescaled consistency index (RC) and homoplasy index (HI).

A preliminary identification of the clades containing our isolates was assessed through an initial ITS single tree containing all species currently accepted in the genus *Diaporthe*. Additionally, we also evaluated the possibility of combining all five loci (ITS, *tef1-α*, *tub2*, *his3*, and *cal*). A comparison of highly supported clades among single locus trees (including solely the phylogenetically closely related species previously selected) was performed to look for phylogenetic concordance among the individual gene trees (Fig. S1-S5).

All the trees were edited in Inkscape Vector software v.0.92 (<https://www.inkscape.org>). (Adobe Systems Inc, San Jose, CA, USA). Sequences generated in this study were deposited in GenBank (Table 2) (www.ncbi.nlm.nih.gov) and phylogenetic trees and alignments were deposited in TreeBASE (www.TreeBASE.org; S28393).

Mating-type assay.

The mating strategy of the new species was determined by a PCR-based method. Primers MAT1-1-1FW and MAT1-1-1-RV were used to amplify part of the *MAT1-1-1* gene, and the primers set MAT2 188F and MAT1-2-1RV was used to amplify part of the *MAT1-2-1* gene, as following the descriptions in subchapter 2.1.

Prevalence of Diaporthe species.

The prevalence of *Diaporthe* species in the *V. corymbosum* plants sampled, was calculated as previously described by Fu et al. (2019). The Isolation Rate (RI) was calculated for each species using the following equation: $RI (\%) = NS/NI \times 100$, where NS was the number of isolates from the same species, and NI was the total number of isolates collected during the survey.

Plant material and pathogenicity tests.

A minimum of three isolates from each species identified and from different locations, whenever possible, were selected to inoculate blueberry plants. Moreover, several other fungal isolates obtained from *V. corymbosum* plants sampled in a previous work (Table 3) (Hilário et al. 2020) and the ex-type strain of *Diaporthe vaccinii* (CBS 160.32) were also selected to perform the pathogenicity tests. This latter strain was obtained from the Westerdijk Fungal Biodiversity Institute in the Netherlands. The pathogenicity trials were performed from 9 June 2020 until 14 July 2020. Three cultivars of blueberry plants currently used in Portuguese plantations were selected: ‘Duke’ – the most cultivated in the northern; ‘Legacy’ – the best suited to the climate in the southern (Pinto 2015); and ‘Spartan’ – alleged to be highly susceptible to infection by *D. vaccinii* (Baker et al. 1995). Nine-month-old potted plants were obtained through micropropagation method, thus assuring

genetic homogeneity. All plants were supplied by Deifil Green Biotechnology LDA (Portugal). After arrival, plants were subjected to a 15-day acclimation period. Both acclimation period and the pathogenicity trials occurred in greenhouse conditions, with daily temperature ranging from 25°C day to 15°C night, controlled photoperiod 16/8 h (day/night) and watered regularly.

For inoculation, a 5-mm-diameter mycelial plug was taken from the active margin of 7-day-old cultures on PDA and placed in the wounded area with the mycelial surface in contact with the cambium. Plugs of sterile PDA were used to inoculate stems of control plants. External symptoms such as stem necrosis, wilting and dieback were assessed weekly and registered. Thirty-five days after inoculation, the bark was removed to measure the length of the internal lesions. Fungi were re-isolated on PDA to verify Koch's postulates. Pieces of wood from the edges of lesions were immersed in 70% ethanol for 3 min and rinsed twice in sterile distilled water. These wood tissues were plated on PDA, incubated at room temperature, and checked daily for fungal growth.

The analyses were performed considering individual isolates and species. One-way analysis of variance (ANOVA) assumptions were verified using a Shapiro–Wilk test. The homogeneity of variances was also checked using the Bartlett's test. As the datasets did not meet ANOVA assumptions, the analysis was performed using the Kruskal–Wallis test. Lesion length means of the different isolates were compared with one another using the Dunn Test with $p < 0.05$. The different species were compared with one another, using the Wilcoxon rank sum test (with $p < 0.05$). Statistical analyses as well as box plots were generated and conducted in R Statistical Software v. 4.0.1 (R Core Team 2021), along with the `GGPLOT2` package (Wickham 2016).

Table 2. List of *Diaporthe* species used in this study.

Species	Strain ¹	Host	Locality	GenBank Accession				
				ITS	<i>tef1-α</i>	<i>tub2</i>	<i>his3</i>	<i>cal</i>
<i>D. acaciigena</i>	CBS 129521	<i>Acacia retinodes</i>	Australia	KC343005	KC343731	KC343973	KC343489	KC343247
	CBS 114015	<i>Pyrus communis</i>	South Africa	KC343010	KC343736	KC343978	KC343494	KC343252
<i>D. ambigua</i>	CBS 123210	<i>Foeniculum vulgare</i>	Portugal	KC343012	KC343738	KC343980	KC343496	KC343254
	CBS 127746	<i>Platanus acerifolia</i>	Italy	KC343014	KC343740	KC343982	KC343498	KC343256
	CAA957	<i>Vaccinium corymbosum</i>	Portugal	MT073278	MT051928	MT051959	MT051887	MT051851
<i>D. amygdali</i>	CBS 115620	<i>Prunus persica</i>	USA	KC343020	KC343746	KC343988	KC343504	KC343262
	CBS 126679	<i>Prunus dulcis</i>	Portugal	KC343022	KC343748	KC343990	KC343506	KC343264
	CBS 111811	<i>Vitis vinifera</i>	South Africa	KC343019	KC343745	KC343987	KC343503	KC343261
	CAA958	<i>Vaccinium corymbosum</i>	Portugal	MT073273	MT051923	MT051955	MT051883	MT051847
	CAA959	<i>Vaccinium corymbosum</i>	Portugal	MT073283	MT051935	MT051970	MT051898	MT051862
	CFCC 52586	<i>Kadsura longipedunculata</i>	China	MH121521	MH121563	MH121600	MH121479	MH121439
	CBS 136969	<i>Vaccinium corymbosum</i>	Italy	KJ160579	KJ160611	KJ160528	MF418350	KJ160548
	CBS 146754	<i>Prunus dulcis</i>	Spain	MT007489	MT006989	MT006686	MT007095	MT006761
<i>D. anacardii</i>	CBS 720.97	<i>Anacardium occidentale</i>	East Africa	KC343024	KC343750	KC343992	KC343508	KC343266
<i>D. angelicae</i>	CBS 111592	<i>Heracleum sphondylium</i>	Austria	KC343027	KC343753	KC343995	KC343511	KC343269
<i>D. australafricana</i>	CBS 113486	<i>Vitis vinifera</i>	South Africa	KC343038	KC343764	KC344006	KC343522	KC343280
	CBS 113487	<i>Vitis vinifera</i>	South Africa	KC343039	KC343765	KC344007	KC343523	KC343281
<i>D. baccae</i>	CBS 136972	<i>Vaccinium corymbosum</i>	Italy	KJ160565	KJ160597	MF418509	MF418264	MG281695
	CBS 142546	<i>Citrus sinensis</i>	Italy	MF418358	MF418437	MF418517	MF418272	MF418192
	CBS 142545	<i>Citrus sinensis</i>	Italy	MF418351	MF418430	MF418510	MF418265	MF418185
<i>D. beckhausii</i>	CBS 138.27	<i>Viburnum</i> sp.	-	KC343041	KC343767	KC344009	KC343525	KC343283
<i>D. chamaeropsis</i>	CBS 454.81	<i>Chamaerops humilis</i>	Greece	KC343048	KC343774	KC344016	KC343532	KC343290
<i>D. cinerascens</i>	CBS 719.96	<i>Ficus carica</i>	Bulgaria	KC343050	KC343776	KC344018	KC343534	KC343292
	CAA821	<i>Vaccinium corymbosum</i>	Portugal	MK792301	MK828073	MK837924	MK871442	MK883829
<i>D. crousii</i>	MUM 19.29	<i>Vaccinium corymbosum</i>	Portugal	MK792311	MK828081	MK837932	MK871450	MK883835
	CAA828	<i>Vaccinium corymbosum</i>	Portugal	MK792317	MK828084	MK837935	MK871453	MK883837

	CAA960	<i>Vaccinium corymbosum</i>	Portugal	MT073274	MT051924	MT051956	MT051884	MT051848
	CAA961	<i>Vaccinium corymbosum</i>	Portugal	MT073275	MT051925	MT051957	MT051885	MT051849
	CAA962	<i>Vaccinium corymbosum</i>	Portugal	MT073301	MT051926	MT051962	MT051890	MT051854
<i>D. cynaroidis</i>	CBS 122676	<i>Protea cynaroides</i>	South Africa	KC343058	KC343784	KC344026	KC343542	KC343300
<i>D. elaeagni</i>	CBS 504.72	<i>Elaeagnus</i> sp.	Netherlands	KC343064	KC343790	KC344032	KC343548	KC343306
	CBS 123208	<i>Foeniculum vulgare</i>	Portugal	KC343104	KC343830	KC344072	KC343588	KC343346
	CBS 111553	<i>Foeniculum vulgare</i>	Spain	KC343101	KC343827	KC344069	KC343585	KC343343
	CPC 28033	<i>Citrus sinensis</i>	Portugal	MF418402	MF418481	MF418562	MF418322	MF418236
<i>D. foeniculina</i>	CBS 187.27	<i>Camelia sinensis</i>	Italy	KC343107	KC343833	KC344075	KC343591	KC343349
	CAA963	<i>Vaccinium corymbosum</i>	Portugal	MT073311	MT051932	MT051965	MT051893	MT051857
	CAA967	<i>Vaccinium corymbosum</i>	Portugal	MT073307	MT051937	MT051973	MT051901	MT051865
	PSCG 030	<i>Pyrus pyrifolia</i>	China	MK626914	MK654864	MK691323	MK726255	MK691211
<i>D. fusicola</i>	PSCG 118	<i>Pyrus pyrifolia</i>	China	MK626910	MK654860	MK691317	MK726250	MK691204
	CBS 120840	<i>Prunus salicina</i>	South Africa	KC343021	KC343747	KC343989	KC343505	KC343263
<i>D. infecunda</i>	CBS 133812	<i>Schinus terebinthifolius</i>	Brazil	KC343126	KC343852	KC344094	KC343610	KC343368
	CAA998	<i>Vaccinium corymbosum</i>	Portugal	MT073276	MT051927	MT051958	MT051886	MT051850
<i>D. hybrida</i>	CAA999 / MUM 21.01	<i>Vaccinium corymbosum</i>	Portugal	MT073280	MT051929	MT051960	MT051888	MT051852
<i>D. leucospermi</i>	CBS 111980	<i>Leucospermum</i> sp.	Australia	JN712460	KY435632	KY435673	KY435653	KY435663
	CAA971	<i>Vaccinium corymbosum</i>	Portugal	MT073313	MT051933	MT051968	MT051896	MT051860
<i>D. longispora</i>	CBS 194.36	<i>Ribes</i> sp.	Canada	KC343135	KC343861	KC344103	KC343619	KC343377
	CBS 142383	<i>Malus domestica</i>	Portugal	KY435638	KY435627	KY435668	KY435648	KY435658
	CAA740	<i>Malus domestica</i>	Portugal	KY435642	KY435629	KY435670	KY435650	KY435660
	CAA752	<i>Malus domestica</i>	Portugal	KY435643	KY435630	KY435671	KY435651	KY435661
	CAA972	<i>Vaccinium corymbosum</i>	Portugal	MT073271	MT051917	MT051953	MT051881	MT051845
<i>D. malorum</i>	CAA973	<i>Vaccinium corymbosum</i>	Portugal	MT073272	MT051918	MT051954	MT051882	MT051846
	CAA974	<i>Vaccinium corymbosum</i>	Portugal	MT073306	MT051919	MT051963	MT051891	MT051855
	CAA975	<i>Vaccinium corymbosum</i>	Portugal	MT073304	MT051920	MT051966	MT051894	MT051858
	CAA976	<i>Vaccinium corymbosum</i>	Portugal	MT073305	MT051921	MT051967	MT051895	MT051859
	CAA977	<i>Vaccinium corymbosum</i>	Portugal	MT073303	MT051922	MT051971	MT051899	MT051863
<i>D. parvae</i>	PSCG 035	<i>Pyrus x bretschneideri</i>	China	MK626920	MK654859	MK691249	MK726211	MK691169

<i>D. passiflorae</i>	CBS 132527	<i>Passiflora edulis</i>	South America	JX069860	KY435633	KY435674	KY435654	KY435664
<i>D. phillipsii</i>	MUM 19.28	<i>Vaccinium corymbosum</i>	Portugal	MK792305	MK828076	MN000351	MK871445	MK883831
	CAA818	<i>Vaccinium corymbosum</i>	Portugal	MK792307	MK828078	MN000352	MK871447	MK883833
<i>D. portugallica</i>	CBS 144228	<i>Camelia sinensis</i>	Portugal	MH063905	MH063911	MH063917	MH063899	MH063893
	CPC 34248	<i>Camelia sinensis</i>	Portugal	MH063906	MH063912	MH063918	MH063900	MH063894
<i>D. pyracanthae</i>	CAA487	<i>Pyracantha coccinea</i>	Portugal	KY435636	KY435626	KY435667	KY435647	KY435657
	CBS142384	<i>Pyracantha coccinea</i>	Portugal	KY435635	KY435625	KY435666	KY435646	KY435656
<i>D. rossmaniae</i>	CAA763	<i>Vaccinium corymbosum</i>	Portugal	MK792291	MK828064	MK837915	MK871433	MK883823
	MUM 19.30	<i>Vaccinium corymbosum</i>	Portugal	MK792290	MK828063	MK837914	MK871432	MK883822
<i>D. rudis</i>	CBS 114436	<i>Laburnum anagyroides</i>	Austria	KC343232	KC343958	KC344200	KC343716	KC343474
	CBS 113201	<i>Vitis vinifera</i>	Portugal	KC343234	KC343960	KC344202	KC343718	KC343476
	CAA979	<i>Vaccinium corymbosum</i>	Portugal	<i>MT073290</i>	<i>MT051930</i>	<i>MT051961</i>	<i>MT051889</i>	<i>MT051853</i>
	CAA984	<i>Vaccinium corymbosum</i>	Portugal	<i>MT073282</i>	<i>MT051931</i>	<i>MT051964</i>	<i>MT051892</i>	<i>MT051856</i>
	CAA987	<i>Vaccinium corymbosum</i>	Portugal	<i>MT073314</i>	<i>MT051934</i>	<i>MT051969</i>	<i>MT051897</i>	<i>MT051861</i>
	CAA991	<i>Vaccinium corymbosum</i>	Portugal	<i>MT073291</i>	<i>MT051936</i>	<i>MT051972</i>	<i>MT051900</i>	<i>MT051864</i>
<i>D. sclerotioides</i>	CBS 296.67	<i>Cucumis sativus</i>	Netherlands	KC343193	KC343919	KC344161	KC343677	KC343435
<i>D. sterilis</i>	CBS 136969	<i>Vaccinium corymbosum</i>	Italy	KJ160579	KJ160611	KJ160528	MF418350	KJ160548
<i>D. stictica</i>	CBS 370.54	<i>Buxus sempervirens</i>	Italy	KC343212	KC343938	KC344180	KC343696	KC343454
<i>Diaporthella corylina</i>	CBS 121124	<i>Corylus</i> sp.	China	KC343004	KC343730	KC343972	KC343488	KC343246

¹Acronyms of culture collection: **CAA** – Personal Culture Collection Artur Alves, University of Aveiro, Aveiro, Portugal; **CBS** – Westerdijk Fungal Biodiversity Institute, Utrecht, The Netherlands; **CFCC** – China Forestry Culture Collection Center, Beijing, China; **CPC** – Personal culture Collection Pedro W. Crous, hosted at CBS; **MUM** – Culture Collection from Micoteca at Universidade of Minho, Center for Biological Engineering, Braga, Portugal. **PSCG** – Personal Culture Collection Y.S. Guo, China. Ex-type isolates are in **bold** face. Newly sequences generated in this study are in italics.

Table 3. Fungal isolates used and obtained in subchapter 2.1.

Species	Isolate
<i>Diaporthe crousii</i>	CAA823
<i>Diaporthe eres</i>	CAA829
	CAA830
<i>Diaporthe leucospermi</i>	CAA762
<i>Diaporthe phillipsii</i>	CAA817
	CAA818

RESULTS

Fungal isolation.

Twelve plantations, harboring a total of 65 280 plants and corresponding to an area of 31 ha, were evaluated in several blueberry growing regions in Portugal (Fig. 1). From these plants, 95 plants from the cultivars 'Duke' ($n = 60$), 'Ozarkblue' ($n = 2$), 'Aurora' ($n = 7$), 'O'Neal' ($n = 1$), 'Gupton' ($n = 6$), 'Legacy' ($n = 11$), 'Bluecrop' ($n = 10$), 'Liberty' ($n = 2$) and 'New Hanover' ($n = 1$) were collected. Symptoms such as dieback, necrosis of twigs and stems were noticed in all sampled plants. The infections advanced in a basipetal form, developing necrosis above young shoots (Fig. 2A). These symptoms were also accompanied by cankers, that initially appeared as reddish to brown lesions on green twigs (Fig. 2B) and later on the aged stems at the base (Fig. 2C). Twig blight symptoms were also visible, developing red to rust lesion-like areas on the newer shoots, and reddish spots around buds (Fig. 2D). Foliage on these diseased plants tended to redden or yellowing, followed by leaf necrosis (Fig. 2E). Additionally, in more advanced states, dieback led to necrosis of the vascular tissues and consequently to twigs death (Fig. 2F). Samples collected from symptomatic blueberry plants led to a collection of 116 isolates with typical diaporthalean colonies (white to dirty white felty mycelium spreading in a radial pattern and reverse with brownish to greyish concentric zones) and micromorphological characteristics typical of the genus *Diaporthe* (alpha and beta conidia).

This genus was isolated from all regions surveyed although with different abundance values: Urgeztes (21.6%), Arcozelo (15.5%), Ourém (11.2%), Águeda and Póvoa de Lanhoso (10.3%), Agrela (9.5%), Mangualde (6.9%), Arouca (6%), Monte Córdova (4.3%), Penafiel (2.6%), Alpiarça and Idanha-a-Nova (0.9%).

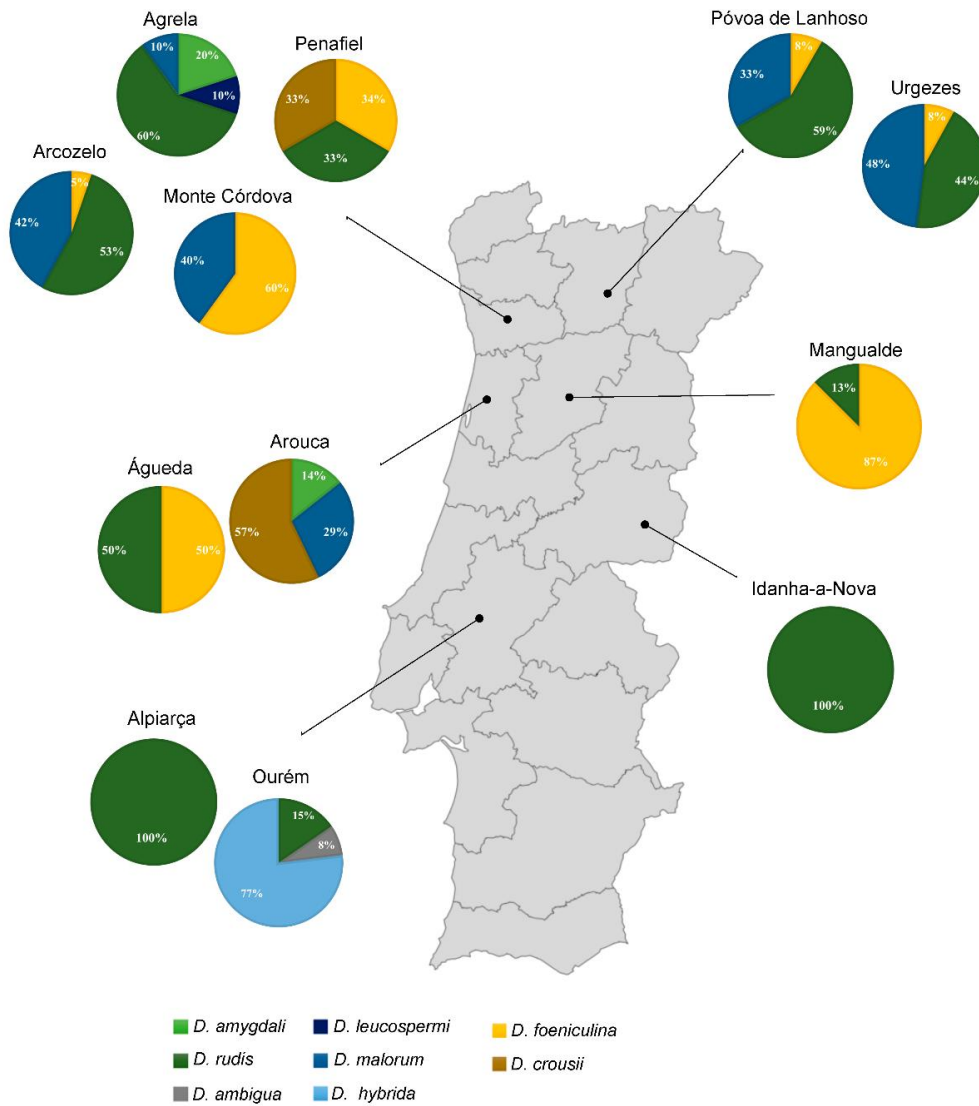


Figure 1. Map of Portugal indicating the distribution and frequency of each *Diaporthe* species within sampled regions.



Figure 2. Symptoms on *Vaccinium corymbosum* with associated *Diaporthe* species. **A.** Necrosis evolving right below a young shoot; **B.** Canker on a green twig. **C.** Canker on older stems developing at the base. **D.** Twig bight with visible red to rust areas. **E.** Leaf discoloration. **F.** Vascular system of a dead twig.

Molecular characterization.

MSP-PCR fingerprinting was performed to evaluate the overall genetic diversity of the 116 fungal isolates. A total of 21 isolates representative of each cluster, and from different geographic regions and cultivars whenever possible, were selected for further molecular characterization (Table 4).

A primary identification using the ITS sequences of our isolates was done using BLASTn. The analysis revealed that our sequences matched to members of *Diaporthe* with high values of identity (98% to 100%), thus confirming the identity of our isolates. Afterwards, a multilocus analysis using the loci ITS, *tef1- α* , *tub2*, *cal* and *his3* was performed, which included those species phylogenetically closely related to our isolates and whose 5 loci are available (Table 2). The 5-loci concatenated alignment contained 2652 characters including gaps (599 from ITS, 458 from *tef1-a*, 513 from *tub2*, 536 from *his3* and 546 from *cal*). Of these 2652 characters, 1429 were constant, 344 were variable and parsimony uninformative and 879 were parsimony informative. MP analysis resulted in 100 equal, most parsimonious trees with TL = 3263 steps, CI = 0.5786, RI = 0.9049, RC = 0.5236 and HI = 0.4789. The analysis included 1 outgroup (*Diaporthella corylina* CBS 121124) and 76 ingroup taxa (22 sequences obtained in this study and 54 *Diaporthe* sequences retrieved from GenBank). The isolates from this study grouped in eight clades (Fig. 3).

Four isolates clustered within the well-supported *Diaporthe rudis* clade (ML/MP/PP = 99/100/1.00); three isolates clustered with *D. crousii* (ML/MP/PP = 100/100/1.00); only one isolate grouped with *D. ambigua* (ML/MP/PP = 100/100/1.00); two isolates fitted in a monophyletic clade containing the species *D. amygdali* (ML/MP/PP = 100/100/1.00); six isolates are deemed to belong to *D. malorum* (ML/MP/PP = 99/100/1.00); and two other isolates (*D. hybrida*) clustered between *D. portugallica* and *D. phillipsii*.

Isolate CAA971 clustered together with the ex-type strains of *D. rossmaniae*, *D. leucospermi* and *D. pyracanthae* forming a highly supported monophyletic clade (ML/MP/PP = 99/100/1.00). A pairwise alignment showed that CAA971 shares polymorphisms either with *D. pyracanthae* or *D. rossmaniae* in *his3*; with *D. leucospermi* in ITS, with *D. pyracanthae* in *tef1- α* ; and with *D. rossmaniae* in *tub2*.

Only in the *cal* locus, CAA971 differs from the remaining three species in the presence of 3 unique polymorphisms. Isolates CAA963 and CAA967 fell within a highly supported clade (ML/MP/PP = 100/100/1.00) containing the type species of *D. foeniculina* and *D. baccae*. A pairwise comparison revealed that our isolates are 100% identical to *D. foeniculina* and *D. baccae* in *tef1- α* and *tub2* loci; 100% identical to *D. foeniculina* in ITS locus; only 3 unique polymorphisms separate our isolates from these species in *cal* locus; and in *his3* locus, it was observed polymorphisms either with *D. baccae* or *D. foeniculina*. The ML trees are presented with ML, MP and PP support values next to the branches, respectively.

Table 4. *Diaporthe* isolates collected from *Vaccinium corymbosum* plants, used in the phylogenetic analysis.

Species	Strain ¹	Cultivar	Symptoms	Location	Mating-type	
					<i>MAT1-1-1</i>	<i>MAT1-2-1</i>
<i>D. ambigua</i>	CAA957	Duke	Dead stem	Ourém	(+)	(+)
	CAA958	Aurora	Twig blight	Arouca	(+)	(-)
<i>D. amygdali</i>	CAA959	Duke	Twig blight	Agrela	(+)	(-)
	CAA960	Aurora	Twig blight	Arouca	(+)	(+)
<i>D. crousii</i>	CAA961	Aurora	Twig blight	Arouca	(+)	(+)
	CAA962	Legacy	Dead stem	Penafiel	(+)	(+)
<i>D. foeniculina</i>	CAA963	Duke	Dead twig	Urgezes	(-)	(+)
	CAA967	Aurora	Dieback	Mangualde	(-)	(+)
<i>D. hybrida</i>	CAA998	Duke	Twig blight	Ourém	(+)	(-)
	CAA999	Duke	Twig blight	Ourém	(+)	(-)
<i>D. leucospermi</i>	CAA971	Duke	Dead twig	Agrela	(+)	(-)
	CAA972	Aurora	Twig blight	Arouca	(-)	(+)
	CAA973	Aurora	Twig blight	Arouca	(-)	(+)
<i>D. malorum</i>	CAA974	Duke	Dieback	Póvoa de Lanhoso	(+)	(-)
	CAA975	Duke	Dead twig	Urgezes	(+)	(-)
	CAA976	Duke	Dead twig	Urgezes	(+)	(-)
	CAA977	Duke	Dieback	Arcozelo	(+)	(-)
<i>D. rudis</i>	CAA979	O'Neal	Stem blight	Ourém	(+)	(+)
	CAA984	Duke	Dead twig	Urgezes	(+)	(+)
	CAA987	Duke	Twig blight	Agrela	(+)	(+)
	CAA991	Duke	Twig blight	Arcozelo	(+)	(+)

¹Acronym of collection: **CAA** – Culture Collection of Artur Alves, University of Aveiro, Portugal.

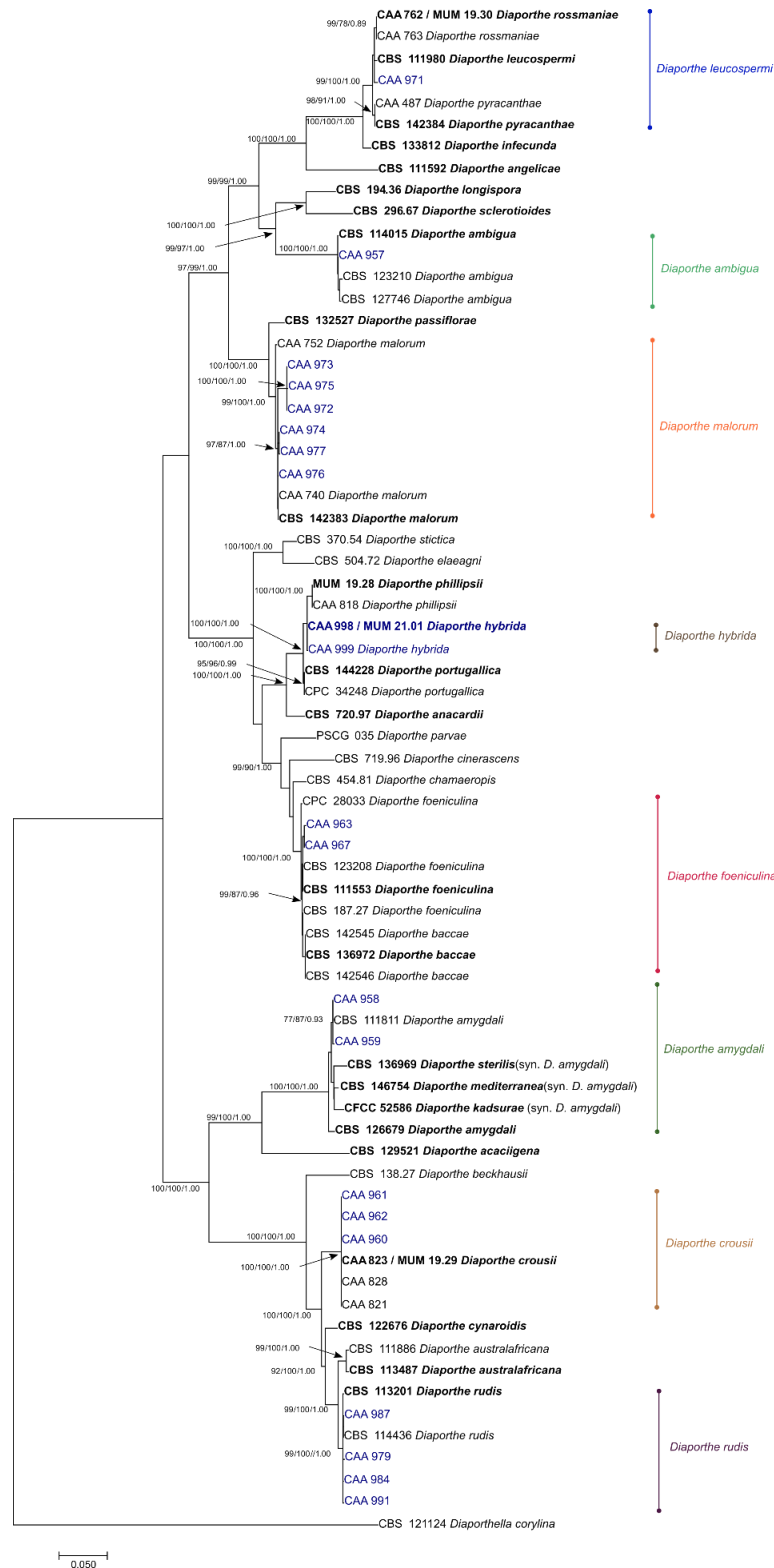


Figure 3. Phylogenetic relationships generated from Maximum Likelihood analysis based on combined ITS, *tef1- α* , *tub2*, *his3* and *cal* sequence data from *Diaporthe* species. The ML tree is drawn to scale and rooted to *Diaporthella corylina*. ML and MP bootstrap values greater than 70% and posterior probabilities (PPs) greater than 0.80 are shown at the nodes. The ex-type strains are in bold.

Distribution and prevalence of Diaporthe species.

Table 5 sums up the total of isolates collected from diseased plants and the prevalence of each species found in this study. Overall, *Diaporthe* species were found in all 95 plants collected showing twig blight and dieback symptoms. From the total 116 diaporthelean isolates, *D. rudis* was the dominant species representing 38.8% of the isolates obtained, followed by *D. malorum* and *D. foeniculina* with an abundance of 25% and 19% respectively. At least two different species were found in ten of the twelve blueberry orchards. *Diaporthe rudis*, *D. foeniculina* and *D. malorum* were found in six surveyed plantations. *Diaporthe ambigua*, *D. leucospermi* and *D. hybrida* were recovered from one orchard only, each one in different regions.

The species collected were also found co-existing with other species in the same plant material, or alone without the co-occurrence of other members of *Diaporthe*. For instance, *D. rudis* was found in association with *D. malorum*, *D. foeniculina*, *D. leucospermi*, *D. crousii* and *D. hybrida*. *Diaporthe amygdali* was also found co-existing with *D. crousii*; *D. leucospermi* was recovered from the same plant material along with *D. malorum*, while *D. ambigua* was only recovered without co-existing with other species (Table S1).

Table 5. Number of isolates and prevalence of each *Diaporthe* species obtained from blueberry orchards.

Species	Number of isolates	Prevalence (%)
<i>D. ambigua</i>	1	0.9%
<i>D. amygdali</i>	3	2.5%
<i>D. crousii</i>	5	4.3%
<i>D. foeniculina</i>	22	19.0%
<i>D. leucospermi</i>	1	0.9%
<i>D. malorum</i>	29	25.0%
<i>D. rudis</i>	45	38.8%
<i>Diaporthe xhybrida</i>	10	8.6%
TOTAL	116	100%

Plant mortality.

Mortality (100%) occurred only for cultivar 'Duke' inoculated with *D. eres* (CAA829) at different days post inoculation (Fig. S6). Additionally, 20% mortality was observed for cultivar 'Duke' inoculated with *D. eres* (CAA830), *D. amygdali* (CAA958, CAA959), *D. malorum* (CAA975), *D. crousii* (CAA962) and *D. hybrida* (CAA998). Moreover, 25% mortality was observed also in 'Duke', after inoculation with *D. hybrida* (CAA998). The cultivar 'Legacy' showed 20% mortality after inoculations with *D. hybrida* (CAA998) and *D. amygdali* (CAA958) (Fig. S7). Isolates CAA962 (*D. crousii*), CAA958 (*D. amygdali*) and CAA830 (*D. eres*) were the only ones to cause 20% mortality in cultivar 'Spartan' (Fig. S8). Besides mortality, plants showed symptoms such as wilting and dead leaves, dieback, extensive discoloration of the outer epidermis, necrosis of the vascular tissues, twig blight and dead twigs (Fig. 4). The remaining plants that survived did not show any of these symptoms, apart from the development of necrotic lesions around the inoculation point at the end of the experiment.

Lesion length measurements.

After 35 days of incubation, the outer bark was carefully removed, and the internal lesions which corresponds to the necrotic woody tissues were measured. Shapiro-Wilk test for normality revealed that the data differed significantly from a normal distribution, for all three cultivars tested ($W = 0.76$, $p < 0.05$ for 'Duke'; $W = 0.65$, $p < 0.05$ for 'Legacy'; $W = 0.78$, $p < 0.05$ for 'Spartan'). Moreover, the homogeneity of variances, an-other assumption of linear tests (Bartlett's test) did not meet a normal distribution with $p < 0.05$ for all cultivars. Thus, the Kruskal-Wallis test was applied, indicating that there are statistically differences among isolates from all three cultivars tested, with $p < 0.05$. Dunn-Test was used to compare all isolates, while the different species were compared with one another, using the Wilcoxon rank test.

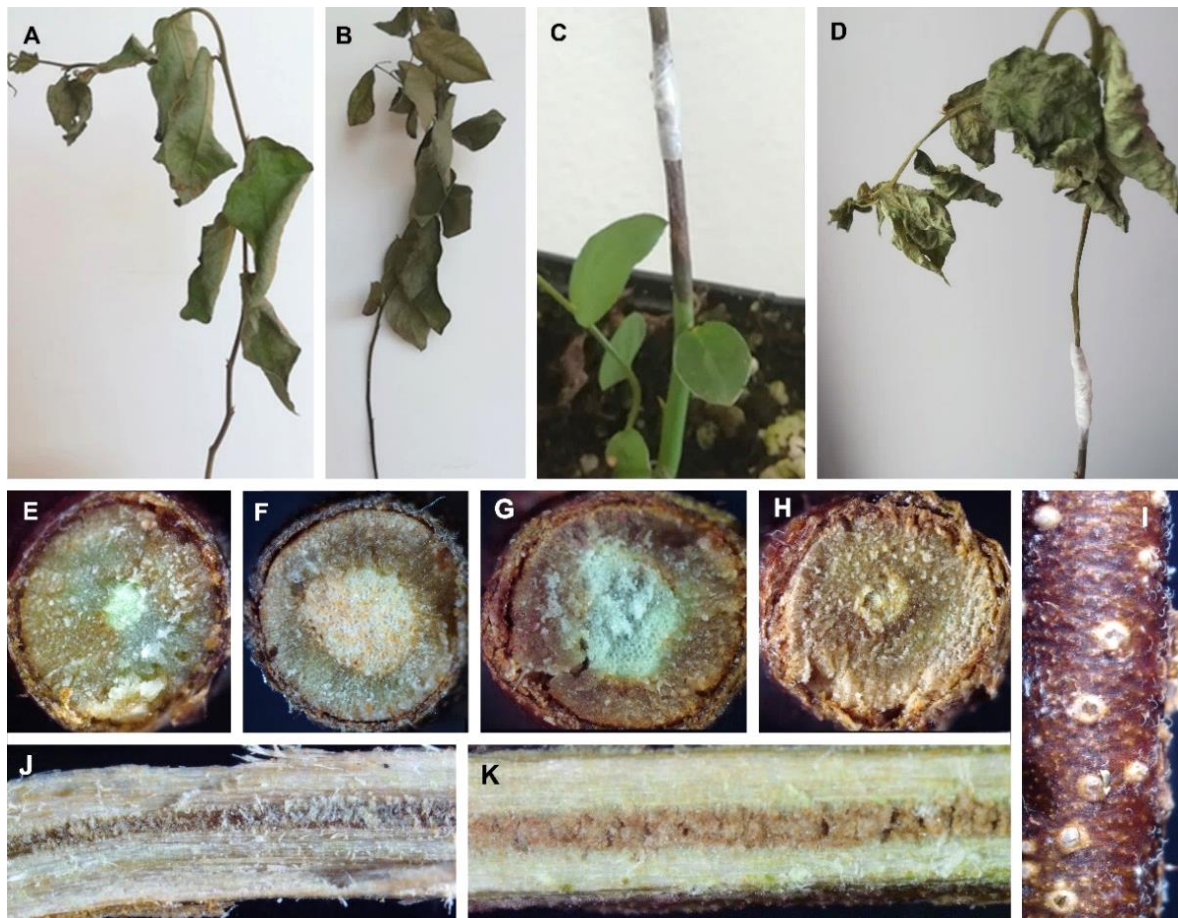


Figure 4. Representative symptoms of twig dieback and lesions induced by inoculation of wounded blueberry plants (cv. ‘Duke’, ‘Spartan’ and ‘Legacy’). **A.** Death plant (cv. ‘Duke’) induced by CAA829. **B.** Death plant (cv. ‘Legacy’) induced by CAA958. **C.** Stem lesion development from the inoculation point (cv. ‘Spartan’) caused by CAA958. **D.** Death plant (cv. ‘Duke’) induced by CAA999. **E, F, G, H.** Cross section of blueberry twigs showing discoloration of the vascular tissues well into the xylem, after infection by CAA830 (cv. ‘Duke’), CAA975 (cv. ‘Duke’), CAA998 (cv. ‘Legacy’), CAA958 (cv. ‘Duke’) respectively. **I.** Pycnidia development of CAA975 on an inoculated twig. **J, K.** Necrotic internal tissues of twigs inoculated with CAA829 (cv. ‘Duke’) and CAA998 (cv. ‘Legacy’).

All *Diaporthe* isolates inoculated on nine-month-year old plants of blueberry cultivars ‘Duke’, ‘Legacy’ and ‘Spartan’, caused necrotic lesions. Differences in aggressiveness were observed among isolates from the same species (Fig. 5), and the differences varied according to the cultivar inoculated. For instance, in cultivar ‘Duke’, isolate CAA975 (*D. malorum*) caused significantly larger lesions (5.9 ± 2.7 cm) than isolate CAA972 (2.4 ± 0.6 cm, $p = 0.0241$). Moreover, in cultivar ‘Legacy’, a homogeneity in the lesion lengths was observed. Nevertheless, a statistically significant difference in the lesion length was observed between isolates of *D. foeniculina*: CAA967 (2.0 ± 0.5 cm) and CAA963 (1.2 ± 0.4 cm, $p = 0.0273$).

Moreover, in cultivar 'Spartan', a statistically significant difference in lesion size was also observed between CAA967 (*D. foeniculina*) (2.4 ± 0.3 cm) and CAA963 (*D. foeniculina*) (1.4 ± 0.5 cm, $p = 0.0181$). It is interesting to note, for instance, that lesions in cultivar 'Spartan', caused by isolate CAA998 (*D. hybrida*) (3.0 ± 1.5 cm) are significantly larger than those caused by its parental species *D. phillipsii* (CAA818) (1.5 ± 0.3 cm, $p = 0.0149$). A similar trend was verified in the cultivar 'Duke': the isolate CAA998 (5.0 ± 3.0 cm) cause lesions significantly larger than those caused by its parental isolates CAA818 (1.9 ± 0.6 cm, $p = 0.0087$) and CAA817 (1.8 ± 0.4 cm, $p = 0.0049$).

When analyzing the different *Diaporthe* species, differences in mean lesion length were observed (Fig. S9). For instance, *D. eres* (isolates CAA829 and CAA830) was the most aggressive species in cultivar 'Duke', which caused the death of all replicates and with significantly larger internal necrotic lesions than any of the other species tested (5.9 ± 1.4 cm), except those of *D. hybrida* (3.5 ± 1.6 cm, $p = 0.0554$). Moreover, there were no statistical differences in the cultivars 'Legacy' and 'Spartan' among lesions caused by strains CBS 160.32, CAA829 and CAA830 (*D. eres*). In general, the cultivar 'Duke' showed larger internal lesions than 'Spartan' and 'Legacy'. The cultivar 'Duke' also presented a great variability between isolates (Fig. 5). Overall, the species *D. eres* and *D. amygdali* induced the longest lesion lengths in all cultivars tested. Contrarily, the smallest lesion size was observed in *D. foeniculina* and *D. leucospermi* (Fig. S9). At the end of the experiment, no lesions were seen in control plants. All the fungal species inoculated were re-isolated, thus verifying Koch's postulates.

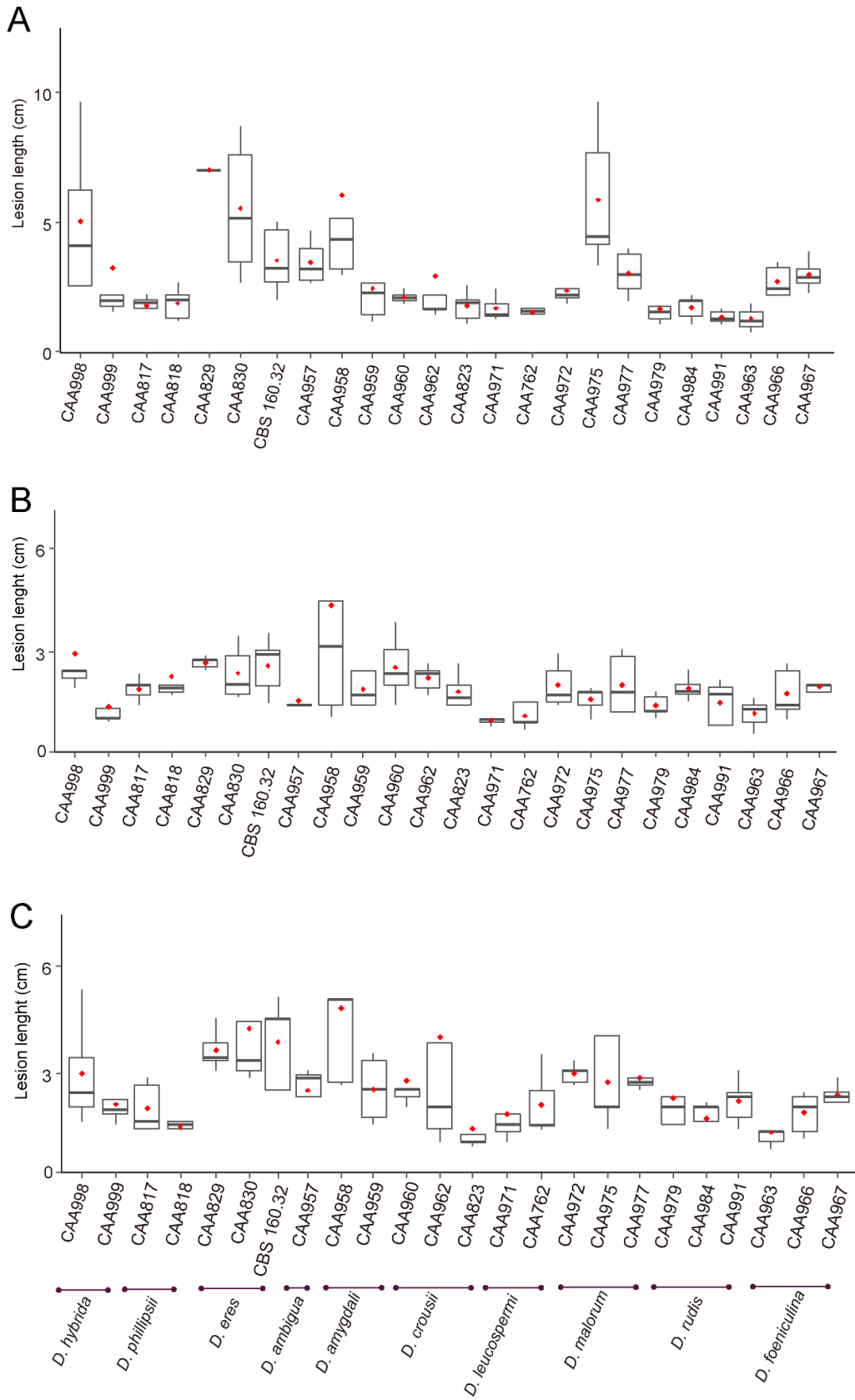


Figure 5. Box plot of lesion length (cm) caused by isolates of *Diaporthe* on twigs of cultivars ‘Duke’ (A), ‘Legacy’ (B) and ‘Spartan’ (C). Black lines in the boxes show medians and red dots represent the means.

TAXONOMY

In this section we provide descriptions and illustrations of the species isolated from *V. corymbosum* plants. Additionally, synonymous names for a few *Diaporthe* species are proposed, which are followed by a brief note based on multi-gene phylogenetic analyses and morphological characters.

Diaporthe ambigua Nitschke, *Pyrenomyces Germanici* 2:311 (1867). Mycobank 193681 (Fig. 6)

Specimen examined: **Portugal. Santarém:** Ourém (39°39'13.5"N 8°35'32.0"W), from dead stems of *V. corymbosum*, July 2019, S. Hilário, living culture: CAA957.

Description: Sexual morph: Perithecial ascomata globose, aggregated, emerging through fennel stems. Perithecial necks black, subcylindrical, tapering towards the apex. Asci unitunicate, cylindrical to clavate, 8-spored, (48.7–)49.5–53.6(–54.7) × (6.9–)7.1–8.1(–8.2) μm, (mean ± S.D. = 51.5 ± 2.4 × 7.6 ± 0.6 μm, *n* = 10). Ascospores hyaline, smooth, fusoid–ellipsoidal, septate, tapering towards both ends, frequently tetraguttulate, (9.5–)10.9–11.5(–12.8) × (2.9–)3.3–3.5(–3.9) μm, (mean ± S.D. = 11.2 ± 0.9 × 3.4 ± 0.2 μm, *n* = 50). Asexual morph: Conidiomata brown, erumpent from fennel stems, extruding white conidial mass. Conidiophores subcylindrical, septate at the base, frequently un-branched, (11.8–)16.2–21.4(–24.4) × (1.2–)1.4–1.8(–2.3) μm, (mean ± S.D. = 18.8 ± 4.2 × 1.6 ± 0.3 μm, *n* = 30). Paraphyses not observed. Alpha conidia ellipsoidal, biguttulate, with an obtuse apex and rounded at the other end, (4.6–)6.0–6.3(–7.3) × (1.9–)2.4–2.6(–3.1) μm, (mean ± S.D. = 6.1 ± 0.6 × 2.5 ± 0.3 μm, *n* = 100). Beta conidia not observed.

Mating type strategy: homothallism,

Culture characteristics: on PDA at 25 °C after 7 days, mycelium flat, spreading with sparse, white to dirty white dense aerial mycelium and with solid patches of olivaceous black; reverse with brownish orange patches in the central part, surrounded by orpiment to buff orange cream areas.

Host range: *Aspalathus linearis*, *Malus domestica*, *Malus sylvestris*, *Prunus salicina*, *Prunus* sp., *Pyrus communis*, *Vitis vinifera*, *Foeniculum vulgare* and *Vaccinium* sp. (Farr & Rossman 2021).

Known distribution: China, Cuba, Germany, Netherlands, South Africa, United Kingdom, United States, Chile, and Portugal (Farr & Rossman 2021).

Notes: *Diaporthe ambigua* was first described on *Pyrus communis* in Germany, and later on apple, pear and plums in South Africa (Smit et al. 1996). Elfar et al. (2013), reported for the first time the presence of this fungus on blueberry plants. This study represents the first report of this pathogen on blueberries in Portugal and Europe.

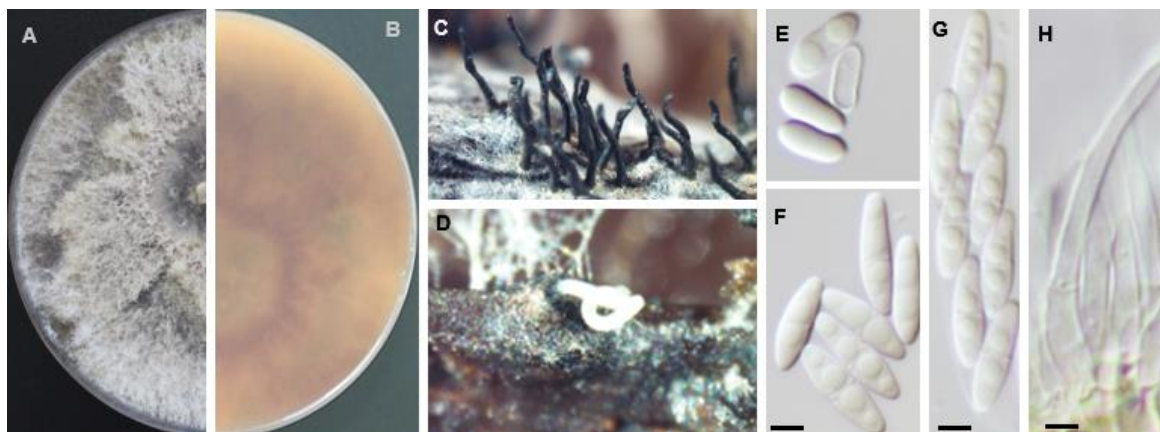


Figure 6. Morphology of *Diaporthe ambigua*. **A, B.** Upper and reverse culture surface respectively (after 7 days at 25 °C). **C.** Perithecial necks emerging from fennel twigs. **D.** Pycnidia oozing white conidial mass. **E.** Alpha conidia. **F.** Ascospores. **G.** 8-spored ascus. **H.** Conidiophores. Bars = 2.5µm.

Diaporthe amygdali (Delacr.) Udayanga, Crous & K.D. Hyde, *Fungal Divers.* **56**:166 (2012). MycoBank MB 800722

Specimen examined: **Portugal. Aveiro;** Arouca (40°54'35.3"N 8°22'49.7"W), from diseased twigs of *V. corymbosum*, 1 April 2019, *P. Pinho*, living culture CAA958. Description & Illustration (Hilário et al. 2021a).

Notes: The clade containing the strain CAA958 comprises the ex-type culture of *D. amygdali* isolated from *Prunus dulcis*, and other synonyms such as *D. sterilis* from *V. corymbosum*, *D. kadsurae* from *Kadsura longipedunculata* and *D. mediterranea* from *P. dulcis*. Our isolates clustered with a taxon isolated from *Vitis vinifera* in South Africa. As stated by Hilário et al. (2021) this clade represents one single species, *D. amygdali*.

Diaporthe crousii Hilário, Santos & Alves, *Mycologia* **55**:207 (2020). MycoBank MB831439 (Fig. 7)

Specimen examined: Portugal. Porto: Penafiel (41°08'07.0"N 8°22'42.5"W), from dead stems of *V. corymbosum*, 7 May 2019, *H. Moreira*, living culture: CAA962.

Description: Sexual morph: Perithecial ascomata globose, solitary or in clusters emerging through pine needles; brown ascomata necks, tapering towards the apex. Asci 8-spored, unitunicate, clavate to subclavate, straight to slightly curved, (31.0–)34.2–36.8(–41.5) × (4.8–)6.0–6.5(–7.7) μm, (mean ± S.D. = 35.5 ± 3.0 × 6.2 ± 0.7 μm, *n* = 30). Ascospores hyaline, smooth, septate, frequently tetraguttulate, ellipsoidal, straight, (10.5–)11.0–12.5(–13.3) × (2.3–)2.5–3.3(–3.7) μm, (mean ± S.D. = 11.7 ± 1.0 × 2.9 ± 0.6 μm, *n* = 50). Asexual morph: Conidiomata brown to black, extruding white conidial mass. Conidiophores hyaline, aggregated, reduced to conidiogenous cells (10.5–)12.8–14.4(–19.0) × (1.3–)1.8–2.2(–2.8) μm, (mean ± S.D. = 13.6 ± 1.9 × 2.0 ± 0.4 μm, *n* = 30). Paraphyses not observed. Alpha conidia hyaline, aseptate, ellipsoid, rounded apex and obtuse to truncate base, rarely biguttulate, (4.6–)5.5–5.7(–6.2) × (1.7–)2.0–2.2(–2.8) μm, (mean ± S.D. = 5.6 ± 0.4 × 2.1 ± 0.2 μm, *n* = 100). Beta conidia and gamma conidia not observed.

Mating type strategy: homothallism

Culture characteristics: Colonies on PDA covering a Petri dish after 7 days at 25 °C, spreading with brown to gray sparse aerial mycelium and with reverse greenish to brownish concentric zone.

Host range: *Vaccinium corymbosum*, *Eucalyptus globulus* (Lopes et al. 2021).

Known distribution: Portugal

Notes: *Diaporthe crousii* was first described as the causal agent of twig canker of blueberries (*V. corymbosum*) and associated to *E. globulus*.

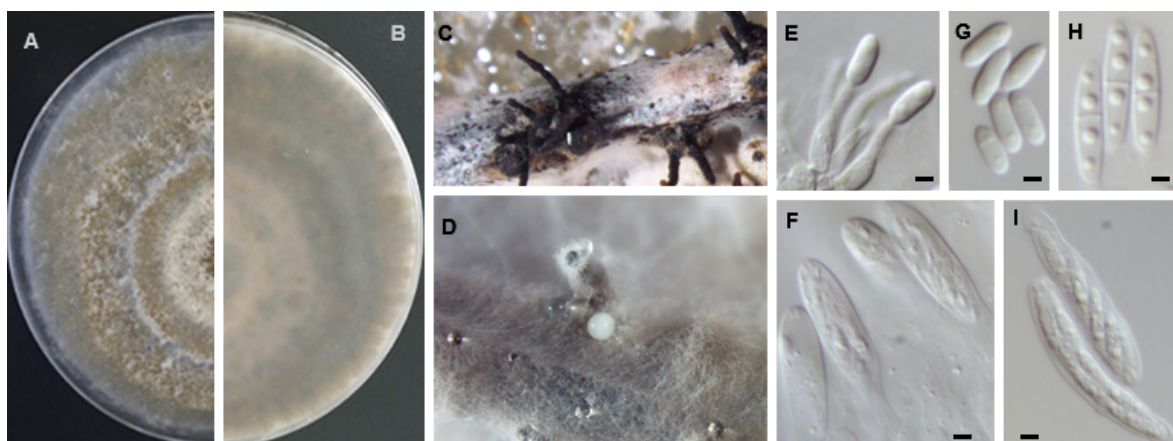


Figure 7. Morphology of *Diaporthe crousii*. **A, B.** upper and reverse culture surface respectively (after 7 days at 25 °C). **C.** Perithecial ascomata and necks emerging through pine needles. **D.** White translucent cirri. **E.** Conidiophores with alpha conidia at their tips. **F.** Immature asci. **G.** Alpha conidia. **H.** Ascospores. **I.** Asci. Bars = 2.5µm

Diaporthe foeniculina Udayanga & Castlebury, **comb. nov.** *Persoonia* **32**:95 (2014). MycoBank MB803929 (Fig. 8)

= *Diaporthe baccae* Lombard, Polizzi & Crous, *Phytopathol. Mediterr.* **53**:295 (2014). MycoBank MB807599

= *Diaporthe ravennica* Thambugala, Camporesi & Hyde, *Fungal Divers.* **82**:296 (2016). MycoBank MB552100

Specimen examined: **Portugal. Viseu:** Mangualde (40°37'43.2"N 7°51'51.8"W), from twig blight of *V. corymbosum*, 30 August 2019, *D. Lopes*, living culture: CAA967

Host range: *Acacia* sp., *Achillea millefolium*, *Ailanthus altissima*, *Arctium minus*, *Asparagus* sp., *Camelia sinensis*, *Castanea sativa*, *Citrus aurantiifolia*, *C. aurantiifolialimon*, *C. bergamia*, *C. japonica*, *C. latifolia*, *C. limon*, *C. lamonia*, *C. maxima*, *C. medica*, *C. mitis*, *C. paradasi*, *C. paradisitriifoliata*, *C. reticulata*, *C. sinensis*, *C. sinensistrifoliata*, *Corylus avellana*, *Cupressus sempervirens*, *Diospyros kaki*, *Ficus benjamina*, *F. carica*, *Foeniculum vulgare*, *Fuchsia excorticata*, *Glycine max*, *Hemerocallis fulva*, *Juglans regia*, *Lunaria rediviva*, *Malus domestica*, *Melilotus officinalis*, *Microcitrus australasica*, *Paraserianthes lophantha*, *Persea americana*, *Prunus amygdalus*, *P. avium*, *Pyrus communis*, *P. pyrifolia*, *Rhus pendulina*, *Ribes nigrum*, *Rosa canina*, *Salix* sp., *Salvia* sp., *Tamarix* sp., *V. corymbosum*, *Vicia* sp., *Vitis vinifera* and *Wisteria sinensis* (Farr & Rossman 2021).

Know distribution: Chile, Croatia, France, Germany, Greece, Iran, Italy, Malta, New Zealand, Portugal, Serbia, South Africa, Spain, Turkey, Uruguay, USA (Farr & Rossman 2021).

Description: Asexual morph: Pycnidial conidiomata, black, erumpent, aggregated or solitary, covered in white mycelium, with yellowish drop-like conidial cirrus oozing from ostiole. Conidiophores hyaline, rarely unbranched, cylindrical, straight to sinuous, reduced to conidiogenous cells, (10.5–)12.0–13.9(–15.0) × (1.4–)1.8–2.4(–3.0) μm, (mean ± S.D. = 12.9 ± 1.5 × 2.1 ± 0.5 μm, *n* = 30). Paraphyses not observed. Alpha conidia aseptate, hyaline, smooth, ellipsoidal, frequently with two, rounded apex and rarely with subtruncate base (6.6–)7.6–8.2(–9.6) × (1.8–)2.3–2.5(–3.0) μm, (mean ± S.D. = 7.9 ± 0.7 × 2.4 ± 0.3 μm, *n* = 100). Beta conidia hyaline, aseptate, eguttulate, slightly curved, abundant, apex acute, base subtruncate, (20.5–)21.5–23.4(–26.9) × (0.9–)1.2–1.4(–1.8) μm, (mean ± S.D. = 22.4 ± 1.9 × 1.3 ± 0.3 μm, *n* = 100). Gamma conidia rare, aseptate, hyaline, rounded apex, (11.9–)11.6–13.0(–13.1) × (1.6–)1.7–1.9(–2.0) μm, (mean ± S.D. = 12.3 ± 0.7 × 1.8 ± 0.2 μm, *n* = 4). Sexual morph: not observed.

Mating type strategy: heterothallism

Culture characteristics: colonies on PDA at 25 °C after 7 days spreading moderate with aerial mycelium, feathery margins, pale brown zones in a radial pattern and re-verse with greenish yellow pigmentation developing in the center.

Notes: Phillips & Santos (Santos et al. 2010) described *Diaporthe neotheicola* in Portugal from *Foeniculum vulgare*. Later, Udayanga & Castlebury (Udayanga et al. 2014) synonymized *D. neotheicola* as *D. foeniculina* and that is the name currently accepted. Posterior to that, Thambugala, Camporesi & Hyde (Dissanayake et al. 2017) described *D. ravennica* as a distinct species phylogenetically distinct from *D. baccae* and *D. foeniculina*. Here we show that *D. foeniculina* and *D. baccae* cluster in a well-supported clade and are closely related. A pairwise comparison showed that *D. foeniculina* and *D. baccae* are similar, since both species differ in 7 nt in ITS (*p*-distance = 0.012), 2 nt of *his3* (*p*-distance = 0.004) and 1 in *cal* (*p*-distance = 0.002). *Tef1-α* and *tub2* sequences from both *D. foeniculina* and *D. baccae* are 100% identical.

Moreover, in the ITS initial tree performed, we noted that *D. ravennica* was very closely related to *D. foeniculina* and *D. baccae*. Due to the absence of *cal* and *his3* sequences, we could not include the species in our phylogenetic analysis. However, we noted that *D. ravennica* is 100% identical to *D. baccae* and *D. foeniculina* based on *tef1- α* and *tub2* loci, and 9 nt (p -distance = 0.015) and 3 nt (p -distance = 0.005) in the ITS locus separate *D. ravennica* from *D. foeniculina* and *D. baccae* respectively. Morphologically, these species are virtually indistinguishable with overlapping micromorphological characters: yellow to pale luteous conidial cirrus; alpha conidia with base subtruncate, with none, two or many guttules; beta conidia curved, base subtruncate, acute apex and with dimensions that match within the same ranges.

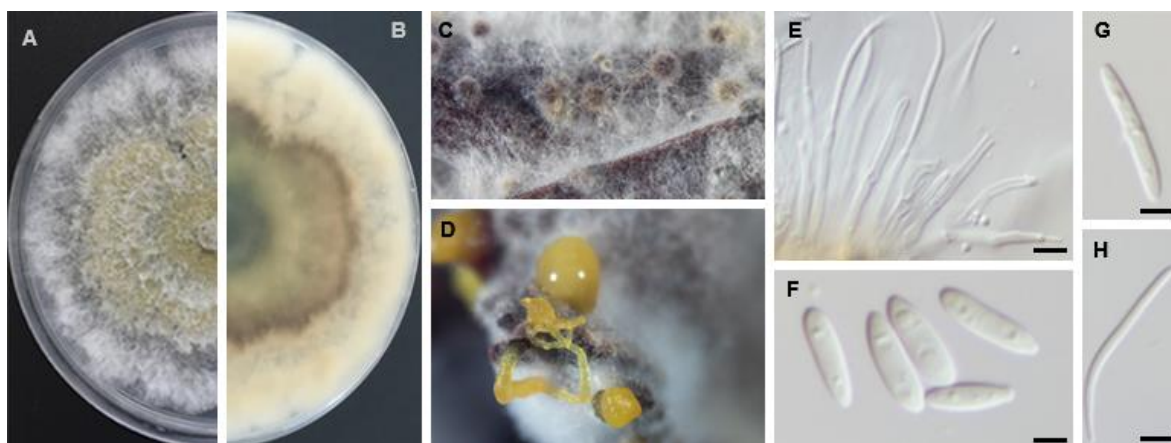


Figure 8. Morphology of *Diaporthe foeniculina*. **A, B.** upper and reverse culture surface respectively (after 7 days at 25 °C). **C.** Conidiomata on pine needles. **D.** Pycnidia oozing orange cirri. **E.** Conidiophores with beta conidia at their tips. **F.** Alpha conidia. **G.** Gamma conidia. **H.** Beta conidia. Bars = 2.5 μ m.

Diaporthe leucospermi Crous & Summerell, *Personia* **27**:32 (2011). MycoBank MB560561 (Fig. 9)

= *Diaporthe pyracanthae* Santos & Alves, *Mycosphere* **8**:489 (2017). MycoBank MB820224

= *Diaporthe rossmaniae* Hilário, Amaral, Santos & Alves, *Mycologia* **55**:207 (2020). MycoBank MB831452

Specimen examined: **Portugal. Porto:** Agrela (41°08'07.0"N 8°28'09.7"W), from a dead twig of *V. corymbosum*, 10 July 2019, S. Hilário, living culture: CAA971.

Host range: *Acer negundo*, *Chamaerops humilis*, *Hydrangea macrophylla*, *Leucospermum* sp., *Pyracantha coccinea*, *Vaccinium corymbosum* (Farr & Rossman 2021).

Known distribution: Australia and Portugal (Farr & Rossman 2021).

Description: Asexual morph: Pycnidial conidiomata, brown to black, embedded on fennel stems and pine needles, aggregated or solitary, covered in white mycelium, oozing white translucent conidial cirrhus. Conidiophores lining the inner cavity, subcylindrical, aseptate, branched, reduced to conidiogenous cells, sometimes bearing beta conidia at their tips (9.9–)10.8–14.1(–15.2) × (1.5–)1.6–2.6(–3.1) μm, (mean ± S.D. = 12.5 ± 2.1 × 2.1 ± 0.6 μm, *n* = 30). Paraphyses not observed. Alpha conidia hyaline, ellipsoid, found infrequent, eguttulate, rounded apex and obtuse base, (4.4–)4.9–5.8(–5.9) × (1.7–)1.9–2.6(–2.3) μm, (mean ± S.D. = 5.4 ± 0.6 × 2.1 ± 0.2 μm, *n* = 10). Beta conidia hyaline, aseptate, smooth, filiform, hooked in apical part, apex acute, base truncate, (22.5–)26.1–28.5(–31.8) × (1.0–)1.1–1.3(–1.5) μm, (mean ± S.D. = 27.3 ± 2.9 × 1.2 ± 0.2 μm, *n* = 100). Gamma conidia infrequent, aseptate, hyaline, rounded apex, (8.1–)7.7–9.1(–8.8) × (1.8–)1.9–2.0(–2.1) μm, (mean ± S.D. = 8.4 ± 0.5 × 2.9 ± 0.1 μm, *n* = 4). Sexual morph: not observed

Mating type strategy: heterothallism

Culture characteristics: colonies on PDA at 25 °C after 7 days spreading large with moderate aerial mycelium, pale olivaceous-grey to smoke-grey with patches of olivaceous black near the margins; reverse straw yellow with gallstone yellow zones.

Notes: Crous & Summerell (Crous et al. 2011) described *D. leucospermi* on leaves of *Leucospermum* sp. in Australia. Santos & Alves (Santos et al. 2017) described *D. pyracanthae* from *Malus domestica* in Portugal as a distinct species based on DNA sequence data and morphological characters. The authors showed that although conidial dimensions of both species are similar, they differ in several nucleotide positions: 3 nucleotides in ITS, 1 nt in *tef1-α*, 8 nt in *tub2* and 2 nt in *his3*. Later, Hilário, Amaral, Santos & Alves (Hilário et al. 2020) described *D. rossmaniae* as a distinct but closely related species to *D. pyracanthae* and *D. leucospermi*. The authors have shown that although culture characteristics are slightly different, alpha and beta conidia dimensions are within the same ranges. Moreover, *D. rossmaniae*

differs from *D. leucospermi* in 3 nt in ITS, 3 in *tef1- α* , 2 nt in *his3* and 1 in *tub2* and from *D. pyracanthae* in 5 nucleotides in *tub2* and 2 in *tef1- α* (Hilário et al. 2020). However, we show in this study that *D. rossmaniae* is phylogenetically indistinguishable from *D. pyracanthae* and *D. leucospermi*.

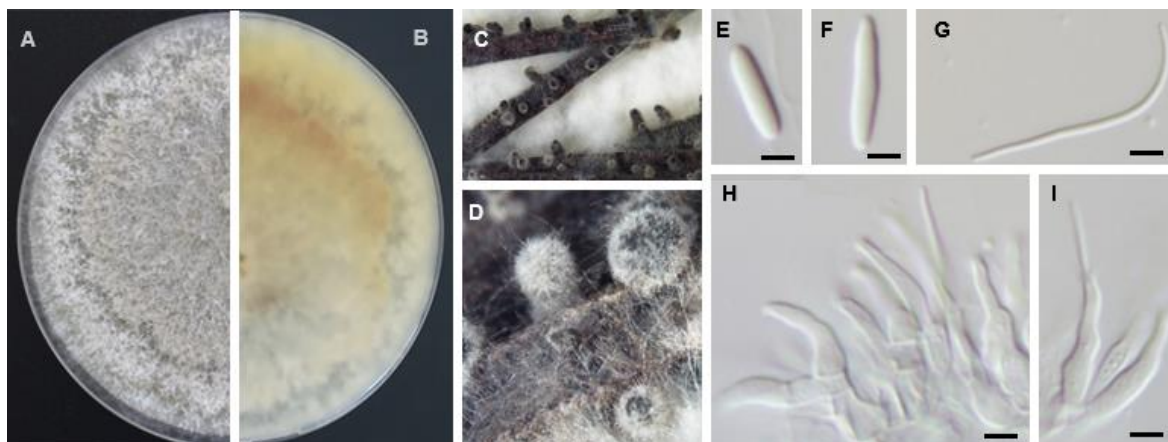


Figure 9. Morphology of *Diaporthe leucospermi*. **A, B.** Upper and reverse culture surface respectively (after 7 days at 25 °C). **C, D.** Conidiomata on pine needles. **E.** Alpha conidia. **F.** Gamma conidia. **G.** Beta conidia. **H.** Conidiophores arising from pseudoparenchyma. **I.** Conidiophores with beta conidia at their tip. Bars = 2.5 μ m

Diaporthe malorum Santos & Alves, *Mycosphere* **8**:489 (2017). MycoBank MB820226

Specimen examined: **Portugal. Aveiro:** Arouca (40°54'35.3"N 8°22'49.7"W) on twigs of *V. corymbosum*, 20 January 2020, S. Hilário, living culture: CAA972, CAA974. Description & Illustration (Hilário et al. 2022).

Host range: *Malus domestica* (Santos et al. 2017), *Eucalyptus globulus* (Lopes et al. 2021), *V. corymbosum*.

Known distribution: Portugal

Notes: The clade comprising *D. malorum* firstly described as the causal agent of twig canker and shoot blight of apples (*M. domestica*), also contains isolates from *E. globulus* and *V. corymbosum*.

Diaporthe rudis (Fr.) Nitschke, *Pyrenomyces Germanici* 2:282 (1870). (Fig. 10)

Specimen examined: **Portugal. Porto:** Arcozelo (41°15'31.8"N 8°28'57.8"W), from twig blight symptoms of *V. corymbosum*, 20 July 2019, S. Hilário, living culture: CAA991

Description: Sexual morph: Perithecial ascomata globose, solitary or in clusters. Perithecial necks brown to black, covered in white mycelium. Asci unitunicate elongate, 8-spored, (48.0–)49.2–53.5(–57.6) × (5.8–)6.0–6.6(–6.9) µm, (mean ± S.D. = 51.3 ± 3.1 × 6.3 ± 0.4 µm, *n* = 10). Ascospores hyaline, elongated, septate, frequently tetraguttulate with larger guttules at center, (9.7–)11.4–11.9(–13.2) × (2.1–)2.7–2.9(–3.6) µm, (mean ± S.D. = 11.6 ± 0.8 × 2.8 ± 0.3 µm, *n* = 50). Asexual morph: Conidiomata brown, erumpent from fennel stems, extruding white conidial mass. Conidiophores not observed. Paraphyses not observed. Alpha conidia ellipsoidal, biguttulate, with an obtuse apex and rounded at the other end, (5.4–)6.1–6.3(–7.0) × (2.1–)2.5–2.6(–2.9) µm, (mean ± S.D. = 6.2 ± 0.3 × 2.5 ± 0.2 µm, *n* = 100). Beta conidia not observed.

Mating type strategy: homothallism

Culture characteristics: In dark at 25 °C for 7 days, colonies on PDA relatively slow growing, white to pale brown zones developing in center, aerial mycelium, reverse with reddish concentric zones.

Host range: *Acer* sp., *Asphodelus albus*, *Aucuba japonica*, *Brugmansia* sp., *Castanea* sp., *Corylus* sp., *Dipsacus fullonum*, *Epilobium* sp., *Eucalyptus globulus*, *Fagus* sp., *Fraxinus* sp., *Holcus* sp., *Hydrangea* sp., *Ileostylis* sp., *Laburnum* sp., *Lupinus* sp., *Malus* sp., *Protea* sp., *Pyrus* sp., *Rosa* sp., *Sambucus* sp., *Salix* sp., *V. corymbosum* and *Vitis vinifera* (Farr & Rossman 2021).

Know distribution: Australia, Canada, Chile, Austria, Germany, Italy, Latvia, Portugal, Spain, Sweden, Switzerland, New Zealand and South Africa (Farr & Rossman 2021).

Notes: Diaporthe rudis, commonly associated to *Vitis vinifera*, it has been reported on a wide range of hosts including blueberries. Compared with the description of Udayanga et al. (2014), our isolate CAA991 has shorter and thinner ascospores ($11.6 \pm 0.8 \times 2.8 \pm 0.3 \mu\text{m}$ vs $13.2 \pm 1.1 \times 3.6 \pm 0.1 \mu\text{m}$), and longer conidiogenous cells. Besides that, beta conidia of isolate CAA991 were not found, whereas it was reported in the ex-type CBS 113201.

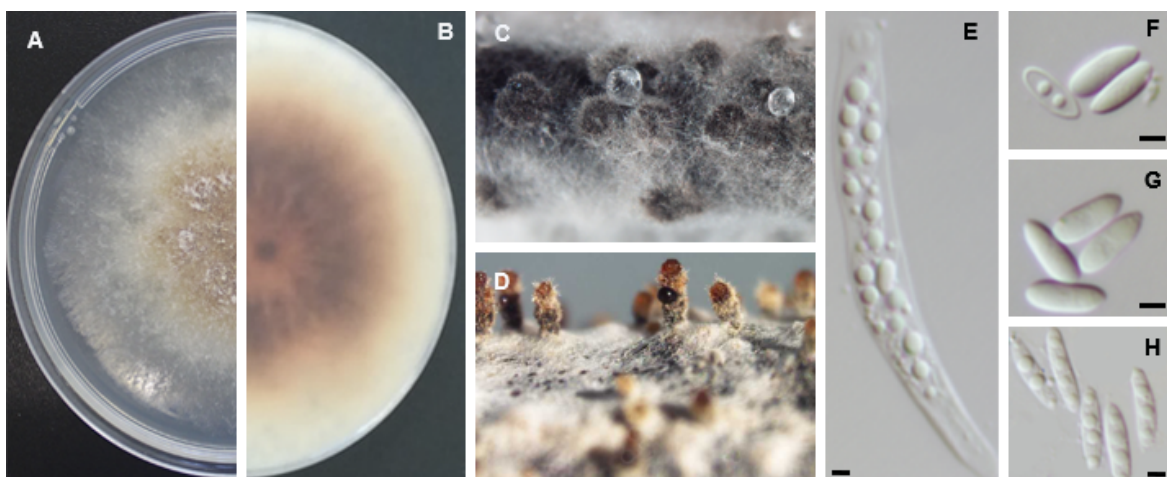


Figure 10. Morphology of *Diaporthe rudis*. **A, B.** upper and reverse culture surface respectively (after 7 days at 25 °C). **C.** Conidiomata on pine needles. **D.** Perithecial ascomata on fennel twigs. **E.** Ascus. **F, G.** Alpha conidia. **H.** Ascospores. Bars = 2.5 μm

Diaporthe hybrida Hilário & Alves *Fungal Biol.* **126**:62 (2022). MycoBank: MB838688

Specimen examined: **Portugal. Santarém:** Ourém (39°39'13.5"N 8°35'32.0"W), on twigs of *V. corymbosum*, 30 January 2020, S. Hilário, living culture: CAA998 (**MUM 21.01**). Description & Illustration (Hilário et al. 2022).

Notes: Diaporthe hybrida was the first hybrid described in this genus (Hilário et al. 2022), from cross between *D. portugallica* (Guarnaccia & Crous 2018) and *D. phillipsii* (Hilário et al. 2020).

DISCUSSION

Although a previous study identified a few species of *Diaporthe* as causal agents of twig blight and dieback diseases in the main blueberry growing region in the Center of Portugal (Hilário et al. 2020), the current study represents the first national survey to evaluate the distribution of *Diaporthe* on several blueberry

cultivars. Additionally, this study also gives an insight into the pathogenicity potential of *Diaporthe* species, including the well-known pathogen *D. vaccinii*, to some blueberry cultivars planted in Portugal.

Diaporthe foeniculina (formerly known as *Phomopsis theicola* and *D. neotheicola*) was first described on *Camellia sinensis* in Italy in 1927 (Santos & Phillips 2009), and since then it has been isolated from several different hosts including *Vitis vinifera*, *Protea* sp., *Pyrus* sp., *Citrus* sp. (Gomes et al. 2013; Mostert et al. 2001; van Niekerk et al. 2005), *Aspalathus linearis* (van Rensburg et al. 2006), *Foeniculum vulgare* (Santos & Phillips 2009) and *Prunus* sp. (Diogo et al. 2010). Later, Elfar et al. (2013) reported for the first time the presence of *D. foeniculina* in Chile, causing stem cankers on blueberries. Hilário et al. (2020) also found *D. foeniculina* occurring as endophyte or latent pathogen in asymptomatic branches and from dead plant material co-existing with *D. rudis*. The pathogenicity testes carried out by Elfar et al. (2013) and Hilário et al. (2020) showed that although causing cankers, it is reasonable to consider *D. foeniculina* as a weak pathogen on *Vaccinium corymbosum* plants.

Diaporthe rudis, (referred to as *D. viticola*) is a recognized fungal pathogen in Europe and New Zealand mostly associated to *Vitis vinifera* (Guarnaccia et al. 2018; Udayanga et al. 2014). This fungus has also been found on several hosts such as *Aucuba japonica*, *Fraxinus excelsior*, *Citrus* sp., *Acer* sp., and *Castanea sativa* and distributed worldwide (Gomes et al. 2013). Despite the presence of *D. rudis* occurring on blueberry plants in the Netherlands (Lombard et al. 2014), it is unclear whether the species was obtained from diseased or healthy plants or if pathogenicity tests were performed. On the contrary, Cardinaals et al. (2018) also isolated *D. rudis* in the Netherlands from shoot blight disease blueberries, whereas Hilário et al. (2020) isolated this species from diseased and asymptomatic plants. The present study records, for the second time, the occurrence of *D. rudis* on *V. corymbosum* in Portugal. Although it was the most dominant species found (38.8%), it may be claimed that the presence of *D. rudis* on blueberry just occurred as a result of high inoculum pressure, since most of the blueberry plantations were located nearby vineyards. Moreover, a recent study demonstrated that *D. rudis* cause minor symptoms on blueberry plants after artificial inoculations (Hilário et al. 2020). Taking

all this into consideration, this raises questions about the real impact of this species on blueberries, suggesting that *D. rudis* may be less prone to be a pathogen on blueberries.

Diaporthe ambigua was initially described on *Pyrus communis* in Germany, later on apple, pear and plums in South Africa (Smit et al. 1996); on grapevines in California (Úrbez-Torres et al. 2013); on *Foeniculum vulgare* in Portugal (Santos & Phillips 2009); on kiwi fruits in Greece (Thomidis et al. 2019) and on *V. corymbosum* in Chile (Elfar et al. 2013). Although *D. ambigua* has been claimed to be highly virulent in shoots, stems, and fruit of blueberries (Elfar et al. 2013) the records of this pathogen on blueberries are limited and unclear. In the present study, *D. ambigua* was recovered from one orchard only. Moreover, in a recent study, Spies et al. (2020) investigated twigs of 145 European olive trees in South Africa showing dieback and found out that *D. ambigua* was only recovered from a single European olive tree, and that its pathogenicity to this host was unknown. This occasional occurrence of *D. ambigua* on olives in South Africa and blueberries in Portugal, allied to the fact that this species has been found on blueberry dead stems, raises the possibility of a saprophytic behavior of *D. ambigua*. Such conclusion has been previously drawn by Santos & Phillips (2009), who proposed that *D. ambigua* may be purely saprophytic, taking advantage of dead plant material to grow.

Diaporthe leucospermi was firstly described from leaves of *Leucospermum* sp. in Australia in 2012 (Crous et al. 2011) and since then, no records of this species have been documented. However, Santos et al. (2010) collected the isolates Ph-C189/1, Ph-C180/1, Ph-C174/1 and Di-C007 from *Hydrangea macrophylla* and *Acer negundo* in Portugal. It is interesting to note that based on ITS and *tef1- α* available sequences, these isolates are deemed to fall within the concept of *D. leucospermi*. A pairwise comparison revealed that the Portuguese isolates are 100% identical to *D. leucospermi* in the ITS region, whereas some polymorphisms are shared among these isolates in *tef1- α* locus. Only 2 nucleotide differences and the presence of a 7 bp insertion (5' CCCCCC 3') in *tef1- α* region of isolates Ph-C189/1 and Di-C007 separate them from *D. leucospermi*, while no polymorphisms were observed among isolates Ph-C180/1 and Ph-C174/1 and *D. leucospermi*. However, further studies including other loci would be needed to resolve the identity of the Portuguese

isolates mentioned above. Later, Santos et al. (2017) and Hilário et al. (2020) described *D. pyracanthae* and *D. rossmaniae* as two different species, but they are shown in this study to be indistinguishable from *D. leucospermi*.

The distribution of *Diaporthe malorum* is only known from Portugal, where it was found in *M. domestica* (Santos et al. 2017) and *E. globulus* (Lopes et al. 2021). The present study reports for the first time the presence of this species in blueberries. *Diaporthe crousii*, firstly described as a pathogen on *V. corymbosum* in Portugal (Hilário et al. 2020), was also found in *E. globulus* (Lopes et al. 2021).

Diaporthe amygdali (= *Phomopsis amygdali*), has been reported worldwide on a wide range of hosts (Udayanga et al. 2012). In a recent study, a monophyletic clade containing *D. amygdali* and closely related species was resolved, by applying the principle of Genealogical Concordance Phylogenetic Species Recognition (GCPSR) and the coalescent-based species delimitation methods (Hilário et al. 2021a). Apart from the report of *D. sterilis* (syn. *D. amygdali*), causing cankers and twig blight on *V. corymbosum* in Italy (Lombard et al. 2014), the present study reports for the second time the presence of *D. amygdali* associated with twig blight of blueberry plants.

Diaporthe hybrida, described as the first hybrid in the genus *Diaporthe* (Hilário et al. 2022) was also pathogenic to blueberry, but the incidence of this species in the survey was low, given that its presence was restricted to one plantation only (Ourém). Therefore, it remains unclear the impact of this new hybrid pathogen on blueberry orchards.

Pathogenicity tests were performed using nine-month-old blueberry plants, that determined the capacity of *Diaporthe* isolates to cause lesions on this crop. All *Diaporthe* species inoculated to blueberry plants cv. 'Duke', 'Legacy' and 'Spartan' were able to cause lesions. The most severe symptoms were detected on blueberry twigs inoculated with *D. eres* (CAA829) in cultivar 'Duke', which caused the death of all replicates. *Diaporthe hybrida* was also found to cause necrosis when inoculated in cultivar Duke. It is noteworthy that this species was able to cause significantly larger lesions than its parental species (*D. phillipsii*) (Hilário et al. 2022), which is corroborated by studies that state that hybrids are thought to be important for the evolution of fungal plant pathogens, increasing their virulence on the host

(Möller & Stukenbrock 2017). As hybridization plays an important role in the spread of pathogenicity traits, further genetic analysis of *D. hybrida* would be essential to establish new insights into the impact of this new virulent pathogen, which may affect blueberry plants. Lombard et al. (2014) have shown that *D. sterilis* (syn. *D. amygdali*) caused brown lesions developing on the green stems and twigs, resulting in twig blight on cultivar 'Legacy'. Likewise, in the present study, the isolate CAA958 (*D. amygdali*) not only caused mortality of one out of five replicates in the cultivar 'Legacy', as caused the longest lesions in this cultivar, when compared to the other *Diaporthe* species. Overall *D. amygdali* and *D. eres* showed to be one of the most virulent species, while *D. ambigua*, *D. foeniculina*, *D. rudis* and *D. leucospermi* yielded the lowest lesion lengths, and thus regarded as the least virulent species.

Although *Diaporthe vaccinii* was earlier considered as a quarantine pathogen for the European Union (EU Regulation 2016/2031), the recent EU Regulation (2019/2072) does not include the species in the current list of EU quarantine pests. However, the impact and pathogenicity potential of *D. vaccinii* was never entirely explored (van Bruggen et al. 2018). It is worthy to note that *D. vaccinii* was not found during our survey across the country, and no records have been reported in Europe in the past few years (EPPO 2021). Nabetani et al. (2017) have shown that *D. vaccinii* might be the major causal agent of twig blight on blueberry plants in British Columbia and found that the cultivar 'Duke' was shown to be more susceptible to *D. vaccinii*. Contrarily, Cardinaals et al. (2018) tested *D. vaccinii* on cultivars 'Duke' and 'Liberty' but revealed that the symptoms caused by this pathogen are insignificant, and thus it may not represent a major threat to commercial blueberry productions. Currently, it is known that it has been eradicated from all European countries where it was earlier detected (Jeger et al. 2017). This can also be a proof that *D. vaccinii* might have been wrongly identified, as also suggested by Lombard et al. (2014) and Elfar et al. (2013), as its identification was previously based on its Phomopsis-like conidia and host association. According to our pathogenicity tests, the cultivar 'Duke' was the most susceptible to *D. eres* infection. Moreover, we also demonstrated that *D. eres* strain CBS 160.32 (syn. *D. vaccinii*) caused similar lesion lengths to *D. eres* strains CAA829 and CAA830, and it was not aggressive, as has been recurrently described in the literature. Such results corroborate the hypothesis

that *D. vaccinii* is a synonym of *D. eres*, and that this species not only harbors intraspecific variability (Hilário et al. 2021b) but also differences in virulence among isolates. Furthermore, it is noteworthy that the pathogenicity trials carried out in this study were based solely on one strain of *D. vaccinii* (ex-type CBS 160.32). This strain has been kept in culture for over 90 years, which might have affected its virulence, leading to loss of its pathogenicity. Therefore, this study provides evidence about the capability of *D. eres* to cause disease on *V. corymbosum*, which is more aggressive than the well-known host-specific strain CBS 160.32. As previously suggested by Cardinaals et al. (2018) and supported by our results, the strain CBS 160.32 might not represent a threat to blueberry orchards in Europe.

It is also worth mentioning that the *Diaporthe* species identified in this study were found to be co-existing in the same plant material with members of *Botryosphaeriaceae* and *Pestalotiopsis*. Such an occurrence is not new, as it has been previously reported (Elfar et al. 2013; Espinoza et al. 2008, 2009; Moral et al. 2017). This should not be overlooked, and it deserves further investigation, given that the species of *Diaporthe*, together with other pathogenic fungi (Lorenzini & Zapparoli 2019), may contribute to cause dieback and twig blight of blueberries.

CONCLUSIONS

The present study is the first evaluation of *Diaporthe* species associated with blueberries from several orchards in Portugal, combining morphology and molecular data, which provide useful information for evaluating pathogenicity of the several species and in different blueberry cultivars. To our knowledge, this study represents also the first report of *D. leucospermi*, *D. amygdali* and *D. malorum* associated with blueberries, and of *D. ambigua* on this host in Europe. We have also demonstrated that strain CBS 160.32 (*D. eres*) did not cause the death of any plant inoculated and that the symptoms caused were minor, when compared to other isolates, indicating that this strain may not be a threat to *Vaccinium* plantations. However, it is important to highlight that *D. amygdali* together with *D. eres* (strains CAA829 and CAA830) were the most aggressive species, indicating the importance of *D. eres* as a pathogen of blueberries. Moreover, pathogenicity studies coupled with morpho-

physiological and biochemical parameters will be required to further clarify the pathogenic role and the impact of *Diaporthe* on the physiology of blueberry.

ACKNOWLEDGMENTS

This research was funded by the Portuguese Foundation for Science and Technology (FCT/MCTES) for financing CESAM (Centre for Environmental and Marine Studies) (UIDP/50017/2020 + UIDB/50017/2020) through national funds, and the PhD grants of Sandra Hilário (SFRH/BD/137394/2018). Liliana Santos is funded by national funds (OE), through FCT in the scope of the framework contract foreseen in the numbers 4, 5 and 6 of the article 23, of the Decree-Law 57/2016, of August 29, changed by Law 57/2017, of July 19.

The authors are thankful to Portuguese producers for supplying the plant material from their plantations: Hugo Botelho and Pedro Pinho (Bfruit Nature Flavors), Hugo Lains (WePlant in Portugal), Nuno Silveira (Visionagro, Lda), Helder Moreira (Valxisto, Unipes-soal, Lda), Jorge Duarte, João Vieira, António Rodrigues, Ana Moreira (Hortitool Consulting, Lda), Marcelo Miranda and Monica (Groselh&Mirtilo), Rui Marinho (Quinta da Hortelã), Odete Gonçalves (Bluepanoply), Diana Lopes and Mara Almeida (Acegrow), and Paulo. We want also to thank Deifil Green Biotechnology LDA for supplying the plant material for the pathogenicity tests, and Eduardo Batista (University of Aveiro) for helping with the inoculation of plants.

REFERENCES

- Baker JB, Hancock JF, Ramsdell DC. **1995**. Screening highbush blueberry cultivars for resistance to *Phomopsis* canker. *HortScience* 30, 586–588.
- Cardinaals J, Wenneker M, Voogd JGB, van Leeuwen GCM. **2018**. Pathogenicity of *Diaporthe* spp. on two blueberry cultivars (*Vaccinium corymbosum*). *EPPO Bulletin* 48, 128–134.
- Crous PW, Summerell BA, Swart L, Denman S, Taylor JE, Bezuidenhout CM, Palm ME, Marinowitz S. **2011**. Fungal pathogens of *Proteaceae*. *Persoonia* 27, 20–45.

- Diogo ELF, Santos JM, Phillips AJL. **2010**. Phylogeny, morphology and pathogenicity of *Diaporthe* and *Phomopsis* species on almond in Portugal. *Fungal Diversity* 44, 107–115.
- Dissanayake AJ, Camporesi E, Hyde KD, Wei Z, Yan JY, Li XH. **2017**. Molecular phylogenetic analysis reveals seven new *Diaporthe* species from Italy. *Mycosphere* 8, 853–877.
- Elfar K, Torres R, Díaz GA, Latorre B. **2013**. Characterization of *Diaporthe australafricana* and *Diaporthe* spp. associated with stem canker of blueberry in Chile. *Plant Disease* 97, 1042–1050.
- European and Mediterranean Plant Protection Organization (EPPO). EPPO A2 List of Pests Recommended for Regulation as Quarantine Pests. Available online https://www.eppo.int/ACTIVITIES/plant_quarantine/A2_list (accessed on 30 May 2021).
- Espinoza JG, Briceño EX, Keith LM, Latorre BA. **2008**. Canker and twig dieback of blueberry caused by *Pestalotiopsis* spp. and a *Truncatella* sp. in Chile. *Plant Disease* 92, 1407–1414.
- Espinoza JG, Briceño EX, Chávez ER, Úrbez-Torres JR, Latorre BA. **2009**. *Neofusicoccum* spp. associated with stem canker and dieback of blueberry in Chile. *Plant Disease* 93, 1187–1194.
- Farr DF, Castlebury LA, Rossman AY. **2002**. Morphological and molecular characterization of *Phomopsis vaccinii* and additional isolates of *Phomopsis* from blueberry and cranberry in the eastern United States. *Mycologia* 94, 494–504.
- Farr DF, Rossman AY. **2021**. Fungal Databases, U.S. National Fungus Collections, ARS, USDA. Available online <https://nt.ars-grin.gov/fungalDATABASES/> (accessed 10 May 2021).
- Food and Agriculture Organization of the United Nations (FAOSTAT). **2021**. Available online: <http://www.fao.org/faostat/en/#home> (accessed on 30 May 2021).
- Fu M, Crous PW, Bai Q, Zhang PF, Xiang J, Guo YS, Zhao FF, Yang MM, Hong N, Xu WX, Wang GP. **2019**. *Colletotrichum* species associated with anthracnose of *Pyrus* spp. in China. *Persoonia* 42, 1–35.

- Gomes RR, Glienke C, Videira SIR, Lombard L, Groenewald JZ, Crous PW. **2013**. *Diaporthe*: A genus of endophytic, saprobic and plant pathogenic fungi. *Persoonia* 31, 1–41.
- Gonçalves C, Guiné RPF, Teixeira D, Gonçalves FJ. **2015**. Evaluation of bioactive phenols in blueberries from different cultivars. *International Journal of Food, Veterinary and Agricultural Engineering* 9, 281–284.
- Guarnaccia V, Groenewald JZ, Woodhall J, Armengol J, Cinelli T, Eichmeier A, Ezra D, Fontaine F, Gramaje D, Gutierrez-Aguirregabiria A, ... Crous, PW. **2018**. *Diaporthe* diversity and pathogenicity revealed from a broad survey of grapevine diseases in Europe. *Persoonia* 40, 135–153.
- Guarnaccia V, Crous PW. **2018**. Species of *Diaporthe* on *Camellia* and *Citrus* in the Azores Islands. *Phytopathologia Mediterranea* 57, 307–319.
- Hilário S, Amaral AI, Gonçalves MFM, Lopes A, Santos L, Alves A. **2020**. Diversity and pathogenicity of *Diaporthe* species on blueberry plants in Portugal, with description of 4 new species. *Mycologia* 112, 293–308.
- Hilário S, Santos L, Alves A. **2021a**. *Diaporthe amygdali*, a species complex or a complex species? *Fungal Biology* 125, 505–518.
- Hilário S, Gonçalves MFM, Alves A. **2021b**. Using genealogical concordance and coalescent-based species delimitation to assess species boundaries in the *Diaporthe eres* complex. *Journal of Fungi* 7, 507.
- Hilário S, Santos L, Phillips AJL, Alves A. **2022**. Caveats of the internal transcribed spacer region as a barcode to resolve species boundaries in *Diaporthe*. *Fungal Biology* 126, 54–74.
- Jeger M, Bragard C, Caffier D, Candresse T, Chatzivassiliou E, Dehnen-Schmutz K, Gilioli G, Grégoire JC, Miret J, MacLeod A, ... van Bruggen AHC. **2017**. Pest risk assessment of *Diaporthe vaccinii* for the EU territory. *EFSA Journal* 15, 1–185.
- Lombard L, Van Leeuwen GCM, Guarnaccia V, Polizzi G, Van Rijswick PCJ, Rosendahl CHM, Gabler J, Crous PW. **2014**. *Diaporthe* species associated with *Vaccinium*, with specific reference to Europe. *Phytopathologia Mediterranea* 53, 287–299.

- Lopes AF, Batista E, Hilário S, Santos L, Alves A. **2021**. Occurrence of *Diaporthe* species in *Eucalyptus globulus*, *Pinus pinaster* and *Quercus suber* in Portugal. *Forest Pathology* 51, e12674.
- Lorenzini M, Zapparoli G. **2019**. *Diaporthe rudis* associated with berry rot of postharvest grapes in Italy. *Plant Disease* 103, 1030.
- Madeira BSP. **2006**. *Cultura do Mirtilo*. Agrobok: Portugal, 2016. pp. 200.
- Mathew FM, Olson TR, Science P, Dakota S. **2018**. Identification of sunflower (*Helianthus annuus*) accessions resistant to *Diaporthe helianthi* and *Diaporthe gulyae*. *Plant Health Progress* 19, 97–102.
- Möller M, Stukenbrock EH. **2017**. Evolution and genome architecture in fungal plant pathogens. *Nature Reviews Microbiology* 15, 756–771.
- Moral J, Agustí-Brisach C, Pérez-Rodríguez M, Xaviér C, Raya MC, Rhouma A, Trapero A. **2017**. Identification of fungal species associated with branch dieback of olive and resistance of table cultivars to *Neofusicoccum mediterraneum* and *Botryosphaeria dothidea*. *Plant Disease* 101, 306–316.
- Mostert L, Crous PW, Kang JC, Phillips AJL. **2001**. Species of *Phomopsis* and a *Libertella* sp. occurring on grapevines with specific reference to South Africa: morphological, cultural, molecular and pathological characterization. *Mycologia* 93, 146–167.
- Nabetani K, Wood BK, Sabaratnam S. **2017**. Role of pycnidia in twig and blossom blight and stem dieback of highbush blueberry caused by *Phomopsis vaccinii* in British Columbia. *Canadian Journal of Plant Pathology* 39, 405–421.
- Pinto R. **2015**. Melhoria das técnicas culturais na produção de mirtilo em substrato. Master Thesis, University of Lisbon, Lisbon, Portugal. Available online <https://www.repository.utl.pt/bitstream/10400.5/11157/1/Tese%20Rita%20Pinto.pdf> (accessed on 21 February 2021).
- Portal do Instituto Nacional de Estatística (INE). **2021**. Estatísticas agrícolas 2020. Available online <https://www.ine.pt/xurl/pub/437147278> (accessed on 10 July 2021).
- R Core Team. **2021**. R: A Language and Environment for Statistical Computing; R Foundation for Statistical Computing: Vienna, Austria. Available online <https://www.R-project.org/> (accessed on 14 February 2021).

- Retamales JB, Hancock JF. **2012**. *Blueberries*; CAB International. pp. 323.
- Rodríguez-Gálvez E, Hilário S, Lopes A, Alves A. **2020**. Diversity and pathogenicity of *Lasiodiplodia* and *Neopestalotiopsis* species associated with stem blight and dieback of blueberry plants in Peru. *European Journal of Plant Pathology* 157, 89–102.
- Santos JM, Correia VG, Phillips AJL. **2010**. Primers for mating-type diagnosis in *Diaporthe* and *Phomopsis*: their use in teleomorph induction in vitro and biological species definition. *Fungal Biology* 114, 255–270.
- Santos JM, Phillips AJL. **2009**. Resolving the complex of *Diaporthe* (*Phomopsis*) species occurring on *Foeniculum vulgare* in Portugal. *Fungal Diversity* 34, 111–125.
- Santos L, Phillips AJL, Crous PW, Alves A. **2017**. *Diaporthe* species on *Rosaceae* with descriptions of *D. pyracanthae* sp. *Mycosphere* 8, 485–511.
- Scarlett KA, Shuttleworth LA, Collins D, Rothwell CT, Guest DI, Daniel R. **2018**. *Botryosphaerales* associated with stem blight and dieback of blueberry (*Vaccinium* spp.) in New South Wales and Western Australia. *Australasian Plant Pathology* 48, 45–57.
- Silva S, Costa EM, Veiga M, Morais R.M, Calhau C, Pintado M. **2020**. Health promoting properties of blueberries: A review. *Critical Reviews in Food Science and Nutrition* 60, 181–200.
- Smit WA, Wingfield MJ, Wingfield BD. **1996**. A new canker disease of apple, pear, and plum rootstocks caused by *Diaporthe ambigua* in South Africa. *Plant Disease* 80, 1331–1335.
- Spies CFJ, Mostert L, Carlucci A, Moyo P, Van Jaarsveld WJ, du Plessis IL, van Dyk M, Halleen F. **2020**. Dieback and decline pathogens of olive trees in South Africa. *Persoonia* 45, 196–220.
- Syme P. **2021**. Werner's nomenclature of colours. A recreation of the original 1821 color guidebook with new cross references, photographic examples, and posters designed by Nicholas Rougeux. Available online <https://www.c82.net/werner/> (accessed on 21 April 2021).

- Thomidis T, Prodromou I, Zambounis A. **2019**. Occurrence of *Diaporthe ambigua* Nitschke causing postharvest fruit rot on kiwifruit in Chrysoupoli Kavala, Greece. *Journal of Plant Pathology* 101, 1295–1296.
- Udayanga D, Castlebury LA, Rossman A, Hyde KD. **2014**. Species limits in *Diaporthe*: a molecular reassessment of *D. citri*, *D. cytospora*, *D. foeniculina* and *D. rudis*. *Persoonia* 32, 83–101.
- Udayanga D, Liu X, Crous PW, McKenzie EH, Chukeatirote E, Hyde KD. **2012**. A multi-locus phylogenetic evaluation of *Diaporthe* (*Phomopsis*). *Fungal diversity* 56, 157–171.
- Udayanga D, Liu X, McKenzie EHC, Chukeatirote E, Bahkali AHA, Hyde KD. **2011**. The genus *Phomopsis*: Biology, applications, species concepts and names of common phytopathogens. *Fungal Diversity* 50, 189–225.
- Úrbez-Torres JR, Peduto F, Smith RJ, Gubler WD. **2013**. *Phomopsis* dieback, a grapevine trunk disease caused by *Phomopsis viticola* in California. *Plant Disease* 97, 1571–1579.
- van Bruggen AHC, West JS, van der Werf W, Potting RPJ, Gardi C, Koufakis I, Zelenev VV, Narouei-Khandan H, Shilder A, Harmon P. **2018**. Input data needed for a risk model for the entry, establishment and spread of a pathogen (*Phomopsis vaccinii*) of blueberries and cranberries in the EU. *Annals of Applied Biology* 172, 126–147.
- van Niekerk JM, Groenewald JZ, Farr DF, Fourie PH, Halleen F, Crous PW. **2005**. Reassessment of *Phomopsis* species on grapevines. *Australasian Plant Pathology* 34, 27–39.
- van Rensburg JCJ, Lamprecht SC, Groenewald JZ, Castlebury LA, Crous PW. **2006**. Characterisation of *Phomopsis* spp. associated with die-back of rooibos (*Aspalathus linearis*) in South Africa. *Studies in Mycology* 55, 65–74.
- Vilka L, Volkova J. **2015**. Morphological diversity of *Phomopsis vaccinii* isolates from cranberry (*Vaccinium macrocarpon* Ait.) in Latvia. *Proceedings of the Latvia University of Agriculture* 33, 8–18.
- Weingartner DP, Klos EJ. **1975**. Etiology and symptomatology of canker and dieback diseases on blueberry caused by *Fusicoccum* and *Diaporthe*. *Phytopathology* 65, 105–110.

- Wickham H. **2016**. *ggplot2: Elegant Graphics for Data Analysis*, 2nd ed.; Springer-Verlag: New York, pp. 268.
- Yang Q, Fan X-L, Guarnaccia V, Tian C-M. **2018**. High diversity of *Diaporthe* species associated with dieback diseases in China, with twelve new species described. *MycoKeys* 39, 97–149.

SUPPLEMENTARY MATERIAL

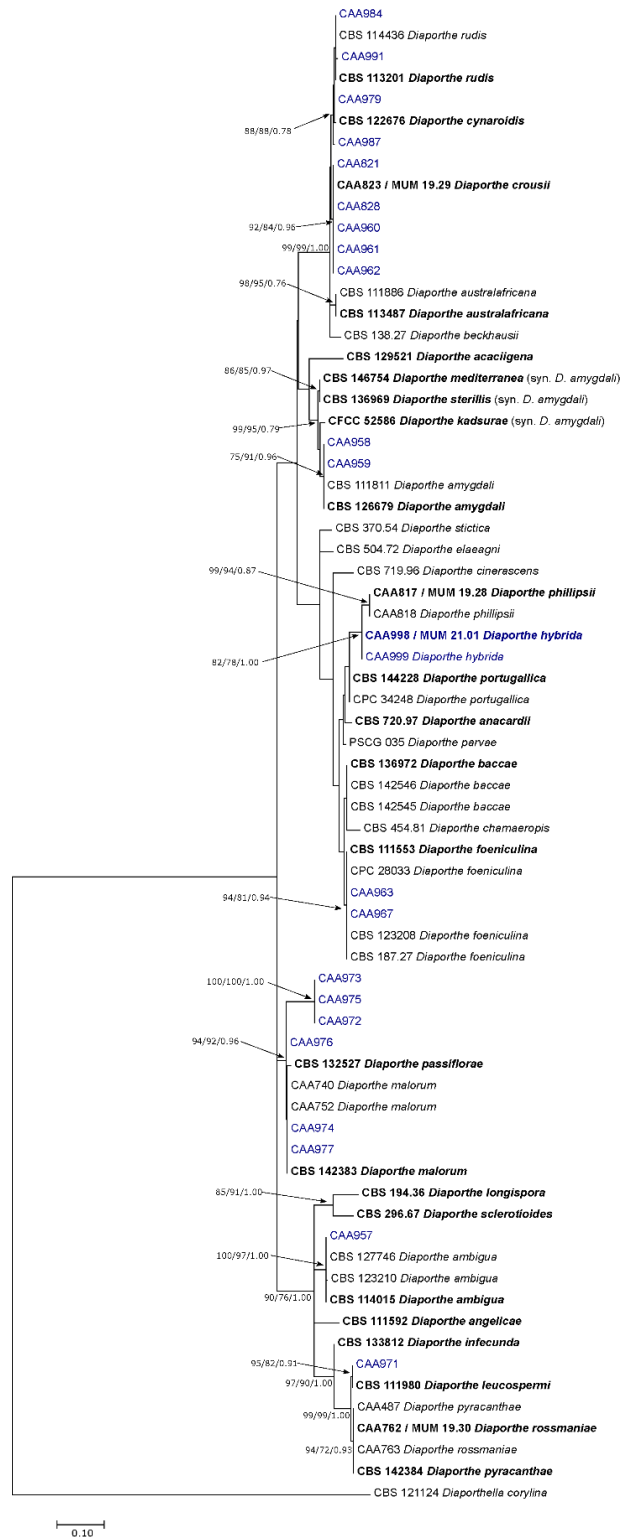


Figure S1. Phylogram generated from Maximum Likelihood analysis based on combined ITS sequence data from *Diaporthe* species. The ML tree is drawn to scale and rooted to *Diaporthella corylina*. ML and MP bootstrap values greater than 70% and posterior probabilities (PPs) greater than 0.80 are shown at the nodes. The ex-type strains are in bold.

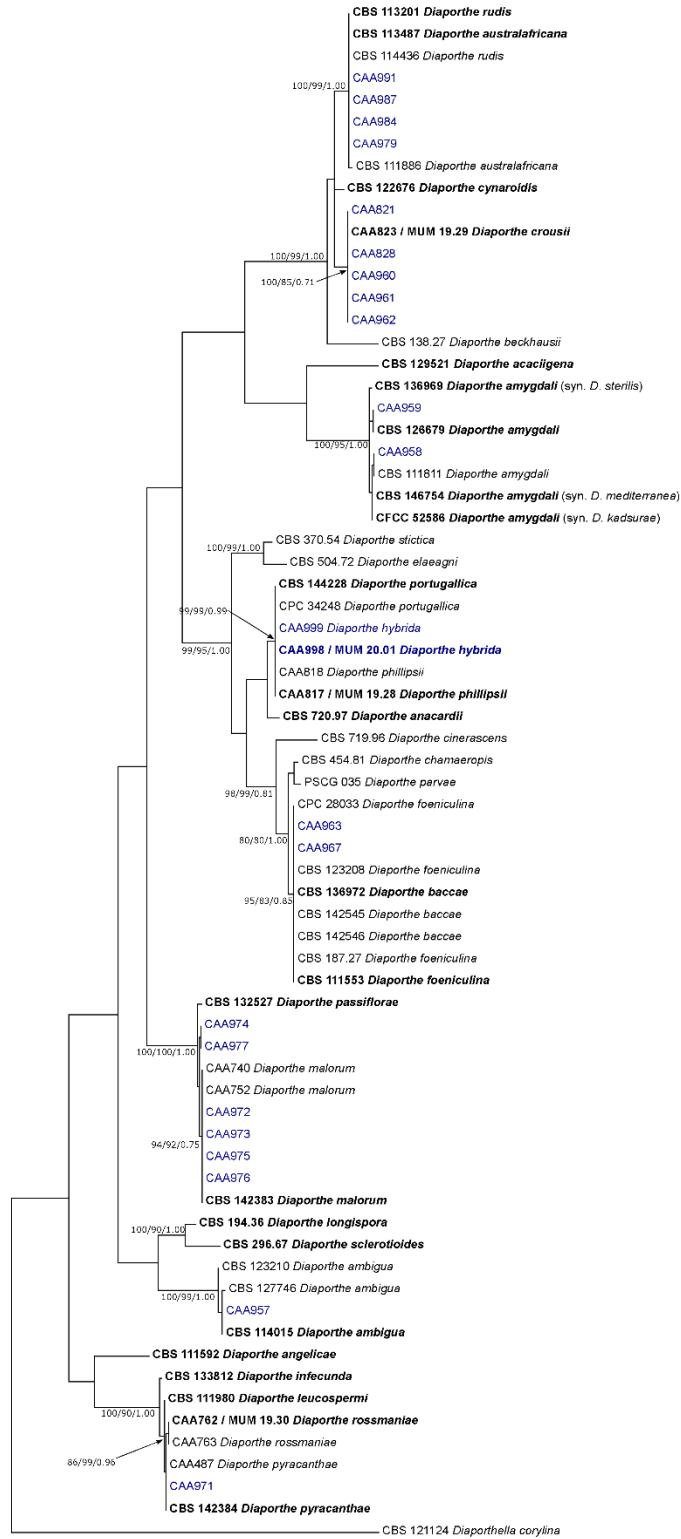


Figure S2. Phylogram generated from Maximum Likelihood analysis based on *tef1-α* sequence data from *Diaporthe* species. The ML tree is drawn to scale and rooted to *Diaporthella corylina*. ML and MP bootstrap values greater than 70% and posterior probabilities (PPs) greater than 0.80 are shown at the nodes. The ex-type strains are in bold.

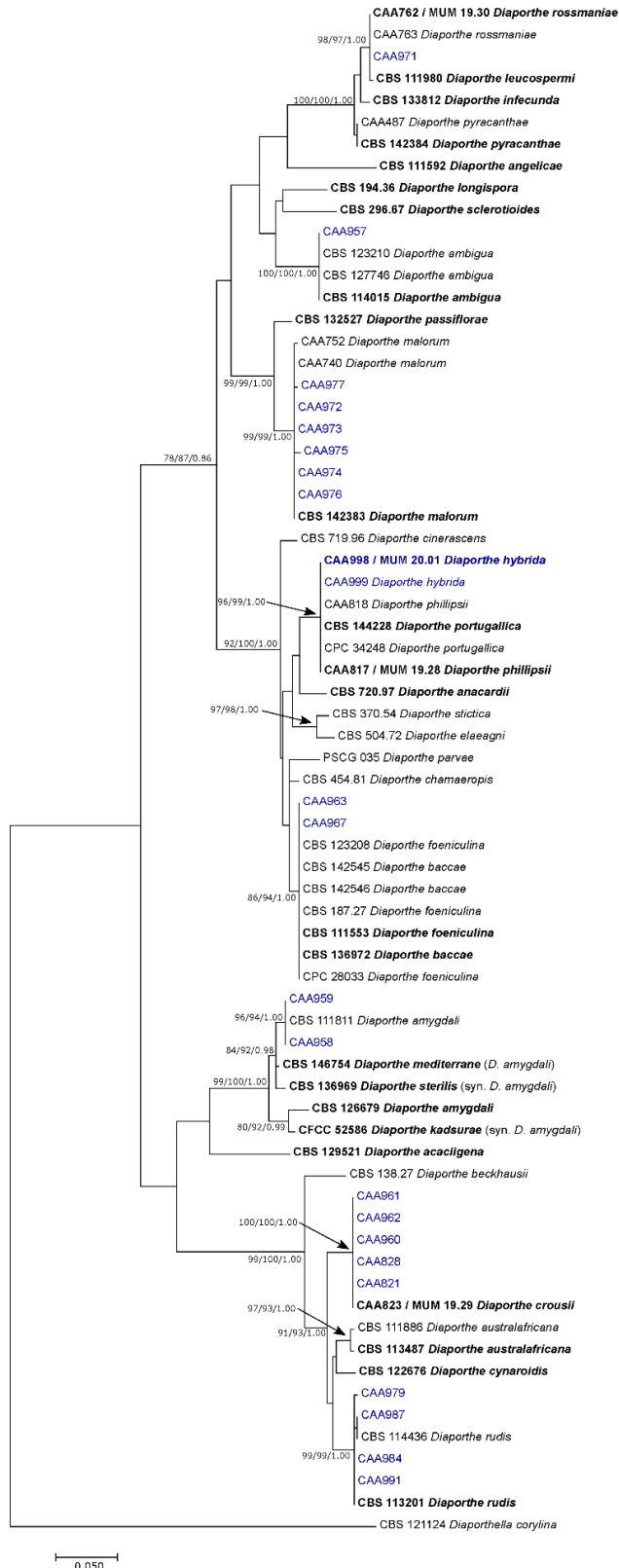


Figure S3. Phylogram generated from Maximum Likelihood analysis based on *tub2* sequence data from *Diaporthe* species. The ML tree is drawn to scale and rooted to *Diaporthella corylina*. ML and MP bootstrap values greater than 70% and posterior probabilities (PPs) greater than 0.80 are shown at the nodes. The ex-type strains are in bold.

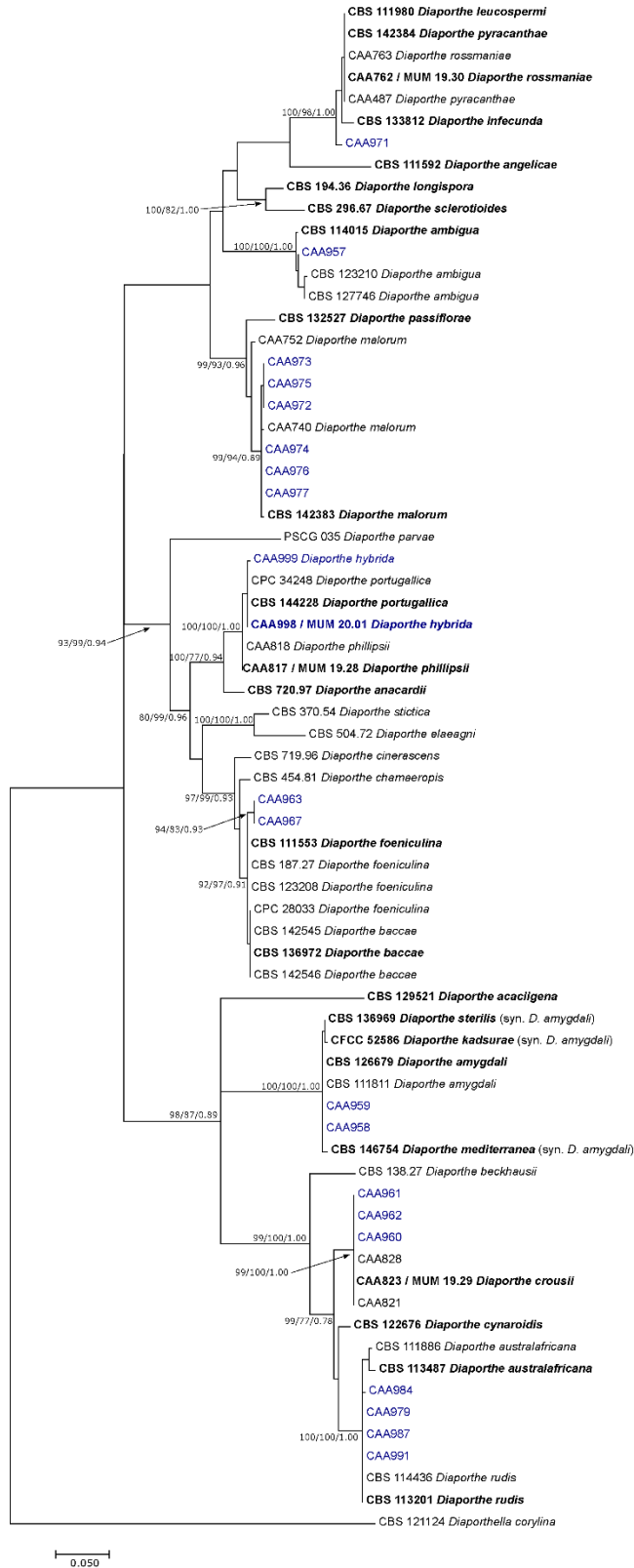


Figure S4. Phylogram generated from Maximum Likelihood analysis based on *cal* sequence data from *Diaporthe* species. The ML tree is drawn to scale and rooted to *Diaporthella corylina*. ML and MP bootstrap values greater than 70% and posterior probabilities (PPs) greater than 0.80 are shown at the nodes. The ex-type strains are in bold.

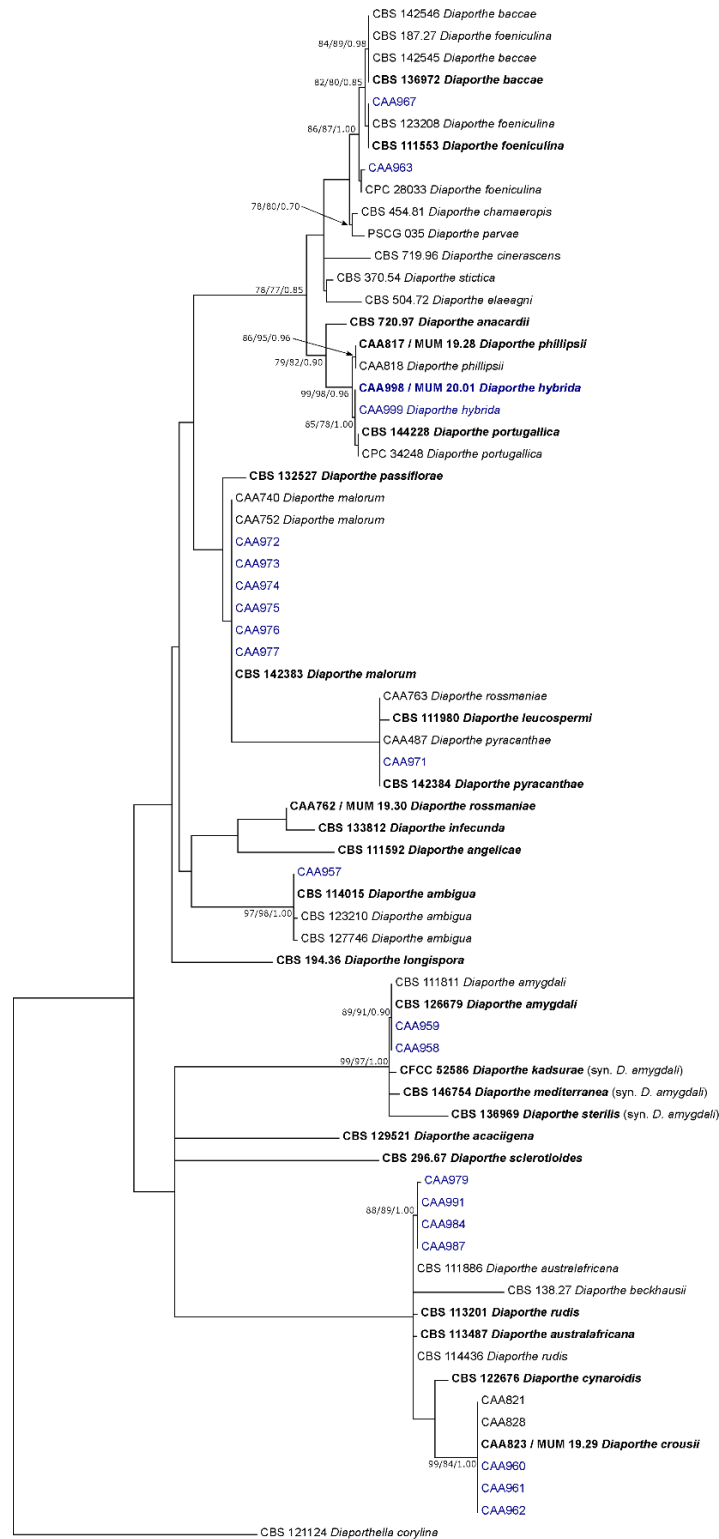


Figure S5. Phylogram generated from Maximum Likelihood analysis based on combined *his3* sequence data from *Diaporthe* species. The ML tree is drawn to scale and rooted to *Diaporthella corylina*. ML and MP bootstrap values greater than 70% and posterior probabilities (PPs) Bayesian analysis greater than 0.80 are shown at the nodes. The ex-type strains are in bold.

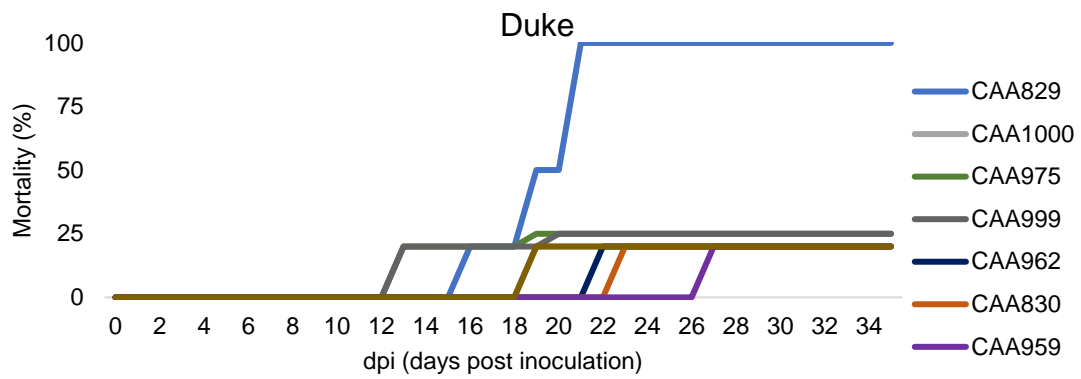


Figure S6. Time course percentage of mortality of cultivar 'Duke', after inoculation with different isolates.

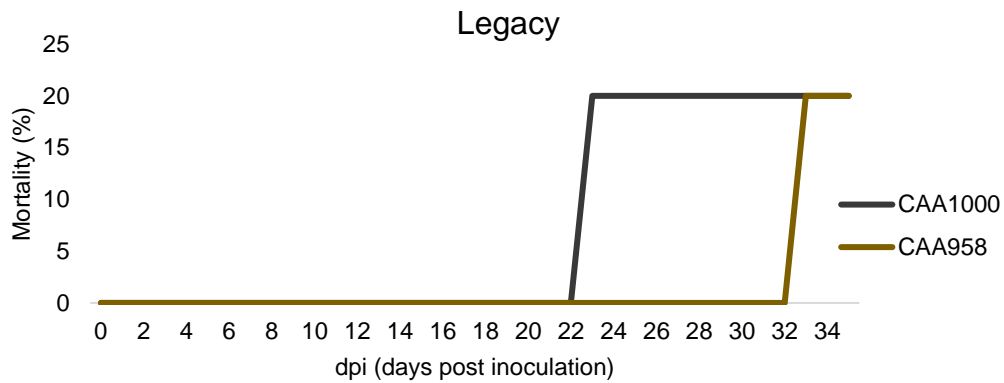


Figure S7. Time course percentage of mortality of cultivar 'Legacy', after inoculation with different isolates.

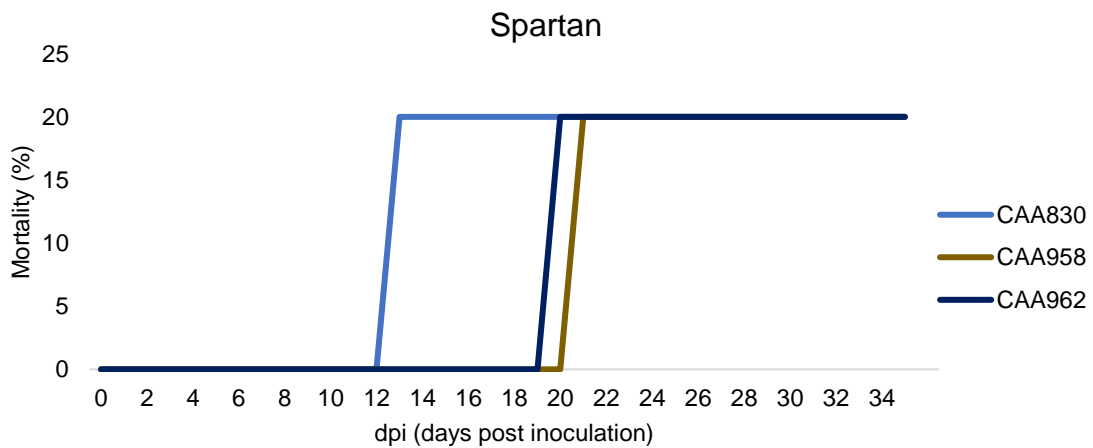


Figure S8. Time course percentage of mortality of cultivar 'Spartan', after inoculation with different isolates.

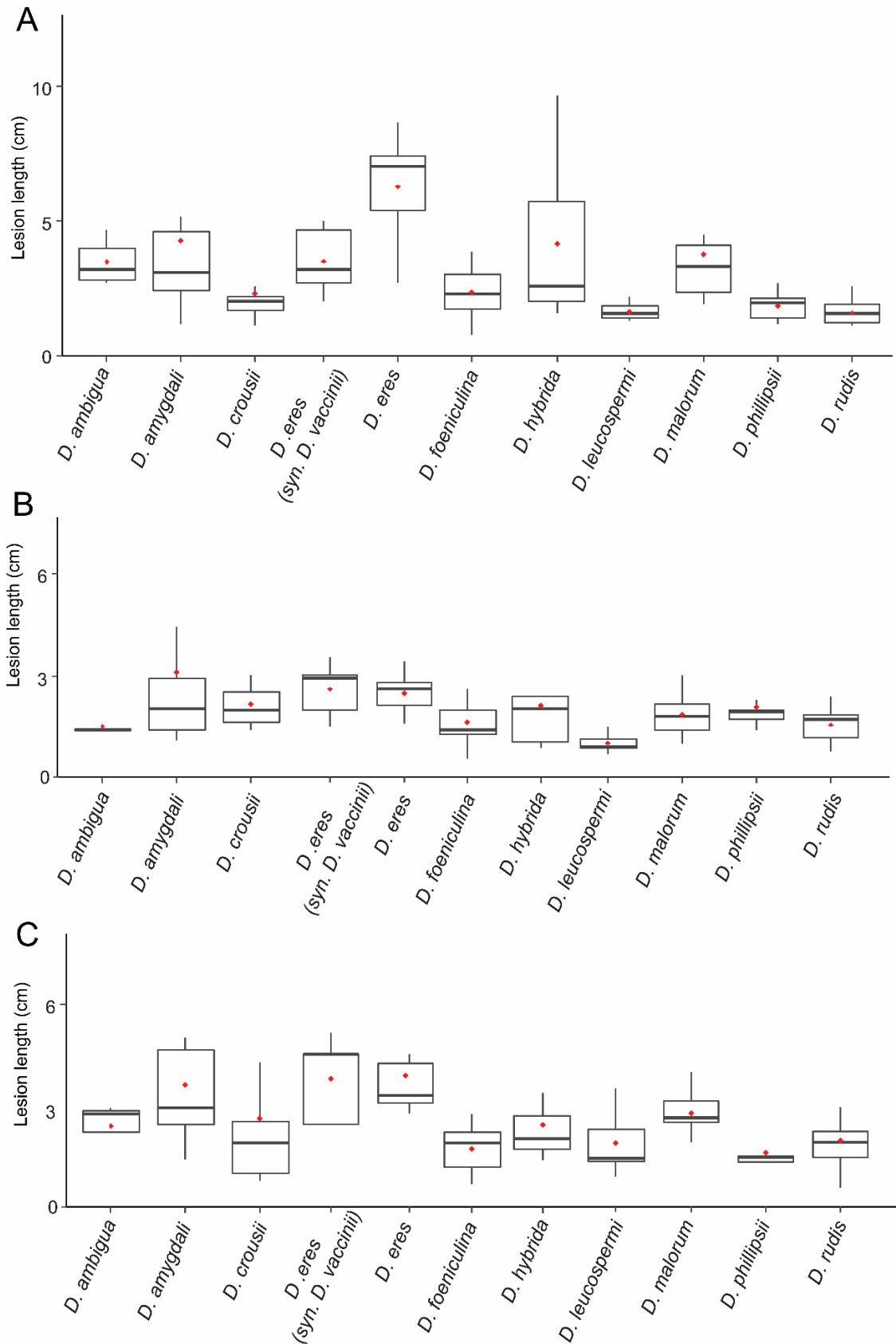


Figure S9. Box plot of lesion length (cm) caused by *Diaporthe* species on blueberry twigs of cultivars 'Duke' (A), 'Legacy' (B) and 'Spartan' (C). Black lines in the boxes show medians, and red dots represent the means. Species were compared according to the Wilcoxon rank sum test.

Table S1. Cases of *Diaporthe* species found alone or co-existing (+) with other species in the same plant material surveyed.


	Plantation	Location	Propagation method	Species
1	Soil plantation	Arouca	Micropropagation	<i>D. malorum</i> ^a <i>D. amygdali</i> + <i>D. crousii</i>
2	Potted plantation	Ourém	Micropropagation	<i>D. ambigua</i> ^a <i>Diaporthe hybrida</i> + <i>D. rudis</i>
3	Soil plantation	Alpiarça	Stem cutting	<i>D. rudis</i> ^a
4	Soil plantation	Penafiel	Micropropagation	<i>D. crousii</i> + <i>D. rudis</i> + <i>D. foeniculina</i>
5	Soil plantation	Póvoa de Lanhoso	Micropropagation	<i>D. malorum</i> ^a <i>D. rudis</i> ^a
6	Soil plantation	Urgezes	Micropropagation	<i>D. rudis</i> + <i>D. malorum</i> + <i>D. foeniculina</i> <i>D. malorum</i> ^a <i>D. rudis</i> ^a
7	Soil plantation	Agrela	Micropropagation	<i>D. rudis</i> + <i>D. foeniculina</i> <i>D. rudis</i> + <i>D. leucospermi</i> + <i>D. malorum</i> <i>D. rudis</i> ^a <i>D. amygdali</i> ^a
8	Soil plantation	Monte Córdova	Micropropagation	<i>D. malorum</i> ^a <i>D. foeniculina</i> ^a
9	Soil plantation	Arcozelo	Micropropagation	<i>D. malorum</i> ^a <i>D. foeniculina</i> ^a <i>D. rudis</i> ^a <i>D. rudis</i> + <i>D. malorum</i>
10	Soil plantation	Idanha-a-Nova	Micropropagation	<i>D. rudis</i> ^a
11	Soil plantation	Águeda	Micropropagation	<i>D. rudis</i> ^a <i>D. foeniculina</i> ^a
12	Soil plantation	Mangualde	Micropropagation	<i>D. rudis</i> ^a <i>D. foeniculina</i> ^a

^aSpecies found without co-occurrence of other members of *Diaporthe*



CHAPTER 3

Coalescent models and phylogenetic networks to
resolve species complexes in *Diaporthe*



SUBCHAPTER 3.1

***Diaporthe amygdali*, a species complex or a complex species?**

Hilário S, Santos L, Alves A.

Fungal Biology 2021 25, 505-518

ABSTRACT

Delimitation of species boundaries within the fungal genus *Diaporthe* has been challenging, but the analyses of combined multilocus DNA sequences has become an important tool to infer phylogenetic relationships and to circumscribe species. However, analyses of congruence between individual gene genealogies and the application of the genealogical concordance principle have been somehow overlooked. We noted that a group of species including *D. amygdali*, *D. garethjonesii*, *D. sterilis*, *D. kadsurae*, *D. ternstroemia*, *D. ovoicicola*, *D. fusicola*, *D. chongqingensis* and *D. mediterranea*, commonly known as *D. amygdali* complex, occupy a monophyletic clade in *Diaporthe* phylogenies but the limits of all species within the complex are not entirely clear. To assess the boundaries of species within this complex we employed the Genealogical Concordance Phylogenetic Species Recognition principle (GCPSR) and coalescence-based models: General Mixed Yule-Coalescent (GMYC) and Poisson Tree Processes (PTP). The incongruence detected between individual gene phylogenies, as well as the results of coalescent methods do not support the recognition of lineages within the complex as distinct species. Moreover, results support the absence of reproductive isolation and barriers to gene flow in this complex, thus providing further evidence that the *D. amygdali* species complex constitutes a single species. This study highlights the relevance of the application of the GCPSR principle, showing that concatenation analysis of multilocus DNA sequences, although being a powerful tool, might lead to an erroneous definition of species limits. Additionally, it further shows that coalescent methods are useful tools to assist in a more robust delimitation of species boundaries in the genus *Diaporthe*.

keywords: Coalescent models; GMYC; Phylogeny; PTP; Systematics; Species delimitation

INTRODUCTION

The genus *Diaporthe* (syn. *Phomopsis*), known to be paraphyletic, encompasses important plant pathogens, endophytes and saprobes widely distributed in tropical and temperate regions (Gao et al. 2017). *Diaporthe* tends to be morphologically conserved and to harbor some phenotypic plasticity (Mostert et al. 2001). For many years, species in this genus were defined based on host association (Rehner & Uecker 1994), unclear linkage of sexual and asexual morphs and morphological traits (Udayanga et al. 2011) which resulted in a proliferation of more than 2000 species names (<http://www.indexfungorum.org/>). Currently, taxonomic studies in the genus *Diaporthe* have been established using molecular techniques such as the use of multi-gene phylogenies, based on the nuclear ribosomal internal transcribed spacer (ITS) region, the translation elongation factor 1-a (*tef1-a*), beta-tubulin (*tub2*), histone (*his3*), and calmodulin (*cal*) loci (Gomes et al. 2013; Santos et al. 2017).

Fusicoccum amygdali (Delacr.) was described based on micromorphological characters (*Fusicoccum*-like aseptate and hyaline conidia) (Crous & Palm 1999), as a canker pathogen on twigs of almond (*Prunus dulcis*) in France (Delacroix 1905). Later, Canonaco in 1936 found this pathogen on almonds and peach (*P. persica*) and named it as *Phomopsis amygdalina*. Tuset & Portilla (1989) studied the morphology and symptomatology of both *F. amygdali* and *P. amygdalina* and considered them to be identical. These authors recognized that the fungal pathogen of almond and peach would be best accommodated in the genus *Phomopsis* and made the new combination *Phomopsis amygdali* (Del.) Tuset & Portilla. More recently, Diogo et al. (2010) isolated strains of *P. amygdali* and proposed a suitable specimen as epitype. With the abolishment of the dual nomenclature in Fungi, Udayanga et al. (2012) accommodated *P. amygdali* within the genus *Diaporthe* and introduced *D. amygdali* as a new species combination. Since the epityfication of *Diaporthe amygdali* (Diogo et al. 2010) several new species morphologically identical and phylogenetically closely related have been described, such as *D. ternstroemia* (Gao et al. 2014), *D. sterilis* (Lombard et al. 2014), *D. ovoicicola*, *D. fusicola* (Gao et al. 2015), *D. garethjonesii* (Hyde et al. 2016), *D. kadsurae* (Yang et al. 2018), *D. chongqingensis* (Guo et al. 2020) and *D. mediterranea* (León et al.

2020). In a recent study, Gao et al. (2016) noted that phylogenetic relationships between some of those species were ambiguous and that molecular variation between them was low, thus raising questions about a putative species complex, named in that study as the *D. amygdali* complex.

Although it has been previously recommended that new species in the genus *Diaporthe* should be carefully introduced (Gao et al. 2017), all these species belonging to the aforementioned complex were described based on the concatenation of sequences from different loci, without following the Genealogical Concordance Phylogenetic Species Recognition (GCPSR) principle, that lies in the comparison of individual gene genealogies to identify phylogenetic concordance between them, detect lack of gene flow between lineages and thus define species limits (Taylor et al. 2000). The delimitation of species boundaries using a multilocus approach is not always straightforward, as genes can harbor different evolutionary histories, leading to discordances between gene trees (Stewart et al. 2014). Processes such as incomplete lineage sorting or recombination are the main causes of these conflicts, misleading the relationships among closely related taxa (Degnan & Rosenberg 2009). Such incongruencies have been commonly detected in a few genera of fungi (Bustamante et al. 2019; Liu et al. 2016), but somehow overlooked in the genus *Diaporthe* (Zapata et al. 2020).

In contrast to the GCPSR criteria, coalescent-based methods such as the General Mixed Yule Coalescent (GMYC) (Pons et al. 2006) and the Poisson Tree Processes (PTP) (Zhang et al. 2013) can infer species trees and thus delimit the species boundaries, even when there is incongruence between gene trees and a lack of reciprocal monophyly among lineages (Carstens & Knowles 2007). Nevertheless, despite the reliable support of these methods to define species boundaries (Bustamante et al. 2019), they have seldomly been used in plant pathogenic fungi (Liu et al. 2016) and have never been applied in the genus *Diaporthe*.

During an investigation of pathogens causing twig blight disease on blueberry in Portugal, we isolated a fungus that resembled *D. amygdali*. Therefore, the purpose of this study was to identify the fungus based on molecular data, and to resolve the boundaries of the *D. amygdali* complex by implementing a polyphasic

approach comprising: 1) single and multilocus phylogenetic analyses; comparison of micromorphological characters; 2) pairwise homoplasy index test; 3) phylogenetic networks, and 4) coalescent-based species delimitation methods.

MATERIAL AND METHODS

Fungal isolation.

Blueberry twigs showing typical *Diaporthe* blight disease symptoms were collected from Aveiro, Arouca (40°54'35.3"N, 8°22'49.7"W) and Porto, Santo Tirso (41°15'28.9"N, 8°28'13.1"W), in the north region of Portugal. Isolations were made following the procedures described in subchapter 2.1.

DNA extraction and PCR amplification.

Genomic DNA extraction and amplification of ITS and the protein coding regions *tef1-a*, *tub2*, *his3* and *cal*, were as described in subchapter 2.1.

Morphological characterization and temperature growth studies.

Given that no fruiting bodies were observed in the samples collected, isolates were induced to sporulate, as described in subchapter 2.1. After sporulation, micromorphological characters and measurements were performed following the description in subchapter 2.2. The alpha conidia and conidiophores length/width (L/W) ratios of our isolates and of the *D. amygdali* complex were calculated and hierarchical clustering analysis using the Ward's method (Murtagh & Legendre 2014) was carried out. The dendrogram was generated and conducted in R Statistical Software v.3.5.3 (R Core Team 2019), along with the `DENDEXTEND` package (Galili 2015).

The influence of temperature on mycelial growth was also assessed. Colony characters, optimal growth rate and growth parameters were calculated as described in subchapter 2.1.

Phylogenetic analyses.

The nucleotide sequences were analyzed, and the phylogenetic trees were constructed based on Maximum Parsimony (MP), Maximum Likelihood (ML) and Bayesian Inference (BI) analyses, as described in subchapter 2.1. For the MP analyses, the following parameters were also calculated: consistency index (CI), retention index (RI), tree length (TL), rescaled consistency index (RC) and homoplasy index (HI).

An initial individual ITS tree, containing all species currently accepted in the genus *Diaporthe*, was generated to determine the taxa closest to our isolates, and to select the species recognized within the *D. amygdali* complex. Apart from these isolates, six well-delimited *Diaporthe* species were included in further analyses. To examine the possibility of a combined dataset, sequences from the five loci were aligned, combined, and a partition homogeneity test was conducted in PAUP* v.4.0b10 (Swofford 2002). Moreover, a comparison of highly supported clades (ML and MP >70% and PPs >0.95) among single-locus trees was performed to detect conflict between individual phylogenies, as previously described by Alves et al. (2008). Furthermore, individual gene trees of the *D. amygdali* complex, comprising all available species for each locus were also constructed. These trees were rooted to *D. pustulata* and *D. acaciigena*. Sequences generated in this study were deposited in GenBank (Table 1) (www.ncbi.nlm.nih.gov). The phylogenetic trees and alignments were deposited in TreeBASE (www.TreeBASE.org; study number S26680).

Pairwise homoplasy index test.

The criterion of incongruence among the five gene genealogies was used to select hypothesized “species”/populations to infer the occurrence of sexual recombination, using the pairwise homoplasy index test (PHI, Φ_w) (Bruen 2005) implemented in SplitsTree v.4.16.1 (Huson & Bryant 2006). The test was performed to determine the recombination level within the complex and between every pair of clades (clade a to clade i, Fig. 1). To detect evidence of intragenic recombination, individual loci were also analyzed by the PHI test. Results of PHI index below a 0.05 threshold ($\Phi_w < 0.05$) indicated significant recombination.

Phylogenetic network analyses.

A phylogenetic network based on the combined dataset of five loci was performed. This analysis was undertaken using the NeighborNet algorithm to evaluate the impact of recombination, implemented in SplitsTree software v.4.16.1 (Huson & Bryant 2006). Additionally, the individual gene alignments used to construct the single locus trees of *D. amygdali* complex, plus four well-delimited species were added to infer the network analyses for each locus.

Coalescent-based species delimitation.

To infer the species boundaries of *Diaporthe amygdali* complex, two coalescent-based methods were performed based on a combined alignment of ITS, *tef1-a*, *tub2*, *his3* and *cal* genes. Firstly, the Poisson Tree Processes (PTP) model, was used to delimit species. The analysis was performed with 500 000 MCMC generations, thinning set to 100, burn-in at 10% and conducted on the web server for PTP (<http://species.h-its.org/ptp/>), using the Newick-format tree produced by MEGA v.7.

General Mixed Yule Coalescent (GMYC) approach was also performed. BEAUTi v.1.10.4 was used to create the xml-formatted input files for *BEAST v1.10.4 (Suchard et al. 2018). Divergence times were estimated under the reconstructed birth-death prior (Gernhard 2008) with a random starting tree and 10 000 000 MCMC generations sampled every 1000 generations. For a better accuracy, species tree estimations were carried out based on an uncorrelated relaxed-clock model assuming a lognormal distribution (Drummond et al. 2006). The convergence of loglikelihood curves ($-\ln$), the adequate effective sample size values (>200) and the burn-in states were confirmed by inspection of the MCMC samples in Tracer v.1.7.1 (Rambaut et al. 2018). The TreeAnnotator v.1.10.4 from *BEAST was used to summarize the resulting trees and to check for maximum clade credibility tree, where the first 1 000 000 generations were discarded as burn-in. The species tree inferred with *BEAST was then visualized with FigTree v.1.4.4 (Rambaut 2018) and converted as Newick-format input file for the GMYC analysis. Given that the multiple threshold approach of GMYC has been developed for larger

data sets with a greater number of lineages (Monaghan et al. 2009), in the present study we only used the single-threshold version. The GMYC web server (<http://species.hits.org/gmyc/>) was then used to fit our tree to the single threshold model.

In order to make assumptions regarding the identity of species of the *D. amygdali* complex whose *tub2*, *cal* and *his3* sequences were not available, a PTP analysis, shown to outperform the GMYC method (Fujisawa & Barraclough 2013) was also performed. This analysis was based on the combined dataset of ITS and *tef1-a* sequences since it comprises all species currently accepted within this complex.

Population genetic diversity.

Diversity indices were calculated for each gene region and the combined sequence dataset to understand the genetic diversity within the *D. amygdali* complex. DnaSP program v.6.12 (Barcelona, Spain) (Rozas et al. 2017) was used to calculate the following parameters for each of the five loci: pairwise nucleotide diversity (p), haplotype diversity (hd), number of haplotypes (h) and the number of polymorphic sites (S). To understand the potential departure from an equilibrium model of evolution (Tajima 1989), the Tajima's D statistical test was performed with a permutation test of 1000 replicates. All these parameters were measured from a partitioned combined dataset of ex-type isolates of five species and 20 taxonomically authenticated isolates belonging to *D. amygdali* complex and for which sequences of ITS, *tef1-a*, *tub2*, *cal* and *his* were available (Table 1).

Table 1. List of *Diaporthe* species used in this study.

Species	Strain ¹	Host	Location	GenBank Accession					
				ITS	<i>tef1-α</i>	<i>tub2</i>	<i>cal</i>	<i>his3</i>	
<i>D. acaciigena</i>	CBS 129521	<i>Acacia retinodes</i>	Australia	KC343005	KC343731	KC343973	KC343247	KC343489	
<i>D. ambigua</i>	CBS 114015	<i>Pyrus communis</i>	South Africa	KC343010	KC343736	KC343978	KC343252	KC343494	
	CBS 123210	<i>Foeniculum vulgare</i>	Portugal	KC343012	KC343738	KC343980	KC343254	KC343496	
	CBS 126680	<i>Prunus dulcis</i>	Portugal	KC343023	KC343749	KC343991	KC343265	KC343507	
	CBS 111811	<i>Vitis vinifera</i>	South Africa	KC343019	KC343745	KC343987	KC343261	KC343503	
	CBS 115620	<i>Prunus persica</i>	USA	KC343020	KC343746	KC343988	KC343262	KC343504	
	CBS 120840	<i>Prunus salicina</i>	South Africa	KC343021	KC343747	KC343989	KC343263	KC343505	
	CBS 126679	<i>Prunus dulcis</i>	Portugal	KC343022	KC343748	KC343990	KC343264	KC343506	
	LC3156	<i>Camelia sinensis</i>	China	KP267861	KP267935	KP293441	-	KP293515	
	LC3204	<i>Camelia sinensis</i>	China	KP267877	KP267951	KP293457	-	KP293530	
	LC3380	<i>Camelia sinensis</i>	China	KP267889	KP267963	KP293469	-	KP293540	
<i>D. amygdali</i>	LC3411	<i>Camelia sinensis</i>	China	KP267895	KP267969	KP293475	-	KP293546	
	LC4153	<i>Camelia sinensis</i>	China	KP267916	KP267990	KP293496	-	KP293563	
	DAL-9	<i>Prunus dulcis</i>	Spain	MT007298	MT006775	MT006472	MT006696	MT007000	
	DAL-70	<i>Prunus dulcis</i>	Spain	MT007339	MT006816	MT006513	MT006703	MT007015	
	DAL-227	<i>Prunus dulcis</i>	Spain	MT007467	MT006944	MT006641	MT006730	MT007064	
	CAA958	<i>Vaccinium corymbosum</i>	Portugal	MT073273	MT051923	MT051955	MT051847	MT051883	
	CAA959	<i>Vaccinium corymbosum</i>	Portugal	MT073283	MT051935	MT051970	MT051862	MT051898	
	<i>D. amygdali</i> (syn. <i>D. chongqingensis</i>)	PSCG 435	<i>Pyrus pyrifolia</i>	China	MK626916	MK654866	MK691321	MK691209	MK726257
		PSCG 436	<i>Pyrus pyrifolia</i>	China	MK626917	MK654867	MK691322	MK691208	MK726256
	<i>D. amygdali</i> (syn. <i>D. fusicola</i>)	CGMCC 3.17087	<i>Lithocarpus glabra</i>	China	KF576281	KF576256	KF576305	KF576233	-
CGMCC 3.17088		<i>Lithocarpus glabra</i>	China	KF576263	KF576238	KF576287	KF576221	-	
PSCG 015		<i>Pyrus pyrifolia</i>	China	MK626915	MK654861	MK691320	MK691210	MK726254	

	PSCG 030	<i>Pyrus pyrifolia</i>	China	MK626914	MK654864	MK691323	MK691211	MK726255
	PSCG 118	<i>Pyrus pyrifolia</i>	China	MK626910	MK654860	MK691317	MK691204	MK726250
	PSCG 178	<i>Pyrus pyrifolia</i>	China	MK626913	MK654862	MK691324	MK691206	MK726251
	PSCG 179	<i>Pyrus pyrifolia</i>	China	MK626912	MK654863	MK691318	MK691207	MK726252
	PSCG 371	<i>Pyrus pyrifolia</i>	China	MK626911	MK654865	MK691319	MK691205	MK726253
<i>D. amygdali</i> (syn. <i>D. garethjonesii</i>)	MFLUCC 12-0542	Unknown dead leaf	Thailand	KT459423	KT459457	KT459441	KT459470	-
	MFLUCC 12-0542B	Unknown dead leaf	Thailand	KT459424	KT459458	KT459442	KT459471	-
<i>D. amygdali</i> (syn. <i>D. kadsurae</i>)	CFCC 52588	<i>Acer</i> sp.	China	MH121522	MH121564	MH121601	MH121440	MH121480
	CFCC 52586	<i>Kadsura longipedunculata</i>	China	MH121521	MH121563	MH121600	MH121439	MH121479
<i>D. amygdali</i> (syn. <i>D. ovoicicola</i>)	CGMCC 3.17092	<i>Lithocarpus glabra</i>	China	KF576264	KF576239	KF576288	KF576222	-
	CGMCC 3.17093	<i>Lithocarpus glabra</i>	China	KF576265	KF576240	KF576289	KF576223	-
	CGMCC 3.17094	<i>Lithocarpus glabra</i>	China	KF576266	KF576241	KF576290	KF576224	-
<i>D. amygdali</i> (syn. <i>D. mediterranea</i>)	DAL-6	<i>Prunus dulcis</i>	Spain	MT007486	MT006986	MT006683	MT006758	MT007092
	CBS 146754	<i>Prunus dulcis</i>	Spain	MT007489	MT006989	MT006686	MT006761	MT007095
	DAL-176	<i>Prunus dulcis</i>	Spain	MT007496	MT006996	MT006693	MT006768	MT007102
	PMM1657	<i>Vitis vinifera</i>	South Africa	KY511331	-	KY511363	-	-
	PMM1660	<i>Vitis vinifera</i>	South Africa	KY511333	-	KY511365	-	-
<i>D. amygdali</i> (syn. <i>D. sterilis</i>)	CBS 136969	<i>Vaccinium corymbosum</i>	Italy	KJ160579	KJ160611	KJ160528	KJ160548	MF418350
	CPC 20575	<i>Vaccinium corymbosum</i>	Italy	KJ160581	KJ160613	KJ160530	KJ160550	-
<i>D. amygdali</i> (syn. <i>D. ternstroemia</i>)	CGMCC 3.15183	<i>Ternstroemia gymnanthera</i>	China	KC153098	KC153089	-	-	-
	CGMCC 3.15184	<i>Ternstroemia gymnanthera</i>	China	KC153099	KC153090	-	-	-
<i>D. beckausii</i>	CBS 138.27	<i>Viburnum</i> sp.	-	KC343041	KC343767	KC344009	KC343283	KC343525
<i>D. malorum</i>	CBS 142383	<i>Malus domestica</i>	Portugal	KY435638	KY435627	KY435668	KY435658	KY435648
	CAA740	<i>Malus domestica</i>	Portugal	KY435642	KY435629	KY435670	KY435660	KY435650

<i>D. pustulata</i>	CBS 109742	<i>Acer pseudoplatanus</i>	Austria	KC343185	KC343911	KC344153	KC343669	KC343427
	CBS 109784	<i>Prunus padus</i>	Austria	KC343187	KC343913	KC344155	KC343671	KC343429
<i>D. rudis</i>	CBS 114436	<i>Laburnum anagyroides</i>	Austria	KC343232	KC343958	KC344200	KC343474	KC343716
	CBS 113201	<i>Vitis vinifera</i>	Portugal	KC343234	KC343960	KC344202	KC343476	KC343718

¹Acronyms of culture collection: **CAA** – Personal Culture Collection Artur Alves, University of Aveiro, Aveiro, Portugal; **CBS** – Westerdijk Fungal Biodiversity Institute, Utrecht, The Netherlands; **CFCC** – China Forestry Culture Collection Center, Beijing, China; **CGMCC** – China General Microbiological Culture Collection Center, Beijing, China; **CPC** – Personal Culture Collection Pedro Crous, housed at CBS; **DAL** – León et al. 2020; **LC** – Personal Culture Collection Lei Cai, State Key Laboratory of Mycology, Institute of Microbiology, Chinese Academy of Sciences, China; **MFLUCC** – Mae Fah Luang University Culture Collection, Chiang Rai, Thailand; **PMM** – Lesuthu et al. 2019; **PSCG** – Guo et al. 2020. Ex-type isolates are highlighted in bold. Newly sequences generated in this study are given in italics.

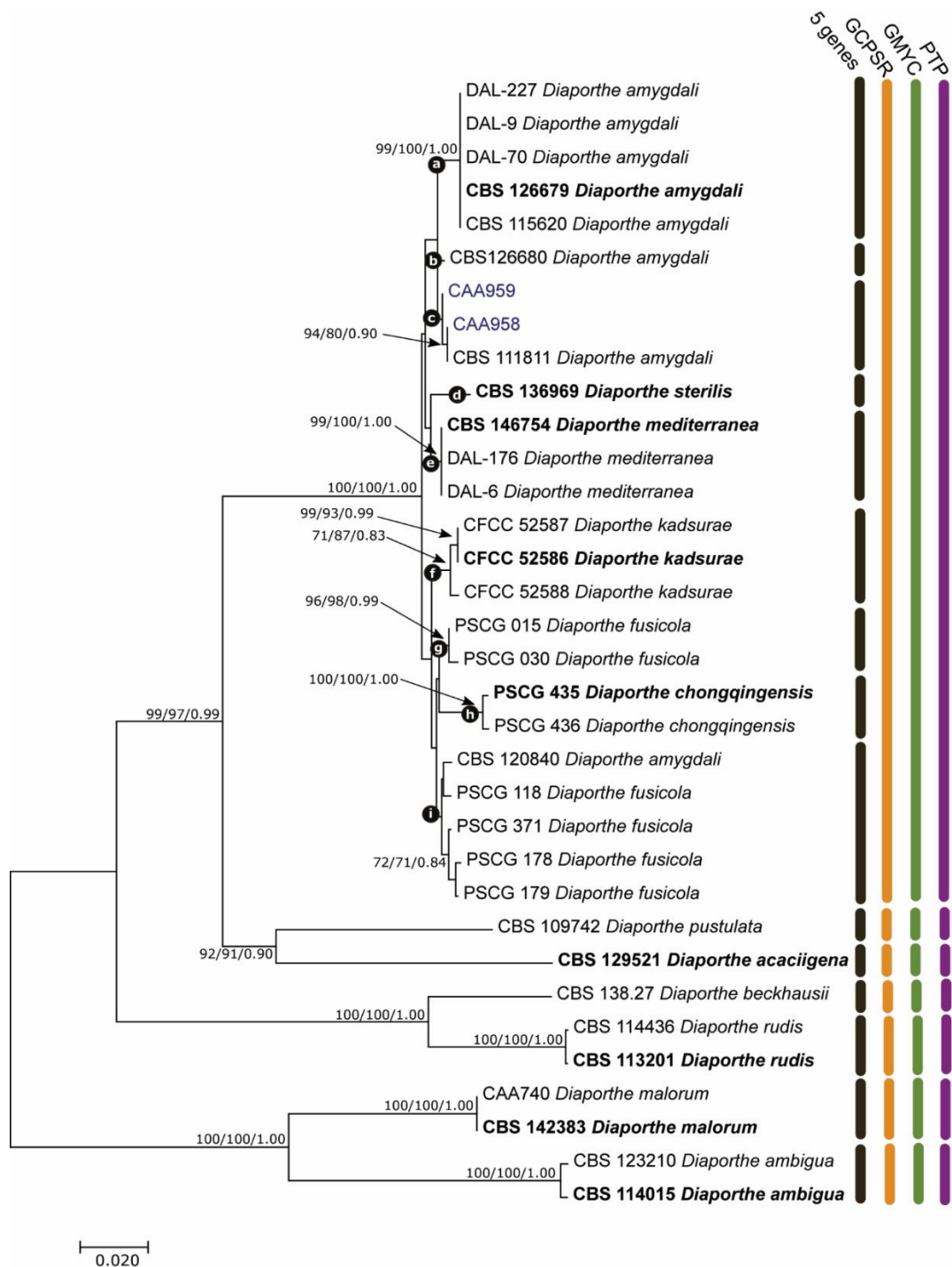


Figure 1. Phylogenetic relationships and species boundaries of *Diaporthe amygdali* complex and related species. The Maximum Likelihood tree is drawn to scale with branch lengths measured in the number of substitutions per site and was constructed based on the Tamura Nei-parameter model assuming a gamma distribution. ML and MP bootstrap values greater than 70% and posterior probabilities (PPs) greater than 0.80 are shown at the nodes. Black bars in the first column at the right present the results of the phylogenetic analysis based on five loci (ITS, *tef1- α* , *tub2*, *his3* and *ca1*). The orange, green and purple columns represent the results after applying the GCPSR principle and the coalescent methods GMYC and PTP respectively. The ex-type strains are in bold. The newly generated sequences are indicated in blue. Black circles represent hypothesized species within the *D. amygdali* complex as inferred by the concatenated gene tree.

RESULTS

Phylogenetic analyses.

Apart from ITS, part of the protein coding genes *tef1-a*, *tub2*, *cal* and *his3* were sequenced and new sequences were deposited in GenBank (Table 1). The individual loci phylograms of the complex (Figs. S1-S5) showed that our isolates belong to a monophyletic clade containing the species *D. fusicola*, *D. ovoicicola*, *D. kadsurae*, *D. garethjonesii*, *D. chongqingensis*, *D. ternstroemia*, *D. mediterranea*, *D. sterilis* and *D. amygdali*, supported by high bootstrap and posterior probability values. However, due to a lack of sequence data from *tub2*, *his3* and *cal* loci, only strains from *D. amygdali* complex for which sequence information was available for all five loci were included in the combined analysis. The partition homogeneity test resulted in a low p -value ($p = 0.01$), indicating that the loci are not suitable to be combined. Moreover, sequences of the five genes were aligned and analyzed separately by Maximum Likelihood, Maximum Parsimony and Bayesian Inference analyses, and the resulting trees were compared. Only ML single locus trees are shown with bootstrap and posterior probabilities given for the well-supported branches (Figs. S6-S10). Relationships among the highly supported clades from all five loci confirmed the tree topologies of the BI and MP trees.

Species delimitation based on GCPSR principle.

Despite the incongruencies between individual gene trees and the result of the partition homogeneity test, a combined multilocus tree was also constructed. The combined alignment comprises 2348 characters (568 characters from ITS, 380 from *tef1-a*, 431 from *tub2*, 500 from *cal*, and 469 from *his3* including alignment gaps). The analysis included 9 well-delimited outgroup taxa and 25 ingroup taxa (2 were obtained in this study and the remaining taxa were retrieved from GenBank) (Table 1). A character-status summary including the percentage of parsimony informative characters and the best nucleotide model for individual and combined analyses is summed up in Table 2.

To understand the boundaries of the *D. amygdali* complex, the GCPSR principle was implemented. The individual gene trees were compared to identify concordant branches. However, this analysis revealed conflicts between tree

topologies. For instance, the isolates CAA958 and CAA959 are paraphyletic in the individual *tef1-a* tree, whereas they are monophyletic in the other single (Figs. S6-S10) and combined trees (Fig. 1). Moreover, strains of *D. fusicola* (Table 1) are distributed throughout the individual phylograms clustering with other species (e.g., with *D. kadsurae* and *D. chongqingensis* in *cal* tree, and with *D. mediterranea* and *D. kadsurae* in *tef1-a* tree) and lacking high bootstrap and posterior probability values on both individual and combined trees. As opposed to this, individual gene trees are concordant and have the same topology for the six well-delimited species (*D. ambigua*, *D. rudis*, *D. malorum*, *D. pustulata*, *D. acaciigena* and *D. beckausii*) denoting no conflicts among the individual phylograms. This provides strong evidence that these clades represent different species. Taking this into consideration, we verified that the point that delimits the transition from concordant branches to incongruity among branches corresponds to the *D. amygdali* species complex (Fig. 1), thus determining the limit of the species. Therefore, by implementing the GCPSR principle, i.e., the comparison of more than one gene genealogy to identify phylogenetic concordance, the hypothesis that *D. amygdali* is a species complex was rejected.

Table 2. Alignment properties and nucleotide substitution models used for phylogenetic analyses.

Character-status summary	Loci and combined alignment					
	ITS	<i>tef1-α</i>	<i>tub2</i>	<i>his3</i>	<i>cal</i>	<i>5 loci</i>
Total characters	568	380	431	469	500	2348
Invariable characters	473	177	275	344	314	1575
Informative characters (%)	76 (13%)	164 (43%)	131 (30%)	105 (22%)	157 (31%)	631 (27%)
Uninformative characters	19	39	25	30	29	142
Tree length (TL)	144	344	240	220	273	1260
Consistency index (CI)	0.7917	0.7994	0.8083	0.7864	0.8681	0.7865
Homoplasy index (HI)	0.2083	0.2006	0.1917	0.2236	0.1319	0.2135
Retention index (RI)	0.8699	0.8705	0.9055	0.8730	0.9341	0.8778
Rescaled consistency index (RC)	0.7098	0.6959	0.7320	0.6865	0.8086	0.6904
Nucleotide substitution models ¹	K2+G	HKY+I	K2+G	KKY+G	T92+I	TN93+G

¹K2: Kimura 2-parameter model; T92: Tamura 3-parameter model; HKY: Hasegawa–Kishino–Yano model; TN93: Tamura Nei-parameter model; G, I: models of evolution assuming a gamma distribution or invariant sites.

Species delimitation based on coalescent methods.

The ultrametric tree obtained from *BEAST using the combined dataset of 5 loci was used for the GMYC analysis. In this analysis, single threshold mode proved to be significantly better suited to the ultrametric tree than the null model ($\log L_{\text{GMYC}}$

= 207.2425 vs $\log L_0 = 204.1522$, with a significant likelihood-ratio test, $p = 0.044$). Moreover, this model fitted the switch in the branching pattern at -0.011039 , leading to an estimate of 7 putative species, where *D. amygdali* complex was recognized as one potential single species (clade 7, Fig. 3). For the PTP analysis, the best-fit ML tree and BI majority-rule consensus topology gave the same results as the GMYC analysis, *i.e.*, the complex was also recognized as a single species (clade 3, Fig. 4). Thus, the coalescent methods gave congruent results with each other and with the GCPSR principle and assigned *D. amygdali* complex as a single species.

Given the lack of *tub2*, *cal* and *his3* sequences for some species of the complex, neither the combined phylogenetic analysis performed, nor the coalescent methods included all species alleged to belong to this complex, as estimated by the initial individual trees (Figs. S1-S5). After analyzing these phylograms, we confirmed that all species fall into a monophyletic clade in all single locus trees, with some internal nodes lacking phylogenetic support. Moreover, from the PTP analysis of ITS and *tef1-a* (Fig. S11), the transition between blue-colored to red-colored branches indicated that all species clustered in a single clade, confirming that the complex should be considered as a population rather than individual species. Lastly, the structure of the phylogenetic networks constructed for each gene (Figs. S12-S16) also demonstrated that this complex should be regarded as a single lineage, since all species group together. Therefore, taking into consideration these aspects, we can consider that all species falling into the *D. amygdali* complex should be recognized as a single species.

Pairwise homoplasy test and phylogenetic networks.

Significant recombination was detected within the *D. amygdali* complex when applying the PHI test ($\Phi_w = 5.2 \times 10^{-7}$), denoting that there was no reproductive isolation within the group. For instance, recombination was verified among strains from clade I (Fig. 1) and the species *D. kadsurae*, *D. amygdali*, *D. sterilis* and *D. mediterranea* (Table S1). Moreover, the pairwise homoplasy index test also confirmed that *tef1-a* and *his3* loci were subjected to a significant rate of recombination (mean = 0.1263, $\Phi_w = 0.027$ and mean = 0.1091, $\Phi_w = 0.022$ respectively). Subsequently, networked relationships within the *D. amygdali*

complex (Fig. 2), are shown with boxes instead of a bifurcating evolutionary tree. The presence of boxes in the network infers the relationships among individuals and imply likelihood of recombination among them. Moreover, based on the relative distance of species and structure of the phylogenetic network, all strains in the *D. amygdali* complex should be regarded as one single species.

Population genetic diversity.

A summary of the genetic diversity and polymorphism indices for each gene region as well as for combined dataset is given in Table 3. Overall, all loci gave low average number of differences per site (p), ranging from 0.008 to 0.026. Haplotype diversity (hd) showed the opposite, with high values for all genes, being the *tub2* locus with the highest indice ($hd = 0.933$). In addition to that, *tef1-a*, *his3* and the combined alignment gave not statistically significant negative Tajima's D values as -0.6168 , -1.3070 and -0.2601 respectively.

Morphological analysis.

Based on published morphological descriptions of eight species belonging to the *D. amygdali* complex (excluding *D. sterilis* which lacks a taxonomic description) and based on morphological observations of our isolates CAA958 and CAA959, a hierarchical clustering analysis was performed using the Ward's method. The dendrogram was constructed based on the ratios of alpha conidia and conidiophores length and width. This analysis divided the taxa into two distinct large clusters in both dendrograms (Fig. S17).

Table 3. Polymorphism and genetic diversity data for the *Diaporthe amygdali* complex.

Loci	Number of haplotypes (h)	Number of polymorphic sites (S)	Haplotype diversity (hd)	Nucleotide diversity (π)	Tajima's D test
ITS	8	18	0.827	0.013	0.1011 ^{ns}
<i>tef1-α</i>	5	15	0.663	0.014	-0.6168 ^{ns}
<i>tub2</i>	14	33	0.933	0.026	0.2334 ^{ns}
<i>his3</i>	7	21	0.827	0.009	-1.3070 ^{ns}
<i>cal</i>	9	12	0.847	0.008	0.1732 ^{ns}
Combined	17	99	0.950	0.014	-0.2601 ^{ns}

^{ns} Not statistically significant.

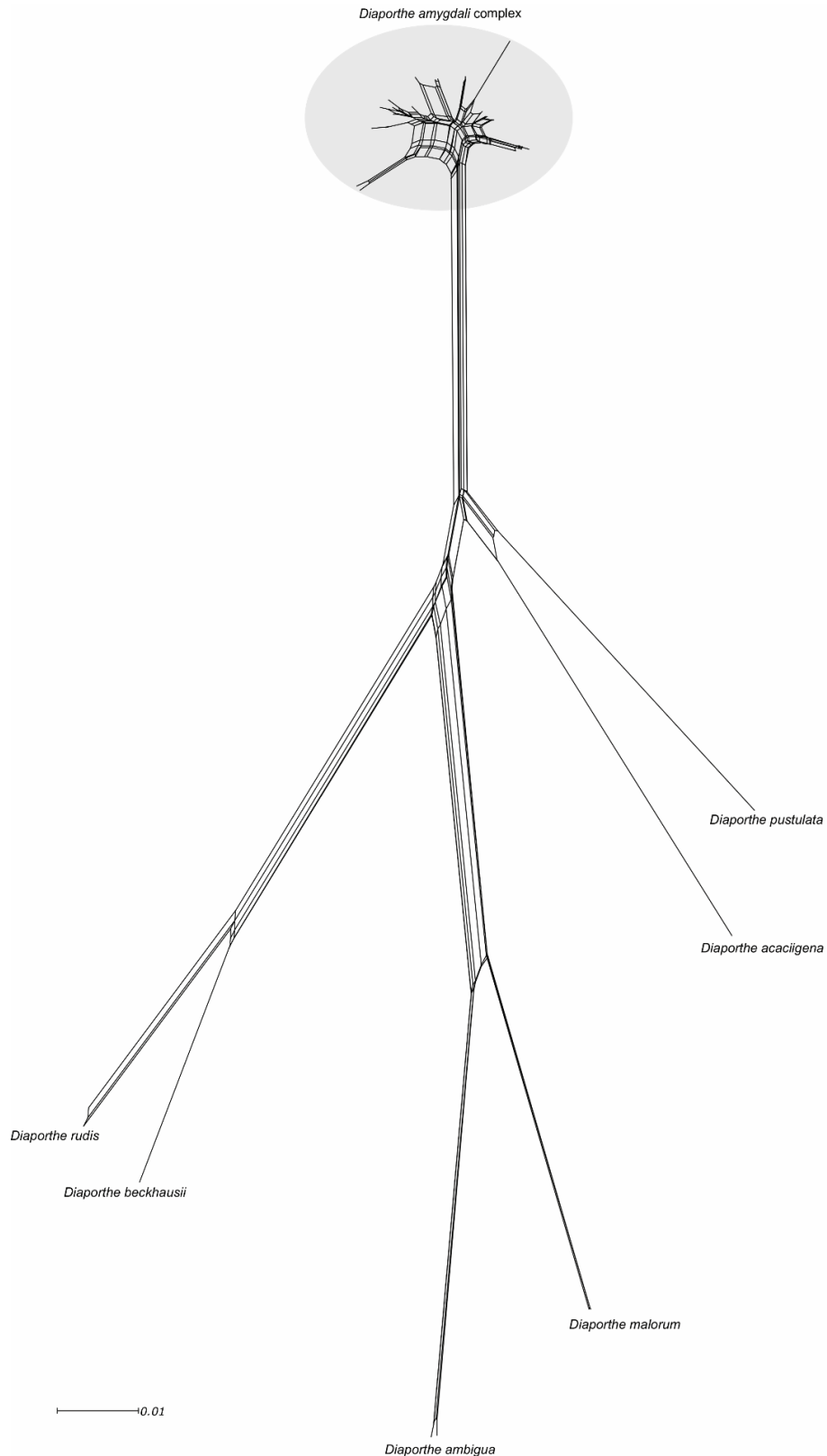


Figure 2. Phylogenetic network from the concatenated data (ITS, *tef1- α* , *tub2*, *his3* and *ca1*) representing the structure of the *Diaporthe amygdali* complex and other well-delimited species, based on the NeighborNet algorithm as inferred by SplitsTree. The scale bar represents the expected number of substitutions per nucleotide position.

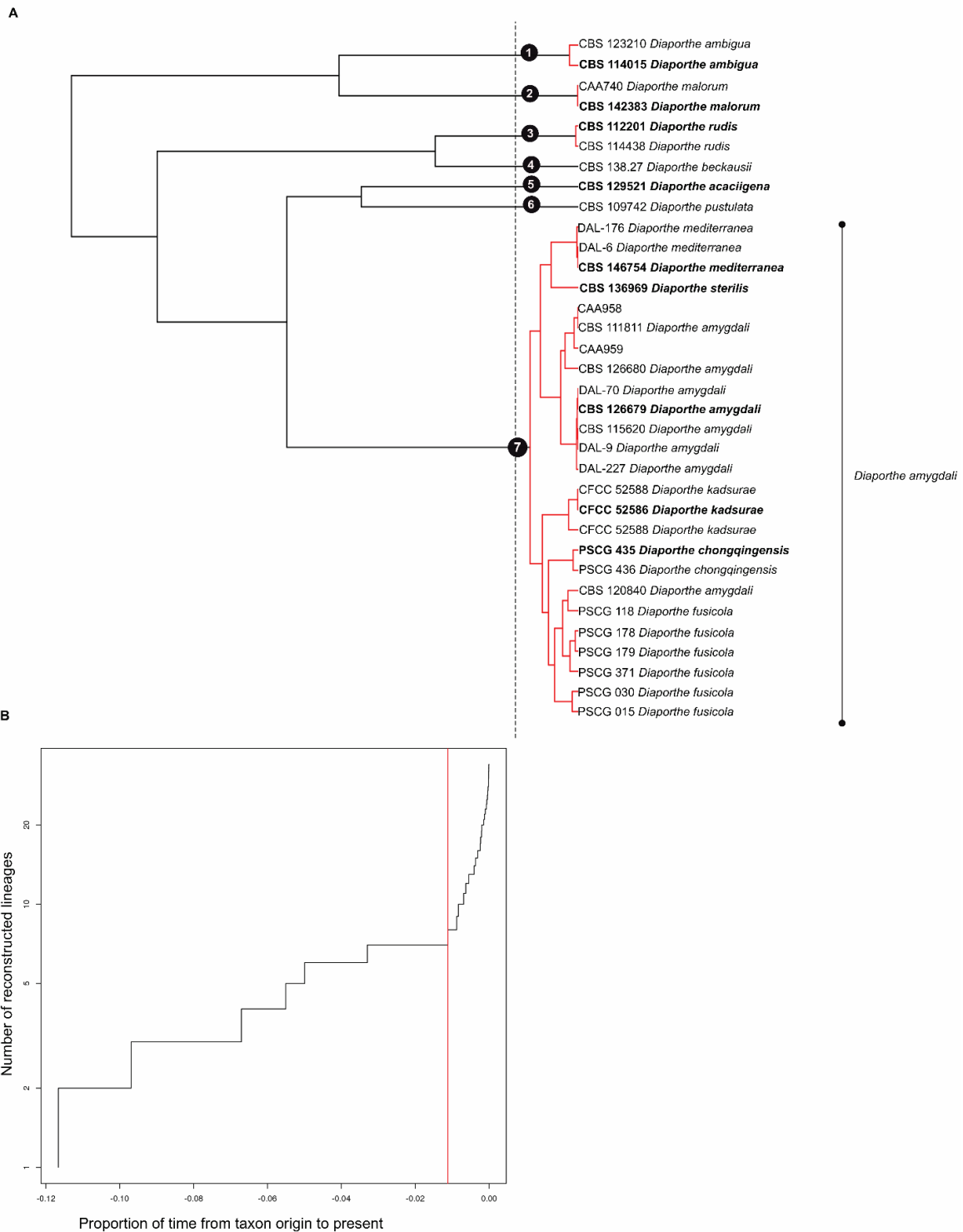


Figure 3. Results of the GMYC analyses for the *Diaporthe amygdali* clade and related taxa. **A.** Ultrametric tree inferred by the single threshold method. Genetic clusters recognized as putative species are highlighted with black circles (1-7). The vertical black dashed line represents the timing of the earliest coalescent event. **B.** Lineage-through-time (LTT) plot for the single threshold analysis of GMYC. Time is expressed as a proportion of the total time since the first evolutionary split event inferred for the taxon. The red line corresponds to the transition from interspecies to intraspecies branching events

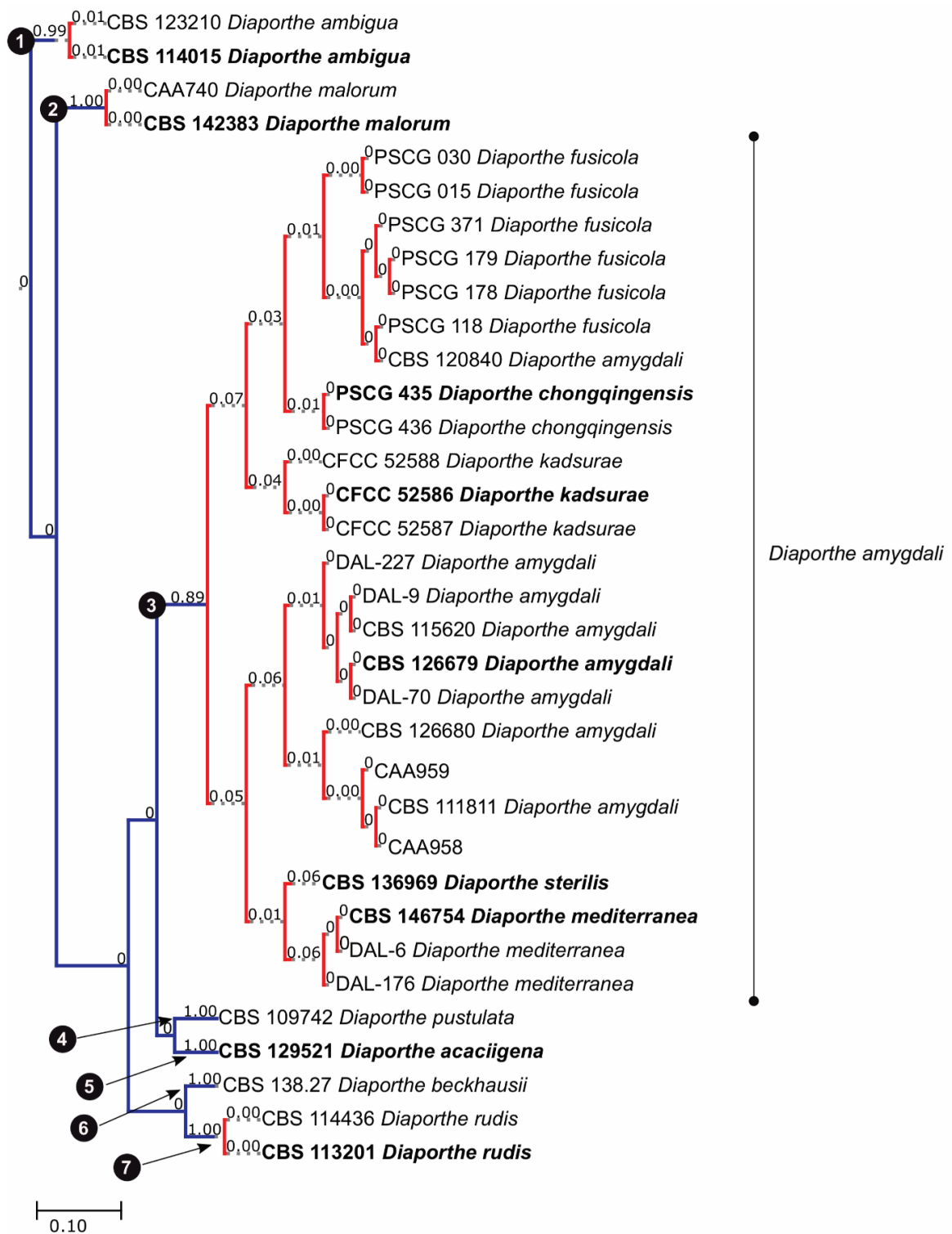


Figure 4. Results of the PTP analyses for the *Diaporthe amygdali* clade and related taxa, based on the Bayesian and Maximum Likelihood topologies. Putative species clusters are indicated using transitions between blue-colored to red-colored branches and represented by black circles (1-7).

TAXONOMY

The present study combined phylogenetic analyses based on the GCPSR principle, GMYC and PTP coalescent methods, and on morphological comparisons to delimit the species boundaries within the *D. amygdali* complex. *Diaporthe amygdali*, *D. chongqingensis*, *D. fusicola*, *D. garethjonesii*, *D. kadsurae*, *D. mediterranea*, *D. ovoicicola*, *D. sterilis* and *D. ternstroemia* are here recognized to be conspecific, *i.e.*, they constitute a single species. In this section, a synopsis with micromorphological characteristics of all these species (Table 4) and synonymous names of *D. amygdali* are provided. Moreover, a detailed description and illustrations of the fungus collected in the present study are also given.

Diaporthe amygdali (Delacr.) Udayanga, Crous & Hyde, *Fungal Divers.* **56**:166 (2012). (Fig. 5).

Basionym: *Fusicoccum amygdali* Delacr., *Bull. Soc. Mycol. France* **21**:182 (1905).

Synonyms: *Phomopsis amygdalina* Canonaco, *Riv. Pat. Veg.* **26**:157 (1936).

= *Phomopsis amygdali* (Delacr.) Tuset & Portilla, *Can. J. Bot.* **67**:1280 (1989).

= *Diaporthe sterilis* Lombard, Polizzi & Crous, *Phytopathol. Mediterr.* **53**:296 (2014).

= *Diaporthe ovoicicola* Gao & Cai, *Fungal Biol.* **119**:298 (2015).

= *Diaporthe fusicola* Gao & Cai, *Fungal Biol.* **119**:300 (2015).

= *Diaporthe ternstroemia* Gao, Sun & Cai, *Fungal Biol.* **119**:306 (2015).

= *Diaporthe garethjonesii* Dissanayake, Tangthirasunun & Hyde, *Fungal Divers.* **80**:209 (2016).

= *Diaporthe kadsurae* Tian & Yang, *MycKeys* **39**:135 (2018).

= *Diaporthe chongqingensis* Guo & Wang, *Persoonia* **45**:146 (2020).

= *Diaporthe mediterranea* León, Rodríguez-Reina & Armengol, *Agronomy* **10**:17 (2020).

Specimens examined: **Portugal. Aveiro**: Arouca, Quinta do Coval (40°54'35.3"N 8°22'49.7"W) from diseased twigs of *V. corymbosum*, 1 April 2019, P. Pinho CAA958. Living culture CAA958 (**MUM 20.33**), deposited in the Micoteca da Universidade do Minho, Portugal

Known distribution: China, France, Greece, Italy, Japan, Portugal, South Africa, Spain, Thailand, Tunisia, Turkey, and USA (Farr & Rossman 2020).

Host range: *Acer* sp., *Camelia sinensis*, *Corylus avellana*, *Lithocarpus glabra*, *Pieris japonica*, *Prunus armeniaca*, *P. dulcis*, *P. persica*, *P. salicina*, *Pyrus pyrifolia*, *Kadsura longipedunculata*, *Ternstroemia gymnanthera*, *Vaccinium corymbosum*, *Vitis vinifera* (Farr & Rossman 2020).

Description: Asexual morph: coelomycetous, black conidiomata broadly spherical, solitary or aggregated, pycnidial-shaped, immersed on pine needles tissue, covered in white to brown mycelium, with yellowish translucent conidial cirrus extruding from ostioles. Conidiophores arising from pseudoparenchyma, hyaline, cylindrical, smooth-walled, densely aggregated, straight to slightly curved, sometimes tapering towards the apex (12.8–)16.6–22.9 × 1.9–2.2(–2.7) mm (mean ± SD = 17.9 ± 5.1 × 2.3 ± 0.4 mm, *n* = 30), reduced to enteroblastic, phialidic, hyaline conidiogenous cells. Paraphyses absent. Alpha conidia found rarely bi-guttulate, hyaline, aseptate, thick-walled, fusoid with one apex acute (4.8–)6–9.1 × 1.5–2.3(–3.0) mm (mean ± SD = 7.0 ± 0.6 × 2.4 ± 0.3 mm, *n* = 100). Gamma conidia infrequent, aseptate, hyaline, fusoid to subcylindrical (11.1–)11.6–13.1 × 1.3–1.5(1.7) mm (mean ± SD = 12.1 ± 1.9 × 1.6 ± 0.2 mm, *n* = 4). Beta conidia not observed. Sexual morph: not found.

Culture characteristics: Pycnidial conidiomata produced in fennel twigs and pine needles in 4 weeks. Colonies spreading on PDA with cottony flattened mycelium with rare gray patches, predominantly smoke gray, dirty white tufts, developing solitary black conidiomata with age and reverse pale olivaceous gray to pale brown zones in a radial pattern; colonies obtained maximum growth of 90 mm diameter at 25 °C after 6 days in the dark (μ_{opt} = 7.6 ± 1.3 mm/day, *n* = 6). No growth at 5 °C. Growth rates at 20 °C and 30 °C were similar. It grew faster at 10 °C than at 35 °C. After 6 days, at 30 °C colonies were observed olivaceous-black, with tufts of dirty white mycelium. Maximum temperature for growth = 33.7 ± 0.5 °C, minimum temperature = 5.1 ± 0.8 °C and optimum temperature = 24.5 ± 1.5 °C.

Additional material examined: Portugal. Porto: Santo Tirso, Agrela (41°15'28.9"N 8°28'13.1"W), isolated from *V. corymbosum* with twig blight symptoms, 24 Jul. 2019, S. Hilário, living culture CAA959.

Notes: The morphology of our isolates correlates with the detailed description of *Phomopsis amygdali* by Tuset & Portilla (1989): conidiomata subglobose, erumpent, dark brown to black, conidia exuding in white to cream drops; conidiophores subcylindrical, hyaline, branched, reduced to phialidic conidiogenous cells that match within the same ranges of dimensions; alpha and gamma conidia dimensions of our isolates match those of *P. amygdali* reported by Mostert et al. (2001); the rarely biguttulate alpha conidia correlate with the description of Delacroix (1905), who noted that *Fusicoccum amygdali* guttulation varied from none to two; the absence of beta conidia in our isolates correlates also with their absence reported by Delacroix (1905), Mostert et al. (2001) and Diogo et al. (2010), and with their scarceness reported by Tuset & Portilla (1989). Culture characteristics are also similar to the ones of *P. amygdali* reported by Mostert et al. (2001) and Diogo et al. (2010): cottony colonies, from smoke gray to pale olivaceous gray, dirty white tufts and a few gray patches on surface, with reverse olivaceous gray and pale brown concentric zones. Cardinal temperatures also correlate the ones reported by Mostert et al. (2001).

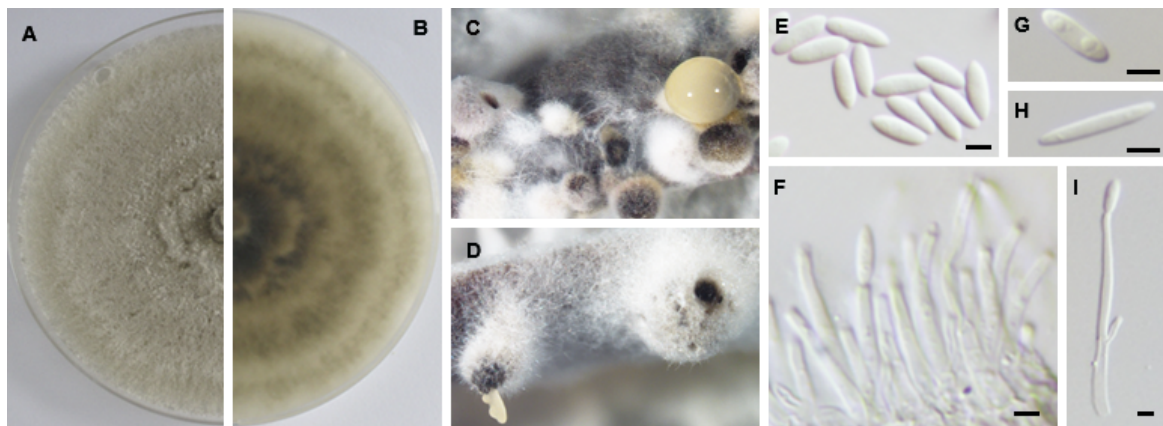


Figure 5. Morphology of *Diaporthe amygdali* from *Vaccinium corymbosum* (CAA958). Upper (A) and reverse (B) culture surface on PDA after 6 days at 25 °C. C, D. Pycnidia on pine needles, oozing conidial cirrhus. E. Alpha conidia. F. Conidiophores aggregated and protruding on pseudoparenchyma. G. Bi-guttulate alpha conidia. H. Gamma conidia. I. Conidiophore with alpha conidia at its tip. Bars = 2.5 μm.

Table 4. Synopsis of micromorphological characteristics of *Diaporthe amygdali* synonyms discussed in this study (Note: *D. sterilis* was not compared due to the absence of taxonomic descriptions).

Species / Isolates	Conidiomata	Conidiophores and conidiogenous cells	Alpha conidia (µm)	Beta conidia (µm)	References
<i>D. amygdali</i> Tuset & Portilla	dark brown to black, separate or aggregated, unilocular pycnidia (180–500 µm diameter)	branched and basal 1–2 septate conidiophores up to 6.6–23.3 × 1.6–5.8 µm, enteroblastic, phialidic, hyaline with collarettes	alpha conidia ellipsoid, rarely fusiform, each end obtuse, 0–2 guttulate (4.9–9.9 × 2.3–3.8 µm)	Observed on the host only. Beta conidia hyaline, filiform, straight, or more often slightly curved (15.3–23.1 × 1.1–1.9 µm)	Tuset & Portilla 1989
<i>D. amygdali</i> (CAA958 and CAA959)	black conidiomata broadly spherical, covered in mycelium; conidial mass yellowish translucent	conidiophores hyaline, cylindrical, aseptate, tapering towards the apex (16.6–22.9 × 1.9–2.2 µm), reduced to phialidic and hyaline conidiogenous cells	alpha conidia rarely biguttulate, hyaline, fusoid with one apex acute (6–8.1 × 1.5–2.3 µm)	not observed	This study
<i>D. chongqingensis</i> Guo & Wang	pycnidial conidiomata globose, solitary or aggregated, wrapped in hyphae (285–744 µm diameter), yellowish translucent conidial mass	conidiophores hyaline, smooth, 1–septate, densely aggregated, unbranched, (6.5–12.5 × 2–6 µm); conidiogenous cells phialidic, hyaline, tapered towards the apex (14–26 × 1.5–2.5 µm)	alpha conidia hyaline, aseptate, fusiform, biguttulate or multi guttulate, acutely round at one end (5.5–7.5 × 2–3 µm)	not observed	Guo et al. 2020
<i>D. fusicola</i> Gao & Cai 2015	pycnidial conidiomata, subglobose to globose (175–500 µm diameter), pycnidial necks hairy, aggregated, translucent yellow conidia cirri	Conidiophores hyaline, branched, septate, straight to sinuous, cylindrical, hyaline, straight or slightly curved, with periclinal, thickening present (11–24.1 × 1.6–2.9 µm)	alpha conidia fusoid, hyaline, mostly biguttulate, tapering towards both ends (5.4–7.9 × 1.6–2.7 µm)	not observed	Gao et al. 2015
<i>D. garethjonesii</i> Dissanayake, Tangthirasunun & Hyde 2016	pycnidial conidiomata, globose, unilocular, black, ostiolate (115 × 85 µm diameter)	conidiophores, hyaline, smooth, cylindrical, straight to sinuous (5–12 × 1–1.5 µm); conidiogenous cells phialidic, cylindrical, slight taper towards apex.	alpha conidia, aseptate, hyaline, smooth, guttulate, fusoid to ellipsoid, tapering towards both ends (5–6 × 2–3 µm)	beta conidia found rare, hyaline, smooth, straight, curved (40–50 × 3–4 µm)	Hyde et al. 2016

<i>D. kadsurae</i> Tian & Yang 2018	conidiomata pycnidial, brown to black, slightly erumpent, nearly flat, unilocular, ostiolate (475–525 µm diameter)	conidiophores, cylindrical, hyaline, unbranched, straight or slightly curved, tapering towards the apex (7–11 × 1.8–2.9 µm)	alpha conidia hyaline, aseptate, oval or fusoid, biguttulate (5.5–7.5 × 2.1–2.9 µm)	not observed	Yang et al. 2018
<i>D. mediterranea</i> (León, Rodríguez-Reina & Armengol 2020)	conidiomata pycnidial, globose or irregular, aggregated, erumpent, dark brown to black (422–632 µm diameter), whitish translucent to creamy conidial drops	conidiophores densely aggregated lining the inner cavity, smooth and hyaline, cylindrical, straight, reduced to conidiogenous cells (12.8–18.2 × 1.8–2.6 µm)	alpha conidia aseptate, fusiform, hyaline, multi-guttulate and acute at both ends (6.1–7.1 × 2.2–2.6 µm)	not observed	León et al. 2020
<i>D. ovoicicola</i> Gao & Cai 2015	pycnidial conidiomata, globose, deeply embedded in the substrate, aggregated, cream conidial drops (140–250 µm diameter)	conidiophores hyaline, single to multiseptate, branched, phialidic, cylindrical, guttulate, tapering towards the apex, straight or slightly curved, (14.2–23.6 × 1.6–2.3 µm)	alpha conidia, hyaline, unicellular, ovoid-fusoid, mostly with one end obtuse and the other acute, 0–2 small guttulate (5.3–8.3 × 1.7–3 µm)	beta conidia hyaline, aseptate, filiform, curved, eguttulate, with rounded ends (16.1–25 × 1.2–1.5 µm)	Gao et al. 2015
<i>D. ternstroemia</i> Gao, Sun & Cai 2014	conidiomata globose (180–390 µm diameter) deeply embedded in PDA, white to dark brown, yellow translucent conidial mass	conidiophores, cylindrical, single to multi-septate, hyaline, branched (13.9–18.2 × 1.8–2.4 µm)	alpha conidia, fusiform to ellipsoidal, obtuse at one end, hyaline, biguttulate (6.2–10.7 × 2.0–3.4 µm)	Not observed	Gao et al. 2014

DISCUSSION

The criteria used to delimit species in the genus *Diaporthe* in recent years have relied mostly on a combination of morphological characterization and multilocus sequence analyses (Gao et al. 2017; Guo et al. 2020; Mostert et al. 2001). However, researchers have been essentially regarding distinct well-supported clades in single and multilocus trees as species (Stewart et al. 2014), disregarding the existence of incongruences between gene trees or without proving the lack of gene flow between populations, which are important factors for determining species status (Taylor et al. 2000). This is particularly important in the genus *Diaporthe*, where high intraspecific variability has been erroneously used to delimit species, thus overestimating species diversity (Gao et al. 2017). In this regard, our study aimed to clearly delimit the boundaries of species included in the *D. amygdali* complex.

One of the main principles of the GCPSR, is that the transition from concordance to conflict when comparing gene genealogies determines the limits of species (Taylor et al. 2000). In order to understand the limits of species within the *D. amygdali* complex, the GCPSR principle was applied in this paper. After analyzing the individual gene genealogies, the phylogenetic discordance was evident in the tree topologies, which showed incongruent positions and conflicting branches. For instance, the isolates CAA958 and CAA959 obtained in this study, and two isolates of *D. kadsurae* were shown to be paraphyletic on the individual *tef1-a* and *cal* trees, whereas they are monophyletic in the other single and combined trees. This indicates that the genes have different evolutionary histories (Kubatko & Degnan 2007), and the concatenation to infer phylogenetic relationships is unsuitable for our dataset. By applying the GCPSR to our dataset, we consider that the *D. amygdali* complex represents a single species, given the observed incongruent subclades within the complex.

The degree of genetic diversity within the complex resolved here, was also evaluated. The overall high diversity of haplotypes above 0.5 and the substantiated low nucleotide diversity observed within the complex, may be indicative of population size expansion (Gazis et al. 2011). Moreover, positive Tajima's D values for ITS, *tub2* and *cal* were observed. This is indicative of a balancing selection,

where the absence of significant recombination for these loci maintains advantageous genetic diversity in the population (Koenig et al. 2019). In contrast, Tajima's D values gave negative for *tef1-a* and *his3* genes and for the combined alignment, which indicates a possible recent population expansion. This suggests an excess of rare alleles in the population that have arisen after the fixation of a new beneficial genetic variant (Korneliussen et al. 2013). Thus, this may be explained by inbreeding events within the population, occurring mainly in *tef1-a* and *his3* loci that showed significant recombination, suggesting that *D. amygdali* is a single entity producing a large number of offspring (Linde 2010). Consequently, this can lead to recently diverged individuals within the complex that retained ancestral polymorphisms, *i.e.*, a population under incomplete lineage sorting, thus explaining the existence of incongruences between gene trees (Stewart et al. 2014).

Taking into consideration that concatenation of genes is not advisable in the presence of conflicts between individual genes trees, coalescent-based species delimitation methods based on the Poisson Tree Processes and the General Mixed Yule Coalescent were applied. In previous studies, authors have applied coalescent methods to estimate the limits of species. For instance, Bustamante et al. (2019) were able to establish the boundaries of the morphologically conserved genus *Beauveria* and confirmed cryptic diversity in five species. Liu et al. (2016) found that species of *Colletotrichum siamense sensu lato* were described as distinct lineages based on the concatenation of genes, whereas those results were not supported when applying the coalescent methods, showing that *C. siamense s. lat.* was not a species complex but a single species. Their outcomes are quite similar to those of our study on *D. amygdali* complex. In the present work, many clades within the *D. amygdali* complex in the concatenated analysis (Fig. 1) were well supported and some of them were previously described as distinct species. However, this overestimation of species was not supported by the coalescent methods, that is the GMYC and PTP analyses inferred that the *D. amygdali* complex should be recognized as single species. Moreover, based on the phylogenetic networks for each locus and the PTP analysis performed for the combined dataset of ITS and *tef1-a*, it seems clear that all species that fall into the *D. amygdali* complex should be regarded as one single species, *i.e.*, *D. amygdali*.

Studies of morphological and ecological characteristics are also used in species delimitation (Liu et al. 2016), although not always obvious as species defined based on these characteristics often comprise more than one species when the Phylogenetic Species Recognition is applied (Harrington & Rizzo 1999; Taylor et al. 2000). The Ecological Species Concepts consists of a set of lineages that occupies a specific niche and that evolves separately from all other lineages (Harrington & Rizzo 1999; Steenkamp et al. 2018). As stated by Liu et al. (2016), distinct species recognized in the phylogenetic tree can be used as guide to diagnose ecological differences among clades. However, in this study, we clearly show a lack of phylo-geographical association among species belonging to the *D. amygdali* complex, as they show a worldwide distribution, *i.e.*, none of the well-supported clades in the complex is restricted to a specific locality (Dissanayake & Phillips 2017). Additionally, the nine clades recognized in the multilocus tree as hypothesized “species”, were tested for genetic exchange. Our results revealed significant genetic recombination within the group and among some of the paired clades, indicating a lack of reproductive isolation. For instance, strains of clades a (host: *Prunus persica* and *P. dulcis*), b (host: *Prunus persica*), d (host: *Vaccinium corymbosum*), e (host: *Prunus dulcis*) and f (host: *Kadsura longipedunculata* and *Acer* sp.) showed recombination with strains of clade i (host: *Prunus salicina* and *Pyrus pyrifolia*). Therefore, these ecological aspects evidence a clear absence of host plant and geographic barriers to gene flow.

The Morphological Species Concept was for many years the dominant concept in *Diaporthe*, where all the described fungi were diagnosed by morphological characters (Rehner & Uecker 1994). However, this approach is no longer suitable in this genus, due to the presence of conserved morphological characters (Mostert et al. 2001; Udayanga et al. 2012). Based on published descriptions, the *D. amygdali* complex shows morphological indistinctiveness. It was shown that all species harbor ovoid to ellipsoid alpha conidia, a common absence of beta conidia, yellowish translucent conidial masses and conidiomata and conidiophore dimensions that lie within the same ranges. Moreover, although the dendrogram of conidial and conidiophores length and width differentiated the species into two different groups, they do not support any of the clades in the

combined and individual phylograms. Therefore, we assume that the differences in conidia and conidiophores size are merely a reflection of variability within *D. amygdali* and character plasticity (Mostert et al. 2001).

Most of the recognized species in the *D. amygdali* complex were proposed based on just a few strains, which might be the main reason for the ambiguous species boundaries in this complex, as advocated by Gao et al. (2016). For example, although the sister clades of *D. sterilis* and *D. amygdali* received strong support values and were well separated in the phylogenetic trees of Lombard et al. (2014), their distinctiveness was not supported in the phylogenetic analyses carried out by Gao et al. (2016) when more strains were strains of the same species, were distributed throughout different clades in the individual phylograms, which probably indicates intraspecific variability within the complex, rather than different taxa. It has therefore been proposed that a large number of strains and ideally from different locations, should always be included to delimitate species or to describe novel taxa in the genus *Diaporthe* (Gao et al. 2016; Liu et al. 2016).

Apart from the *D. amygdali* complex discussed here, several other complexes in the genus *Diaporthe* seem to have lineages with similar morphological characteristics. For instance, the *D. eres* species complex is shown to harbor common rod-shaped conidia (Udayanga et al. 2014); *D. sojae* complex showing oval conidia with obtusely rounded ends (Udayanga et al. 2015) and *D. arecae* complex that display typically acutely rounded conidia (Guo et al. 2020). Harrington & Rizzo (1999) advocated that the Phylogenetic Species Recognition diagnoses species as “the smallest aggregation of populations with a common lineage that share unique, diagnosable phenotypic characters”. Although this concept can be particularly difficult in fungi (Taylor et al. 2000), by following this description and taking into consideration that these complexes seem to correlate with their DNA phylogeny, it is plausible that these species complexes may represent a single species with high intraspecific variability, characteristic of the genus *Diaporthe* (Gomes et al. 2013). Therefore, the use of coalescent methods should be considered in future studies as an important tool to resolve the boundaries of species complexes in *Diaporthe*.

CONCLUSIONS

In the present study, molecular analyses based on GCPSR, and coalescent methods (GMYC and PTP) provide strong evidence that *D. amygdali* is a single species rather than a species complex. Moreover, the pairwise homoplasy index test and the comparison of morphological and ecological characters, have strengthened the fact that reproductive isolation and geographical or host plant barriers to gene flow are absent. This study has also demonstrated that the identification of species in *Diaporthe* might be overestimated, assuming that all well-supported clades have been accepted as distinct species when using the concatenation of multilocus DNA sequences. Therefore, we highly recommend that the individual gene genealogies must always be checked for incongruencies and carefully analyzed prior to the description of new taxa. Moreover, we also propose that sequencing all five loci currently accepted in the genus *Diaporthe* (ITS, *tef1-a*, *tub2*, *his3*, *cal*) should be considered in future studies to make them available for other researchers. It is also clear that multiple strains from different origins should be included in the analyses to assess intraspecific variation. Lastly, upcoming studies including the coalescent methods GMYC and PTP should be implemented in the genus *Diaporthe* to provide accurate information to restructure the phylogenetic relationships between species. This approach will be of the utmost importance to identify the species more precisely, which might revolutionize the current knowledge of the boundaries of *Diaporthe* species as we known them.

ACKNOWLEDGMENTS

The authors are thankful to the Portuguese Foundation for Science and Technology (FCT/MCTES) for financing CESAM (Centro de Estudos do Ambiente e do Mar) (UIDP/50017/2020 + UIDB/50017/2020) through national funds, and the PhD grant of Sandra Hilário (SFRH/BD/137394/2018). Liliana Santos is funded by national funds (OE), through FCT in the scope of the framework contract foreseen in the numbers 4, 5 and 6 of the article 23, of the Decree-Law 57/2016, of August 29, changed by Law 57/2017, of July 19. We want to acknowledge Hugo Botelho and Pedro Pinho (Bfruit nature flavors, Portugal), Jorge Duarte (Hortitool Consulting, Lda) and Ana Moreira for supplying the plant material from their plantations.

REFERENCES

- Bruen TC. **2005**. A simple and robust statistical test for detecting the presence of recombination. *Genetics* 172, 2665–2681.
- Bustamante DE, Oliva M, Leiva S, Mendoza JE, Bobadilla L, Angulo G, Calderon MS, **2019**. Phylogeny and species delimitations in the entomopathogenic genus *Beauveria* (Hypocreales, Ascomycota), including the description of *B. peruviana* sp. nov. *MycoKeys* 58, 47–68.
- Canonaco A. **1936**. Il seccume dei rameti di mandorlo in relazione ad alcuni micromiceti. *Rivista di Patologia Vegetale* 26, 145–164.
- Carstens BC, Knowles LL. **2007**. Estimating species phylogeny from gene-tree probabilities despite incomplete lineage sorting: an example from *Melanoplus grasshoppers*. *Systematic Biology* 56, 400–411.
- Crous PW, Palm ME. **1999**. Reassessment of the anamorph genera *Botryodiplodia*, *Dothiorella* and *Fusicoccum*. *Sydowia* 51, 161–175.
- Degnan JH, Rosenberg NA. **2009**. Gene tree discordance, phylogenetic inference and the multispecies coalescent. *Trends in Ecology & Evolution* 24, 332–340.
- Delacroix G. **1905**. Sur une maladie des amandiers en Provence. *Bulletin Trimestriel de Société Mycologique de France* 21, 180–185.
- Diogo ELF, Santos JM, Phillips AJL. **2010**. Phylogeny, morphology and pathogenicity of *Diaporthe* and *Phomopsis* species on almond in Portugal. *Fungal Diversity* 44, 107–115.
- Dissanayake A, Phillips AJL. **2017**. Advances in understanding *Diaporthe*. *Mycosphere* 8, 7019.
- Drummond AJ, Ho SYW, Phillips MJ, Rambaut A. **2006**. Relaxed phylogenetics and dating with confidence. *PLoS Biology* 4, e88.
- Farr DF, Rossman AY. **2020**. Fungal Databases, U.S. National Fungus Collections, ARS. USDA. Available online <https://nt.ars-grin.gov/fungal-databases/> (accessed on 14 July 2020).
- Fujisawa T, Barraclough TG. **2013**. Delimiting species using single-locus data and the Generalized Mixed Yule Coalescent approach: a revised method and evaluation on simulated data sets. *Systematic Biology* 62, 707–724.

- Galili T. **2015**. dendextend: an R package for visualizing, adjusting, and comparing trees of hierarchical clustering. *Bioinformatics* 31, 3718–3720.
- Gao YH, Liu F, Cai L. **2016**. Unravelling *Diaporthe* species associated with *Camellia*. *Systematic Biodiversity* 14, 102–117.
- Gao YH, Liu F, Duan W, Crous PW, Cai L. **2017**. *Diaporthe* is paraphyletic. *IMA Fungus* 8, 163–187.
- Gao YH, Su Y, Sun W, Cai L. **2015**. *Diaporthe* species occurring on *Lithocarpus glabra* in China, with descriptions of five new species. *Fungal Biology* 119, 295–309.
- Gao YH, Sun W, Su YY, Cai L. **2014**. Three new species of *Phomopsis* in Gutianshan nature reserve in China. *Mycological Progress* 13, 111–121.
- Gazis R, Rehner S, Chaverri P. **2011**. Species delimitation in fungal endophyte diversity studies and its implications in ecological and biogeographic inferences. *Molecular Ecology* 20, 3001–3013.
- Gernhard T. **2008**. The conditioned reconstructed process. *Journal of Theoretical Biology* 253, 769–778.
- Gomes RR, Glienke C, Videira SIR, Lombard L, Groenewald JZ, Crous PW. **2013**. *Diaporthe*: a genus of endophytic, saprobic and plant pathogenic fungi. *Persoonia* 31, 1–41.
- Guo YS, Crous PW, Bai Q, Fu M, Yang MM, Wang XH, Du YM, Hong N, Xu WX, Wang GP. **2020**. High diversity of *Diaporthe* species associated with pear shoot canker in China. *Persoonia* 45, 132–162.
- Harrington TC, Rizzo DM. **1999**. Defining species in the fungi. In: Worrall JJ, ed. *Structure and Dynamics of Fungal Populations*. Dordrecht, Netherlands: Springer. p. 43–71.
- Huson DH, Bryant D. **2006**. Application of phylogenetic networks in evolutionary studies. *Molecular Biology and Evolution* 23, 254–267.
- Hyde KD, Hongsanan S, Jeewon R, Bhat DJ, McKenzie EHC, Jones EBG, Rungtiwa P, Ariyawansa HA, Saranyaphat B, Zhao Q, ... Tanaka K. **2016**. Fungal diversity notes 367–492, taxonomic and phylogenetic contributions to fungal taxa. *Fungal Diversity* 80, 1–270.

- Koenig D, Hagmann J, Li R, Bemm F, Slotte T, Neuffer B, Wright SI, Weigel D. **2019**. Long-term balancing selection drives evolution of immunity genes in *Capsella*. *eLife* 8, e43606.
- Korneliussen TS, Moltke I, Albrechtsen A, Nielsen R. **2013**. Calculation of Tajima's D and other neutrality test statistics from low depth next-generation sequencing data. *BMC Bioinformatics* 14, 289.
- Kubatko LS, Degnan JH. **2007**. Inconsistency of phylogenetic estimates from concatenated data under coalescence. *Systematic Biology* 56, 17–24.
- León M, Berbegal M, Rodríguez-Reina J, Elena G, Abad-Campos P, Ramón-Albalat A, Olmo D, Vicent A, Luque J, Miarnau X, ... Armengol J. **2020**. Identification and characterization of *Diaporthe* spp. Associated with twig cankers and shoot blight of almonds in Spain. *Agronomy* 10, 1062.
- Lesuthu P, Mostert L, Spies CFJ, Moyo P, Regnier T, Halleen F. **2019**. *Diaporthe nebulae* sp. nov. and first report of *D. cynaroidis*, *D. novem*, and *D. serafiniae* on grapevines in South Africa. *Plant Disease* 103, 808–817.
- Linde CC. **2010**. Population genetic analyses of plant pathogens: new challenges and opportunities. *Australasian Plant Pathology* 39, 23–28.
- Liu F, Wang M, Damm U, Crous PW, Cai L. **2016**. Species boundaries in plant pathogenic fungi: a *Colletotrichum* case study. *BMC Evolutionary Biology* 16, 81.
- Lombard L, van Leeuwen GCM, Guarnaccia V, Polizzi G, van Rijswijk PCJ, Rosendahl CHM, Gabler J, Crous PW. **2014**. *Diaporthe* species associated with *Vaccinium*, with specific reference to Europe. *Phytopathologia Mediterranea* 53, 287–299.
- Monaghan MT, Wild R, Elliot M, Fujisawa T, Balke M, Inward DJG, Lees DC, Ranaivosolo R, Eggleton P, Barraclough TG, Vogler AP. **2009**. Accelerated species inventory on Madagascar using coalescent-based models of species delineation. *Systematic Biology* 58, 298–311.
- Mostert L, Crous PW, Kang JC, Phillips AJL. **2001**. Species of *Phomopsis* and a *Libertella* sp. occurring on grapevines with specific reference to South Africa: morphological, cultural, molecular and pathological characterization. *Mycologia* 93, 146–167.

- Murtagh F, Legendre P. **2014**. Ward's hierarchical agglomerative clustering method: which algorithms implement Ward's criterion? *Journal of Classification* 31, 274–295.
- Pons J, Barraclough T, Gomez-Zurita J, Cardoso A, Duran D, Hazell S, Kamoun S, Sumlin W, Vogler A. **2006**. Sequence-based species delimitation for the DNA taxonomy of undescribed insects. *Systematic Biology* 55, 595–609.
- R Core Team. **2019**. R: A language and environment for statistical computing. R foundation for statistical computing. Austria, Vienna. Available online <https://www.R-project.org/>.
- Rambaut A. **2018**. FigTree, a graphical viewer of phylogenetic trees. Available online <http://tree.bio.ed.ac.uk/software/figtree>.
- Rambaut A, Drummond AJ, Xie D, Baele G, Suchard MA. **2018**. Posterior summarisation in Bayesian phylogenetics using Tracer 1.7. *Systematic Biology* syy032.
- Rehner SA, Uecker FA. **1994**. Nuclear ribosomal internal transcribed spacer phylogeny and host diversity in the coelomycete *Phomopsis*. *Canadian Journal of Botany* 72, 1666–1674.
- Rozas J, Ferrer-Mata A, Sánchez-DelBarrio JC, Guirao-Rico S, Librado P, Ramos-Onsins SE, Sánchez-Gracia A. **2017**. DnaSP 6: DNA sequence polymorphism analysis of large data sets. *Molecular Biology and Evolution* 34, 3299–3302.
- Santos L, Alves A, Alves R. **2017**. Evaluating multi-locus phylogenies for species boundaries determination in the genus *Diaporthe*. *PeerJ* 5, e3120.
- Steenkamp ET, Wingfield MJ, McTaggart AR, Wingfield BD. **2018**. Fungal species and their boundaries matter e definitions, mechanisms and practical implications. *Fungal Biology Reviews* 32, 104–116.
- Stewart JE, Timmer LW, Lawrence CB, Pryor BM, Peever TL. **2014**. Discord between morphological and phylogenetic species boundaries: incomplete lineage sorting and recombination results in fuzzy species boundaries in an asexual fungal pathogen. *BMC Evolutionary Biology* 14, 38.
- Suchard MA, Lemey P, Baele G, Ayres DL, Drummond AJ, Rambaut A. **2018**. Bayesian phylogenetic and phylodynamic data integration using BEAST 1.10. *Virus Evolution* 4 vey016.

- Tajima F. **1989**. Statistical method for testing the neutral mutation hypothesis by DNA polymorphism. *Genetics* 123, 585–595.
- Taylor JW, Jacobson DJ, Kroken S, Kasuga T, Geiser DM, Hibbett DS, Fisher MC, **2000**. Phylogenetic species recognition and species concepts in fungi. *Fungal Genetics and Biology* 31, 21–32.
- Tuset JJ, Portilla MAT. **1989**. Taxonomic status of *Fusicoccum amygdali* and *Phomopsis amygdalina*. *Canadian Journal of Botany* 67, 1275–1280.
- Udayanga D, Castlebury LA, Rossman AY, Chukeatirote E, Hyde, K.D. **2014**. Insights into the genus *Diaporthe*: phylogenetic species delimitation in the *D. eres* species complex. *Fungal Diversity* 67, 203–229.
- Udayanga D, Castlebury LA, Rossman AY, Chukeatirote E, Hyde KD. **2015**. The *Diaporthe sojae* species complex: Phylogenetic reassessment of pathogens associated with soybean, cucurbits and other field crops. *Fungal Biology* 119, 383–407.
- Udayanga D, Liu XZ, Crous PW, McKenzie EHC, Chukeatirote E, Hyde KD. **2012**. A multi-locus phylogenetic evaluation of *Diaporthe* (*Phomopsis*). *Fungal Diversity* 56, 157–171.
- Udayanga D, Liu X, McKenzie EHC, Chukeatirote E, Bahkali AHA, Hyde KD. **2011**. The genus *Phomopsis*: biology, applications, species concepts and names of common phytopathogens. *Fungal Diversity* 50, 189–225.
- Yang Q, Fan XL, Guarnaccia V, Tian CM. **2018**. High diversity of *Diaporthe* species associated with dieback diseases in China, with twelve new species described. *MycKeys* 39, 97–149.
- Zapata M, Palma MA, Aninat MJ, Piontelli E. **2020**. Polyphasic studies of new species of *Diaporthe* from native forest in Chile, with descriptions of *Diaporthe araucanorum* sp. nov., *Diaporthe foikelawen* sp. nov. and *Diaporthe patagonica* sp. nov. *International Journal of Systematic and Evolutionary Microbiology* 70, 3379–3390.
- Zhang J, Kapli P, Pavlidis P, Stamatakis A. **2013**. A general species delimitation method with applications to phylogenetic placements. *Bioinformatics* 29, 2869–2876.

SUPPLEMENTARY MATERIAL

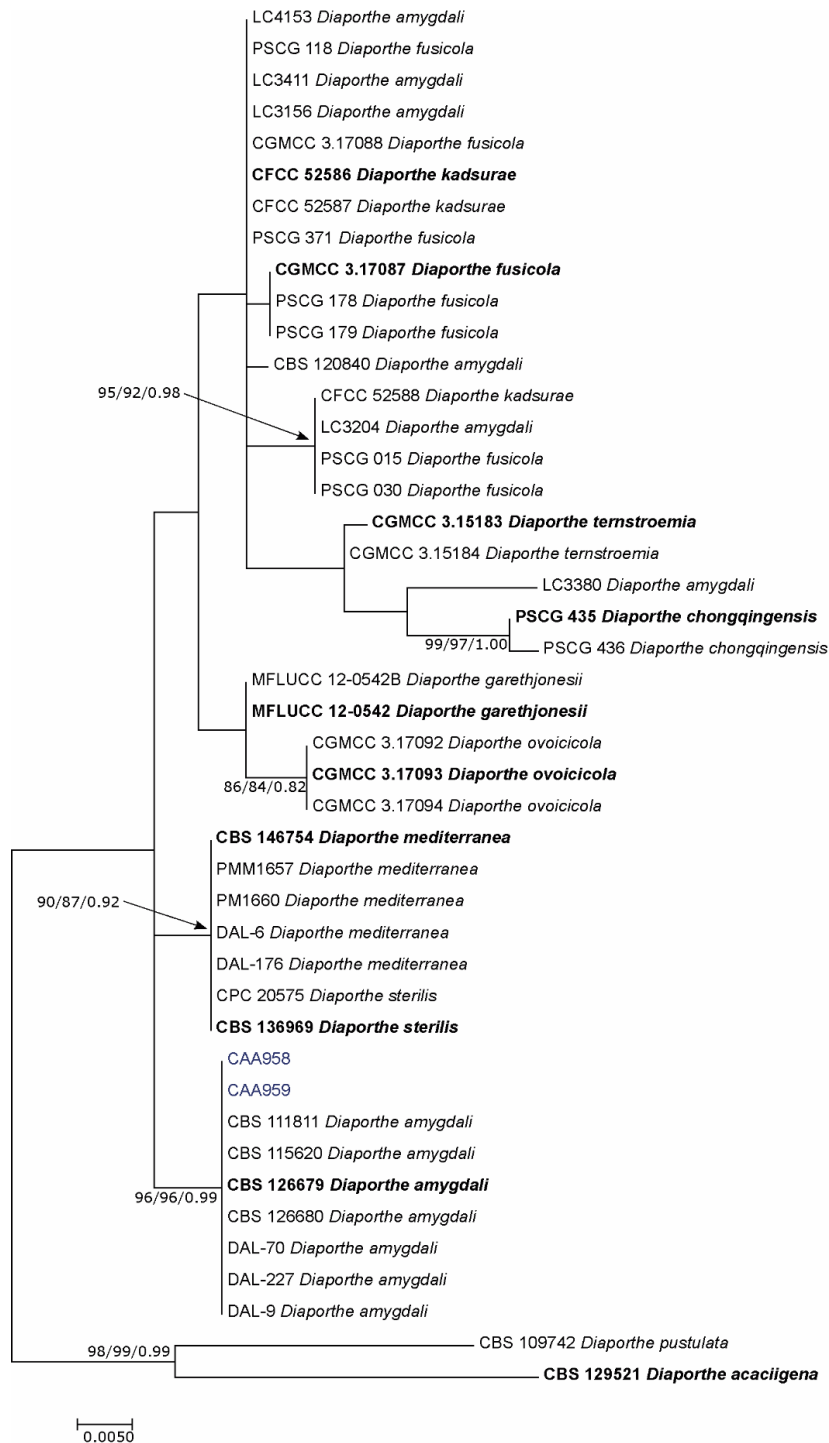


Figure S1. Phylogram generated from maximum likelihood analysis based on ITS sequence data for all strains of the *Diaporthe amygdali* species complex. The ML tree was constructed based on the Kimura 2-paramter model assuming a gamma distribution and rooted to *D. pustulata* an *D. acaciigena*. ML and MP bootstrap values greater than 70% and posterior probabilities greater than 0.80 are shown at the nodes. The ex-type strains are in bold. The newly generated sequences are indicated in blue.

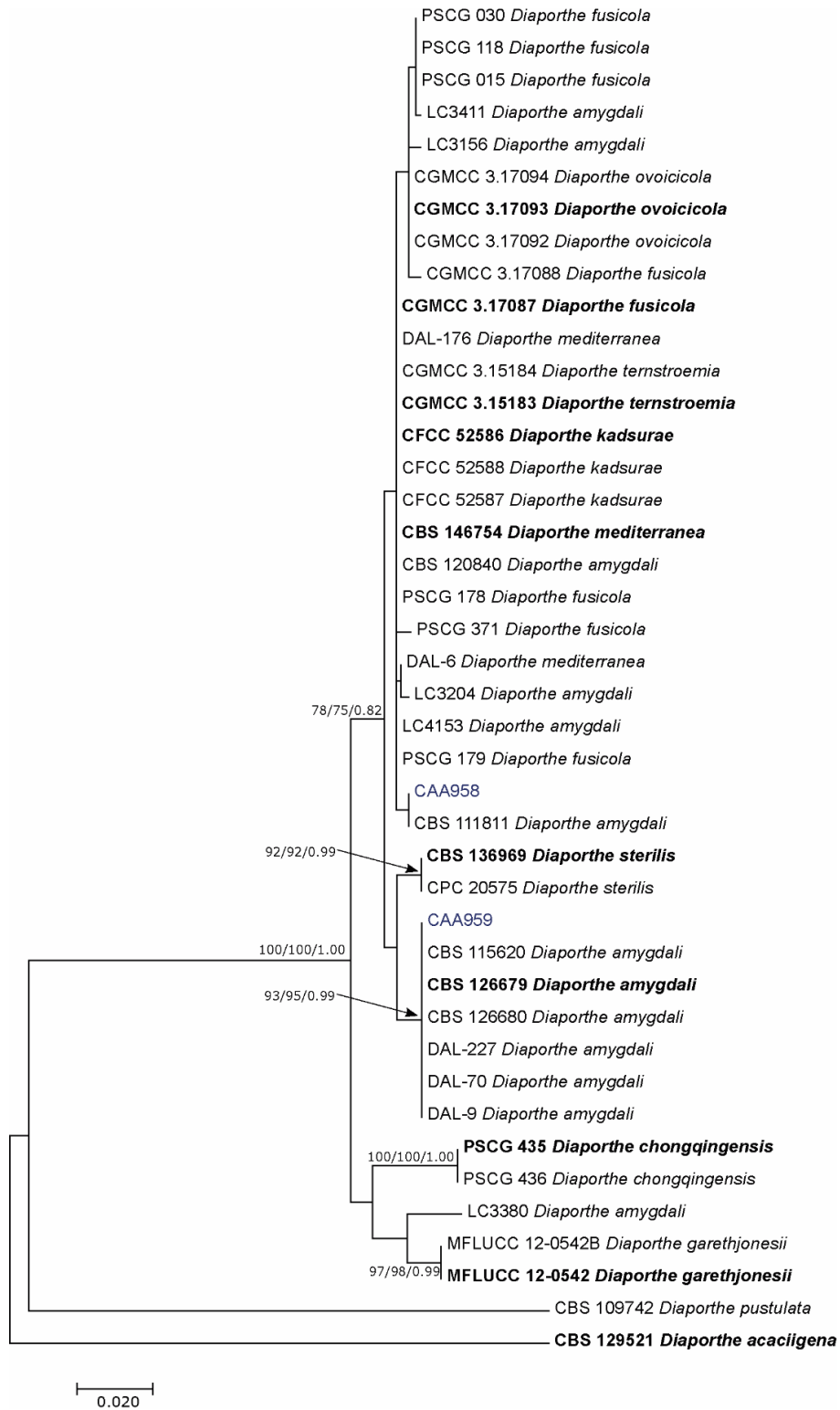


Figure S2. Phylogram generated from maximum likelihood analysis based on *tef1- α* sequence data for all strains of the *Diaporthe amygdali* species complex. The ML tree was constructed based on the Kimura 2-parameter model and rooted to *D. pustulata* and *D. acaciigena*. ML and MP bootstrap values greater than 70% and posterior probabilities greater than 0.80 are shown at the nodes. The ex-type strains are in bold. The newly generated sequences are indicated in blue.

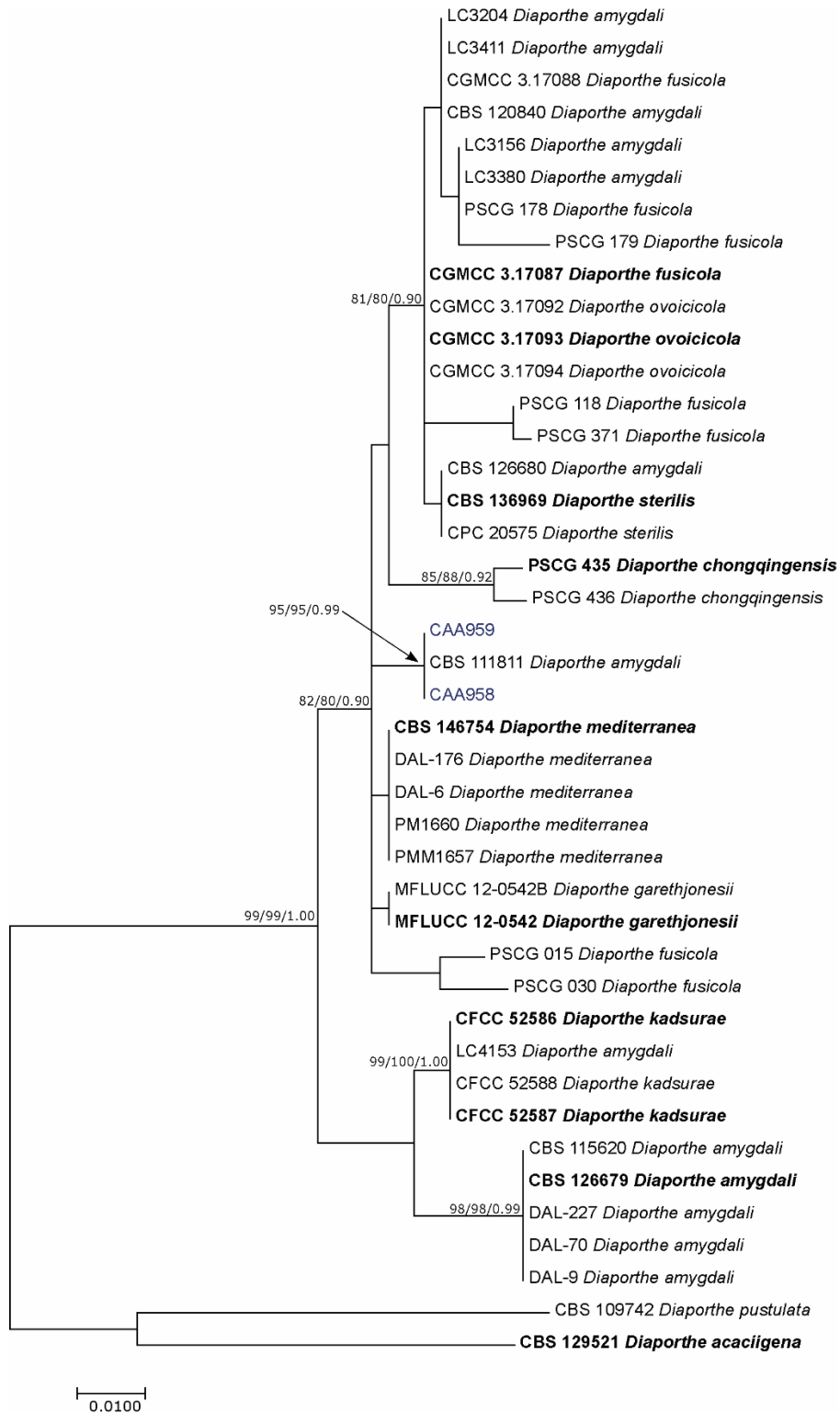


Figure S3. Phylogram generated from maximum likelihood analysis based on *tub2* sequence data for all strains of the *Diaporthe amygdali* species complex. The ML tree was constructed based on the Tamura 3-parameter model assuming a gamma distribution and rooted to *D. pustulata* and *D. acaciigena*. ML and MP bootstrap values greater than 70% and posterior probabilities greater than 0.80 are shown at the nodes. The ex-type strains are in bold. The newly generated sequences are indicated in blue.

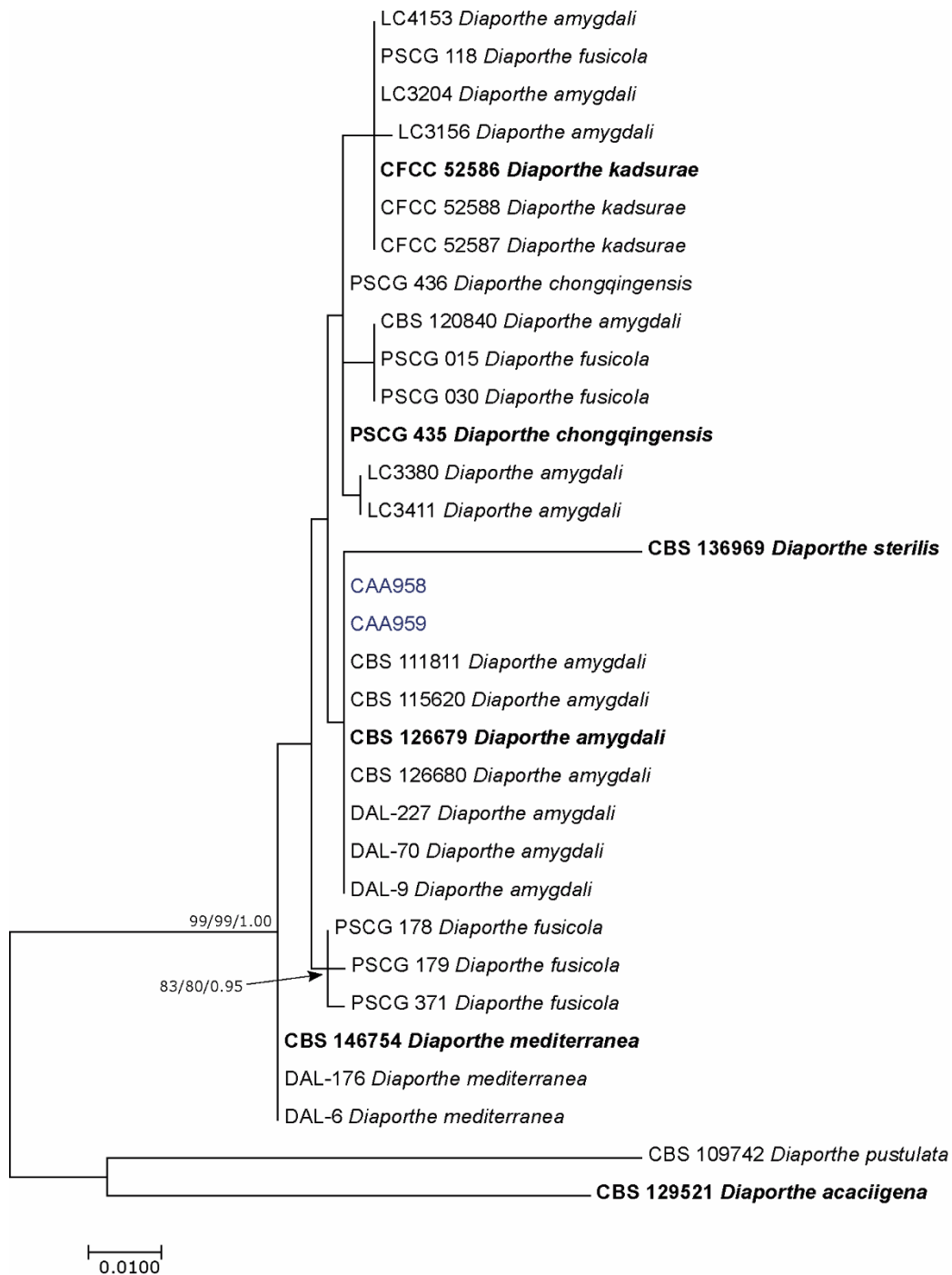


Figure S4. Phylogram generated from maximum likelihood analysis based on *his3* sequence data for all strains of the *Diaporthe amygdali* species complex. The ML tree was constructed based on the Hasegawa–Kishino–Yano model assuming a gamma distribution and rooted to *D. pustulata* and *D. acaciigena*. ML and MP bootstrap values greater than 70% and posterior probabilities greater than 0.80 are shown at the nodes. The ex-type strains are in bold. The newly generated sequences are indicated in blue.

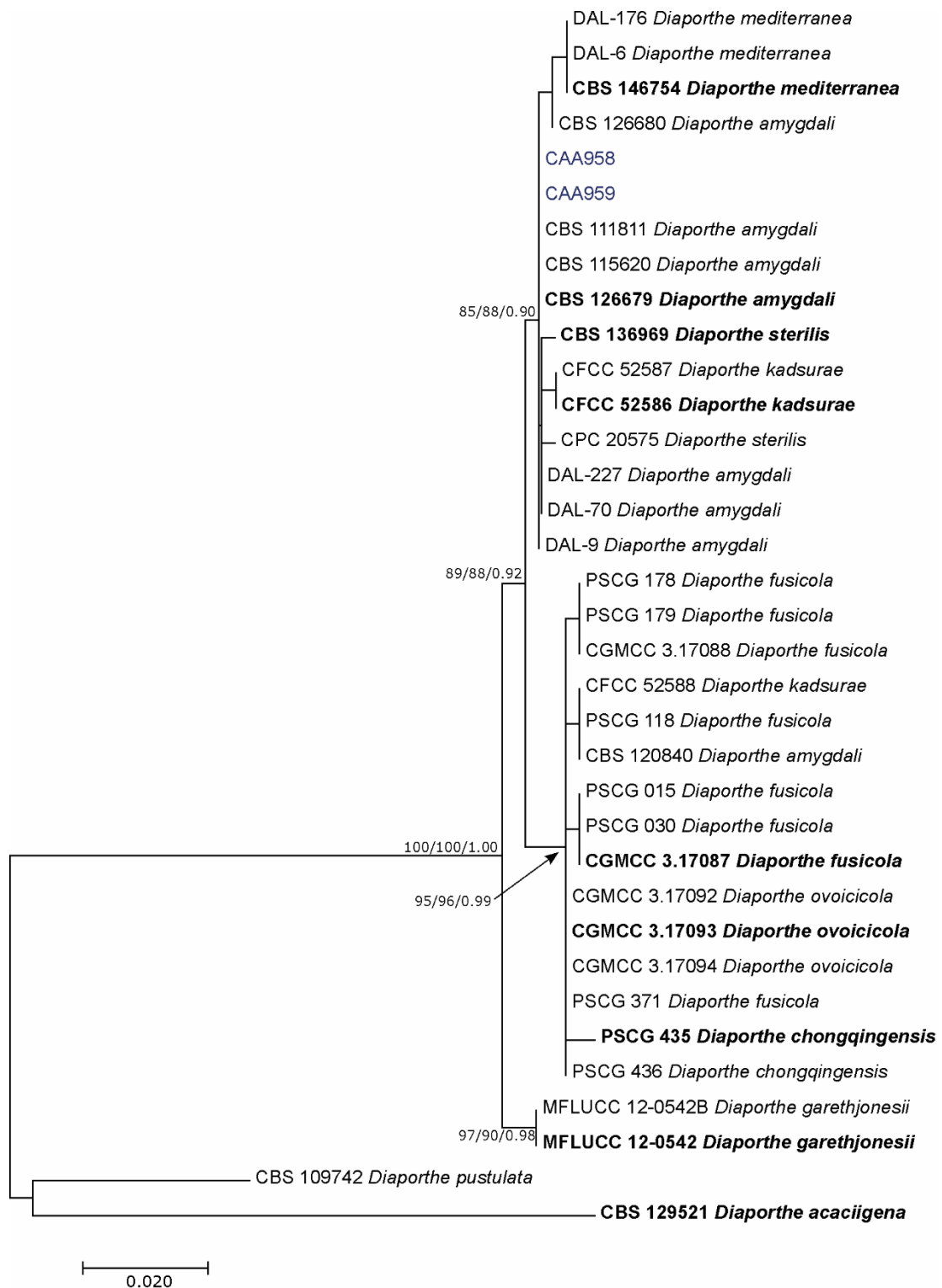


Figure S5. Phylogram generated from maximum likelihood analysis based on *cal* sequence data for all strains of the *Diaporthe amygdali* species complex. The ML tree was constructed based on the Kimura 2-parameter model and rooted to *D. pustulata* and *D. acaciigena*. ML and MP bootstrap values greater than 70% and posterior probabilities greater than 0.80 are shown at the nodes. The ex-type strains are in bold. The newly generated sequences are indicated in blue.

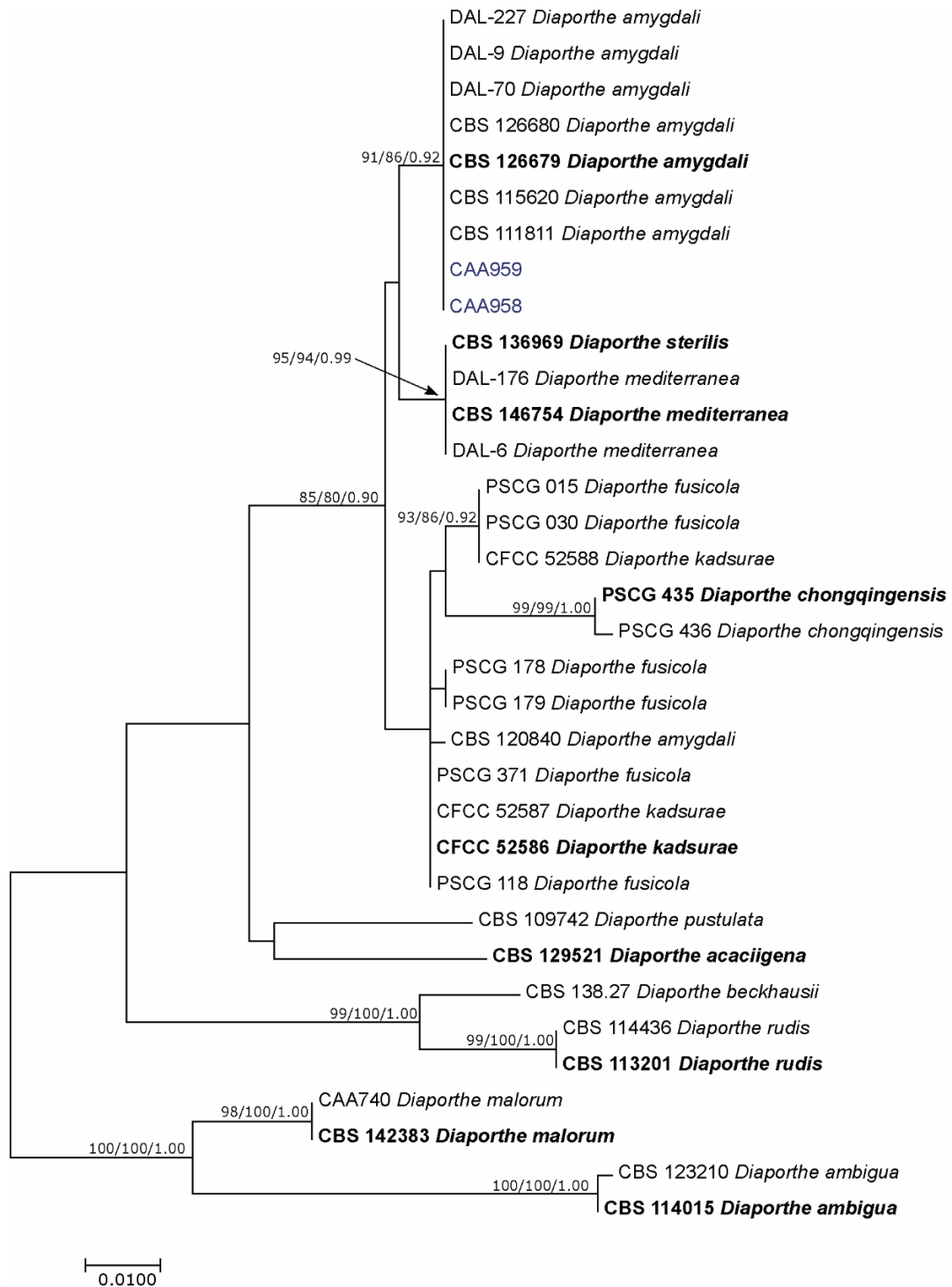


Figure S6. Phylogram generated from maximum likelihood analysis based on ITS sequence data for *Diaporthe amygdali* species complex and related species. The ML tree was constructed based on the Kimura 2-parameter model assuming a gamma distribution. ML and MP bootstrap values greater than 70% and posterior probabilities greater than 0.80 are shown at the nodes. The ex-type strains are in bold. The newly generated sequences are indicated in blue.

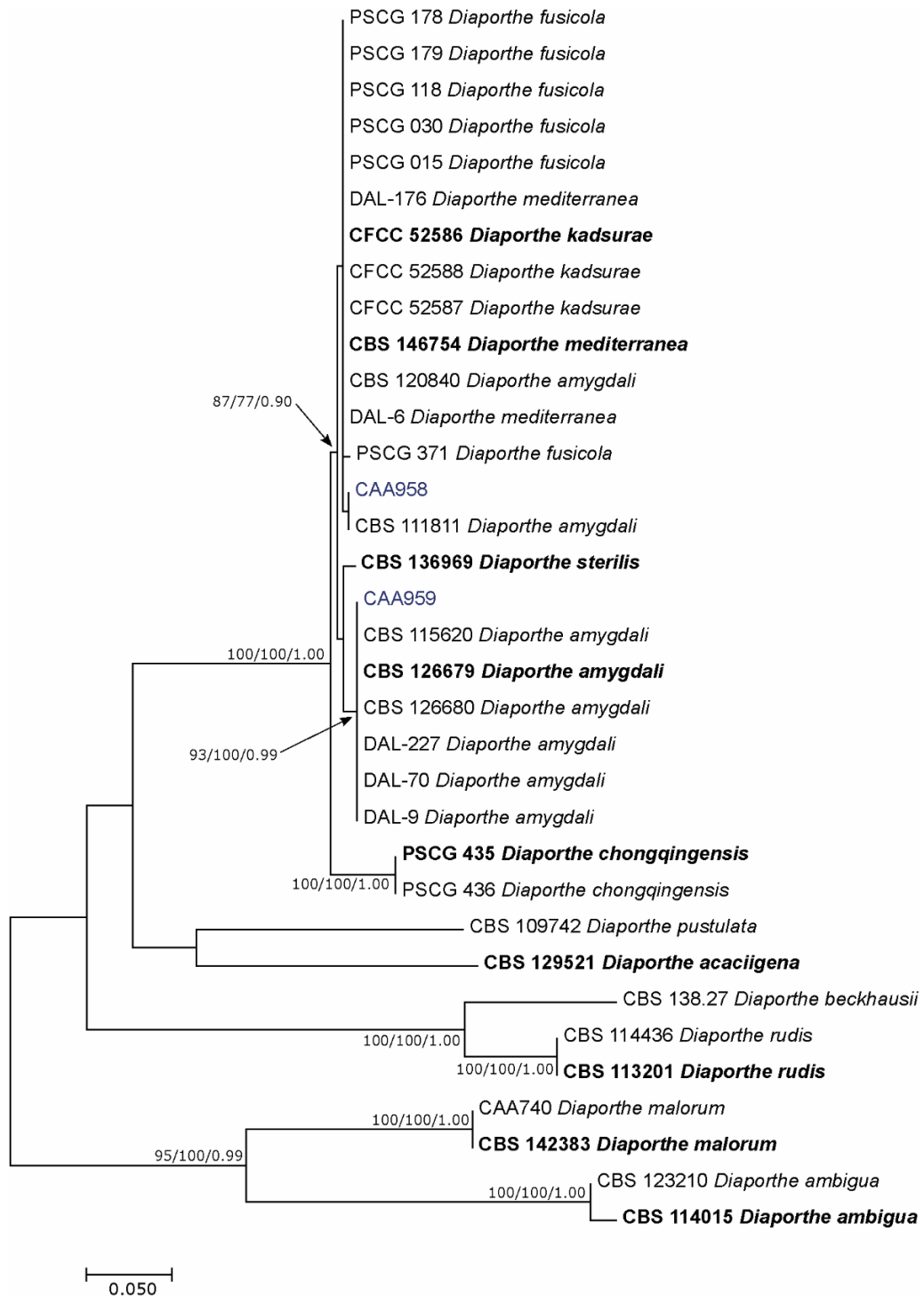


Figure S7. Phylogram generated from maximum likelihood analysis based on *tef1- α* sequence data for *Diaporthe amygdali* species complex. The ML tree was constructed based on the Hasegawa–Kishono–Yano model assuming invariant sites. ML and MP bootstrap values greater than 70% and posterior probabilities greater than 0.80 are shown at the nodes. The ex-type strains are in bold. The newly generated sequences are indicated in blue.

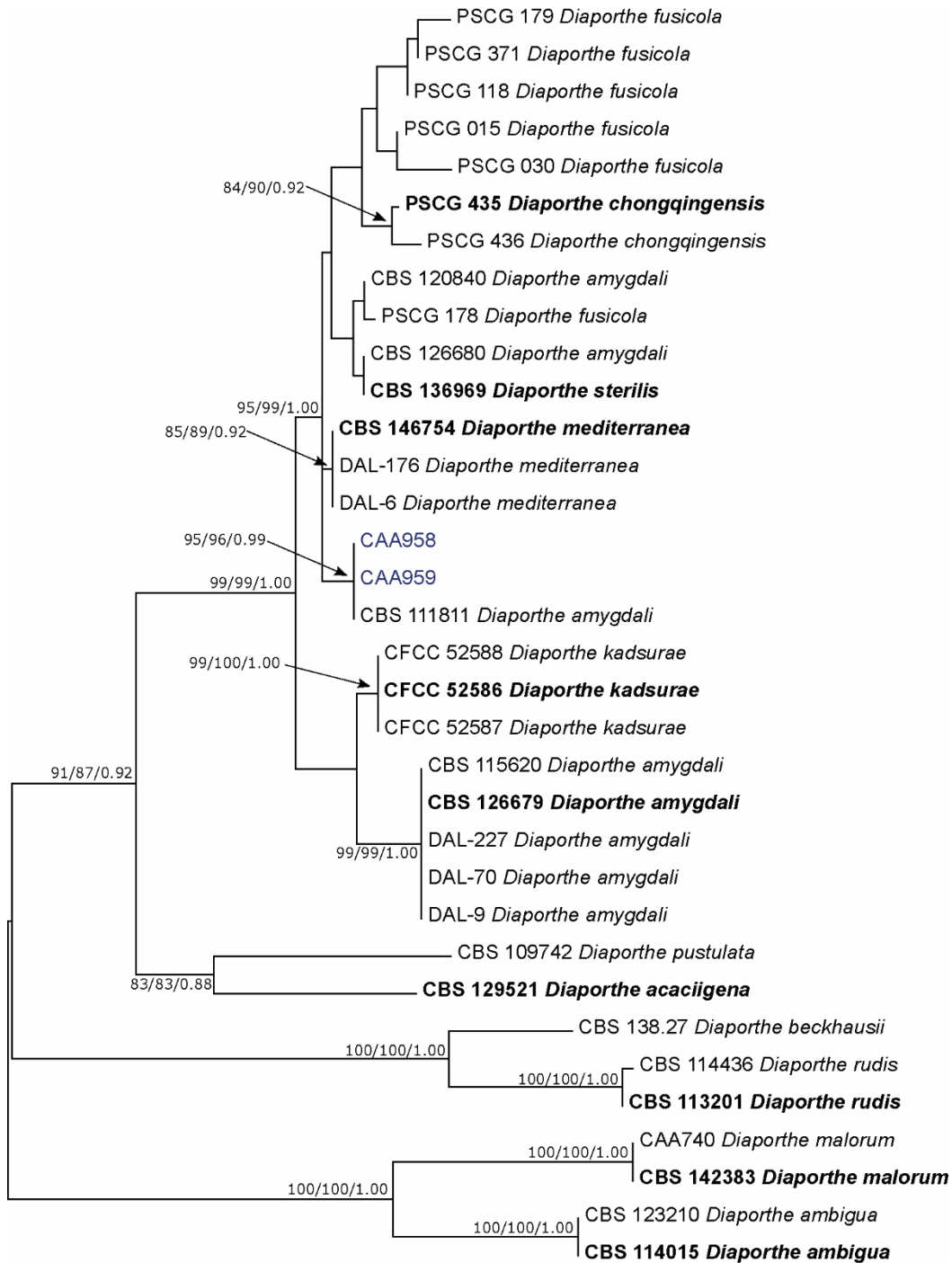


Figure S8. Phylogram generated from maximum likelihood analysis based on *tub2* sequence data for *Diaporthe amygdali* species complex. The ML tree was constructed based on the Kimura 2-parameter model assuming a gamma distribution. ML and MP bootstrap values greater than 70% and posterior probabilities greater than 0.80 are shown at the nodes. The ex-type strains are in bold. The newly generated sequences are indicated in blue.

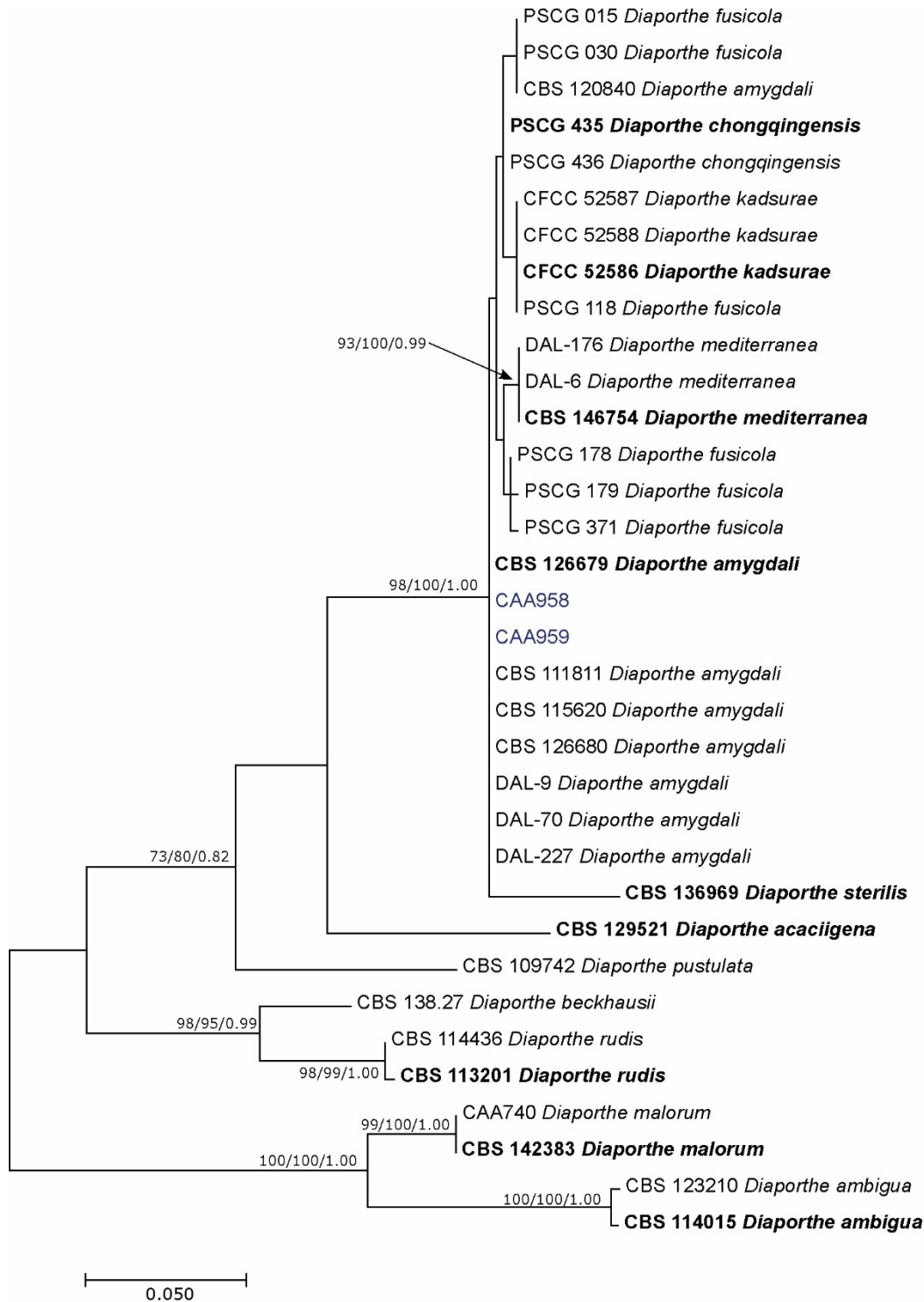


Figure S9. Phylogram generated from maximum likelihood analysis based on *his3* sequence data for *Diaporthe amygdali* species complex. The ML tree was constructed based on the Hasegawa–Kishono–Yano model assuming a gamma distribution. ML and MP bootstrap values greater than 70% and posterior probabilities greater than 0.80 are shown at the nodes. The ex-type strains are in bold. The newly generated sequences are indicated in blue.

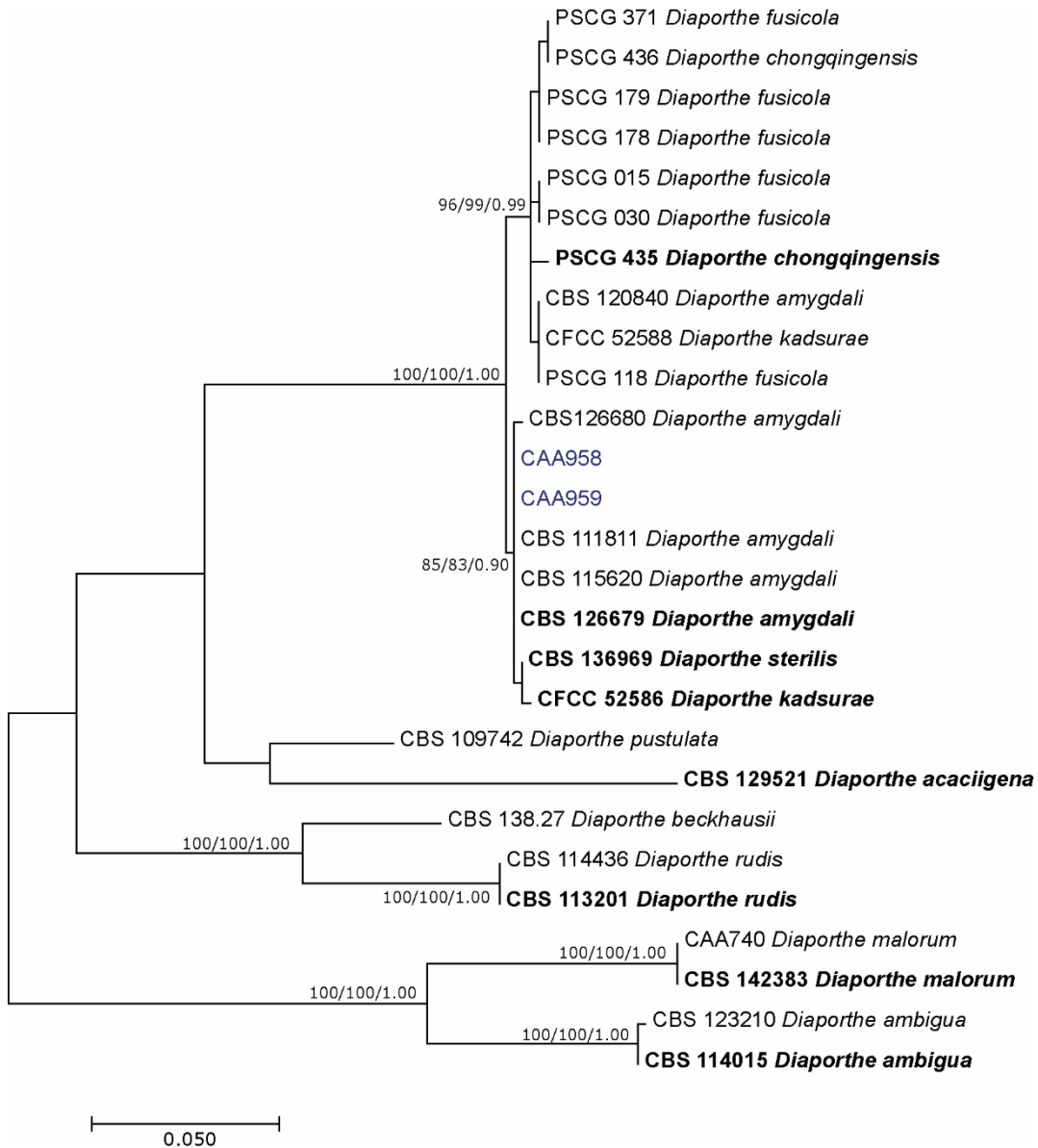


Figure S10. Phylogram generated from maximum likelihood analysis based on *cal* sequence data for *Diaporthe amygdali* species complex. The ML tree was constructed based on the Tamura 3-model assuming invariant sites. ML and MP bootstrap values greater than 70% and posterior probabilities greater than 0.80 are shown at the nodes. The ex-type strains are in bold. The newly generated sequences are indicated in blue

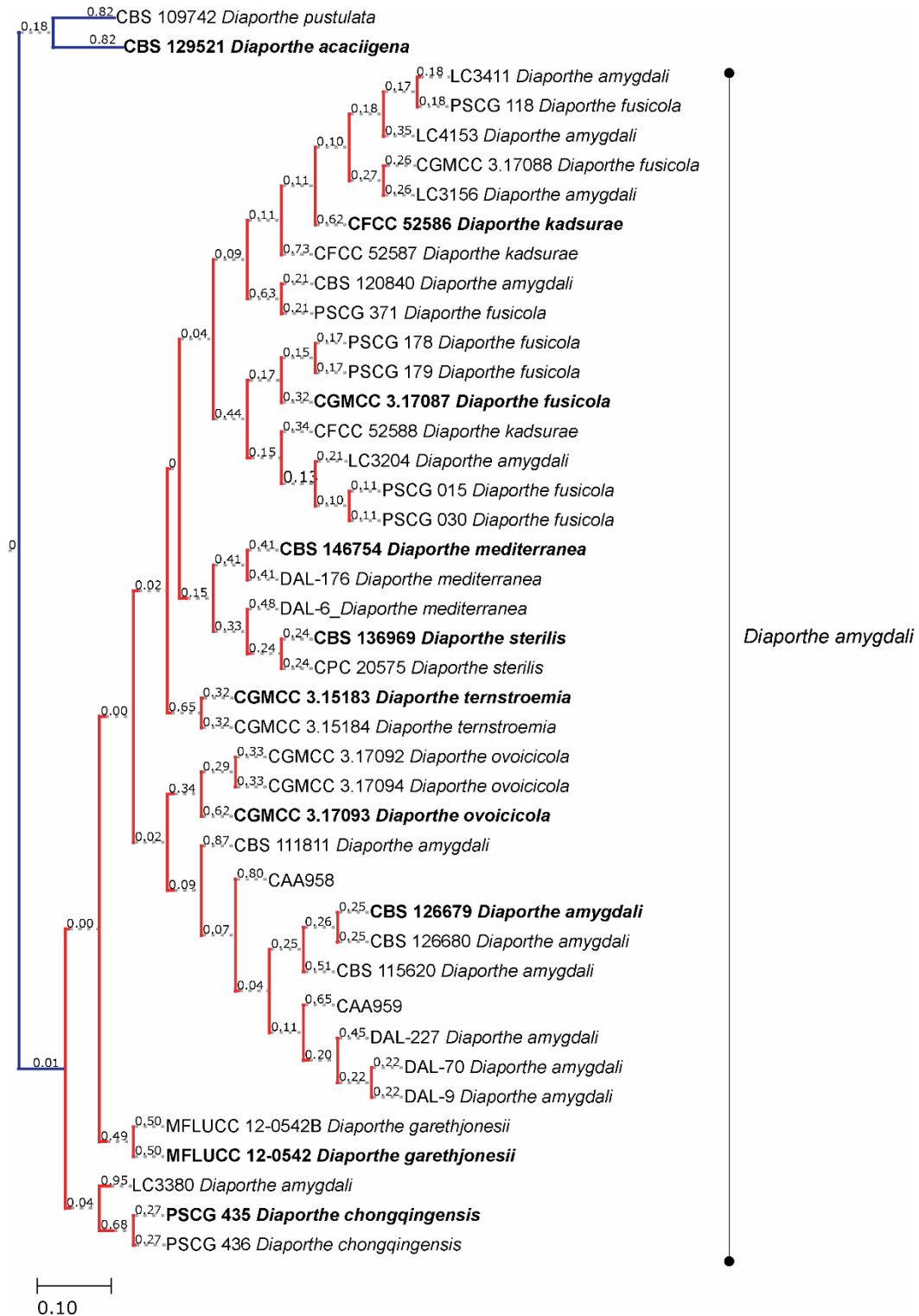


Figure S11. Results of the PTP analysis for the *Diaporthe amygdali* complex based on combined ITS and *tef1-α*. The tree was rooted to *D. pustulata* and *D. acaciigena*. Putative species clusters are indicated using transitions between blue-colored to red-colored branches.

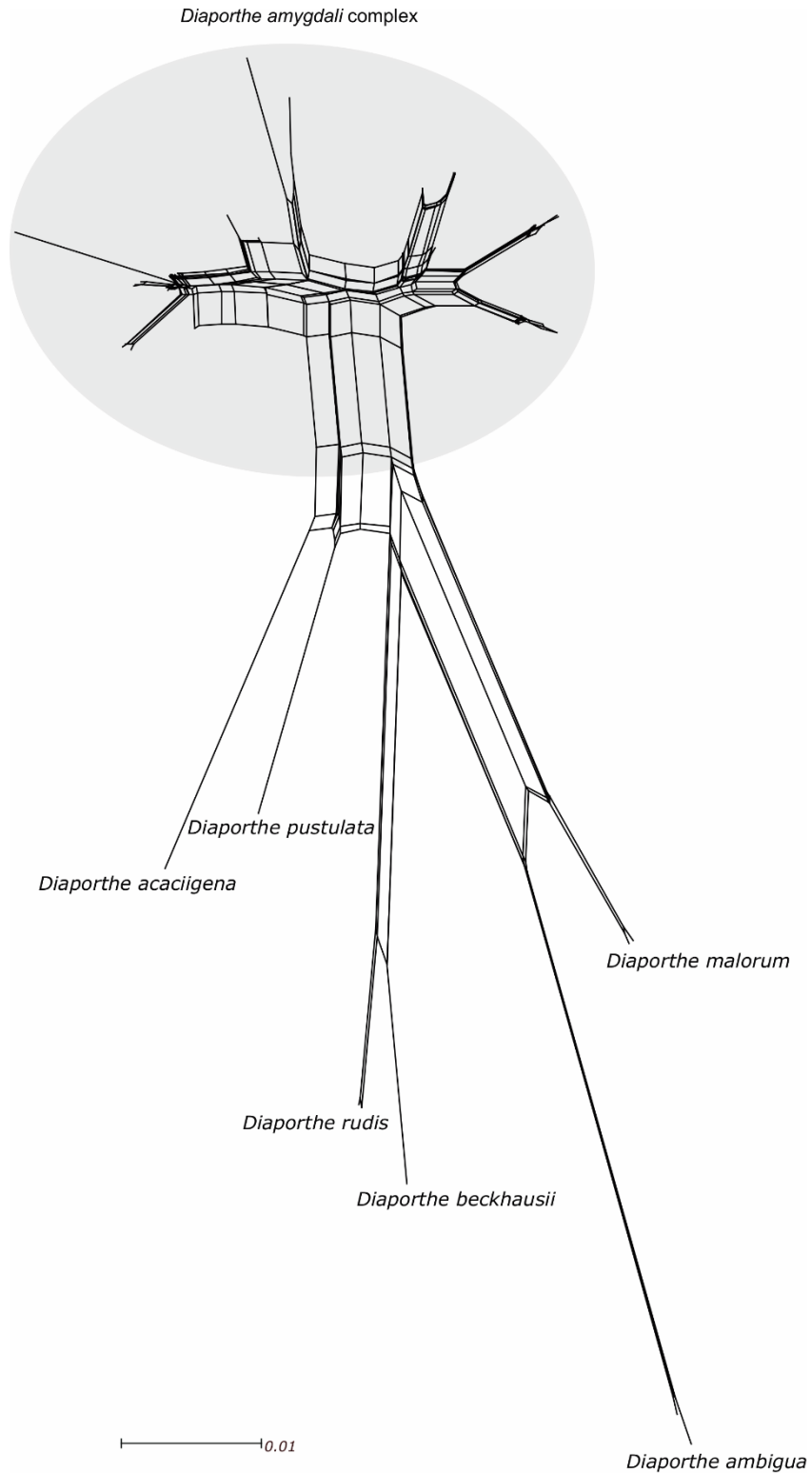


Figure S12. Phylogenetic network from ITS locus, representing the structure of the *Diaporthe amygdali* complex and other well-delimited species, based on the GTR model, as inferred by SplitsTree. The scale bar represents the expected number of substitutions per nucleotide position.

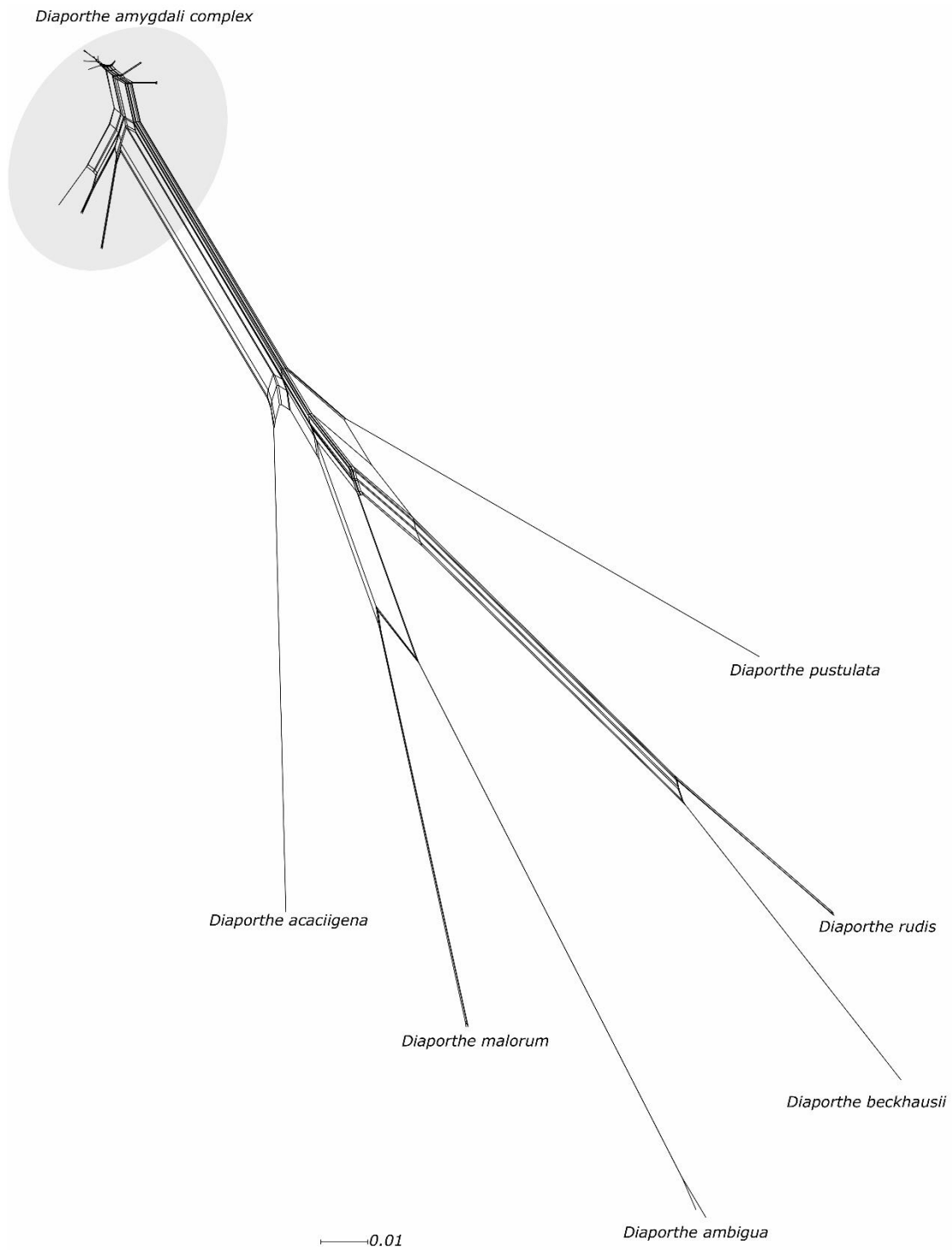


Figure S13. Phylogenetic network from *tef1- α* locus, representing the structure of the *Diaporthe amygdali* complex and other well-delimited species, based on the GTR model, as inferred by SplitsTree. The scale bar represents the expected number of substitutions per nucleotide position.

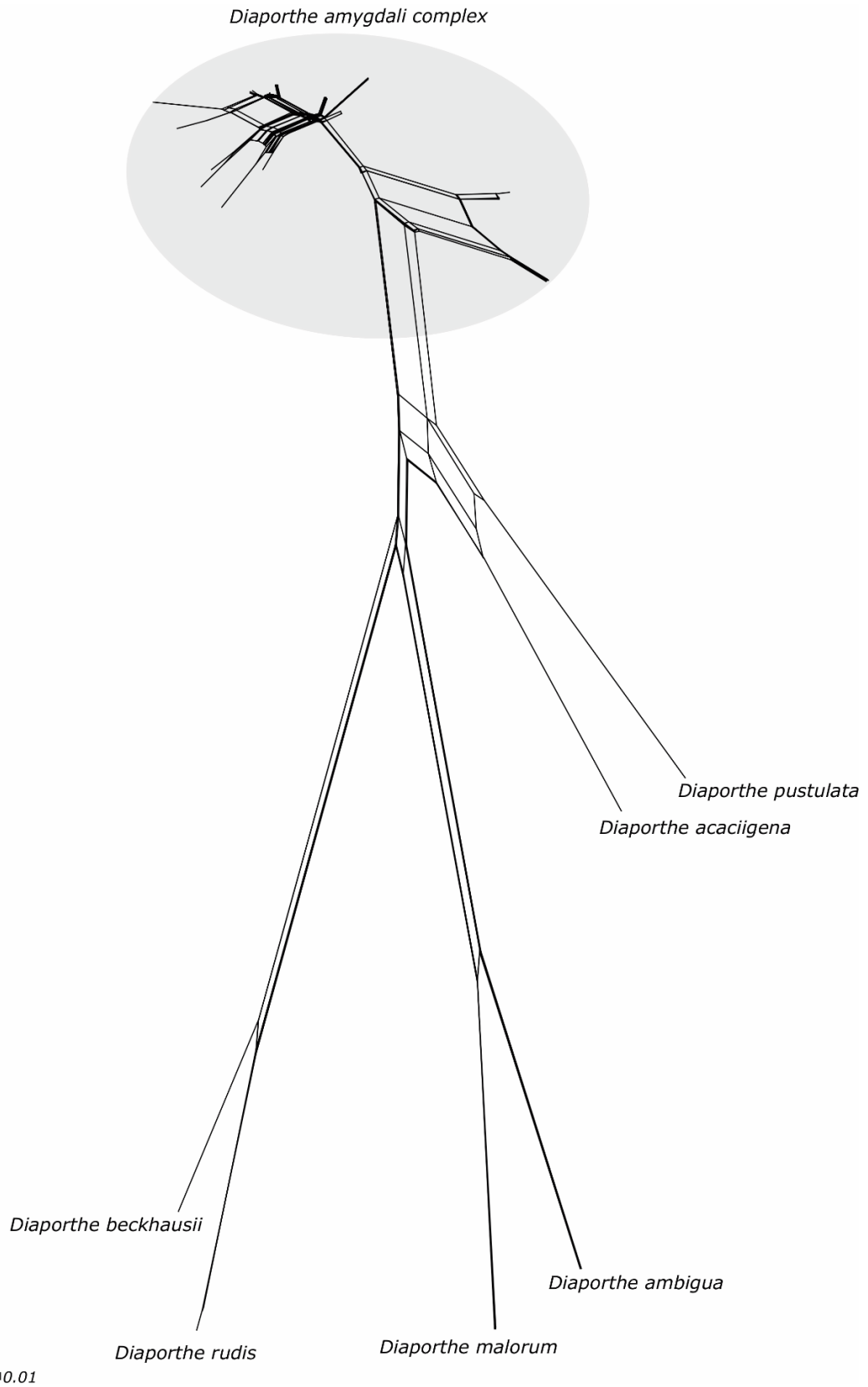


Figure S14. Phylogenetic network from *tub2* locus, representing the structure of the *Diaporthe amygdali* complex and other well-delimited species, based on the GTR model, as inferred by SplitsTree. The scale bar represents the expected number of substitutions per nucleotide position.

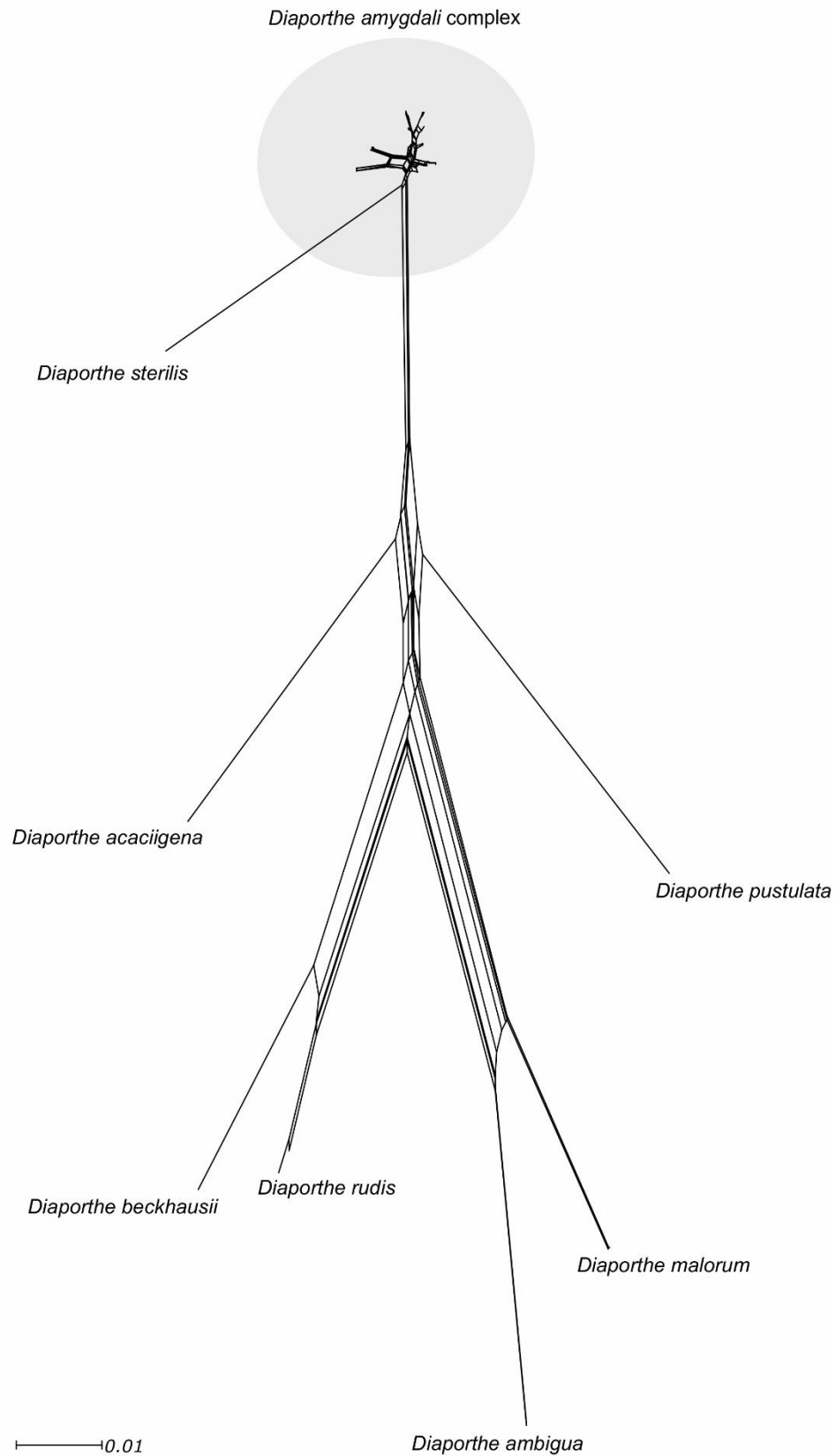


Figure S15. Phylogenetic network from *his3* locus, representing the structure of the *Diaporthe amygdali* complex and other well-delimited species, based on the GTR model, as inferred by SplitsTree. The scale bar represents the expected number of substitutions per nucleotide position.

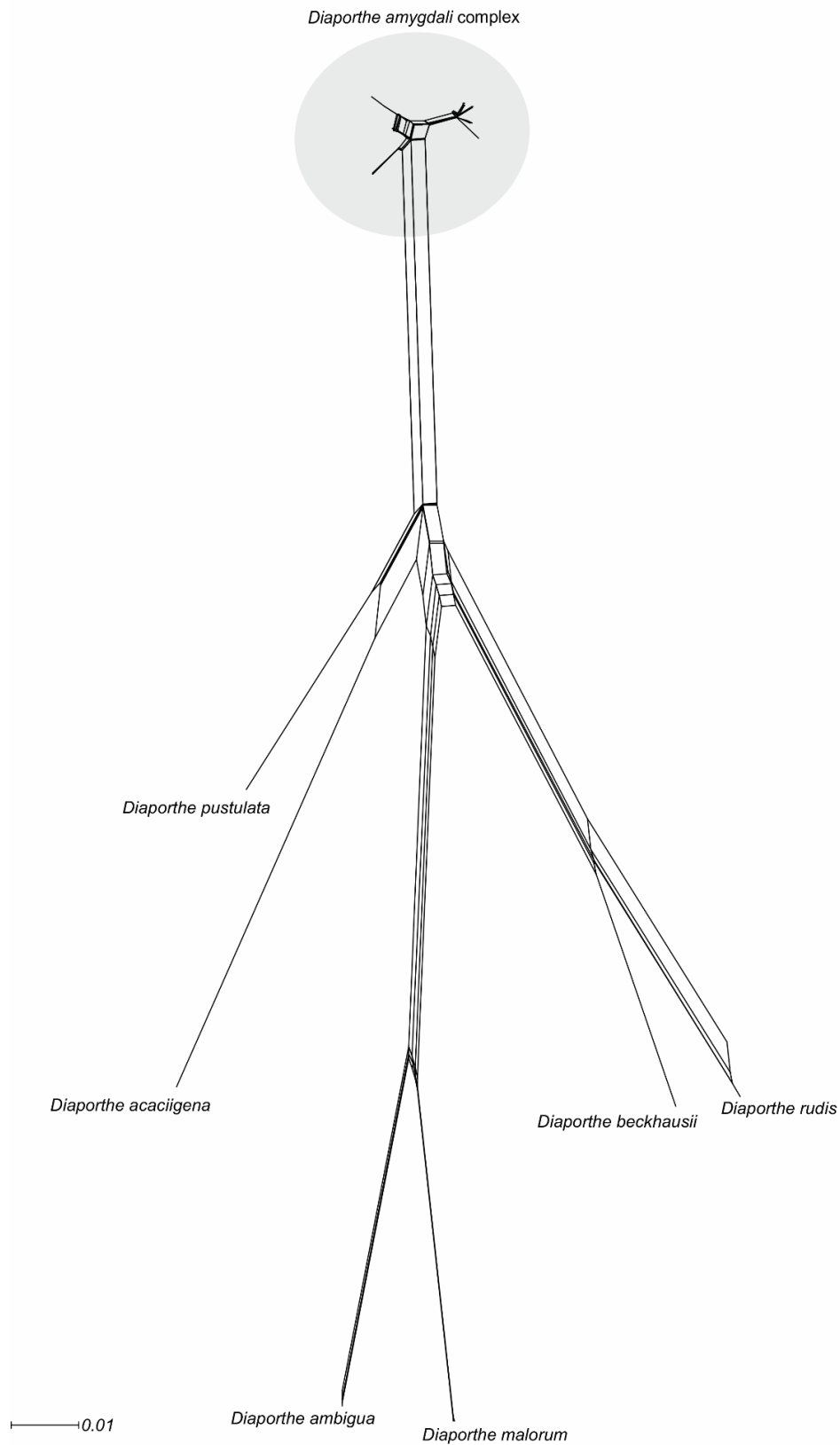


Figure S16. Phylogenetic network from *cal* locus, representing the structure of the *Diaporthe amygdali* complex and other well-delimited species, based on GTR model, as inferred by SplitsTree. The scale bar represents the expected number of substitutions per nucleotide position.

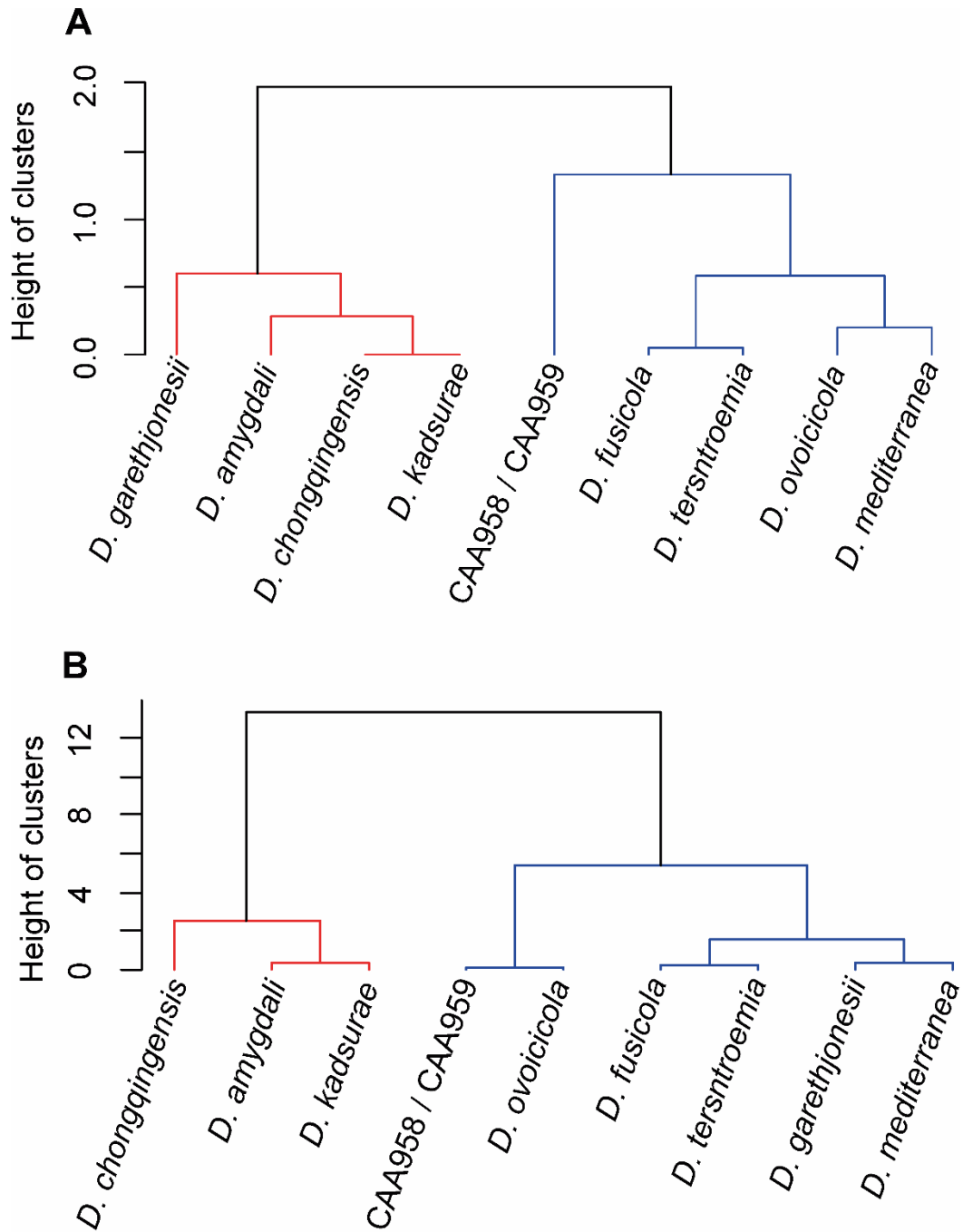


Figure S17. Dendrogram from the hierarchical clustering analysis based on the Ward's method showing the distribution of the lengths and width ratio (L/W) of alpha conidia (**A**) and conidiophores (**B**) of species and isolates from the *Diaporthe amygdali* complex. Red and blue colors represent the two different clusters, based on the micromorphological descriptions.

Table S1. Pairwise homoplasy index (PHI) of paired clades in *Diaporthe amygdali* complex, based on the concatenation of five loci.

Clades	a	b	c	d	e	f	g	h	i
a	Grey								
b	Green	Green							
c	Grey	Grey	Grey						
d	Green	Green	Grey	Green					
e	Grey	Green	Grey	Green	Grey				
f	Grey	Green	Green	Green	Grey	Grey			
g	Grey	Green	Grey	Green	Grey	Grey	Grey		
h	Grey	Green	Grey	Grey	Grey	Grey	Grey	Grey	
i	Orange	Orange	Grey	Orange	Orange	Orange	Orange	Grey	Orange

Note: Squares highlighted in orange stands for significant recombination; Grey squares indicate no recombination; Green squares indicate that PHI test was not performed as only one isolate is available, or there are too few informative characters.

SUBCHAPTER 3.2

Using genealogical concordance and coalescent-based species delimitation to assess species boundaries in the *Diaporthe eres* complex

Hilário S, Gonçalves MFM, Alves A.

Journal of Fungi 2021 7, 507

ABSTRACT

DNA sequence analysis has been of the utmost importance to delimit species boundaries in the genus *Diaporthe*. However, the common practice of combining multiple genes, without applying the genealogical concordance criterion, has complicated robust delimitation of species, given that phylogenetic incongruence between loci has been disregarded. Despite the several attempts to delineate the species boundaries in the *D. eres* complex, the phylogenetic limits within this complex remain unclear. In order to bridge this gap, we employed the Genealogical Phylogenetic Species Recognition principle (GCPSR), the coalescent-based model Poisson Tree Processes (PTP) and evaluated the presence of recombination within the *D. eres* complex. Based on the GCPSR principle, it was evident the presence of incongruence between individual gene genealogies, *i.e.*, conflicting nodes and branches lacking phylogenetic support. Moreover, the results of the coalescent model identified *D. eres* complex as a single species, which was not consistent with the current large number of species within the complex recognized in phylogenetic analyses. The absence of reproductive isolation and barriers to gene flow, the high haplotype and low nucleotide diversity indices within the above-mentioned complex, suggest that *D. eres* constitutes a population, rather than different lineages. Therefore, we argue that a cohesive approach comprising the genealogical concordance criteria and methods to detect recombination must be implemented in future studies to circumscribe species in the genus *Diaporthe*.

keywords: GCPSR; PTP; Species delimitation; Taxonomy

INTRODUCTION

A reliable and accurate identification of fungal plant pathogens is of the utmost importance in disease diagnosis to implement effective management and

quarantine strategies (Wingfield et al. 2012). However, one crucial aspect in recognizing a fungal species, is correctly defining a species (Hyde et al. 2020). Although molecular approaches have changed our perception of fungal diversity (Lücking & Hawksworth 2018), difficulties in understanding the evolutionary processes in fungi have arisen, thus turning a correct definition of a fungal species a prevailing challenge to mycologists (Gao et al. 2017; Lücking et al. 2020).

The Genealogical Concordance Phylogenetic Species Recognition (GCPSR), introduced by Taylor et al. (2000), relies in the comparison of individual gene genealogies to identify incongruences, and it has been particularly useful to delimit the species boundaries in morphologically conserved fungi (Liu et al. 2016). However, the common approach of concatenating sequence data to delimit species without following the GCPSR principle (Inderbitzin et al. 2020; Taylor et al. 2000) has been overestimating the true diversity of species, since each clade in combined trees is frequently recognized as a distinct lineage (Achari et al. 2020; Stewart et al. 2014). Moreover, species boundaries in closely related taxa can be somehow difficult to determine through multilocus sequence data, as some alleles are not expected to be reciprocally monophyletic in the initial stages of speciation, resulting in phylogenetic incongruences (Liu et al. 2016; Rannala & Yang 2020). As an alternative, the delimitation of species using multi-species coalescent models, provides a more comprehensive insight into the speciation events, as it can estimate species boundaries even in the presence of incongruence between individual genealogies (Carstens & Knowles 2007).

Some authors have already advocated that the description of fungal species needs to be based on approaches that employ a combination of several methods: phylogenetic analysis following the genealogical concordance (GCPSR) (Taylor et al. 2000), coalescence models such as Poisson Tree Processes (PTP) (Zhang et al. 2013), and splits graphs (Phylogenetic networks) (Hyde et al. 2020). Nevertheless, despite the usefulness of the above-mentioned methods to support the boundaries of species, there are only a few studies in fungi, namely in *Colletotrichum* (Liu et al. 2016), *Beauveria* (Bustamante et al. 2019) and more recently in *Diaporthe* (Hilário et al. 2020).

Diaporthe species are associated with a wide range of plant hosts as pathogens, endophytes or saprobes of crops, ornamentals, and forest trees (Fan et al. 2018; Guarnaccia et al. 2018; Yang et al. 2018). Species identification in the genus *Diaporthe* has evolved from host association and morphology (Mostert et al. 2001; Rehner & Uecker 1994), to the widespread adoption of DNA sequencing (Gomes et al. 2013). Currently, the nuclear ribosomal internal transcribed spacer (ITS), the translation elongation factor 1- α (*tef1- α*), beta-tubulin (*tub2*), histone H3 (*his3*), and calmodulin (*cal*) genes are the most used molecular loci in this genus, that currently counts with the description of over 200 species supported by ex-type cultures and supplementary DNA sequences (Gao et al. 2017; Marin-Felix et al. 2019).

Diaporthe eres, is the type species of the genus and was originally described by Nitschke (1870), from *Ulmus* sp. in Germany (Udayanga et al. 2014). In 1933, Wehmeyer listed several synonyms under *D. eres* based on morphological characters. Later, based on molecular data, few of these synonyms were accepted by several authors (Gomes et al. 2013; Udayanga et al. 2014). Udayanga et al. (2014), attempted to define the species limits of *D. eres* and closely related species based on the concatenation of seven loci and designated an epitype specimen for *D. eres*. Despite the attempts by several authors to re-examine the *D. eres* complex, its boundaries are not entirely understood (Guarnaccia et al. 2018; Guo et al. 2020; Yang et al. 2018). In several studies, many species have been demonstrated to be synonymous of the *D. eres* species, based on multi-locus analyses such as *D. biguttusis*, *D. camptothecicola*, *D. castaneae-mollissimae*, *D. cotoneastri*, *D. ellipicola*, *D. longicicola*, *D. mahothocarpus*, *D. momicola* and *Phomopsis fukushii* (Guo et al. 2020; Udayanga et al. 2014; Yang et al. 2018). In a recent study, Chaisiri et al. (2021) found that *D. henanensis*, *D. lonicerae* and *D. rosicola* were also synonyms of *D. eres*, based on the GCPSR principle coupled with haplotype network analysis and population genetic diversity. Although *D. eres* has been regarded as a minor pathogen, it is also considered one of the main causal agents of cankers on grapevines (Guarnaccia et al. 2018), blueberries (Lombard et al. 2014) and apple trees (Ali et al. 2020). Lopes et al. (2021) reported the occurrence of *D. eres* in forest trees but found some difficulties in the interpretation of their

phylogenetic analyses and delimitation of the species in the *D. eres* complex. Therefore, the this study aimed clarify the limits of the *D. eres* species complex by implementing several distinct methods such as: single and multilocus phylogenetic analyses; the genealogical concordance principle; coalescent-based species delimitation methods (PTP); phylogenetic networks; pairwise homoplasy index test and comparison of morphological characters.

MATERIAL AND METHODS

Fungal isolates.

In 2007, a survey was conducted to inspect for the presence of *Diaporthe* species associated with ornamental plants in Portugal. Twigs and leaves of *Banksia* sp. showing blight symptoms typical of *Diaporthe* were collected. Fungal isolates, which it was collected a fungus that resembled *D. eres*, were obtained by the methods described in subchapter 2.1. Moreover, isolates CAA954 and CAA1001 obtained previously from *Quercus suber* and *Pinus pinaster* and identified as *D. eres* (Lopes et al. 2021) were also included in this study. Cultures were maintained in the collection of Artur Alves (CAA), University of Aveiro (Portugal) on potato dextrose agar (PDA) (Merck, Darmstadt, Germany). The isolates used in this study are listed in Table 1.

DNA extraction and PCR amplification.

Genomic DNA extraction and amplification of ITS and the protein coding regions *tef1-a*, *tub2*, *his3* and *cal*, were as described in subchapter 2.1.

Phylogenetic analyses.

The nucleotide sequences were analyzed, and the phylogenetic trees for the *D. eres* species complex were constructed based on Maximum Parsimony (MP), Maximum Likelihood (ML) and Bayesian Inference (BI) analyses, as described in subchapter 2.1. For the MP analyses, the parameters consistency index (CI), retention index (RI), tree length (TL), rescaled consistency index (RC) and homoplasy index (HI) were calculated.

Besides species of the *D. eres* complex, the phylogenetic analyses included also six well-delimited *Diaporthe* species. To examine the possibility of a combined dataset, sequences from the five loci were aligned, combined, and the Incongruence Length Difference was performed as described in subchapter 3.1. Moreover, the highly supported clades in individual genealogies were also compared to detect conflict among them as described in subchapter 3.1. Individual gene trees of the *D. eres* species complex, comprising all available species for each locus were also constructed. These trees were rooted to *Diaporthe citri* and *D. citrichinensis*. The sequence generated in this study was deposited in GenBank (Table 1). (www.ncbi.nlm.nih.gov). The phylogenetic tree and alignments were deposited in TreeBASE (www.TreeBASE.org; S27078).

Pairwise homoplasy index test and phylogenetic network analysis.

The concatenated five loci tree was used to infer the occurrence of sexual recombination within the *D. eres* complex, through the pairwise homoplasy index test (PHI) (Bruen 1990) implemented in SplitsTree v.4.16.1 (www.splitstree.org) (Huson & Bryant 2006). To detect intragenic recombination, individual loci were also analyzed using the PHI test. Significant recombination was considered with a PHI index below 0.05 ($\Phi_w < 0.05$). The relationships between closely related taxa were visualized by constructing a phylogenetic network from the concatenated dataset of five loci, using the LogDet transformation and the NeighborNet algorithm options implemented in SplitsTree v.4.16.1.

Species delimitation analyses.

To infer the species boundaries of *Diaporthe eres* complex, coalescence-based methods were performed based on the combined alignment of ITS, *tef1- α* , *tub2*, *his3* and *cal* genes. Firstly, the single Poisson Tree Processes model (PTP) (Zhang et al. 2013), was used. The newick-format tree produced by MEGA v.7 was used for the PTP analysis with the following parameters: 500 000 MCMC generations, thinning set to 100, burn-in at 50 000 generations and conducted on the web server for PTP (<http://species.h-its.org/ptp/>). Secondly, the multi-rate PTP (mPTP), which can accommodate data sets comprised of species with different

levels of molecular diversity (Kapli et al. 2017) was also conducted on the web server for mPTP (<http://mptp.h-its.org>), using the same newick-format tree as for the single PTP analysis.

Population genetic diversity.

The genetic diversity of the *Diaporthe eres* complex was calculated from a combined dataset of 19 ex-type species and 21 taxonomically authenticated isolates belonging to the complex, as described in subchapter 3.1.

Morphology of the Diaporthe eres species complex.

The alpha conidia, beta conidia and conidiophores length/width (L/W) ratios of all current species belonging to the *Diaporthe eres* complex were calculated, following the descriptions in subchapter 3.1.

Table 1. List of *Diaporthe* species used in this study.

Species	Strain ¹	Host	Country	GenBank Accession				
				ITS	<i>tef1-α</i>	<i>tub2</i>	<i>his3</i>	<i>cal</i>
<i>D. ambigua</i>	CBS 114015	<i>Pyrus communis</i>	South Africa	KC343010	KC343736	KC343978	KC343494	KC343252
	CBS 123210	<i>Foeniculum vulgare</i>	Portugal	KC343012	KC343738	KC343980	KC343496	KC343254
<i>D. amygdali</i>	CBS 126679	<i>Prunus dulcis</i>	Portugal	KC343022	KC343748	KC343990	KC343506	KC343264
	CBS 115620	<i>Prunus persica</i>	USA	KC343020	KC343746	KC343988	KC343504	KC343262
<i>D. citri</i>	CBS 134239	<i>Citrus cinensis</i>	USA	KC357553	KC357522	KC357456	MF418280	KC357488
	CBS 135422	<i>Citrus</i> sp.	USA	KC843311	KC843071	KC843187	MF418281	KC843157
<i>D. eres</i>	CPC 29331	<i>Vitis vinifera</i>	France	MG281034	MG281555	MG281207	KC343631	KC343389
	CBS 138594	<i>Ulmus laevis</i>	Germany	KJ210529	KJ210550	KJ420799	KC343637	KC343395
	CBS 143344	<i>Vitis vinifera</i>	Czech Republic	MG281020	MG281541	MG281193	MG281366	MG281715
	CAA756	<i>Banksia</i> sp.	Portugal	<i>MW040531</i>	<i>MW052385</i>	<i>MW091320</i>	<i>MW052384</i>	<i>MW091319</i>
	CAA954	<i>Pinus pinaster</i>	Portugal	MN190309	MT309431	MT309457	MT309440	MT309448
	CAA1001	<i>Quercus suber</i>	Portugal	MT237172	MT309432	MT309458	MT309441	MT309449
	CBS 146.46	<i>Alnus</i> sp.	Netherlands	KC343008	KC343734	KC343976	KC343492	KC343250
<i>D. eres</i> (syn. <i>D. alnea</i>)	CBS 159.47	<i>Alnus</i> sp.	Netherlands	KC343009	KC343735	KC343977	KC343493	KC343251
<i>D. eres</i> (syn. <i>D. alleghaniensis</i>)	CBS 495.72	<i>Betula alleghaniensis</i>	Canada	FJ889444	GQ250298	KC843228	KC343491	KC343249
<i>D. eres</i> (syn. <i>D. betulae</i>)	CFCC 50469	<i>Betula platyphylla</i>	China	KT732950	KT733016	KT733020	KT732999	KT732997
	CFCC 50470	<i>Betula platyphylla</i>	China	KT732951	KT733017	KT733021	KT733000	KT732998
<i>D. eres</i> (syn. <i>D. betulina</i>)	CFCC 52562	<i>Betula platyphylla</i>	China	MH121497	MH121539	MH121579	MH121457	MH121421
	CFCC 52561	<i>Betula platyphylla</i>	China	MH121496	MH121538	MH121578	MH121456	MH121421
<i>D. eres</i> (syn. <i>D. bicincta</i>)	CBS 121004	<i>Juglans</i> sp.	USA	KC343134	KC343860	KC344102	KC343618	KC343376
<i>D. eres</i> (syn. <i>D. biguttusis</i>)	CGMCC 3.17081	<i>Lithocarpus glabra</i>	China	KF576282	KF576257	KF576307	-	-
<i>D. eres</i> (syn. <i>D. brevicancrria</i>)	CBS 146962	<i>Picea pungens</i>	USA	MN136180	MN136153	MN136190	MN136178	MN136129
	MIFCC 305	<i>Picea glauca</i>	USA	MN136184	MN136151	MN136188	MN136176	MN136127

<i>D. eres</i> (syn. <i>Diaporthe</i> cf. <i>nobilis</i>)	CBS 124030	<i>Malus pumila</i>	New Zealand	KC343149	KC343875	KC344117	KC343633	KC343391
	CBS 134470	<i>Castanea sativa</i>	Australia	KC343146	KC343872	KC344114	KC343630	KC343388
	CBS 587.79	<i>Pinus pentaphylla</i>	Japan	KC343153	KC343879	KC344121	KC343637	KC343395
<i>D. eres</i> (syn. <i>D. camptothecicola</i>)	CFCC 51632	<i>Camptotheca acuminata</i>	China	KY203726	KY228887	KY228893	KY228881	KY228877
	CFCC 51633	<i>Camptotheca acuminata</i>	China	KY203727	KY228888	KY228894	KY228882	KY228878
<i>D. eres</i> (syn. <i>D. castaneae-mollissimae</i>)	DNP128	<i>Vaccinium corymbosum</i>	China	KC763096	KJ210561	KJ420801	KJ420852	KJ435040
<i>D. eres</i> (syn. <i>D. celeris</i>)	CBS 143349	<i>Vitis vinifera</i>	UK	MG281017	MG281538	MG281190	MG281363	MG281712
	CBS 143350	<i>Vitis vinifera</i>	UK	MG281018	MG281539	MG281191	MG281364	MG281713
<i>D. eres</i> (syn. <i>D. celastrina</i>)	CBS 139.27	<i>Celastrus</i> sp.	USA	KC343047	KC343773	KC344015	KC343531	KC343289
<i>D. eres</i> (syn. <i>D. chensiensis</i>)	CFCC 52567	<i>Abies chensiensis</i>	China	MH121502	MH121544	MH121584	MH121462	MH121426
	CFCC 52568	<i>Abies chensiensis</i>	China	MH121503	MH121545	MH121585	MH121463	MH121427
<i>D. eres</i> (syn. <i>D. cotoneastris</i>)	CBS 135428	<i>Juglans cinerea</i>	USA	KC843328	KC843121	KC843229	KC343630	KC343388
	CBS 439.82	<i>Cotoneaster</i> sp.	UK	KC343090	KC343816	KC344058	KC343574	KC343332
<i>D. eres</i> (syn. <i>D. ellipicola</i>)	CGMCC 3.17084	<i>Lithocarpus glabra</i>	China	KF576270	KF576245	KF576291	-	-
<i>D. eres</i> (syn. <i>D. fukushii</i>)	CBS 116953	<i>Pyrus pyrifolia</i>	New Zealand	KC343147	KC343873	KC344115	KC343631	KC343389
	CBS 116954	<i>Pyrus pyrifolia</i>	Japan	JQ807469	JQ807418	KJ420819	KJ420868	KJ435023
<i>D. eres</i> (syn. <i>D. helixis</i>)	CBS 138596	<i>Hedera helix</i>	France	KJ210538	KJ210559	KJ420828	KJ420875	KJ435043
<i>D. eres</i> (syn. <i>D. longicicola</i>)	CGMCC 3.17089	<i>Lithocarpus glabra</i>	China	KF576267	KF576242	KF576291	-	-
	CGMCC 3.17090	<i>Lithocarpus glabra</i>	China	KF576268	KF576243	KF576292	-	-
<i>D. eres</i> (syn. <i>D. mahothocarpus</i>)	CGMCC 3.15181	<i>Lithocarpus glabra</i>	China	KC153096	KC153087	KF576312	-	-
<i>D. eres</i> (syn. <i>D. maritima</i>)	DAOMC 250563	<i>Picea rubens</i>	Canada	KU552027	KU552022	KU574616	-	-
<i>D. eres</i> (syn. <i>D. momicola</i>)	MFLUCC 16-0113	<i>Prunus persica</i>	China	KU557563	KU557631	KU557587	-	KU557611
	MFLUCC 16-0114	<i>Prunus persica</i>	China	KU557564	KU557632	KU557588	-	KU557612

<i>D. eres</i> (syn. <i>D. neilliae</i>)	CBS 144.27	<i>Sapiraea</i> sp.	USA	KC343144	KC343870	KC344112	KC343628	KC343386
<i>D. eres</i> (syn. <i>D. padina</i>)	CFCC 52590	<i>Prunus padus</i>	China	MH121525	MH121567	MH121604	MH121483	MH121443
	CFCC 52591	<i>Malus domestica</i>	China	MH121526	MH121568	MH121605	MH121484	MH121444
<i>D. eres</i> (syn. <i>D. phragmitis</i>)	CBS 138897	<i>Phragmites australis</i>	China	KP004445	-	KP004507	KP004503	-
<i>D. eres</i> (syn. <i>D. pulla</i>)	CBS 338.89	<i>Hedera helix</i>	Yugoslavia	KC343152	KC343878	KC344120	KC343636	KC343394
<i>D. eres</i> (syn. <i>D. rosicola</i>)	MFLU 17-0646	<i>Rosa</i> sp.	UK	MG828895	MG829270	MG843877	-	MG829274
	CBS 160.32	<i>Vaccinium macrocarpon</i>	USA	AF317578	GQ250326	KC344196	KC343712	KC343470
<i>D. eres</i> (syn. <i>D. vaccinii</i>)	CBS 135436	<i>Vaccinium corymbosum</i>	USA	AF317570	JQ807380	KC843225	KJ420877	KC849457
	CAA829	<i>Vaccinium corymbosum</i>	Portugal	MK792306	MK828077	MK837928	MK871446	MK883832
<i>D. eres</i> (syn. <i>D. vacuae</i>)	MUM 19.31	<i>Vaccinium corymbosum</i>	Portugal	MK792309	MK828080	MK837931	MK871449	MK883834
	CBS 123208	<i>Foeniculum vulgare</i>	Portugal	KC343104	KC343830	KC344072	KC343588	KC343346
<i>D. foeniculina</i>	CBS 111553	<i>Foeniculum vulgare</i>	Spain	KC343101	KC343827	KC344069	KC343585	KC343343
	CAA740	<i>Malus domestica</i>	Portugal	KY435642	KY435629	KY435670	KY435650	KY435660
<i>D. malorum</i>	CBS 142383	<i>Malus domestica</i>	Portugal	KY435638	KY435627	KY435668	KY435648	KY435658
	CFCC 51634	<i>Senna bicapsularis</i>	China	KY203722	KY228883	KY228889	KY228879	KY228873
<i>D. sennicola</i>	CFCC 51635	<i>Senna bicapsularis</i>	China	KY203723	KY228883	KY228889	KY228879	KY228873

¹Acronyms of culture collection: **CAA** – Personal Culture Collection Artur Alves, University of Aveiro, Aveiro, Portugal; **CBS** – Westerdijk Fungal Biodiversity Institute, Utrecht, The Netherlands; **CFCC** – China Forestry Culture Collection Center, Beijing, China; **CGMCC** – China General Microbiological Culture Collection Center, Beijing, China; **CMW** – Forestry and Agricultural Biotechnology Institute, University of Pretoria, South Africa; **CPC** – Personal Culture Collection Pedro Crous, housed at CBS; **DAOMC** – The Canadian Collection of Fungal Cultures, Canada; **DNP** – Isolates in SMML culture collection, USDA-ARS, Beltsville, USA; **MFLU** – Herbarium of Mae Fah Luang University, Thailand; **MIFCC** – Michigan Isolate Fungal Culture Collection, Michigan, USA; **MUM** – Culture Collection from Micoteca da Universidade do Minho, Center for Biological Engineering of University of Minho, Braga, Portugal. Ex-type isolates are in bold. The newly sequences generated in this study are in italics

RESULTS

Phylogenetic analyses and informative characters.

The individual gene trees of the complex (Figs. S1-S5) showed that the isolates used in this study cluster in a clade containing 29 species, designated here as the *D. eres* species complex. The partition homogeneity test for both 5-loci and 4-loci combined alignments resulted in a low p-value ($p = 0.01$), indicating that the genes are unsuitable to be combined. Nevertheless, despite the observed incongruences, multilocus analyses were constructed based on 5 and 4 loci. The 5 loci combined alignment comprises 2364 characters (537 characters from ITS, 387 from *tef1- α* , 430 from *tub2*, 522 from *cal*, and 488 from *his3*, including alignment gaps and indel coding); and the 4 loci combined alignment is comprised of 1827 characters (387 from *tef1- α* , 430 from *tub2*, 522 from *cal*, and 488 from *his3*, including alignment gaps and indel coding). Both analyses included 12 well-delimited outgroup taxa and 40 ingroup taxa (3 from this study and 37 taxa were retrieved from GenBank) (Table 1). The parsimony informative characters and the nucleotide models used for each analysis is summed up in Table 2. Moreover, sequences of the five genes were aligned and analyzed separately by ML, MP and BI analyses, and the resulting trees were compared (Figs. S6-S10). The ML, MP and BI analyses resulted in trees topologically similar.

According to the informative characters provided by the MP analyses, *tef1-a* displayed the highest informative sequences followed by *cal*, *tub2* and *his3* loci. ITS presented the lowest percentage, indicating that this locus is unreliable for the delimitation of the *D. eres* species. The combined four loci dataset (*tef1-a*, *tub2*, *cal*, and *his3*) showed better delimitation for *D. eres* compared to the dataset of five loci dataset (Fig. 1), confirming that the ITS locus is not the appropriate locus to delineate species in this genus.

Species delimitation based on the GCPSR principle.

The isolates from this study clustered in a highly supported clade on both 5-loci (ML/MP/PP = 100/100/1.00) (Fig. 1) and 4-loci (ML/MP/PP = 99/99/1.00) (Fig. S11) phylogenies, respectively.

Table 2. Alignment properties and nucleotide substitution models used for phylogenetic analyses.

Character-status summary	Loci and combined alignments						
	ITS	<i>tef1-α</i>	<i>tub2</i>	<i>his3</i>	<i>cal</i>	4 loci	5 loci
Total characters	537	387	430	488	522	1827	2364
Invariable characters	434	183	273	342	307	1104	1539
Informative characters (%)	92 (17%)	184 (47%)	143 (33%)	116 (23%)	200 (38%)	649 (35%)	735 (31%)
Uninformative characters	11	20	14	30	15	74	90
Tree length (TL)	206	366	255	280	356	1358	1647
Consistency index (CI)	0.6359	0.7486	0.7686	0.7036	0.8090	0.7018	0.6594
Homoplasy index (HI)	0.3641	0.2514	0.2314	0.2964	0.1910	0.2982	0.3406
Retention index (RI)	0.8727	0.8892	0.8959	0.8683	0.9037	0.8554	0.8311
Rescaled consistency index (RC)	0.5549	0.6657	0.6886	0.6109	0.7311	0.6003	0.5480
Nucleotide substitution models ²	K2+G	HKY	K2+G	KKY+G	T92+G	TN93+G	TN93+G

²K2: Kimura 2-parameter model; T92: Tamura 3-parameter model; HKY: Hasegawa–Kishino–Yano model; TN93: Tamura Nei-parameter model; G: models of evolution assuming a gamma distribution.

To assess species boundaries in the *D. eres* complex, the GCPSR principle was applied. Our results revealed conflicts between individual phylogenies, with several nodes lacking phylogenetic support. For example, *D. vaccinii* is closely related to *D. celeris* in the *tub2* tree (Fig. S8), but it is a sister species to *D. camptothecicola* (previously synonymized with *D. eres*) in the ITS individual phylogram (Fig. S6). Moreover, a lack of high bootstrap and posterior probability values on both individual and combined trees in several branches were observed, revealing poor phylogenetic support among the species. It is also evident that isolates from the same species cluster in different clades in the same individual gene tree. For instance, two isolates of *D. alnea* are phylogenetically distant in the *tub2* tree (Figure S8), while they group together in the remaining individual phylograms. The same seems to occur with some isolates of *D. eres*: the isolates CBS 116953 and MAFF625034 (formerly described as *D. fukushii*) and two isolates of *D. camptothecicola*, previously synonymized with *D. eres* do not cluster together in the ITS single locus tree (Fig. S6). It is also notable from our analyses that the ex-type of *D. alnea* (CBS 146.46) is a close relative to *D. allenghaniensis* in the *tub2* tree (Fig. S8), whereas they are different taxa in the remaining individual and combined trees. Moreover, the species *D. brevicancra* is phylogenetically indistinguishable from *D. celastrina* and *D. maritima* in the individual *cal* tree (Fig. S10). Thus, by

implementing the GCPSR principle that lies on the comparison of more than one gene genealogy to identify phylogenetic concordance, we verified that the node delimiting the transition from concordant branches to incongruence corresponds to the *D. eres* complex (Fig. 1). As estimated by the initial individual trees (Fig. S1-S5), the species *D. maritima*, *D. phragmitis* and *D. rosicola* belong to the *D. eres* species complex. However, given the lack of some sequences for these species, they were not included in the 4-loci and 5-loci phylogenetic analyses. However, by analyzing the individual gene trees and given their position within the complex, we advocate that the aforementioned species should also be assigned to *D. eres*. Contrarily, individual gene trees are concordant regarding the six well-delimited species (*D. citri*, *D. sennicola*, *D. malorum*, *D. foeniculina*, *D. ambigua* and *D. amygdali*) indicating that there are no conflicts among the individual phylograms. This provides solid evidence that these clades represent different species.

Species delimitation based on Poisson Tree Processes (PTP).

Given the lack of *tef1- α* , *cal* and *his3* sequences for some species of the complex, the coalescent model applied included only those species whose five loci were available. Both single PTP and mPTP analyses gave congruent results and recognized the *D. eres* complex as a single species. From the analyses, the transition between blue-colored to red-colored branches (in single PTP, Fig. 2), and the transition from green-colored to red-colored (in multi-rate PTP, Fig. 3) evidenced that all species were comprised in one clade only, showing that the complex should be considered as a population rather than different taxa. In addition to that, a PTP analysis was also performed based on the 4-loci combined alignment (Fig. S12), excluding the ITS data, to understand whether the delimitation of species would be the same. This result corroborates the one from the PTP analysis based on the alignment of 5 genes, indicating that the ITS region did not affect the species delimitation, contrarily to the phylogenetic analysis. Therefore, we can consider that all species currently accepted in the *D. eres* complex should be recognized as a single species.

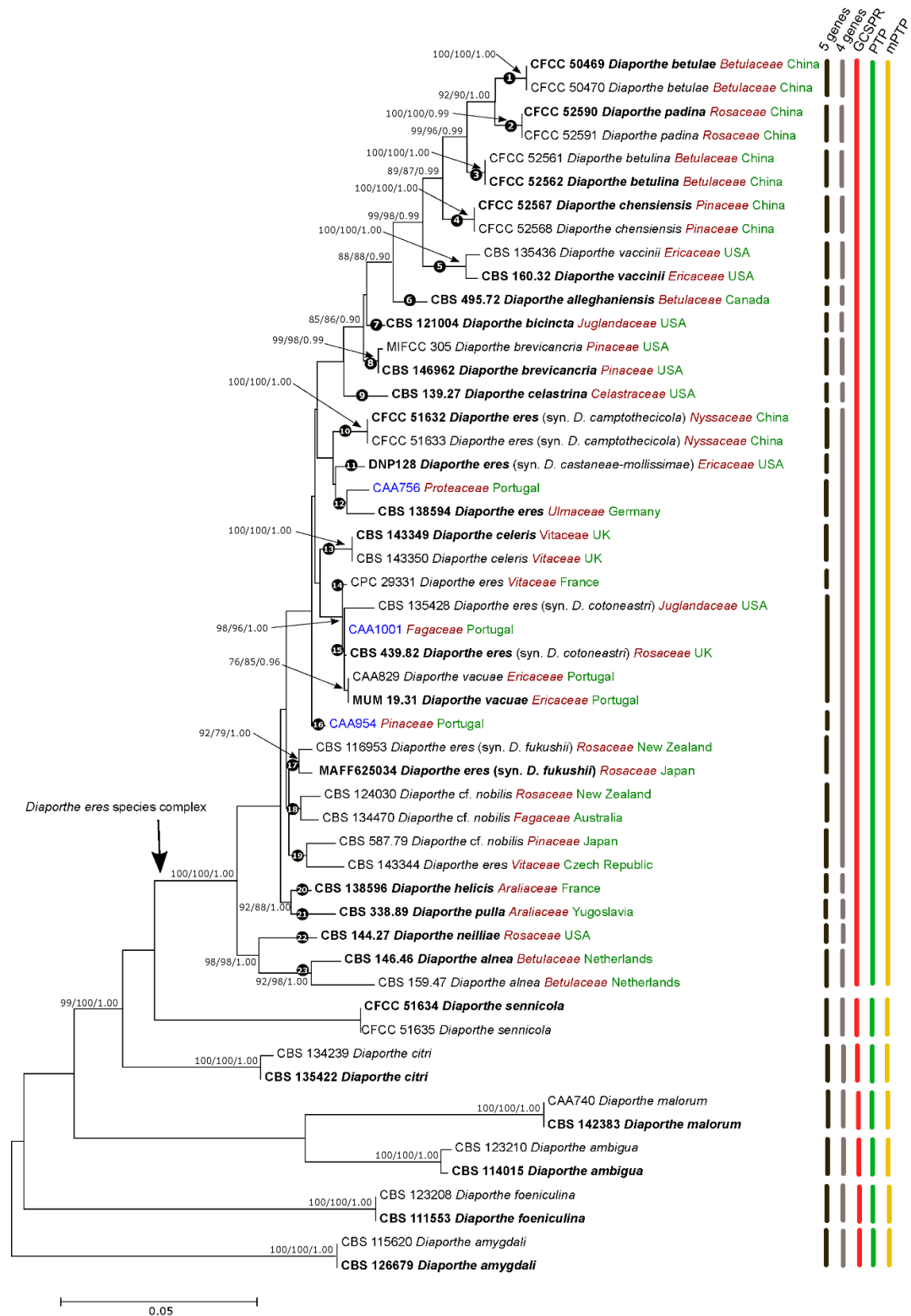


Figure 1. Maximum Likelihood (ML) tree of the *Diaporthe eres* complex and related species, based on ITS *tef1- α* , *tub2*, *his3* and *cal* loci. The ML tree is drawn to scale and was constructed based on the Tamura Nei-parameter model assuming a gamma distribution. ML and MP bootstrap values greater than 70% and posterior probabilities (PPs) greater than 0.80 are shown at the nodes. The ex-type strains are in bold. The isolates from this study are indicated in blue. Species name is followed by the family of the host where it was isolated from (red) and country of origin (green).

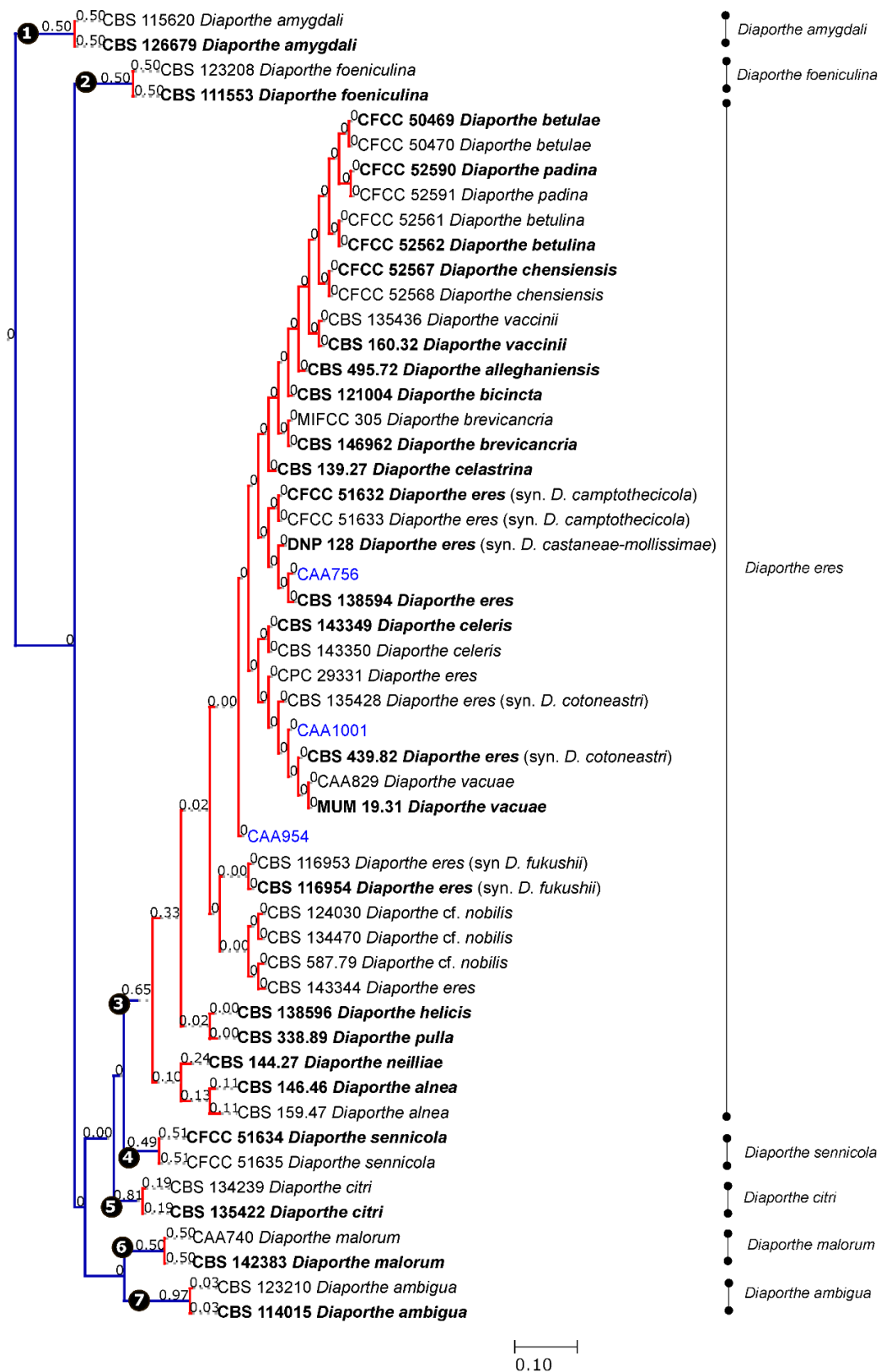


Figure 2. Results of the single PTP analyses for the *Diaporthe eres* species complex and related taxa, based on Bayesian and Maximum Likelihood topologies. Putative species clusters are indicating using transitions between blue-colored to red-colored branches and represented by circles (1-7). The isolates obtained in this study are indicated in blue.

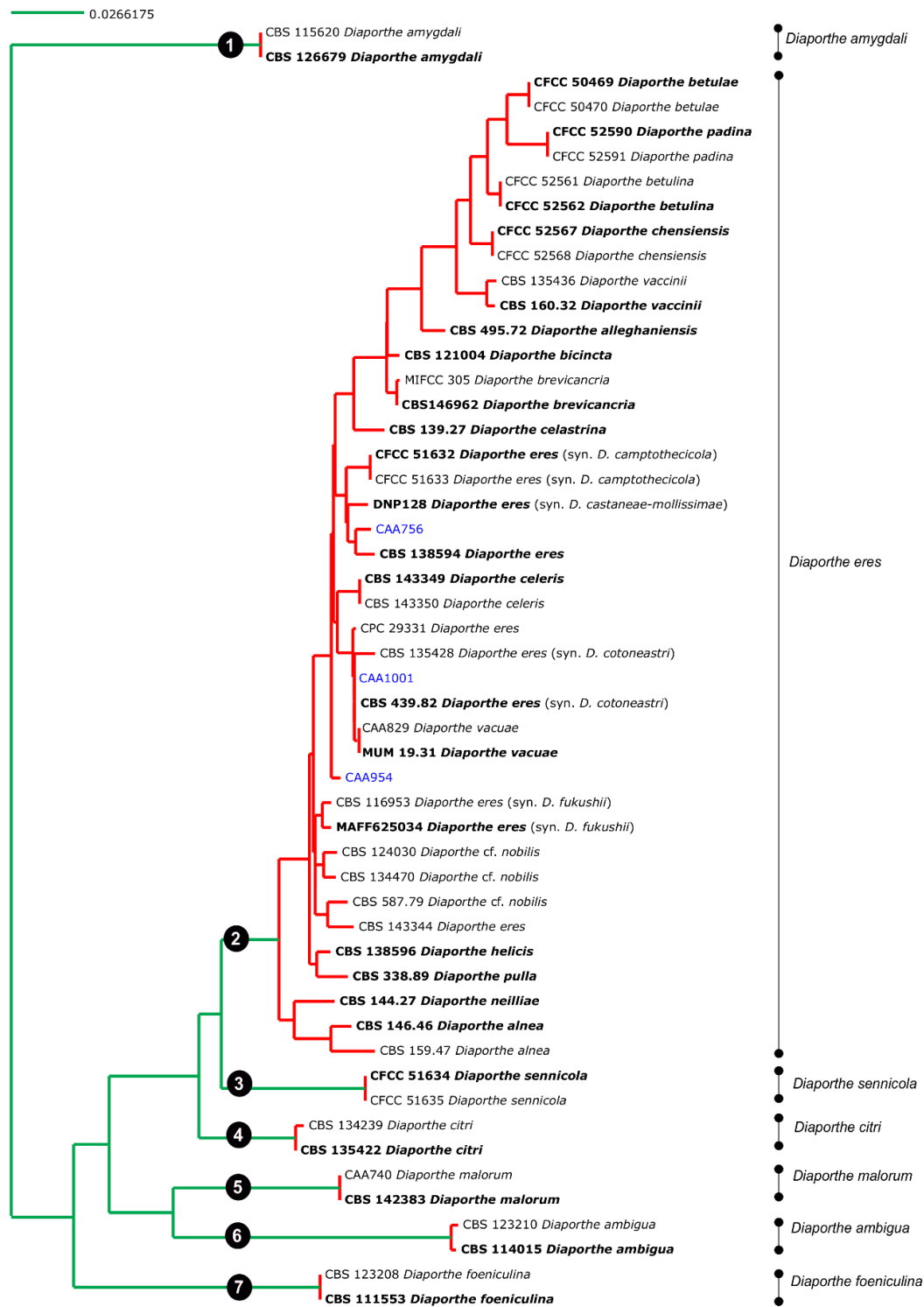


Figure 3. Results of the mPTP analysis for the *Diaporthe eres* species complex and related taxa. Putative species clusters are indicated using transitions between green-colored to red-colored branches. The isolates obtained in this study are indicated in blue.

Pairwise homoplasmy test and phylogenetic networks.

Significant recombination was detected within the *D. eres* complex when applying the PHI test ($\Phi_w = 0$), denoting that there was no reproductive isolation within the group. Moreover, the pairwise homoplasmy index test also confirmed that ITS and *tub2* loci have a significant rate of recombination ($\Phi_w = 1.098 \times 10^{-7}$ and $\Phi_w = 4.175 \times 10^{-6}$, respectively). Subsequently, the network relationships in the *D. eres* complex (Fig. 4) are shown with boxes, indicating the occurrence of recombination within the group. Additionally, based on the relative distance of species and structure of the phylogenetic network, all species in *D. eres* complex should be regarded as one single species.

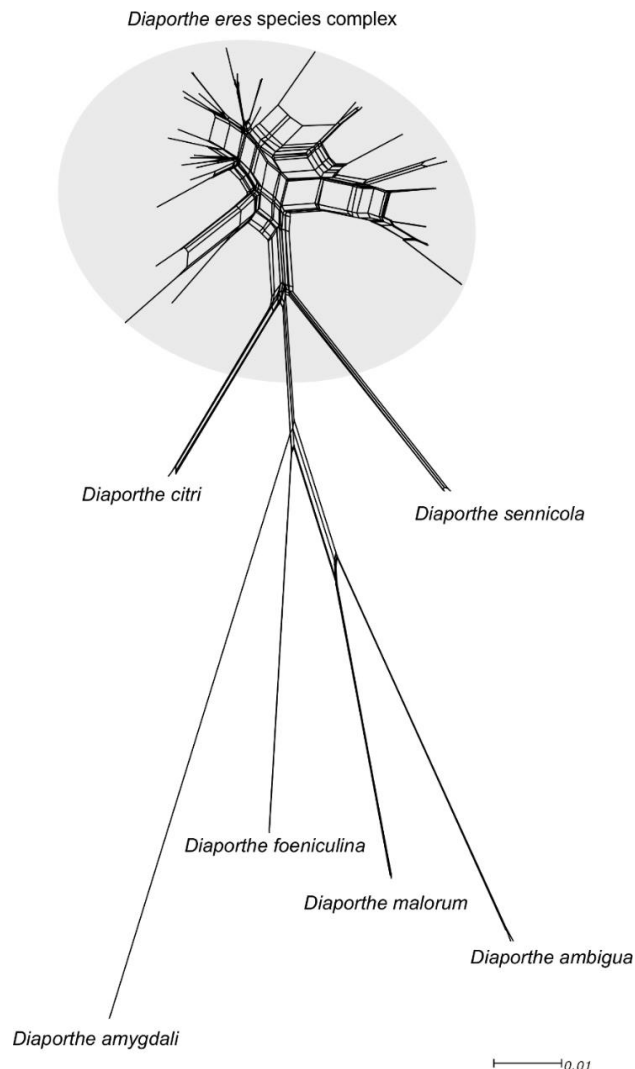


Figure 4. Phylogenetic network from the concatenated data (ITS, *tef1- α* , *tub2*, *his3* and *cal*) representing the structure of *Diaporthe eres* species complex and other well-delimited species, based on the LogDet transformation and the NeighborNet algorithm, inferred by SplitsTree. The scale bar represents the expected number of substitutions per nucleotide position.

Population genetic diversity.

The genetic diversity data for each gene region as well as for the combined dataset is summarized in Table 3. In this analysis, all loci showed a low number of nucleotide diversity ($\pi = 0.009$ to $\pi = 0.025$) and high values for all genes ($hd = 0.882$ to $hd = 0.966$). In addition to that, *tef1- α* , *his3*, *tub2*, *cal* and the combined five and four loci alignments gave not statistically significant negative Tajima's D values.

Table 3. Polymorphism and genetic diversity data for the *Diaporthe eres* species complex.

Loci	Number of haplotypes (h)	Polymorphic sites (S)	Haplotype diversity (hd)	Nucleotide diversity (π)	Tajima's D test
ITS	18	35	0.948	0.025	0.6097
<i>tef1-α</i>	19	43	0.966	0.019	-1.6281
<i>tub2</i>	17	43	0.943	0.022	-0.7208
<i>his3</i>	13	44	0.882	0.021	-1.0077
<i>cal</i>	12	13	0.921	0.009	-0.3513
5 loci ³	25	178	0.990	0.019	-0.7359
4 loci ⁴	24	143	0.988	0.018	-1.0881

³Combined alignment based on ITS, *tef1- α* , *tub2*, *his3* and *cal* loci; ⁴Combined alignment based, *tef1- α* , *tub2*, *his3* and *cal* loci. Note: all Tajima's D test gave not statistically significant values.

Morphology of the *Diaporthe eres* species complex.

Based on published morphological descriptions of twenty-five species belonging to the *D. eres* complex (excluding *D. neilliae* which lacks a taxonomic description of the asexual morph), a hierarchical clustering analysis was performed using the Ward's method. The dendrogram was constructed based on the ratios of alpha and beta conidia, and conidiophores length and width (Fig. 5).

TAXONOMY

The present study combined phylogenetic analyses based on the genealogical concordance principle (GCPSR), coalescence (PTP and mPTP) and morphological comparisons to delimit the species boundaries in the *D. eres* complex. According to the aforementioned analyses, the *D. eres* complex constitutes a single species, rather than different lineages. In order to compare and study the micromorphological characteristics of all these species, a synopsis of conidiomata, conidiogenous cells and conidia characteristics is provided in Table 4.

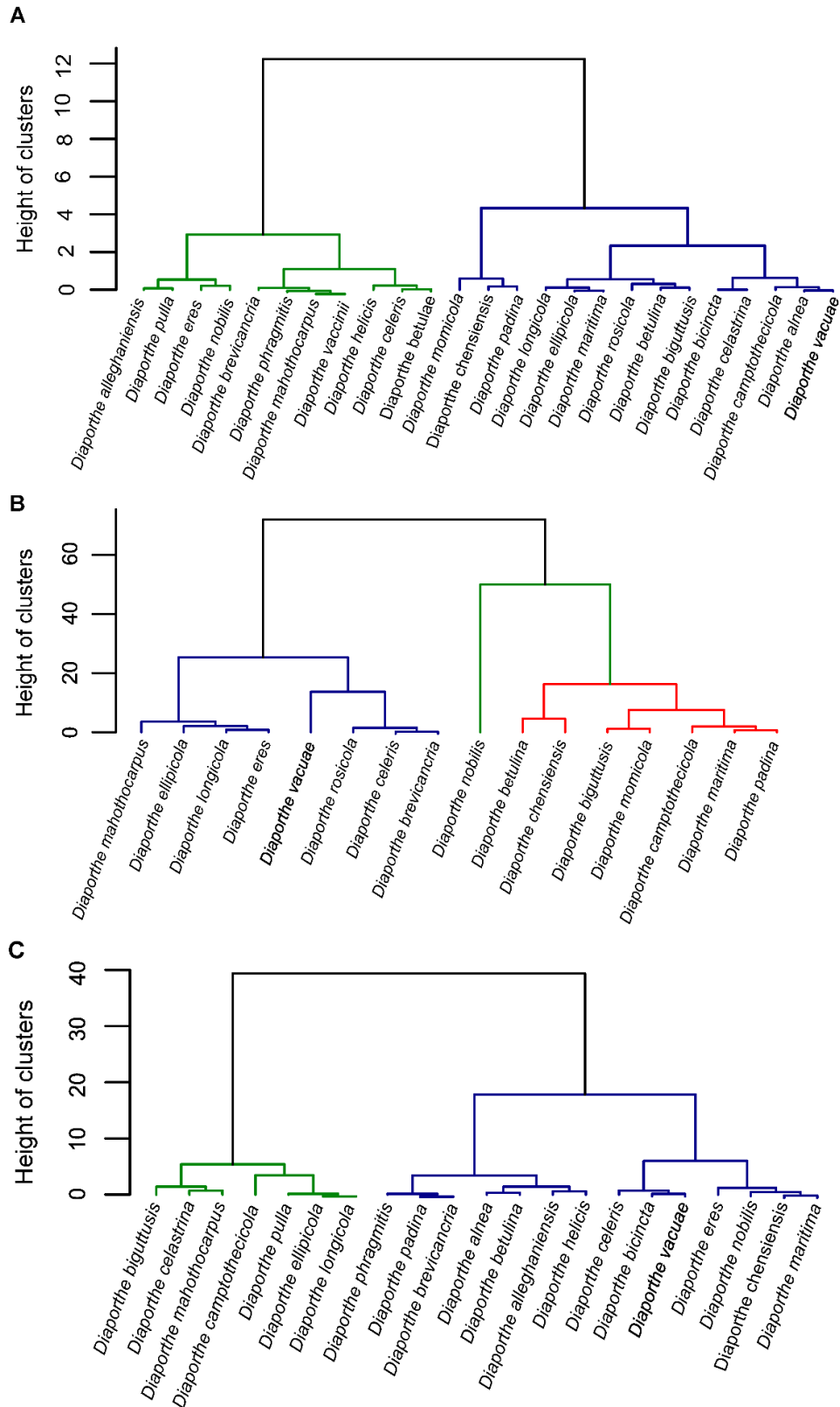


Figure 5. Dendrogram from the hierarchical clustering analysis based on the Ward's method showing the distribution of the lengths and width ratio (L/W) of alpha conidia (A), beta conidia (B) and conidiophores (C) of all species isolates from the *Diaporthe eres* complex. Green, blue and red colors represent the different clusters based on the micromorphological descriptions.

Diaporthe eres Nitschke, *Pyrenomycetes Germanici* **2**:245 (1870)
 = *Phoma oblonga* Desm., *Annl's Sci. Nat., Bot., sér. 3*, **22**:218 (1853)
 = *Diaporthe alnea* Fuckel, *Jahrb. nassau. Ver. Naturk* **23–24**:207 (1870)
 = *Diaporthe pulla* Nitschke, *Pyrenomycetes Germanici* **2**:249 (1870)
 = *Diaporthe helicis* Niessl, *Verh. Naturforsch. Ver., Brünn* **16**:50 (1876)
 = *Diaporthe nobilis* Saccardo & Spegazzini, *Michelia* **1**:386 (1878)
 = *Diaporthe bicincta* (Cooke & Peck) Sacc., *Syll. fung (Abellini)* **1**:622 (1882)
 = *Diaporthe neilliae* Peck, *Ann. Rep. N.Y. St. Mus. nat. Hist.* **39**:52 (1887)
 = *Diaporthe celastrina* (Ellis & Barthol), *J. Mycol.* **8**:173 (1902)
 ≡ *Phomopsis oblonga* (Desm.) Traverso, *Fl. ital. crypt., Pars 1*: 248 (1906)
 = *Phomopsis velata* Sacc. Traverso, *Fl. ital. crypt. (Florence)* **2**:248 (1906)
 = *Diaporthe vaccinii* Shear, *Bull. - U.S., Dep. Agric* **258**:7 (1931)
 = *Diaporthe alleghaniensis* Arnold, *Can. J. Bot.* **45**:787 (1967)
 ≡ *Diaporthe cotoneastri* Udayanga, Crous & Hyde, *Fungal Divers.* **56**:166 (2012)
 ≡ *Diaporthe castaneae-mollisimae* Udayanga, Crous & Hyde, *Fungal Divers.* **56**:166 (2012)
 = *Diaporthe phragmitis* Crous, *Fungal Planet* **283**:219 (2014)
 = *Diaporthe biguttusis* Gao & Cai, *Fungal Biol.* **119**:300 (2015)
 = *Diaporthe ellipicola* Gao & Cai, *Fungal Biol.* **119**:300 (2015)
 = *Diaporthe longicicola* Gao & Cai, *Fungal Biol.* **119**:303 (2015)
 = *Diaporthe mahothocarpus* Gao & Cai, *Fungal Biol.* **119**:306 (2015)
 = *Diaporthe betulae* Tian & Fan, *Phytotaxa* **269**:96 (2016)
 = *Diaporthe maritima* Tanney, *Fungal Biol.* **120**:1454 (2016)
 = *Diaporthe camptothecicola* Tian & Yang, *Mycotaxon* **132**:595 (2017)
 = *Diaporthe momicola* Dissanayake, Li & Hyde, *Mycosphere* **8**:541 (2017)
 = *Diaporthe fukushii* Dissanayake, Phillips & Hyde, *Mycosphere* **8**:1130 (2017)
 = *Diaporthe betulina* Tian & Yang, *Myckeys* **39**:121 (2017)
 = *Diaporthe chensiensis* Tian & Yang, *Myckeys* **39**:127 (2017)
 = *Diaporthe padina* Tian & Yang, *Myckeys* **39**:137 (2017)
 = *Diaporthe celeris* Guarnaccia, Woodhall & Crous, *Persoonia* **40**:146 (2018)
 = *Diaporthe rosicola* Wanasinghe, Jones & Hyde, *Fungal Divers.* **89**:187 (2018)
 = *Diaporthe vacuae* Hilário, Santos & Alves, *Mycologia* **55**:207 (2021)

= *Diaporthe brevicancra* Sakalidis & Medina-Mora, *Phytopathology* **111**:515 (2020)

Typification: as described by Udayanga et al. (2014) – *Diaporthe eres*, Germany, Nordrhein-Westfalen, Munsterland, Munster Botanical Gardens, on twigs of *Ulmus* sp., June 1865, T. Nitschke, (lectotype B 70 0009145); Carpinion forest, on dead, attached, corticated twigs of *Ulmus laevis*, 5 January 2013, R. Jarling, comm. R. Schumacher (epitype BPI 892912, ex-epitype culture AR5193 = CBS 138594). *Phoma oblonga*, France, on twigs of *Ulmus campestris*, unknown collector (bound specimen of Desmazieres, *Plantes Cryptogames du Nord de la France*, Ed. 2, ser. 2. No. 60 in BPI). Germany, Carpinion forest, on dead, attached, corticated twigs of *Ulmus laevis*, 5 January 2013, R. Jarling, comm. R. Schumacher (epitype BPI 892913, ex-epitype culture AR5196 = CBS 138595). *Phomopsis castaneae-mollissimae*, China, Taian, Shangdong, leaf of *Castanea mollissima*, April 2006, S.X. Jiang (CLS 0612, holotype not seen, ex-type culture BYD1 = DNP128), ex-isotype culture BYD4 = DNP129. *Diaporthe cotoneastri*, UK, Scotland, Ayr, on *Cotoneaster* sp., May 1982, H. Butin (isotype CBS-H 7633 not seen, ex-isotype culture CBS 439.82). *Phomopsis fukushii*, Japan, Ibaraki, on *Pyrus pyrifolia*, August 1994, S. Kanematsu, (neotype BPI 892933, ex-neotype culture MAFF625034 = AR3672).

Known distribution: Austria, China, France, Germany, Italy, Japan, Korea, Latvia, Lithuania, Netherlands, New Zealand, Poland, Portugal, Russia, Serbia, South Africa, UK, USA, Yugoslavia (Farr & Rossman 2021).

Host range: *Abutilon* sp., *Acer campestre*, *Acer nugundo*, *Alliaria officinalis*, *Allium giganteum*, *Arctium* sp., *Banksia* sp., *Betula alleghaniensis*, *Camelia sinensis*, *Castanea mollissima*, *C. sativa*, *Celastrus scandens*, *Chamaecyparis thyoides*, *Citrus* sp., *Cotoneaster* sp., *Cornus florida*, *Corylus avellana*, *Cucumis* sp., *Daphne lauriola*, *Eucalyptus globulus*, *Fraxinus excelsior*, *Glycine max*, *Hedera helix*, *Hordeum* sp., *Ilex aquifolium*, *Juglans cinerea*, *J. regia*, *Juniperus* sp., *Laburnum* sp., *Laurus nobilis*, *Magnolia* sp., *Malus pumila*, *M. silvestris*, *Opuntia* sp., *Osmanthus aquifolium*, *Oxydendrum arboreum*, *Phaseolus vulgaris*, *Picea pungens*, *P. glauca*, *P. abies*, *Pinus pantepylla*, *P. pinaster*, *Prunus persica*, *P. cerasus*, *P. nume*, *Pyrus pyrifolia*, *Quercus suber*, *Rhododendron* sp., *Rubus* sp., *Rumex hydrolapathum*, *Salix* sp., *Sassafras albida*, *Skimmia japonica*, *Sorbus*

aucuparia, *Tilis cordata*, *Ulmus minor*, *U. laevis*, *U. campestris*, *Vaccinium corymbosum*, *V. macrocarpon*, *Viburnum lantana*, *Vitis vinifera*, *Wisteria sinensis*, *Ziziphus jujuba* (Farr & Rossman 2021).

Description: Both sexual and asexual morphs of *D. eres* have been previously described and illustrated by Udayanga et al. (2014). Briefly, sexual morph characterized by having perithecia, black, globose or irregular, clustered in groups, immersed in host tissue with long necks, 300–700 μm long. Asci (39–)48.5–58.5(–61) \times (6.5–)7–9(–11) μm (mean \pm SD = $53 \pm 5 \times 8.0 \pm 0.7$), unitunicate, 8-spored, sessile, elongate to clavate. Ascospores (11–)12.5–14.5(–15.5) \times 3–4 μm (mean \pm SD = $13.5 \pm 1 \times 3.5 \pm 0.3$), hyaline, two-celled, often 4-guttulate, with larger guttules at center and smaller ones at the ends, elongated to elliptical; asexual morph with pycnidia 200–250 μm diameter, globose, embedded in tissue, erumpent at maturity, with a 200–300 μm long, black, elongated neck, often with yellowish, conidial cirrus extruding from ostiole, walls parenchymatous, consisting of 3–4 layers of medium brown texture angularis. Conidiophores 10–15 \times 2–3 μm , hyaline, smooth, unbranched, ampulliform, straight to sinuous. Conidiogenous cells phialidic, cylindrical, slightly tapering towards the apex. Paraphyses absent. Alpha conidia (6–)6.5–8.5(–9) \times 3–4 μm (mean \pm SD = $7.5 \pm 0.5 \times 2.5 \pm 0.5$), abundant in culture, aseptate, hyaline, smooth, ovate to ellipsoidal, often biguttulate, base sub-truncate. Beta conidia (18–)22–28(29) \times 1–1.5 μm (mean \pm SD = $25 \pm 2 \times 1.3 \pm 0.3$), aseptate, hyaline, smooth, fusiform to hooked, base sub-truncate.

Notes: The micromorphology of the asexual morph of all species belonging to the *D. eres* complex match the original description of *D. eres* reported by Udayanga et al. (2014): pycnidia embedded in tissue, irregularly distributed over agar surface, producing abundant and black stromata at maturity, covered in white mycelium, and oozing yellowish conidial cirrus from ostioles. Cultural characteristics are also similar to those reported by Udayanga et al. (2014): colonies spreading on PDA in a radial pattern with white, aerial, cottony mycelium, sometimes with brown aerial mycelium at the center, becoming grey at edges of plate, and reverse white to ivory color concentric zones, becoming brownish to black with age; conidiophores, alpha conidia and beta conidia with dimensions that correlates with the ones reported by those authors. Although the asexual morph of

D. neilliae was not recorded by Udayanga et al. (2014), the sexual morph was compared to the one of *D. eres*: perithecia and ascospores of *D. neilliae* that match within the same ranges as those of *D. eres*, and asci of *D. neilliae* were reported to be slightly shorter than those of *D. eres* ($45 \pm 5 \times 8.5 \pm 0.7 \mu\text{m}$ for *D. neilliae* vs. $53 \pm 5 \times 8.0 \pm 0.7$ for *D. eres*).

Table 4. Synopsis of morphological characteristics of *Diaporthe eres* synonymous discussed in this study. (Note: the taxonomic description of *D. neilliae* was not included as its asexual morph is unknown). The newly synonymous introduced in the present study are marked with an asterisk.

Species	Conidiomata	Conidiophores and conidiogenous cells	Alpha conidia (µm)	Beta conidia (µm)	References
<i>D. alleghaniensis</i> Arnold 1967*	Conidiomata small, with a conical shape, 200-250 µm diameter	Conidiophores 9–15 × 1–2 µm, hyaline, unbranched, ampulliform, cylindrical to sub-cylindrical. Conidiogenous phialidic, cylindrical, slightly tapering towards apex	Alpha conidia 7–9 × 3–4 µm, aseptate, hyaline, smooth, ovate to ellipsoidal, biguttulate or multiguttulate, base sub-truncate.	Not observed	Udayanga et al. 2014
<i>D. alnea</i> Fuckel 1870* = <i>Phomopsis alnea</i>	Pycnidia with 100–200 µm diameter, globose to subglobose, embedded in tissue, erumpent at maturity	Conidiophores 9–16 × 1–2 µm, hyaline, unbranched, ampulliform, cylindrical to sub-cylindrical. Conidiogenous cells phialidic, cylindrical, tapering towards the apex	Alpha conidia 8–10 × 2–3 µm, aseptate, hyaline, smooth, ellipsoidal, biguttulate or multiguttulate, base subtruncate	Not observed	Udayanga et al. 2014
<i>D. betulae</i> Tian & Fan 2016*	Conidiomatal stromata immersed, erumpent, separate, conical, with a single locule	Conidiophores reduced to phialidic conidiogenous cells hyaline, straight or slightly curved	Alpha conidia hyaline, ellipsoidal, aseptate, smooth, biguttulate, 8.5–11.5 × 3.5–4.5 µm	Not observed	Du et al. 2016
<i>D. betulina</i> Tian & Yang 2018*	Conidiomata pycnidial, conical, immersed and erumpent through the bark surface, 290–645 µm diameter	Conidiophores 12.5–17.5 × 1.5–2 µm, cylindrical, hyaline, phialidic, branched, straight or slightly curved	Alpha conidia hyaline, aseptate, ellipsoidal to fusiform, biguttulate, acute at both ends, 8–10 × 2.5–3 µm	Beta conidia hyaline, aseptate, filiform, straight, eguttulate, tapering towards one apex, 26–32.5 × 1 µm	Yang et al. 2018
<i>D. bicincta</i> Cooke & Peck 1882*	Pycnidia with 200–300 µm diameter, globose, erumpent at maturity, conidial cirrhous extruding from ostiole	Conidiophores 7–12 × 1–2 µm, hyaline, smooth, unbranched, cylindrical to sub-cylindrical. Conidiogenous cells 0.5–1 µm diameter, phialidic, cylindrical, tapering towards the apex.	Alpha conidia 9–12 × 2–3.5 µm, aseptate, hyaline, ovate to ellipsoidal, biguttulate or multiguttulate, base subtruncate.	Not observed	Udayanga et al. 2014

<i>D. biguttusis</i> Gao & Cai 2015*	Pycnidial conidiomata, dark brown, globose clustered, 79–227 µm diameter	Conidiophores 11.5–27.1 × 1.4–2.3 µm, cylindrical, single to multi-septate, densely aggregated, slightly tapering towards the apex.	Alpha conidia hyaline, biguttulate, fusiform or oval, with both ends obtuse, 5.9–8.5 × 1.9–2.6 µm	Beta conidia hyaline, aseptate, filiform, hamate, eguttulate, tapering towards both ends, 28.1–37.9 × 1.3–2.0 µm	Gao et al. 2015
<i>D. brevicancris</i> Sakalidis & Medina-Mora 2021*	Pycnidia dark brown to black, emerged in host tissue, solitary or aggregated, often with creamy yellow conidial cirrus, 236–368 µm diameter	Conidiophores hyaline, reduced to conidiogenous cells phialidic, and narrowing towards the apex 7.1–17.5 × 1.0–2.4 µm	Alpha conidia, hyaline, aseptate, oblong to ellipsoid, often biguttulate with a sub-truncated base, 4.4–8.6 × 1.3–3.3 µm	Beta conidia aseptate, hyaline, smooth, mostly convex at one end, hooked, 12.4–27.4 × 0.9–2.1 µm	Sakalidis et al. 2021
<i>D. camptothecicola</i> Tiang & Yang 2017	Conidiomatal pycnidia immersed or slightly erumpent through bark surface, sparse, globose to ovoid, with 560 µm diameter	Conidiophores (8.3–)12.5–15.8(–17.0) × 0.9–1.2 µm hyaline, unbranched, smooth, cylindrical, straight, or slightly curved, conidiogenous cells enteroblastic, phialidic.	Alpha conidia hyaline, aseptate, oblong, biguttulate, (4.6–)5.5–7.0(–7.5) × 1.5–1.8 µm	Beta conidia hyaline, aseptate, filiform with obtuse ends, 19.5–28.3 × 1.0 µm	Yang et al. 2017
<i>D. celsastrina</i> Ellis & Barthol 1902*	Pycnidia with 200–300 µm diameter, globose, embedded in tissue, erumpent at maturity conidial cirrus extruding from ostiole;	Conidiophores 7–21 × 1–2 µm, hyaline, smooth, unbranched, ampulliform, cylindrical. Conidiogenous cells 0.5–1 µm diam, phialidic, cylindrical, terminal, slightly tapering towards apex.	Alpha conidia 9–12 × 2–3.5 µm, aseptate, hyaline, ellipsoidal, biguttulate, multiguttulate, or eguttulate, base subtruncate	Not observed	Udayanga et al. 2014
<i>D. celeris</i> Guarnaccia, Woodhall & Crous 2018*	Conidiomata pycnidial, globose or irregular, solitary, erumpent, dark brown to black, 350–650 µm diam, with yellowish translucent to brown conidial cirrus	Conidiophores hyaline, smooth, unbranched, cylindrical, straight, 5–18 × 1–3 µm. Conidiogenous cells phialidic, hyaline, cylindrical, 5–8 × 1–2 µm, tapering towards the apex.	Alpha conidia, aseptate, fusiform, hyaline, mono- to biguttulate and acutely rounded at both ends, 5.5–7.5 × 2–3 µm	Beta conidia hyaline, eguttulate, filiform, curved, tapering towards both ends, 16–22.5 × 1–2 µm	Guarnaccia et al. 2018

<i>D. chensiensis</i> Tian & Yang 2018*	Conidiomata pycnidial, immersed in bark, slightly erumpent discoid, ostiolate, 200–325 µm diameter	Conidiophores 8.5–13 2–3 µm, cylindrical, hyaline, phialidic, unbranched, straight or slightly curved, tapering towards the apex	Alpha conidia hyaline, aseptate, smooth, ellipsoidal, biguttulate, rounded at both ends, 6.5–11 × 2–2.2 µm	Beta conidia present on the host only, hyaline, eguttulate, smooth, filiform, 21–28.5 × 0.8–1.1 µm	Yang et al. 2018
<i>D. ellipicola</i> Gao & Cai 2015	Pycnidial conidiomata, globose, 141–338 µm diameter, erumpent, single or clustered, extruding yellowish translucent conidial droplets from the ostioles.	Conidiophores cylindrical, branched, septate, hyaline, 12–22.4 × 1.1–2 µm, phialidic, cylindrical, straight, slightly tapering towards the apex.	Alpha conidia 6–8.7 × 2–3 µm, aseptate, hyaline, smooth, biguttulate, oval, ellipsoid rounded at both ends.	Beta conidia 23.4–35.5 × 1.4–2 µm, hyaline, curved	Gao et al. 2015
<i>D. eres</i> Nitschke 1870 = <i>D. castaneae-mollisimae</i> = <i>D. cotoneastri</i> = <i>D. fukushi</i>	Pycnidia 200–250 µm diameter, globose, embedded in tissue, erumpent at maturity, often with yellowish, conidial cirrus extruding from ostiole.	Conidiophores 10–15 × 2–3 µm, hyaline, smooth, unbranched, ampulliform, straight to sinuous. Conidiogenous cells 0.5–1 µm diameter, phialidic, cylindrical, slightly tapering towards the apex.	Alpha conidia (6–)6.5–8.5(–9) × 3–4 µm, aseptate, hyaline, smooth, ovate to ellipsoidal, often biguttulate, base subtruncate.	Beta conidia 18–29 × 1–1.5 µm, aseptate, hyaline, smooth, fusiform to hooked, base sub-truncate	Udayanga et al. 2014
<i>D. heliciis</i> Niessl 1876* = <i>D. nitschkei</i>	Pycnidia with 200–300 µm diameter, globose, embedded in tissue, erumpent at maturity, often with white conidial cirrus extruding from ostiole	Conidiophores (6–)8–15 (16.5) × 1–2 µm, hyaline, smooth, unbranched, ampulliform, cylindrical to clavate. Conidiogenous cells phialidic, cylindrical, tapering towards the apex	Alpha conidia (5.5–)6–8 (9.5) × 2.5–3.5 µm, aseptate, hyaline, smooth, cylindrical to ellipsoidal, biguttulate or multiguttulate, base subtruncate	Not observed	Udayanga et al. 2014
<i>D. longicicola</i> Gao & Cai 2015	Conidiomata pycnidial, globose to subglobose, 500–750 µm diameter, dark brown to black, covered with white mycelium	Conidiophores 14.1–22.5 × 1.3–2 µm, hyaline, branched, densely aggregated, cylindrical, tapering towards the apex	Alpha conidia 5.3–10.4 × 1.5–3.1 µm, with two big guttulate or 2–3 small guttulate, hyaline, ellipsoid or clavate, with one end obtuse and the other end acute and elongate	Beta conidia filiform, hyaline, hamate or curved, aseptate, 25–32.2 × 1.2–2 µm	Gao et al. 2015

<i>D. mahothocarpus</i> Gao & Cai 2015 = <i>Phomopsis mahothocarpus</i>	Conidiomata globose, 200–350 µm diameter, ostiolate, deeply embedded in culture, aggregated in clusters	Conidiophores 15.5–21.8 × 1.6–2.2 µm, cylindrical, hyaline, branched, septate, straight or slightly curved	Alpha conidia 5.5–8.0 × 1.8–2.9 µm, hyaline, aseptate, oval or fusiform, usually with one guttule at each end	Beta conidia 21.1–28.5 × 1.2–1.9 µm, aseptate, filiform, hyaline, curved, eguttulate, with obtuse ends	Gao et al. 2014
<i>D. maritima</i> Tanney 2016*	Conidiomata pycnidial, globose to subglobose, unilocular/multilocular, aggregated, dark brown to black, ostiolate, up to 300 µm diameter, with yellowish conidial mass	Conidiogenous cells phialidic, subcylindrical to ampulliform, straight to sinuous, cylindrical or slightly tapering towards the apex, (8.5–)9–12.5(–16) × 2–3 µm	Alpha conidia aseptate, hyaline, smooth, oblong to fusiform or ellipsoidal, apex rounded, base subtruncate, bi- to multiguttulate (10–)11–12.5(–13.5) × (3–)3.5–4 µm	Beta conidia aseptate, hyaline, smooth, straight to hamiform or uncinata 29–40 × 1–2 µm	Tanney et al. 2016
<i>D. momicola</i> Dissanayake, Li & Hyde 2017	Conidiomata up to 350 µm diameter, solitary or in groups with black cylindrical ostiolate necks, subglobose	Conidiophores reduced to conidiogenous cells	Alpha conidia 6.5–9.5 × 1.5–2 µm, hyaline, smooth, biguttulate, fusiform to oval, tapered at both ends, cylindrical to ellipsoidal	Beta conidia 20–32 × 1–1.5 µm, scattered among the alpha conidia	Dissanayake et al. 2017
<i>D. nobilis</i> Saccardo & Spegazzini 1878	Conidiomata pycnidial, scattered to confluent, uniloculate, dark brown to black, broadly spherical to flattened, 650–700 µm high and 400–500 µm wide	Conidiophores thin walled, brown, vertically aligned, multicellular, 2–6 µm wide, elongate. Conidiogenous cells formed at the apex of the conidiophores cylindrical, straight or curved.	Alpha conidia 7–9 × 3–5 µm, aseptate, cylindrical or ellipsoidal, obtuse at both ends, hyaline, generally biguttulate	Beta conidia 20–30 × 0.3–0.8 µm, filiform, blunt at one end, pointed and usually curved at the other, hyaline, one-celled	Li et al. 2017
<i>D. padina</i> Tian & Yang 2017*	Conidiomata pycnidial, immersed in bark, scattered, slightly erumpent, light brown, one ostiole, 330–520 µm diameter	Conidiophores 5.5–12.5 × 1–1.5 µm, hyaline, unbranched, cylindrical, straight or slightly curved	Alpha conidia hyaline, aseptate, ellipsoidal to fusiform, eguttulate, 7–8 × 1.5–2 µm	Beta conidia hyaline, filiform, straight or hamate, eguttulate, base truncate, 21–24 × 1 µm	Yang et al. 2018
<i>D. phragmitis</i> Crous 2014*	Conidiomata pycnidial, globose, up to 250 µm diam, black, erumpent, exuding creamy	Conidiophores hyaline, smooth, septate, rarely branched, densely aggregated, cylindrical, 20–30 × 3–4 µm. Conidiogenous	Alpha conidia aseptate, hyaline, smooth, multi- or bi-guttulate, fusoid to ellipsoid, tapering towards both ends, base	Not observed	Crous et al. 2014

	conidial droplets from central ostioles	cells phialidic, cylindrical, terminal, intercalary	subtruncate, 6–8.5 × 2–3 μm		
<i>D. pulla</i> Nitschke 1870* = <i>Phoma pulla</i> = <i>Phomopsis pulla</i>	Pycnidia with 200–300 μm diameter, globose, embedded in tissue, erumpent at maturity, black stromata, with bright yellow conidial cirrus	Conidiophores 10–25 × 1–2 μm, hyaline, unbranched, cylindrical to clavate. Conidiogenous cells phialidic, cylindrical, slightly tapering towards the apex	Alpha conidia (6–)6.5–7.5 (8) × (2–)2.5–3.5(–4) μm, aseptate, hyaline, smooth, cylindrical to ellipsoidal, biguttulate or multi-guttulate, base subtruncate	Not observed	Udayanga et al. 2014
<i>D. rosicola</i> Wanasinghe, Jones & Hyde 2018*	Conidiomata pycnidial, 120–160 μm diameter, solitary, semi-immersed, unilocular, globose, dark brown, ostiolate	Conidiophores hyaline, smooth, unbranched, cylindrical, straight to sinuous. Conidiogenous cells phialidic, cylindrical, slightly tapering towards the apex	Alpha conidia 7–9.5 × 2.4–3 μm, hyaline, biguttulate, fusiform or oval, both ends, obtuse	Beta conidia 12–22 × 1.2–1.6 μm, hyaline, aseptate, filiform, tapering towards both ends	Wanasinghe et al. 2018
<i>D. vaccinii</i> Shear 1931* = <i>Phomopsis vaccinii</i>	Conidiomata superficial, scattered, black, spherical to irregular, uniloculate, with ostiole circular, exuding white to yellowish cirrus	Conidiogenous cells enteroblastic, phialidic, with conidiophores short, 1–2 septa or multiseptate, branched.	Alpha conidia 5.9–11.3 × 2.1–3.9 μm, hyaline, fusiform, straight, guttulate, aseptate,	Beta conidia hyaline, filiform, straight or curved, eguttulate, aseptate.	Farr et al. 2002
<i>D. vacuae</i> Hilário, Santos & Alves 2020*	Pycnidial conidiomata, brown to black, broadly spherical, covered in white mycelium, with yellowish conidial cirrus extruding from ostiole	Conidiophores reduced to conidiogenous cells, hyaline, smooth and straight to sinuous, broadening in the base, slightly tapering toward the apex (10.9 ± 2.2 × 1.8 ± 0.3) μm	Alpha conidia infrequent, hyaline, smooth, cylindrical, 9.3 ± 1.1 × 2.6 ± 0.3 μm	Beta conidia hyaline, 1-celled, smooth, filiform, frequently hooked in apical part, apex acute, 27.4 ± 2.3 × 1.6 ± 0.2 μm	Hilário et al. 2020

DISCUSSION

In recent years, the use of multilocus DNA sequence data, coupled with morphology and ecology has been widely employed to establish robust species boundaries in the genus *Diaporthe* (Gao et al. 2017; Santos et al. 2017). Nevertheless, given that several authors have identified distinct species based on the concatenation of genes, without looking for incongruences between individual gene genealogies (Stewart et al. 2014), the number of species in *Diaporthe* has been increasing considerably. This is largely attributed to the intraspecific variability in the genus, where each clade has been incorrectly recognized as a distinct lineage (Gomes et al. 2013; Udayanga et al. 2011).

Although the ITS region is considered the primary barcode for fungi (Schoch et al. 2012), it has been argued by several authors that this ribosomal DNA region harbors a high variability, and therefore it is believed to be uninformative to resolve species within the *D. eres* complex (Crouch et al. 2009). Considering this, the ITS region has been excluded from the phylogenetic analysis, and currently the concatenation of *tef1- α* , *tub2*, *his3* and *cal* loci has been widely used to resolve species in the aforementioned complex (Fan et al. 2018; Gomes et al. 2013; Guo et al. 2020; Udayanga et al. 2014; Yang et al. 2018).

Despite Udayanga et al. (2014) have proven that the concatenation of seven loci to resolve the *D. eres* complex, excluding the discordant ITS data, resulted in a robust tree congruent with the other single genes, the same was not verified in the present study. By applying the GCPSR principle, the genealogical concordance among genes must be verified (Taylor et al. 2000). However, incongruent nodes, conflicting branches, and the lack of phylogenetic support in some branches were observed in the individual phylograms versus the 4-loci and 5-loci combined trees. For example, isolates of *D. eres* (e.g., MAFF265034 and CFCC 51632, previously known as *D. fukushii* and *D. camptothecicola*, respectively) did not cluster together on the individual ITS tree but formed a monophyletic clade in the remaining individual and combined trees. Moreover, it was also evident that the species *D. brevicancra* was phylogenetically indistinguishable from *D. celastrina* on the individual *cal* locus. Hence, by applying the genealogical concordance we verified that the node delimiting the *D. eres* complex, represents the transition from

concordant branches to incongruence, thus indicating that this complex of species represents one single species, *D. eres*. These incongruences observed between the individual gene genealogies confirm that the loci may harbor different evolutionary histories (Kubatko & Degnan 2007), thus making the concatenation of genes an inappropriate approach to infer the phylogenetic relationships within the *D. eres* complex.

Bearing in mind that the Ecological Species Concept recognizes species as of a group of individuals that occupies a specific niche (Steenkamp et al. 2018), the use of phylogenetic approaches based on multiple loci aids to reveal ecological patterns of diversification among clades (Gazi et al. 2011; Liu et al. 2016). However, in the present study, we demonstrate that the species belonging to the *D. eres* complex are distributed worldwide, thus lacking a correlation between the genetic divergence of the complex and its ecological niche. Despite *D. pulla* is restricted to a specific locality (Yugoslavia), it was previously shown to belong to an unresolved sub-clade, which Gomes et al. (2013) referred as *D. nobilis* complex. Later, Udayanga et al. (2014) showed that many of the isolates in the aforementioned complex clustered within *D. eres* based on the GCPSR principle. Additionally, given the genetic differences between *D. pulla* with its closest relative *D. helicis*, Udayanga et al. (2014) suggested that these two species should be designated as distinct lineages. However, according to our results, *D. pulla* and *D. helicis* belong to *D. eres* complex and are thus synonymized here with *D. eres*.

Although the Morphological Species Concept was historically the dominant concept in the genus *Diaporthe* (Rehner & Uecker 1994), the presence of conserved morphological characters made this concept inadequate to delineate species in this genus (Mostert et al. 2001). Based on the taxonomic description of the *D. eres* complex, it was evident a clear absence of morphological distinctiveness. Overall, species harbor oblong to ellipsoid alpha conidia, a common presence of beta conidia, creamy to yellowish conidial cirrus, conidiomata shapes and conidiophores dimensions that match within the same ranges. Despite the dendrograms of the length and width ratios distinguished the species into different groups, these are not correlated to any of the clades in the combined gene trees. Moreover, despite the higher variability in the L/W ratios observed for beta conidia,

this might simply represent a character plasticity of *Diaporthe*, rather than an indication of morphospecies. For instance, temperatures above 30 °C or the dextrose concentration (a component of the PDA medium) seems to influence the production of this type of conidia (Mostert et al. 2020). Culture characteristics are also quite identical among the recognized “species” within the *D. eres* complex: aerial mycelium cottony with yellowish gray to brownish-gray coloration, margin regular, producing abundant black stromata at maturity in culture and oozing yellow cirrus. Therefore, we consider those micromorphological characters as minor differences among species, demonstrating only a high character variation within the *D. eres* complex. As stated by Hyde et al. (2020), the recognition of significant recombination within closely related taxa should be considered as a method to justify a species. Therefore, the *D. eres* species complex was tested to disclose the presence of genetic recombination. Our results proved that significant genetic exchange occur within the complex, indicating that there is no reproductive isolation between some of the putative species recognized on the 5-loci combined tree. The genetic diversity within the *D. eres* complex was also estimated. Low nucleotide diversity values in addition to high haplotype diversity indices indicate a high number of closely related haplotypes (Mendez-Harclerode et al. 2007). Moreover, although *tef1- α* locus showed the highest informative characters to resolve the *D. eres* complex, as also corroborated by previous studies (Chaisiri et al. 2021; Udayanga et al. 2014), the Tajima’s D test gave negative values for *tef1- α* locus and the remaining genes (except for the ITS locus) which is indicative of inbreeding events within the population occurring at these loci. Therefore, this suggests that *D. eres* complex is a population that may have undergone a recent expansion, producing a large number of offspring (Manawasinghe et al. 2019; Mendez-Harclerode et al. 2007). In a recent study, Chaisiri et al. (2021) have also shown high levels of haplotype diversity within the five loci among *D. eres*, thus reflecting high genetic diversity. The neutrality Tajima’s test run by these authors has similarly shown negative values which suggests a population expansion in *D. eres* isolates. Such population expansion showed in the present study might be explained by inbreeding events among some species of the complex, occurring mainly in *tub2* and ITS loci which showed significant genetic recombination. Therefore, taking into

consideration the lack of gene flow, the absence of supporting phenotypic, geographic, and ecological differences, the recent divergence and the possibility of incomplete lineage sorting of the *D. eres* complex may be considered as ongoing evolving lineages (Boluda et al. 2019).

Given the existence of conflicts between individual gene trees, the impossibility to combine genes and the lack of phenotypic distinctiveness, we attempted to delimit the species boundaries of the *D. eres* species complex through coalescent-based models. This latter approach involves understanding how several species are related by modeling the genealogical history of individuals with a common ancestor (Pons et al. 2006; Zhang et al. 2013). The General Mixed-Yule Coalescent (GMYC) and the Poisson Tree Processes (PTP) models are widely used to identify branching patterns between divergence and intraspecific diversification and thus to distinguish between species and populations (Matute & Sepúlveda 2019). However, the GMYC model can overestimate the number of taxa, particularly in species with a strong intraspecific genetic structure (Boluda et al. 2019). An important advantage on using PTP analyses (both single and multi-rate) is that it models speciation events in terms of the number of nucleotide substitutions (Zhang et al. 2013). Therefore, it avoids the compute-intensive process of generating time-calibrated ultrametric trees, which are required as an input for GMYC analysis. Another drawback of this latter analysis is the choice of the molecular clock, which is essential to infer the timing of evolutionary divergence events in a given phylogeny (Ho & Duchêne 2014). However, this is somehow difficult to predict, as fossil evidence remains scarce for fungi (Berbee & Taylor 2010). For this reason, PTP analyses are considered to yield more accurate delimitations than GMYC (Tang et al. 2014), and that was the one currently adopted in the present study. According to our results, the highly supported clades recognized as distinct species in the combined 5-loci and 4-loci trees were not concordant with the coalescent methods, as both single and multi-rate PTP analyses inferred that *D. eres* complex should be recognized as a single species. Furthermore, based on the phylogenetic network performed, it is notable that the species within the *D. eres* complex are linked with boxes which is an indicative for the presence of recombination. For this reason, we considered that all species falling into the *D. eres* complex should be regarded as

one single species, *i.e.*, *D. eres*, rather than different taxa. According to Yang et al. (2018), the species *D. maritima*, *D. phragmitis* and *D. rosicola* belong to the *D. eres* species complex. Given the lack of sequences available for some loci, these species could not be included in the analyses. Nevertheless, considering that these species fall into the *D. eres* complex based in the individual genealogies performed, and knowing that Chasiri et al. (2021) have synonymized *D. rosicola* as *D. eres*, which we also corroborate in the present study, we feel comfortable to consider *D. maritima* and *D. phragmitis* as synonymous of *D. eres*.

Of particular relevance is the synonymization of *D. vaccinii* with *D. eres*. *Diaporthe vaccinii* has been regarded as a common and important pathogen of *Vaccinium* species, especially in the USA where it has been originally reported (Lombard et al. 2014). In Europe it is a quarantine organism and is regarded as eradicated from all countries where it was previously detected (Jeger et al. 2017). We recognize the potential impact that our proposal may have in the plant pathology community, but the results from the integrative approach performed in this study provide strong evidence that *D. vaccinii* cannot be regarded as a distinct species from *D. eres*. Previous studies recognize that both species are morphologically indistinguishable and phylogenetically very closely related (Fan et al. 2018; Guo et al. 2020; Yang et al. 2018). Thus, it is not unreasonable to accept that they represent a single species.

The species *D. vaccinii* was described in an epoch where host association was regarded as an important character to delimit species. It is now widely accepted that most (if not all) species of *Diaporthe* are not host specific (Mostert et al. 2001; Rehner & Uecker 1994), and *D. vaccinii* is one of the rare exceptions still accepted. Recognizing it as a synonym of *D. eres* means that its status as a major pathogen of blueberry would need to be reassessed. Previous studies (Cardinaals et al. 2018) have suggested that *D. vaccinii* was probably not a major threat to blueberry production in Europe and that its status as a quarantine organism should be reappraised.

Following the most common species concept used in fungi, the Phylogenetic Species Concept (PSC) (Taylor et al. 2000), a species is assigned to a phylogenetic cluster that shares a most recent common ancestor and it differs phenotypically from

its closest relatives (Achari et al. 2020; Inderbitzin et al. 2020). However, this is not always observed in the genus *Diaporthe*, as in the case of the *Diaporthe eres* complex, that was shown in this study to display little or no morphological variation. Moreover, the incongruences observed among the individual genealogies, turn the concatenation of multiple loci an inappropriate approach to delimit species. For this reason, we reckon that the genealogical concordance allied to the recognition of significant recombination among species must be applied in future studies to delimit the species boundaries in the genus *Diaporthe*.

CONCLUSIONS

In the present study, the phylogenetic analyses based on the GCPSR principle and the coalescent-based species model PTP proves that the *D. eres* complex is a population with evolving lineages, rather than a complex composed of distinct species. Furthermore, the pairwise homoplasy index test and the comparison of morphological and ecological characters, have highlighted the absence of gene flow within the population, given that there is no evidence neither of reproductive isolation nor geographical barriers. This study suggests that the identification of species in *Diaporthe* has been largely overestimated, since the use of multilocus DNA sequences has been widely used without comparing the individual genealogies to look for incongruent nodes. This has been particularly important in the genus *Diaporthe*, given the presence of a high intra-specific variability that might have been erroneously regarded as an aspect to describe novel taxa. Hence, individual gene genealogies must always be compared to look for incongruences among them. Once incongruent branches or a lack of phylogenetic support are observed, careful assumptions need to be made prior the description of new species in the genus *Diaporthe*. We also recommend that several strains from different locations should be included in the analyses, whenever possible, in the attempt to assess the intraspecific variation. Moreover, bearing in mind that the ITS region is the primary barcode for fungi, and it has been adopted as the genetic marker of choice for species delimitation, we advocate that this ribosomal region should not be excluded from the phylogenetic analyses, but carefully analyzed along with the other protein coding genes used in the genus *Diaporthe* such as *tef1- α* ,

tub2, *his3* and *cal* loci. In addition, further studies based on the coalescent models should also be implemented in the genus *Diaporthe* to provide stronger support to infer the phylogenetic relationships between cryptic species. Large-scale whole genome sequencing must also be considered in the future to provide insights into the validity of the current five loci used for molecular identification in the genus *Diaporthe*, as well as to identify new markers to be used in the delimitation of species in this genus, or even to develop a genome-based taxonomy approach to delimit species in the genus.

ACKNOWLEDGMENTS

The authors are thankful to the Portuguese Foundation for Science and Technology (FCT/MCTES) for financing CESAM (Centre for Environmental and Marine Studies) (UIDP/50017/2020 + UIDB/50017/2020) through national funds, and the PhD grants of Sandra Hilário (SFRH/BD/137394/2018) and Micael Gonçalves (SFRH/BD/129020/2017).

REFERENCES

- Achari SR, Kaur J, Dinh Q, Mann R, Sawbridge T, Summerell BA, Edwards J. **2020**. Phylogenetic relationship between Australian *Fusarium oxysporum* isolates and resolving the species complex using the multispecies coalescent model. *BMC Genomics* 21, 248.
- Ali S, Renderos W, Bevis E, Hebb J, Abbasi PA. **2020**. *Diaporthe eres* causes stem cankers and death of young apple rootstocks in Canada. *Canadian Journal of Plant Pathology* 42, 218–227.
- Berbee ML, Taylor JW. **2010**. Dating the molecular clock in fungi—how close are we? *Fungal Biology Reviews* 24, 1–16.
- Boluda CG, Rico VJ, Divakar PK, Nadyeina O, Myllys L, McMullin RT, Zamora JC, Scheidegger C, Hawksworth DL. **2019**. Evaluating methodologies for species delimitation: the mismatch between phenotypes and genotypes in lichenized fungi (*Bryoria* sect. *Implexae*, *Parmeliaceae*). *Persoonia* 42, 75–100.
- Bruen TC. **2005**. A simple and robust statistical test for detecting the presence of recombination. *Genetics* 172, 2665–2681.

- Bustamante DE, Oliva M, Leiva S, Mendoza JE, Bobadilla L, Angulo G, Calderon MS. **2019**. Phylogeny and species delimitations in the entomopathogenic genus *Beauveria* (Hypocreales, Ascomycota), including the description of *B. peruviansis* sp. nov. *MycKeys* 58, 47–68.
- Cardinaals J, Wenneker M, Voogd JGB, van Leeuwen GCM. **2018**. Pathogenicity of *Diaporthe* spp. on two blueberry cultivars (*Vaccinium corymbosum*). *EPPO Bulletin* 48, 128–134.
- Carstens BC, Knowles LL. **2007**. Estimating species phylogeny from gene-tree probabilities despite incomplete lineage sorting: an example from *Melanoplus* grasshoppers. *Systematics Biology* 56, 400–411.
- Chaisiri C, Liu X, Lin Y, Fu Y, Zhu F, Luo C. **2021**. Phylogenetic and haplotype network analyses of *Diaporthe eres* species in China based on sequences of multiple loci. *Biology* 10, 179.
- Crouch JA, Clarke BB, Hillman BI. **2009**. What is the value of ITS sequence data in *Colletotrichum* systematics and species diagnosis? A case study using the falcate-spored gramminicolous *Colletotrichum* group. *Mycologia* 101, 648–656.
- Crous PW, Wingfield MJ, Schumacher RK, Summerell BA, Giraldo A, Gené J, Guarro J, Wanasinghe DN, Hyde KD, Camporesi E, ... Groenewald JZ. **2014**. Fungal Planet description sheets: 281–319. *Persoonia* 33, 212–289.
- Dissanayake AJ, Zhang W, Liu M, Hyde KD, Zhao WS, Li XH, Yan JY. **2017**. *Diaporthe* species associated with peach tree dieback in Hubei, China. *Mycosphere* 8, 533–549.
- Du Z, Fan XL, Hyde KD, Yang Q, Liang YM, Tian CM. **2016**. Phylogeny and morphology reveal two new species of *Diaporthe* from *Betula* spp. in China. *Phytotaxa* 269, 90–102.
- Fan X, Yang Q, Bezerra JD, Alvarez LV, Tian C. **2018**. *Diaporthe* from walnut tree (*Juglans regia*) in China, with insight of the *Diaporthe eres* complex. *Mycological Progress* 17, 841–853.
- Farr DF, Castlebury LA, Rossman AY. **2002**. Morphological and molecular characterization of *Phomopsis vaccinii* and additional isolates of *Phomopsis* from blueberry and cranberry in the eastern United States. *Mycologia* 94, 494–504.

- Farr DF, Rossman AY. **2021**. *Fungal Databases, U.S. National Fungus Collections*, ARS, USDA. Available online <https://nt.ars-grin.gov/fungal databases/> (accessed on 08 April 2021).
- Galili T. **2015**. dendextend: an R package for visualizing, adjusting, and comparing trees of hierarchical clustering. *Bioinformatics* 31, 3718–3720.
- Gao YH, Liu F, Duan W, Crous PW, Cai L. **2017**. *Diaporthe* is paraphyletic. *IMA Fungus* 8, 163–187.
- Gao YH, Su YY, Sun W, Cai L. **2015**. *Diaporthe* species occurring on *Lithocarpus glabra* in China, with descriptions of five new species. *Fungal Biology* 119, 295–309.
- Gao YH, Sun W, Su YY, Cai L. **2014**. Three new species of *Phomopsis* in Gutianshan nature reserve in China. *Mycological Progress* 13, 111–121.
- Gazis R, Rehner S, Chaverri P. **2011**. Species delimitation in fungal endophyte diversity studies and its implications in ecological and biogeographic inferences. *Molecular Ecology* 20, 3001–3013.
- Gomes RR, Glienke C, Videira SIR, Lombard L, Groenewald JZ, Crous PW. **2013**. *Diaporthe*: A genus of endophytic, saprobic and plant pathogenic fungi. *Persoonia* 31, 1–41
- Guarnaccia V, Groenewald JZ, Woodhall J, Armengol J, Cinelli T, Eichmeier A, Ezra D, Fontaine F, Gramaje D, Gutierrez-Aguirregabiria A, ... Crous PW. **2018**. *Diaporthe* diversity and pathogenicity revealed from a broad survey of grapevine diseases in Europe. *Persoonia* 40, 135–153.
- Guo YS, Crous PW, Bai Q, Fu M, Yang MM, Wang XH, Du YM, Hong N, Xu WX, Wang GP. **2020**. High diversity of *Diaporthe* species associated with pear shoot canker in China. *Persoonia* 45, 132–162.
- Hilário S, Amaral I, Gonçalves FM, Lopes A, Santos L, Alves A. **2020**. Diversity and pathogenicity of *Diaporthe* species on blueberry plants in Portugal, with description of 4 new species. *Mycologia* 112, 293–308.
- Hilário S, Santos L, Alves A. **2021**. *Diaporthe amygdali*, a species complex or a complex species? *Fungal Biology* 125, 505–518.
- Ho SY, Duchêne S. **2014**. Molecular-clock methods for estimating evolutionary rates and timescales. *Molecular Ecology* 23, 5947–5965.

- Huson DH, Bryant D. **2006**. Application of phylogenetic networks in evolutionary studies. *Molecular Biology and Evolution* 23, 254–267.
- Hyde KD, Jeewon R, Chen YJ, Bhunjun CS, Calabon MS, Jiang HB, Lin C-G, Norphanphoun C, Sysouphathong P, Pem D, ... Lumyong, S. **2020**. The numbers of fungi: is the descriptive curve flattening?. *Fungal Divers* 103, 219–271.
- Inderbitzin P, Robbertse B, Schoch CL. **2020**. Species identification in plant-associated prokaryotes and fungi using DNA. *Phytobiomes Journal* 4, 103–114.
- Jeger M, Bragard C, Caffier D, Candresse T, Chatzivassiliou E, Dehnen-Schmutz K, Gilioli G, Grégoire JC, Miret J, MacLeod A, ... van Bruggen AHC. **2017**. Pest risk assessment of *Diaporthe vaccinii* for the EU territory. *EFSA Journal* 15, 1–185.
- Kapli P, Lutteropp S, Zhang J, Kobert K, Pavlidis P, Stamatakis A, Flouri T. **2017**. Multi-rate Poisson tree processes for single-locus species delimitation under maximum likelihood and Markov chain Monte Carlo. *Bioinformatics* 33, 1630–1638.
- Kubatko LS, Degnan JH. **2007**. Inconsistency of phylogenetic estimates from concatenated data under coalescence. *Systematic Biology* 56, 17–24.
- Li Y, Tan P, Zhao DG. **2017**. *Diaporthe nobilis*, a new record on *Camellia sinensis* in Guizhou Province, China. *Mycosphere* 8, 1–8.
- Liu F, Wang M, Damm U, Crous PW, Cai L. **2016**. Species boundaries in plant pathogenic fungi: a *Colletotrichum* case study. *BMC Evolutionary Biology* 16, 81.
- Lombard L, van Leeuwen GCM, Guarnaccia V, Polizzi G, van Rijswijk PCJ, Rosendahl CHM, Gabler J, Crous PW. **2014**. *Diaporthe* species associated with *Vaccinium*, with specific reference to Europe. *Phytopathologia Mediterranea* 53, 287–299.
- Lopes AF, Batista E, Hilário S, Santos L, Alves A. **2021**. Occurrence of *Diaporthe* species in *Eucalyptus globulus*, *Pinus pinaster* and *Quercus suber* in Portugal. *Forest Pathology* e12674.
- Lücking R, Aime MC, Robbertse B, Miller AN, Ariyawansa HA, Aoki T, Cardinali G, Crous PW, Druzhinia IS, Geiser DM, ... Schoch CL. **2020**. Unambiguous

- identification of fungi: where do we stand and how accurate and precise is fungal DNA barcoding? *IMA Fungus* 11, 14.
- Lücking R, Hawksworth DL. **2018**. Formal description of sequence-based voucherless Fungi: promises and pitfalls, and how to resolve them. *IMA Fungus* 9, 143–165.
- Manawasinghe IS, Dissanayake A, Liu M, Wanasinghe D, Xu J, Zhao W, Zhang W, Zhou Y, Hyde KD, Brooks S, Yan J. **2019**. High genetic diversity and species complexity of *Diaporthe* associated with grapevine dieback in China. *Frontiers in Microbiology* 10, 1936.
- Marin-Felix Y, Hernández-Restrepo M, Wingfield MJ, Akulov A, Carnegie AJ, Cheewangkoon R, Gramaje D, Groenewald JZ, Guarnaccia V, Halleen F, ... Crous, P.W. Genera of phytopathogenic fungi: GOPHY 2. *Studies in Mycology* 92, 47–133.
- Matute DR, Sepúlveda VE. **2019**. Fungal species boundaries in the genomics era. *Fungal Genetics and Biology* 131, 103249.
- Mendez-Harclerode FM, Strauss RE, Fulhorst CF, Milazzo ML, Ruthven DC, Bradley RD. **2007**. Molecular evidence for high levels of intrapopulation genetic diversity in woodrats (*Neotoma micropus*). *Journal of Mammalogy* 88, 360–370.
- Mostert L, Crous PW, Kang JC, Phillips AJL. **2001**. Species of *Phomopsis* and a *Libertella* sp. occurring on grapevines with specific reference to South Africa: Morphological, cultural, molecular and pathological characterization. *Mycologia* 93, 146–167.
- Murtagh F, Legendre P. **2014**. Ward's hierarchical agglomerative clustering method: which algorithms implement Ward's criterion? *Journal of Classification* 31, 274–295.
- Pons J, Barraclough T, Gomez-Zurita J, Cardoso A, Duran D, Hazell S, Kamoun S, Sumlin W, Vogler A. **2006**. Sequence-based species delimitation for the DNA taxonomy of undescribed insects. *Systematic Biology* 55, 595–609.
- R Core Team. **2021**. *R: A language and environment for statistical computing*. R Foundation for Statistical Computing, Vienna, Austria. <https://www.R-project.org/>.

- Rannala B, Yang Z. **2020**. Species Delimitation. In *Phylogenetics in the Genomic Era*; Scornavacca, C., Delsuc, F., Galtier, N., eds.; No commercial publisher, Authors open access book. <https://hal.inria.fr/PGE>, chapter 5.5; pp. 1–18.
- Rehner SA, Uecker FA. **1994**. Nuclear ribosomal internal transcribed spacer phylogeny and host diversity in the coelomycete *Phomopsis*. *Canadian Journal of Botany* **72**, 1666–1674.
- Rozas J, Ferrer-Mata A, Sánchez-DelBarrio JC, Guirao-Rico S, Librado P, Ramos-Onsins SE, Sánchez-Gracia A. **2017**. DnaSP 6: DNA sequence polymorphism analysis of large data sets. *Molecular Biology and Evolution* **34**, 3299–3302.
- Sakalidis M, Medina-Mora CM, Shin K, Fulbright DW. **2021**. Characterization of *Diaporthe* spp. associated with spruce decline on Colorado blue spruce in Michigan. *Phytopathology* **111**, 509–520.
- Santos L, Alves A, Alves R. **2017**. Evaluating multi-locus phylogenies for species boundaries determination in the genus *Diaporthe*. *Peer J* **5**, e3120.
- Schoch CL, Seifert KA, Huhndorf S, Robert V, Spouge JL, Levesque CA, Chen W. Fungal Barcoding Consortium. **2012**. Nuclear ribosomal internal transcribed spacer (ITS) region as a universal DNA barcode marker for Fungi. *Proceedings of the National Academy of Sciences of the United States of America* **109**, 6241–6246.
- Steenkamp ET, Wingfield MJ, McTaggart AR, Wingfield BD. **2018**. Fungal species and their boundaries matter – Definitions, mechanisms and practical implications. *Fungal Biology Reviews* **32**, 104–116.
- Stewart JE, Timmer LW, Lawrence CB, Pryor BM, Peever TL. **2014** Discord between morphological and phylogenetic species boundaries: incomplete lineage sorting and recombination results in fuzzy species boundaries in an asexual fungal pathogen. *BMC Evolutionary Biology* **14**, 38.
- Tajima F. **1989**. Statistical method for testing the neutral mutation hypothesis by DNA polymorphism. *Genetics* **123**, 585–595.
- Tang CQ, Humphreys AM, Fontaneto D, Barraclough TG, Paradis E. **2014**. Effects of phylogenetic reconstruction method on the robustness of species delimitation using single-locus data. *Methods in Ecology and Evolution* **5**, 1086–1094.

- Tanney JB, McMullin DR, Green BD, Miller JD, Seifert KA. **2016**. Production of antifungal and antiinsectan metabolites by the *Picea* endophyte *Diaporthe maritima* sp. nov. *Fungal Biology* 120, 1448–1457.
- Taylor JW, Jacobson DJ, Kroken S, Kasuga T, Geiser DM, Hibbett DS, Fisher MC. **2000**. Phylogenetic species recognition and species concepts in fungi. *Fungal Genetics and Biology* 31, 21–32.
- Udayanga D, Castlebury LA, Rossman AY, Chukeatirote E, Hyde KD. **2014**. Insights into the genus *Diaporthe*: phylogenetic species delimitation in the *D. eres* species complex. *Fungal Diversity* 67, 203–229.
- Udayanga D, Liu X, McKenzie EHC, Chukeatirote E, Bahkali AHA, Hyde KD. **2011**. The genus *Phomopsis*: Biology, applications, species concepts and names of common phytopathogens. *Fungal Diversity* 50, 189–225.
- Wanasinghe DN, Phukhamsakda C, Hyde KD, Jeewon R, Lee HB, Jones EG, Tibpromma S, Tennakoon DS, Jayasiri SC, Gafforov Y, ... Karunarathna SC. **2018**. Fungal diversity notes 709–839: taxonomic and phylogenetic contributions to fungal taxa with an emphasis on fungi on *Rosaceae*. *Fungal Diversity* 89, 1–236.
- Wingfield MJ, De Beer ZW, Slippers B, Wingfield BD, Groenewald JZ, Lombard L, Crous PW. **2012**. One fungus, one name promotes progressive plant pathology. *Molecular Plant Pathology*, 13, 604–613.
- Yang Q, Fan XL, Du Z, Liang YM, Tian CM. **2017**. *Diaporthe camptothecicola* sp. nov. on *Camptotheca acuminata* in China. *Mycotaxon* 132, 591–601.
- Yang Q, Fan XL, Guarnaccia V, Tian CM. **2018**. High diversity of *Diaporthe* species associated with dieback diseases in China, with twelve new species described. *MycoKeys* 39, 97–149.
- Zhang J, Kapli P, Pavlidis P, Stamatakis A. **2013**. A general species delimitation method with applications to phylogenetic placements. *Bioinformatics* 29, 2869–2876.

SUPPLEMENTARY MATERIAL

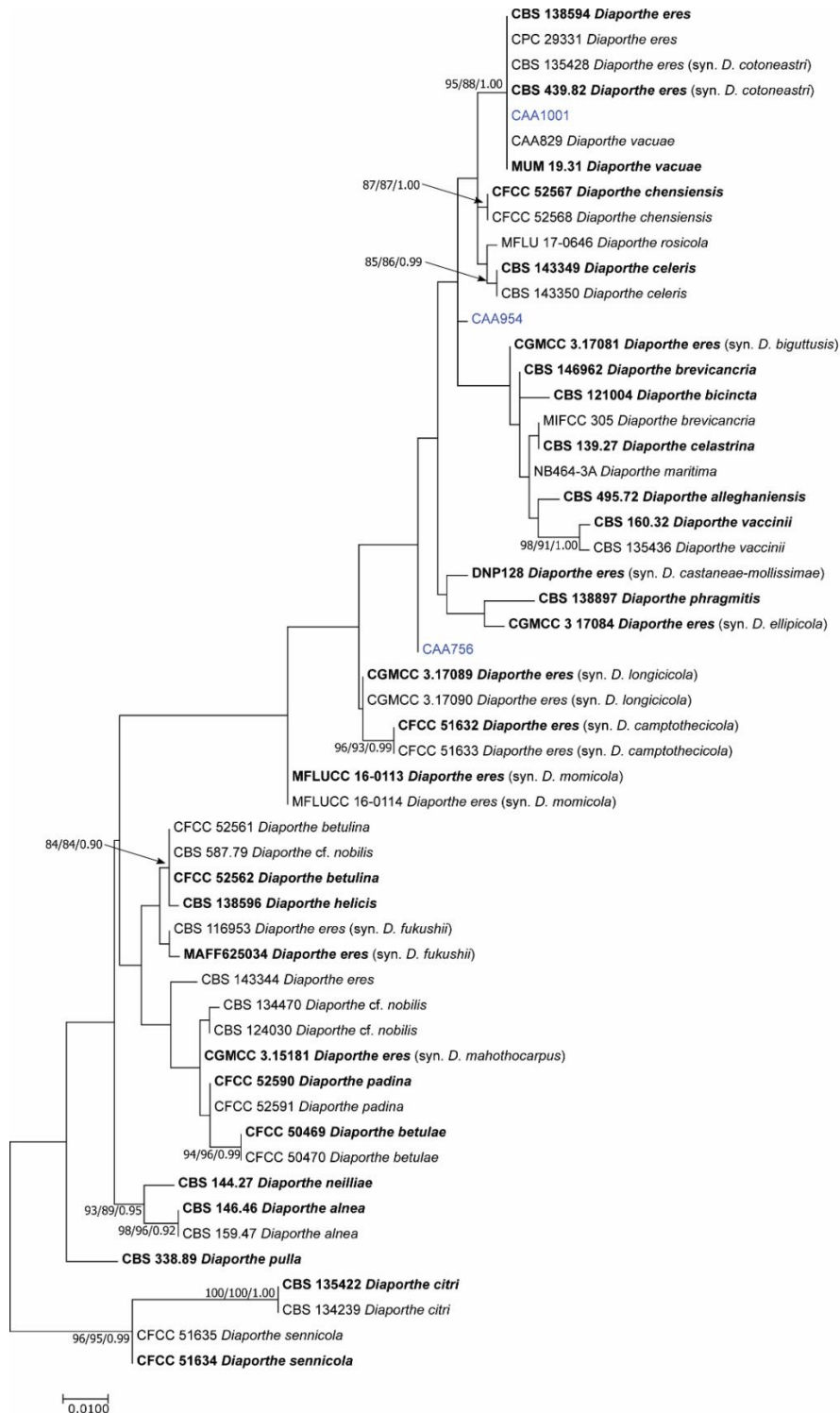


Figure S1. Maximum Likelihood tree based on ITS sequence data for all species of the *Diaporthe eres* species complex. The ML tree was constructed based on the Kimura 2-parameter model assuming a gamma distribution. ML and MP bootstrap values greater than 70% and posterior probabilities (PPs) greater than 0.80 are shown at the nodes. The ex-type strains are in bold. The newly generated sequences are indicated in blue.

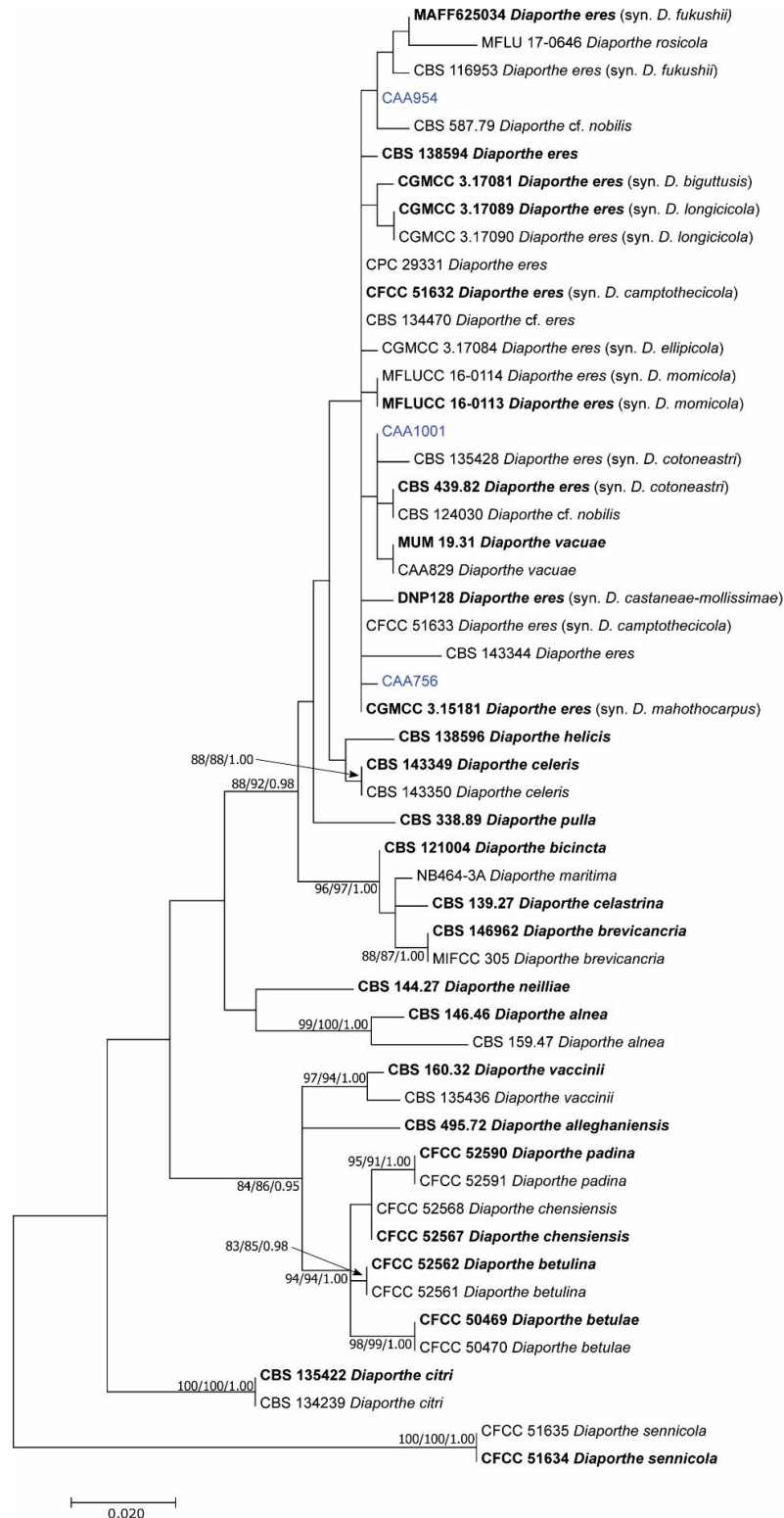


Figure S2. Maximum Likelihood tree based on *tef1-α* sequence data for all species of the *Diaporthe eres* species complex. The ML tree was constructed based on the Kimura 2-paramter model assuming uniform rates. ML and MP bootstrap values greater than 70% and posterior probabilities (PPs) greater than 0.80 are shown at the nodes. The ex-type strains are in bold. The newly generated sequences are indicated in blue.

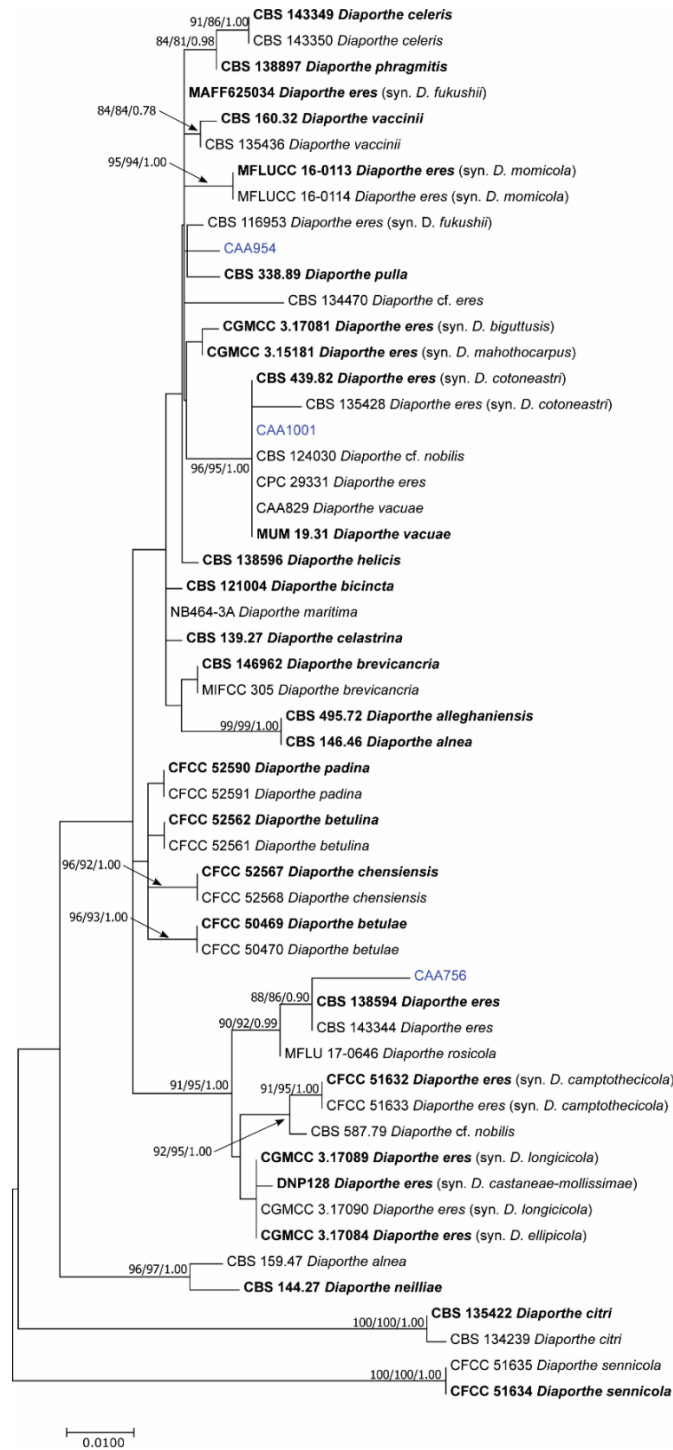


Figure S3. Maximum Likelihood tree based on *tub2* sequence data for all species of the *Diaporthe eres* species complex. The ML tree was constructed based on the Kimura 2-parameter model assuming a gamma distribution. ML and MP bootstrap values greater than 70% and posterior probabilities (PPs) greater than 0.80 are shown at the nodes. The ex-type strains are in bold. The newly generated sequences are indicated in blue

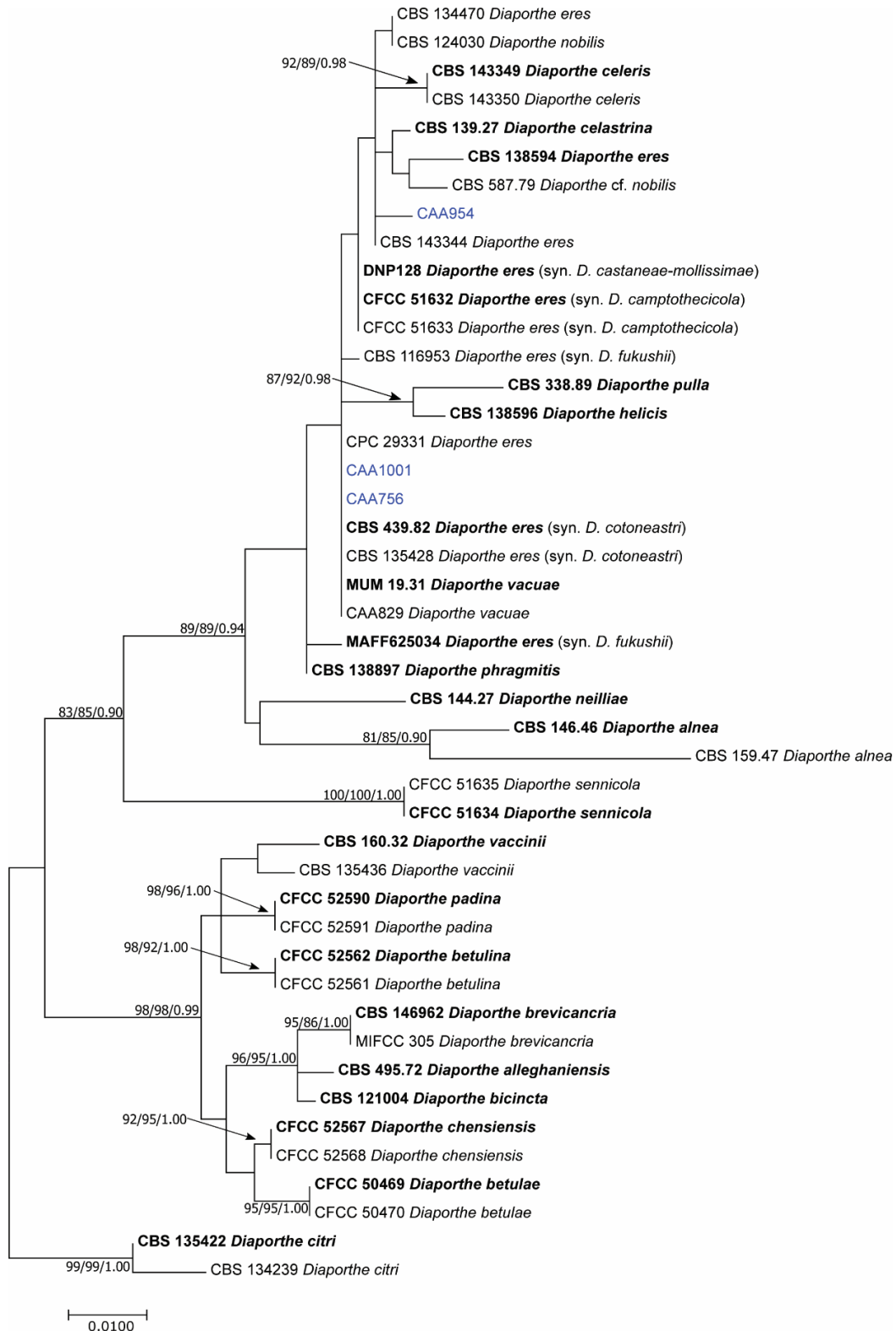


Figure S4. Maximum Likelihood tree based on *his3* sequence data for all species of the *Diaporthe eres* species complex. The ML tree was constructed based on the Hasegawa-Kishino-Yano model assuming a gamma distribution. ML and MP bootstrap values greater than 70% and posterior probabilities (PPs) greater than 0.80 are shown at the nodes. The ex-type strains are in bold. The newly generated sequences are indicated in blue.

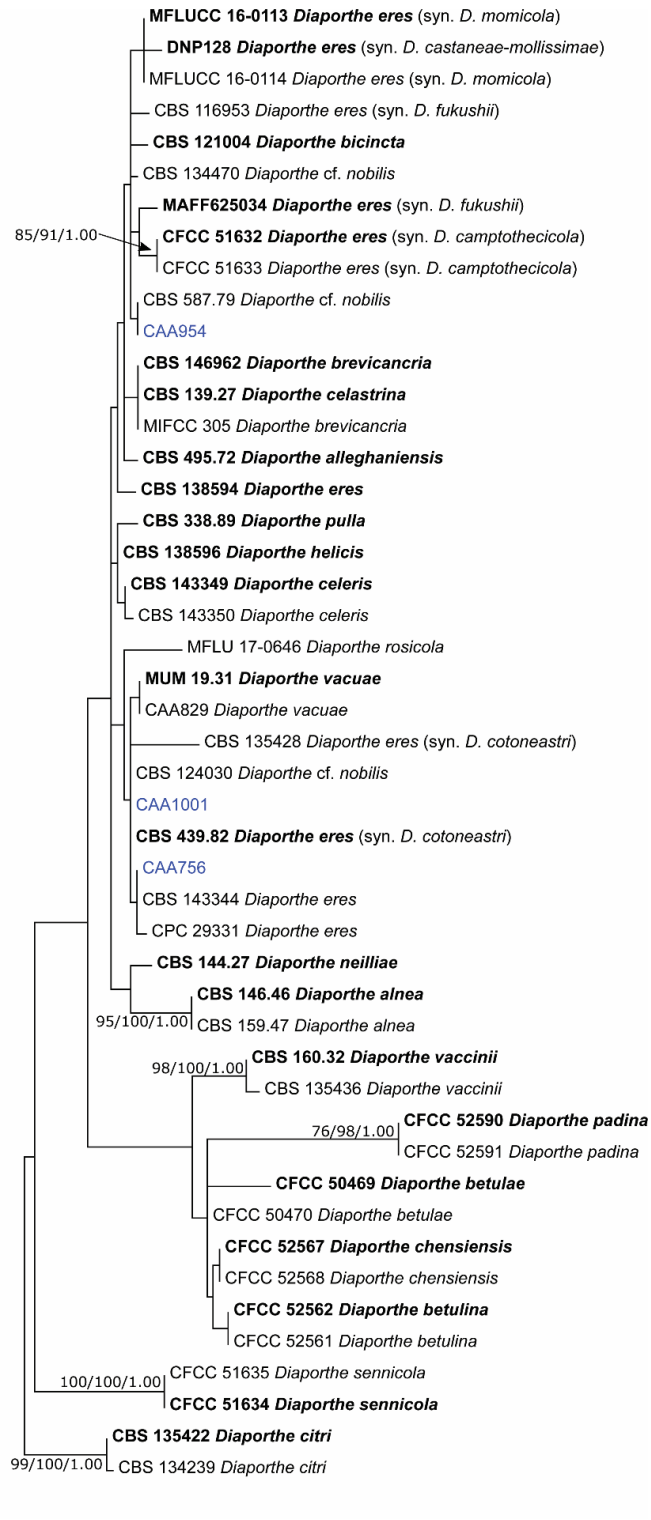


Figure S5. Maximum Likelihood tree based on *cal* sequence data for all species of the *Diaporthe eres* species complex. The ML tree was constructed based on the Tamura 3-parameter model assuming a gamma distribution. ML and MP bootstrap values greater than 70% and posterior probabilities (PPs) greater than 0.80 are shown at the nodes. The ex-type strains are in bold. The newly generated sequences are indicated in blue.

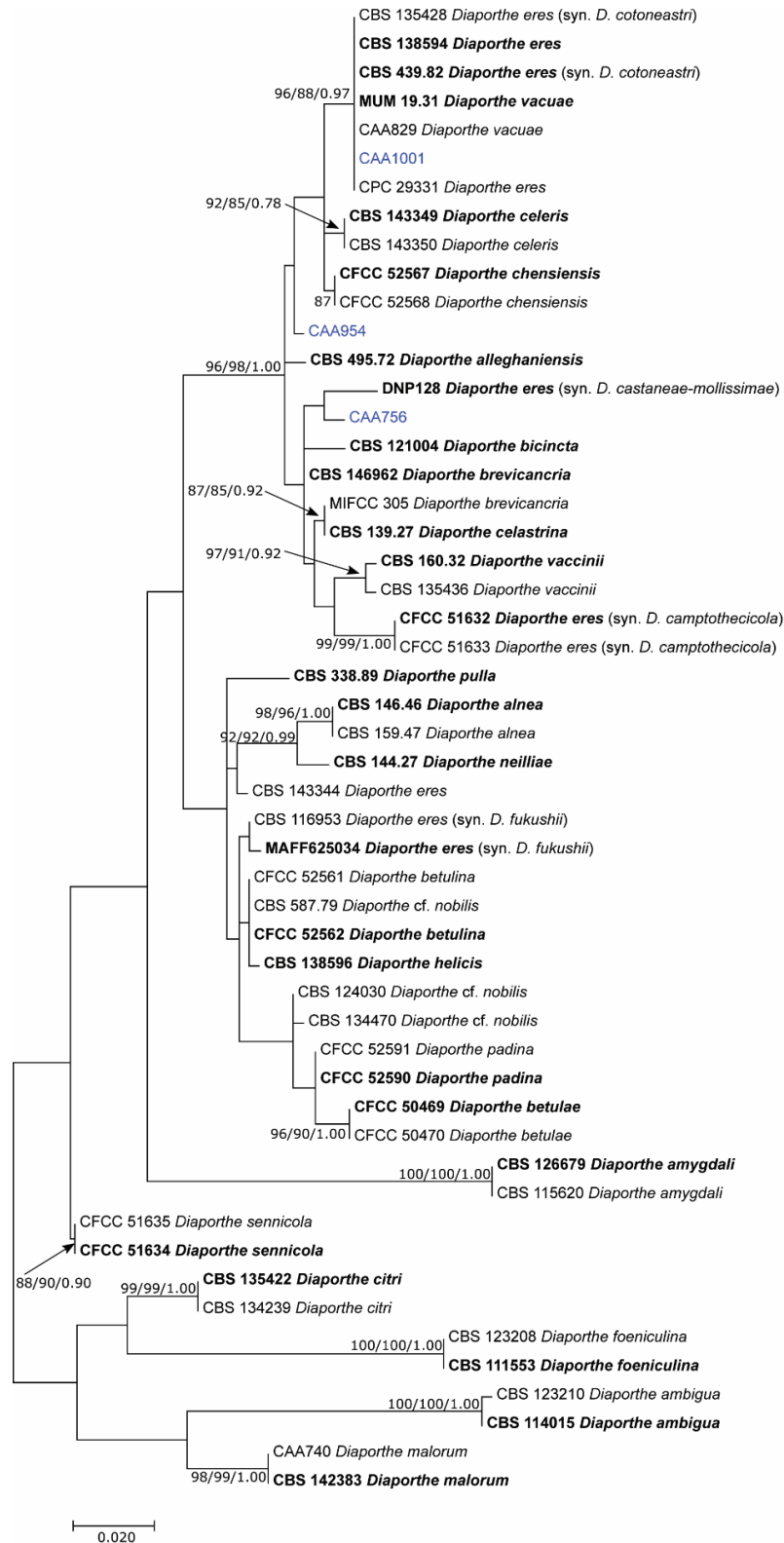


Figure S6. Maximum Likelihood tree based on ITS sequence data for the *Diaporthe eres* species complex and related species. The ML tree was constructed based on the Kimura 2-paramter model assuming a gamma distribution and invariant sites. ML and MP bootstrap values greater than 70% and posterior probabilities (PPs) greater than 0.70 are shown at the nodes. The ex-type strains are in bold. The isolates from this study are indicated in blue.

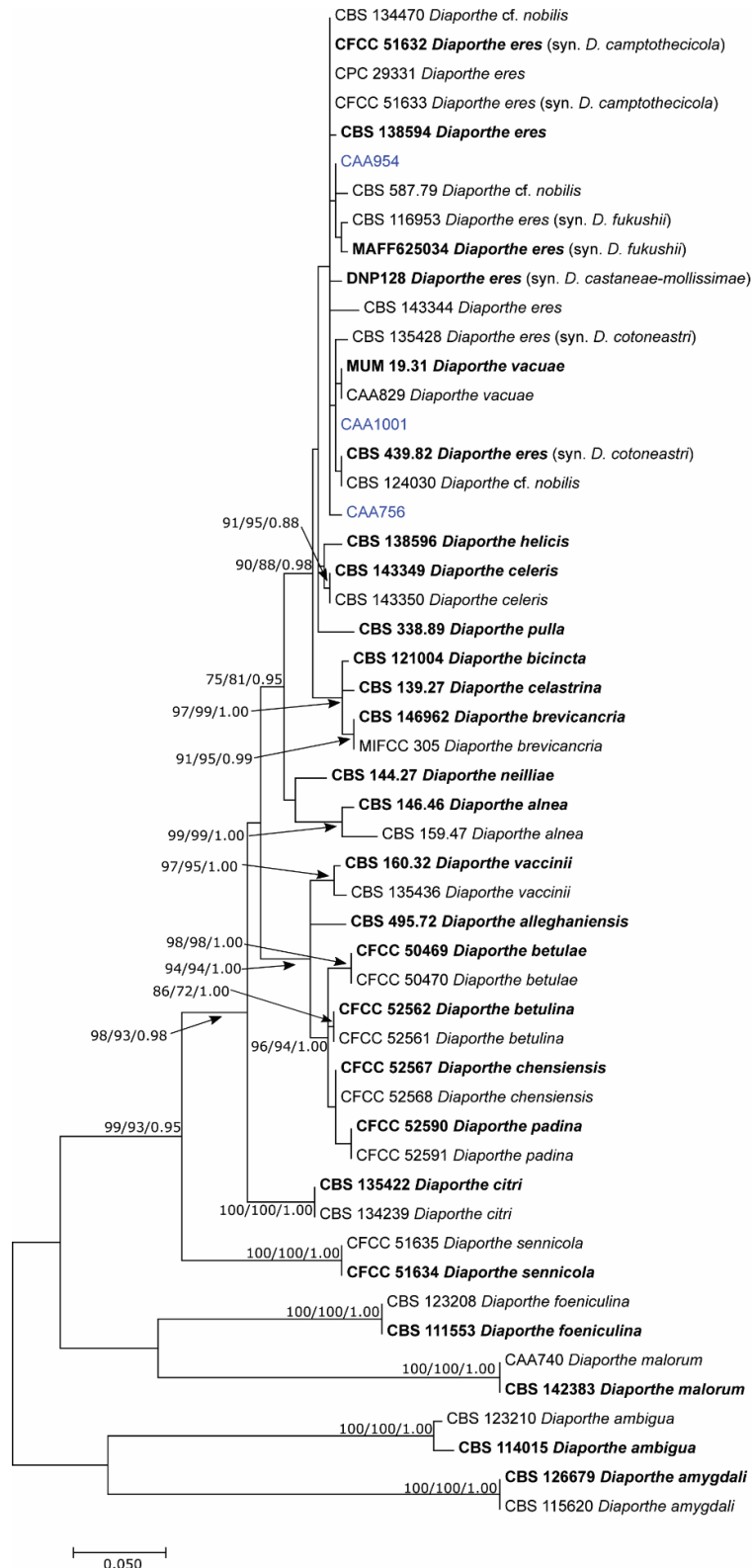
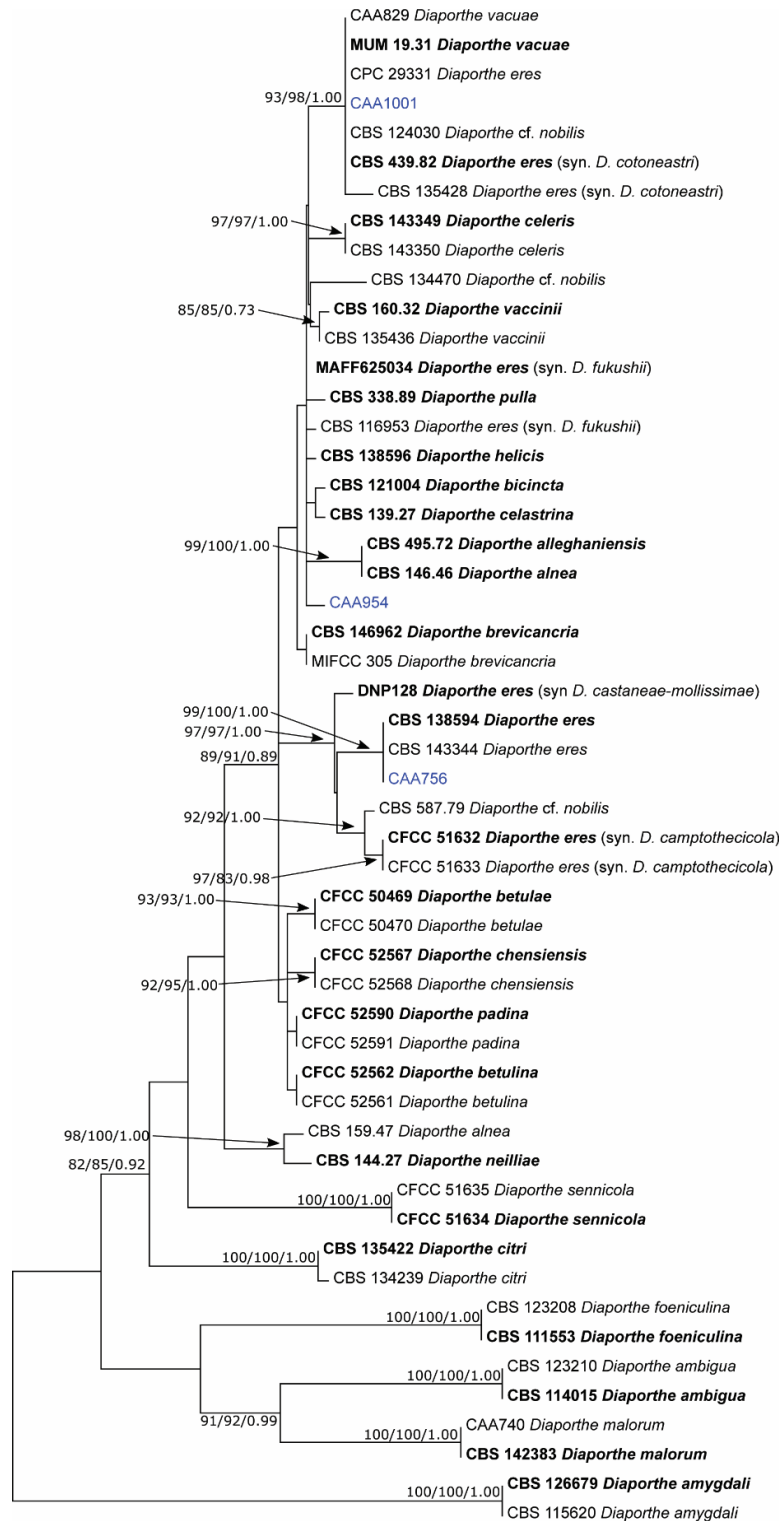


Figure S7. Maximum Likelihood tree based on *tef1-α* sequence data for the *Diaporthe eres* species complex and related species. The ML tree was constructed based on the Hasegawa-Kishino-Yano model assuming uniform rates. ML and MP bootstrap values greater than 70% and posterior probabilities (PPs) greater than 0.70 are shown at the nodes. The ex-type strains are in bold. The isolates from this study are indicated in blue.



0.020

Figure S8. Maximum Likelihood tree based on *tub2* sequence data for the *Diaporthe eres* species complex and related species. The ML tree was constructed based on the Kimura 2-parameter model assuming a gamma distribution and invariant sites. ML and MP bootstrap values greater than 70% and posterior probabilities (PPs) greater than 0.70 are shown at the nodes. The ex-type strains are in bold. The isolates from this study are indicated in blue.

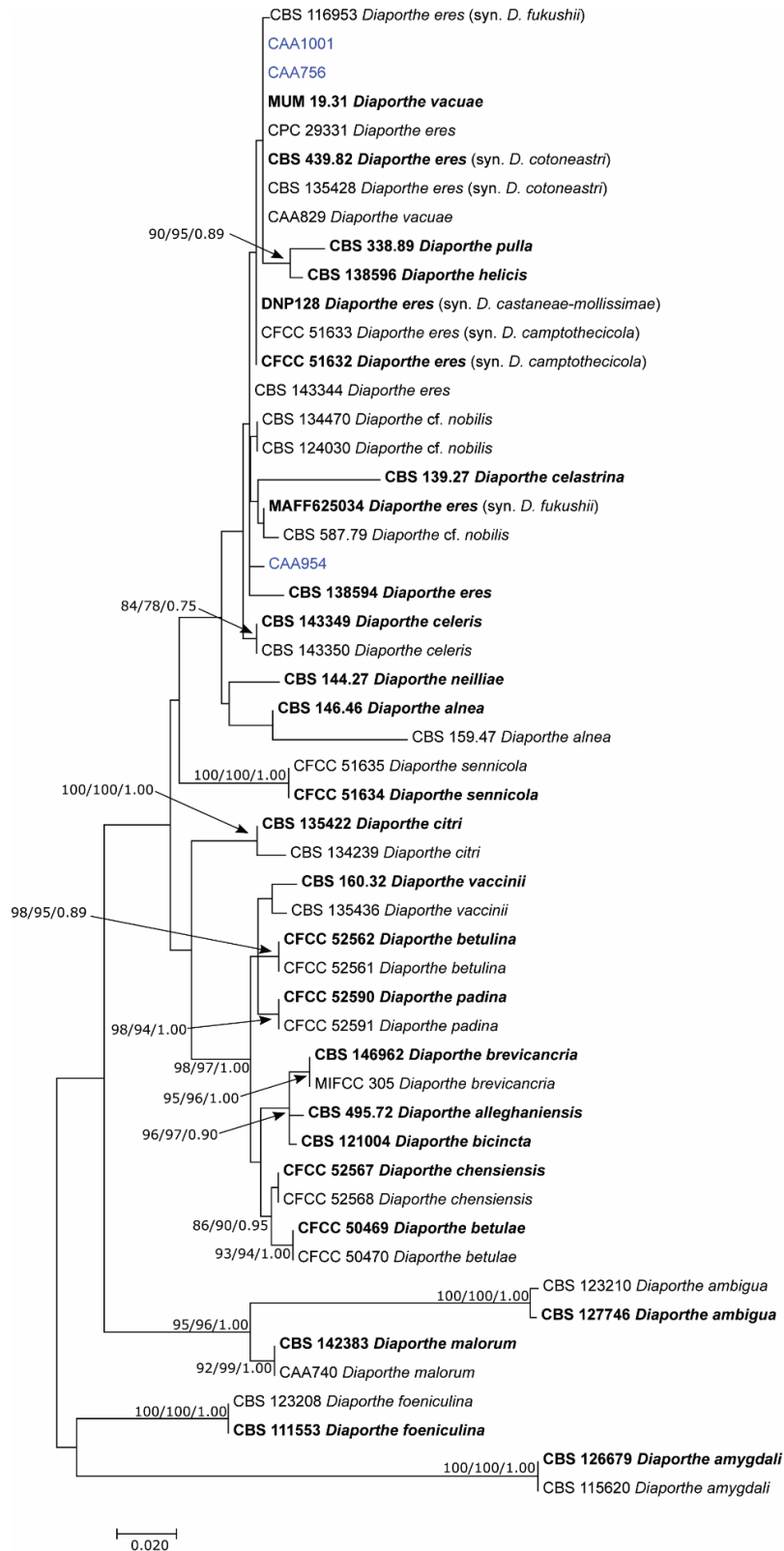


Figure S9. Maximum Likelihood tree based on *his3* sequence data for the *Diaporthe eres* species complex and related species. The ML tree was constructed based on the Hasegawa-Kishino-Yano model assuming a gamma distribution and invariant sites. ML and MP bootstrap values greater than 70% and posterior probabilities (PPs) greater than 0.70 are shown at the nodes. The ex-type strains are in bold. The isolates from this study are indicated in blue.

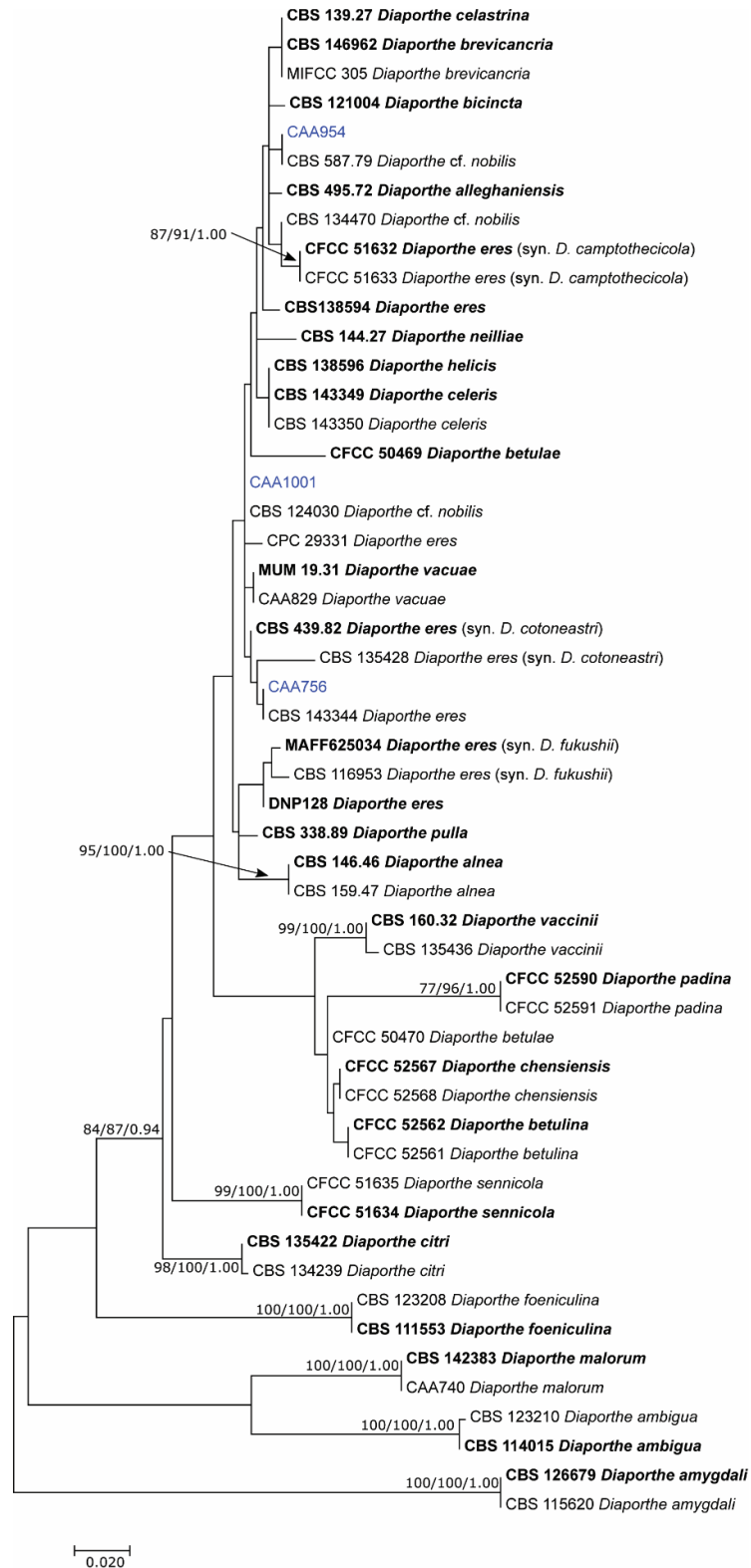


Figure S10. Maximum Likelihood tree based on *cal* sequence data for the *Diaporthe eres* species complex and related species. The ML tree was constructed based on the Tamura 3-parameter model assuming a gamma distribution and invariant sites. ML and MP bootstrap values greater than 70% and posterior probabilities (PPs) greater than 0.70 are shown at the nodes. The ex-type strains are in bold. The isolates from this study are indicated in blue.

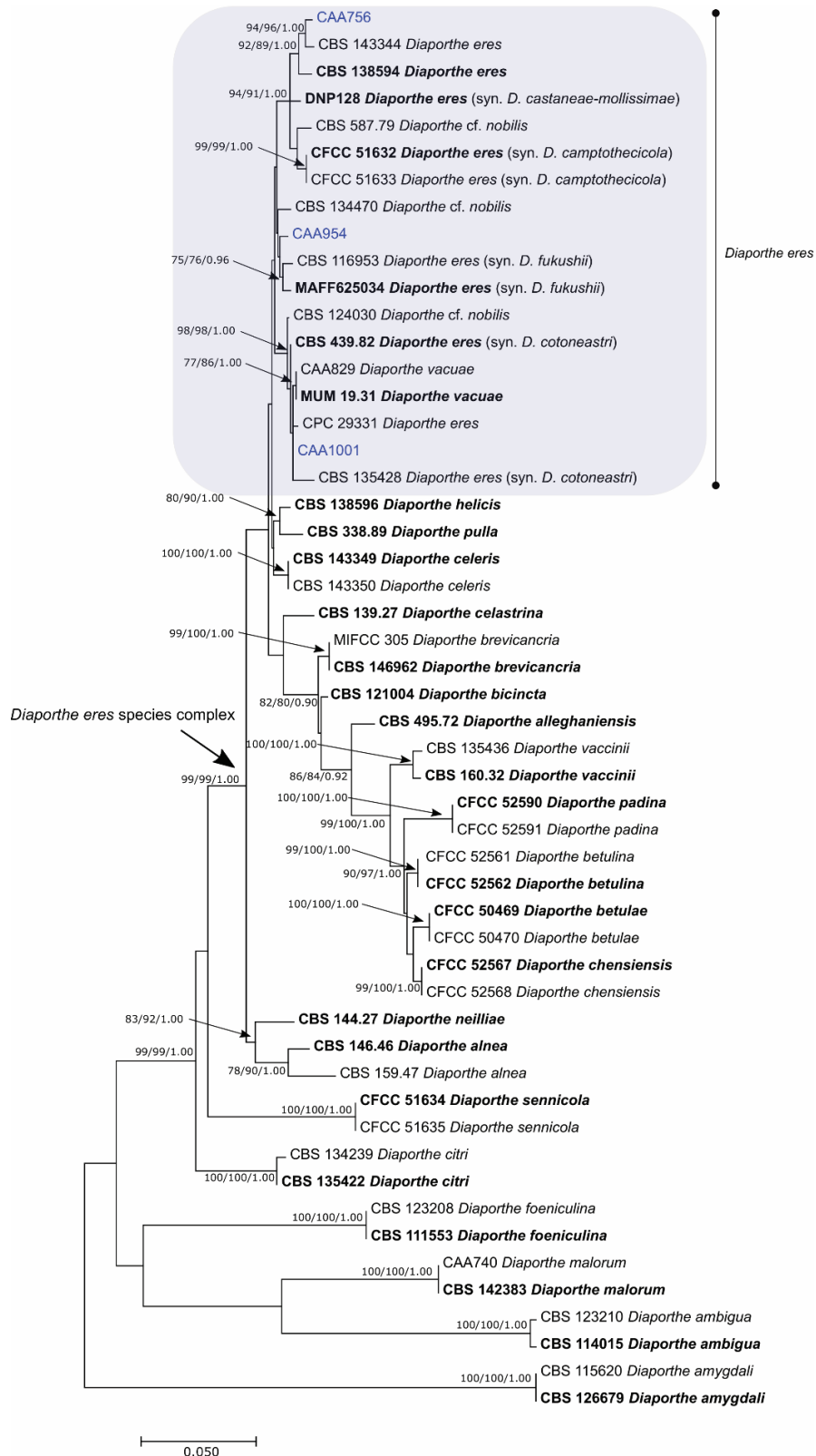


Figure S11. Maximum Likelihood tree based on *tef-α*, *tub2*, *his3* and *cal* sequence data for the *Diaporthe eres* species complex and related species. The ML tree was constructed based on the Kimura 2-paramter model assuming a gamma distribution and invariant sites. ML and MP bootstrap values greater than 70% and posterior probabilities (PPs) greater than 0.70 are shown at the nodes. The ex-type strains are in bold. The isolates from this study are indicated in blue.

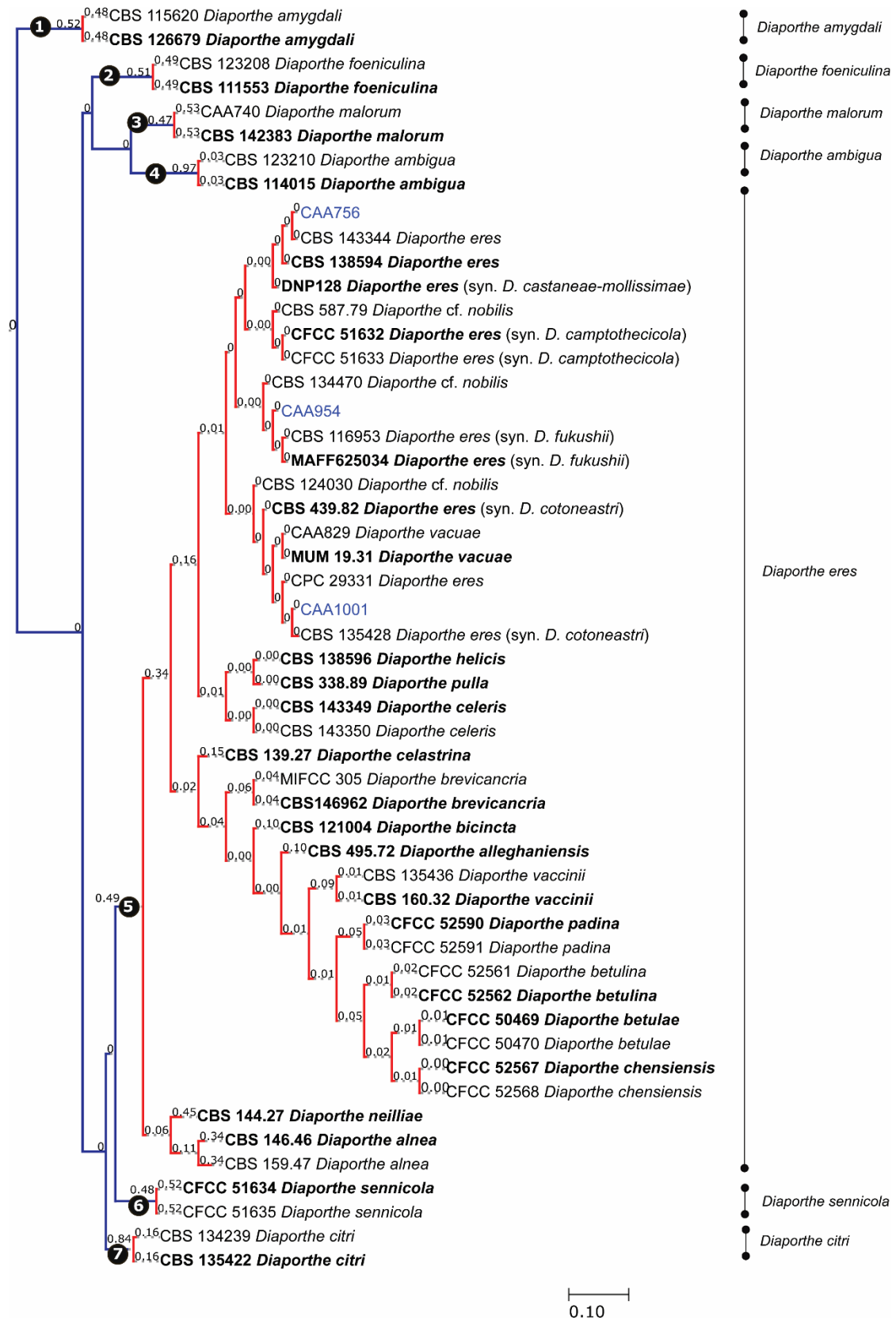


Figure S12. Results of the single PTP analyses for the *Diaporthe eres* species complex and related taxa, based on *tef1- α* , *tub2*, *his3* and *cal* loci on Bayesian and Maximum Likelihood topologies. Putative species clusters are indicating using transitions between blue-colored to red-colored branches and represented by circles (1-7). The isolates obtained in this study are indicated in blue.



CHAPTER 4

Case studies towards an intraspecific and
intragenomic variation in the Internal Transcribed
Spacer region

Caveats of the Internal Transcribed Spacer region as a barcode to resolve species boundaries in *Diaporthe*

Hilário S, Santos L, Phillips AJL, Alves A.

Fungal Biology **2022** 126, 54-74

ABSTRACT

Species in *Diaporthe* are largely reported as important plant pathogens. Identification of species in this genus has been complemented by morphological and molecular features. However, one important factor delaying this process is the struggle to formulate robust species concepts to create adequate international phytosanitary measures. Regardless of the wide use of the internal transcribed spacer (ITS) rRNA region, established as the primary DNA barcode for fungi, the tendency for intraspecific variation has been reported, misleading interpretation of phylogenetic analyses. Therefore, the present study aimed to illustrate, using specific examples, how the ITS region may be problematic for species delimitation. We showed that the ITS region is highly variable, with strains of *D. malorum* and *D. novem* falling into more than one clade, which if analyzed on their own, would be likely recognized as distinct taxa. Divergent ITS paralogs were also proven to coexist within the genome of *D. novem*. We also suggest that ITS may have escaped from concerted evolution or has undergone a duplication event. Furthermore, this study reports for the first time the existence of a putative hybrid in the genus *Diaporthe*. Our findings offer new clues towards the intraspecific and intragenomic variation in the ITS region, raising questions about its value for barcoding, *i.e.*, identifying species in the genus *Diaporthe*. Therefore, we recommend that the ITS region be analyzed cautiously and always compared for congruence prior to description of novel taxa.

keywords: DNA barcode; Hybridization; ITS polymorphisms; *Phomopsis*; Phylogeny

INTRODUCTION

Diaporthe (syn. *Phomopsis*) represents a cosmopolitan group of fungi with diverse ecological behaviors, including saprotrophs, endophytes, and plant pathogens some causing significant diseases on a wide range of economically important crops (e.g., grapevines, citrus, soybean, sunflower, blueberries) (Dissanayake & Phillips 2017; Gao et al. 2017; Guarnaccia et al. 2018; Lombard et al. 2014; Murali et al. 2006). Moreover, this genus is also regarded as a potential source of secondary metabolites that can be used in a variety of applications (Xu et al. 2021; Yan et al. 2018).

The species concept traditionally applied in *Diaporthe* was the morphological species concept in which several characters of both sexual and asexual morphs (e.g., size and shape of ascomata and conidiomata, conidiophore size, septation and branching, size and shape of ascospores and conidia) defined taxa (Rehner & Uecker 1994; Udayanga et al. 2011). In the past, association with a specific host was considered a reliable trait for species recognition (Uecker 1988) which led to an explosion of species names. A search of MycoBank (www.mycobank.org; accessed on 20 October 2020) and Index Fungorum (www.speciesfungorum.org; accessed on 20 October 2020) revealed more than 1000 epithets for *Diaporthe* and over 900 for *Phomopsis*. However, several studies have confirmed that the same *Diaporthe* species can be found on different hosts and co-occur on the same host adopting a different ecological behavior (e.g., endophytic and pathogenic) (Guarnaccia & Crous 2018; Hilário et al. 2020; Torres et al. 2016). Moreover, morphological characters within this genus are known to exhibit extensive plasticity (Mostert et al. 2001). Thus, identification of species based solely on host association and morphology is no longer acceptable in *Diaporthe* and many of the published names based on such characters are thought to be synonyms (Fan et al. 2018; Gao et al. 2017).

With the introduction of DNA sequence analysis and multiple gene genealogies, the Phylogenetic Species Concept has been widely applied (Steenkamp et al. 2018; Taylor et al. 2000) in the description of novel taxa and has unveiled cryptic species in *Diaporthe* (Udayanga et al. 2014a). The most recent taxonomic studies in this genus have relied mostly on the analysis of five loci: ITS rRNA (internal transcribed spacer region of the nuclear ribosomal DNA) and the

protein coding genes *tef1- α* (translation elongation factor 1-alpha), *tub2* (β -tubulin), *his3* (histone 3) and *cal* (calmodulin) (Gomes et al. 2013; Santos et al. 2017a), which provide a robust approach to resolve *Diaporthe* species (Guarnaccia & Crous 2018).

Notwithstanding the recognized role of ITS in fungal identification and classification (Schoch et al. 2012; Vu et al. 2019), its utility for species delimitation has been disputed and the recognized pitfalls somehow neglected by some authors (Gazis et al. 2011). While a recent study has demonstrated that the ITS sequences deposited in the National Center for Biotechnology Information may harbor technical errors or atypical chimeric sequences (Baturó-Cieřniewska et al. 2020), some studies in the past have shown an intragenomic heterogeneity of rRNA in several genera (Hibbett et al. 2011), thus limiting the utility of ITS. It was first reported by O'Donnell & Cigelnik (1997) in the important plant pathogen *Fusarium* and since then, polymorphisms in the rRNA region have been found in other filamentous fungi (e.g., *Ceratocystis*) (Harrington et al. 2014), yeasts (e.g., *Candida*) (Zhao et al. 2015) and in mushrooms (e.g., *Amanita*) (Hughes et al. 2018). Further studies have also documented sequence divergence within a genome by up to 15% (Hughes et al. 2018; Li et al. 2013), which undoubtedly have implications on phylogenetic reconstruction, thus raising questions about the use of ITS to delineate species. ITS intraspecific variability within individuals of some genera including *Diaporthe* are seldom documented (Santos et al. 2010; Udayanga et al. 2014a), not thoroughly explored and overlooked, as many authors still use the ITS as the sole locus to define species boundaries in *Diaporthe* (Dayarathne et al. 2020; Li et al. 2020). For this reason, taxonomic studies in this genus remain an everlasting challenge, due to a copious number of species being described each year (Gao et al. 2017).

During an extensive survey of the diversity of *Diaporthe* species associated with a range of host plants in Portugal, a large collection of isolates was obtained. In the process of identifying some of these isolates we came across a set of challenges posed by the ITS region. Therefore, with this study we aimed to: (1) illustrate the existence of intraspecific and intragenomic variation in the ITS region within and between individuals, providing case studies; (2) describe the existence of possible hybridization between species; (3) propose guidelines for a more rational outline on how to delimit species and establish novel taxa in the genus *Diaporthe*.

MATERIAL AND METHODS

Fungal isolation.

Between 2007 and 2019, a survey was conducted to determine the presence of *Diaporthe* species associated with diverse hosts including weeds (*Foeniculum vulgare*), ornamental trees (*Magnolia soulangeana*), fruit crops (*Vaccinium corymbosum*) and forest trees (*Eucalyptus globulus*) in Portugal. Branch and twig portions showing dieback and blight symptoms typical of *Diaporthe*, were collected from several regions in Portugal: Porto (Felgueiras, Penafiel, Santo Tirso), Braga (Póvoa de Lanhoso, Urgezes), Viana do Castelo (Ponte da Barca), Aveiro (Arouca, Gafanha da Nazaré) and Santarém (Ourém).

Isolations were made from single ascospores, conidia or by directly plating out pieces of plant and wood tissues (2-5mm) on potato dextrose agar plates, following the procedures in subchapter 2.1.

DNA extraction and PCR amplification.

Genomic DNA extraction, microsatellite-primed PCR (MSP-PCR) fingerprinting and amplification of ITS and the protein coding regions *tef1-a*, *tub2*, *his3* and *cal*, were as described in subchapter 2.1.

Mating type assays.

To diagnose the mating strategy of *Diaporthe* isolates used in this study, a PCR-based method was performed to amplify the *MAT1-1-1* and *MAT1-2-1* genes, following the descriptions in subchapter 2.1.

Phylogenetic analyses.

The nucleotide sequences were analyzed, and the phylogenetic trees were constructed based on Maximum Parsimony (MP), Maximum Likelihood (ML) and Bayesian Inference (BI) analyses, as described in subchapter 2.1. For the MP analyses, the following parameters were also calculated: consistency index (CI), retention index (RI), tree length (TL), rescaled consistency index (RC) and homoplasy index (HI).

A preliminary identification of the critical clades containing our isolates was assessed through an initial ITS tree containing all species accepted in the genus *Diaporthe*. We also evaluated the possibility of combining all five (ITS, *tef1- α* , *tub2*, *his3*, and *cal*) and four (*tef1- α* , *tub2*, *his3*, and *cal*) loci. A comparison of highly supported clades (bootstrap values $\geq 70\%$ and Bayesian posterior probabilities ≥ 0.95) among single locus trees was performed to look for incongruencies between individual phylogenies (Alves et al. 2008). All the trees presented here were graphically processed in Inkscape Vector software v.0.92 (<https://www.inkscape.org>) (Adobe Systems Inc, San Jose, CA, USA). Sequences generated in this study were deposited in GenBank (www.ncbi.nlm.nih.gov) (Table 1) and phylogenetic trees and alignments were deposited in TreeBASE (www.TreeBASE.org; study number S27489).

Mating experiments.

Isolates with opposite mating-types were selected to perform *in vitro* mating experiments following the method described by Brayford (1990) with slight modifications. A 5-mm-diameter mycelial plug of each isolate was inoculated on 2% WA and $\frac{1}{4}$ PDA plates, containing small fragments of autoclaved wild fennel twigs and pine needles, and incubated at room temperature under diffuse daylight for approximately 3 months. Matings were considered successful when perithecia containing ascospores were formed.

To determine the viability of ascospores, these were carefully taken from the perithecia with a sterile scalpel, placed in a drop of sterile water with the support of a Nikon stereomicroscope SMZ1500 (Nikon, Tokyo, Japan), spread over $\frac{1}{4}$ PDA plates and incubated overnight for 24 hours. After this period, at least eight single germinating ascospores were transferred to fresh PDA plates and stored at 25 °C in the dark. ITS sequences of the progenies (F1) from successful crossings were then sequenced and analyzed.

Table 1. *Diaporthe* isolates from *Magnolia soulangeana*, *Vaccinium corymbosum*, *Foeniculum vulgare* and *Eucalyptus globulus* used in this study.

Species	Strain ¹	Host	Strain source ²	Location	GenBank Accession					Mating-type	
					ITS	<i>tef1-α</i>	<i>tub2</i>	<i>his3</i>	<i>cal</i>	MAT1-1-1	MAT1-2-1
<i>D. malorum</i>	CAA375	<i>M. soulangeana</i>	SC	Felgueiras	MT073269	MT051938	MT051987	MT051913	MT051877	(-)	(+)
	CAA378	<i>M. soulangeana</i>	SC	Felgueiras	MT073270	MT051939	MT051988	MT051914	MT051878	(-)	(+)
	CAA972	<i>V. corymbosum</i>	SC	Arouca	MT073271	MT051917	MT051953	MT051881	MT051845	(-)	(+)
	CAA973	<i>V. corymbosum</i>	SC	Arouca	MT073272	MT051918	MT051954	MT051882	MT051846	(-)	(+)
	CAA974	<i>V. corymbosum</i>	SC	Póvoa de Lanhoso	MT073306	MT051919	MT051963	MT051891	MT051855	(+)	(-)
	CAA975	<i>V. corymbosum</i>	SC	Urgezes	MT073304	MT051920	MT051966	MT051894	MT051858	(+)	(-)
	CAA976	<i>V. corymbosum</i>	SC	Urgezes	MT073305	MT051921	MT051967	MT051895	MT051859	(+)	(-)
	CAA977	<i>V. corymbosum</i>	SC	Santo Tirso	MT073303	MT051922	MT051971	MT051899	MT051863	(+)	(-)
	CAA951	<i>E. globulus</i>	SC	Penafiel	MN190306	MT309428	MT309454	MT309437	MT309445	(+)	(-)
	CAA953	<i>E. globulus</i>	SC	Ponte da Barca	MN190308	MT309430	MT309456	MT309439	MT309447	(+)	(-)
<i>D. novem</i>	CAA149	<i>F. vulgare</i>	SA	Aveiro	MT073315	MT051940	MT051974	MT051902	MT051866	(-)	(+)
	CAA159	<i>F. vulgare</i>	SA	Aveiro	MT073320	MT051941	MT051975	MT051903	MT051867	(-)	(+)
	CAA160	<i>F. vulgare</i>	SA	Aveiro	MT073321	MT051942	MT051976	MT051904	MT051868	(-)	(+)
	CAA162	<i>F. vulgare</i>	SA	Aveiro	MT073323	MT051943	MT051977	MT051905	MT051869	(+)	(-)
	CAA164	<i>F. vulgare</i>	SA	Aveiro	MT073325	MT051944	MT051978	MT051906	MT051870	(+)	(-)
	CAA165	<i>F. vulgare</i>	SA	Aveiro	MT073326	MT051945	MT051979	MT051907	MT051871	(+)	(-)
	CAA168	<i>F. vulgare</i>	SA	Aveiro	MT073329	MT051946	MT051980	MT051908	MT051872	(+)	(-)
	CAA262	<i>F. vulgare</i>	SA	Gafanha da Nazaré	MT073334	MT901027	MT901028	MT901026	MT901025	(-)	(+)
	CAA263	<i>F. vulgare</i>	SC	Gafanha da Nazaré	MT073335	MT051947	MT051981	MT051909	MT051873	(+)	(-)

	CAA264	<i>F. vulgare</i>	SC	Gafanha da Nazaré	<i>MT073336</i>	<i>MT051948</i>	<i>MT051982</i>	<i>MT051910</i>	<i>MT051874</i>	(+)	(-)
	CAA293	<i>F. vulgare</i>	SA	Aveiro	<i>MT073341</i>	<i>MT051950</i>	<i>MT051984</i>	<i>MT051911</i>	<i>MT051876</i>	(+)	(-)
	CAA295	<i>F. vulgare</i>	SA	Aveiro	<i>MT073342</i>	<i>MT051950</i>	<i>MT051984</i>	<i>MT051912</i>	<i>MT051876</i>	(-)	(+)
	CAA300 clone1				<i>MT221241</i>						
	CAA300 clone2				<i>MT221237</i>						
	CAA300 clone3	<i>F. vulgare</i>	SA	Aveiro	<i>MT221240</i>	<i>MT051952</i>	<i>MT051986</i>	<i>MT051916</i>	<i>MT051880</i>	(+)	(-)
	CAA300 clone4				<i>MT221238</i>						
	CAA300 clone5				<i>MT221239</i>						
<i>Diaporthe xepithet</i>	CAA998	<i>V. corymbosum</i>	SC	Ourém	<i>MT073276</i>	<i>MT051927</i>	<i>MT051958</i>	<i>MT051886</i>	<i>MT051850</i>	(+)	(-)
	CAA999	<i>V. corymbosum</i>	SC	Ourém	<i>MT073280</i>	<i>MT051929</i>	<i>MT051960</i>	<i>MT051888</i>	<i>MT051852</i>	(+)	(-)

¹Acronym of collection: **CAA** – Personal culture Collection Artur Alves, Universidade de Aveiro, Portugal; ²**SA** – strains isolated from single ascospore; **SC** – strains isolated from single conidia. GenBank accession numbers generated in this study are in italics.

Morphology and culture characteristics.

After asexual morph sporulation and *in vitro* mating experiments, both conidiomata and ascomata were crushed in a drop of sterile water on a microscope slide, the water allowed to evaporate and replaced with 100% lactic acid. Micromorphological characters and measurements were performed following the description in subchapters 2.1 and 2.2.

Population genetic diversity and haplotype network analysis.

Among the identified species, only *Diaporthe novem* and *D. malorum* showed intraspecific variability. For both species, diversity indices were calculated for each gene region and the combined sequence dataset to understand genetic diversity. DnaSP v.6.12 (Barcelona, Spain) (Librado & Rozas 2009) was used to calculate the following parameters: number of haplotypes, pairwise nucleotide diversity (π), haplotype diversity (hd) and the number of polymorphic sites (S). To understand the potential departure from an equilibrium model of evolution, Tajima's D statistical test (Tajima 1989) was calculated with a permutation test of 1000 replicates. Moreover, to measure the amount of genetic variation among populations in the ITS region, the fixation index (F_{ST}) (Wright 1951) was also calculated.

To infer the analysis of population genetic data at the intraspecific level, *Diaporthe malorum* and *D. novem* haplotype networks were constructed using POPART (Leigh & Bryant 2015) under the median-joining network method for the ITS region. Statistically significant splits were obtained at a 95% confidence level. Networks were manually edited in Inkscape Vector software v.0.92 (<https://www.inkscape.org>).

RESULTS

Fungal isolation.

During the survey, several plants and trees from nine localities in Portugal, were inspected for symptoms such as dieback, twig and branch blight: *Magnolia soulangeana* ($n = 2$), *E. globulus* ($n = 2$), *F. vulgare* ($n = 8$) and *V. corymbosum* ($n = 5$), leading to a collection of 17 diseased twigs and branches. From these samples, an assemblage of 82 isolates with micromorphological and culture characteristics

typical of *Diaporthe*, were obtained. All isolates were induced to sporulate and within 4–6 weeks produced pycnidia oozing white and translucent yellow conidial cirrhi on both pine needles and fennel stems. After three months, the mating assays resulted in the formation of perithecia with long necks at the intersection zone between the two fungal isolates, and exuding white translucent spores mass.

Phylogenetic analyses.

MSP-PCR fingerprinting was performed to assess genetic diversity within the collection of isolates from the different hosts. A total of 25 isolates representative of each cluster, and when possible, from different geographic regions, were selected for further molecular characterization. A primary identification using the ITS rRNA region was done using BLASTn assigning the isolates to the genus *Diaporthe*. These isolates were further characterized based on a multilocus analysis, including the ITS and the protein coding genes *tef1- α* , *tub2*, *his3* and *cal*. The sequences newly generated in this study were deposited in GenBank (Table 1).

Sequences of the five genes were aligned and analyzed separately. Phylogenetic trees obtained from maximum likelihood, maximum parsimony and Bayesian analyses were compared for the placement of each isolate, topology and clade stability. Relationships among the highly supported clades from the three analyses were topologically similar. Therefore, ML single locus trees are shown with bootstraps and posterior probabilities (ML/MP/PP) given for those well-supported branches and represented in Fig. 1 (ITS) and Figs. S1-S4 (*tef1-a*, *tub2*, *his3* and *cal*). Furthermore, a combined alignment of all four loci excluding ITS (Fig. S5), and a combined alignment of the five (Fig. 2) were also performed, including those *Diaporthe* species phylogenetically closely related to our isolates (Table 2).

All the analyses included an outgroup (*Diaporthella corylina* CBS 121124) and 56 ingroup taxa (25 sequences obtained in this study and 31 *Diaporthe* sequences from GenBank). The ITS, *tef1-a*, *tub2*, *his3* and *cal* individual dataset consisted of 2617 characters (587 for ITS, 450 for *tef1-a*, 508 for *tub2*, 531 for *his3* and 541 for *cal*). The 4-locus combined alignment comprised 2030 characters. All individual and combined datasets included alignment gaps and indel coding. Alignment properties, and nucleotide substitution models are provided in Table 3.

Table 2. *Diaporthe* species used in the phylogenetic analyses. Ex-type isolates are highlighted in bold.

Species	Strain ¹	Host	Location	GenBank Accession				
				ITS	<i>tef1-α</i>	<i>tub2</i>	<i>cal</i>	<i>his3</i>
<i>D. alangii</i>	CFCC 52556	<i>Alangium kurzii</i>	China	MH121491	MH121533	MH121573	MH121415	MH121451
<i>D. anacardii</i>	CBS 720.97	<i>Anacardium occidentale</i>	East Africa	KC343024	KC343750	KC343992	KC343266	KC343508
<i>D. angelicae</i>	CBS 111592	<i>Heracleum sphondylium</i>	Austria	KC343027	KC343753	KC343995	KC343269	KC343511
<i>D. arctii</i>	CBS 139280	<i>Arctium lappa</i>	Germany	KJ590736	KJ590776	KJ610891	KJ612133	KJ659218
<i>D. baccae</i>	CBS 136972	<i>Vaccinium corymbosum</i>	Italy	KJ160565	KJ160597	MF418509	MG281695	MF418264
<i>D. chamaeropsis</i>	CBS 454.81	<i>Chamaerops humilis</i>	Greece	KC343048	KC343774	KC344016	KC343290	KC343532
<i>D. cuppatea</i>	CBS 117499	<i>Aspalathus linearis</i>	South Africa	KC343057	KC343783	KC344025	KC343299	KC343541
<i>D. foeniculina</i>	CBS 111553	<i>Foeniculum vulgare</i>	Spain	KC343101	KC343827	KC344069	KC343343	KC343585
<i>D. inconspicua</i>	CBS 133813	<i>Maytenus ilicifolia</i>	Brazil	KC343123	KC343849	KC344091	KC343365	KC343607
<i>D. lusitanicae</i>	CBS 123213	<i>Foeniculum vulgare</i>	Portugal	KC343137	KC343863	KC344105	KC343379	KC343621
	CBS 123212	<i>Foeniculum vulgare</i>	Portugal	KC343136	KC343862	KC344104	KC343378	KC343620
<i>D. malorum</i>	CBS 142383	<i>Malus domestica</i>	Portugal	KY435638	KY435627	KY435668	KY435658	KY435648
	CAA740	<i>Malus domestica</i>	Portugal	KY435642	KY435629	KY435670	KY435660	KY435650
	CAA752	<i>Malus domestica</i>	Portugal	KY435643	KY435630	KY435671	KY435661	KY435651
<i>D. neoarctii</i>	CBS 109490	<i>Ambrosia trifida</i>	USA	KC343145	KC343871	KC344113	KC343387	KC343629
<i>D. novem</i>	CBS 127270	<i>Glycine max</i>	Croatia	KC343156	KC343882	KC344124	KC343398	KC343640
	CBS 127271	<i>Glycine max</i>	Croatia	KC343157	KC343883	KC344125	KC343399	KC343641
	CPC 28169	<i>Citrus aurantiifolia</i>	Italy	MF418429	MF418508	MF418589	MF418263	MF418349
	CPC 28167	<i>Citrus aurantiifolia</i>	Italy	MF418428	MF418507	MF418588	MF418262	MF418348
	CPC 28165	<i>Citrus aurantiifolia</i>	Italy	MF418427	MF418506	MF418587	MF418261	MF418347
	CPC 26188	<i>Citrus japonica</i>	Italy	MF418426	MF418505	MF418586	MF418260	MF418346
	CBS 127269	<i>Glycine max</i>	Croatia	KC343155	KC343881	KC344123	KC343397	KC343639
	CBS 354.71	<i>Polygonatum odoratum</i>	Romania	KC343158	KC343884	KC344126	KC343400	KC343642
	<i>D. passiflorae</i>	CBS 132527	<i>Passiflora edulis</i>	South America	JX069860	KY435633	KY435674	KY435664
<i>D. phaseolorum</i>	CBS 139281	<i>Phaseolus vulgaris</i>	USA	KJ590738	KJ590739	KJ610893	KJ612135	KJ659220
<i>D. phillipsii</i>	MUM 19.28	<i>Vaccinium corymbosum</i>	Portugal	MK792305	MK828076	MN000351	MK871445	MK883831
	CAA818	<i>Vaccinium corymbosum</i>	Portugal	MK792307	MK828078	MN000352	MK871447	MK883833
<i>D. portugallica</i>	CBS 144228	<i>Camelia sinensis</i>	Portugal	MH063905	MH063911	MH063917	MH063893	MH063899
	CPC 34248	<i>Camelia sinensis</i>	Portugal	MH063906	MH063912	MH063918	MH063894	MH063900

<i>D. subordinaria</i>	CBS 101711	<i>Plantago lanceolata</i>	New Zealand	KC343213	KC343939	KC344181	KC343455	KC343697
	CBS 464.90	<i>Plantago lanceolata</i>	South Africa	KC343214	KC343940	KC344182	KC343456	KC343698
<i>Diaporthella corylina</i>	CBS 121124	<i>Corylus</i> sp.	China	KC343004	KC343730	KC343972	KC343246	KC343488

¹Acronyms of culture collections: **CAA** – Personal culture Collection Artur Alves, Universidade de Aveiro, Portugal; **CBS** – Westerdijk Fungal Biodiversity Institute, Utrecht, the Netherlands; **CFCC** – China Forestry Culture Collection Center; **CPC** – Personal culture Collection Pedro W. Crous, hosted at CBS; **MUM** – Fungal culture Collection from Micoteca da Universidade do Minho, Portugal.

Table 3. Alignment properties from individual and combined phylograms

Parsimony characters summary	ITS	<i>tef1-α</i>	<i>tub2</i>	<i>his3</i>	<i>cal</i>	4 loci	5 loci
Total characters	587	450	508	531	541	2030	2617
Invariable characters	423	187	305	371	292	1155	1578
Informative characters	103 (18%)	175 (39%)	116 (23%)	107 (20%)	165 (31%)	563 (28%)	666 (25%)
Uninformative characters	61	88	87	53	84	312	373
Tree length (TL)	327	516	349	302	446	1654	2024
Consistency index (CI)	0.6453	0.7481	0.7536	0.7020	0.7578	0.7249	0.6966
Homoplasy index (HI)	0.3547	0.2519	0.2464	0.2980	0.2422	0.2751	0.3034
Retention index (RI)	0.9109	0.9346	0.9419	0.9197	0.9425	0.9330	0.9241
Rescaled consistency index (RC)	0.5878	0.7059	0.7098	0.6456	0.7143	0.6763	0.6438
Nucleotide substitution model ¹	K2+G+I	HKY+G	T92+G	TN93+G	T92+I	TN93+G	TN93+G

¹ K2 – Kimura parameter model; HKY– Hasegawa–Kishono–Yano model; T92 – Tamura 3-parameter model; TN93 – Tamura-Nei parameter model; G, I – models of evolution assuming a gamma distribution and invariant sites.

The ITS phylogeny was not clear to resolve the limits of *Diaporthe novem* and *D. malorum* isolates, given that these did not cluster together resulting in three and two monophyletic clades, respectively. Two sets of isolates from single ascospores (CAA159 to CAA168; CAA295 and CAA300) were collected from twigs of *F. vulgare* in different locations but each set derived from the same individual plant. The single ascospore-derived isolates had different ITS sequences and were placed in three different major groups in the ITS phylogram (Fig. 1, clades a, b, c). However, they were determined to be the same phylogenetic species, as all isolates fell within the clade containing *D. novem* in the individual *tef1- α* , *tub2*, *his3* and *cal* (Figs. S1-S4) phylograms, and in the 4-locus combined ML tree (Fig. S5).

In the case of *D. malorum*, isolates CAA975 and CAA976 were obtained from the same twig of *V. corymbosum*. However, based on the ITS phylogram, both isolates are deemed to represent two different taxa as they were placed on two different highly supported clades (Fig. 1 clades d, e). These clades also separate the isolates CAA951 and CAA953, from *E. globulus* as two distinct taxa. However, as opposed to the ITS tree, all other individual and 4-loci phylogenetic trees clearly assigned these isolates to the species *D. malorum*.

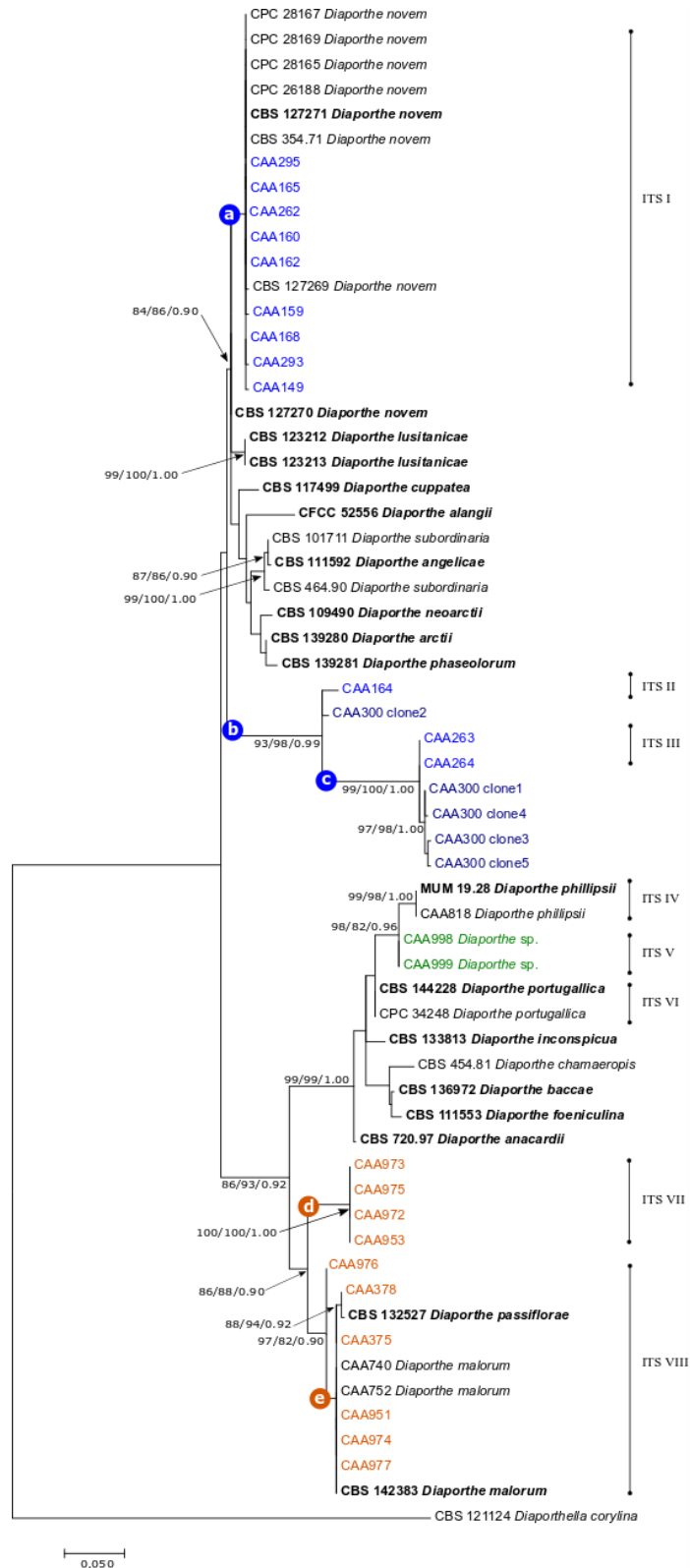


Figure 1. Maximum Likelihood phylogenetic tree obtained from ITS sequences data from *Diaporthe* species. The tree was built using the Kimura parameter model assuming invariant sites and a gamma distribution and rooted to *Diaporthella corylina*. ML/MP/PP bootstrap support and posterior probabilities values are given at the nodes. The values are shown only for those nodes that received support in at least two of the phylogenetic inference methods. Ex-type isolates are in bold.

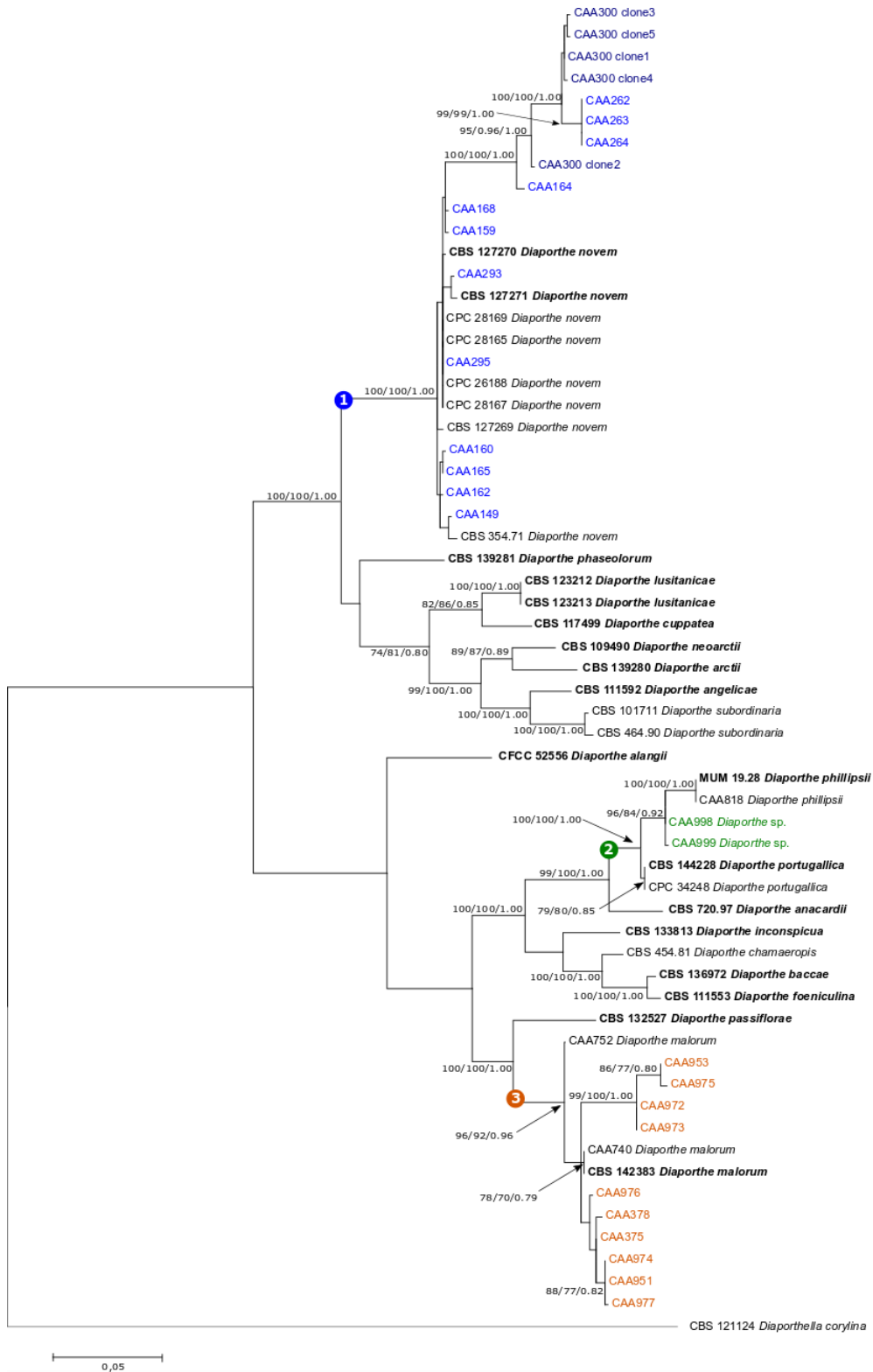


Figure 2. Maximum Likelihood phylogenetic tree obtained from ITS, *tef1- α* , *tub2*, *his3* and *cal* sequences data from *Diaporthe* species. The tree was built using the Tamura-Nei parameter model assuming a gamma distribution and rooted to *Diaporthella corylina*. ML/MP/PP bootstrap support and posterior probabilities values are given at the nodes. The values are shown only for those nodes that received support in at least two of the phylogenetic inference methods. Ex-type isolates are in bold.

The remaining isolates (CAA998 and CAA999) formed a separate clade in the 4-loci (ML/MP/PP = 78/96/0.90) and 5-loci (ML/MP/PP = 96/84/0.92) combined analyses, located between *D. portugallica* and *D. phillipsii*. The molecular identification of these isolates was uncertain given their position in the individual phylograms (Fig. 1 and Figs. S1-S4). A comparison of sequences of all five loci of CAA998 and CAA999 with those of *D. phillipsii* and *D. portugallica* showed that these strains share polymorphisms in *his3*, *cal* and ITS loci with the above-mentioned species, and no fixed polymorphisms were found. Besides, the *tef1-a* and *tub2* sequences of CAA998 and CAA999 were 100% identical with those of *D. portugallica* and *D. phillipsii*.

ITS rRNA cloning.

The fragment covering the rRNA ITS1-5.8S-ITS2 regions of isolate CAA300 was amplified by PCR. When we tried to determine the sequence of the purified PCR product by direct sequencing, we found that overlapping peaks appeared at certain positions in the sequencing chromatograms when either ITS1 or ITS4 were used as the sequencing primers (Fig. 3). To detect these polymorphisms, the ITS amplicon from isolate CAA300 was cloned and 17 clones containing target fragments were randomly selected and sequenced.

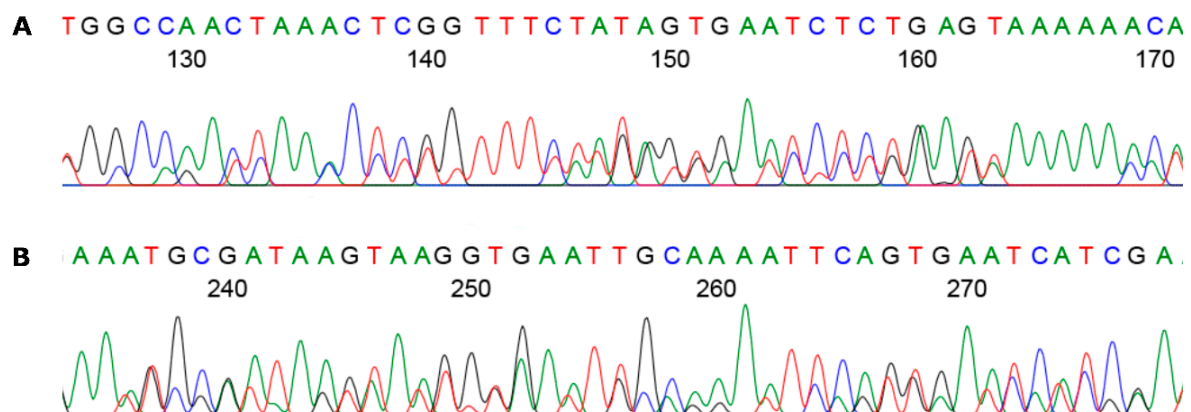


Figure 3. Sequencing chromatogram of PCR product of the rRNA ITS1-5.8S-ITS2 region of *Diaporthe novem* strain CAA300 using ITS1 (**A**) and ITS4 (**B**) as the sequencing primers, showing overlapped peaks.

Clear sequence chromatograms without overlapping peaks were obtained for every clone. In total, 5 different ITS copies were detected within the genome of CAA300, which are represented in Fig. 1. However, only one ITS copy was found to be quite different from the remaining 4 clones, with a divergence of 35 to 39 nucleotides.

Case Studies.

1. Intraspecific ITS variability.

The *Rosaceae* pathogen described in Portugal, *Diaporthe malorum* (Santos et al. 2017b), was introduced based on a unique ITS sequence, referred to in this study as ITS VIII (Fig. 1). Identical ITS sequence, was found in isolates of *D. malorum* from *M. soulangeana*, *E. globulus* and *V. corymbosum*. In addition, a second ITS sequence type (ITS VII) was found in isolates from *V. corymbosum* and *E. globulus*. Two other ITS variants (designated as ITS II and III, respectively) were found in isolates of *D. novem* from *F. vulgare* in Portugal.

The major observation in the ITS phylogram (Fig. 1), was the splitting of isolates of *D. malorum* CAA375 to CAA977 into two sub-clades (highlighted in orange in clades d, e). Moreover, the isolates of *D. novem* CAA149 to CAA295 fell into three distinct sub-clades (highlighted in blue in clades a, b, c, Fig. 1). Pairwise alignments showed that within each ITS group there were no nucleotide differences in the ITS region, 18 nucleotide differences (3.0%) exist between groups VII and VIII, 56 nucleotide differences (9.4%) between groups I and III, 33 (6.2%) differences between groups I and II, and 40 nucleotide differences (7.5%) between groups II and III. These differences were mainly in the ITS1, except for groups I and II where the differences were largely present in the ITS2.

The individual phylograms of *tef1- α* , *tub2*, *his3* and *cal* (Figs. S1-S4) assigned the set of strains CAA375 to CAA977 in the clade containing *D. malorum*. Additionally, strains CAA149 to CAA295 were clustered in a well-supported clade, fitted within the concept of *D. novem*. Likewise, in the 4-loci phylogram (Fig. S5) these clades were also highly supported by bootstrap and posterior probability values, thus indicating a close relationship with *D. novem* (ML/MP/PP = 100/100/1.00) and *D. malorum* (ML/MP/PP = 96/98/1.00). The 5-loci combined

phylogram clustered all these isolates mentioned above in a similar fashion to the ITS tree, where different clades were formed as demonstrated in Fig. 2.

2. Intrasporocarpic and intragenomic ITS heterogeneity.

Strains CAA159, CAA160, CAA162, CAA164, CAA165 and CAA168 (ITS I and II, Fig. 1) originated from individual sibling ascospores isolated from the same perithecium. Based on the MSP-PCR fingerprinting, these isolates had similar banding patterns and clustered together. Therefore, it was expected that all these isolates would also group together in the phylogenetic analyses. However, isolate CAA164 showed a distinct ITS sequence from all isolates represented in Fig. 1 (clade a), representing a distinct ITS type (clade b). Additionally, a third ITS type (clade c) comprising the isolates CAA263 and CAA264 was also detected.

Analysis of the ITS region of these strains revealed 173 bp span for ITS1 and 151 bp for ITS2 region (including gaps) with the intermediate 5.8S rRNA partition spanning 164 bp. In a pairwise alignment, isolate CAA164 was shown to share polymorphisms in the ITS1 portion with the isolates collected in this study from clade a, including the type strain of *D. novem* and polymorphisms in the ITS2 portion with strains from clade c. For instance, 34 nucleotides out of 173 bp in ITS1 (19.6%) are shared with *D. novem*, whereas 26 nucleotides out of 151 in ITS2 (17%) are shared with isolates with the ITS type III. Moreover, 2 nucleotides out of 164 in 5.8S (1.2%) are shared with *D. novem* and another 3 nucleotides from IT1-5.8S-ITS2 region (0.6%) were new in the sequence of CAA164.

Likewise, the ITS clones from isolate CAA300 did not cluster together. Clone 1, clone 3, clone 4 and clone 5 clustered in a highly supported clade, containing the isolates CAA263 and CAA264 (ML/MP/PP = 99/100/1.00). Nevertheless, clone 2 appeared as a sister taxon of CAA164. Individual phylogenetic analyses of *tef1- α* , *tub2*, *his3* and *cal* with the type species of *D. novem* yielded one clade only (Figs. S1-S4), consistent with the recognized species limits. However, sequence analyses of individual five clones from isolate CAA300 revealed rare ITS variants that did not cluster in the ITS phylogram according to the expected species grouping. Four sequences (*i.e.*, clones 1, 3, 4 and 5, Fig. 1) showed to be phylogenetically most distant from that of the type strain of *D. novem* (CBS 127271).

For instance, these clones showed 65 to 69 bp mismatches, equivalent to a divergence of 13.4% to 14.2% with the type strain. Moreover, the ITS sequence from clone 2 showed 30 nucleotide differences from of the type strain of *D. novem* (CBS 127271) (6% divergent) and 35 to 39 nucleotides (7.4% to 8.2% divergent) separate clone 2 from the remaining clones.

There are three other interesting cases: (1) clone 2 yielded one ITS variant very similar to that from strain CAA164 (single ascospore isolate), with 8 nucleotide differences, which reflects 1.7% divergence; (2) clones 1, 3, 4 and 5 were phylogenetically closely related to strains CAA263 and CAA264 (single conidium isolates) (clade c, Fig. 1), with 6 to 10 nucleotide differences (diverging by 1.2% to 2%); (3) although isolates CAA300 and CAA295 are sibling ascospores (isolated from the same perithecium), all clones of CAA300 were different from CAA295 by up to 69 nucleotides, representing a divergence of 14.2% between sibling ascospores.

3. Hybridization in *Diaporthe*.

Strains of a *Diaporthe* sp. (CAA998 and CAA999) did not cluster with any recognized *Diaporthe* species in the 4-loci (Fig. S5) and 5-loci (Fig. 2) combined analyses but appeared to cluster between *D. portugallica* and *D. phillipsii*. Individual gene genealogies were inconclusive as CAA998 and CAA999 clustered either with one or the other species. A pairwise comparison of the ITS regions revealed an intriguing outcome (Fig. 4). Inspection of the ITS alignment revealed that isolates CAA998 and CAA999 share polymorphisms in ITS1 with *D. phillipsii* and polymorphisms in ITS2 with *D. portugallica*. For instance, 12 nucleotides out of 176 bp in ITS1 (6.8%) are shared with *D. phillipsii*, whereas 11 nucleotides out of 157 in ITS2 (7%) are shared with *D. portugallica* (Fig. 4). Therefore, *Diaporthe* sp. may have arisen from hybridization between *D. portugallica* and *D. phillipsii*.

```

CBS 144228 Diaporthe portugallica TCATTGCTGGAACGCGCCCTGGCGCACCCAGAAACCCTTTGTGAACCTTATACCTTACTG
CAA998 Diaporthe sp. ....
CAA999 Diaporthe sp. ....
MUM 19.28 Diaporthe phillipsii ....

CBS 144228 Diaporthe portugallica TTGCCTCGGCGCAGGCCGTCCCCTATGGGGTCCCTTGGAG---ACAAGGAGCAGCCGGCC
CAA998 Diaporthe sp. ....C.C....TTGTCTC.A
CAA999 Diaporthe sp. ....C.C....TTGTCTC.A
MUM 19.28 Diaporthe phillipsii ....C.C....TTGTCTC.A

CBS 144228 Diaporthe portugallica GGTGGCCAAATTAACCTCTGTTTTCACACTGAAACTCTGAGTACAAAACATAAATGAATCA
CAA998 Diaporthe sp. ....CC
CAA999 Diaporthe sp. ....CC
MUM 19.28 Diaporthe phillipsii ....CC

CBS 144228 Diaporthe portugallica AAACCTTCAACAACGGATCTCTTGGTTCTGGCATCGATGAAGAACGCAGCGAAATGCGAT
CAA998 Diaporthe sp. ....
CAA999 Diaporthe sp. ....
MUM 19.28 Diaporthe phillipsii ....

CBS 144228 Diaporthe portugallica AAGTAATGTGAATTGCAGAATTCAGTGAATCATCGAATCTTTGAACGCACATTGCGCCCT
CAA998 Diaporthe sp. ....
CAA999 Diaporthe sp. ....
MUM 19.28 Diaporthe phillipsii ....

CBS 144228 Diaporthe portugallica CTGGTATTCGGAGGGCATGCCTGTTCGAGCGTCATTTCAACCCTCAAGCCTGGCTTGGT
CAA998 Diaporthe sp. ....
CAA999 Diaporthe sp. ....
MUM 19.28 Diaporthe phillipsii ....

CBS 144228 Diaporthe portugallica GATGGGGCACTGCCTGTGTAATAA--AGGCGAGGCCCTGAAATACAGTGGCGAGCTCGCCAGGA
CAA998 Diaporthe sp. ....C.GTAAA--AGG
CAA999 Diaporthe sp. ....C.GTAAA--AGG
MUM 19.28 Diaporthe phillipsii ....T.TCCCCAGGAA

CBS 144228 Diaporthe portugallica CTCCTGAGCGTAGTAGTTAAACCCCTCGCTTTGGAAGGCCTGGCGGTGCCCTGCCCTTAAAC
CAA998 Diaporthe sp. ....
CAA999 Diaporthe sp. ....
MUM 19.28 Diaporthe phillipsii ....

CBS 144228 Diaporthe portugallica CCCAACTCTTGAAAAATTGACCTCGGATCAGGTAGGAATACCCGCTGAACTTAA
CAA998 Diaporthe sp. ....
CAA999 Diaporthe sp. ....
MUM 19.28 Diaporthe phillipsii ....

```

Figure 4. Alignment of the nuclear ribosomal DNA of *Diaporthe portugallica* and *D. phillipsii* ex-types and the putative hybrids CAA998 and CAA999. Nucleotide sites in the upper line shaded in light and black grey indicate the ITS1 and ITS2 sequences, respectively. Framed sites indicate shared polymorphisms with the parental sequences. Conserved positions are indicated by a dot and gaps are indicated by a hyphen.

Mating type diagnosis and mating experiments.

The PCR-based mating type diagnostic assay revealed that heterothallism was the predominant mating strategy among all isolates tested. This assay was also useful to select isolates with opposite mating-types to perform the *in vitro* matings. Approximately three months after inoculation, 52% (11/21) of the crossings between

isolates with the same ITS type and with different ITS types resulted in the formation of perithecia with viable ascospores (Fig. 5).

A

ITS population	ITS I	CAA159*								
		CAA160*								
		CAA162*	+	+						
		CAA165*	-	+						
		CAA262			nd	nd				
		CAA295			nd	nd				
	ITS II	CAA164*	-	-			+	+		
	ITS III	CAA263	nd	nd			-	-		
		CAA264	nd	nd			+	-		
			CAA159*	CAA160*	CAA162*	CAA165*	CAA262	CAA295	CAA164*	CAA263
		ITS I						ITS II	ITS III	
		ITS population								

B

ITS population	ITS VII	CAA953						
		CAA972	-					
		CAA975		+				
	ITS VIII	CAA740	nd		nd			
		CAA752	-		+			
		CAA974	nd	+		-	+	
		CAA977	nd	+		nd	-	
			CAA953	CAA972	CAA975	CAA740	CAA752	CAA974
		ITS VII			ITS VIII			
		ITS population						

Figure 5. Mating experiments between some isolates from ITS populations of *D. novem* (A) and *D. malorum* (B). Squares highlighted in grey represent sexual incompatibility. Single ascospores isolates obtained from the same perithecium are represented by a superscript asterisk. -, No perithecia; +, perithecia with viable ascospores; nd, not determined.

Several *MAT1-1-1* and *MAT1-2-1* isolates from clades a, b and c (Fig. 1) were selected and crossed with each other, regardless of their ITS sequence. For instance, isolate CAA164 (ITS II) could be mated with CAA295 and CAA262 (ITS I). Moreover, from the subset of 6 sibling single ascospore isolates (CAA159 to CAA168) only 50% (3/6) of the crossings resulted in the formation of perithecia. Due to the absence of mating-type compatibility, isolates from ITS I (clade a) and III (clade c) could not be crossed with CAA164 (ITS II) (Fig. 5A).

Isolates of *D. malorum* were successfully crossed with opposite mating-types, comprising those from ITS VII and VIII (Fig. 1). Isolates with the same ITS type mated with other isolates with the same ITS type as well as those from different ITS types (Fig. 5B). The ITS sequences from the F1 progenies, comprising a total

of 43 isolates, were analyzed. In crossings between isolates CAA295 (ITS I) and CAA264 (ITS III), both ITS I and ITS III F1 isolates were obtained. Regardless of the ITS types from the parental isolates, we observed that from the remaining crossings, the F1 offspring from the same perithecium inherited the ITS from only one parental isolate.

Polymorphism and population structure analysis.

To understand the genetic diversity of *D. malorum* and *D. novem* isolates, analyses were conducted using DnaSP v.6.12. A summary of genetic diversity and polymorphism indices for each gene region as well as for the combined dataset is given in Table 4.

Table 4. Polymorphism and genetic diversity data of *Diaporthe novem* and *D. malorum* isolates obtained from Portugal.

Species	Gene	n ¹	bp ²	h ³	S ⁴	hd ⁵	π ⁶	TD ⁷
<i>Diaporthe novem</i>	ITS	16	538	10	61	0.867	0.060	2.387
	<i>tef1-α</i>	16	327	2	1	0.233	0.001	-0.448
	<i>tub2</i>	16	530	4	6	0.725	0.004	0.599
	<i>his3</i>	16	470	2	1	0.325	0.001	0.156
	<i>cal</i>	16	499	2	3	0.400	0.002	0.948
	5-loci	16	2364	15	72	0.992	0.014	2.147
	4-loci	16	1826	9	11	0.858	0.002	0.647
<i>Diaporthe malorum</i>	ITS	10	542	3	18	0.644	0.018	2.408
	<i>tef1-α</i>	10	333	2	3	0.556	0.005	2.057
	<i>tub2</i>	10	502	3	3	0.378	0.001	-1.562
	<i>his3</i>	10	429	1	0	0	0	-
	<i>cal</i>	10	405	1	0	0	0	-
	5 loci	10	2292	7	24	0.933	0.005	1.919
	4 loci	10	1750	4	6	0.711	0.001	0.284

¹Number of sequences (n). ²Total number of sites (bp). ³Number of haplotypes (h). ⁴Number of polymorphic sites (S). ⁵Haplotype diversity (hd). ⁶Average nucleotide diversity (π). ⁷Tajima's D statistical test (TD)

ITS gave the highest average number of differences per site for *D. novem* and *D. malorum* (0.060 and 0.018 respectively), whereas *tef1-α* and *his3* gave the lowest (0.001) for *D. novem*, and *his3* and *cal* (0.0) for *D. malorum*. Haplotype diversity (hd) was highest for the ITS for both *D. novem* and *D. malorum* (0.867 and 0.644) respectively and lowest for *tef1-α* (0.233) in *D. novem*, and for *cal* and *his3* in *D. malorum* (hd = 0). In addition to that, besides the combined analyses, for *D. novem*, ITS, *tub2*, *his3* and *cal* gave positive Tajima's D values as 2.387, 0.599, 0.156 and 0.948, respectively. For *D. malorum*, only ITS and *tef1-α* gave positive

values (2.408 and 2.057, respectively), apart from the combined analyses. Wright's F_{ST} statistics (F_{ST}) gave high values ($F_{ST} = 0.99$) for *D. novem* ITS populations and negative values ($F_{ST} = -0.21$) for *D. malorum* ITS populations.

ITS sequences obtained in this study were used to generate Median-joining networks of *D. malorum* (Fig. 6A) and *D. novem* (Fig. 6B) populations, thus representing haplotypes of both species from the different regions they were collected. Results from the haplotype networks shows that the different haplotypes of *D. malorum* and *D. novem* were not correlated to any specific geographic distribution, being distributed in several locations.

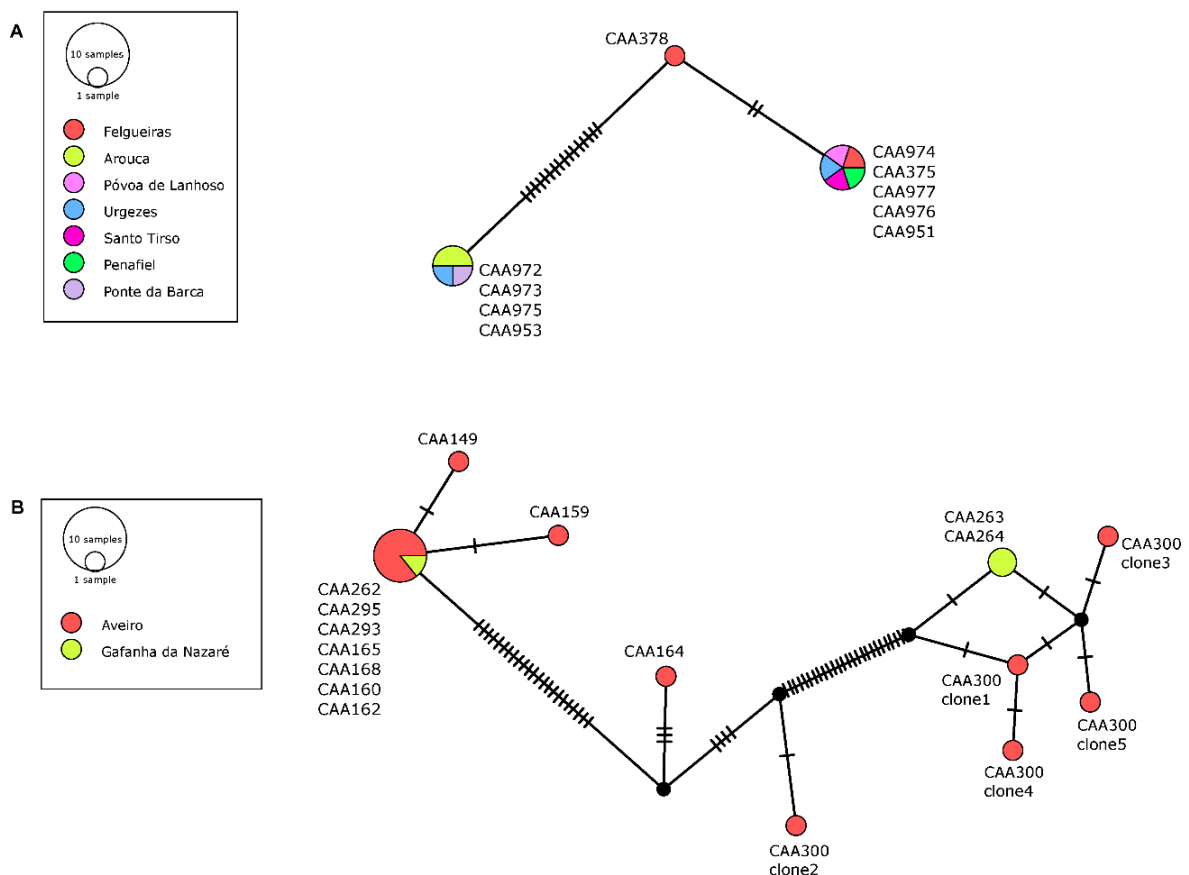


Figure 6. Median joining networks constructed for Internal Transcribed Spacer (ITS) sequences representing haplotypes of *Diaporthe malorum* (A) and *D. novem* (B) isolated from different Portuguese regions. The size of the circle indicates frequency of sequences belonging to a particular haplotype (smallest circle = 1 sequence, to largest circle = 7 sequences). Black dots are median vectors presumed unsampled or missing intermediates. Hatch marks along the network branches indicate the number of mutations.

Morphological characterization.

Representative isolates with different ITS types from clade 1 and clade 3 (Fig. 1), fitting within the concept of *D. novem* and *D. malorum* respectively, were morphologically characterized based on their asexual morphs (Table 5). After 4-6 weeks, pycnidia were brown to black, globose and rarely cone-shaped, solitary or aggregated, always covered with mycelium, immersed in pine needles and fennel stems partially erumpent and extruding white or translucent yellowish conidial masses (Fig. 7 and 8). Colonies of *D. malorum* on PDA after 7 days at 25 °C flat with irregular growth, aerial mycelium white to pale brown and reverse yellowish to brown with concentric zones (Fig. 7), and reverse turning black olivaceous gray after 15 days at 25 °C in darkness. Conidiophores were cylindrical to subcylindrical, hyaline, with hyaline conidiogenous cells attached to the apex of conidiophores lining the inner cavity of pycnidia. Conidiogenous cells phialidic, slightly curved, hyaline and tapering towards the apex. Alpha conidia unicellular, fusiform, hyaline, rarely bi-guttulate. Beta conidia hyaline, filiform, with rounded base, apex acute, frequently hooked in apical part.

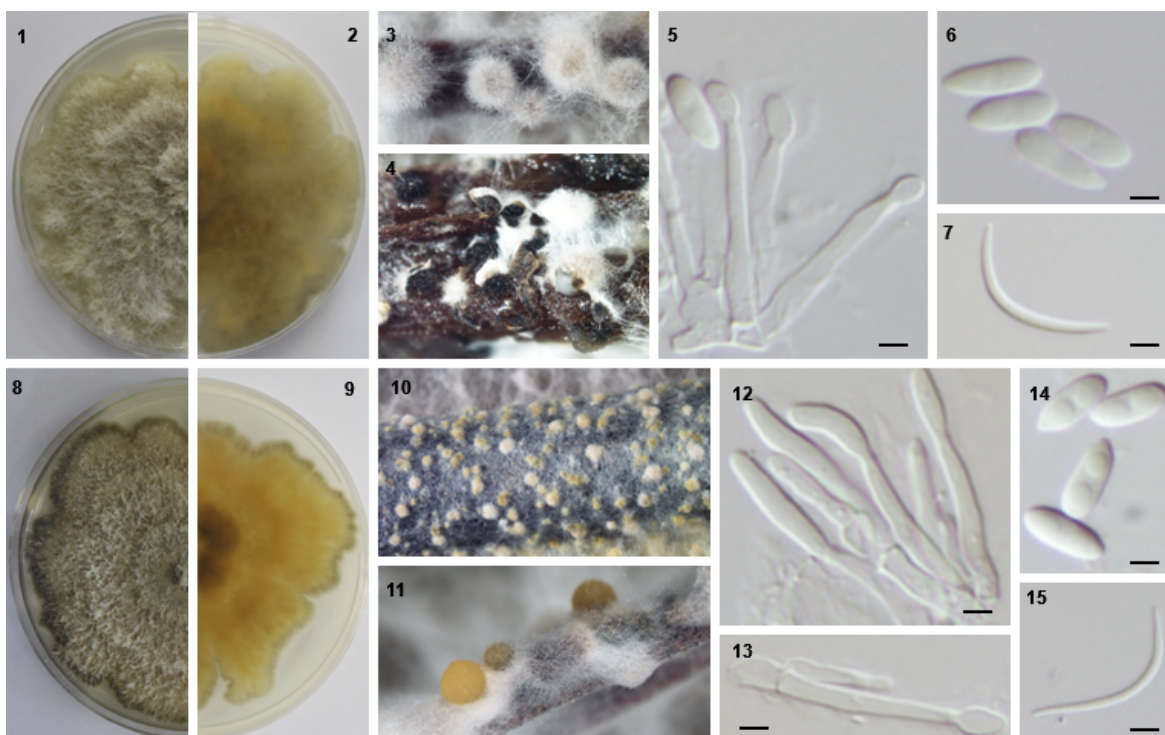


Figure 7. Morphology of *Diaporthe malorum* isolates CAA972 (1-7) and CAA974 (8-15) from *Vaccinium corymbosum*. 1, 8. Upper culture surface. 2, 9. Reverse culture surface. Both on PDA, 25 °C and 7 days. 3, 4, 11. Pycnidia developing on pine needles exuding conidial cirrus. 10. Pycnidia developing on fennel twigs. 5, 12, 13. Conidiophores with developing conidiogenous cells. 6, 14. Alfa conidia. 7, 15. Beta conidia. Bars: = 2.5 µm.

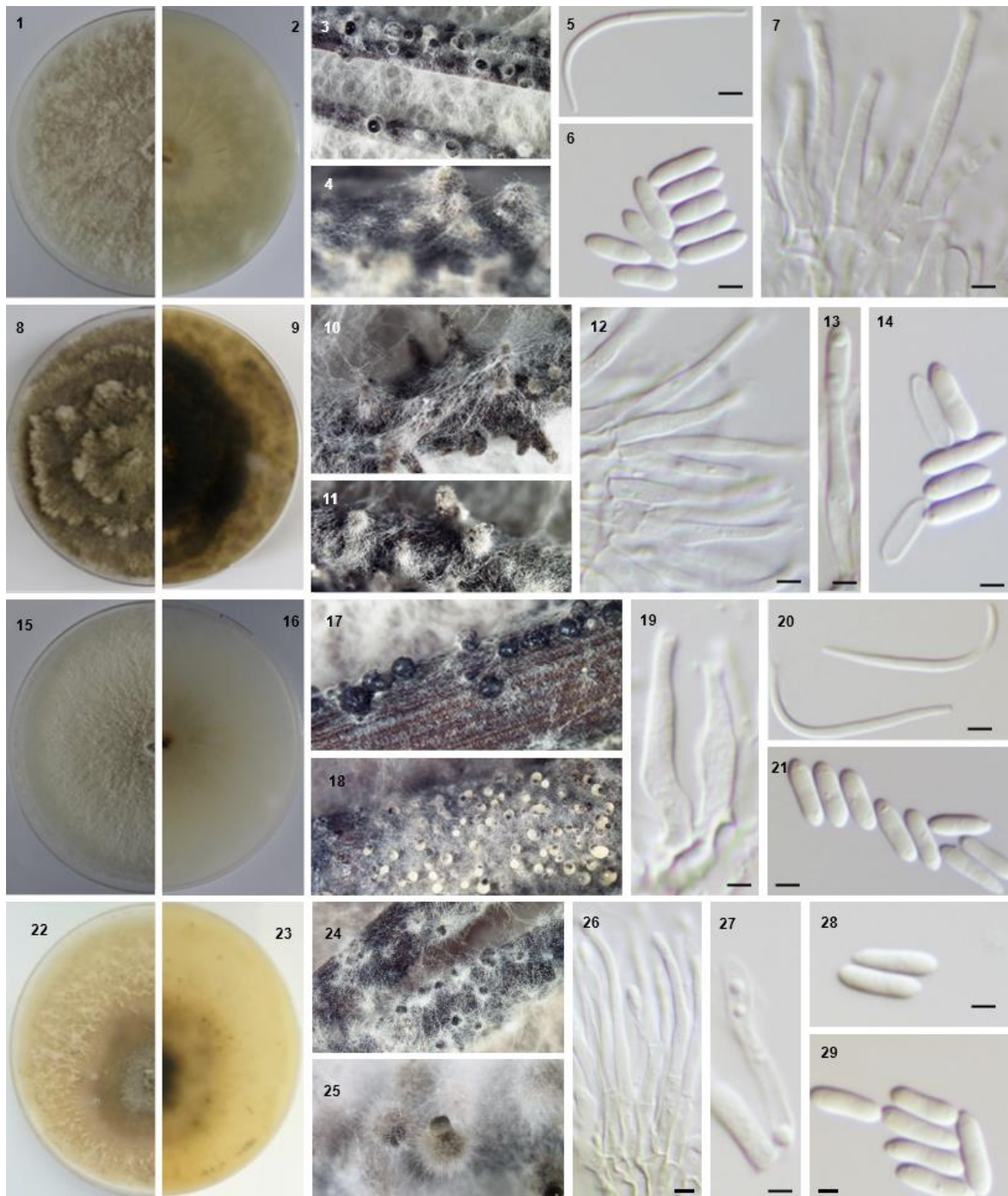


Figure 8. Morphology of *Diaporthe novem* isolates CAA162 (1-7), CAA164 (8-14), CAA263 (15-21) and CAA300 (22-29) from *Foeniculum vulgare*. 1, 8, 15, 22. Upper culture surface. 2, 9, 16, 23. Reverse culture surface. Both on PDA, 25 °C and 7 days. 3, 4, 10, 11, 24, 25. Pycnidia developing on pine needles. 17, 18. Pycnidia developing on fennel twigs exuding conidial cirrus. 5, 20. Beta conidia. 6, 14, 21, 28, 29. Alfa conidia. 7, 12, 19, 26. Conidiogenous layer with developing conidiophores. 13, 27. Conidiophore with developing conidia. Bars: 2.5 µm.

Colonies of *D. novem* exhibited some variability. On PDA, colonies were commonly with greyish white aerial mycelium and yellowish grey zones, with reverse skimmed milk to wine yellow, turning pale brown to black with age (Fig. 8).

Sometimes, colonies found growing with a radial pattern, wax yellow to blackish brown felted aerial mycelium. Conidiophores cylindrical, hyaline, densely aggregated, thick walled, broadening in the base, with hyaline conidiogenous cells attached to the apex of conidiophores. Alpha conidia oval to subcylindrical, hyaline, frequently bi-guttulate, aseptate. Beta conidia, when found, were hyaline, filiform, hooked in apical part.

Nearly 6 weeks after sporulation, pycnidia of isolates CAA998 and CAA999 were black, covered in white mycelium and exuding yellow cirrhi. Colonies spreading with aerial mycelium olivaceous green with gallstone yellow on the reverse after 7 days at 25 °C and becoming dark with age. At 30 °C, developed brown colonies with radial concentric zones.

TAXONOMY

In this section we provide a detailed morphological description and illustrations of the putative hybrid from *V. corymbosum*. We also supply a detailed description of the sexual morph of *D. malorum*, which has been obtained and described for the first time after *in vitro* crossing of opposite mating types.

Diaporthe xhybrida S. Hilário & A. Alves **nothosp. nov.** (Fig. 9)

MycoBank: MB838688

Typification: **Portugal. Santarém:** Ourém (39°39'13.5"N 8°35'32.0"W) from diseased *Vaccinium corymbosum* twigs, April 2019, H. Lains (holotype **AVE-F-12**, a dried culture sporulating on fennel stems, deposited in the Herbarium Universitatis Aveirensis from Universidade de Aveiro, Portugal). Ex-type culture **MUM 21.01** (=CAA958), deposited in the Micoteca da Universidade do Minho, Braga, Portugal.

Etymology: Named after its hybrid origin, resulting from cross between *D. portugallica* and *D. phillipsii*.

Known distribution: Portugal.

Mating type strategy: Heterothallism.

Description: known only from the type strain. Asexual morph: pycnidial conidiomata, produced on pine needles or fennel twigs on ¼ strength PDA within 4-6 weeks, mostly solitary with yellow conidial cirrhous extruding from the ostioles; conidiophores hyaline, smooth, densely aggregated, thick walled, cylindrical, straight to slightly curved with conidiogenous cells in the ends (mean \pm S.D. = $12.3 \pm 2.7 \times 1.8 \pm 0.2 \mu\text{m}$, $n = 30$); paraphyses hyaline, subcylindrical, straight, 1-septate and branched (mean \pm S.D. = $35.4 \pm 7.7 \times 1.4 \pm 0.5 \mu\text{m}$, $n = 20$); alpha conidia aseptate, rarely found bi- guttulate, hyaline, acute at both ends and sometimes with rounded ends (mean \pm S.D. = $7.0 \pm 0.6 \times 2.4 \pm 0.3 \mu\text{m}$, $n = 100$), L/W ratio of 3.0 ± 0.5 ; beta conidia found rare, hyaline, aseptate, smooth, filiform, apex acute, slightly curved, hooked in apical part (mean \pm S.D. = $20.5 \pm 0.3 \times 1.2 \pm 0.3 \mu\text{m}$, $n = 4$), L/W ratio of 16.6 ± 0.1 ; gamma conidia not observed. Sexual morph: Not observed.

Culture characteristics: Colonies on PDA spreading with moderate aerial olivaceous green superficial mycelium, flattened and dense, turning gallstone yellow on the reverse, covering a Petri dish in 7 days at 25 °C. After the fourth day, the growth was faster at 25 °C. It grew better at 30 °C than at 10 °C; No growth was observed at 5 °C nor at 35 °C; *Diaporthe xhybrida* developed brown to black mycelium with concentric zones at 30 °C after 7 days in the dark.

Additional material examined: **Portugal. Santarém:** Ourém (39°39'13.5"N 8°35'32.0"W), from diseased *V. corymbosum* twigs, April 2019, *H. Lains*, living culture CAA999. Both holotype strain and isolate CAA999 were collected from the same plant material.

Notes: Morphologically, *Diaporthe xhybrida* differs from *D. portugallica* and *D. phillipsii* in its larger alpha conidia ($7.0 \pm 0.6 \times 2.4 \pm 0.3 \mu\text{m}$ vs $6.8 \pm 0.7 \times 2.2 \pm 0.2 \mu\text{m}$ for *D. phillipsii* vs $6.6 \pm 0.8 \times 2.2 \pm 0.3 \mu\text{m}$ for *D. portugallica*) and in the presence of beta conidia, which is not known neither in *D. portugallica* nor in *D. phillipsii*. *Diaporthe xhybrida* also differs from *D. phillipsii* and *D. portugallica* in colony characters (reverse gallstone yellow vs reverse white to ivory color for *D. phillipsii* vs reverse pale brown for *D. portugallica*) (Guarnaccia & Crous 2018; Hilário et al. 2020). *Diaporthe xhybrida* clusters with *D. portugallica* in the *his3* and *cal* single gene trees. However, the isolates CAA998 and CAA999 cluster with both *D. portugallica* and *D. phillipsii* in *tef1- α* and *tub2* trees, as there are no nucleotide

differences in the sequences among *tef1-α* and *tub2* loci. Additionally, *Diaporthe xhybrida* shares polymorphisms in the ITS1 sequence with *D. phillipsii* and polymorphisms in the ITS2 sequence with *D. portugallica*. Therefore, *Diaporthe xhybrida* described here has been arisen from hybridization between *D. portugallica* and *D. phillipsii*.

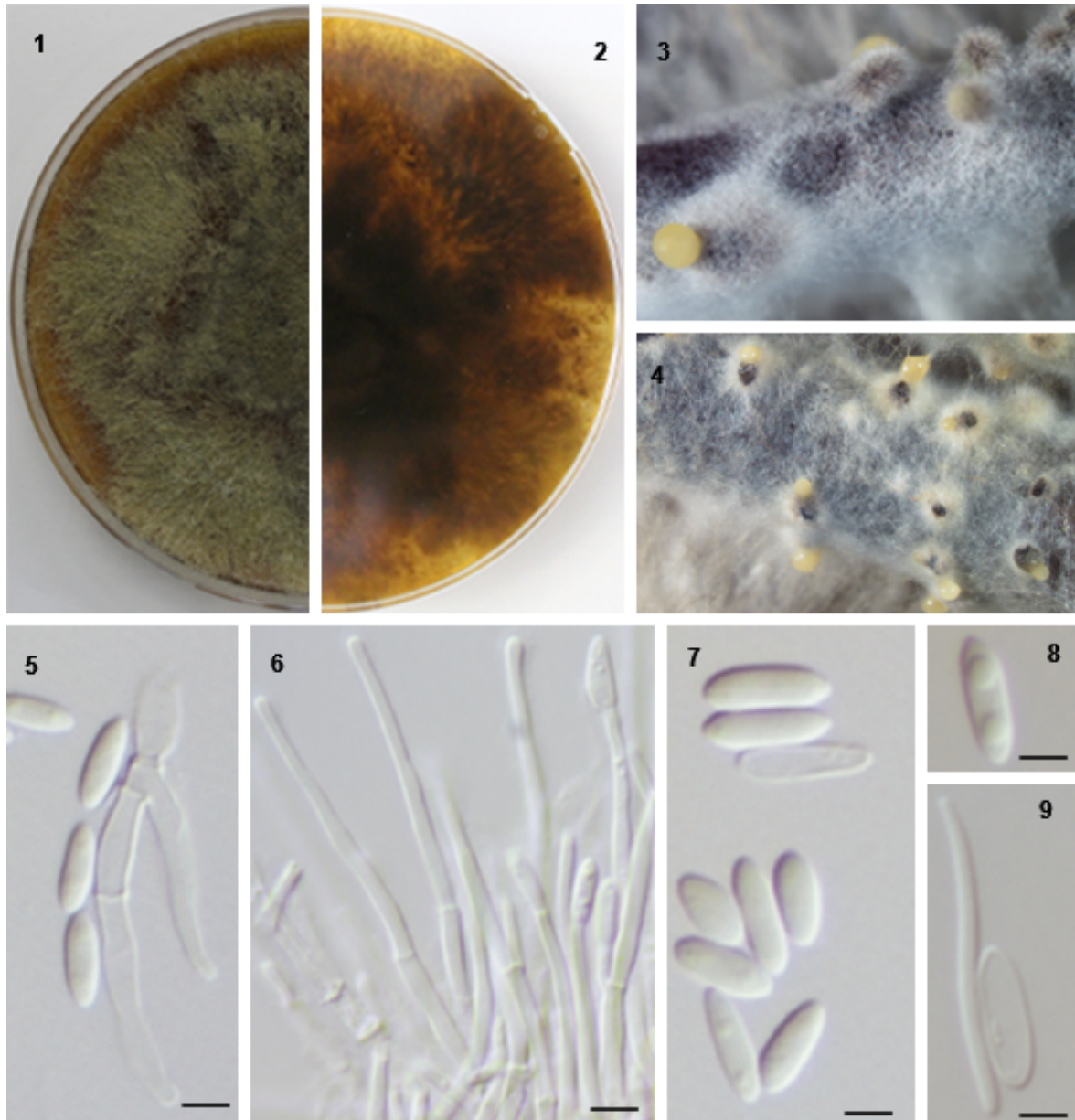


Figure 9. Morphology of *Diaporthe xhybrida* from *Vaccinium corymbosum*. **1.** Upper culture surface. **2.** Reverse culture surface. Both on PDA, 25 °C and 7 days. **3, 4.** Pycnidia developing on pine needles and fennel twigs in culture exuding yellow conidial cirrhuses. **5.** Alpha conidia and branched conidiophores. **6.** Conidiophores and 1-septate paraphyses. **7, 8.** Alpha conidia. **9.** Left: beta conidia, Right: alpha conidia. Bars = 2.5 μm.

Diaporthe malorum L. Santos & A. Alves, *Mycosphere* **8**:489 (2017) (Fig. 10)

MycoBank: MB820226

Specimens examined: **Portugal. Aveiro:** Arouca (40°54'35.3"N 8°22'49.7"W) from *V. corymbosum* twigs, April 2019, P. Pinho; **Portugal. Braga:** Urgeztes (41°25'24.5"N 8°17'35.1"W) from *V. corymbosum* twigs, July 2019, S. Hilário; perithecia on *Foeniculum vulgare* stems in culture obtained from cross between CAA972 (MAT1-2-1) and CAA975 (MAT1-1-1).

Known distribution: Portugal (Santos et al. 2017b).

Host range: *Eucalyptus globulus* (Lopes et al. 2021), *Malus domestica* (Santos et al. 2017b), *Magnolia soulangeana* and *V. corymbosum*.

Mating type strategy: Heterothallism.

Description: Sexual morph: Perithecial ascomata, globose, solitary or aggregated, black and ostiolate exuding a translucent white spores mass; black long necks emerging through fennel stems and covered with dirty white to brown mycelium; asci (36.2–)37.1–47.2(–48.3) × (5.7–)6.2–7.3(–7.4) μm mean ± S.D. = 42.1 ± 5.8 × 6.7 ± 0.6 μm, *n* = 10), L/W ratio of 6.3 ± 1.1, 8-spored, unitunicate, clavate to subclavate, straight to slightly curved with visible apical ring; ascospores (9.9–)10.7–11.0(–12.8) × (2.4–)2.7–2.8(–3.2) μm (mean ± S.D. = 10.8 ± 0.6 × 2.8 ± 0.2 μm, *n* = 100), L/W ratio of 3.9 ± 0.3, septate, hyaline, cylindrical, frequently eguttulate to tetra-guttulate.

Culture characteristics: Colonies on PDA spreading with moderate aerial superficial mycelium flattened and dense, ranging from white, dirty white to smoke grey, yellowish grey at the margins, sometimes with irregular growth; turning buff orange, yellow to orange white and cream yellow to pale brown on the reverse.

Notes: Perithecia formed in culture with viable ascospores only after crossing isolates with opposite mating-types, as diagnosed by PCR.

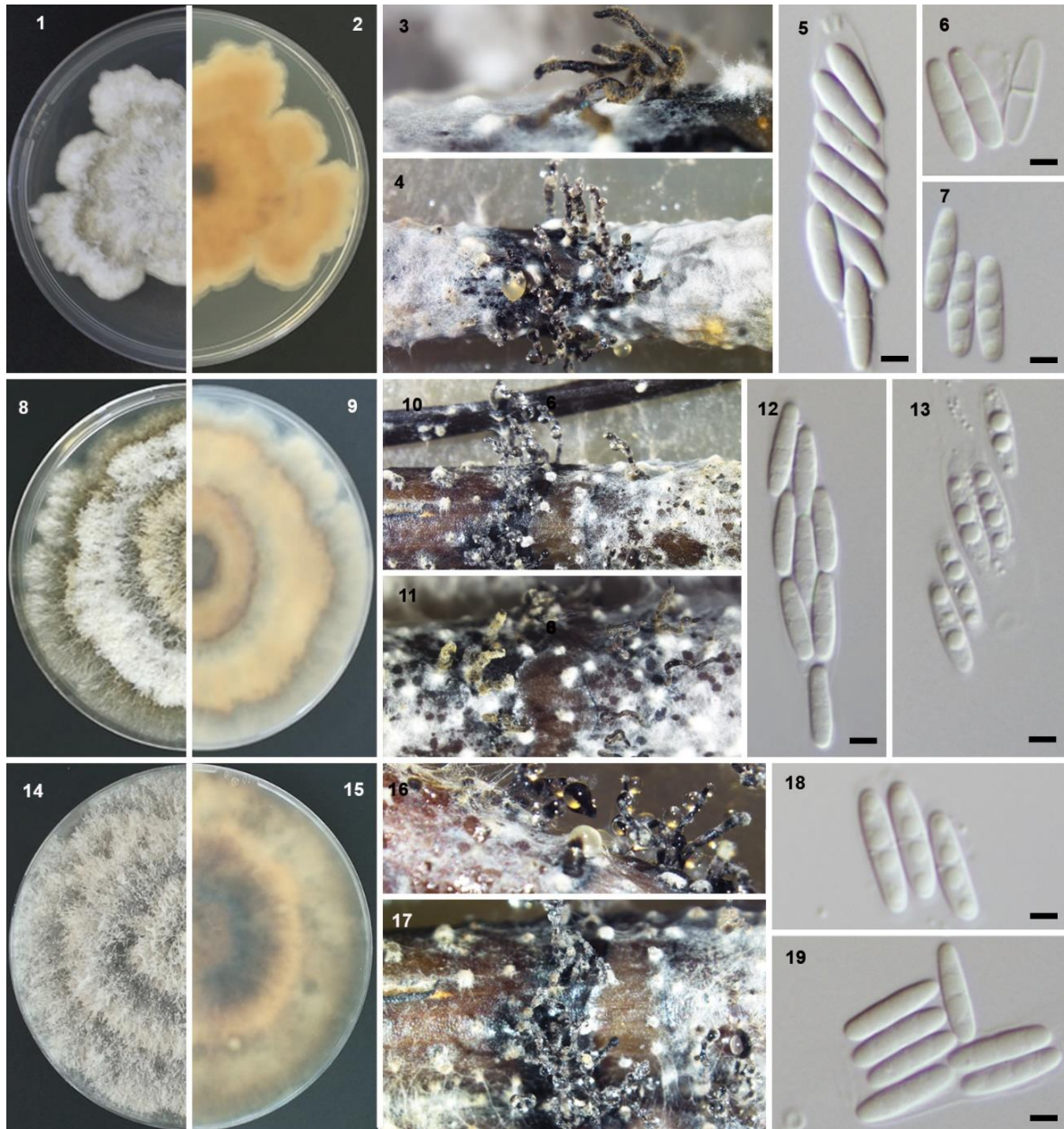


Figure 10. Morphology of *Diaporthe malorum* progenies from crosses between CAA972 x CAA975 (1-7), CAA752 x CAA974 (8-9) and CAA972 vs CAA977 (14-19). 1, 8, 14. Upper culture surface. 2, 9, 15. Reverse culture surface. Both on PDA, 25 °C and 7 days. 3, 4, 10, 11, 16, 17. Perithecial ascomata and necks emerging through fennel twigs on culture. 5, 12. Asci with 8 ascospores. 6, 7, 13. Septate and tetraguttulate ascospores. 19. Ascospores and visible apical ring. Bars = 2.5 µm.

Table 5. Synopsis of characters of *Diaporthe malorum*, *D. novem* and their representative isolates from the different ITS populations.

Species / Isolates	Conidiomata	Conidiophores and conidiogenous cells	Alpha conidia (µm)	Beta conidia (µm)	Culture characteristics on PDA	References
<i>D. malorum</i>	Conidiomata pycnidial, dark brown, superficial, solitary or more frequently aggregated, opening via a central ostiole, exuding a creamy to white conidial cirrus.	Conidiophores lining the inner cavity, subcylindrical, hyaline, smooth, reduced to conidiogenous cells. Conidiogenous cells phialidic, hyaline, and smooth, subcylindrical with apical taper.	Hyaline, aseptate, smooth, fusiform, rarely bi-guttulate, ellipsoid, rounded apex and obtuse to truncate base, mean ± S.D. = 6.3 ± 0.5 × 2.2 ± 0.3 µm, n = 100)	Infrequent, hyaline, aseptate, smooth, filiform, frequently hooked in apical part, apex acute, base truncate, mean ± S.D. = 21.5 ± 2.1 × 1.3 ± 0.3 µm, n = 50).	Colonies spreading flat, with sparse to moderate aerial mycelium, sometimes with a reddish exudate; growing with pale brown to brown, reverse pale brown to dark reddish-brown mycelia	Santos et al. 2017
CAA972	Conidiomata pycnidial, dark brown, broadly spherical, solitary or aggregated, covered in white mycelium, exuding a translucent white conidial cirrus	Conidiophores cylindrical, hyaline, smooth, straight, slightly broadening in the base, mean ± S.D. = 13.9 ± 1.8 × 1.8 ± 0.2 µm, n = 30), conidiogenous cells phialidic, tapering towards the apex, hyaline, smooth, mean ± S.D. = 2.5 ± 0.2 × 1.2 ± 0.2 µm, n = 30)	Hyaline, aseptate, smooth, fusiform, rarely bi-guttulate, ellipsoid, apex apiculate to obtuse, mean ± S.D. = 6.9 ± 0.6 × 2.3 ± 0.2 µm, n = 100)	Beta conidia infrequent aseptate, smooth, filiform, rounded ends, apex acute, frequently hooked in apical part, mean ± S.D. = 19.1 ± 1.0 × 1.5 ± 0.2 µm, n = 100).	Colonies spreading flat, irregular growth, with aerial ivory white to pale brown mycelium and reverse yellowish to olivaceous gray zones	This study
CAA974	Conidiomata pycnidial, broadly spherical, solitary or aggregated, covered in white to yellowish mycelium, exuding a yellow conidial cirrus from ostioles	Conidiophores cylindrical, hyaline, smooth, straight, slightly broadening in the base, mean ± S.D. = 13.1 ± 1.2 × 1.9 ± 0.2 µm, n = 30), conidiogenous cells phialidic, straight or slightly curved, tapering towards the apex,	Hyaline, aseptate, smooth, fusiform, frequently bi-guttulate, ellipsoid, apex apiculate to obtuse, mean ± S.D. = 6.7 ± 0.5 × 2.5 ± 0.3 µm, n = 100)	Beta conidia infrequent aseptate, smooth, filiform, rounded ends, apex acute, frequently hooked in apical part, mean ± S.D. = 19.3 ± 0.9 × 1.3 ± 0.2 µm, n = 100).	Colonies spreading flat, irregular growth, with aerial white to pale brown mycelium, brown to black mycelium at the marginal area and reverse yellowish to brown concentric zones	This study

		hyaline, smooth, mean \pm S.D. = $7 \pm 0.8 \times 1.2 \pm 0.6 \mu\text{m}$, n = 30)				
<i>D. novem</i>	Conidiomata pycnidial, cone-shaped	Cylindrical, hyaline, smooth, uni- to bicellular, $5.3\text{--}10.4 \times 1.9\text{--}3.2 \mu\text{m}$. Conidiogenous cells phialidic, clavate to filiform, tapering towards the apex, periclinal thickening present.	Unicellular, oval to cylindrical, with obtuse ends, hyaline, biguttulate, mean \pm S.D. = $7.4 \pm 0.6 \times 2.2 \pm 0.1 \mu\text{m}$ (n = 100).	Beta-conidia hyaline, aseptate, filiform, curved, eguttulate, with rounded ends, mean \pm S.D. = $32.6 \pm 2.4 \times 1.1 \pm 0.1 \mu\text{m}$ (n = 100).	-	Santos et al. 2011
CAA162	Conidiomata pycnidial, broadly spherical, dark, superficial, solitary, or aggregated, covered in white mycelium, exuding a translucent white conidial cirrus.	Conidiophores cylindrical, densely aggregated, hyaline, smooth, reduced to conidiogenous cells, tapering towards the apex, thick walled, mean \pm S.D. = $21.5 \pm 2.5 \times 2.5 \pm 0.3 \mu\text{m}$ (n = 30).	Oval to subcylindrical with obtuse ends, hyaline, frequently biguttulate, aseptate, continuous or rarely found constricted at the center, mean \pm S.D. = $6.8 \pm 0.7 \times 2.2 \pm 0.2 \mu\text{m}$ (n = 100).	Beta-conidia hyaline, aseptate, filiform, one-celled, frequently hooked in apical part, apex acute mean \pm S.D. = $34.2 \pm 3.1 \times 1.5 \pm 0.2 \mu\text{m}$, n = 100).	Colonies originally flat with greyish white aerial mycelium with yellowish grey zones and reverse skimmed milk white and to ash grey zones, turning brown with age.	This study
CAA164	Brown to black conidiomata pycnidial, cone-shaped emerging from pine needles, solitary or in clusters, covered in white mycelium	Conidiophores cylindrical, hyaline, smooth, densely aggregated, thick walled, straight, tapering towards the apex, reduced to conidiogenous cells, mean \pm S.D. = $16.6 \pm 3.7 \times 2.4 \pm 0.5 \mu\text{m}$ (n = 30).	Oval to subcylindrical, hyaline, smooth, aseptate, frequently biguttulate, rounded apex, obtuse to truncate, continuous or rarely found constricted at the center, mean \pm S.D. = $7.2 \pm 0.6 \times 2.4 \pm 0.3 \mu\text{m}$ (n = 100).	Not observed	Colonies growing with a radial pattern, wax yellow to blackish brown aerial and felted mycelium, becoming felted and reverse with pale brown to black zones.	This study
CAA264	Black conidiomata pycnidial, superficial, broadly spherical, solitary or aggregated, exuding a translucent white to	Conidiophores cylindrical, thick walled, hyaline, straight, smooth, densely aggregated, broadening in the base, slightly tapering towards	Oval to subcylindrical, hyaline, smooth, aseptate, frequently biguttulate, rounded apex, obtuse to truncate, continuous or rarely	Beta-conidia hyaline, aseptate, filiform, one-celled, frequently hooked in apical part, apex acute, mean \pm S.D. =	Colonies spreading with flattened white to greyish white mycelium in the center and reverse with white at the	This study

	yellow conidial cirrus	the apex, reduced to conidiogenous cells, mean \pm S.D. = $12.4 \pm 1.6 \times 3.4 \pm 1.5 \mu\text{m}$ (n = 30).	found constricted at the center, mean \pm S.D. = $6.6 \pm 0.6 \times 2.4 \pm 0.2 \mu\text{m}$ (n = 100).	$30.1 \pm 2.4 \times 1.9 \pm 0.3 \mu\text{m}$, n = 100)	margins and pale saffron yellow rays in the center, turning brown with age	
CAA300	Black conidiomata pycnidial, solitary and frequently aggregated, exuding a translucent white conidial cirrus	Conidiophores cylindrical, thick walled, hyaline, straight, densely aggregated, slightly tapering towards the apex, reduced to conidiogenous cells, mean \pm S.D. = $22.2 \pm 4.1 \times 1.7 \pm 0.3 \mu\text{m}$ (n = 30).	Oval to subcylindrical, hyaline, aseptate, rarely bi-guttulate, rounded apex, obtuse to truncate, mean \pm S.D. = $7.4 \pm 0.6 \times 2.4 \pm 0.2 \mu\text{m}$ (n = 100).	Not observed	Colonies spreading with flattened white to wine yellow mycelium, developing a pale olivaceous gray concentric zone and reverse lemon yellow with brown pigmentation with age	This study

DISCUSSION

In this study, we provide evidence that significant intraspecific variation in the ITS regions of the ribosomal RNA gene cluster exist among individuals of the species *D. novem* and *D. malorum*. In addition, intragenomic variation in the ITS region was shown to occur within the genome of a single isolate of *D. novem*. Moreover, intrasporocarpic variation was also shown to exist among sibling ascospores of *D. novem*. This study is also the first to show the occurrence of hybridization between species in the genus *Diaporthe*.

The rRNA ITS region is one of the most frequently used molecular markers in fungi because of the rapid accumulation of mutations but with limited intraspecific variation (Schoch et al. 2012). However, several studies have shown a higher than average intraspecific and intrasporocarpic variability in the ITS region (Kovács et al. 2011; Lindner & Banik 2011; Nilsson et al. 2008; Santos et al. 2010; Simon and Weiß 2008; Smith et al. 2007).

Santos and colleagues (2010) were the first to study the intraspecific variation in the ITS region between single ascospore isolates in the genus *Diaporthe* from *Hydrangea macrophylla* in Azores Islands (Portugal). They assessed ITS sequence variation in 10 ascospores from the same perithecium and detected polymorphism when analyzing the ITS gene tree, where 2 different populations were formed. However, the single gene tree from *tef1-a* data assigned all these isolates within a single well-supported clade. They have proven that these isolates were interfertile and therefore were considered as belonging to the same biological species. Later, Udayanga et al. (2014a) assigned these isolates as a species belonging to the *D. eres* complex. These later authors, besides proving that ITS showed the lowest phylogenetic informativeness, observed also a high intraspecific variability in this region and decided to exclude it from the analyses. Since then, many authors have followed this approach and nowadays ITS is no longer used to delimit species in the *D. eres* species complex (Fan et al. 2018; Guo et al. 2020; Yang et al. 2018). However, this case of intraspecific variation reported by Santos et al. (2010) was never thoroughly examined. Here we show that it was not a sporadic occurrence, and that this phenomenon could be probably common in *Diaporthe*.

In the present study, three different ITS types designated I, II and III were recovered from *D. novem* isolated from *F. vulgare* in Aveiro (Portugal) and derived from sibling ascospores. These differences were confined to the ITS1 and ITS2 regions, and minor differences were noticed in the conserved 5.8S region of the isolate with the ITS type II. Moreover, it was shown that these ITS types, even if belonging to sibling ascospores, reflected an intraindividual sequence divergence of 6.2%. Interestingly, Stadler et al. (2014) have also observed the same in *Xylaria hypoxylon*, where single ascospore isolates were also derived from the same perithecium, resulting in three different ITS genotypes. Two other ITS types referred to in this study as VII and VIII were recovered from *D. malorum* isolated from 3 different hosts (*V. corymbosum*, *M. soulangeana* and *E. globulus*) and collected from different regions in Portugal. An intraspecific ITS variability involved ITS types VII and VIII, that diverged by up to 3.0%. However, this sequence heterogeneity was not observed in either the 4-loci phylogram or in the individual trees of protein-coding genes (*tef1- α* , *tub2*, *his3* and *cal*) as the isolates from ITS I, II and III groups fell within a highly supported clade containing *D. novem* and the isolates from ITS groups VII and VIII fitted within the concept of *D. malorum*. Thus, we can comfortably affirm that the ITS region harbors a high intraspecific variability, and it is prone to introduce variation in the analyses, overestimating the true diversity of species.

Recently, Hosseini et al. (2020) isolated strains of *D. novem* from soybean in France. The authors also noticed incongruences between the ITS sequence of a given isolate versus its respective *tef1- α* and *tub2* sequences, as it formed a separated branch in the ITS phylogram and was distantly related to the type strain of *D. novem*. These authors pointed out that such outcome could be due to a special mutation event that changed several bases in the ITS region, or to hybridization between *D. novem* and another *Diaporthe* species that was not part of their study. Interestingly, after a pairwise comparison among our isolates from *F. vulgare* with the one from soybean, we noted that this latter isolate had an ITS sequence very similar to the one from strains within clade c (CAA263 and CAA264) with 10 nucleotide differences, reflecting similarity of 98%. When compared to the type strain of *D. novem*, the isolate from soybean showed 90% similarity. This result

corroborates the hypothesis of ongoing recombination events among strains of *D. novem*, rather than hybridization.

It is noteworthy that some isolates of *D. novem* distributed in the clades a, b and c (e.g., CAA159 to CAA168) from *F. vulgare*, as well as those of *D. malorum* from clades c and d (e.g., CAA975 and CAA976) from *V. corymbosum*, despite their splitting in the ITS phylogeny, were recovered from the same location. Therefore, we can affirm that different ITS sequences may occur in the same geographic region (Fig. 6), and even within isolates from the same host (Udayanga et al. 2014a). We also detected no evidence of host specialization, given that the two reported ITS types of *D. malorum* were collected from three different hosts, and that our isolates of *D. novem* were collected from *F. vulgare*, whereas the one from France was collected from *Glycine max* (Hosseini et al. 2020).

Mating experiments showed that isolates from clades a, b and c (Fig. 1) can mate successfully, resulting in perithecia with viable ascospores isolates (F1), regardless of their different ITS sequences. Therefore, it is reasonable to assume that there are no reproductive barriers between the tested isolates, proving that they can be regarded as belonging to the same biological species. The same is true for isolates from clades c and d (Fig. 1). Despite their distinctions in the ITS phylogeny, mating was reported between isolates from ITS groups VII and VIII (Fig. 5) indicating that they constitute a single biological species. Surprisingly, the two ITS types from the parental species were not found in the same F1 progeny, indicating that these ITS types may be independently segregated in meiotic events as also reported previously (Santos et al. 2010).

Although polymorphisms of the ITS rRNA, have rarely been reported in pathogenic fungi, its occurrence seems to be more common than previously recognized. It was first reported by O'Donnell and Cigelnik (1997) who found intragenomic ITS variability in plant pathogenic *Fusarium*. Further studies have meanwhile reported these polymorphisms in the filamentous fungal genera *Ceratocystis* (Harrington et al. 2014) and *Ophiocordyceps* (Li et al. 2013), in yeasts such as *Candida* (Zhao et al. 2015), *Pichia* (Wu et al. 2016) and *Xanthophyllomyces* (Fell et al. 2007), in the truffle-like fungi *Terfezia* (Kovács et al. 2011) and also in the Basidiomycota, e.g., *Amanita* (Hughes et al. 2018) and *Laetiporus* (Lindner & Banik

2011). The sequence divergence observed does not usually exceed 3% (Kovács et al. 2011; Smith et al. 2007). However, Stadler et al. (2020), stated that an intragenomic variation by up to 15% may occur, leading to an erroneous overestimation of novel taxa. The study carried out by Stadler et al. (2020) was based on high quality genomes obtained through using third generation sequence technologies and constitutes the first direct proof of this intragenomic variation.

The present study shows for the first time, the occurrence of intragenomic ITS variation in the genus *Diaporthe*, particularly within an isolate of *D. novem*. Some of the divergent ITS sequences observed among the clones of CAA300 were greater than 14% divergent from the type strain of *D. novem*. Sequence comparison of all clones generated indicates that the polymorphic ITS sequences of isolate CAA300 arose from different isolates with different ITS types. For instance, clone 2 appears to be closely related to CAA164, while clones 1, 3, 4 and 5 were very close to CAA263 and CAA264. Therefore, we presume that these ITS sequences share the same evolutionary history as the strains they clustered with in the ITS and multigene trees. Furthermore, we hypothesize that this intragenomic heterozygosity observed in isolate CAA300 might be the result of two events: (1) from an intragenomic recombination among strains of *D. novem*, where copies seem to have escaped concerted evolution and present copies of the ancestral individuals; and (2) the existence of pseudogenes that are free from selective pressure (Hughes et al. 2018; Li et al. 2017; Tremble et al. 2019). Although not yet observed in filamentous fungi, the existence of extrachromosomal rRNA may also contribute to intragenomic variation (Lindner & Banik 2011) and thus, should not be disregarded as a putative hypothesis that deserves further investigation.

Taking into consideration all these cases reported in *D. novem* and *D. malorum* we advocate that the most plausible reason for this variability is an intergenomic recombination among strains of these species, merely representing novel haplotypes rather than novel taxa. We also hypothesize that these species may be too recently evolved to have had time to eliminate variation in the gene tandem repeats of nuclear ribosomal DNA (Harrington et al. 2014) or an ongoing speciation event may have started recently in the lineages (Tremble et al. 2019).

Although fungal hybrids are rare in nature they have been previously reported (Cruywagen et al. 2017). The inheritance of nucleotides of the ITS1 and ITS2 sequences from the parental species has been previously documented in plants, after an event of hybridization (Chiang et al. 2001). Two isolates of a *Diaporthe* sp. (CAA998 and CAA999) obtained from *Vaccinium corymbosum* could not be clearly attributed to any of the currently known species as shown in our phylogenetic analyses, since there were incongruences in the ITS versus other genes. Moreover, the small differences seen between *D. portugallica*, *D. phillipsii* and isolates CAA998 and CAA999 could likely represent one single species with an intraspecific genetic variability. However, one intriguing observation in our results was the apparent inheritance of nucleotides in *Diaporthe xhybrida*, in the ITS1 sequence from *D. phillipsii* and in the ITS2 sequence from *D. portugallica* (Fig. 4). Therefore, the hypothesis that those taxa could represent one single species was discarded. A reasonable explanation to the occurrence of this ITS type V is the hybridization between *D. portugallica* and *D. phillipsii*, where the retention of both parental ITS types led to a single composite sequence (Kanzi et al. 2020). This event may have happened through sexual reproduction or exchange of genetic material by fusion of their vegetative hyphae in a parasexual cycle (Olson & Stenlid 2002).

The genetic diversity between the populations of *D. novem* and *D. malorum* was evaluated. In addition, we used a median-joining network, in which the number of mutations separate haplotypes (Manawasinghe et al. 2019). The calculated haplotype diversities of *D. novem* were higher than 0.5 for ITS, *tub2* and the combined dataset, whereas for *D. malorum*, these high values were observed for ITS, *tef1- α* and the combined dataset, reflecting high genetic diversity at these loci. Tajima's D indicates how much population variation can be constant over time (Tajima 1989), whereas migration rates estimated from Wright's F_{ST} , are often used to infer patterns of gene flow (Linde 2010). Negative Tajima's values were observed for *tef1- α* (*D. novem*) and *tub2* (*D. malorum*), which may be a signal of a possible population expansion at these loci, explained by a neutral process of evolution. As opposed to this, Tajima's D gave positive values for all other loci and the combined sequences. This may be indicative of a departure from the Hardy–Weinberg equilibrium, explained by selective pressure causing a possible recent population

contraction (Manawasinghe et al. 2019). This is validated by high F_{ST} values for the populations of *D. novem* ($F_{ST} = 0.99$) indicating that this species is producing a large number of offspring, leading to individuals within the population being quite related to the ancestry with a low allelic frequency (Linde 2010). In contrast, *D. malorum* populations gave negative F_{ST} values ($F_{ST} = -0.21$). These results are indicative of high levels of gene flow among individuals over a large geographic range, preventing the formation of gene pools (Bortolotto et al. 2011). This is also corroborated by the network analyses (Fig. 6), where we clearly show a wide distribution of *D. malorum* across several regions in the country.

Another problem also encountered in the genus *Diaporthe*, is the notable disagreement of the optimal set of loci to be used for species identification, as multiple studies have used different gene combinations to resolve the species boundaries in this genus (Gao et al. 2015, 2016, 2017; Udayanga et al. 2014a, b; Yang et al. 2018). Given that *Diaporthe* contains numerous cryptic species and harbors a high intraspecific variability, it has been suggested in previous studies that a multi-locus sequence analyses including the ITS, *tef1- α* , *tub2*, *his3* and *cal* genes should always be considered (Gomes et al. 2013; Santos et al. 2017a). Although the ITS performs poorly for species resolution in some genera, due to either high intraspecific variability or low interspecific variability (or both), it is still widely used (Baturó-Cieśniewska et al. 2020; Crous et al. 2021; Lücking et al. 2020; Udayanga et al. 2014a). This is mainly due to the high availability of ITS sequences in public databases and the limited number of sequences of additional markers for some taxa (Crous et al. 2021; Hongsanan et al. 2018). However, one of the main problems of using the ITS region in *Diaporthe*, is the high intraspecific variability in this region that has been regarded as indicative to describe new taxa (Gao et al. 2017; Udayanga et al. 2014a). For example, several authors have been describing new species based solely on ITS (Dayarathne et al. 2020; Li et al. 2020), ITS, *tef1- α* or *tub2* (Wrona et al. 2020), ITS and *tub2* (Nabetani et al. 2017) or ITS and *tef1- α* (Cardinaals et al. 2018), without analyzing the existence of intraspecific variability. Therefore, it is of paramount importance that phylogenetic analyses always be cautiously interpreted to avoid the overestimation of species diversity (Gao et al. 2017).

Guidelines for an appropriate species delimitation in the genus Diaporthe.

In the present study we propose some recommendations for a most suitable species delimitation in the genus *Diaporthe*, considering the guidelines previously provided by Jeewon and Hyde (2016) and more recently by Crous et al. (2021):

1. It is important to adopt a large sampling size and add as many isolates as possible to determine intraspecific variation (Liu et al. 2016).
2. It is recommended that ITS sequence data should be carefully interpreted. Although Vu et al. (2019) have predicted that 99.6% is the optimal identity threshold to discriminate filamentous fungal species, there is no consensus on the percent identity that is needed for a confident identification (Crous et al. 2021). For instance, while in the genus *Ceraceosorus* ITS identity within species was found to be less than 90% (Kijpornyongpan and Aime 2016), a genomic study of *Hypoxylon fragiforme* showed that ITS paralogs shared less than 97% identity within a genome (Stadler et al. 2020). Likewise, in the present study we have shown that sequences from individuals of the same species may differ by 3.0% to 9.4%, and that ITS paralogs were observed to have a variation by up to 14%.
3. To avoid the overestimation of fungal species, the Genealogical Concordance Phylogenetic Species Concept principle must be applied. This method relies in the comparison of individual gene genealogies to identify concordant branches between them (Taylor et al. 2000). Thus, gene genealogies must result in similar topologies when using Maximum Parsimony, Maximum Likelihood, and Bayesian inference (Crous et al. 2021; Hongsanan et al. 2018) with bootstrap values greater than 70% and Bayesian posterior probability values above 0.90 (Gazis et al. 2011; Taylor et al. 2000).
4. Phylogenetic relationships of novel taxa should also include a comparison with closely related taxa whenever available, to determine nucleotide differences between sister taxa (Jeewon & Hyde 2016).
5. Although the Phylogenetic Species Concept has been widely applied in the description of new species and unveiled cryptic speciation in the

genus *Diaporthe* (Fan et al. 2018; Udayanga et al. 2014a, b), molecular data combined with morphological characteristics should also be favored, as has been already applied in this genus, providing a more robust framework to establish novel species (Gomes et al. 2013; Gao et al. 2017; Guarnaccia et al. 2018; Guo et al. 2020; Mostert et al. 2001; Yang et al. 2018).

6. An integrative approach including also coalescent-based methods and analyses to detect recombination allows a more robust and reliable delimitation of species in *Diaporthe* (Hilário et al. 2021a, b).

CONCLUSIONS

Even though the ITS region seems to be effective for species identification in several genera, we cannot assume that it will work equally well with all the species in any given genus. In this study we have shown that both intraspecific and intragenomic variation of the ITS region occurs in *Diaporthe* more often than it is reported in literature, thus questioning its validity for molecular identification. Moreover, we have demonstrated that ITS shows a high variability that may be explained by a failure of concerted evolution, ongoing speciation events or intergenomic recombination among individuals of the same species. This study is also the first to report a possible hybridization in the genus *Diaporthe* that deserves further investigation, as hybridization plays an important role in the potential spread of pathogenicity traits and in the evolution of new pathogenic lineages with important ecological adaptations. Furthermore, genetic analysis of a more global range of *D. portugallica* and *D. phillipsii* and the use of more variable molecular markers would be essential to establish if this suspected interspecific hybridization has occurred regularly or whether it was a single event. Taking all this into consideration, we recommend that the ITS region must be analyzed carefully prior to new species description. In addition, we endorse the importance of sequencing other loci such as *tef1- α* , *tub2*, *his3* and *cal*, as multi-locus DNA analyses have revealed a promising approach to delineate species boundaries in *Diaporthe*.

The above findings have illustrated that ITS, the most variable region of the ribosomal genes may harbor some pitfalls and therefore, should be cautiously

analyzed before drawing any conclusions regarding the identity of a possibly new taxa. Moreover, the examples of polymorphic rRNA sequences that we have shown to occur in the genus *Diaporthe* should not be ignored and should be thoroughly examined in other groups of filamentous fungi. Phylogenomic analyses may also be helpful in future studies to resolve incongruent phylogenetic relationships and to better estimate species diversity in fungi, rather than recognize novel taxa based on ITS sequences.

ACKNOWLEDGMENTS

Thanks are due to the Portuguese Foundation for Science and Technology (FCT/MCTES) for the financial support to CESAM (Centro de Estudos do Ambiente e do Mar) (UIDB/AMB/50017/2020 + UIDP/AMB/50017/2020) through national funds, and the PhD grant of Sandra Hilário (SFRH/BD/137394/2018). Liliana Santos is funded by national funds (OE), through FCT in the scope of the framework contract foreseen in the numbers 4, 5 and 6 of the article 23, of the Decree-Law 57/2016, of August 29, changed by Law 57/2017, of July 19. Alan JL Phillips acknowledges the support from UIDB/04046/2020 and UIDP/04046/2020 Centre grants from FCT, Portugal (to BioISI).

The authors are thankful to Hugo Botelho and Pedro Pinho (Bfruit Nature Flavors), Hugo Lains (WePlant in Portugal), Jorge Duarte (Hortitool Consulting, Lda), João Vieira, António Rodrigues, Marcelo Miranda and Monica (Groselh&Mirtilo) for kindly supplying the blueberry plants from their plantations. We want also to acknowledge Eduardo Batista (PhD student, University of Aveiro) for the samples collected from Ponte da Barca and Penafiel.

REFERENCES

- Baturo-Cieśniewska A, Pusz W, Patejuk K. **2020**. Problems, limitations, and challenges in species identification of Ascomycota members on the basis of ITS regions. *Acta Mycologia* 55, 1–18.
- Bortolotto E, Bucklin A, Mezzavilla M, Zane L, Patarnello T. **2011**. Gone with the currents: lack of genetic differentiation at the circum-continental scale in the Antarctic krill *Euphausia superba*. *BMC Genetetics* 12, 1–18.

- Brayford D. **1990**. Variation in *Phomopsis* isolates from *Ulmus* species in the British Isles and Italy. *Mycological Research* 94, 691–697.
- Cardinaals J, Wenneker M, Voogd JGB, van Leeuwen GCM. **2018**. Pathogenicity of *Diaporthe* spp. on two blueberry cultivars (*Vaccinium corymbosum*). *Bulletin OEPP/EPPO* 48, 128–134.
- Chiang TY, Hong KH, Peng CI. **2001**. Experimental hybridization reveals biased inheritance of the internal transcribed spacer of the nuclear ribosomal DNA in *Begonia xtaipeiensis*. *International Journal of Plant Research* 114, 343–351.
- Crous PW, Rossman AY, Aime C, Allen C, Burgess T, Groenewald JZ, Castlebury L, **2021**. Names of phytopathogenic fungi: a practical guide. *Phytopathology* 111, 1500–1508.
- Cruywagen EM, Slippers B, Roux J, Wingfield MJ. **2017**. Phylogenetic species recognition and hybridisation in *Lasiodiplodia*: a case study on species from baobabs. *Fungal Biology* 121, 420–436.
- Dayarathne MC, Jones EBG, Maharachchikumbura SSN, Devadatha B, Sarma VV, Khongphinitbunjong K, Chomnunti P, Hyde KD. **2020**. Morpho-molecular characterization of microfungi associated with marine based habitats. *Mycosphere* 11, 1–188.
- Dissanayake AJ, Phillips AJL. **2017**. Advances in understanding *Diaporthe* (Editorial). *Mycosphere*, 8, 7019.
- Fan X, Yang Q, Bezerra JD, Alvarez LV, Tian C. **2018**. *Diaporthe* from walnut tree (*Juglans regia*) in China, with insight of the *Diaporthe eres* complex. *Mycological Progress* 17, 841–853.
- Fell JW, Scorzetti G, Stätzell-Tallman A, Boundy-Mills K. **2007**. Molecular diversity and intragenomic variability in the yeast genus *Xanthophyllomyces*: the origin of *Phaffia rhodozyma*? *FEMS Yeast Research* 7, 1399–1408.
- Gao Y, Liu F, Duan W, Crous PW, Cai L. **2017**. *Diaporthe* is paraphyletic. *IMA Fungus* 8, 163–187.
- Gazis R, Rehner S, Chaverri P. **2011**. Species delimitation in fungal endophyte diversity studies and its implications in ecological and biogeographic inferences. *Molecular Ecology* 20, 3001–3013.

- Gomes RR, Glienke C, Videira SIR, Lombard L, Groenewald JZ, Crous PW. **2013**. *Diaporthe*: A genus of endophytic, saprobic and plant pathogenic fungi. *Persoonia* 31, 1–41.
- Guarnaccia V, Crous PW. **2018**. Emerging citrus diseases in Europe, caused by species of *Diaporthe*. *IMA Fungus* 8, 317–334.
- Guarnaccia V, Groenewald JZ, Woodhall J, Armengol J, Cinelli T, Eichmeier A, Ezra D, Fontaine F, Gramaje D, Gutierrez-Aguirregabiria A, ... Crous PW. **2018**. *Diaporthe* diversity and pathogenicity revealed from a broad survey of grapevine diseases in Europe. *Persoonia* 40, 135–153.
- Guo YS, Crous PW, Bai Q, Fu M, Yang MM, Wang XH, Du YM, Hong N, Xu WX, Wang GP. **2019**. High diversity of *Diaporthe* species associated with pear shoot canker in China. *Persoonia* 45, 132–162.
- Harrington TC, Kazmi MR, Al-Sadi AM, Ismail SI. **2014**. Intraspecific and intragenomic variability of ITS rDNA sequences reveals taxonomic problems in *Ceratocystis fimbriata* sensu stricto. *Mycologia* 106, 224–242.
- Hibbett DS, Ohman A, Glotzer D, Nuhn M, Kirk P, Nilsson RH. **2011**. Progress in molecular and morphological taxon discovery in fungi and options for formal classification of environmental sequences. *Fungal Biology Reviews* 25, 38–47.
- Hilário S, Amaral AI, Gonçalves MFM, Lopes A, Santos L, Alves A. **2020**. Diversity and pathogenicity of *Diaporthe* species on blueberry plants in Portugal, with description of 4 new species. *Mycologia* 112, 293–308.
- Hilário S, Gonçalves MFM, Alves A. **2021a**. Using genealogical concordance and coalescent-based species delimitation to assess species boundaries in the *Diaporthe eres* complex. *Journal of Fungi* 7, 507.
- Hilário S, Santos L, Alves A. **2021b**. *Diaporthe amygdali*, a species complex or a complex species?. *Fungal Biology* 125, 505–518.
- Hosseini B, El-Hasan A, Link T, Voegelé RT. **2020**. Analysis of the species spectrum of the *Diaporthe/Phomopsis* complex in European soybean seeds. *Mycological Progress* 19, 455–469.
- Hughes KW, Tulloss RH, Petersen RH. **2018**. Intragenomic nuclear RNA variation in a cryptic *Amanita* taxon. *Mycologia* 110, 93–103.

- Jeewon R, Hyde KD. **2016**. Establishing species boundaries and new taxa among fungi: recommendations to resolve taxonomic ambiguities. *Mycosphere* 7, 1669–1677.
- Kanzi AM, Trollip C, Wingfield MJ, Barnes I, Van der Nest MA, Wingfield BD. **2020**. Phylogenomic incongruence in *Ceratocystis*: a clue to speciation?. *BMC Genomics* 21, 1–11.
- Kijpornyongpan T, Aime MC. **2016**. Rare or rarely detected? *Ceraceosorus guamensis* sp. nov.: A second described species of *Ceraceosorales* and the potential for underdetection of rare lineages with common sampling techniques. *Antonie van Leeuwenhoek* 109, 127–1139.
- Kovács GM, Balázs TK, Calonge FD, Martin MP. **2011**. The diversity of *Terfezia* desert truffles: new species and a highly variable species complex with intrasporocarpic nrDNA ITS heterogeneity. *Mycologia* 103, 841–853.
- Leigh JW, Bryant D. **2015**. POPART: full-feature software for haplotype network construction. *Methods in Ecology and Evolution* 6, 1110–1116.
- Li W-J, McKenzie EHC, Liu J-KJ, Bhat DJ, Dai DQ, Camporesi E, Tian Q, Maharachchikumbura SSN, Luo ZL, Shang Q-J, ... Hyde KD. **2020**. Taxonomy and phylogeny of hyaline-spored coelomycetes. *Fungal Diversity* 100, 279–801.
- Li Y, Jiao L, Yao YJ. **2013**. Non-concerted ITS evolution in fungi, as revealed from the important medicinal fungus *Ophiocordyceps sinensis*. *Molecular Phylogenetics and Evolution* 68, 373–379.
- Li Y, Yang RH, Jiang L, Hu XD, Wu ZJ, Yao YJ. **2017**. rRNA pseudogenes in filamentous ascomycetes as revealed by genome data. *G3: Genes, Genomes, Genetics* 7, 2695–2703.
- Librado P, Rozas J. **2009**. DnaSPv5: a software for comprehensive analysis of DNA polymorphism data. *Bioinformatics* 25, 1451–1452.
- Linde CC. **2010**. Population genetic analyses of plant pathogens: new challenges and opportunities. *Australasian Plant Pathology* 39, 23–28.
- Lindner DL, Banik MT. **2011**. Intragenomic variation in the ITS rDNA region obscures phylogenetic relationships and inflates estimates of operational taxonomic units in genus *Laetiporus*. *Mycologia* 103, 731–740.

- Liu F, Wang M, Damm U, Crous PW, Cai L. **2016**. Species boundaries in plant pathogenic fungi: a *Colletotrichum* case study. *BMC Evolutionary Biology* 16, 81.
- Lombard L, Van Leeuwen GCM, Guarnaccia V, Polizzi G, Van Rijswijk PCJ, Rosendahl CHM, Gabler J, Crous PW. **2014**. *Diaporthe* species associated with *Vaccinium*, with specific reference to Europe. *Phytopathologia Mediterranea* 53, 287–299.
- Lopes AF, Batista E, Hilário S, Santos L, Alves A. **2021**. Occurrence of *Diaporthe* species in *Eucalyptus globulus*, *Pinus pinaster* and *Quercus suber* in Portugal. *Forest Pathology* 51, e12674.
- Lücking R, Aime MC, Robbertse B, Miller AN, Ariyawansa HA, Aoki T, Cardinali G, Crous PW, Druzhinina IS, Geiser DM, ... Schoch CL. **2020**. Unambiguous identification of fungi: where do we stand and how accurate and precise is fungal DNA barcoding?. *IMA Fungus* 11, 1–32.
- Manawasinghe IS, Dissanayake A, Li X, Liu M, Wanasinghe D, Xu J, Zhao W, Zhang W, Zhou Y, Hyde K, ... Yan J. **2019**. High genetic diversity and species complexity of *Diaporthe* associated with grapevine dieback in China. *Frontiers in Microbiology* 10, 1936.
- Mostert L, Crous PW, Kang JC, Phillips AJL. **2001**. Species of *Phomopsis* and a *Libertella* sp. occurring on grapevines with specific reference to South Africa: morphological, cultural, molecular and pathological characterization. *Mycologia* 93, 146–167.
- Murali T, Suryanarayanan T, Geeta R. **2006**. Endophytic *Phomopsis* species: host range and implications for diversity estimates. *Canadian Journal of Microbiology* 52, 673–680.
- Nabetani K, Wood BK, Sabaratnam S. **2017**. Role of pycnidia in twig and blossom blight and stem dieback of highbush blueberry caused by *Phomopsis vaccinii* in British Columbia. *Canadian Journal of Plant Pathology* 39, 405–421.
- Nilsson RH, Kristiansson E, Ryberg M, Hallenberg N, Larsson KH. **2008**. Intraspecific ITS variability in the kingdom *Fungi* as expressed in the international sequence databases and its implications for molecular species identification. *Evolutionary Bioinformatics* 4, EBO–S653.

- O'Donnell K, Cigelnik E. **1997**. Two divergent intragenomic rDNA ITS2 types within a monophyletic lineage of the fungus *Fusarium* are nonorthologous. *Molecular Phylogenetics and Evolution* 7, 103–116
- Olson Å, Stenlid J. **2002**. Pathogenic fungal species hybrids infecting plants. *Microbes and Infection* 4, 1353–1359.
- Rehner SA, Uecker FA. **1994**. Nuclear ribosomal internal transcribed spacer phylogeny and host diversity in the coelomycetes *Phomopsis*. *Canadian Journal of Botany* 72, 1666–1674.
- Santos JM, Correia VG, Phillips AJL. **2010**. Primers for mating-type diagnosis in *Diaporthe* and *Phomopsis*: their use in teleomorph induction in vitro and biological species definition. *Fungal Biology* 114, 255–270.
- Santos JM, Vrandečić K, Cosić J, Duvnjak T, Phillips AJL. **2011**. Resolving the *Diaporthe* species occurring on soybean in Croatia. *Persoonia* 27, 9–19.
- Santos L, Alves A, Alves R. **2017a**. Evaluating multi-locus phylogenies for species boundaries determination in the genus *Diaporthe*. *Peer J* 5, e3120.
- Santos L, Phillips AJL, Crous PW, Alves A. **2017b**. *Diaporthe* species on Rosaceae with descriptions of *D. pyracanthae* sp. *Mycosphere* 8, 485–511.
- Schoch CL, Seifert KA, Huhndorf S, Robert V, Spouge JL, Levesque CA, Chen W, Fungal Barcoding Consortium. **2012**. Nuclear ribosomal internal transcribed spacer (ITS) region as universal DNA barcode marker for Fungi. *Proceedings of the National Academy of Sciences USA* 109, 6241–6246.
- Simon UK, Weiß M. **2008**. Intragenomic variation of fungal ribosomal genes is higher than previously thought. *Molecular and Biology Evolution* 25, 2251–2254.
- Smith ME, Douhan GW, Rizzo DM. **2007**. Intra-specific and intra-sporocarp ITS variation of ectomycorrhizal fungi as assessed by rDNA sequencing of sporocarps and pooled ectomycorrhizal roots from a *Quercus* woodland. *Mycorrhiza* 18, 15–22.
- Stadler M, Hawksworth DL, Fournier J. **2014**. The application of the name *Xylaria hypoxylon*, based on *Clavaria hypoxylon* of Linnaeus. *IMA Fungus* 5, 57–66.

- Stadler M, Lambert C, Wibberg D, Kalinowski J, Cox RJ, Kolařík M, Kuhnert E. **2020**. Intragenomic polymorphisms in the ITS region of high-quality genomes of the *Hypoxylaceae* (Xylariales, Ascomycota). *Mycological Progress* 19, 235–245.
- Tajima F. **1989**. Statistical method for testing the neutral mutation hypothesis by DNA polymorphism. *Genetics* 123, 585–595.
- Taylor JW, Jacobson DJ, Kroken S, Ka T, Geiser DM, Hibbett DS, Fisher MC. **2000**. Phylogenetic species recognition and species concepts in fungi. *Fungal Genetics and Biology* 31, 21–32.
- Torres C, Camps R, Aguirre R, Besoain XA. **2016**. First report of *Diaporthe rudis* in Chile causing stem-end rot on ‘Hass’ avocado fruit imported from California, USA. *Plant Disease* 100, 1951.
- Tremble K, Suz LM, Dentinger BT. **2019**. Lost in Translation: population genomics and long-read sequencing reveals relaxation of concerted evolution of the ribosomal DNA cistron. *bioRxiv* 811216.
- Udayanga D, Castlebury LA, Rossman AY, Chukeatirote E, Hyde KD. **2014a**. Insights into the genus *Diaporthe*: phylogenetic species delimitation in the *D. eres* species complex. *Fungal Diversity* 67, 203–229.
- Udayanga D, Castlebury LA, Rossman A, Hyde KD. **2014b**. Species limits in *Diaporthe*: a molecular reassessment of *D. citri*, *D. cytospora*, *D. foeniculina* and *D. rudis*. *Persoonia* 32, 83–101.
- Udayanga D, Liu X, McKenzie EHC, Chukeatirote E, Bahkali AHA, Hyde KD. **2011**. The genus *Phomopsis*: Biology, applications, species concepts and names of common phytopathogens. *Fungal Diversity* 50, 189–225.
- Uecker FA. **1988**. A world list of *Phomopsis* names with notes on nomenclature, morphology and biology. *Mycologia Memoir* 13, 1–231.
- Vu D, Groenewald M, de Vries M, Gehrman T, Stielow B, Eberhardt U, Al-Hatmi A, Groenewald JZ, Cardinali G, Houbraeken J, ... Verkley GJM. **2019**. Large-scale generation and analysis of filamentous fungal DNA barcodes boosts coverage for kingdom Fungi and reveals thresholds for fungal species and higher taxon delimitation. *Studies in Mycology* 92, 135–154.
- Wright S. **1951**. The genetical structure of populations. *Annals of Eugenics* 15, 323–354.

- Wrona CJ, Mohankumar V, Schoeman MH, Tan YP, Shivas RG, Jeff-Ego OS, Akinsanmi OA. **2020**. *Phomopsis* husk rot of macadamia in Australia and South Africa caused by novel *Diaporthe* species. *Plant Pathology* 69, 911–921.
- Wu ZW, Wang QM, Liu XZ, Bai FY. **2016**. Intragenomic polymorphism and intergenomic recombination in the ribosomal RNA genes of strains belonging to a yeast species *Pichia membranifaciens*. *Mycology* 7, 102–111.
- Xu TC, Lu YH, Wang JF, Song ZQ, Hou YG, Liu SS, Liu CS, Wu SH. **2021**. Bioactive secondary metabolites of the genus *Diaporthe* and anamorph *Phomopsis* from terrestrial and marine habitats and endophytes: 2010–2019. *Microorganisms* 9, 217.
- Yan DH, Song X, Li H, Luo T, Dou G, Strobel G. **2018**. Antifungal activities of volatile secondary metabolites of four *Diaporthe* strains isolated from *Catharanthus roseus*. *Journal of Fungi* 4, 65.
- Yang Q, Fan X-L, Guarnaccia V, Tian C-M. **2018**. High diversity of *Diaporthe* species associated with dieback diseases in China, with twelve new species described. *MycKeys* 39, 97–149.
- Zhao Y, Tsang CC, Xiao M, Cheng J, Xu Y, Lau SK, Woo PC. **2015**. Intra-genomic internal transcribed spacer region sequence heterogeneity and molecular diagnosis in clinical microbiology. *International Journal of Molecular Sciences* 16, 25067–25079.

SUPPLEMENTARY MATERIAL

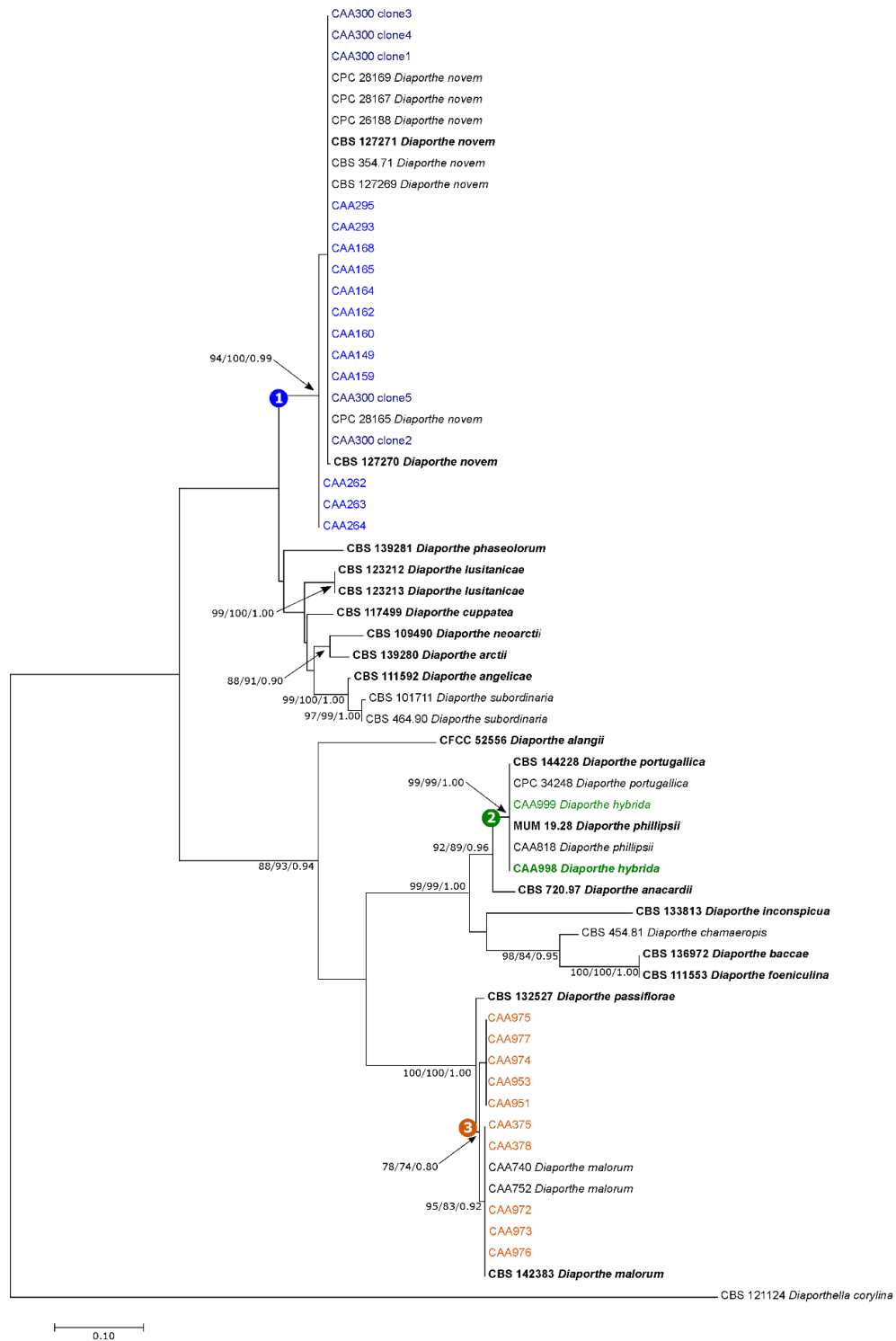


Figure S1. Maximum Likelihood phylogenetic tree obtained from *tef1-α* sequences data from *Diaporthe* species. The tree was built using the Hasegawa–Kishino–Yano parameter model a gamma distribution and rooted to *Diaporthella corylina*. ML/MP/PP bootstrap support and posterior probabilities values are given at the nodes. The values are shown only for those nodes that received support in at least two of the phylogenetic inference methods. Ex-type isolates are in bold.

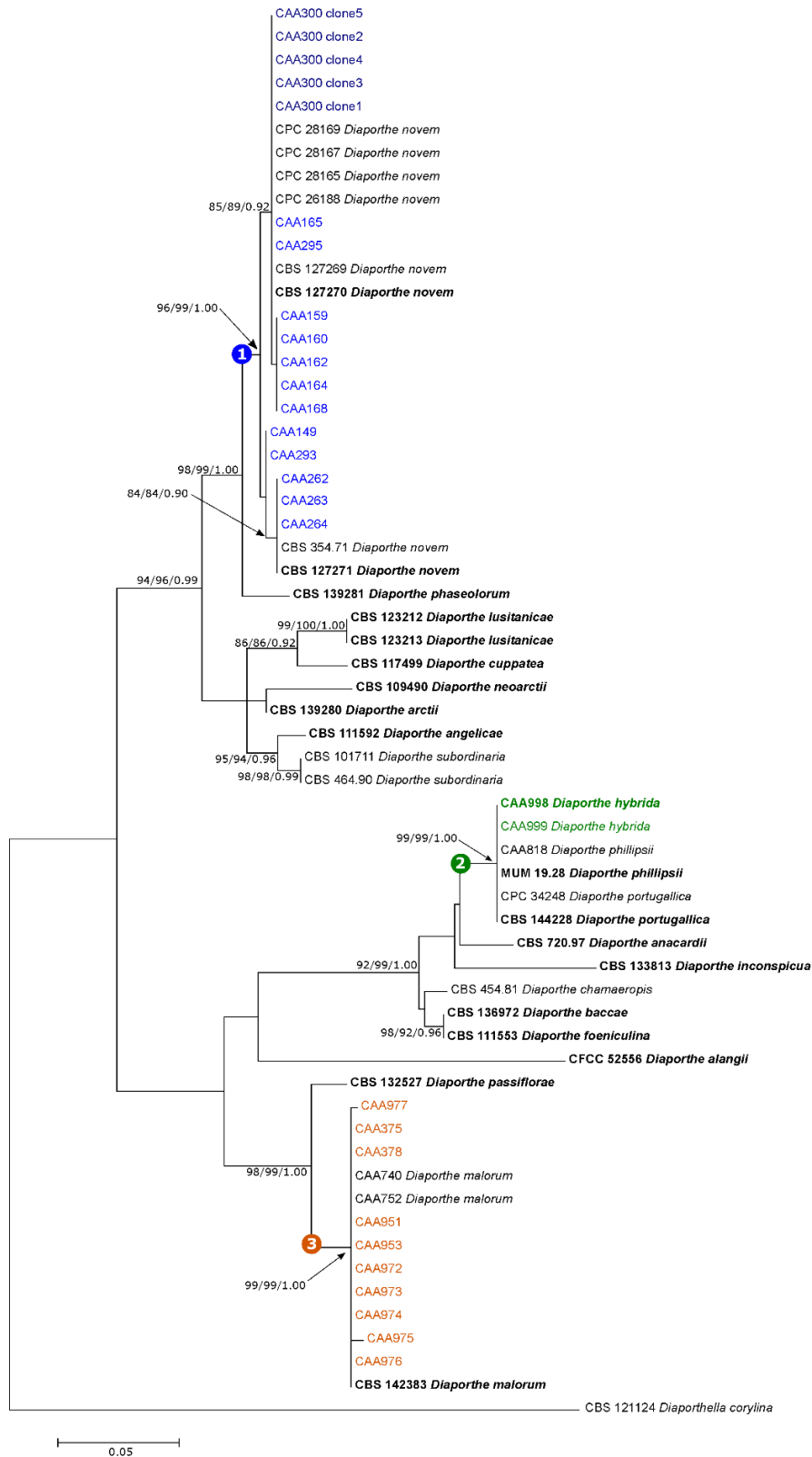


Figure S2. Maximum Likelihood phylogenetic tree obtained from *tub2* sequences data from *Diaporthe* species. The tree was built using the Tamura 3-parameter model assuming a gamma distribution and rooted to *Diaporthella corylina*. ML/MP/PP bootstrap support and posterior probabilities values are given at the nodes. The values are shown only for those nodes that received support in at least two of the phylogenetic inference methods. Ex-type isolates are in bold.

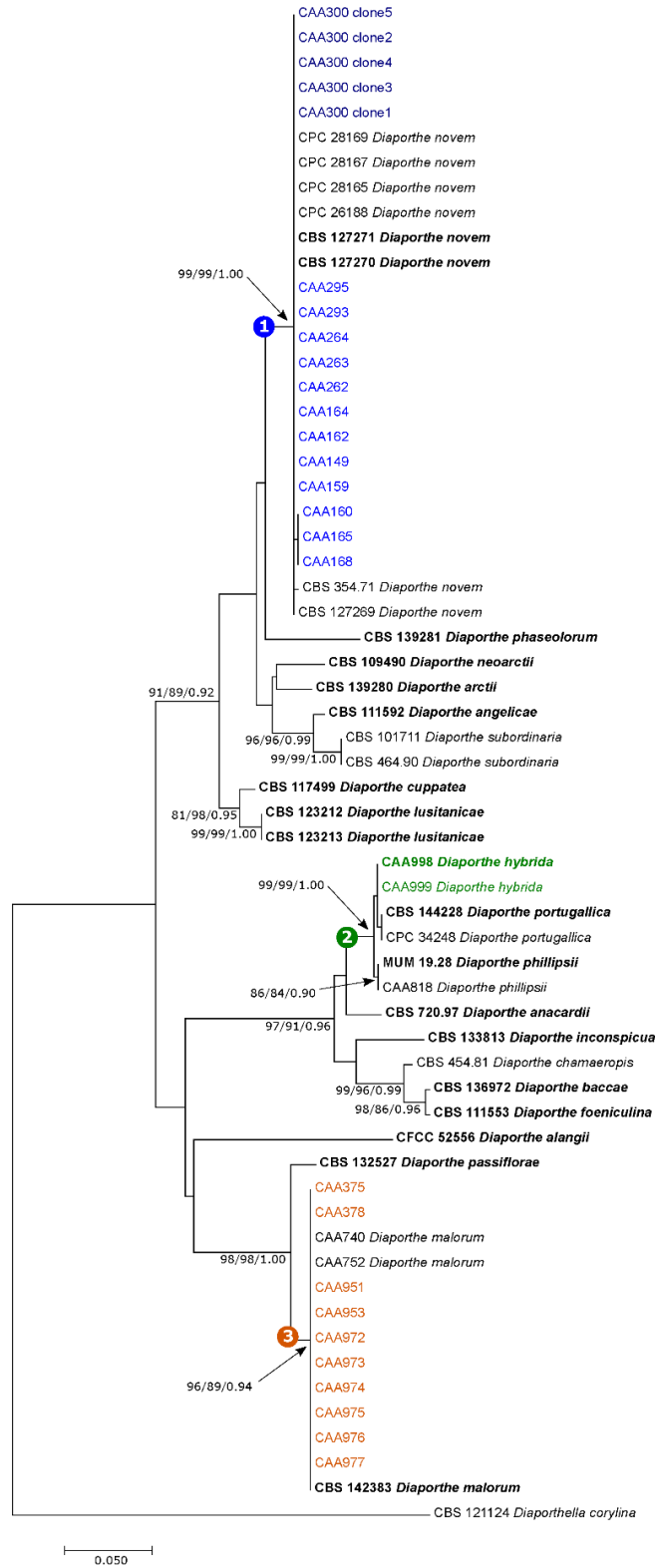


Figure S3. Maximum Likelihood phylogenetic tree obtained from *his3* sequences data from *Diaporthe* species. The tree was built using the Tamura-Nei parameter model assuming a gamma distribution and rooted to *Diaporthella corylina*. ML/MP/PP bootstrap support and posterior probabilities values are given at the nodes. The values are shown only for those nodes that received support in at least two of the phylogenetic inference methods. Ex-type isolates are in bold.

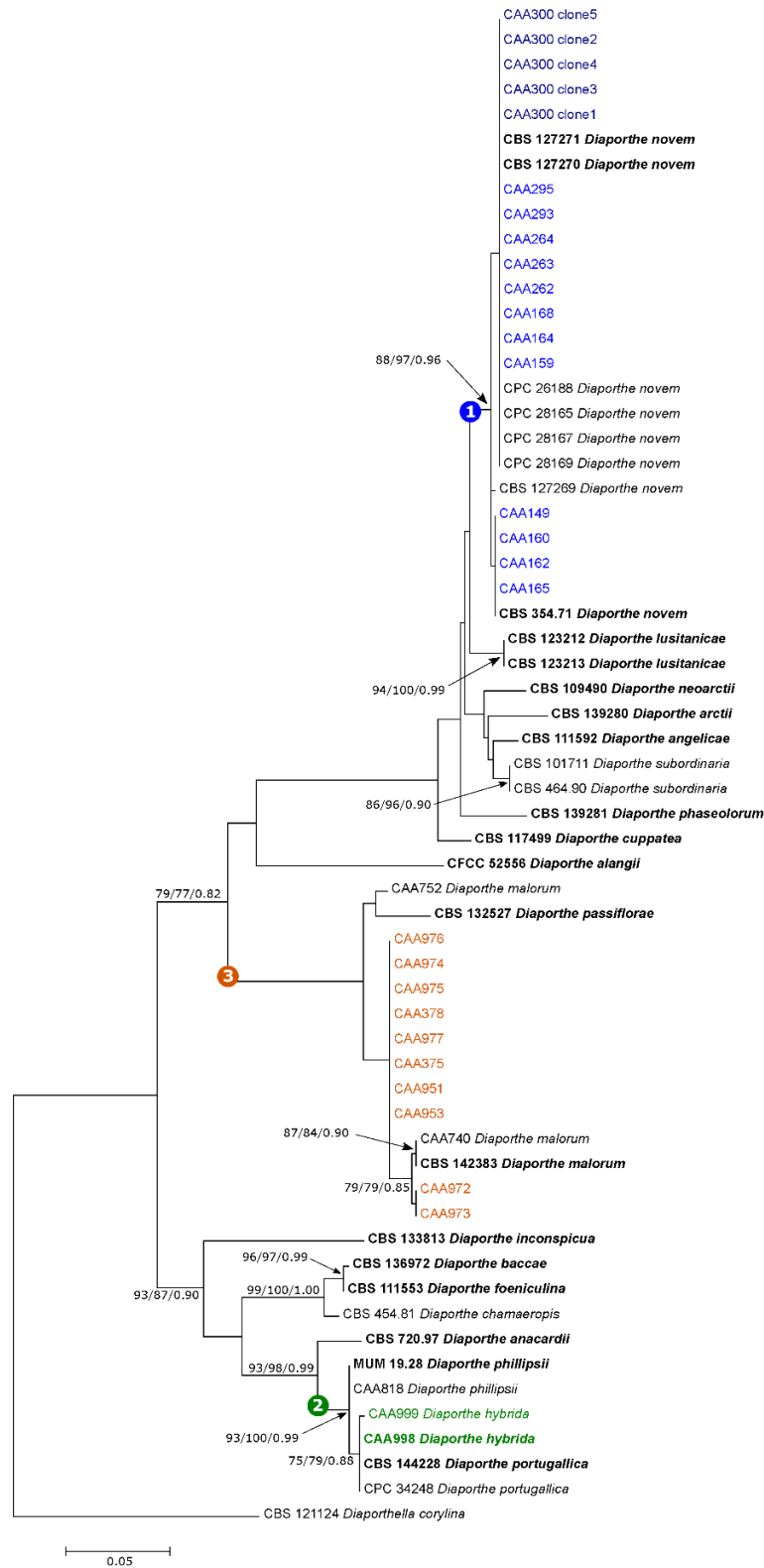


Figure S4. Maximum Likelihood phylogenetic tree obtained from *cal* sequences data from *Diaporthe* species. The tree was built using the Tamura 3-parameter model assuming invariant sites and rooted to *Diaporthella corylina*. ML/MP/PP bootstrap support and posterior probabilities values are given at the nodes. The values are shown only for those nodes that received support in at least two of the phylogenetic inference methods. Ex-type isolates are in bold.

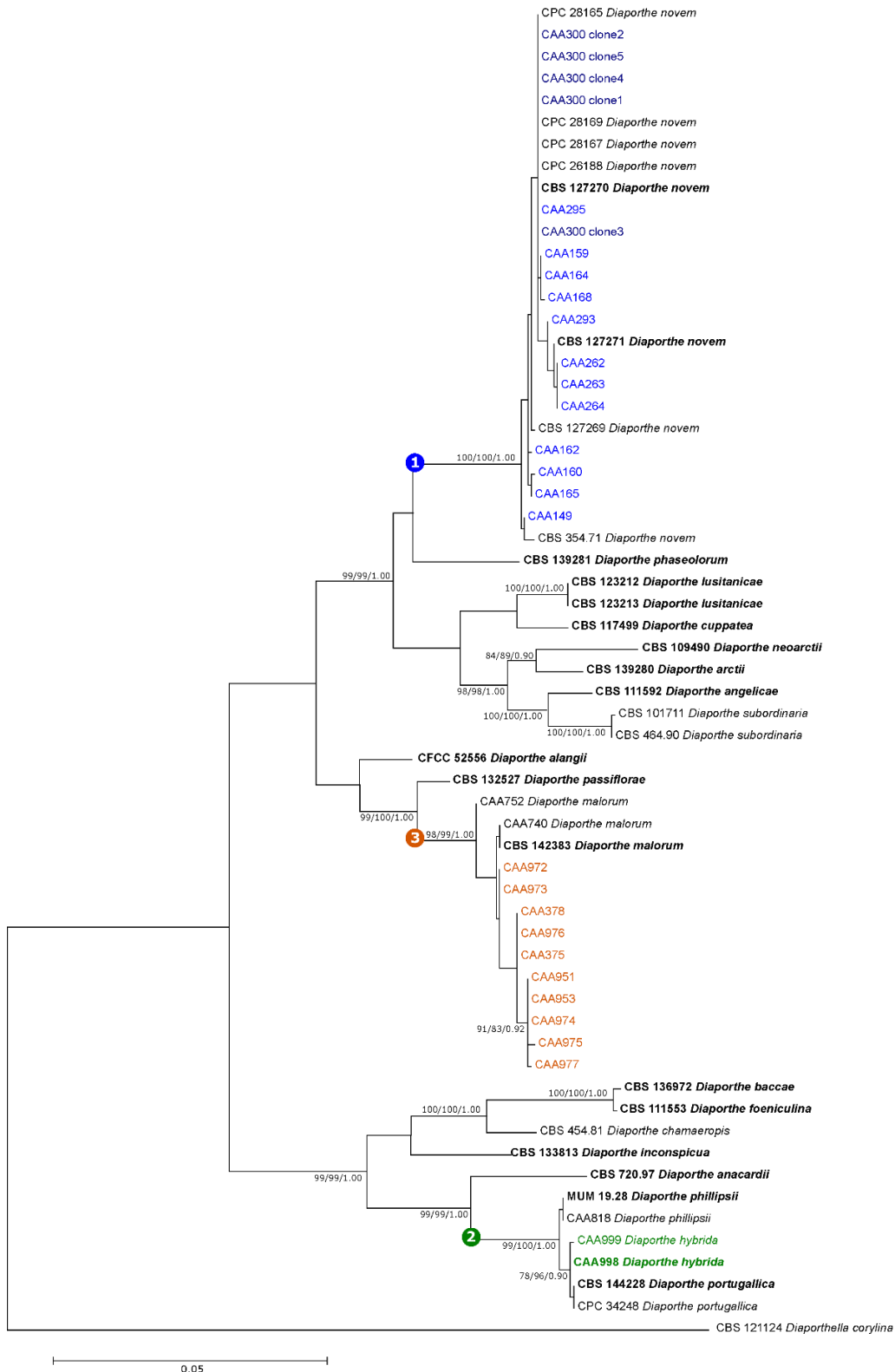



Figure S5. Maximum Likelihood phylogenetic tree obtained from *tef1- α* , *tub2*, *his3* and *cal* sequences data from *Diaporthe* species. The tree was built using the Tamura-Nei parameter model assuming a gamma distribution and rooted to *Diaporthella corylina*. ML/MP/PP bootstrap support and posterior probabilities values are given at the nodes. The values are shown only for those nodes that received support in at least two of the phylogenetic inference methods. Ex-type isolates are in bold.



CHAPTER 5

Physiological performance of blueberries under biotic
and abiotic stresses



The impact of two *Diaporthe* spp. on *Vaccinium corymbosum* physiological performance under different water availability scenarios

Hilário S, Pinto G, Monteiro P, Santos L, Alves A.

European Journal of Plant Pathology (in press)

ABSTRACT

Blueberries (*Vaccinium corymbosum* L.) are cultivated worldwide and represent an important asset for the Portuguese economy. Pathogens infection and water deficit are known to affect crops productivity worldwide, thus limiting plant yield or fruit quality. *Diaporthe* is a cosmopolitan genus comprising plant pathogens and endophytes, that may switch their behavior to a pathogenic phase when the host is under environmental stimuli (e.g., drought, precipitation). Given the scarce physiological studies on blueberry plant-pathogen interactions, in this study we aimed to evaluate the effect of *Diaporthe amygdali* and *D. eres* on 9-month-old clonal blueberries under two different water scenarios: well-watered (WW) and water deficit (WD). Morphological (lesion length) and physiological parameters (water status, leaf gas exchange, photosynthetic pigments, proline, phenolic compounds, flavonoids, starch, total soluble sugars, and lipid peroxidation) were assessed. Our results suggest that the irrigation regime applied was not sufficient to cause a severe stress on plants. Under WW conditions, plants inoculated with *D. eres* may have used malondialdehyde content (MDA) as a signaling molecule. Although *D. amygdali* has caused plant mortality, this study demonstrates that under WW conditions, plants manage to deal with pathogen attack, thus maintaining their physiological performance. This study also demonstrates that the interaction between fungal pathogens and water limitations seem to stimulate plant defense, through the accumulation of proline. Our findings offer crucial insights to understand how blueberry plants cope with the infection by species of *Diaporthe*, and how plants can adapt to climate changes in the Mediterranean area (e.g., water scarcity).

Keywords: blueberry; *Diaporthe amygdali*; *Diaporthe eres*; plant performance; plant-pathogen interaction; water limitation

INTRODUCTION

Blueberries (*Vaccinium corymbosum* L.) are a small-fruit crop largely cultivated and commercialized due to their fruits' health benefits (Silva et al. 2020). In Portugal, blueberry production has increased during the last 20 years, being currently the 7th biggest producer worldwide (FAOSTAT 2022), with a total planted area of 2490 ha and a production of 15 418 tons (INE 2021). In Europe the total blueberry production increased from 47 970 tons in 2010 to 168 472 tons in 2020 (FAOSTAT 2022), due to the efforts to develop new genotypes more adapted to several climates, such as the Mediterranean (Mazzoni et al. 2020).

The reported decrease of rainfall has limited the availability of water, which has proven to be a problem in crops from the Mediterranean region (del Pozo et al. 2019). This situation is especially serious for the root-hairless blueberry plants, which are rapidly affected by water deprivation, leading to a reduction of their growth and fruit quality (Jiménez-Donaire et al. 2020). In this regard, such topic has attracted the attention of researchers in the last years. Recent studies have evaluated the response of blueberry plants to drought stress aiming to understand its effect in yield and fruit quality (Ortega-Farias et al. 2021), to select drought resistant cultivars (Balboa et al. 2020), and to validate if propagation methods have a role in plants' response (Mazurek et al. 2021). Although seldom explored, a few studies assessed blueberry fitness in response to water deficit. These studies reported a decrease in shoot growth (Mingeau et al. 2001), stomatal closure and reduction in gas exchange (Rho et al. 2012), low water potentials (Lobos et al. 2018) and decreased chlorophyll concentration (Yu et al. 2015).

The dissemination of pathogens is another threat causing severe economic losses in agriculture (Baldi and Porta 2020). *Diaporthe* is one of the most common genera of endophytic fungi or latent pathogens, found in a wide range of hosts (Gomes et al. 2013; Hilário et al. 2020). It is worth mentioning that this "friendly" behavior may switch to a pathogenic stage that can occur in situations in which the host fitness may be compromised (e.g., excessive pruning, lack of rainfall) (Hrycan et al. 2020). Most of the studies on the pathogenicity on blueberry plants are solely based on the evaluation of the symptoms and disease development under optimal growth conditions (Cardinaals et al. 2018; Guarnaccia et al. 2021; Hilário et al.

2020). In a recent study, Hilário et al. (2021b) showed that *D. amygdali* strain CAA958 was one of the most aggressive species to blueberry plants, while *Diaporthe eres* strain CBS 160.32 (syn. *D. vaccinii*), no longer listed as a quarantine organism (EU Regulation 2019/2072), was confirmed to cause minor symptoms. Although Roloff et al (2004) demonstrated that photosynthetic rates on blueberry plants decreased in the presence of the fungus *Septoria albopunctata*, the interaction of the pathosystem *V. corymbosum*/*Diaporthe* spp. is yet to be unveiled.

In the field, stresses rarely occur independently. Drought stress can have different outcomes on plant performance such as increase the plant susceptibility to pathogens by triggering disease outbreaks (Ghanbary et al. 2021), can provide endurance to some plants (Pandey et al. 2017) or even reduce disease susceptibility (Swinfield et al. 2012). The combination of both drought stress and fungal infection results in a complex interaction of shared and/or unique molecular and physiological responses (Sinha et al. 2019) as reported for other abiotic combination (Correia et al. 2018). The downregulation of the photosynthetic machinery (e.g., stomatal closure, turgor loss) (Hazrati et al. 2016; Morales et al. 2013), the upregulation of stress-responsive genes, and increased accumulation of osmoprotectants (e.g., proline, carbohydrates) (Chen and Jiang 2010) are some of the molecular responses common to both stresses. These outcomes and the molecular responses mentioned above depend on the order in which drought and fungal infection are imposed, the pathogen, the timing and severity of drought, which avoid drawing solid conclusions on host-pathogen interactions (Hossain et al. 2019; Ramegowda and Senthil-Kumar, 2015).

Considering blueberry importance, the expansion of this crop into areas with water limitation (Balboa et al. 2020), the cosmopolitan behaviour of species in the genus *Diaporthe* (Dissanayake et al. 2020) and the increased plants susceptibility to *Diaporthe* infection (Hulke et al. 2019; Kim et al. 2015), it is essential to understand the host physiological responses to these environmental stimuli. This knowledge is important to further select cultivars displaying resistance to drought and to fungal infection, aiming to guarantee the sustainability of the agriculture sector (Toscano et al. 2019).

Therefore, this study was designed to explore if water limitation after inoculation changes disease progression and host-pathogen interaction using two fungal species with different levels of aggressiveness. We aimed to evaluate the physiological fitness of *V. corymbosum* cultivar 'Duke' after infection with *D. eres* strain CBS 160.32 and *D. amygdali* strain CAA958 under well-watered (WW) and water deficit conditions (WD). Symptoms progression and key morpho-physiological indicators of primary (growth) and secondary metabolism (defense) such as the water status content, leaf gas exchange related parameters, phenolic and flavonoids compounds, proline, starch, total soluble sugars and malondialdehyde content were assessed.

MATERIAL AND METHODS

Fungal isolates.

Diaporthe amygdali CAA958 was obtained from *Vaccinium corymbosum* plants sampled in a previous study on the species of *Diaporthe* occurring in association with this host in Portugal (Hilário et al. 2021b). Strain CBS 160.32 (*D. eres*, syn. *D. vaccinii*) was obtained from the Westerdijk Fungal Biodiversity Institute, Netherlands. *Diaporthe amygdali* strain CAA958 was selected once it showed to be one of the most aggressive species on blueberry plants, as described by Hilário et al. (2021b). *Diaporthe eres* CBS 160.32, formerly recognized as *D. vaccinii* (Hilário et al. 2021a), and previously listed as a quarantine organism in Europe was also selected as it proved to be less aggressive. Cultures were maintained in 15% glycerol at -80°C at the University of Aveiro (Portugal). When needed these were grown on potato dextrose agar for 7 days at 25°C (PDA, Merck, Germany).

Plant material.

Blueberry plants from cultivar 'Duke' (one the most widely cultivated in Portugal), were obtained from micropropagation from the breeding program of Deifil, Biotechnology (Braga, Portugal). Sixty clonal plants, with 9 months, were transplanted to 1L plastic pots filled with 3:2 (w/w) peat:perlite mixture. Potted plants were subjected to a 20-day acclimation period with a temperature of 25/20°C and a 16/8h (day/night) photoperiod. During the acclimatation period, plants were watered

every 2 days to maintain 75% field capacity (FC) and fertilized two times at the transplantation day and before the inoculation day with a N:P:K nutrient solution (5:8:10; Frutifol L12, Nufarm, Portugal). After the acclimation period, plants were placed inside a climate chamber (Fitoclima 1200, Aralab, Portugal), with a temperature of 25/20°C, a 16/8 h (day/night) photoperiod, a steady relative humidity (RH) of 60/65% and a photosynthetic photon flux density (PPFD) of approximately 400 $\mu\text{mol m}^{-2} \text{s}^{-1}$. To minimize the effects of environmental heterogeneity, pots were randomly arranged and moved during the entire experiment.

Plant inoculation procedure.

Plant inoculation was initiated by surface disinfection of the stem with 70% ethanol. A shallow wound was made 5 cm above the soil surface using a sterile scalpel, removing the bark, and exposing the cambium. Mycelial plugs (5 mm diameter) from the active margin of one-week-old fungal cultures grown on PDA at 25°C were placed into the wound with the mycelial surface facing the cambium and sealed with Parafilm® to prevent desiccation. Plugs of sterile PDA were similarly applied into wounds on stems of control plants. Ten replicate plants were randomly assigned to each treatment.

Experimental design.

For this experiment, three treatments were considered for each one of the water conditions: well-watered (WW) and water deficit (WD). For each water treatment, ten plants were inoculated with *D. amygdali* strain CAA958, ten inoculated with *D. eres* strain CBS 160.32 and ten mock-inoculated. The WW plants were subjected to water supplied every evening until soil water content reached around 75% FC. The WD regime was established by withholding water supply until the soil water content reached around 30% of FC (which lasted 9 days) and thereafter kept at this target. Pots from both water regimes were gravimetrically monitored through daily weighing and watered to maintain the soil water targeted (if necessary). Soil water content corresponding to 100% FC was previously determined by weighing soil-filled pots after full watering (till runoff) and after drying for 3 days at 80 °C. Each treatment (inoculated and non-inoculated plants) was

sampled as soon as 50% mortality was observed in one treatment (Fig. 1). Healthy leaves from five plants ($n=5$) displaying typical disease symptoms (dieback and stem necrosis) were selected from each treatment, and immediately frozen in liquid nitrogen and stored at -80°C for further analysis.

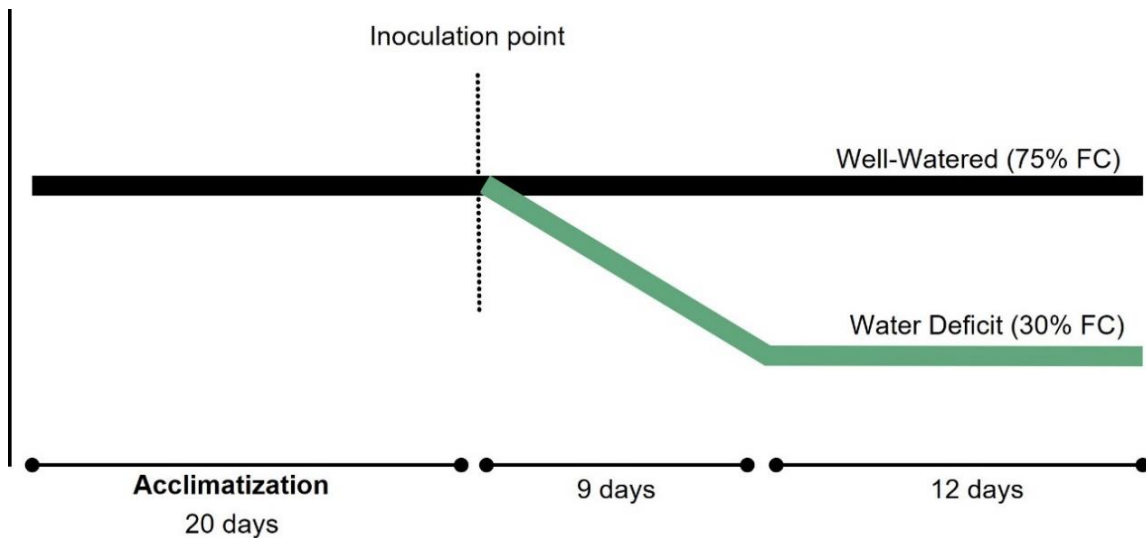


Figure 1. Experimental design implemented to evaluate the physiological performance of blueberry plants (cultivar 'Duke'), inoculated with two fungal species and under different water regimes: well-watered (WW, 75% FC) and water deficit (WD, 30% FC).

Disease progression.

During the entire experiment, the disease progression was evaluated. The development of external symptoms such as stem lesions, necrosis, foliar chlorosis, and wilting was assessed weekly. At the end of the experiment that lasted 21 days, the length of the internal lesions was measured by removing the external bark. Pieces of wood from the edges of lesions were immersed in 70% ethanol for 1 min, rinsed in sterile distilled water and blotted dry on sterile filter paper. Disinfected plant tissue was placed on PDA and incubated at room temperature for one week to verify Koch's postulates.

Water status.

For leaf relative water content (RWC) fresh weight (FW) tissue was recorded in three leaf discs with 11 mm in diameter. Discs were transferred to tubes with distilled water and maintained overnight in the dark at 4°C . After 24 hours, the turgid weight (TW) was registered. Leaf discs were then dried at 50°C for one week to obtain the dry weight (DW) and shoot water potential (Ψ_{md} , MPa) was measured

with a Schölander-type pressure chamber (PMS Instrument Co., Corvallis, OR). RWC was measured according to Smart and Bingham (1974).

Leaf gas exchange measurements.

Stomatal conductance (g_s , $\text{mmol H}_2\text{O m}^{-2} \text{s}^{-1}$), transpiration rate (E , $\text{mmol H}_2\text{O m}^{-2} \text{s}^{-1}$), net CO_2 assimilation rate (A , $\mu\text{mol CO}_2 \text{m}^{-2} \text{s}^{-1}$) and intercellular CO_2 concentration content (C_i , ppm) were measured in five plants per treatment using an LCpro-SD portable infrared gas analyzer (ADC BioScientific Ltd., UK) equipped with a broad photosynthesis chamber. The following conditions were maintained inside the chamber during all measurements: ambient CO_2 concentration and humidity; air flux: $200 \mu\text{mol/s}$; block temperature: $26.5 \pm 0.7^\circ\text{C}$. To determine the saturation light intensity A/PPFD (photosynthetic photon flux density; light response curves of CO_2 assimilation), response curves were performed with the following PPFD: 2000, 1500, 1000, 750, 500, 250, 100, 50 and $0 \mu\text{mol m}^{-2} \text{s}^{-1}$. After A/PPFD data analysis, punctual measurements at saturation light intensity were performed at $1000 \mu\text{mol m}^{-2} \text{s}^{-1}$. Data were recorded when the measured parameters were stable (8–10min). Measurements were carried out in five biological replicates per treatment and isolate used.

Biochemical parameters.

Photosynthetic pigments, total soluble sugars, and starch.

Photosynthetic pigments, total soluble sugars and starch were determined following the descriptions of López-Hidalgo et al. (2020). Briefly, 1mL of cold (4°C) 80% ethanol was added to 70 mg frozen tissue and ground for 30 sec. Samples were centrifuged at $10\,000g$ for 10 min at 4°C and the originated pellets (for starch quantification) and supernatants (for photosynthetic pigments and total soluble sugars quantification) were separated and used for further quantifications.

From the supernatant, 300 μl was diluted in 80% cold ethanol (1:1) for photosynthetic pigments determination. Chlorophyll A, chlorophyll b and carotenoid contents were quantified and calculated according to López-Hidalgo et al. (2020). Briefly, 150 μl of the diluted sample were transferred to 96-well microplate and

absorbances were measured at 470, 649 and 664nm, in a microplate reader (Synergy HT, BioTek Instruments, Winooski, VT, USA).

Both total soluble sugars and starch were determined using the anthrone method following the procedure described by López-Hidalgo et al. (2020). Samples were transferred to a 96-well microplate and the absorbance was read at 625 nm, in a microplate reader. Total soluble sugars content was calculated against a D-glucose standard curve in 80% ethanol (1–0 mg/ml). Starch content was calculated with a D-glucose in 30% perchloric acid standard curve (1–0 mg/ml).

Malondialdehyde (MDA) content.

Lipid peroxidation, estimated by the amount of malondialdehyde (MDA), was quantified using the method described by Heath and Packer (1968), with minor modifications. Briefly, MDA was extracted from 75mg of frozen leaves, homogenized in 5mL of TCA (trichloroacetic acid) 0.1% (v/v) and centrifuged at 12,000g for 15 min at 4°C. Afterwards, 1 ml of supernatant was mixed with 4 ml of 0.5% of thiobarbituric acid (TBA) in 20% TCA and incubated at 95°C for 30 min. The absorbance was read at 532 and 600 nm. MDA content was determined applying the formula described by Heath and Packer (1968).

Proline quantification.

Proline content was determined as described by Bates et al. (1973) with slight modifications. Plant tissue (70 mg) from five biological replicates per treatment was homogenized with 1.5ml of sulphosalicylic acid (3%, w/v). Following centrifugation (10 min, 10,000g, 4 °C), 1ml of supernatant was collected, and 1ml of ninhydrin acid and 1ml of glacial acetic acid were added. After incubation at 100°C and cooling, 2 ml of toluene were added to the solution and absorbance was read at 520nm. Free proline content was calculated against a D-proline standard curve (0–0.5 mg/ml).

Total phenolic content and flavonoids quantification.

Extraction was conducted as described by Dinis et al. (2012) with slight modifications. Briefly, 40mg of frozen leaves were homogenized in 1.5mL of MeHO 70% and kept in an orbital shaker at 700 rpm for 1h at 25°C. Samples were

centrifuged at 10,000g at 4°C for 15min and the supernatant was collected. This process was repeated at least 4 times, until we obtain a final volume of 6 ml. Samples were then stored at -80°C for further quantification.

Total phenolic content was estimated by Folin–Ciocalteu’s method adapted from Singleton et al. (1999). A total of 20µL of supernatant, 90µL of distilled water and 10µL of Folin–Ciocalteu reagent solution were added to a 96-well microplate and left in the dark at room temperature for 6min. Then, 80µL of 7% sodium carbonate solution were added to each well and incubated in the dark at room temperature for 2h. The absorbance was measured at a wavelength of 750nm. Gallic acid was used as standard to build a calibration curve (0–1 mg/mL).

Total flavonoid content was measured following the aluminum chloride colorimetric assay adapted from Chang et al. (2002). A total of 60µL of supernatant 28µL of 5% sodium nitrite solution were added to a 96-well microplate and left in the dark at room temperature for 6min. Then, 28µL of 10% aluminum chloride solution was added to each well and incubated again for 6min in the dark. After that, 120µL of 4% sodium hydroxide solution was added to each well and gently shook. The absorbance was measured at 370nm. Catechin was used as standard to calculate calibration curve (0–0.5 mg/mL).

Statistical analysis.

Before analysis, data were checked for normality with the Shapiro-Wilk test. As data meet ANOVA assumptions, two-way analysis of variance (ANOVA) followed by Bonferroni’s multiple comparison tests was employed to identify significant differences between plants inoculated with *D. eres* CBS 160.32 and *D. amygdali* CAA958 under well-watered and water deficit conditions ($p \leq 0.05$) (Table 1). Considering that plant response was dependent on the inoculation (Table 2), data were analyzed, and one-way ANOVA followed by a Tukey test as a post-hoc multiple comparisons ($p \leq 0.05$) was performed to evaluate the fungal effect in each water treatment (Table 2). All analyses were performed using SigmaPlot for Windows (Systat Software for Windows v. 14.5 Systat Software Inc., Chicago, IL, USA).

RESULTS

Disease progression.

Twenty-one days after inoculation, mortality rates (50%) occurred only for plants inoculated with *D. amygdali* under WD conditions (Fig. 2). Besides the development of necrosis in the inoculation site, plants showed wilting of leaves and discoloration of the outer epidermis. The remaining plants that survived, like in the other treatments, did not show any of these symptoms, besides the development of lesions around the inoculation point at the end of the experiment. *Diaporthe eres* did not cause death of any plant.

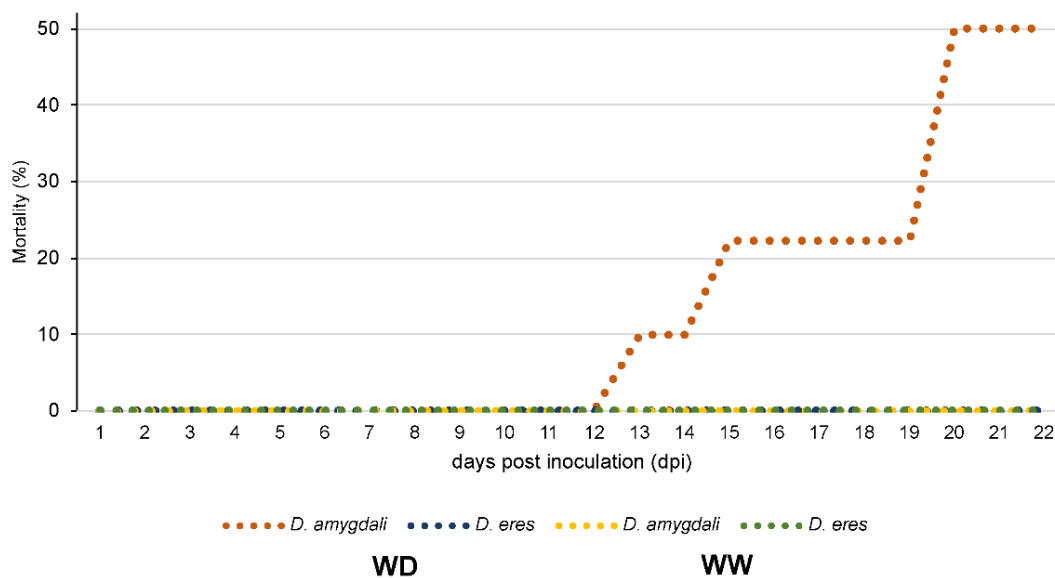


Figure 2. Blueberry mortality after inoculation with *Diaporthe amygdali* and *D. eres* under WD (water deficit) and WW (well-watered) treatments. Day 1 corresponds to the inoculation day.

Necrosis length.

Overall, *D. amygdali* showed larger lesion lengths in both WW and WD conditions (Fig. 3) alongside with wilting of leaves and necrosis of the internal vascular tissues. Moreover, *D. eres* (1.0 ± 0.3 cm) and *D. amygdali* (1.4 ± 0.3 cm) exhibited also significantly larger necrosis on WD conditions, compared to the WW treatment (0.8 ± 0.3 cm, $p = 0.001$; 1.2 ± 0.6 cm, $p = 0.043$, respectively) (Fig. 3).

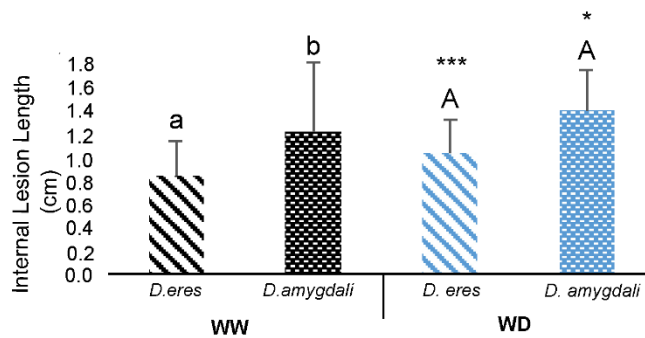


Figure 3. Internal lesion lengths caused by *Diaporthe eres* and *D. amygdali* under well-watered (WW) and water deficit (WD) conditions. Data are presented as mean \pm SD. Capital and lowercase letters indicate differences between inoculated plants within each water treatment ($p \leq 0.05$). The asterisks indicate differences between WW and WD treatments (* $p \leq 0.05$. *** $p \leq 0.001$).

Water potential.

No significant differences were observed within the WD treatment (Fig. 4). Non-inoculated plants under WD treatment displayed a decrease of water potential ($\Psi_{md} = -0.2$ MPa), compared to those non-inoculated under WW conditions ($\Psi_{md} = -0.3$ MPa). Moreover, the inoculation with *D. eres* influenced that water potential, since an increase was observed under WW conditions ($\Psi_{md} = -0.4$ MPa) (Fig. 4, Table 1).

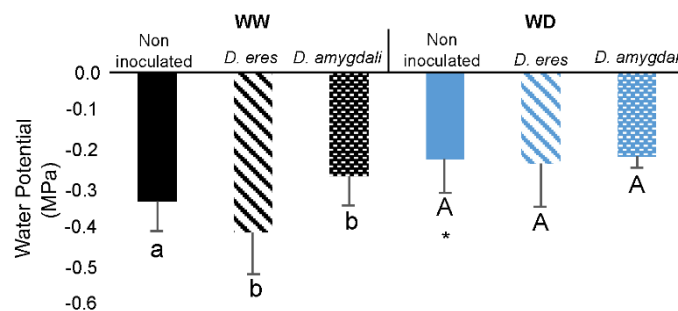


Figure 4. Shoot water potential of blueberry plants (Ψ_{md}) under well-watered (WW) and water deficit (WD) conditions and inoculated with *Diaporthe eres* and *D. amygdali*. Data are presented as mean \pm SD. Capital and lowercase letters indicate differences between inoculated plants within each water treatment ($p \leq 0.05$). The asterisk indicates differences between WW and WD treatments (* $p \leq 0.05$).

Relative water content (RWC).

No significant differences on RWC were observed within the WW treatment (Fig. 5). Under WD conditions, inoculation with both fungal species induced a significant decrease in RWC values, compared to the non-inoculated plants.

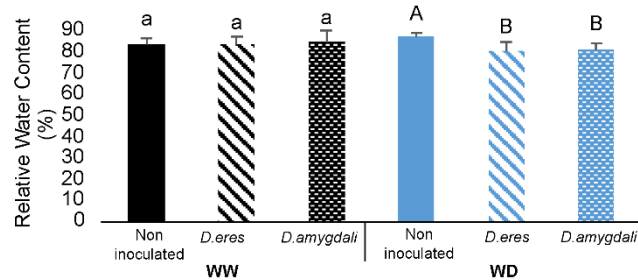


Figure 5. Relative water content (RWC) of blueberry plants under well-watered (WW) and water deficit (WD) conditions and inoculated with *Diaporthe eres* and *D. amygdali*. Data are presented as mean \pm SD. Capital and lowercase letters indicate differences between inoculated plants within each water treatment ($p \leq 0.05$).

Table 1. Two-way ANOVA summary table for morphological and physiological parameters considering two water availability scenarios (well-watered and water deficit) and inoculation (*Diaporthe eres*, *D. amygdali* infection and mock inoculation) as fixed factors. *F* value and *p*-value are shown for each source of variation (water availability – WA; inoculation – I, and their interaction (WA \times I). NS, non-significant. * $p \leq 0.05$. ** $p \leq 0.01$. *** $p \leq 0.001$.

Parameter	<i>F</i>			<i>p</i>			<i>Sig.</i>		
	WA	I	WA \times I	WA	I	WA \times I	WA	I	WA \times I
Starch	1.87	3.79	5.180	0.190	0.044	0.018	NS	*	*
Total soluble sugars	1.84	3.36	28.89	0.192	0.057	<0.001	NS	NS	***
MDA	19.68	11.17	8.37	0.001	<0.001	0.003	***	***	**
Proline	79.58	33.63	36.48	<0.001	<0.001	<0.001	***	***	***
Chlorophyll A	0.54	6.69	4.35	0.472	0.007	0.03	NS	**	*
Chlorophyll b	2.03	4.25	1.87	0.171	0.031	0.182	NS	*	NS
Carotenoids	0.64	4.63	1.66	0.434	0.024	0.218	NS	*	NS
Phenolic compounds	6.64	3.07	0.38	0.017	0.065	0.686	*	NS	NS
Flavonoids	5.37	0.64	0.55	0.031	0.535	0.586	*	NS	NS
Gs	5.67	15.26	4.96	0.026	<0.001	0.016	*	***	*
A	18.73	33.89	4.88	<0.001	<0.001	0.017	***	***	*
Ci	10.02	11.47	0.00	0.004	<0.001	0.997	**	***	NS
E	2.4	11.42	4.89	0.128	<0.001	0.016	NS	***	*
Ψ_{md}	6.69	8.35	8.84	0.019	0.003	0.003	*	**	**
Internal lesion	20.26	10.34	0.08	<0.001	0.005	0.786	***	**	NS
RWC	0.70	2.15	3.2	0.410	0.138	0.059	NS	NS	NS

Leaf gas exchange measurements.

It is visible a negative impact of water treatment and inoculation on leaf gas exchange parameters (Table 1). Under WW conditions, CO₂ assimilation rate (A) (Fig. 6A), stomatal conductance (gs) (Fig. 6C) and transpiration rate (E) (Fig. 6D), were affected after inoculation for both *D. eres* and *D. amygdali*. An increase in intercellular CO₂ concentration (Ci) was observed upon inoculation with *D. eres* (Fig. 6B). In the WD conditions, plants showed a similar response profile. Inoculated plants presented higher Ci values in WD treatment, compared to the non-inoculated plants, whereas A, gs and E rates were negatively affected by both fungal species. Non-inoculated plants showed a decrease in A under WD conditions ($3.1 \pm 1.2 \mu\text{mol CO}_2 \text{ m}^{-2}\text{s}^{-1}$), compared to the WW conditions ($5.3 \pm 1.6 \mu\text{mol CO}_2 \text{ m}^{-2}\text{s}^{-1}$). Additionally, plants inoculated with *D. amygdali* and exposed to WD showed a significantly lower rate of the foliar CO₂ assimilation ($1.4 \pm 0.4 \mu\text{mol CO}_2 \text{ m}^{-2}\text{s}^{-1}$) when compared to the respective treatment under WW conditions ($2.6 \pm 1.0 \mu\text{mol CO}_2 \text{ m}^{-2}\text{s}^{-1}$, $p = 0.034$).

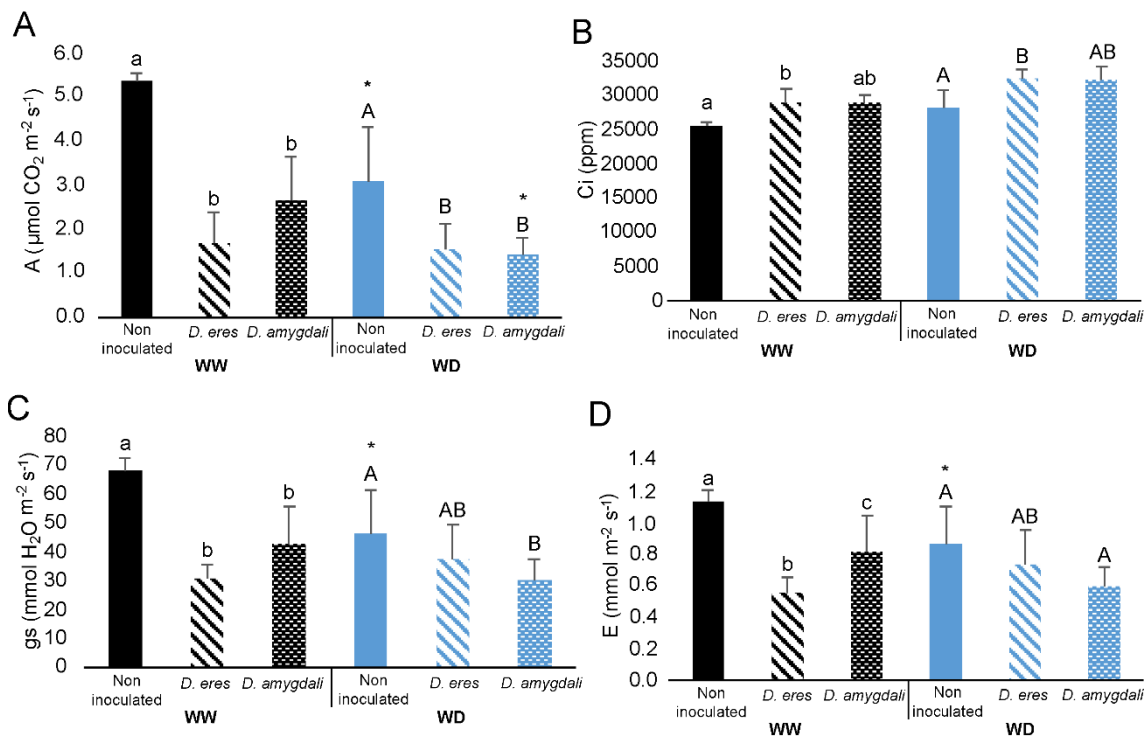


Figure 6. Foliar net CO₂ assimilation rate (A) (A), intercellular CO₂ concentration (Ci) (B), stomatal conductance (gs) (C) and transpiration rate (E) (D) of blueberry plants under well-watered (WW) and water deficit (WD) conditions and inoculated with *Diaporthe eres* and *D. amygdali*. Data are presented as mean \pm SD. Capital and lowercase letters indicate differences between inoculated plants within each water treatment ($p \leq 0.05$). The asterisk indicates differences between WW and WD treatments ($*p \leq 0.05$).

Photosynthetic pigments content.

Under WW conditions, no significant differences were found in chlorophyll b (Fig. 7B) and carotenoids (Fig. 7C) content in inoculated plants, regardless of the fungal species. However, *Diaporthe* inoculation showed an effect in chlorophyll a (Table 1). This pigment was significantly smaller in plants inoculated with *D. eres* (3.4 ± 0.5 nmol gFW⁻¹) and *D. amygdali* (4.9 ± 1.9 nmol gFW⁻¹), than in non-inoculated plants (7.8 ± 0.8 nmol gFW⁻¹) (Fig. 7A). In plants under WD conditions, no significant differences in chlorophyll a were observed (Fig. 7A). Additionally, the interaction between the two factors (inoculation and water regime) had a negative impact in chlorophyll b and carotenoids content. Plants inoculated with *D. eres* under WW conditions had significantly higher contents of chlorophyll b (4.6 ± 0.4 nmol gFW⁻¹) and carotenoids (2.4 ± 0.1 nmol gFW⁻¹), compared to the respective treatment under WD conditions (chlorophyll b: 3.1 ± 0.6 nmol gFW⁻¹, $p = 0.011$; carotenoids: 1.8 ± 0.5 nmol gFW⁻¹, $p = 0.048$) (Fig. 7B, Table 2).

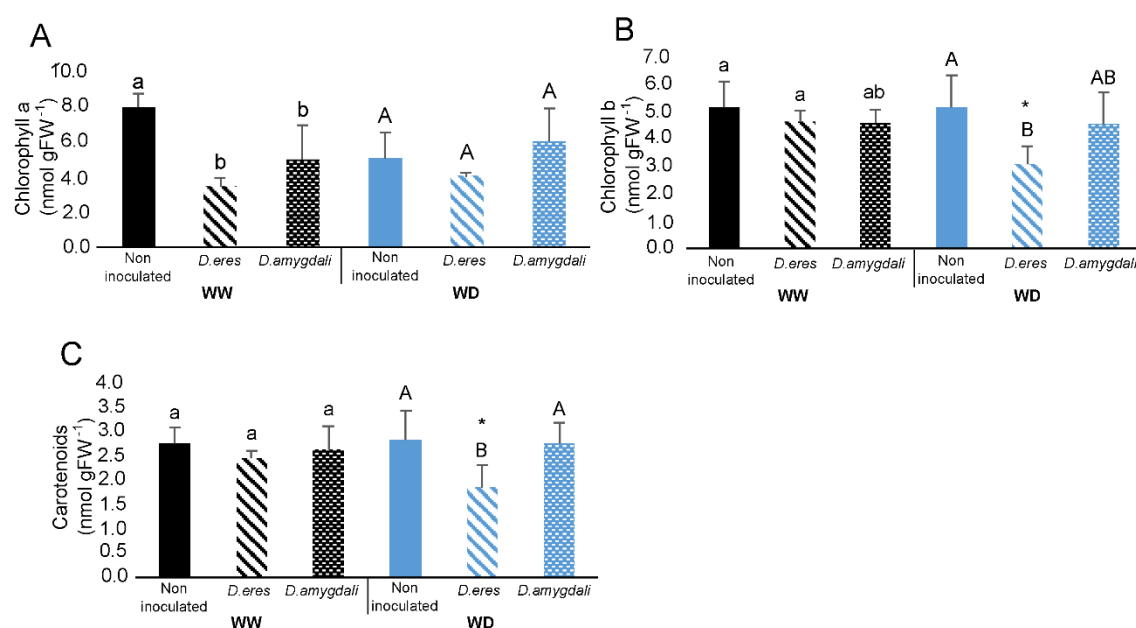


Figure 7. Chlorophyll a, b, and carotenoids content of blueberry plants under well-watered (WW) and water deficit (WD) conditions and inoculated with *Diaporthe eres* and *D. amygdali*. Data are presented as mean \pm SD. Capital and lowercase letters indicate differences between inoculated plants within each water treatment ($p \leq 0.05$). The asterisk indicates differences between WW and WD treatments ($*p \leq 0.05$).

Table 2. One-way ANOVA analysis for morphological and physiological parameters considering the inoculation of *Diaporthe eres* and *D. amygdali*, under well-watered and water deficit conditions. NS, non-significant. * $p \leq 0.05$. ** $p \leq 0.01$. *** $p \leq 0.001$.

Parameter	<i>Diaporthe eres</i>			<i>Diaporthe amygdali</i>		
	F	P	Sig.	F	p	Sig.
Starch	1.12	0.326	NS	5.81	0.047	*
Total soluble sugars	17.98	0.005	**	30.44	0.003	**
MDA	53.52	0.001	***	0.18	0.686	NS
Proline	129.22	<0.001	***	76.54	<0.001	***
Chlorophyll a	4.15	0.097	NS	0.59	0.466	NS
Chlorophyll b	15.46	0.011	*	0.00	0.984	NS
Carotenoids	6.76	0.048	*	0.14	0.716	NS
Phenolic compounds	0.44	0.525	NS	3.97	0.081	NS
Flavonoids	2.51	0.164	NS	0.51	0.499	NS
Gs	1.41	0.269	NS	3.52	0.097	NS
A	0.10	0.758	NS	6.57	0.034	*
Ci	2.35	0.164	NS	3.93	0.083	NS
E	2.92	0.126	NS	3.48	0.099	NS
Ψmd	4.98	0.067	NS	1.13	0.349	NS
Internal lesion	25.04	0.001	***	5.78	0.043	*
RWC	1.84	0.211	NS	1.88	0.208	NS

Malondialdehyde content.

The inoculation with *D. eres* under WW conditions influenced the MDA content (Fig. 8, Table 2). Significant differences were found in *D. eres* inoculated plants under WW conditions, exhibiting higher MDA content (60.1 ± 7.3 nmol gFW⁻¹) when compared to WD scenario (22.2 ± 6.4 nmol gFW⁻¹, $p = 0.001$) (Fig. 8, Table 2). Moreover, a significant interaction between the factors was found (Table 1). Under WW conditions, plants inoculated with *D. eres* showed significantly higher MDA content when compared to those inoculated with *D. amygdali* (23.5 ± 12.2 nmol gFW⁻¹) and to the non-inoculated plants (26.4 ± 10.6 nmol gFW⁻¹). No significant differences were observed in WD treatments.

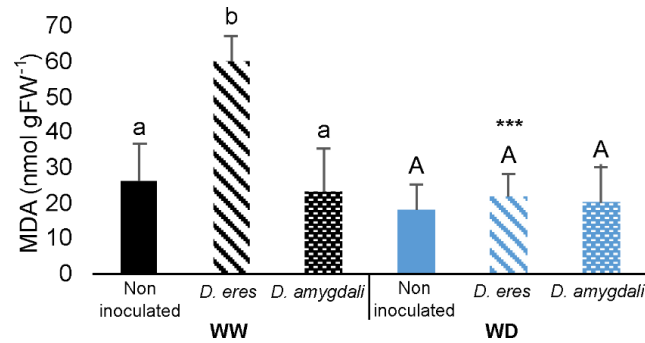


Figure 8. MDA content of blueberry plants under well-watered (WW) and water deficit (WD) conditions and inoculated with *Diaporthe eres* and *D. amygdali*. Data are presented as mean \pm SD. Capital and lowercase letters indicate differences between inoculated plants within each water treatment ($p \leq 0.05$). The asterisks indicate differences between WW and WD treatments ($***p \leq 0.001$).

Phenolic compounds and flavonoids content.

Under WW conditions, phenolics content in plants inoculated with *D. eres* (38.6 mg gFW⁻¹) and *D. amygdali* (35.1 mg gFW⁻¹) was significantly smaller, compared to the non-inoculated plants (43.2 mg gFW⁻¹) (Fig. 9B). No significant differences were observed in flavonoids contents within each treatment (Fig. 9A). Additionally, the availability of water had also an effect on antioxidants content on blueberries (Table 1). In non-inoculated plants and under WW conditions, the content of phenolic compounds (43.2 \pm 7.4 mg gFW⁻¹) and flavonoids (27.4 \pm 6.8 mg gFW⁻¹) were significantly higher compared to the non-inoculated plants under WD conditions (34.3 \pm 5.7 mg gFW⁻¹, $p = 0.017$; 20.9 \pm 4.9 mg gFW⁻¹, $p = 0.031$) respectively (Fig.9B, Table 2).

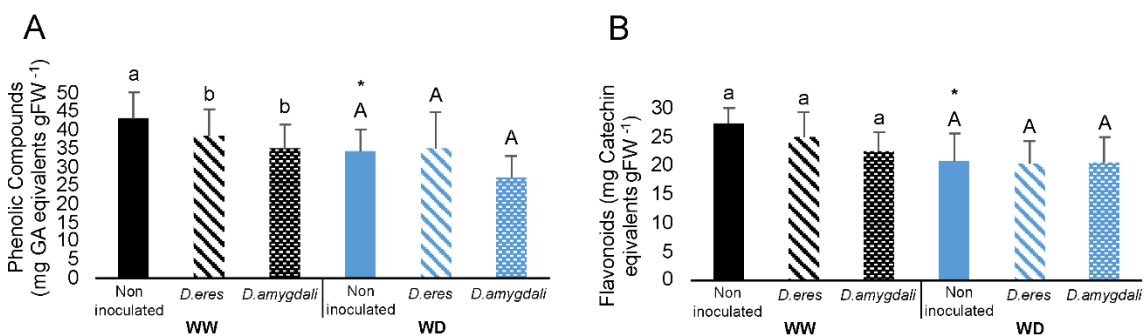


Figure 9. Phenolic compounds (A) and flavonoids (B) content of blueberry plants under well-watered (WW) and water deficit (WD) conditions and inoculated with *Diaporthe eres* and *D. amygdali*. Data are presented as mean \pm SD. Capital and lowercase letters indicate differences between inoculated plants within each water treatment ($p \leq 0.05$). The asterisk indicates differences between WW and WD treatments ($*p \leq 0.05$).

Proline content.

It is visible that the water treatment did not affect the proline content, whereas the interaction between inoculation and water regime applied (Table 1). Regarding the WW, no significant differences were observed for proline content (Fig. 10) in inoculated and non-inoculated plants. Proline content was significantly higher in WD treated plants inoculated with *D. eres* ($105.3 \pm 4.0 \text{ mg g}^{-1}$, $p \leq 0.001$) and *D. amygdali* ($104.0 \pm 10.7 \text{ mg g}^{-1}$, $p \leq 0.001$) (Table 2). However, WD non-inoculated plants maintained the same the profile of WW plants.

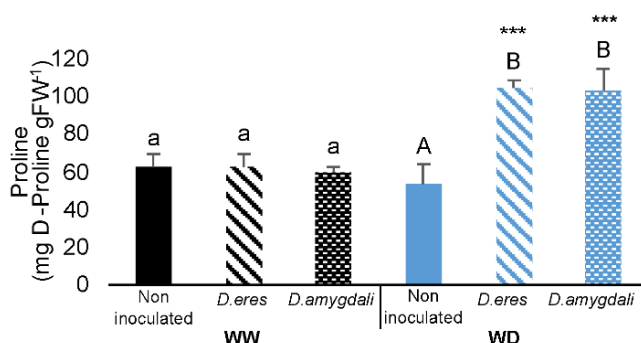


Figure 10. Proline content of blueberry plants under well-watered (WW) and water deficit (WD) conditions and inoculated with *Diaporthe eres* and *D. amygdali*. Data are presented as mean \pm SD. Capital and lowercase letters indicate differences between inoculated plants within each water treatment ($p \leq 0.05$). The asterisks indicate differences between WW and WD treatments ($*** p \leq 0.001$).

Total soluble sugars and starch content.

The inoculation with *D. amygdali* showed a negative effect on total soluble sugars content (Table 2). Plants inoculated with this fungus and under WW conditions showed lower content of soluble sugars ($0.6 \pm 0.1 \text{ mg gFW}^{-1}$), compared to the non-inoculated plants ($0.9 \pm 0.09 \text{ mg gFW}^{-1}$). Moreover, a significant interaction was observed between both inoculation and water regime factors. Plants under WD conditions and inoculated with *D. amygdali* exhibited higher total sugars content ($1.2 \pm 0.1 \text{ mg gFW}^{-1}$), compared to those exposed to WW ($0.6 \pm 0.1 \text{ mg gFW}^{-1}$, $p = 0.003$), while plants inoculated with *D. eres* showed lower sugars content ($0.6 \pm 0.03 \text{ mg gFW}^{-1}$), compared to the respective WW condition ($1.0 \pm 0.2 \text{ mg gFW}^{-1}$, $p = 0.005$).

Regarding the starch content, no significant differences were observed in starch content within plants under WW conditions (Fig 11B). Nevertheless, the

starch content in plants exposed to the WD treatment was significantly affected after inoculation with *D. amygdali* only. Additionally, a significant interaction between water and inoculation was found (Table 2). Inoculated plants with *D. amygdali* exhibited a significant increase in starch content ($1.3 \pm 0.5 \text{ mg gFW}^{-1}$), compared to the respective WW treatment ($0.7 \pm 0.4 \text{ mg gFW}^{-1}$, $p = 0.047$ (Fig. 11)

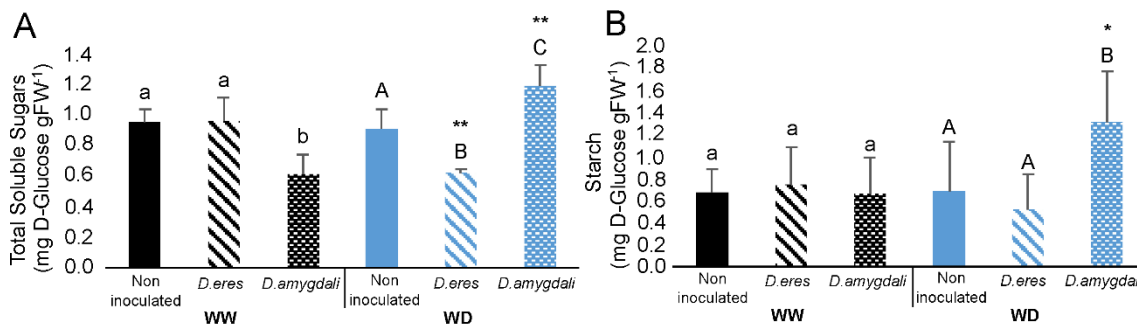


Figure 11. Total soluble sugars (A) and starch (B) content of blueberry plants under well-watered (WW) and water deficit (WD) conditions and inoculated with *Diaporthe eres* and *D. amygdali*. Data are presented as mean \pm SD. Capital and lowercase letters indicate differences between inoculated plants within each water treatment ($p \leq 0.05$). The asterisks indicate differences between WW and WD treatments (** $p \leq 0.01$. *** $p \leq 0.001$).

DISCUSSION

To our knowledge, this is the first study to explore the pathosystem *V. corymbosum*/*Diaporthe* spp., under two water regimes. Our results indicate that although *D. eres* and *D. amygdali* were able to colonize hosts' tissues, infected blueberry plants responded differently to the pathogens. This study also highlights the role of water availability in infection of blueberry plants by *Diaporthe* that seems to occur in a pathogen type-dependent manner.

Water deficit conditions impacted plant physiological performance. Some studies have shown under 45–50% of FC blueberry plants suffer of moderate water stress, which negatively affects their physiological and biochemical characteristics (Balboa et al. 2020; Chen et al. 2017). For instance, Chen et al. (2017) showed that chlorophyll content of blueberry decreased, while the MDA content increased under drought stress conditions. Additionally, Balboa et al. (2020) demonstrated that proline content increased in all cultivars tested under WD conditions. Rho et al. (2012) proved that cultivar 'Bluecrop' was highly sensitive to WD, given the observed rapid stomatal closure and reduced gas exchange. Lobos et al. (2018)

also stated that under severe WD conditions, cultivar 'Brigitta' displays water potentials ranging from -0.9 MPa to -1.2 MPa. However, our results indicate that although we have applied a stricter water regime (30% FC), this was not sufficient for plants of cultivar 'Duke' to reflect severe changes at physiological and biochemical levels, given for instance the observed high values of water potential (ranging from -0.2 MPa to -0.4 MPa).

One of the main effects of the water regime applied was a decrease in phenolic compounds and flavonoids. Although flavonoids and phenolic compounds content can be accumulated in plants under abiotic stresses, such as drought, (Naikoo et al. 2019, Laoué et al. 2022), environmental stress can also cause a decrease in the content of phenols (Król et al. 2014). Therefore, it is suggested that the antioxidant system component was not activated, and thus was not involved in plant defense as a strategy to cope with water limitation. Moreover, the leaf gas exchange was negatively affected by the water regime applied through the decrease in g_s , E , A rates which might be considered as a water save strategy (Bertolino et al. 2019; Morato de Moraes et al. 2020). Such results might explain the ability of cultivar 'Duke' to adapt to water-stress conditions (Molnar et al. 2022).

Under WW conditions, blueberry plants responses depend on the pathogen inoculated. Based on the lesion lengths observed in this study, *D. amygdali* CAA958 was the most aggressive, while *D. eres* CBS 160.32 caused minor symptoms as previously demonstrated by Hilário et al. (2021), suggesting that strain CBS 160.32 does not seem to pose a threat to blueberry plants. One of the plant responses to pathogen infection is the imbalance of photosynthesis (Rojas et al. 2014). The results showed that plants inoculated with both *D. eres* and *D. amygdali* under WW conditions exhibited a decrease in A , g_s and E , and an increase in C_i . The increase of C_i may be caused by a reduction of the activity of photosynthetic machinery components that limited CO_2 assimilation probably due to oxidative stress (Munné-Bosch & Peñuelas 2004). This may suggest that *D. eres* and *D. amygdali* were able to negatively affect the photosynthetic apparatus of blueberries as reported for other pathosystems (Amaral et al. 2019). Moreover, Roloff et al. (2004) showed that infection of blueberry plants by *Septoria albopunctata* had a significant negative effect on photosynthesis, with net assimilation rate decreasing as disease severity

increased. Furthermore, the observed decrease in chlorophyll a after *D. eres* and *D. amygdali* infection may also help explaining the decrease in photosynthetic performance. Chlorophylls are the main pigments in plant photosynthetic apparatus, responsible for the energy absorption and the transfer of electron chains (ETR) (Gu et al. 2017). The decrease in chlorophyll a content may lead to a lower capacity to absorb energy, thus causing a decrease in the net CO₂ assimilation rate, as observed in our study. The photosynthetic capacity of maize leaves is inhibited by infection with *Colletotrichum musae* and *Fusarium moniliforme* and is accompanied by a decrease in chlorophylls content (Costa Pinto et al. 2000). Another aspect to consider is that the production of phytotoxins by fungi (e.g., alternariol), may have an impact on the photosynthetic apparatus (Demuner et al. 2013). Therefore, as suggested by Linaldeddu et al. (2009), the decrease in the net photosynthetic rate and the total chlorophylls, regardless of the lesion size observed, could be explained by the production of diffusible toxins.

Stress usually leads to oxidative stress induced by increased reactive oxygen species (ROS) production, which is indicated by the accumulation of MDA (Xu & Zhou 2006). However, it is important to note that lipid peroxidation can also result from increased lipoxygenase activity, caused by a pathogen invasion (Morales & Munné-Bosch 2019). In fact, in this study we observed an increase in MDA content in plants under WW conditions and inoculated with *D. eres*. Besides the minor symptoms and the null mortality observed, it is suggested that MDA might have acted as a signaling molecule rather than a response to lipid peroxidation (Morales & Munné-Bosch, 2019) in plants inoculated with *D. eres*.

It is recognized that sugars play a key role in plant defense, supplying energy for cellular defense against pathogens (Nabavi et al. 2020). Nevertheless, either a decrease or an increase may happen in the level of sugars in infected tissues (Berger et al. 2007). Our results show that the total soluble sugars content decreased in plants under WW conditions and infected with *D. amygdali*. Considering that this pathogen was shown to be the most aggressive, it is plausible that the enhanced sugar metabolism from the plant to cope with fungal infection may have caused changes in the composition of carbohydrates, thus causing a reduction of their content (Morkunas & Ratajczak 2014).

Water deficit conditions may change pathogen behavior impacting plant responses. Previous studies have shown that low water availability results in physiological and metabolic changes in several agricultural crops, weakening the host defense and increasing disease susceptibility (Ghanbary et al. 2021). Such changes can cause oxidative damage to membrane lipids and decreases in stomatal conductance, photosynthetic rate, and chlorophyll concentration (Ghanbary et al. 2017; Yang & Luo 2021). Although investigations into the effects of stress scenarios on disease development caused by *Diaporthe* are limited, stress of host plant (e.g., transplant shock, excessive pruning, freeze injury) may affect the transition from the endophytic to pathogenic phase (Hrycan et al. 2020). Hulke et al. (2019) found that increases in average precipitation enhanced disease incidence of *Phomopsis* stem blight of sunflowers caused by *D. helianthi*. Moreover, Kim et al. (2015) found also that severe frost and frequent wind events increased *Citrus* trees susceptibility to *D. citri* infection. In the present study, under WD conditions, *D. amygdali* CAA958 not only caused larger lesions than *D. eres*, as also caused 50% plant mortality. Thus, it is suggested that water availability may be considered a key factor to enhance the pathogenicity of *D. amygdali*. Moreover, the mortality observed might also have been caused by the presence of phytotoxins such as the Fusicoccin, identified in *D. amygdali* and recently detected on the genome of *D. amygdali* strain CAA958 (Hilário et al. 2022). Although this toxin induces opening of stomata and uncontrolled transpiration (Marra et al. 2021), we have observed a stomatal closure through the decrease of g_s and E in plants inoculated with *D. amygdali*. However, this hypothesis cannot be overlooked, and further studies should be considered to evaluate the effect that Fusicoccin may pose to blueberry plants. Despite the differences in aggressiveness, inoculated plants with both pathogens under WD conditions showed a decrease in A, g_s and E, and an increase in Ci when compared to WD non-inoculated plants, revealing stomatal limitations and impacts at metabolic level. For instance, plants inoculated with *D. amygdali* CAA958 reflected an increase in proline, starch, and total soluble sugars content, whereas plants inoculated with *D. eres* CBS 160.32 showed a decrease in total soluble sugars content.

Under abiotic or biotic stresses, plants remobilize starch to provide energy and carbon, when photosynthesis may be limited (Thalmann & Santelia 2017). According to our results, under WD conditions, plants inoculated with *D. amygdali* CAA958, seem to invest their photo-assimilated energy (total soluble sugars and starch) to maintain cell turgor and to protect them against oxidative stress and membrane injury (Chen & Jiang 2010). Proline accumulation has been reported as a key metabolite, functioning as a compatible osmolyte and a signaling molecule that contributes to cellular osmotic adjustment, ROS detoxification and protection of membrane integrity (Hayat et al. 2012; Kavi Kishor & Sreenivasulu 2014). Our results showed high levels of proline on plants inoculated under WD conditions. Such result is corroborated by Balboa et al. (2020), who also showed the same trend in different blueberry cultivars, upon WD stress. This suggests that proline would act more as a signaling molecule rather than an osmoprotectant after pathogen infection and under water limitation (Hayat et al. 2012). Although MDA content was lower in plants inoculated with *D. amygdali* CAA958 and *D. eres* CBS 160.32 under WD conditions, this does not imply that an increase in ROS production did not occur: 1) the presence of scavenging enzymes in fungal pathogens are determinant in detoxification of ROS to ensure a successful infection, as already reported in the fungus *Magnaporthe oryzae* (Apel & Hirt 2004; Huang et al. 2011, 2019); 2) proline accumulation may act as an antioxidant to scavenge intracellular ROS (Hossain et al. 2014).

CONCLUSIONS

The study of the pathogens and plants as an interacting system, coupled with experimental systems with stresses combinations, is essential to unveil how plants cope with a pathogen attack or global change scenarios. The present study is the first to explore the pathosystem *V. corymbosum*/*Diaporthe* spp., under WW and WD conditions. Our study evidenced that *D. eres* CBS 160.32, previously regarded as a quarantine organism, was the least aggressive species and therefore should not be considered as a threat to blueberry plants. Nevertheless, our results highlighted that *D. eres* CBS 160.32 was able to alter practically all parameters analyzed, on both WD and WW treatments, which may eventually impact the health

of the plants. Therefore, this suggests that lesion size is not related to physiological alterations, and thus cannot be considered as the main measure of pathogen aggressiveness. Our findings also support that *D. eres* CBS 160.32 and *D. amygdali* CAA958 may act as latent pathogens, given the minor symptoms and null mortality rates under WW conditions. Nevertheless, as plants inoculated with *D. amygdali* CAA958 showed 50% mortality under WD conditions, it is suggested that water availability may be a key factor for the pathogenicity of this species.

Furthermore, future studies including RNA sequencing (RNA-Seq) technology should be conducted to unveil blueberry defense mechanisms upon fungal infection and water availability. This approach coupled with more physiological studies, may support the selection of resistant traits to design innovative plant protection strategies under global change scenarios that may hamper agriculture sustainability.

ACKNOWLEDGMENTS

Thanks are due to the Portuguese Foundation for Science and Technology (FCT/MCTES) for the financial support to CESAM (Centro de Estudos do Ambiente e do Mar) (UIDP/50017/2020 + UIDB/50017/2020 + LA/P/0094/2020) through national funds, and the PhD grants of Sandra Hilário (SFRH/BD/137394/2018) and Pedro Monteiro (SFRH/BD/143879/2019). Liliana Santos is funded by national funds (OE), through FCT in the scope of the framework contract foreseen in the numbers 4, 5 and 6 of the article 23 of the Decree-Law 57/2016, of August 29, changed by Law 57/2017, of July 19. The authors are also thankful to Deifil Green Biotechnology LDA (Braga, Portugal) for supplying the plant material for the assays.

REFERENCES

- Amaral J, Correia B, António C, Rodrigues AM, Gómez-Cadenas A, Valledor L, Hancock RD, Alves A, Pinto G. **2019**. *Pinus* susceptibility to pitch canker triggers specific physiological responses in symptomatic plants: an integrated approach. *Frontiers in Plant Science* 10, 509.
- Apel K, Hirt H. **2004**. Reactive oxygen species: metabolism, oxidative stress, and signal transduction. *Annual Review of Plant Biology* 55, 373–399.

- Balboa K, Ballesteros GI, Molina-Montenegro MA. **2020**. Integration of physiological and molecular traits would help to improve the insights of drought resistance in highbush blueberry cultivars. *Plants* **9**, 1457.
- Baldi P, La Porta N. **2020**. Molecular approaches for low-cost point-of-care pathogen detection in agriculture and forestry. *Frontiers in Plant Science* **11**, 570862.
- Bates LS, Waldren RP, Teare ID. **1973**. Rapid determination of free proline for water-stress studies. *Plant Soil* **39**, 205e207.
- Berger S, Sinha AK, Roitsch T. **2007**. Plant physiology meets phytopathology: plant primary metabolism and plant–pathogen interaction. *Journal of Experimental Botany* **58**, 4019–4026.
- Bertolino LT, Caine RS, Gray JE. **2019**. Impact of stomatal density and morphology on water-use efficiency in a changing world. *Frontiers in Plant Science* **10**, 225.
- Cardinaals J, Wenneker M, Voogd JGB, van Leeuwen GCM. **2018**. Pathogenicity of *Diaporthe* spp. on two blueberry cultivars (*Vaccinium corymbosum*). *EPPO Bulletin* **48**, 128–134.
- Chang C-C, Yang M-H, Wen H-M, Chern J-C. **2002**. Estimation of total flavonoid content in propolis by two complementary colorimetric methods. *Journal of Food and Drug Analysis* **10**, 178–182.
- Chen H, Jiang J-G. **2010**. Osmotic adjustment and plant adaptation to environmental changes related to drought and salinity. *Environmental Reviews* **18**, 309–319.
- Chen X, Qiu L, Guo H, Wang Y, Yuan H, Yan D, Zheng B. 2017. Spermidine induces physiological and biochemical changes in southern highbush blueberry under drought stress. *Brazilian Journal of Botany* **40**, 841–851.
- Costa Pinto LSR, Azevedo JL, Pereira JO, Carneiro Vieira ML, Labate CA. **2000**. Symptomless infection of banana and maize by endophytic fungi impairs photosynthetic efficiency. *New Phytologist* **147**, 609–615
- del Pozo A, Brunel-Saldias N, Engler A, Ortega-Farias S, Acevedo-Opazo C, Lobos GA, Jara-Rojas R, Molina-Montenegro MA. **2019**. Climate change impacts and

- adaptation strategies of agriculture in Mediterranean-climate regions (MCRs). *Sustainability* 11, 2769.
- Dinis LT, Oliveira MM, Almeida J, Costa R, Gomes-Laranjo J, Peixoto F. **2012**. Antioxidant activities of chestnut nut of *Castanea sativa* Mill. (cultivar 'Judia') as function of origin ecosystem. *Food Chemistry* 132, 1–8.
- Dissanayake AJ, Chen YY, Liu JKJ. **2020**. Unravelling *Diaporthe* species associated with woody hosts from Karst Formations (Guizhou) in China. *Journal of Fungi* 6, 251.
- Demuner AJ, Barbosa LCA, Miranda ACM, Geraldo GC, da Silva CM, Giberti S, Bertazzini M, Forlani G. **2013**. The fungal phytotoxin alternariol 9-methyl ether and some of its synthetic analogues inhibit the photosynthetic electron transport chain. *Journal of Natural Products* 76, 2234–2245.
- FAOSTAT. **2022**. Food and Agriculture Organization of the United Nations. Available online: <http://www.fao.org/faostat/en/#home> (accessed on 15 March 2022).
- Ghanbary E, Fathizadeh O, Pazhouhan I, Zarafshar M, Tabari M, Jafarnia S, Parad GA, Bader MKF. **2021**. Drought and pathogen effects on survival, leaf physiology, oxidative damage, and defense in two middle eastern oak species. *Forests* 12, 247.
- Ghanbary E, Kouchaksaraei MT, Mirabolfathy M, Modarres Sanavi SAM, Rahaei, M. **2017**. Growth and physiological responses of *Quercus brantii* seedlings inoculated with *Biscogniauxia mediterranea* and *Obolarina persica* under drought stress. *Forest Pathology* 47, e12353.
- Gomes RR, Glienke C, Videira SIR, Lombard L, Groenewald JZ, Crous PW. **2013**. *Diaporthe*: a genus of endophytic, saprobic and plant pathogenic fungi. *Persoonia* 31, 1–41.
- Gu J, Zhou Z, Li Z, Chen Y, Wang Z, Zhang H, Yang J. **2017**. Photosynthetic properties and potentials for improvement of photosynthesis in pale green leaf rice under high light conditions. *Frontiers in Plant Science* 8, 1082.
- Guarnaccia V, Brondino L, Garibaldi A, Gullino ML. **2021**. Leaf anthracnose and defoliation of blueberry caused by *Colletotrichum helleniense* in Northern Italy. *Phytopathologia Mediterranea* 60, 479-491.

- Hayat S, Hayat Q, Alyemeni MN, Wani AS, Pichtel J, Ahmad A. **2012**. Role of proline under changing environments. *Plant Signaling & Behavior* 7, 1456–1466.
- Hazrati SZ, Tahmasebi-Sarvestani SA, Modarres-Sanavy M, Mokhtassi-Bidgoli A, Nicola S. **2016**. Effects of water stress and light intensity on chlorophyll fluorescence parameters and pigments of *Aloe vera* L. *Plant Physiology and Biochemistry* 106, 141–148.
- Heath RL, Packer L. **1968**. Photoperoxidation in isolated chloroplasts. *Archives of Biochemistry and Biophysics* 125, 189e198.
- Hilário S, Amaral AI, Gonçalves MFM, Lopes A, Santos L, Alves A. **2020**. *Diaporthe* species associated with twig blight and dieback of *Vaccinium corymbosum* in Portugal, with description of four new species. *Mycologia* 112, 293–308.
- Hilário S, Gonçalves MFM, Fidalgo C, Tacão M, Alves A. **2022**. Genome analyses of two blueberry pathogens: *Diaporthe amygdali* CAA958 and *Diaporthe eres* CBS 160.32. *Journal of Fungi* 8, 804.
- Hilário S, Gonçalves MFM, Alves A. **2021a**. Using genealogical concordance and coalescent-based species delimitation to assess species boundaries in the *Diaporthe eres* complex. *Journal of Fungi* 7, 507.
- Hilário S, Santos L, Alves A. **2021b**. Diversity and pathogenicity of *Diaporthe* species revealed from a survey of blueberry orchards in Portugal. *Agriculture* 11, 1271
- Hossain MA, Hoque MA, Burritt DJ, Fujita M. **2014**. Proline protects plants against abiotic oxidative stress: biochemical and molecular mechanisms. In: Ahmad P, ed. *Oxidative damage to plants*. San Diego, CA: Academic Press, Elsevier Inc. p. 477–522.
- Hossain M, Veneklaas EJ, Hardy GESJ, Poot P. **2019**. Tree host–pathogen interactions as influenced by drought timing: linking physiological performance, biochemical defence and disease severity. *Tree Physiology* 39, 6–18.
- Huang K, Czymbek KJ, Caplan JL, Sweigard JA, Donofrio NM. **2011**. Suppression of plant-generated reactive oxygen species is required for successful infection by the rice blast fungus. *Virulence* 2, 559–562.
- Huang H, Ullah F, Zhou DX, Yi M, Zhao Y. 2019. Mechanisms of ROS regulation of plant development and stress responses. *Frontiers in Plant Science* 10, 800.

- Hulke BS, Markell SG, Kane NC, Mathew FM. 2019. *Phomopsis* stem canker of sunflower in North America: Correlation with climate and solutions through breeding and management. *Oilseeds & fats, Crops and Lipids* 26, 13.
- Hrycan J, Hart M, Bowen P, Forge T, Urbez-Torres JR. 2020. Grapevine trunk disease fungi: their roles as latent pathogens and stress factors that favour disease development and symptom expression. *Phytopathologia Mediterranea* 59, 395–424.
- Portal do Instituto Nacional de Estatística (INE). 2021. Estatísticas agrícolas 2020. 2021. Available online <https://www.ine.pt/xurl/pub/437147278> (accessed on 15 March 2022).
- Jiménez-Donaire MDP, Giráldez JV, Vanwalleghem T. 2020. Impact of climate change on agricultural droughts in Spain. *Water* 12, 3214.
- Kavi Kishor PB, Sreenivasulu N. 2014. Is proline accumulation per se correlated with stress tolerance or is proline homeostasis a more critical issue? *Plant, Cell & Environment* 37, 300–311.
- Kim KH, Kim GH, Son KI, Koh YJ. 2015. Outbreaks of yuzu dieback in Goheung Area: possible causes deduced from weather extremes. *The Plant Pathology Journal* 31, 290.
- Król A, Amarowicz R, Weidner S. 2014. Changes in the composition of phenolic compounds and antioxidant properties of grapevine roots and leaves (*Vitis vinifera* L.) under continuous of long-term drought stress. *Acta Physiologiae Plantarum* 36, 1491–1499.
- Laoué J, Fernandez C, Ormeño E. 2022. Plant flavonoids in mediterranean species: a focus on flavonols as protective metabolites under climate stress. *Plants* 11, 172.
- Linaldeddu BT, Sirca C, Spano D, Franceschini A. 2009. Physiological responses of cork oak and holm oak to infection by fungal pathogens involved in oak decline. *Forest Pathology* 39, 232-238.
- Lobos TE, Retamales JB, Ortega-Farías S, Hanson EJ, López-Olivari R, Mora ML. 2018. Regulated deficit irrigation effects on physiological parameters, yield, fruit quality and antioxidants of *Vaccinium corymbosum* plants cv. Brigitta. *Irrigation Science* 36, 49–60.

- López-Hidalgo C, Meijón M, Lamelas L, Valledor L. **2021**. The rainbow protocol: A sequential method for quantifying pigments, sugars, free amino acids, phenolics, flavonoids and MDA from a small amount of sample. *Plant, Cell & Environment* 6, 1977–1986.
- Marra A, Camoni AL, Visconti A, Fiorillo A, Evident A. **2021**. The surprising story of Fusicoccin: A wilt-inducing phytotoxin, a tool in plant physiology and a 14-3-3-targeted drug. *Biomolecules* 11, 1393.
- Mazurek M, Siekierzyńska A, Jacek B, Litwińczuk W. **2021**. Differences in response to drought stress among highbush blueberry plants propagated conventionally and by tissue culture. *Plant Biosystems - An International Journal Dealing with all Aspects of Plant Biology* 155, 172–178.
- Mazzoni L, Balducci F, Di Vittori L, Scalzo J, Capocasa F, Zhong CF, Forbes-Hernandez TY, Giampieri F, Battino M, Mezzetti B. **2020**. Yield and nutritional quality of highbush blueberry genotypes trialled in a Mediterranean hot summer climate. *Journal of the Science of Food and Agriculture* 100, 3675–3686.
- Mingeau M, Perrier C, Ameglio T. **2001**. Evidence of drought-sensitive periods from flowering to maturity on highbush blueberry. *Scientia Horticulturae* 89, 23–40.
- Molnar S, Clapa D, Mitre V. **2022**. Response of the five highbush blueberry cultivars to in vitro induced drought stress by polyethylene glycol. *Agronomy* 12, 732.
- Morales CG, Pino MT, del Pozo A. **2013**. Phenological and physiological responses to drought stress and subsequent rehydration cycles in two raspberry cultivars. *Scientia Horticulturae* 162, 234–241.
- Morales M, Munné-Bosch S. **2019**. Malondialdehyde: facts and artifacts. *Plant Physiology* 180, 1246–1250.
- Morato de Moraes DH, Mesquita M, Bueno AM, Flores RA, Elias de Oliveira HF, de Lima FSR, de Melo Prado R, Battisti R. **2020**. Combined effects of induced water deficit and foliar application of silicon on the gas exchange of tomatoes for processing. *Agronomy* 10, 1715.
- Morkunas I, Ratajczak L. **2014**. The role of sugar signaling in plant defense responses against fungal pathogens. *Acta Physiologiae Plantarum* 36, 1607–1619.


- Munné-Bosch S, Peñuelas J. **2004**. Drought-induced oxidative stress in strawberry tree (*Arbutus unedo* L.) growing in Mediterranean field conditions. *Plant Science* 166, 1105–1110.
- Naikoo MI, Dar MI, Raghib F, Jaleel H, Ahmad B, Raina A, Khan FA, Naushin F. **2019**. Role and regulation of plants phenolics in abiotic stress tolerance: An overview. In: Khan MIR, Reddy PS, Ferrante A, Khan NA, eds. *Plant Signaling Molecules*. Woodhead Publishing, Elsevier Inc. p. 157–168.
- Nabavi S, Samec D, Tomczyk M, Milella L, Russo D, Habtemariam S, Suntar I, Rastrelli L, Daglia M, Xiao J, ... Shirooie S. **2020**. Flavonoid biosynthetic pathways in plants: versatile targets for metabolic engineering. *Biotechnology Advances* 39, 107461.
- Ortega-Farias S, Espinoza-Meza S, López-Olivari R, Araya-Alman M, Carrasco-Benavides M. **2021**. Effects of different irrigation levels on plant water status, yield, fruit quality, and water productivity in a drip-irrigated blueberry orchard under Mediterranean conditions. *Agricultural Water Management* 249, 106805.
- Pandey P, Irulappan V, Bagavathiannan MV, Senthil-Kumar M. **2017**. Impact of combined abiotic and biotic stresses on plant growth and avenues for crop improvement by exploiting physio-morphological traits. *Frontiers in Plant Science* 8, 537.
- Ramegowda V, Senthil-Kumar M. **2015**. The interactive effects of simultaneous biotic and abiotic stresses on plants: mechanistic understanding from drought and pathogen combination. *Journal of Plant Physiology* 176, 47–54.
- Rho H, Yu DJ, Kim SJ, Lee HJ. **2012**. Limitation factors for photosynthesis in 'Bluecrop' highbush blueberry (*Vaccinium corymbosum*) leaves in response to moderate water stress. *Journal of Plant Biology* 55, 450–457.
- Rojas CM, Senthil-Kumar M, Tzin V, Mysore K. **2014**. Regulation of primary plant metabolism during plant-pathogen interactions and its contribution to plant defense. *Frontiers in Plant Science* 5, 17.
- Roloff I, Scherm H, Van Iersel MW. **2004**. Photosynthesis of blueberry leaves as affected by *Septoria* leaf spot and abiotic leaf damage. *Plant Disease* 88, 397–401.
- Silva S, Costa EM, Veiga M, Morais RM, Calhau C, Pintado M. **2020**. Health

- promoting properties of blueberries: A review. *Critical Reviews in Food Science and Nutrition* 60, 181–200.
- Singleton VL, Orthofer R, Lamuela-Raventós RM. **1999**. Analysis of total phenols and other oxidation substrates and antioxidants by means of folin-ciocalteu reagent. *Methods in Enzymology* 299, 152–178.
- Sinha R, Irulappan V, Mohan-Raju B, Suganthi A, Senthil-Kumar M. **2019**. Impact of drought stress on simultaneously occurring pathogen infection in field-grown chickpea. *Scientific Reports* 9, 1–15.
- Smart RE, Bingham GE. **1974**. Rapid estimates of relative water content. *Plant Physiology* 53, 258–260.
- Swinfield T, Lewis O, Bagchi R, Freckleton R. **2012**. Consequences of changing rainfall for fungal pathogen-induced mortality in tropical tree seedlings. *Ecology and Evolution* 2, 1408–1413.
- Thalman M, Santelia D. **2017**. Starch as a determinant of plant fitness under abiotic stress. *New Phytologist* 214, 943–951.
- Toscano S, Ferrante A, Romano D. **2019**. Response of Mediterranean ornamental plants to drought stress. *Horticulturae* 5, 6.
- Xu ZZ, Zhou GS. **2006**. Combined effects of water stress and high temperature on photosynthesis, nitrogen metabolism and lipid peroxidation of a perennial grass *Leymus chinensis*. *Planta* 224, 1080–1090.
- Yang H, Luo P. **2021**. Changes in photosynthesis could provide important insight into the interaction between wheat and fungal pathogens. *International Journal of Molecular Sciences* 22, 8865.
- Yu DJ, Rho H, Kim SJ, Lee HJ. **2015**. Photosynthetic characteristics of highbush blueberry (*Vaccinium corymbosum* cv. Bluecrop) leaves in response to water stress and subsequent re-irrigation. *The Journal of Horticultural Science and Biotechnology* 90, 550–556.



CHAPTER 6

Genome sequencing of two relevant *Diaporthe*
pathogens to blueberry plants



Genome analyses of two blueberry pathogens: *Diaporthe amygdali* CAA958 and *Diaporthe eres* CBS 160.32

Hilário S, Gonçalves MFM, Fidalgo C, Tacão M, Alves A
Journal of Fungi 2022 8, 804

ABSTRACT

The genus *Diaporthe* includes pathogenic species distributed worldwide and affecting a wide variety of hosts. *Diaporthe amygdali* and *Diaporthe eres* have been found to cause cankers, dieback, or twig blights on economically important crops such as soybean, almond, grapevine, and blueberry. Despite their importance as plant pathogens, the strategies of species of *Diaporthe* to infect host plants are poorly explored. To provide a genomic basis of pathogenicity, the genomes of *D. amygdali* CAA958 and *D. eres* CBS 160.32 were sequenced and analyzed. Cellular transporters involved in the transport of toxins, ions, sugars, effectors, and genes implicated in pathogenicity were detected in both genomes. Hydrolases and oxidoreductases were the most prevalent carbohydrate-active enzymes (CAZymes). However, analyses of the secreted proteins revealed that the secretome of *D. eres* CBS 160.32 is represented by 5.4% of CAZymes, whereas the secreted CAZymes repertoire of *D. amygdali* CAA958 represents 29.1% of all secretomes. Biosynthetic gene clusters (BGCs) encoding compounds related to phytotoxins and mycotoxins were detected in *D. eres* and *D. amygdali* genomes. The core gene clusters of the phytotoxin Fusicoccin A in *D. amygdali* are reported here through a genome-scale assembly. Comparative analyses of the genomes from 11 *Diaporthe* species revealed an average of 874 CAZymes, 101 secondary metabolite BGCs, 1640 secreted proteins per species, and genome sizes ranging from 51.5 to 63.6 Mbp. This study offers insights into the overall features and characteristics of *Diaporthe* genomes. Our findings enrich the knowledge about *D. eres* and *D. amygdali*, which will facilitate further research into the pathogenicity mechanisms of these species.

keywords: CAZymes; *Diaporthe*; effectors; Fusicoccin A; virulence factors; whole genome sequencing

INTRODUCTION

The intercontinental movement of pathogens along with crop or forestry products can promote the emergence of new pathogens in new ecological niches (Möller & Stukenbrock 2017). However, although the diseases associated with these pathogens may be known, the mechanisms relating to infection biology and pathogenicity/virulence are not entirely understood. In these cases, sequencing of fungal genomes has been widely implemented by mycologists and plant pathologists (Aylward et al. 2017). A genome analysis can provide a first attempt to identify genes associated with different pathogenic strategies, to understand disease biology, improve methods and strategies for disease diagnosis (Aylward et al. 2017; Ellwood et al. 2010).

The genus *Diaporthe* encompasses species behaving as endophytes, saprobes, and pathogens that play an important role in plant pathology (Gomes et al. 2013). Currently more than 300 species supported by DNA sequences are distributed worldwide and have been reported on several hosts causing diseases in agriculture and forestry (Bhunjun et al. 2022; Gao et al. 2017; Guo et al. 2020). For example, *Diaporthe eres* (syn. *D. castaneae-mollissimae*) was reported to cause leaf blight and leaf spot of *Castanea mollissima* (Udayanga et al. 2012), *D. eres* (syn. *D. vaccinii*) was reported to cause twig blight of blueberries (Farr et al. 2002) and *D. amygdali* is known to cause cankers on almond and peach (Varjas et al. 2017). Moreover, it is also recognized that the symptoms caused by *D. amygdali* might be associated with the production of a phytotoxin, Fusicoccin A (Marra et al. 2021).

Studies on *Diaporthe* have been mostly focused on the identification of plant pathogens and endophytes, their pathogenicity (Guarnacci et al 2018; Hilário et al. 2020, and their metabolites (Singh et al. 2011; Tanney et al. 2016. Although there are 25 published genomes currently available in NCBI database (<https://www.ncbi.nlm.nih.gov/>), and 6 genomes deposited in JGI Portal database (<https://genome.jgi.doe.gov/portal/>), there is still a lack of in-depth studies on the genomes of species of *Diaporthe*. Nevertheless, recent studies using genomic and transcriptomic approaches have been carried out to understand how species of *Diaporthe* infect their hosts. For instance, Mena et al. (2022) revealed insights into

the molecular traits involved in pathogenicity of *D. caulivora* on soybean plants. Gai et al. (2021) demonstrated that the genome sequencing of *Diaporthe* species that are responsible for melanose on citrus (*D. citri*, *D. citriasiana* and *D. citrichinensis*), provided resources to unveil the molecular mechanism of fungicide resistance, pathogen-host interaction, and population genome-related research of this relevant plant pathogen.

Recently, Hilário et al. (2021a) showed that *D. amygdali* CAA958 was one of the most aggressive species to blueberry plants. Moreover, CBS 160.32 the ex-type strain of *D. vaccinii* (syn. *D. eres*) was previously recognized as a threat to blueberry plantations and thus was listed as a quarantine organism in Europe (Hilário et al. 2021b). Therefore, to understand how *Diaporthe* species invade the hosts, we aimed to identify pathogenicity-related genes, candidate effectors, cellular transporters, biosynthetic metabolite gene clusters (BGCs), and carbohydrate-active enzymes (CAZymes), by sequencing and analyzing the genomes of *D. eres* CBS 160.32 and *D. amygdali* CAA958. Additionally, a comparative analysis was performed to gain knowledge on the strategies of *Diaporthe* species to successfully entry and colonize their plant host. For this, we analyzed the genomes of nine important plant pathogens, namely *D. ampelina* DA912 (Morales-Cruz et al. 2015), *D. batatas* CRI 302-4 (Yang et al. 2022), *D. capsici* GY-Z16 (Fang et al. 2020), *D. caulivora* D57 (Mena et al. 2022), *D. citri* ZJUD2, *D. citriasiana* ZJUD30, *D. citrichinensis* ZJUD34 (Gai et al. 2021), *D. helianthi* DHEL01 (Baroncelli et al. 2016a) and *D. longicolla* MSPL 10–6 (Li et al. 2017), whose annotations are available and/or published on public databases.

MATERIAL AND METHODS

Fungal material and culture conditions.

Diaporthe amygdali strain CAA958, was collected from diseased twigs of *Vaccinium corymbosum* in Portugal (Hilário et al. 2021c), stored in a glycerol solution (15%) at –80°C and maintained in the culture collection of Micoteca of University of Minho, hosted at Center for Biological Engineering, Braga, Portugal. *Diaporthe eres* strain CBS 160.32, previously known as *D. vaccinii* (Hilário et al. 2021b), was isolated from *V. macrocarpon* in the USA. It was obtained from the CBS

collection of the Westerdijk Fungal Biodiversity Institute, Netherlands. Both strains were cultured on Potato Dextrose Agar (PDA) medium (Merck, Darmstadt, DE, Germany) at 25°C for seven days, prior to DNA extraction.

DNA extraction.

Mycelia of *D. amygdali* CAA958 and *D. eres* CBS 160.32 were obtained from cultures grown on 50 ml of fresh Potato Dextrose Broth medium (PDB, Merck, Darmstadt, DE, Germany) at 25°C for seven days. The mycelium was filtered using sterile filter paper and was ground to a fine powder in liquid nitrogen. DNA was extracted according to Pitcher et al. (1989). The integrity of DNA was assessed using electrophoresis on 0.8% agarose gel and quantified using a Nanodrop 2000 Spectrophotometer (Thermo Fisher Scientific Inc., Waltham, MA, USA).

Genome sequencing, assembly and prediction.

Diaporthe amygdali CAA958 and *D. eres* CBS 160.32 genomes were sequenced from 100 ng of genomic DNA by Genome Sequencer Illumina HiSeq (2 × 150 bp paired-end reads) with NovaSeq 6000 S2 PE150 XP (Eurofins, Belgium). Adaptor contamination and low-quality reads were removed from output reads using the Trimmomatic software v.0.39 (Bolger et al. 2014). The quality of the reads was assessed using FastQC program (Babraham, Bioinformatics, 2016). The genome was assembled using SPAdes v.3.14 with kmer size values of 21, 33, 55 and 77 (Bankevich et al. 2012). QUAST web interface (<http://cab.cc.spbu.ru/quast/>) was used to assess the quality of the assembly. Assembly completeness was assessed using Benchmarking Universal Single-Copy Orthologs (BUSCO v5.3.2) (<https://busco.ezlab.org/>). Gene prediction was performed with Augustus v.3.3.3 (Stanke et al. 2004), using *Diaporthe helianthi* gene models as training set with default parameters..

Dispersed repeat sequences and non-coding tRNA annotation.

Dispersed repeat sequences were masked throughout the genome with the Repeat Masking option (RepeatMasker v.4.0.9) (Smit et al. 2015) implemented in OmicsBox software v.1.4.12 (<https://www.biobam.com/omicsbox>). Tandem repeat

sequences (TRs) were located across the genome using the software Tandem Repeats Finder (TRF) (<http://tandem.bu.edu/cgi-bin/trdb/trdb.exe>) (Gelfand et al. 2007). The tRNAs regions were predicted using the tRNAscan-SE tool (<http://lowelab.ucsc.edu/tRNAscan-SE/>) with default parameters (Lowe and Eddy 1997).

Gene annotation and functional analyses.

The predicted genes were functionally annotated with OmicsBox software using Blast2Go v.1.2.14 (Götz et al. 2008), against the NCBI's nonredundant (Nr) database, the Kyoto Encyclopedia of Genes and Genomes (KEGG) and Gene Ontology (GO) Consortium (<http://geneontology.org>). The protein sequences were classified based on InterProScan and the Evolutionary Genealogy of Genes: Non-supervised 105 Orthologous Groups (EggNOG) databases. The analyses were performed using an e-value threshold of 1×10^{-3} .

The prediction of secreted proteins, including signal peptides, was carried out with SignalP 5.0 (Armenteros et al. 2019), with default parameters. Predicted proteins with signal-peptide were used to identify putative membrane proteins with DeepTMHMM v.1.0.8 (<https://dtu.biolib.com/DeepTMHMM>) (Hallgreen et al. 2022), and proteins with no transmembrane structure were selected as secreted proteins. Additionally, EffectorP v.3.0 was used to predict fungal effectors (<https://effectorp.csiro.au/>) (Sperschneider et al. 2022). To identify proteins involved in pathogenicity, the predicted secretome was used as a query for BlastP search against the pathogen-host interaction database, with a cut-off e-value set at 1×10^{-5} (PHI-database v.4.10) (<http://www.phi-base.org/>), that catalogues verified pathogenicity, virulence, and effector genes from fungal, oomycete and bacterial pathogens (Urban et al. 2020). Biosynthetic gene clusters encoding for secondary metabolites were predicted using the web-based application antiSMASH v.5.0 (<https://fungismash.secondarymetabolites.org/>), using strictness 'relaxed' option to detect well-defined clusters and partial clusters with functional parts (Blin et al. 2019). Carbohydrate-active enzymes were predicted using the web-based application dbCAN HMMs 5.0 (<http://bcb.unl.edu/dbCAN2/blast.php>) with default settings (Yin et al. 2012). Transporters were identified with a BlastP analysis against

the Transporter Classification Database (Saier et al. 2016), using an e-value threshold of 1×10^{-5} . Geneious Prime v.2021.0.3 (<https://www.geneious.com>) was used to BlastP against PHI and Transporter Classification databases.

Comparative analyses.

Nine other fungal genomes were included for comparative analyses (*D. ampelina* DA912, *D. batatas* CRI 302-4, *D. capsici* GY-Z16, *D. caulivora* D57, *D. citri* ZJUD2, *D. citriasiana* ZJUD30, *D. citrichinensis* ZJUD34, *D. helianthi* DHEL01 and *D. longicolla* MSPL 10–6. These genomes, whose annotations are publicly available, were used to perform a comparison of GC content, genome size, BUSCO completeness, predicted proteins, abundance of CAZymes and BGCs. These taxa include mainly pathogens of citrus (Gai et al. 2021), grapevine (Morales-Cruz et al. 2015), soybean (Li et al. 2017; Mena et al. 2022), sunflower (Baroncelli et al. 2016a), sweet potato (Yang et al. 2022) and walnut (Fang et al. 2020).

RESULTS

Genome assembly and genomic characteristics.

Sequencing of *D. amygdali* CAA958 generated more than 23 million reads with 71×fold genome coverage, while sequencing of *D. eres* CBS 160.32 generated over 24 million reads, with approximately 59×fold coverage. The overall assembly statistics for both genomes are summed up in Table 1. Briefly, *D. amygdali* CAA958 genome was estimated at 51.5 Mbp and with 15,818 predicted coding sequences from which 55.7% encode for hypothetical proteins ($n = 8807$). The *D. eres* CBS 160.32 genome size was estimated to be 60.8 Mbp, (15.2% larger than *D. amygdali* CAA958) and has 4.1% more predicted coding sequences ($n = 16\ 499$) and 13.6% more hypothetical proteins than *D. amygdali* ($n = 10\ 195$).

Table 1. Genome assembly overview and gene statistics for the genome of *Diaporthe amygdali* CAA958, and *Diaporthe eres* CBS 160.32

Genome Features	<i>D. amygdali</i>	<i>D. eres</i>
Genome assembled	51.5 Mbp	60.8 Mbp
Number of contigs (> 500 bp)	267	2524
Largest contig length	4 327 563 bp	1 105 552 bp
N50 contig length	1 008 325 bp	169 851 bp
N75 contig length	622 097 bp	74 774 bp
GC content	52.1%	47.6%
BUSCO completeness	98.3%	98.4%
Predicted genes	15 818	16 499
Predicted proteins with signal peptides	1874	1806
Secreted proteins	1562	1616
Candidate effectors	109	98
Total length of coding genes	23 649 268 bp	24 024 391
Average length of predicted genes	1495 bp	1456 bp
Total length of predicted genes / Genome assembled	45.9%	39.5%
Average number of exons per gene	3	3
Average number of introns per gene	2	2

*BUSCO - Benchmarking Universal Single-Copy Orthologs

Repetitive sequences are grouped into Tandem Repeats (TRs) and Dispersed Repeats (DRs). The total length of DRs in *D. eres* CBS 160.32 and *D. amygdali* CAA958 was estimated at 799 386 bp and 571 940 bp, respectively. Regarding the TRs, 8639 sequences, accounting for 0.95% of the whole genome, were predicted for *D. amygdali* CAA958 and 33 522 TRs, covering 3.68%, were estimated in the genome of *D. eres* CBS 160.32 (Table 2). Among the predicted tRNAs in the *D. amygdali* CAA958 genome, 8 tRNAs were predicted as possible pseudogenes and 154 as anti-codon, while for *D. eres* CBS 160.32, it was predicted 19 possible pseudogenes and 158 anti-codon tRNAs.

Table 2. Statistical results for repetitive sequences, tandem repeats and tRNAs in the *Diaporthe amygdali* CAA958 and *Diaporthe eres* CBS 160.32

Type ^a	<i>D. amygdali</i>			<i>D. eres</i>			
	Number (n)	Total Length (bp)	Genome content (%)	Number (n)	Total Length (bp)	Genome content (%)	
Interspersed and terminal repeats	LTRs	131	12 096	0.0235	140	12 642	0.0208
	DNA transposons	174	9942	0.0193	143	11 693	0.0192
	LINEs	18	1207	0.0023	21	1611	0.0027

SINEs	0	0	0	0	0	0
Rolling circles	4	243	0.0005	0	0	0
Small RNA	55	8582	0.0167	52	8523	0.0140
Satellites	25	1927	0.0037	18	1434	0.0024
Simple repeats	11 895	486 262	0.9445	15 264	686 233	1.1289
Low complexity	1067	51 681	0.1004	1571	77 250	0.1271
TOTAL	13 369	571 940	1.1109	17 209	799 386	1.3151
Tandem repeats	8639	478 007	0.9459	33 522	2 237 060	3.6802
tRNAs	162	15 038	0.0292	177	17 216	0.0283

^aSINEs – short interspersed nuclear elements; LINEs – long interspersed nuclear elements; LTRs – long terminal repeats.

Gene prediction and functional annotation.

The genome of *D. amygdali* CAA958 was estimated at 15 818 genes and *D. eres* CBS 160.32 at 16 499 genes annotated according to the NCBI's nonredundant protein (Nr), UniProt/Swiss-Prot, EggNOG, KEGG, GO databases (Table S1 and Table S2). From the total 14 012 predicted proteins in *D. amygdali* CAA958, a signal peptide was identified in 1874 (14.4%) proteins (Table S3) and a transmembrane structure was detected in 3122 (19.7%) (Table S4). From those proteins with signal peptide and no transmembrane structure, 1562 (31.7%) were selected as secreted proteins (secretome) (Table S5). In the genome of *D. eres* CBS 160.32, 14 625 (88.6%) proteins were predicted, from which 1806 (12.3%) had signal peptide, 3220 (22.0%) proteins were identified with transmembrane structure, and 1616 (11.1%) were selected as secreted proteins.

Functional analysis (GO, Biological Process) of *D. amygdali* CAA958 (Table S1) and *D. eres* CBS 160.32 (Table S2) revealed that most genes are involved in cellular and metabolic processes, localization (establishment of cellular component location) and biological regulation (Fig. 1). In both genomes genes included in cellular process category were mostly classified as chaperones, or being participating in posttranslational modification or protein turnover, intracellular trafficking, secretion, and vesicular transport, signal transduction mechanisms, cell wall and cell cycle control, cytoskeleton, and others, that include defense mechanisms, nuclear and extracellular structure, and cell motility. Regarding the metabolic process category, genes of both species are largely involved in the

transport and metabolism of carbohydrates, biosynthesis, transport and catabolism of secondary metabolites, amino acids, energy production and conversion, metabolism of lipids and inorganic ions. In GO, Molecular Functions, genes are mostly involved in catalytic activity, binding, and transporter activity. Within the catalytic activity, genes are classified as participating in oxidoreductase, hydrolase, and transferase. Analyses of Cellular Component (GO) shows that most genes are involved in cellular anatomical entity, membrane, cytoplasm, and nucleus.

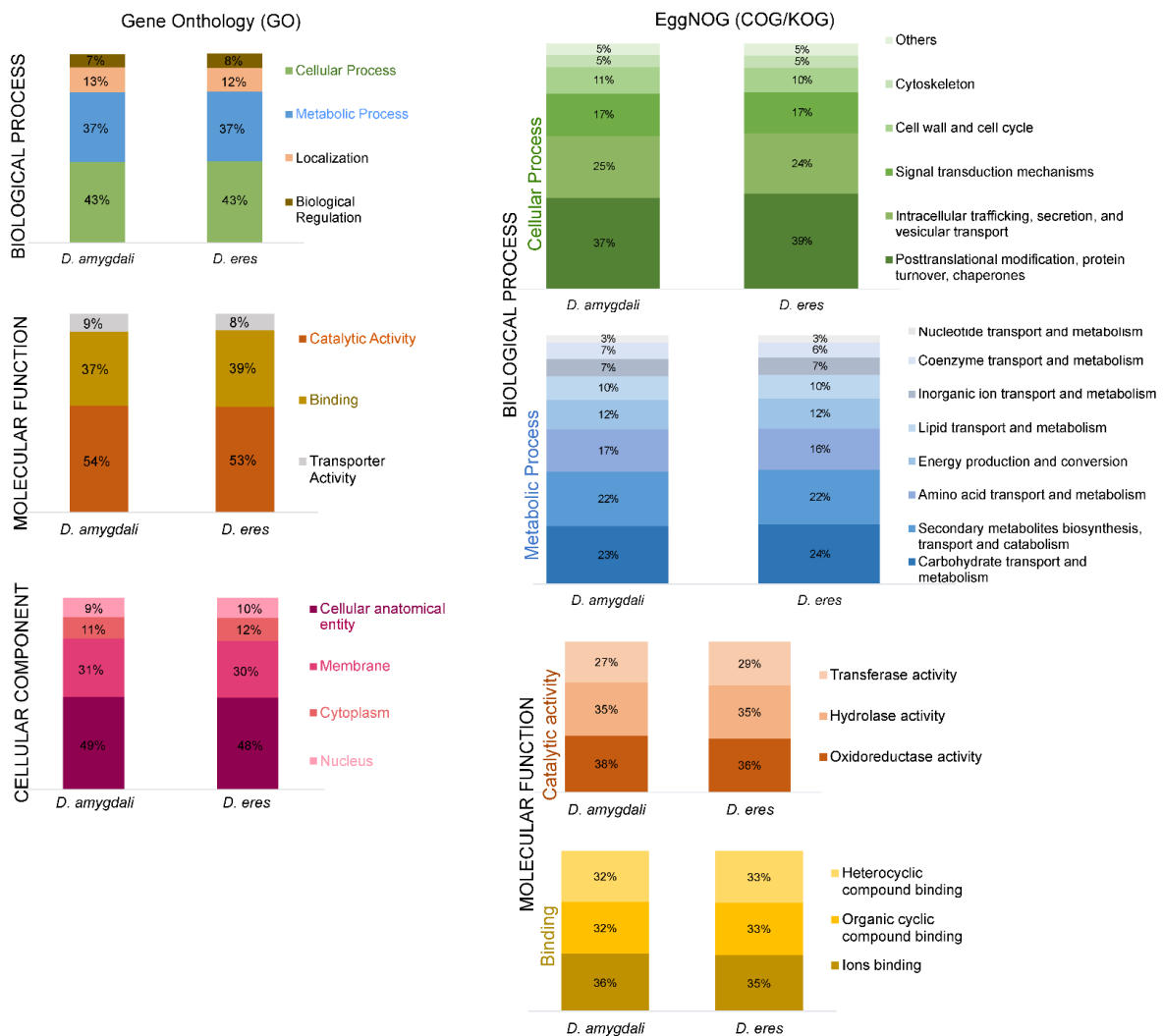


Figure 1. Gene Ontology (GO) and EggNOG functional annotation (right panel) of *Diaporthe amygdali* CAA958 and *Diaporthe eres* CBS 160.32.

Fusicoccin A biosynthesis.

Fusicoccin A is a phytotoxin produced by *D. amygdali*. We identified the genes involved in its biosynthesis, located at 2 different loci. The core gene clusters for Fusicoccin A comprises 13 genes that were found only in the genome of *D.*

amygdali CAA958. The clusters include a *PaFS* fusicoccadiene synthase, five cytochrome P450s (*PaP450-1*, *PaP450-2*, *PaP450-3*, *PaP450-4*, *PaP450-5*), two O-acetyltransferases (*PaAT-1*, *PaAT-2*), a methyltransferase (*PaMT*), a prenyltransferase (*PaPT*), an alpha-ketoglutarate dependent dioxygenase, a glycosyltransferase (*PaGT*) and a short-chain dehydrogenase/reductase (Fig. 2). The schematic organization of the loci was created using the free software SnapGene Viewer 4.0.1 (<https://www.snapgene.com/>).

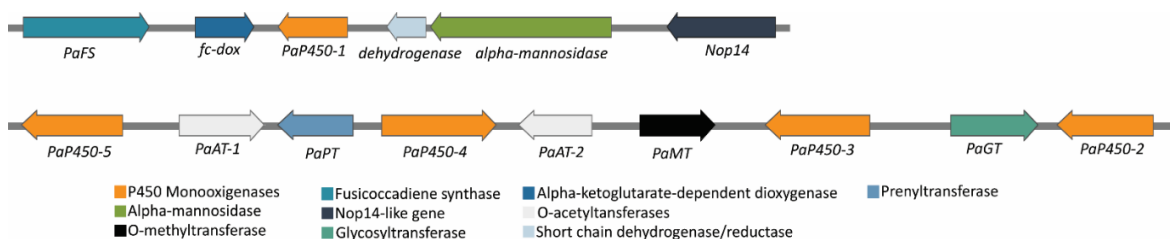


Figure 2. Fusicoccin A biosynthetic gene clusters found in *Diaporthe amygdali* CAA958. Grey horizontal lines represent genomic sequences. Color coded arrows represent the predictive function of different genes. Arrows indicate the direction of transcription of the gene.

Virulence factors, effectors and strategies to overcome host responses.

From the predicted secretome of *D. eres* CBS 160.32, we identified 88 genes encoding for CAZymes (5.4%), 458 secreted proteins were identified in the pathogen–host interaction (PHI) database [44] (28.1%) (Table S6). From these secreted proteins, 98 were identified as effector candidates (20%) including carboxylesterases, lipases, peptidases, and glycosyl hydrolases and several hypothetical proteins (Table S7). In the secretome of *D. amygdali* CAA958, we identified 454 genes encoding for CAZymes (29.1%), 469 in the PHI-database (29%) (Table S6) and 109 effectors (5.6%) such as pectate lyases, cellulases, endopolygalacturanases, cutinases and laccases (Table S7). Some predicted effectors were also found on both *D. eres* and *D. amygdali* genomes including the CFEM domain (Common in Fungal Extracellular Membrane), necrosis and ethylene-inducing peptide 1 (Nep1)-like proteins (NLP), metalloproteases, pectinesterases and acetylxylan esterases. Moreover, genes encoding for proteins with potential roles in the pathogenesis such as the velvet complex, virulence protein sorting and proteases were also identified on both genomes (Table 3). Genes encoding proteins that are produced to overcome immune plant defenses were also

detected on both genomes analyzed, such as genes encoding arylsulfatases, salicylate hydroxylase, tyrosinase, homogentisate dioxygenase (HGD), fumarylacetoacetate hydrolase (FMH), cytochrome P450 monooxygenases superfamily and flavin-containing monooxygenases..

Table 3. Putative proteins involved in fungal pathogenesis, identified in the genome of *Diaporthe eres* CBS 160.32 and *Diaporthe amygdali* CAA958.

Putative protein	<i>D. amygdali</i> CAA958	<i>D. eres</i> CBS 160.32	Function	Reference
Acid aspartase	√	×	Role in the mechanisms of virulence during fungal infection, participating in the degradation of the host's physical barriers	Figueiredo et al. 2021
Aminobutyrate aminotransferase	√	√	Metabolization of γ -aminobutyric acid, providing pathogen nitrogen requirements during infection	Félix et al. 2019
Aminopeptidase, Carboxypeptidase	√	√	Protease required by fungi for host peptide degradation during pathogenesis.	Madhu et al. 2020
Cerato-ulmi	√	×	Hydrophobic proteins secreted by filamentous fungi (<i>Ophiostoma</i> species). It possesses properties of a wilt toxin in susceptible elms, such as <i>Ulmus americana</i> .	Bettini et al. 2014; Temple et al. 2000
Chitin synthases	√	√	Enzymes that serve as a pathogen-associated molecular pattern (PAMP), triggering immune responses in host plants. Reported in <i>Magnaporthe oryzae</i> , <i>Botrytis cinerea</i> , <i>Fusarium graminearum</i> and <i>F. verticillioides</i> .	Kong et al. 2012
Metalloprotease	√	√	Zinc-chelating protease that play an essential role in microbial pathogenesis. In <i>M. oryzae</i> , is an effector that trigger host defense response.	Huang et al. 2020
Nudix proteins	√	√	Important virulence components manipulating host defense mechanisms.	Dong & Wang 2016
Siderophores	√	√	Chelators synthesized to be involved in iron uptake, intracellular transport, and storage. Essential virulence factors allowing the fungus to overcome severe iron limitation imposed by the host.	Silva et al. 2020
Subtilisin-like serine protease	√	√	Protease that are released in infected plant host to degrade pathogenesis-related proteins and to disrupt host cell membranes.	Figueiredo et al. 2018
Tripeptidyl-peptidase	√	×	Acidification of the microenvironment in the host, facilitating the proliferation of the pathogen.	Reichard et al. 2006
Velvet proteins	√	√	Promotion of chromatin accessibility and expression of biosynthetic gene clusters involved in pathogenicity as mycotoxins, pigments, and hormones	López-Berges et al. 2013
Virulence protein SSD1	√	√	Important for <i>M. grisea</i> to colonize rice leaves, leading to evasion and tolerance of the host immune response.	Tanaka et al. 2007; Thammahong et al. 2019

Vacuole protein sorting (VPS)	√	√	Proteins involved in the delivery of soluble vacuolar compounds, metabolite storage and osmoregulation. Essential for fungal growth and pathogenesis.	Palmer 2011
-------------------------------	---	---	---	-------------

Cellular transporters.

All protein classification (TC) classes were detected in our analyses: TC 1, TC 2, TC 3, TC 4, TC 5, TC 8 and TC 9 (Table 4). A total of 2325 and 2238 genes encoding for transporters were identified (Table S8) in *D. amygdali* CAA958 and *D. eres* CBS 160.32, respectively, accounting for 14.7% and 13.6% of the total predicted genes for. Overall, the electrochemical potential-driven transporters (TC 2) were the most prominent group, and in both genomes represent an average of 42% of the annotated transporters, followed by the primary active transporters (TC 3, average = 17%) and channels and pores (TC 1, average = 16%). The TC 2 was the largest category of cellular transporters identified in *D. eres* CBS 160.32 and *D. amygdali* CAA958 (Table 4). Both genomes encode transporters involved in the transport of zinc (e.g., *zrt1*, *zrt2*, *zrt3*), sulfur (e.g., *mup1*, *mup3*), siderophores (e.g., *mirB*), and MFS transporters (Major Facilitator Superfamily) such as sugar/H⁺ symporter (e.g., *stl1*), glucose/xylose symporter, inositol, and glycerol transporters. On both genomes, we also detected genes encoding for ABC transporters (TC 3) that confer antifungal resistance to fluconazole (e.g., *fcr1*) and voriconazole (e.g., *atrF*). Some accessory factors involved in transport (TC 8) were found on *D. eres* and *D. amygdali* genomes, such as genes encoding tetraspanin (e.g., *pls1* and *tsp3*) and peroxiredoxins (e.g., *prx1*) transporters.

Table 4. Number of genes predicted to code for transporters in the genome of *Diaporthe amygdali* CAA958 and *Diaporthe eres* CBS 160.32.

Transporter class	<i>D. amygdali</i>	<i>D. eres</i>
Channels and pores (TC 1)	348	348
Electrochemical potential-driven transporters (TC 2)	973	911
Primary active transporters (TC 3)	366	371
Group translocators (TC 4)	48	39
Transmembrane electron carriers (TC 5)	14	13
Accessory factors involved in transport (TC 8)	270	266
Incompletely characterized transport systems (TC 9)	306	290
TOTAL	2325	2238

Comparative analyses.

Predicted genes and genome statistics.

Most published genomes of *Diaporthe* do not have available functional annotations, thus we have chosen *D. ampelina* DA912, *D. batatas* CRI 302-4, *D. capsici* GY-Z16, *D. caulivora* D57, *D. citri* ZJUD2, *D. citriasiana* ZJUD30, *D. citrichinensis* ZJUD34, *D. helianthi* DHEL01 and *D. longicolla* MSPL 10–6 to perform a comparative analysis. These species were chosen mainly due to their importance as plant pathogens, and to their annotation's availability on public databases and published works. Overall, the genomic features vary among the analyzed species regarding their GC content, genome size, and BUSCO completeness. The GC content ranges from 43.9% to 52.9%, where *D. helianthi* DHEL01 displayed 17% less GC content (43.9%) than *D. caulivora* D57 (52.9%). The number of predicted genes ranged from 10 704 (*D. ampelina* DA 912) to 18 385 (*D. caulivora* DS7), where *D. ampelina* has 41.8% less genes than *D. caulivora*. The size of the genomes had an average of 57.1 Mbp per species, ranging from 51.5 Mbp in *D. amygdali* CAA958 to 63.6 Mbp in *D. helianthi* DHEL01, being the genome of *D. amygdali* 19% smaller than *D. helianthi* (Table 5). A near completeness of the assemblies was also verified by BUSCO analyses, which reported an average of 98.4% of completeness among all species analyzed. The number of secreted proteins showed an average of 1640 per species, and from 2043 in *D. citrichinensis* ZJUD34 to 1224 in *D. batatas* CRI 302-4.

Table 5. Genomic features of the *Diaporthe* species analyzed. (ND – no data)

Species	Strain	Host	BUSCO* completeness %	Genome size (Mb)	GC content %	Predicted genes	Secreted Proteins	CAZymes	BGCs	GenBank Accession number
<i>Diaporthe ampelina</i>	DA912	Grapevine	98.7	53.4	52.8	10 704	ND	696	105	LWAD01000000
<i>Diaporthe amygdali</i>	CAA958	Blueberry	98.3	51.5	52.1	15 818	1562	856	86	This study
<i>Diaporthe batatas</i>	CRI 302-4	Sweet potato	97.9	54.4	50.6	13 037	1224	941	91	JAHWGW000000000
<i>Diaporthe capsici</i>	GY-Z16	Walnut	98.4	57.6	51.3	14 425	1488	843	103	WNXA000000000
<i>Diaporthe caulivora</i>	D57	Soybean	97.8	57.8	52.9	18 385	1501	ND	ND	ND
<i>Diaporthe citri</i>	ZJUD2	Citrus	98.5	59.6	47.9	15 218	1860	847	98	JADAZQ000000000
<i>Diaporthe citriasiana</i>	ZJUD30	Citrus	99.2	52.4	52.0	13 839	1643	796	89	JADWDH000000000
<i>Diaporthe citrichinensis</i>	ZJUD34	Citrus	98.3	54.5	54.1	15 928	2043	925	110	JADAZR000000000
<i>Diaporthe eres</i> (syn. <i>D. vaccinii</i>)	CBS 160.32	Blueberry	98.4	60.8	47.6	16 499	1616	859	88	This study
<i>Diaporthe helianthi</i>	DHEL01	Sunflower	98.3	63.6	43.9	13 139	1433	764	67	MAVT02000001
<i>Diaporthe longicolla</i>	MSPL 10–6	Soybean	98.2	62.0	48.6	16 597	1535	1221	174	AYRD000000000

*BUSCO - Benchmarking Universal Single-Copy Orthologs

CAZymes.

A total of 857 and 859 genes encoding for putative CAZymes were identified in the *D. amygdali* and *D. eres* genomes, respectively, using the HMMER database (Table 6; Table S9-S10). The glycoside hydrolases (GH) are by far the largest family. About 404 and 398 protein-coding genes belonging to more than 65 different glycoside hydrolases, made up approximately 47% of *D. amygdali* and 46% of *D. eres* cell-wall degrading repertoire, respectively. The main GH subfamilies detected on both *D. amygdali* and *D. eres* genomes were β -glucosidases (GH3), endo- β -1,4-glucanases/cellulases (GH5), α -amylases (GH13), xyloglucan transglucosylases (GH16), chitinases (GH18), polygalacturonases (GH28) and β -xylosidase/ α -L-arabinofuranosidases (GH43). Regarding glycosyltransferases (GT), GT1 (uridine diphosphate UDP-glycosyltransferase) and GT2 (cellulose/chitin synthase) were the most abundant. Carbohydrate-binding modules (CBM) families involved in starch-binding (CBM20) and L-rhamnose-binding (CBM67), were also the most abundant in both genomes analyzed. Among the auxiliary activity (AAs) family, cellobiose dehydrogenases (AA3), xylo- and cello-oligosaccharide oxidases (AA7) and copper-dependent lytic polysaccharide monooxygenases (AA9) were the most predominant. Regarding the carbohydrate-esterases (CE) subfamilies, acetylxylan esterases (CE1) and cutinases (CE5) were the most abundant, while the pectase lyases PL1 and PL3 (polysaccharide lyases) were also the most prominent families on *D. amygdali* and *D. eres* genomes.

Table 6. Predicted genes encoding for CAZymes in the genomes of *Diaporthe amygdali* CAA958 and *Diaporthe eres* CBS 160.32.

Classes	Total number of genes		Secreted CAZymes	
	<i>D. amygdali</i>	<i>D. eres</i>	<i>D. amygdali</i>	<i>D. eres</i>
GT	107	108	3	10
GH	404	398	235	40
CBM	20	25	11	4
AA	230	225	131	26
CE	63	66	44	5
PL	33	37	30	3
TOTAL	857	859	454	88

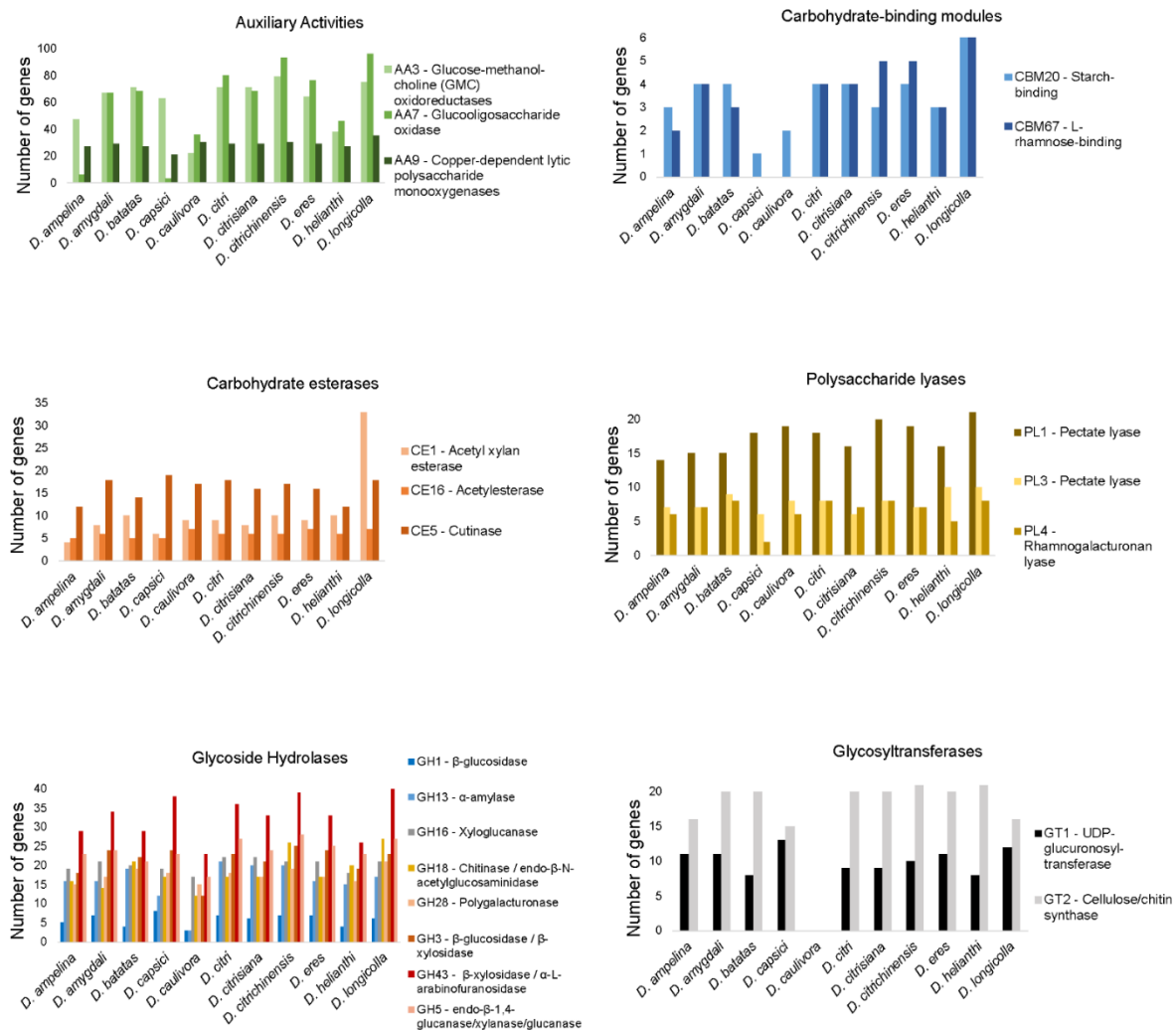


Figure 3. Number of predicted genes encoding for the most abundant carbohydrate-active enzymes families in all genomes of the analyzed *Diaporthe* species.

Overall, the total number of CAZymes per species were 874, ranging from 696 in *D. ampelina* to 1221 in *D. longicolla*. Although all classes of CAZymes were detected, glycoside hydrolases and auxiliary activities were the two groups with the most predicted proteins. Families AA3, AA7, AA9, CBM20, CBM67, CE1, CE16, CE5, PL1, PL3, PL4, GH1, GH13, GH16, GH18, GH43, GT1 and GT2 were the most abundant among all species analyzed (Fig. 3). Overall, *D. longicolla* displayed the highest CAZymes content including the families AA7, CBM20, CBM67, CE1, PL1 and GH43, followed by *D. citrichinensis* with an abundance of AA7, CBM67, PL1, GH18 and GH28 families. Contrarily, the GT1 family was most predominant in *D. capsici* and *D. longicolla* genomes.

BGCs.

There are 86 and 88 BGCs involved in the secondary metabolism of *D. amygdali* and *D. eres*, respectively (Table S11). The BGCs identified on *D. amygdali* genome encode 10 terpenes, 3 indoles, 36 t1PKs (type 1 polyketide synthases), 10 NRPS (non-ribosomal peptide synthase), 6 t1PKs-NRPS, 11 NRPS-like, 2 t1PKs-indole, and one of each: siderophore, Fungal-RiPP, t1PKS-NRPS-indole, NRPS-NRPS-like, t1PKs-t3PKs, t3PKs, “other” and other-t1PKs. Of these 86 BGCs, clusters 1, 21 and 24 have 100% similarity with known BGCs, such as fusarin (mycotoxin), clavatic acid (anti-cancer) and alternariol (phytotoxic and antifungal), respectively. Clusters 2, 12, 24 and 41 showed homologies with fusarielin H (anti-fungal) (25%), betaenone (37%) and alternapyrone (40%) (phytotoxins) and squalestatin (anti-fungal) (40%).

In *D. eres*, the 88 BGCs identified encode for 8 terpenes, 5 indoles, 35 t1PKs (type 1 polyketide synthases), 10 NRPS (non-ribosomal peptide synthase), 6 t1PKs-NRPS, 12 NRPS-like, 2 terpene-NRPS-like, 2 t1PKs-NRPS-like, 2 t1PKs-NRPS-indole, and one of each: siderophore, Fungal-RiPP, NRPS-like-indole, t1PKS-terpene, t1PKs-indole and ‘other’. From the 88 secondary metabolite gene clusters identified, clusters 179, 197 and 297 have 100% similarity with known BGCs, such as the phytotoxins alternariol, mellein and ACT-Toxin II, respectively. Clusters 271, 268 and 134 were also found to have homologies with the phytotoxins alternapyrone (40%) and cercosporin (31%), and with PR-toxin (mycotoxin) (50%), respectively.

Moreover, other BGCs encoding for betaenone, cercosporin, and PR-toxin were detected among the genomes analyzed, but with a similarity ranging from 22% to 60%, indicating that some genes may be truncated. *Diaporthe eres* cluster 268 showed a gene similarity of 31% with cercosporin cluster, and it contains only three genes responsible for the biosynthesis of this compound: *ctb3* (cercosporin toxin biosynthesis protein), *ctb1* (PKS) and *ctb2* (O-methyltransferase). Cluster 12 from *D. amygdali* and cluster 360 from *D. eres* showed 37% similarity with the betaenone BGCs and contain a HR-PKS, an enoyl reductase, a short-chain dehydrogenase reductase and a cytochrome P450 but lacking a dehydrogenase and a FAD-dependent oxidase. Cluster 271 of *D. eres* contains genes involved in PR toxin biosynthesis: a terpene cyclase, an aristolochene synthase, an oxidoreductase, an

oxidase, two P450 monooxygenases, a transferase, and two dehydrogenase enzymes.

The genomes analyzed were rich in gene clusters that are involved in the synthesis of secondary metabolites, with an average of 101 per species. *Diaporthe longicolla* contains the highest number of BGCs ($n = 174$) and *D. helianthi* has the lowest ($n = 67$). *Diaporthe amygdali* and *D. eres* contains 38.5% and 49.4% fewer BGCs than *D. longicolla*, respectively. Overall, all species were estimated with an average of 101 BGCs per species. Type 1 polyketide synthases were the most abundant type of gene clusters, followed by NRPS, NRPS-like, terpenes, and t1PKs-NRPS (Fig. 4). Several BGCs encoding phytotoxins with 100% similarity with known BGCs were detected in the genomes analyzed. For example, fusarin BGC was found on *D. batatas*, *D. helianthi*, *D. longicolla* and *D. amygdali*; alternariol BGC was detected in *D. amygdali*, *D. destruens*, *D. eres* and *D. capsici*, and mellein BGC was also found in *D. eres*, *D. capsici*, *D. destruens* and *D. longicolla*. It is worthy to note that the ACT-toxin BGC was detected only in *D. batatas*, *D. capsici*, *D. citrisiana* and *D. eres*.

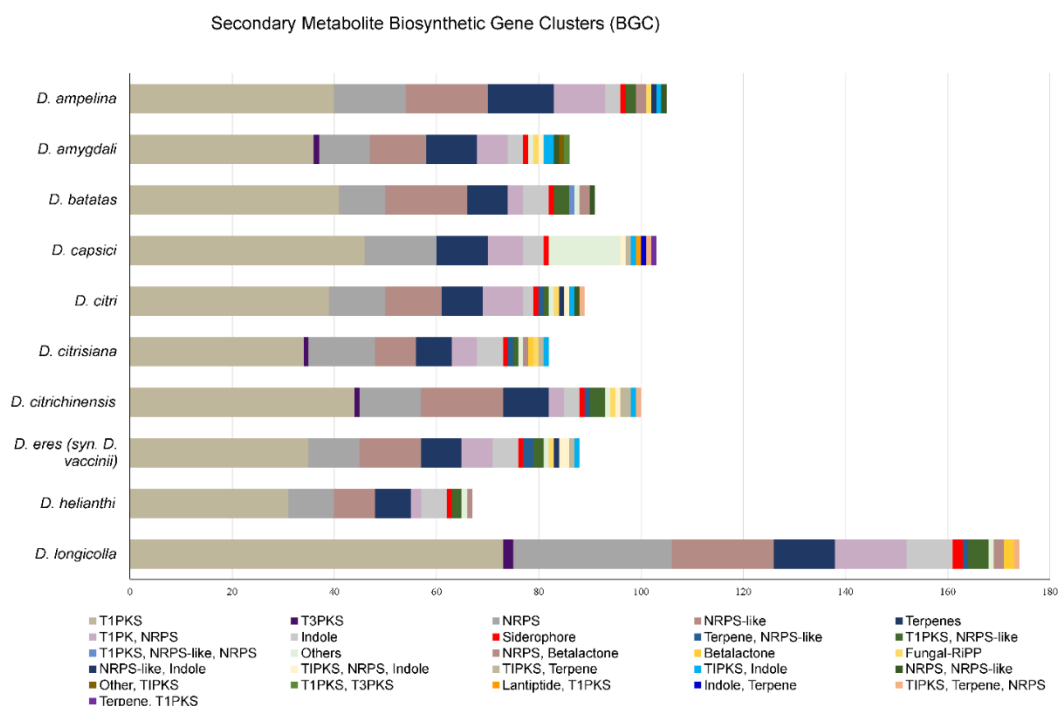


Figure 4. Biosynthetic gene clusters (BGC) identified in the genomes of *Diaporthe* analyzed. *Diaporthe caulivora* BGCs are not included because the genome is not publicly available.

DISCUSSION

The genomes of *D. eres* CBS 160.32 and *D. amygdali* CAA958 were sequenced, analyzed, and compared with the genomes of *D. ampelina* DA912, *D. batatas* CRI 302-4, *D. capsici* GY-Z16, *D. caulivora* D57, *D. citri* ZJUD2, *D. citriasiana* ZJUD30, *D. citrichinensis* ZJUD34, *D. helianthi* DHEL01 and *D. longicolla* MSPL 10–6, to understand the main strategies that *Diaporthe* species use to infect and colonize their hosts.

While plants develop defense mechanisms against fungal pathogens, fungi develop strategies to attack their hosts and to manipulate plant immune responses (Yan et al. 2018). Effectors such as the CFEM domain, NEP1-like protein and metalloproteases, which are known to manipulate the host's hypersensitive response, acting as toxins to induce plant cell death, thereby favoring early pathogen colonization, were detected on both *D. amygdali* CAA958 and *D. eres* CBS 160.32 genomes (Nagel et al. 2021). Vacuole protein sorting (VPS) enhancing stress resistance to survive within the host (Palmer 2011), virulence protein SSD1 involved in tolerance to host immune response (Thammahong et al. 2019) and subtilisin-like serine protease participating in the degradation of pathogenesis-related proteins produced by the host (Figueiredo et al. 2018) are among the pathogenicity genes detected on *D. eres* and *D. amygdali* genomes.

Fungi can quickly adapt to changing environments and develop strategies to overcome immune plant defenses, due to their genetic flexibility (Eschenbrenner et al. 2020). Sulfur is an essential element required for the growth and function of all fungal cells (Paietta 2004; Traynor et al. 2019). To overcome severe nutrient limitation imposed by the host (e.g., sulfur), fungi exhibit responses to alleviate the nutrient deficiency (Paietta 2004). This includes transport systems (e.g., sulfate and methionine permease) allowing the uptake of the sulfate produced, and sulfate starvation-induced (SSI) proteins (e.g., arylsulfatase), involved in sulfur scavenging from the environment (Li et al. 2019). Given that genes encoding for sulfur transporters and arylsulfatases were identified in the genomes of *D. amygdali* and *D. eres*, it is suggested that both species may take advantage of sulfur from their hosts for a successful infection, thus ensuring fungal survival in the host's microenvironment. Moreover, genes encoding for salicylate hydroxylase,

tyrosinase, homogentisate dioxygenase (HGD), and fumarylacetoacetate hydrolase (FMH) (Cregut et al. 2013; Gonçalves et al. 2019), were also identified. The presence of these genes supports the idea that *D. eres* and *D. amygdali* may be able to degrade salicylic acid and plant phenylpropanoid precursors, which are produced by the host as defense mechanisms (Gonçalves et al. 2019). Genes encoding for the biosynthesis of carbohydrates inositol (e.g., inositol 5-phosphatase) and mannitol (e.g., mannitol-1-phosphate 5-dehydrogenase) were also detected, involved in the inositol phosphate metabolism, and fructose and mannose metabolism pathways, respectively. In fungi, inositol plays a major role in metabolic adaptation, fungal virulence, and sexual development (Murry et al. 2021). Reynolds (2009) reported the importance of inositol acquisition in the biology and pathogenesis of some fungal pathogens (e.g., *Candida albicans*). Moreover, it is reported that some fungal plant pathogens use mannitol to detoxify reactive oxygen species (ROS) produced by plants (Meena et al. 2015). This suggests that both *D. amygdali* and *D. eres* may take advantage of inositol to proliferate and cause infection in their hosts, and mannitol to counteract ROS-mediated defenses produced by the host.

A high number of cellular transporters annotated on both *Diaporthe* species were identified, suggesting the ability to transport molecules to enhance pathogenicity, secondary metabolites, and sugars into the cell (Stergiopoulos et al. 2002). The access to sugars that are released from complex plant polysaccharides, relies on the ability of fungi to secrete a large amount of sugar transporters from the MFS transporters (TC.2) (Nogueira et al. 2018) In fact, the TC 2 was the largest category identified in *D. eres* and *D. amygdali*. Sugar/H⁺ symporter, glucose/xylose symporter, inositol and glycerol transporters can recognize and transport more than one type of sugar such as xylose, glucose and cellobiose into the cell (Colabardini et al. 2014). The high number of annotated transporters detected, is corroborated by studies on other fungi colonizing plants such as the *Botryosphaeriaceae*, that ranges from 3,143 in *Dothiorella sarmentorum* to 2,185 in *D. iberica* (Garcia et al. 2021). In addition to the transport of sugars, peroxiredoxin and tetraspanin transporters were also detected. Rocha et al. (2018) suggested that peroxiredoxin plays an important role in development and pathogenicity of *Aspergillus fumigatus*

and *M. oryzae*. Jimenez-Jimenez et al. (2019) have also stated that tetraspanins are crucial for appressorium-mediated penetration into the host, and act as coordinators of the infection process of *M. oryzae* and *Botrytis cinerea*. Therefore, we suggest that *D. eres* CBS 160.32 and *D. amygdali* CAA958 display traits in the genomes to support virulence and persistence into the hosts.

Fusicoccin A is a diterpene-glucoside, discovered in 1964 as a fungal phytotoxin, produced by *Fusicoccum amygdali* (syn. *D. amygdali*) (Noike et al. 2012a), whose structure was characterized in 1968 (Ohkanda 2021). From a draft genome of *Phomopsis amygdali* (syn. *D. amygdali*) strain Niigata-2, Noike et al. (2012b) suggested that Fusicoccin biosynthetic genes are located at 2 different loci: one containing four genes and the other nine genes. In fact, our results showed that these two gene clusters involved in the biosynthesis of Fusicoccin are composed of 13 genes and were detected in *D. amygdali* CAA958. Fusicoccin A is known to induce irreversible opening of stomata, causing uncontrolled transpiration, leading to the development of cankers on branches, as well as the chlorosis and necrosis of distal leaves in almonds and peach trees (Marra et al. 2021; Ohkanda 2021). When tested on stems/twigs or detached leaves, Fusicoccin can also cause the stomatal opening in a wide range of plants such as: tobacco (*Nicotiana tabacum*), sorghum (*Sorghum bicolor*), cucumber (*Cucumis sativa*) and lucerne (*Medicago sativa*) (Noike et al. 2012b; Turner & Graniti 1969). It is interesting to note that some studies outlined that Fusicoccin may also contribute to improve plant physiological performance (Marra et al. 2021). For instance, some biological activities are attributed to this diterpene-glucoside such as the induction of abscission (Feldman et al. 1971), potassium uptake (Lanfermeijer and Prins 1994), cell enlargement or stimulation of seed germination (Ballio et al. 1981). Thus, this suggests that besides its reported phytotoxicity, Fusicoccin can also be used as plant growth regulators in agriculture, as well as biochemical agents for plant physiology (Chen et al. 2022).

The results hinted at a possible correlation between the number of genes and the genome size of the *Diaporthe* species considered in this study. Most fungal species with available genomes exhibit a genome size that ranges from 30 Mbp to 40 Mbp range (average = 37.2 Mbp), while genome sizes of sequenced plant pathogenic ascomycetes are slightly larger (average = 39.4 Mbp) (Aylward et al.

2017; Garcia et al. 2012). However, our results show large genome size among all *Diaporthe* species analyzed, falling within the 51.5–63.6 Mbp range, with an average of 57.1 Mbp. Although still poorly understood, some studies have revealed that large genome size and high numbers of genes are common in fungal plant pathogens (Ohm et al. 2012). Such outcome might be explained by the presence of genes related to host colonization traits (e.g., production of CAZymes, peroxidases) that are under high selective pressure, which may result in gene duplication events that play important roles in fungal evolution and adaptation (Baroncelli et al. 2016b; Garcia et al. 2021).

For a successful infection, pathogens may need to break the plant cell wall that is composed of polysaccharides such as cellulose, beta-glucans, hemicellulose, and pectin (Morales-Cruz et al. 2015; Rafiei et al. 2021). Plant pathogens display a wide variety of CAZymes that are involved in the degradation of these plant polysaccharides (Lombard et al. 2014). All genomes analyzed in this study had abundant numbers of CAZymes (an average of 874 per species), being the GHs the most predominant. GHs functions of β -glucosidases, β -xylosidases, amylases, glucanases and L-arabinofuranosidase, and endo- β -1,4-cellulases were present in all *Diaporthe* species used in this study, thus playing an important role in fungal pathogenicity. For instance, endo- β -1,4-cellulases is one of the families commonly found in *Neofusicoccum parvum* (Morales-Cruz et al. 2015), while pectinases, hemicellulases and cellulases secreted by *Valsa mali* are crucial in apple infection (Yan et al. 2018). In the same way as the GH, AA functions such as cellobiose dehydrogenase and gluco-oligosaccharide oxidase, that assist the lignocellulolytic enzymes in the degradation of plant biomass, were also abundant among all *Diaporthe* species analyzed. Moreover, CBMs that bind to glycoside hydrolases, to enhance plant cell wall degradation (e.g., L-rhamnose-binding and starch-binding) and PLs degrading glycosaminoglycans and pectin were also detected among all species analyzed. Our results corroborate previous studies that state that the capacity of plant cell wall degradation is linked to fungal lifestyle (necrotrophic, hemibiotrophic and biotrophic) (Lyu et al. 2015; Wang et al. 2022). For instance, some authors have documented that higher numbers of hydrolytic enzymes are most prominent in hemibiotrophs (e.g., *M. oryzae*, *D. longicolla*, *N. parvum*),

necrotrophs (e.g., *B. cinerea*), saprobes (e.g., *Paraphaeosphaeria sporulosa*) and endophytes/latent pathogens (e.g., *Periconia macrospinosa*) than in biotrophs (Garcia et al. 2021; Li et al. 2017; Lyu et al. 2015). Therefore, given that species of *Diaporthe* are hemibiotrophs (Udayanga et al. 2011) it is expected that all species analyzed exhibit a high number of CAZymes.

The proportion of CAZymes in the *D. amygdali* secretome (29.1%), is consistent with previous reports in other *Diaporthe* species such as *D. capsici* and *D. citri* (30.7%), *D. caulivora* (30.6%), and *D. longicolla* (31.4%) emphasizing the importance of CAZymes in *Diaporthe* pathogenicity (Mena et al. 2022). Nevertheless, the proportion of CAZymes in the secretome of *D. eres* CBS 160.32 was estimated at 5.4%, which is quite low when comparing with the species mentioned above (average = 30.5%). The low number of secreted hydrolytic enzymes may explain the lack of pathogenicity of *D. eres* CBS 160.32, which is consistent with studies that categorizes this species as a weak pathogen on blueberry plants (Cardinaals et al. 2018; Hilário et al. 2021a).

Moreover, hemibiotrophic plant pathogens usually possess higher numbers of genes involved in the biosynthesis of secondary metabolites than biotrophic pathogens (Howlett 2006). In fact, an abundance of BGCs was found in all species analyzed. These secondary metabolites can be toxic polyketides, non-ribosomal peptides, terpenes, and indoles that induce plant cell death and lead to disease development (Nagel et al. 2021). The genomes of *Diaporthe* analyzed contained many BGCs, especially t1PKS, NRPS, NRPS-like and terpenes. Although the products of some clusters are unknown, some of them could be determined. These compounds included phytotoxins (alternariol, mellein, ACT-toxin II) and mycotoxins (fusarin). Although ACT-toxin is recognized as a host specific toxin from citrus infecting *A. alternata* (Tsuge et al. 2013), it is worthy to note that the ACT-toxin producing gene cluster was detected in *D. eres* and *D. capsici*. However, the ACT-toxin II BGC has also been detected in species of *Botryosphaeriaceae* (Nagel et al. 2021). Therefore, it is suggested that the genes from the cluster responsible for the biosynthesis of the ACT toxin, may have been acquired from horizontal gene transfer, as previously suggested by Wang et al. (2019).

CONCLUSIONS

This study represents the first report of the *Diaporthe amygdali* and *D. eres* genome sequence. Pathogenicity factors, effectors, cellular transporters of sugars and ions, phytotoxins and CAZymes were identified on both genomes. The number of CAZymes identified in the secretome of *D. eres* CBS 160.32 suggest that hydrolytic enzymes may not be the most relevant mechanism adopted by this species as a strategy to infect plant hosts. The comparative genome analyses revealed that species of *Diaporthe* exhibit a great diversity in the number of hydrolases, transferases, lyases and oxidoreductases. These are responsible for the breakdown or modification of plant cell wall polysaccharides, suggesting the ability to surpass the plant cell wall. The high number of predicted CAZymes may reflect an ecological selection and adaptation of these fungi to efficiently degrade the available biomass as carbon source. The genomic data of *D. amygdali* CAA958 and *D. eres* CBS 160.32 will add valuable information for further research on the mechanisms of *Diaporthe* that are involved in pathogenicity. Plant pathogen genomes alone are not sufficient to unravel pathogen-host interactions. Therefore, future studies using Dual RNA sequencing (RNA-Seq) technology, which allow for the analyses of both host and pathogen transcriptomes, may provide a better insight into the biology of pathogen infection, as well as host defense mechanisms.

ACKNOWLEDGMENTS

This research was funded by the Portuguese Foundation for Science and Technology (FCT/MCTES) for financing CESAM (Centre for Environmental and Marine Studies) (UIDP/50017/2020 + UIDB/50017/2020 + LA/P/0094/2020) through national funds, and individual grants to Sandra Hilário (SFRH/BD/137394/2018), Micael Gonçalves (SFRH/BD/129020/2017), Cátia Fidalgo (CEECIND/01373/2018) and Marta Tação (CEECIND/00977/2020).

DATA AVAILABILITY

All data generated and analyzed in this study are included in this article and its supplementary information files. The Whole Genome Shotgun project of *Diaporthe amygdali* and *D. eres* have been deposited in GenBank under the

accession number JAJATV000000000 and JAJATR000000000, respectively. The raw sequencing data for the *D. amygdali* genome and the assembly reported in this paper is associated with NCBI BioProject PRJNA718179, BioSample SAMN18524398 and SRA SRR14151706 within the GenBank. The data for *D. eres* genome and the assembly is associated with NCBI BioProject PRJNA763766, BioSample SAMN21449118 and SRA SRR16214651.

REFERENCES

- Armenteros JJA, Tsirigos KD, Sønderby CK, Petersen TN, Winther O, Brunak S, von Heijne G, Nielsen H. **2019**. SignalP 5.0 improves signal peptide predictions using deep neural networks. *Nature Biotechnology* 37, 420–423.
- Aylward J, Steenkamp ET, Dreyer LL, Roets F, Wingfield BD, Wingfield MJ. **2017**. A plant pathology perspective of fungal genome sequencing. *IMA Fungus* 8, 1–15.
- Ballio A, Michelis MI, Lado P, Randazzo G. **1981**. Fusicoccin structure-activity relationships: Stimulation of growth by cell enlargement and promotion of seed germination. *Physiologia Plantarum* 52, 471–475.
- Bankevich A, Nurk S, Antipov D, Gurevich AA, Dvorkin M, Kulikov AS, Lesin VM, Nikolenko SI, Pham S, Prjibelski AD, ... Pevzner PA. **2012**. SPAdes: a new genome assembly algorithm and its applications to single-cell sequencing. *Journal of Computational Biology* 19, 455–477.
- Baroncelli R, Amby DB, Zapparata A, Sarrocco S, Vannacci G, Le Floch G, Harrison RJ, Holub E, Sukno SA, Sreenivasaprasad A, ... Thon MR. **2016b**. Gene family expansions and contractions are associated with host range in plant pathogens of the genus *Colletotrichum*. *BMC Genomics* 17, 555.
- Baroncelli R, Scala F, Vergara M, Thon MR, Ruocco M. **2016a**. Draft whole-genome sequence of the *Diaporthe helianthi* 7/96 strain, causal agent of sunflower stem canker. *Genomics Data* 10, 151–152.
- Bettini PP, Frascella A, Kolařík M, Comparini C, Pepori AL, Santini A, Scala F, Scala A. **2014**. Widespread horizontal transfer of the cerato-ulmin gene between *Ophiostoma novo-ulmi* and *Geosmithia* species. *Fungal Biology* 118, 663–674.

- Bhunjun CS, Niskanen T, Suwannarach N, Wannathes N, Chen YJ, McKenzie EH, Maharachchikumbura SS, Buyck B, Zhao CL, Fan YG, ... Lumyong S. **2022**. The numbers of fungi: are the most speciose genera truly diverse?. *Fungal Diversity* 114, 387–462.
- Blin K, Shaw S, Steinke K, Villebro R, Ziemert N, Lee SY, Medema MH, Weber T. **2019**. AntiSMASH 5.0: updates to the secondary metabolite genome mining pipeline. *Nucleic Acids Research* 47, W81–W87.
- Bolger AM, Lohse M, Usadel B. **2014**. Trimmomatic: a flexible trimmer for Illumina sequence data. *Bioinformatics* 30, 2114–2120.
- Cardinaals J, Wenneker M, Voogd B, Van Leeuwen M. **2018**. Pathogenicity of *Diaporthe* spp. on two blueberry cultivars (*Vaccinium corymbosum*). *EPPO Bulletin* 48, 128–134.
- Chen H, Singh H, Bhardwaj N, Bhardwaj SK, Khatri M, Kim KH, Peng W. **2022**. An exploration on the toxicity mechanisms of phytotoxins and their potential utilities. *Critical Reviews in Environmental Science and Technology* 52, 395–435.
- Colabardini AC, Nicolas L, Ries A, Brown NA, Fernanda T, Savoldi M, Goldman MHS, Menino JF, Rodrigues F, Goldman GH. **2014**. Functional characterization of a xylose transporter in *Aspergillus nidulans*. *Biotechnology for Biofuels* 7, 46.
- Cregut M, Piutti S, Slezack-Deschaumes S, Benizri E. **2013**. Compartmentalization and regulation of arylsulfatase activities in *Streptomyces* sp., *Microbacterium* sp. and *Rhodococcus* sp. soil isolates in response to inorganic sulfate limitation. *Microbiological Research* 168, 12–21.
- Dong S, Wang Y. **2016**. Nudix Effectors: A common weapon in the arsenal of plant pathogens. *PLoS Pathogens* 12, e1005704.
- Ellwood SR, Liu Z, Syme RA, Lai Z, Hane JK, Keiper F, Moffat CS, Oliver RP, Friesen TL. **2010**. A first genome assembly of the barley fungal pathogen *Pyrenophora teres f. teres*. *Genome Biology* 11, 1–14.
- Eschenbrenner CJ, Feurtey A, Stukenbrock EH. **2020**. Population genomics of fungal plant pathogens and the analyses of rapidly evolving genome compartments. In *Statistical Population Genomics*; Dutheil JY, Ed.; Humana, New York, USA; pp. 337–355.

- Fang X, Qin K, Li S, Han S, Zhu T. **2020**. Whole genome sequence of *Diaporthe capsici*, a new pathogen of walnut blight. *Genomics* 112, 3751–3761.
- Farr DF, Castlebury LA, Rossman AY. **2002**. Morphological and molecular characterization of *Phomopsis vaccinii* and additional isolates of *Phomopsis* from blueberry and cranberry in the eastern United States. *Mycologia* 94, 494–504.
- Feldman AW, Graniti A, Sparapano L. **1971**. Effect of fusicoccin on abscission, cellulase activity and ethylene production in citrus leaf explants. *Physiological Plant Pathology* 1, 115–122.
- Félix C, Meneses R, Gonçalves MFM, Tilleman L, Duarte AS, Jorrín-Novo JV, Van de Peer Y, Deforce D, Van Nieuwerburgh F, Esteves AC, Alves A. **2019**. A multi-omics analysis of the grapevine pathogen *Lasiodiplodia theobromae* reveals that temperature affects the expression of virulence-and pathogenicity-related genes. *Scientific Reports* 9, 1–12.
- Figueiredo L, Santos RB, Figueiredo A. **2021**. Defense and offense strategies: the role of aspartic proteases in plant–pathogen interactions. *Biology* 2, 75.
- Figueiredo J, Sousa Silva M, Figueiredo A. **2018**. Subtilisin-like proteases in plant defence: the past, the present and beyond. *Molecular Plant Pathology* 19, 1017–1028.
- Gai Y, Xiong T, Xiao X, Li P, Zeng Y, Li L, Riely BK, Li H. **2021**. The genome sequence of the Citrus melanose pathogen *Diaporthe citri* and two Citrus-related *Diaporthe* Species. *Phytopathology* 111, 779–783.
- Gao Y, Liu F, Duan W, Crous PW, Cai L. **2017**. *Diaporthe* is paraphyletic. *IMA Fungus* 8, 153–187.
- Garcia JF, Lawrence DP, Morales-Cruz A, Travadon R, Minio A, Hernandez-Martinez R, Rolshausen PE, Baumgartner K, Cantu D. **2021**. Phylogenomics of plant-associated *Botryosphaeriaceae* species. *Frontiers in Microbiology* 12, 587.
- Gelfand Y, Rodriguez A, Benson G. **2007**. TRDB—the tandem repeats database. *Nucleic Acids Research* 35, D80–D87.

- Gomes RR, Glienke C, Videira SIR, Lombard L, Groenewald JZ, Crous PW. **2013**. *Diaporthe*: A genus of endophytic, saprobic and plant pathogenic fungi. *Persoonia* 31, 1–41.
- Gonçalves MFM, Nunes RB, Tilleman L, Van de Peer Y, Deforce D, Van Nieuwerburgh F, Esteves AC, Alves A. **2019**. Dual RNA sequencing of *Vitis vinifera* during *Lasiodiplodia theobromae* infection unveils host–pathogen interactions. *International Journal of Molecular Sciences* 20, 6083.
- Götz S, García-Gómez JM, Terol J, Williams TD, Nagaraj SH, Nueda MJ, Robles M, Talón M, Dopazo J, Conesa A. **2008**. High-throughput functional annotation and data mining with the Blast2GO suite. *Nucleic Acids Research* 36, 3420–3435.
- Guarnaccia V, Groenewald JZ, Woodhall J, Armengol J, Cinelli T, Eichmeier A, Ezra D, Fontaine F, Gramaje D, Gutierrez-Aguirregabiria A, ... Crous PW. **2018**. *Diaporthe* diversity and pathogenicity revealed from a broad survey of grapevine diseases in Europe. *Persoonia* 40, 135–153.
- Guo YS, Crous PW, Bai Q, Fu M, Yang MM, Wang XH, Du YM, Hong N, Xu WX, Wang GP. **2020**. High diversity of *Diaporthe* species associated with pear shoot canker in China. *Persoonia* 45, 132-162.
- Hallgren J, Tsirigos KD, Pedersen MD, Armenteros JJA, Marcotili P, Nielsen H, Krogh A, Winther O. **2022**. DeepTMHMM predicts alpha and beta transmembrane proteins using deep neural networks. *BioRxiv*, Preprint. <https://doi.org/10.1101/2022.04.08.487609> (accessed on 4 May 2022).
- Hilário S, Amaral AI, Gonçalves MFM, Lopes A, Santos L, Alves A. **2020**. Diversity and pathogenicity of *Diaporthe* species on blueberry plants in Portugal, with description of 4 new species. *Mycologia* 112, 293–308.
- Hilário S, Gonçalves FM, Alves A. **2021b**. Using genealogical concordance and coalescent-based species delimitation to assess species boundaries in the *Diaporthe eres* complex. *Journal of Fungi* 7, 507.
- Hilário S, Santos L, Alves A. **2021a**. Diversity and pathogenicity of *Diaporthe* species revealed from a survey of blueberry orchards in Portugal. *Agriculture* 11, 1271.

- Hilário S, Santos L, Alves A. **2021c**. *Diaporthe amygdali*, a species complex or a complex species? *Fungal Biology* 125, 505–518.
- Howlett BJ. **2006**. Secondary metabolite toxins and nutrition of plant pathogenic fungi. *Current Opinion in Plant Biology* 9, 371–375.
- Huang A, Lu M, Ling E, Li P, Wang C. **2020**. A M35 family metalloprotease is required for fungal virulence against insects by inactivating host prophenoloxidasases and beyond. *Virulence* 11, 222–237.
- Jimenez-Jimenez S, Hashimoto K, Santana O, Aguirre J, Kuchitsu K, Cárdenas L. **2019**. Emerging roles of tetraspanins in plant intercellular and inter-kingdom communication. *Plant Signaling and Behavior* 14, e1581559.
- Kong LA, Yang J, Li GT, Qi LL, Zhang YJ, Wang CF, Zhao WS, Xu JR, Peng YL. **2012**. Different chitin synthase genes are required for various developmental and plant infection processes in the rice blast fungus *Magnaporthe oryzae*. *PLoS Pathogens* 8, e1002526.
- Lanfermeijer FC, Prins H. **1994**. Modulation of H⁺-ATPase activity by fusicoccin in plasma membrane vesicles from oat (*Avena sativa* L.) roots (A comparison of modulation by fusicoccin, trypsin, and lysophosphatidylcholine). *Plant Physiology* 104, 1277–1285.
- Li S, Darwish O, Alkharouf NW, Musungu B, Matthews BF. **2017**. Analysis of the genome sequence of *Phomopsis longicolla*: a fungal pathogen causing *Phomopsis* seed decay in soybean. *BMC Genomics* 18, 688.
- Li Q, Gao Y, Yang A. **2019**. Sulfur homeostasis in plants. *International Journal of Molecular Sciences* 21, 8926.
- Lombard V, Golaconda Ramulu H, Drula E, Coutinho PM, Henrissat B. **2014**. The carbohydrate-active enzymes database (CAZy) in 2013. *Nucleic Acids Research* 42, D490–D495.
- López-Berges MS, Hera C, Sulyok M, Schäfer K, Capilla J, Guarro J, Di Pietro A. **2013**. The velvet complex governs mycotoxin production and virulence of *Fusarium oxysporum* on plant and mammalian hosts. *Molecular Microbiology* 87, 49–65.

- Lowe TM, Eddy SR. **1997**. tRNAscan-SE: a program for improved detection of transfer RNA genes in genomic sequence. *Nucleic Acids Research* 25, 955–964.
- Lyu X, Shen C, Fu Y, Xie J, Jiang D, Li G, Cheng J. **2015**. Comparative genomic and transcriptional analyses of the carbohydrate-active enzymes and secretomes of phytopathogenic fungi reveal their significant roles during infection and development. *Scientific Reports* 5, 15565.
- Madhu SN, Sharma S, Gajjar DU. **2020**. Identification of proteases: carboxypeptidase and aminopeptidase as putative virulence factors of species complex. *Open Microbiology Journal* 14, 266-277.
- Marra A, Camoni AL, Visconti A, Fiorillo A, Evident A. **2021**. The Surprising story of Fusicoccin: a wilt-inducing phytotoxin, a tool in plant physiology and a 14-3-3-Targeted Drug. *Biomolecules* 11, 1393. Möller M, Stukenbrock EH. **2017**. Evolution and genome architecture in fungal plant pathogens. *Nature Reviews Microbiology* 15, 756–771.
- Meena M, Prasad V, Zehra A, Gupta VK, Upadhyay RS. **2015**. Mannitol metabolism during pathogenic fungal–host inter-actions under stressed conditions. *Frontiers in Microbiology* 6, 1019.
- Mena E, Garaycochea S, Stewart S, Montesano M, Ponce De León I. **2022**. Comparative genomics of plant pathogenic *Diaporthe* species and transcriptomics of *Diaporthe caulivora* during host infection reveal insights into pathogenic strategies of the genus. *BMC Genomics* 23, 175.
- Murry R, Traxler L, Pötschner J, Krüger T, Kniemeyer O, Krause K, Kothe E. **2021**. Inositol signaling in the basidiomycete fungus *Schizophyllum commune*. *Journal of Fungi* 7, 470.
- Morales-Cruz A, Amrine KCH, Blanco-Ulate B, Lawrence DP, Travadon R, Rolshausen PE, Baumgartner K, Cantu D. **2015**. Distinctive expansion of gene families associated with plant cell wall degradation, secondary metabolism, and nutrient uptake in the genomes of grapevine trunk pathogens. *BMC Genomics* 16, 1–22.
- Nagel JH, Wingfield MJ, Slippers B. **2021**. Increased abundance of secreted hydrolytic enzymes and secondary metabolite gene clusters define the

- genomes of latent plant pathogens in the *Botryosphaeriaceae*. *BMC Genomics* 22, 589.
- Nogueira KM, de Paula RG, Antoniêto ACC, Dos Reis TF, Carraro CB, Silva AC, Almeida F, Rechia CGV, Goldman GH, Silva RN. **2018**. Characterization of a novel sugar transporter involved in sugarcane bagasse degradation in *Trichoderma reesei*. *Biotechnology for Biofuels* 11, 84.
- Noike M, Liu C, Ono Y, Hamano Y, Toyomasu T, Sassa T, Kato N, Dairi T. **2012b**. An enzyme catalyzing O-Prenylation of the glucose moiety of Fusicoccin A, a diterpene glucoside produced by the fungus *Phomopsis amygdali*. *Chembiochem* 13, 566-573.
- Noike M, Ono Y, Araki Y, Tanio R, Higuchi Y, Nitta H, Hamano Y, Toyomasu T, Sassa T, Kato N, ... Dairi T. **2012a**. Molecular breeding of a fungus producing a precursor diterpene suitable for semi-synthesis by dissection of the biosynthetic machinery. *Plos One* 7, e42090.
- Ohkanda J. **2021**. Fusicoccin: A chemical modulator for 14-3-3 proteins. *Chemistry Letters* 50, 57–67.
- Ohm RA, Feau N, Henrissat B, Schoch CL, Horwitz BA, Barry KW, Condon BJ, Copeland AC, Dhillon B, Glaser F, ... Grigoriev IV. **2012**. Diverse lifestyles and strategies of plant pathogenesis encoded in the genomes of eighteen *Dothideomycetes* fungi. *PLoS Pathogens* 8, e1003037.
- Paietta JV. **2004**. Regulation of sulfur metabolism in mycelial fungi. In *The Mycota III: Biochemistry Molecular Biology 2nd Edition*; Brambl R, Marzluf GA, Eds.; Springer, Berlin, Germany; pp. 369–383.
- Palmer GE. **2011**. Vacuolar trafficking and *Candida albicans* pathogenesis. *Communicative and Integrative Biology* 4, 240–242.
- Paolinelli-Alfonso M, Villalobos-Escobedo JM, Rolshausen P, Herrera-Estrella A, Galindo-Sánchez C, López-Hernández JF, Hernandez-Martinez R. **2016**. Global transcriptional analysis suggests *Lasiodiplodia theobromae* pathogenicity factors involved in modulation of grapevine defensive response. *BMC Genomics* 17, 615.
- Pitcher DG, Saunders NA, Owen RJ. **1989**. Rapid extraction of bacterial genomic DNA with guanidium thiocyanate. *Letters in Applied Microbiology* 8, 151–156.

- Rafiei V, Véléz H, Tzelepis G. **2021**. The role of glycoside hydrolases in phytopathogenic fungi and oomycetes virulence. *International Journal of Molecular Sciences* 22, 9359.
- Reichard U, Léchenne B, Asif AR, Streit F, Grouzmann E, Jousson O, Monod M. **2006**. Sedolisins, a new class of secreted proteases from *Aspergillus fumigatus* with endoprotease or tripeptidyl-peptidase activity at acidic pHs. *Applied and Environmental Microbiology* 72, 1739–1748.
- Reynolds TB. **2009**. Strategies for acquiring the phospholipid metabolite inositol in pathogenic bacteria, fungi, and protozoa: making it and taking it. *Microbiology* 155, 1386.
- Rocha MC, de Godoy KF, Bannitz-Fernandes R, Fabri JHM, Barbosa MMF, de Castro PA, Almeida F, Goldman GH, da Cunha AF, Netto LE, ... Malavazi I. **2018**. Analyses of the three 1-Cys peroxiredoxins from *Aspergillus fumigatus* reveal that cytosolic Prx1 is central to H₂O₂ metabolism and virulence. *Scientific Reports* 8, 12314.
- Saier Jr MH, Reddy VS, Tsu BV, Ahmed MS, Li C, Moreno-Hagelsieb G. **2016**. The transporter classification database (TCDB): recent advances. *Nucleic Acids Research* 44, D372–D379.
- Silva MG, de Curcio JS, Silva-Bailão MG, Lima RM, Tomazett MV, de Souza AF, Cruz-Leite VRM, Sbaraini N, Bailão AM, Rodrigues F, ... Almeida Soares CM. **2020**. Molecular characterization of siderophore biosynthesis in *Paracoccidioides brasiliensis*. *IMA Fungus* 11, 11.
- Singh SK, Strobel GA, Knighton B, Geary B, Sears J, Ezra D. **2011**. An endophytic *Phomopsis* sp. possessing bioactivity and fuel potential with its volatile organic compounds. *Microbial Ecology* 61, 729–739.
- Smit AFA, Hubley R, Green P. **2015**. RepeatMasker Open-4.0. 2018. Institute for Systems Biology. Available online <http://www.repeat-masker.org> (accessed on 10 February 2021).
- Sperschneider J, Dodds PN. **2022**. EffectorP 3.0: prediction of apoplasmic and cytoplasmic effectors in fungi and oomycetes. *Molecular Plant Microbe Interactions* 35, 146–156.

- Stanke M, Steinkamp R, Waack S, Morgenstern B. **2004**. AUGUSTUS: a web server for gene finding in eukaryotes. *Nucleic Acids Research* 32, 309–312.
- Stergiopoulos I, Zwiars LH, De Waard MA. **2002**. Secretion of natural and synthetic toxic compounds from filamentous fungi by membrane transporters of the ATP-binding cassette and major facilitator superfamily. *European Journal of Plant Pathology* 108, 719–734.
- Tanaka S, Yamada K, Yabumoto K, Fujii S, Huser A, Tsuji G, Koga H, Dohi K, Mori M, Shiraishi T, ... Kubo Y. **2007**. *Saccharomyces cerevisiae* SSD1 orthologues are essential for host infection by the ascomycete plant pathogens *Colletotrichum lagenarium* and *Magnaporthe grisea*. *Molecular Microbiology* 64, 1332–1349.
- Tanney JB, McMullin DR, Green BD, Miller JD, Seifert KA. **2016**. Production of antifungal and antiinsectan metabolites by the *Picea* endophyte *Diaporthe maritima* sp. nov. *Fungal Biology* 120, 1448–1457.
- Temple B, Horgen PA. **2000**. Biological roles for cerato-ulmin, a hydrophobin secreted by the elm pathogens, *Ophiostoma ulmi* and *O. novo-ulmi*. *Mycologia* 92, 1–9.
- Thammahong A, Dhingra S, Bultman KM, Kerkaert JD, Cramer RA. **2009**. An Ssd1 homolog impacts trehalose and chitin biosynthesis and contributes to virulence in *Aspergillus fumigatus*. *mSphere* 4, e00244-19.
- Traynor AM, Sheridan KJ, Jones GW, Calera JA, Doyle S. **2019**. Involvement of sulfur in the biosynthesis of essential metabolites in pathogenic fungi of animals, particularly *Aspergillus* spp.: molecular and therapeutic implications. *Frontiers in Microbiology* 10, 2859.
- Tsuge T, Harimoto Y, Akimitsu K, Ohtani K, Kodama M, Akagi Y, Egusa M, Yamamoto M, Otani H. **2013**. Host selective toxins produced by the plant pathogenic fungus *Alternaria alternata*. *FEMS Microbiology Reviews* 37, 44–66.
- Turner NC, Graniti A. **1969**. Fusicochin: a fungal toxin that opens stomata. *Nature* 223, 1070–1071.

- Udayanga D, Liu X, Crous PW, McKenzie EH, Chukeatirote E, Hyde KD. **2012**. A multi-locus phylogenetic evaluation of *Diaporthe* (*Phomopsis*). *Fungal Diversity* 56, 157–171.
- Udayanga D, Liu X, McKenzie EHC, Chukeatirote E, Bahkali AHA, Hyde KD. **2011**. The genus *Phomopsis*: Biology, applications, species concepts and names of common phytopathogens. *Fungal Diversity* 50, 189–225.
- Urban M, Cuzick A, Seager J, Wood V, Rutherford K, Venkatesh SY, De Silva N, Martinez MC, Pedro H, Yates AD, Hassani-Pak K. **2020**. PHI-base: the pathogen–host interactions database. *Nucleic Acids Research* 48, D613–D620.
- Varjas V, Vajna L, Izsépi F, Nagy G, Pájtli É. **2017**. First report of *Phomopsis amygdali* causing twig canker on almond in Hungary. *Plant Disease* 101, 1674.
- Wang M, Fu H, Ruan R. **2019**. A small horizontally transferred gene cluster contributes to the sporulation of *Alternaria alternata*. *Genome Biology and Evolution* 12, 3436–3444.
- Wang Y, Wu J, Yan J, Guo M, Xu L, Hou L, Zou Q. **2022**. Comparative genome analysis of plant ascomycete fungal pathogens with different lifestyles reveals distinctive virulence strategies. *BMC Genomics* 23, 34.
- Yan JY, Zhao WS, Chen Z, Xing QK, Zhang W, Chethana KT, Xue MF, Xu JP, Phillips AJL, Wang Y, ...Li XH. **2018**. Comparative genome and transcriptome analyses reveal adaptations to opportunistic infections in woody plant degrading pathogens of *Botryosphaeriaceae*. *DNA Research* 25, 87–102.
- Yang Y, Yao X, Xhang X, Zou H, Chen J, Fang B, Huang L. **2022**. Draft genome sequence of *Diaporthe batatatis* causing dry rot disease in sweet potato. *Plant Disease* 106, 737–740.
- Yin Y, Mao X, Yang J, Chen X, Mao F, Xu Y. **2012**. dbCAN: a web resource for automated carbohydrate-active enzyme annotation. *Nucleic Acids Research* 40, W445–W451.


SUPPLEMENTARY MATERIAL

The supplementary tables of this chapter (S1–S11) are deposited in an excel file named “Supplementary Material Chapter 6”.



CHAPTER 7

Final Considerations



GENERAL DISCUSSION

The blueberry (*Vaccinium corymbosum*) is native to North America, and its production in Portugal started in the 1990s. Since 2007 blueberry crop production has increased exponentially to supply the European markets, and nowadays it is a highly profitable crop to Portugal (Madeira 2016). However, the intercontinental spread of blueberry plant material has resulted in an increase of diseases caused mainly by fungi (Lombard et al. 2014). Among these, members of the genus *Diaporthe* represent an important role as plant pathogens in blueberry plant (Gomes et al. 2013). Moreover, species of *Diaporthe* can asymptotically colonize plant tissues, living as endophytes or opportunistic pathogens, that behave as hitchhiking organisms upon plant material spread (Fisher et al. 2012).

Blueberry twig blight and dieback symptoms typical of *Diaporthe* have been occasionally observed in Portugal, although based solely on the observation of symptoms in the field. Therefore, with this thesis we contributed to disclose the diversity of species of *Diaporthe* associated to these symptoms, as well as to disclose their pathogenic potential on blueberry plants.

As described in Chapter 2, this thesis aimed to study the occurrence of *Diaporthe* species on blueberry plants, in Portugal, showing twig blight and dieback symptoms. For that, first, the survey was carried out in one of the major Portuguese regions of blueberry production (Sever do Vouga, Aveiro). Then, the survey was scaled-up and implemented across the country, attempting to cover different geographical locations. The isolates obtained were assigned to known species such as *D. foeniculina*, *D. rudis*, *D. malorum*, *D. amygdali* and *D. ambigua*. Additionally, four new species were described, such as *D. rossmaniae*, *D. vacuae*, *D. phillipsii* and *D. crousii*. *Diaporthe hybrida* was also found during this survey, and it was reported as the first hybrid in the genus *Diaporthe*. Moreover, some taxonomic ambiguities were resolved and *D. rossmaniae* was synonymized with *D. leucospermi*. *Diaporthe amygdali*, *D. hybrida*, *D. rossmaniae* (syn. *D. leucospermi*) and *D. malorum* are reported for the first time on diseased blueberries in Portugal and worldwide. Whereas the presence of *D. rudis*, *D. foeniculina* and *D. ambigua* have been already reported on this crop mainly in the Netherlands (Cardinaals et al. 2018; Lombard et al. 2014), Italy (Guarnaccia et al. 2020) and Chile (Elfar et al.

2013). Although *D. vaccinii* (syn. *D. eres*) was claimed to be observed in Portugal based on the observation of symptoms (Madeira 2016), it was not found during our survey.

Besides the few studies on the diversity of *Diaporthe* species associated to blueberry plants, their pathogenicity is often underestimated or untested. For instance, *D. ambigua* was claimed to be one of the least virulent species on blueberry plants, but the records of this pathogen are limited (Elfar et al. 2013). The occasional occurrence of *D. ambigua* on blueberry plants and its low level of aggressiveness demonstrated in Chapter 2, is corroborated by Santos & Phillips (2009) and Spies et al. (2020) who suggested that *D. ambigua* may have a saprophytic behavior. Lombard et al. (2014) reported the presence of *D. rudis* on blueberry plants, but it is uncertain whether pathogenicity tests were performed. According to our pathogenicity assays, performed in greenhouse conditions (Chapter 2), all *Diaporthe* species caused symptoms on blueberry plants cultivars 'Bluecrop', 'Duke', 'Legacy' and 'Spartan'. Overall, in our study, *D. vacuae* (syn. *D. eres*) and *D. amygdali* showed to be the most aggressive species, whereas *D. ambigua*, *D. foeniculina*, *D. rudis* and *D. leucospermi* exhibited the smallest lesions and are thus considered as weak pathogens. Although Nabetani et al. (2017) considered *D. vaccinii* (syn. *D. eres*) as the major cause of twig blight on blueberries, this pathogen was regarded as one of the least aggressive to blueberry plants, and thus not considered a threat to blueberry plants (Cardinaals et al. 2018; Chapter 2, 5). This difference in aggressiveness might be associated with the different *D. vaccinii* isolates used in these studies. For instance, for the pathogenicity assays, Nabetani et al (2017) used isolates that were recovered from symptomatic *V. corymbosum* plants, and Cardinaals et al. (2018) used isolates that were recovered from *V. oxycoccus* and *V. macrocarpon* plants. In Chapters 2, and 5, the ex-type strain CBS 160.32 from *V. macrocarpon* was used.

The early and accurate detection and identification of fungal plant pathogens is crucial to mitigate or prevent disease outbreaks, that may result in economic losses (Hariharan and Prasannath 2021). Therefore, a more detailed phylogenetic study was applied in Chapter 3, to assist in a more accurate species delimitation of

D. amygdali (one of the most aggressive species), and *D. vaccinii* (syn. *D. eres*) (given its quarantine status at the time of this study).

The delimitation of species in the genus *Diaporthe* is not always simple. Over the last years the genus *Diaporthe* has received considerable attention and several new species have been described (Sun et al. 2021; Wang et al. 2021). To better estimate the species boundaries in *Diaporthe*, several authors have adopted a five-loci dataset which includes the ITS region and part of the *tef1- α* , *tub2*, *his3* and *cal* genes, for the construction of multi-locus phylogenetic analyses (Gomes et al., 2013; Guo et al. 2020; Santos et al. 2017). The identification of species has been largely based on the application of the Phylogenetic Species Concept (PSC) that diagnoses species as “the smallest aggregation of populations with a common lineage that share unique, diagnosable phenotypic characters” (Harrington and Rizzo 1999). However, this cannot be taken as granted for the genus *Diaporthe*, given the presence of morphological indistinctiveness as demonstrated in Chapter 3, for the *D. amygdali* and *D. eres* species complexes. Moreover, besides the application of multiple gene genealogies and its concatenation, the PSC should also be combined with the GCPSR principle, as well as looking for incongruencies among individual gene genealogies. Gene concatenation, if not checked for incongruencies, results in gene trees that reflects levels of incomplete lineage sorting or recombination, which may overrate the true fungal diversity (Mendes and Hahn 2018). Accordingly, the results shown in Chapter 3 suggest that the actual number of species in *Diaporthe* has been largely overestimated, since they are described based on well-supported clades that are accepted as distinct taxa.

The application of phylogenetic networks, studies on population genetic diversity, studies to detect recombination among individuals, and the GCPSR principle applied in this thesis (Chapter 3), revealed to be fundamental to circumscribe the boundaries of *D. amygdali* and *D. eres* species complexes (Fig. 1). Additionally, the construction of species trees based on coalescent-based delimitation methods (mostly PTP as it is time-calibrated independent) revealed also to be a promising tool to delimit species, when dealing with conflicts among gene trees and when the concatenation of genes is an inappropriate approach. In Chapter 3, we showed clear evidence that *D. amygdali* and *D. eres* are complex

species harboring high rates of intraspecific variability and that must be regarded as a single species. In this chapter, *D. vaccinii* (formerly regarded as a quarantine organism) was synonymized with *D. eres*, which corroborates previous studies conducted by Lombard et al. (2014) and Elfar et al. (2013), who suggested that *D. vaccinii* might have been wrongly identified.

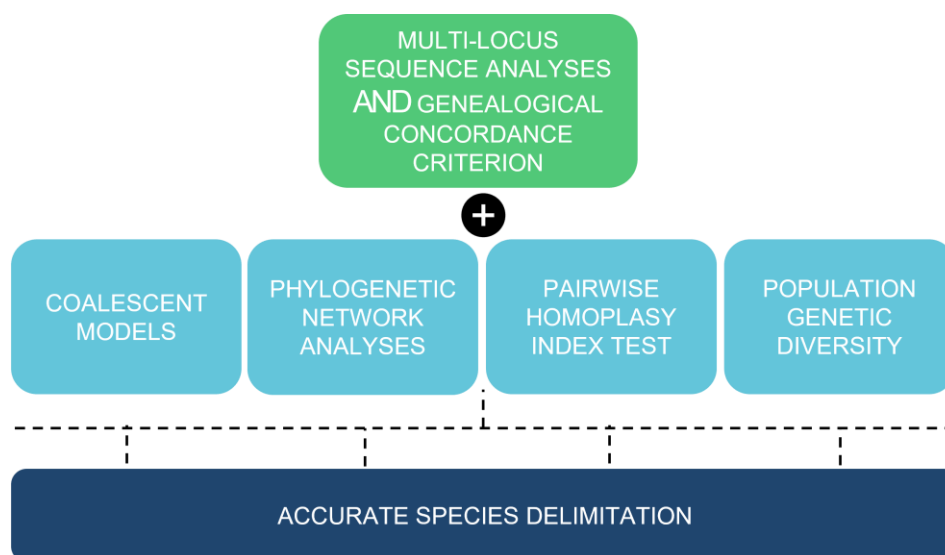


Figure 1. Representation of the main steps to consider an accurate species delimitation in the genus *Diaporthe*. The arrows do not represent a workflow.

Taking into consideration the challenges encountered in Chapter 3 related the high variability in the ITS region, a more detailed study to uncover the pitfalls of this ribosomal DNA region was conducted (Chapter 4). Despite the recognized low discriminatory power of ITS, this region has been accepted as the primary DNA barcode for fungi (Schoch et al. 2012). Nevertheless, some studies have demonstrated an intragenomic variation of the ITS region in several genera, raising questions about the usefulness of ITS (Hibbett et al. 2011). The results of this thesis evidenced the occurrence of intrasporocarpic ITS variability, intragenomic ITS heterogeneity, intraspecific ITS variability and hybridization events in the genus *Diaporthe* (Fig. 2). Such findings may be explained by a failure of concerted evolution in the ITS region, ongoing speciation events or even recombination among individuals, as previously advocated by Tremble et al. (2019).

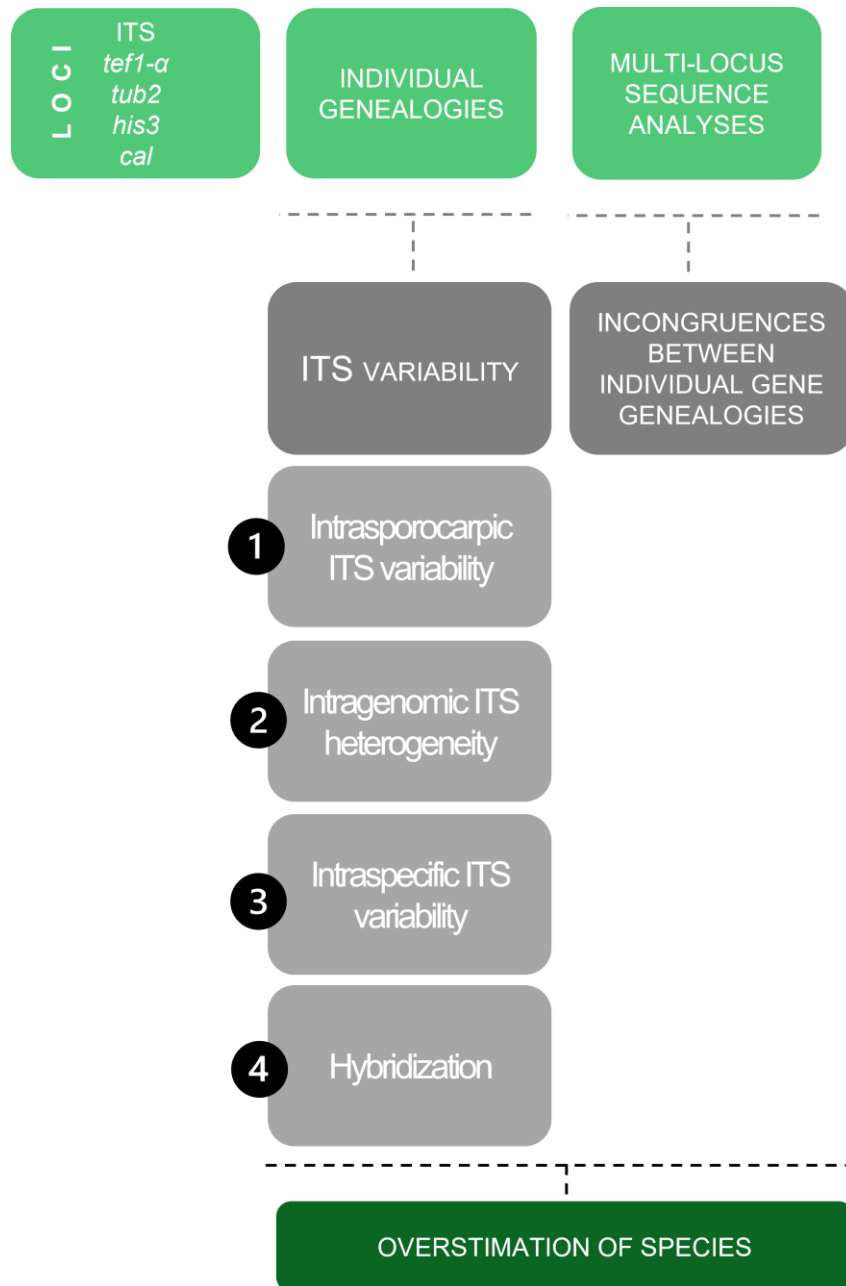


Figure 2. Schematic representation for the construction of phylogenetic trees in the genus *Diaporthe*, the main pitfalls (1–4) associated to the use of the ITS region on species delimitation.

Moreover, apart from this variation in the ITS region, this thesis demonstrated that hybridization may have occurred between *D. portugallica* and *D. phillipsii*, by reporting the first hybrid in the genus *Diaporthe* (*D. hybrida*). Therefore, the possibility of hybridization in the genus *Diaporthe* may reveal a lack of reproductive barriers between these 2 species, and thus be regarded as the same biological species. These results highlight the importance to:

1. Add as many isolates as possible in the phylogenetic analyses of *Diaporthe* to determine intraspecific variation.
2. Analyze the ITS region before the description of any new taxa.
3. Apply the GCPSR principle so that gene genealogies result in similar topologies.
4. Implement a cohesive approach including phylogenetic analyses, phylogenetic networks, and coalescent-based methods to allow a reliable delimitation of species.

Another important aspect is the need to investigate the physiological plant responses to fungal infection coupled with water scarcity. Since the dissemination of pathogens and the limited water availability are a threat that can cause economic losses in agriculture (del Pozo et al. 2019). This is particularly important in crops from the Mediterranean area, including the blueberry plant, which are under an acute lack of precipitation (Tramblay et al. 2020). Although previous studies demonstrated that low water availability may increase fungal disease susceptibility (Ghanbary et al. 2021), the effects of stress scenarios (e.g., drought) on disease development caused by *Diaporthe* is still poorly explored. Moreover, it is also important to highlight that species of the genus *Diaporthe* can switch from an endophytic to a pathogenic stage when the host is under environmental stimuli (Hrycan et al. 2020). In this regard, in Chapter 5, we assessed for the first time the interaction of the pathosystem *V. corymbosum* / *Diaporthe* spp. to understand whether disease susceptibility is enhanced by water deficit conditions.

Despite the observed lesions and mortality rates caused by *D. eres* and *D. amygdali* infection, the lesion size might not be directly related to physiological disorders. In this regard, the assessment of fungal pathogenicity should include additional parameters that evaluate the physiological performance of the plant. Moreover, this study is also in line with the concept that species of *Diaporthe* are endophytes or latent pathogens that can live in plants without causing any symptoms until some environmental stimuli induces a switch in the lifestyle (Gomes et al. 2013). Considering this, is it plausible that under optimal growth conditions (well-watered), blueberry plants may have counteracted pathogen attack. For instance, plants inoculated with *D. eres* (syn. *D. vaccinii*), the least aggressive

pathogen, showed an increase in MDA content and a stability on the antioxidant content under well-watered conditions. This evidences that plants used MDA as a signaling molecule and that the antioxidant system was not activated as a strategy to cope with *D. eres* infection.

On the other hand, under an environmental stress imposed by climate change (e.g., water limitation), plants response could change. In fact, the higher mortality rate caused by *D. amygdali* under water deficit conditions reported in this research, suggested that this pathogen acted as latent pathogen, transitioning to a pathogenic phase after the host was exposed to water limitation. Nevertheless, the plant has also managed to respond to the pathogen attack under such conditions. In fact, water deficit plants inoculated with both *D. eres* and *D. amygdali* showed, for instance, stomatal limitations, high levels of proline, total soluble sugars, and starch. Such outcomes indicate that proline may act as a signaling molecule rather than an osmoprotectant to cope with pathogen infection, while total soluble sugars and starch may be used by infected plants to maintain cell turgor and to protect them against oxidative stress.

Overall, this chapter highlights that:

1. Water limitation can trigger disease caused by species of *Diaporthe*.
2. Water availability is considered a key factor for the pathogenicity of *D. amygdali*.
3. Water deficit conditions impacted plant physiological performance to trigger a water save strategy.
4. The irrigation regime applied was not sufficient to cause severe stress on blueberry plants.

To find clues on the pathogenicity factors that may be related to *Diaporthe* infection on blueberry plants, and to add more valuable information to the genome database of *Diaporthe*, the genomes of *D. amygdali* and *D. eres* (syn. *D. vaccinii*) were sequenced, annotated, and analyzed (Chapter 6). Our findings underline genomic signatures that allow both species to successfully invade the host plant through the presence of:

1. CAZymes produced by fungi to degrade plant cell wall polysaccharides (e.g., pectins, celluloses, lignins), ensuring a successful entry into the host.
2. BGCs encoding for toxic metabolites that injures plant cells and enhances disease progression. (e.g., alternariol, Fusicoccin A, ACT-toxin II).
3. Cellular transporters allowing fungi to transport ions (e.g., zinc, sulfur, copper), molecules to enhance pathogenicity (e.g., peroxiredoxin, tetraspanin) and sugars resulting from plant polysaccharides degradation (e.g., glucose, xylose, inositol, and glycerol).
4. Pathogenicity factors (e.g., acid aspartate, aminopeptidase) and candidate effectors (e.g., carboxylesterases, pectate lyases, laccases) that facilitates the host to be infected.

The genome analysis revealed also that although *D. amygdali* and *D. eres* (syn. *D. vaccinii*) showed abundant number of CAZymes, their proportion in the secretome of *D. eres* (syn. *D. vaccinii*) was estimated at 5.4%, while *D. amygdali* is represented by 29.1%. Such result is congruent with other studies in *Diaporthe* (Mena et al. 2022) and denotes the importance of CAZymes in the pathogenicity of *D. amygdali*, whereas secreted hydrolytic enzymes might not be essential for the pathogenicity of *D. eres* (syn. *D. vaccinii*). This result, allied to the fact that *D. vaccinii* was for many years wrongly regarded as a threat to blueberry plantations is now consistent with studies that categorizes this species as a weak pathogen on blueberry plants (Cardinaals et al. 2018; Chapter 2, 5). Moreover, this outcome also corroborates the new European Union (EU) Regulation of 29 November 2019 (2019/2072), that has no longer included *D. vaccinii* into the list of EU quarantine pests.

FUTURE PERSPECTIVES

Despite the contribution of the present thesis to the knowledge of species of *Diaporthe* on blueberry plants in the North and Centre of Portugal, and their pathogenesis, integration of omics approaches should be undertaken to unveil the mechanisms used by these fungal species during the infection process. As the

interaction between plants and their pathogens is a dynamic process, it would be important to use transcriptomics, proteomics, and metabolomics to detect *Diaporthe*-specific transcripts, proteins, and metabolites, respectively, involved in the infection process. Moreover, the application of the Dual RNA sequencing (RNA-Seq) is also a promising approach since it allows not only the detection of pathogen-specific transcripts, but also a thorough insight into the biology of pathogen infection, as well as host defense mechanisms.

The results obtained in this thesis suggest that water limitation triggers a strategy to avoid water losses and can enhance *D. amygdali* infection on blueberry plants. Nevertheless, a study using a stricter water regime, coupled with omics and Dual RNA-Seq approaches would be valuable to understand how blueberry plants cope with the infection by species of *Diaporthe* under climate changes in the Mediterranean (e.g., drought).

Diaporthe is considered one of the most common genera with endophytic species. To explore the dynamics of *Diaporthe* under different environmental conditions (e.g., drought or high salinity) using culture-independent methodologies, would be an interesting future work. This would offer insights into the endophytic community to evaluate how these species can survive in such environments and to study their plant growth-promoting potential. Omics approaches, at this stage, will be crucial to understand adaptation patterns of the endophytic community in response to environmental stimuli: key genes and transcripts, metabolites and proteins that may help plants to thrive in such conditions.

Several species of *Diaporthe* are important plant-pathogens. To facilitate the diagnosis of diseases caused by these fungi, it is crucial to develop accurate diagnostic methods. Considering the availability of a large amount of DNA sequences for many species, it is possible to develop species-specific primers for diagnostic tests. Given that species of *Diaporthe* can co-occur with members of the family *Botryosphaeriaceae* it would be essential to perform Real-Time PCR assays for the diagnosis and quantification of co-infections on blueberry plants.

REFERENCES

- Cardinaals J, Wenneker M, Voogd B, Van Leeuwen M. **2018**. Pathogenicity of *Diaporthe* spp. on two blueberry cultivars (*Vaccinium corymbosum*). *EPPO Bulletin* 48, 128–134.
- del Pozo A, Brunel-Saldias N, Engler A, Ortega-Farias S, Acevedo-Opazo C, Lobos GA, Jara-Rojas R, Molina-Montenegro MA. **2019**. Climate change impacts and adaptation strategies of agriculture in Mediterranean-climate regions (MCRs). *Sustainability* 11, 2769.
- Elfaz K, Torres R, Díaz GA, Latorre B. **2013**. Characterization of *Diaporthe australafricana* and *Diaporthe* spp. associated with stem canker of blueberry in Chile. *Plant Disease* 97, 1042–1050.
- Fisher, M.C., Gurr, S.J., Cuomo, C.A., Blehert, D.S., Jin, H., Stukenbrock, E.H., Stajich, J.E., Kahmann, R., Boone, C., Denning, D.W. & Gow, N.A. (2020). Threats posed by the fungal kingdom to humans, wildlife, and agriculture. *MBio* 11, e00449-20.
- Ghanbary E, Fathizadeh O, Pazhouhan I, Zarafshar M, Tabari M, Jafarnia S, Parad GA, Bader MKF. **2021**. Drought and pathogen effects on survival, leaf physiology, oxidative damage, and defense in two Middle Eastern oak species. *Forests* 12, 247.
- Gomes, R.R., Glienke, C., Videira, S.I.R., Lombard, L., Groenewald, J.Z. & Crous, P.W. (2013). *Diaporthe*: A genus of endophytic, saprobic and plant pathogenic fungi. *Persoonia* 31, 1–41.
- Guarnaccia V, Martino I, Tabone G, Brondino L, Gullino ML. **2020**. Fungal pathogens associated with stem blight and dieback of blueberry in northern Italy. *Phytopathologia Mediterranea* 59, 229-245.
- Guo, Y.S., Crous, P.W., Bai, Q., Fu, M., Yang, M.M., Wang, X.H., Du, Y.M., Hong, N., Xu, W.X. & Wang, G.P. (2020). High diversity of *Diaporthe* species associated with pear shoot canker in China. *Persoonia* 45, 132-162.
- Hariharan G, Prasannath K. **2021**. Recent advances in molecular diagnostics of fungal plant pathogens: a mini review. *Frontiers in Cellular and Infection Microbiology* 10, 829.

- Harrington TC, Rizzo DM. **1999**. Defining species in the fungi. In: Worrall JJ, ed. *Structure and dynamics of fungal populations*. Dordrecht, Netherlands: Springer. p. 43–71.
- Hibbett DS, Ohman A, Glotzer D, Nuhn M, Kirk P, Nilsson RH. **2011**. Progress in molecular and morphological taxon discovery in fungi and options for formal classification of environmental sequences. *Fungal Biology Reviews* 25, 38–47.
- Hrycan J, Hart M, Bowen P, Forge T, Urbez-Torres JR. **2020**. Grapevine trunk disease fungi: their roles as latent pathogens and stress factors that favour disease development and symptom expression. *Phytopathologia Mediterranea* 59, 395-424.
- Lombard L, Van Leeuwen GCM, Guarnaccia V, Polizzi G, Van Rijswijk PCJ, Rosendahl CHM, Gabler J, Crous PW. **2014**. *Diaporthe* species associated with *Vaccinium*, with specific reference to Europe. *Phytopathologia Mediterranea* 53, 287–299.
- Madeira BSP. **2016**. Cultura do Mirtilo. Lisboa: Publindústria, Agrobook.
- Mendes FK, Hahn MW. **2018**. Why concatenation fails near the anomaly zone. *Systematic Biology* 67, 158–169.
- Nabetani K, Wood B, Sabaratnam S. **2017**. Role of pycnidia in twig and blossom blight and stem dieback of highbush blueberry caused by *Phomopsis vaccinii* in British Columbia. *Canadian Journal of Plant Pathology* 39, 405–421.
- Santos L, Alves A, Alves, R. **2017**. Evaluating multi-locus phylogenies for species boundaries determination in the genus *Diaporthe*. *Peer J* 5, e3120.
- Schoch, C.L., Seifert, K.A., Huhndorf, S., Robert, V., Spouge, J.L., Levesque, C.A., Chen, W., & Fungal Barcoding Consortium. Nuclear ribosomal internal transcribed spacer (ITS) region region as universal DNA barcode marker for Fungi. *Proceedings of the National Academy of Sciences of the United States of America* 109, 6241-6246.
- Sun W, Huang S, Xia J, Zhang X, Li Z. **2021**. Morphological and molecular identification of *Diaporthe* species in south-western China, with description of eight new species. *MycologyKeys* 77, 65.
- Tramblay Y, Koutroulis A, Samaniego L, Vicente-Serrano SM, Volaire F, Boone A, Le Page M, Llasat MC, Albergel C, Burak S, ... Polcher J. **2020**. Challenges for

drought assessment in the Mediterranean region under future climate scenarios. *Earth-Science Reviews* 210, 103348.

Tremble K, Suz LM, Dentinger BT. **2019**. Lost in Translation: population genomics and long-read sequencing reveals relaxation of concerted evolution of the ribosomal DNA cistron. *bioRxiv* 811216.

Wang X, Guo Y, Du Y, Yang Z, Huang X, Hong N, Xu W, Wang G. **2021**. Characterization of *Diaporthe* species associated with peach constriction canker, with two novel species from China. *MycKeys* 80, 77.